Nonlinear analysis methods in neural field models

Romain Veltz

UNIVERSITY OF PARIS-EST

DOCTORAL SCHOOL MSTIC

MATHEMATIQUES ET SCIENCES ET
TECHNOLOGIES DE L'INFORMATION ET
DE LA COMMUNICATION

P H D T H E S I S

to obtain the title of

PhD of Science

of the University of Paris Est

Specialty : Computer Science

Defended by

Romain Veltz

Nonlinear analysis methods in neural field models

Thesis Advisors:

- Olivier Faugeras
- Renaud Keriven

prepared at INRIA Sophia Antipolis, NeuroMathComp Team

defended on 16th, December 2011

Committee:

Reviewers:	Paul Bressloff	-	University of Utah
	Gérard Iooss	-	Laboratoire J. A. Dieudonné, Nice
Examinators:	Nicolas Brunel	-	Laboratoire de Neurophysique et Physiologie, Paris
	Frédéric Chavane	-	INT, Marseille
	Pascal Chossat	-	Laboratoire J. A. Dieudonné, Nice
	Yves Frégnac	-	UNIC, Gif-sur-Yvette, France

Abstract

This thesis deals with mesoscopic models of cortex called neural fields. The neural field equations describe the activity of neuronal populations, with common anatomical / functional properties. They were introduced in the 1950s and are called the equations of Wilson and Cowan. Mathematically, they consist of integro-differential equations with delays, the delays modeling the signal propagation and the passage of signals across synapses and the dendritic tree. In the first part, we recall the biology necessary to read this thesis and derive the main equations. Then, we study these equations with the theory of dynamical systems by characterizing their equilibrium points and dynamics in the second part. In the third part, we study these delayed equations in general, by giving formulas for the bifurcation diagrams, by proving a center manifold theorem, and by computing the principal normal forms. We apply these results to one-dimensional neural fields which allows a detailed study of the dynamics. Finally, in the last part, we study three models of visual cortex. The first two models are from the literature and describe respectively a hypercolumn, *i.e.* the basic element of the first visual area (V1) and a network of such hypercolumns. The third model is a new model of V1 which generalizes the two previous models while allowing a detailed study of specific effects of delays.

Résumé

Cette thèse traite de modèles mésoscopiques de cortex appelés champs neuronaux. Les équations des champs neuronaux décrivent l'activité corticale de populations de neurones, ayant des propriétés anatomiques/fonctionnelles communes. Elles ont été introduites dans les années 1950 et portent le nom d'équations de Wilson et Cowan. Mathématiquement, elles consistent en des équations intégro-différentielles avec retards, les retards modélisant les délais de propagation des signaux ainsi que le passage des signaux à travers les synapses et l'arbre dendritique. Dans la première partie, nous rappelons la biologie nécessaire à la compréhension de cette thèse et dérivons les équations principales. Puis, nous étudions ces équations du point de vue des systèmes dynamiques en caractérisant leurs points d'équilibres et la dynamique dans la seconde partie. Dans la troisième partie, nous étudions de façon générale ces équations à retards en donnant des formules pour les diagrammes de bifurcation, en prouvant un théorème de la variété centrale et en calculant les principales formes normales. Nous appliquons tout d'abord ces résultats à des champs neuronaux simples mono-dimensionnels qui permettent une étude détaillée de la dynamique. Enfin, dans la dernière partie, nous appliquons ces différents résultats à trois modèles de cortex visuel. Les deux premiers modèles sont issus de la littérature et décrivent respectivement une hypercolonne, *i.e.* l'élément de base de la première aire visuelle (V1) et un réseau de telles hypercolonnes. Le dernier modèle est un nouveau modèle de V1 qui généralise les deux modèles précédents tout en permettant une étude poussée des effets spécifiques des retards.

Acknowledgements

My first words are for my two supervisors Olivier Faugeras and Renaud Keriven. Thank you Olivier for your confidence in my work. I was told researching is a year of sadness for an instant happiness during discovery. Hopefully for me, you shattered this point of view by your eagerness to understand, your tireless curiosity, your honesty and your patience. These qualities have been an outstanding support when the solution does not want to come, when the numerics are too long and the set of ideas is empty. This will be my toolbox for researching and a constant help in everyday life. Thank you Renaud for your help, your patience and your presence. I am forever indebted to you.

I would also like to thank the members of my committee: Paul Bressloff, Nicolas Brunel, Frédéric Chavane, Pascal Chossat, Yves Frégnac and Gérard Iooss. Your work has been a constant source of inspiration for my research. I would like to deeply thank my reviewers Paul Bressloff and Gérard Iooss for taking the time to read carefully, comment and criticize this long Thesis. I warmly thank Frédéric Chavane and Yves Frégnac for your patience in answering my questions about biology. I would like to express my respect and sympathy to Pascal Chossat: your always insightful and precise comments have been a constant help in my work. Finally, I would like to thank Nicolas Brunel for accepting to be in my committee despite extremely busy schedule. Your sound comments on my manuscript have helped me to improve the quality of the exposition.

I would like to thank Mike Henderson and Eric Phipps for your support in my use of the Trilinos-Multifario libraries. Most of the work in this Thesis would have been impossible without these wonderful tools.

I would also like to thank Elias Jarlebringin who provided his program for computing the eigenvalues in delay differential equations.

Thank you Sylvain and Joan for the skiing adventures, it cost me one board but it was worth the fun. Many thanks to Manu for the paragliding and sailing, to Sapna for your everlasting good mood, to Nico for the 4L and other delightful moments, to François for your kindness, to Maria-Jose for all the breakfasts, to Claudio for the parties, to Greg for the nights in conferences, to Emilien for the DWS, to James for your French, to Manu for the lunch time, to Anne-Charlotte for your joyful mood, to Mathieu for the sleeping bag, to Geoffroy for the cigars, to Johny for being always present, to DD for the yerba mate. I am also indebted to Rudy and Christel for going out by all weathers.

My last words are for my family and more particularly for my parents and my sister. Thank you my parents for your constant support and love. Thank you for all the joy disregard for the events. Thank you for your education, for all the moments we passed together... I can't wait for the upcoming ones! I am proud to be part of your legacy. To my sister, thank you for making me better by the special link that binds us together.

Finally I want to cheer my little Magali, for accepting me the way I am. Thank you for your patience in the never ending writing and for all the rest that is inappropriate to write... You are my favourite person.

This work was partially supported by the ERC grant 227747 - NERVI, the EC IP project #015879 - FACETS and the EU FET-Proactive FP7 research project 269921 BrainScaleS.

To Guillaume,
For your constant support,
For our friendship.

Introduction

Les faits mathématiques dignes d'être étudiés, ce sont ceux qui, par analogie avec d'autres faits, sont susceptibles de nous conduire à la connaissance d'une loi mathématique de la même façon que les faits expérimentaux nous conduisent à la connaissance d'une loi physique.
([Poincaré 1924])

This Thesis is oriented toward the study of mesoscopic models of cortical activity as part of the world of computational neuroscience. Computational neuroscience is a relatively new field which aims at understanding the brain functions with different interdisciplinary points of view such as mathematics, physics, computer vision, electrical engineering...

The brain is composed, among other things, of a large number of neurons which are densely connected by synapses. It is a electrochemical machinery whose basic elements (the neurons) begin to be understood and modelled, even if the models are analytically intractable. For example, the description in a single synapse requires dozens of variables to describe various quantities such as ions concentrations or membrane potentials. Hence, the simulation at the molecular level of interconnected neurons is already a formidable numerical task. It is difficult to imagine what will be the outcome for the understanding of information processing in the brain for example. Indeed, such a simulation (see [Markram 2006, Izhikevich 2008]) would produce terabytes of data and it is not obvious that the model would be easier to understand than the brain itself. It is very unlikely that it would yield *working principles* (for example the efficient coding principle as in [Barlow 1961]) and *general laws* (the organic evolution theory by C.Darwin or in physics the laws of electrodynamics for example) of a brain theory. These laws are essential for attacking questions related to information processing in the brain. Instead of this very precise modelling, another approach is to understand the activity (to be defined) of a population of neurons which share similar properties (shape of the neuron, cell type...) or the activity of functional populations of neurons which share similar functional properties (like being most responsive for the same stimulus). Note that the labelling of neurons by their functional properties rather than by their intrinsic properties is a short-cut to describe the network. Indeed, the functional properties are only consequences of the neurons being embedded in the network that we want to study and of the set of stimuli that are used to produce the functional responses. This implies that we have to be careful about the "meaning" of the cortical activity when studying these networks for a set of stimuli different from the one used to define the functional properties (see section 11.3.3). In this Thesis, we will study the two types of networks, the ones where the populations are labelled by a functional property (see for example chapter 9) and the ones where the functional properties

are not used to label the population (see chapter 11). The modeling of population of neurons with neural fields equations, as pursued in this Thesis, is related to the mean field approach whose goal is to derive a closed set of equations for a few macroscopic variables from the huge set of equations describing each individual neuron in the network. The link, which should be provided by a mean field theory, between the spiking neural network equations and the neural fields equations is still missing (but see [Roxin 2005]). Nevertheless, we will study the "simple" neural fields equations as a first approximation. These neural fields equations describe the mean membrane potential of populations of neurons that are distributed in the cortex.

From an experimental point of view, this type of modeling seems well suited (see for example [Grimbert 2008]) for voltage sensitive dye optical imaging data which measures the "mean" cortical activity of neurons in the visual cortex in behaving animals.

The most appealing aspect of the neural fields (resp. mean field) modelling is that the models are amenable to a mathematical study. Indeed, the number of equations and parameters is usually small enough to apply tools from dynamical systems for example. This allows to explore more thoroughly the different parameter regimes and simplify the study/discovery of working principles by assuming that the working principles extend from the detailed description to the neural fields description. Obviously, this approach is likely to work if the mean field equations are simple enough for an analytical study, but sophisticated enough to account for some important biological facts. In fact, we will not look for working principles but do the opposite: we will *assume* a specific working principle and adjust the neural fields to agree with this principle. Then we will look at the cortical activity that is specific to this assumed working principle and see if it agrees with biology (see part IV).

The goal of this Thesis is the study of the neural fields equations. It is made of four parts, part I is an introduction to biology and to the neural field equations. The next two parts are "theoretical" while part IV deals with the application to visual cortex models of the tools developed in the theoretical parts II and III. In particular, the models are adjusted to operate in a particular working regime and the consequences of this regime are drawn. The two parts II and III are largely independent and part IV concerning the models can be read without a deep understanding of the two "theoretical" parts.

Part II: Stationary cortical states

The neural fields equations are a system of ordinary differential equations in a sophisticated phase space. They display stationary solutions which are interpreted as stationary cortical activities. In these equations, there is a term which describes the external stimulus. Hence, given a stimulus, these equations can predict what is the cortical activity corresponding to the stimulus. However, depending on the

parameters, the neural field equations can have multiple stationary solutions which are all cortical representations of the stimulus. If more than one stable solution exists, we will show how to label one of these cortical activities as the "main" representation of the stimulus and the other as *neural illusions*. This part focuses on the study of the stationary solutions. More precisely, we apply topological tools coupled to bifurcation theory to study the number of stationary solutions as well as their dependency on various parameters. We use multi-parameters numerical continuation to compute these solutions. Two numerical examples are presented.

Part III: Delayed neural field equations

In part II, the delays were neglected. There are now taken into account. In our modelling with neural field equations, we consider two main types of delays. The first is the propagation delay coming from the finite propagation speed of signals along axons. The second is an *effective* delay: it is a convenient/cheap way to model the synaptic and dynamical spike generation processes. The first chapter of this part deals with the general theory of delayed neural field equations. The next two chapters are more computational: we derive computer programs to compute eigenvalues, bifurcation diagrams and normal forms that are used in the last chapter dealing with neural networks with simple geometry. In particular, these studies provide an understanding of the relative contribution of effective/propagation delays in the dynamics of the delayed neural fields.

Part IV: Application to models study

This part concerns the applications of the tools, developed in the two previous parts, to three models of visual cortex. We apply the "theoretical" results about the stationary solutions to two models taken from the literature. The first one, the Ring Model of orientation tuning is an hypercolumn model, *i.e.* one of the basic elements of the primary visual cortex area. The second model is based on experimental optical imaging data given by the laboratory of F.Chavane. In particular, the relative importance of feed-forward input (from the LGN) and recurrent computations (done by the cortex) in the emergence of the cortical activity is investigated. The last application is a new model of V1 which generalizes the two previous examples and allows a tractable study of the effect of the delays with the use of the tools developed in the second part.

Introduction (Version française)

> *Les faits mathématiques dignes d'être étudiés, ce sont ceux qui, par analogie avec d'autres faits, sont susceptibles de nous conduire à la connaissance d'une loi mathématique de la même façon que les faits expérimentaux nous conduisent à la connaissance d'une loi physique*
> ([Poincaré 1924])

L'objectif de cette thèse est l'étude de modèles mésoscopiques de l'activité corticale, elle s'inscrit dans le cadre des neurosciences computationnelles. Le monde des neurosciences computationnelles est relativement jeune et a pour objectif la compréhension des fonctions du cerveaux du point de vue des mathématiques, de la physique, de la vision par ordinateur ou encore de l'électrotechnique.

Le cerveau est composé, entre autres, d'un grand nombre de neurones connectés par des synapses. C'est un système électro-chimique dont les éléments de base commencent à être compris et modélisés. Ces modèles n'admettent généralement pas de solution analytique. Par exemple, la description d'une seule synapse requiert l'utilisation de dizaines de variables pour décrire les concentrations ioniques par exemple. Ainsi, la simulation au niveau moléculaire d'un ensemble de neurones interconnectés est déjà un formidable problème numérique. Il est difficile d'imaginer quelles seraient les retombées d'une telle simulation pour la compréhension du traitement de l'information par le cerveau. En effet, une telle simulation (voir [Markram 2006, Izhikevich 2008]) produirait des téraoctets de données et il n'est pas évident que ce modèle soit plus facile à comprendre que le cerveau lui-même. Il est peu problable que cette méthode donne lieu à des principes de fonctionnement (comme le principe du codage efficace énoncé dans [Barlow 1961]) ou des lois générales (comme la théorie de l'évolution de C.Darwin ou les lois de l'électrodynamique en physique) d'une théorie du cerveau. Ces lois sont essentielles pour aborder des questions comme le traitement de l'information dans le cerveau par exemple. Au lieu de cette modélisation très précise, une autre approche consiste a comprendre l'activité (à définir) d'une population de neurones qui partagent des propriétés anatomiques (forme du neurone, type de cellule...) ou l'activité de populations fonctionnelles de neurones qui partagent des propriétés fonctionnelles (comme être sélectif à un stimulus particulier). On peut remarquer qu'indexer des neurones par leurs propriétés fonctionnelles est un raccourci pour décrire le réseau. En effet, les propriétés fonctionnelles des neurones sont issues du réseau que l'on étudie et de l'ensemble des stimuli utilisés pour produire des réponses fonctionnelles. Dans cette Thèse, nous étudierons les deux types de réseaux : ceux où les populations sont indexées par des propriétés fonctionnelles (voir par exemple le chapitre 9) et ceux où les populations sont indexées par des propriétés anatomiques (voir chapitre 11). La modélisation de populations de neurones avec des équations

de champs neuronaux, ainsi fait dans cette thèse, est reliée à l'approche du champ moyen dont le but est d'approcher, par un ensemble d'équations décrivant un nombre restreint de variables macroscopiques, l'énorme ensemble d'équations qui décrivent chaque neurone du réseau. Le lien rigoureux, qui serait donné par une théorie de champ moyen, entre les équations des réseaux de neurones à potentiel d'action et les équations des champs neuronaux, reste à trouver (voir [Roxin 2005]). Néanmoins, nous étudierons, dans cette thèse, les équations (simples) des champs neuronaux en supposant qu'elles sont une approximation de réseaux de neurones à potentiel d'action dans une certaine plage de fonctionnement. Ces équations des champs neuronaux décrivent le potentiel membranaire moyen d'une population de neurones distribués dans le cortex.

L'aspect le plus intéressant de la modélisation par les champs neuronaux est que les modèles peuvent être mathématiquement étudiés. En effet, le nombre d'équations et de paramètres est généralement assez petit pour permettre l'usage des outils de la théorie des systèmes dynamiques. Cela permet d'explorer les effets des différents paramètres et simplifie l'étude des principes de fonctionnement en supposant que ces principes sont aussi décrits par les équations des champs neuronaux, *i.e.* que la description est assez précise. Cette approche est valable si les équations de champ moyen sont assez simples pour permettre une étude analytique mais assez précises pour tenir compte de faits biologiques essentiels. En fait, nous procéderons de la sorte : nous étudierons des principes de fonctionnement présupposés et ajusterons les champs neuronaux pour qu'ils satisfassent ces principes. Ensuite, nous étudierons l'activité corticale produite par ces champs neuronaux et vérifierons si elle est en accord avec la biologie (voir la partie IV).

Le but de cette thèse est donc l'étude des équations des champs neuronaux. Elle est composée de quatre parties, la partie I étant une introduction aux équations des champs neuronaux. Les deux parties qui suivent sont des parties "théoriques" tandis que la dernière partie IV traite des applications, aux modèles de cortex visuel, des outils développés dans les deux parties théoriques II et III. Les modèles sont ajustés pour fonctionner dans un régime particulier et les conséquences de ce régime de fonctionnement sont étudiées. Les deux parties II et III sont largement indépendantes et la partie IV, concernant les modèles, peut être abordée sans une compréhension détaillée des deux parties théoriques.

Partie II: les états stationnaires corticaux

Les champs neuronaux sont décrits par un système d'équations différentielles ordinaires dans un espace des phases abstrait. Leurs solutions stationnaires sont interprétées comme des activités stationnaires corticales. Dans ces équations, on trouve un terme qui décrit le stimulus (extérieur). Ainsi, étant donné un stimulus, ces équations prédisent l'activité corticale correspondant à ce stimulus. Cependant, selon les paramètres, le nombre de telles activités peut être supérieur à un et chacune de ces activités est une représentation du stimulus. Se pose alors la question de

savoir laquelle est la représentation principale “choisie” par le cortex. Si plusieurs solutions stationnaires sont stables, nous étudions quelle est, parmi ces activités corticales stationnaires, celle qui correspond à la représentation principale du stimulus, les autres étant interprétées comme des *illusions neuronales*. Cette partie se concentre donc sur l'étude des solutions stationnaires. Plus précisement, nous appliquons des outils topologiques couplés à la théorie des bifurcations pour étudier le nombre de solutions stationnaires ainsi que leur dépendence en les différents paramètres. Nous utilisons un programme de continuation numérique pour le calcul des solutions stationnaires. Deux exemples numériques sont présentés.

Partie III : les équations des champs neuronaux avec retards

Dans la partie précédente, les retards ont été négligés : on les prend maintenant en compte. Deux types de retard sont considérés dans notre modélisation. Le premier type de retard est le retard de propagation qui provient de la vitesse (finie) de propagation des signaux dans les axones. Le second type de retard est un retard *effectif* : c'est une façon simple de modéliser la naissance du potentiel d'action par l'interaction des différentes dynamiques synaptiques et neuronales. Le premier chapitre concerne la théorie générale des équations des champs neuronaux avec retards. Dans les deux chapitres suivants, nous donnons des programmes pour calculer les valeurs propres, les diagrammes de bifurcation et les formes normales. Ces programmes sont utilisés dans le dernier chapitre qui concerne l'étude de réseaux neuronaux simples où le cortex est de monodimensionnel. Cette dernière étude permet de comprendre le rôle respectif des delais effectifs et des delais de propagation dans la dynamique des champs neuronaux à retards.

Partie IV: application à l'étude de modèles de cortex visuel

Cette dernière partie concerne l'application, des outils développés dans les deux parties précédentes, à trois modèles de cortex visuel. Nous appliquons les outils concernant les solutions stationnaires à deux modèles issus de la littérature. Le premier, le Ring Model est un modèle d'hypercolonne, une des structures fondamentales de la première aire visuelle. Le second modèle, décrivant un réseau d'hypercolonnes, est basé sur des données expérimentales. Nous étudions le poids relatif de l'entrée thalamique et des calculs effectués par le réseau récurrent dans l'émergence de la réponse corticale. Le dernier modèle est un nouveau modèle de V1 qui généralise les deux modèles précédents tout en permettant une étude analytique des effets des retards en utilisant les outils de la seconde partie.

Contents

Part I

Introduction to the biology/modeling of the visual cortex

Chapter 1

Introduction to the biology of vision

Contents

The goal of this chapter is not to present a snapshot of the biology of vision at the present time. This would be impossible and most information would not prove useful for the rest of our study (despite being of great interest). Also, because of the huge literature, giving some advice concerning which references to read is very difficult. Hence, I will expose what I read and hopefully, it will be convenient for most of the readers. Readers that have not been introduced to the neurosciences biology should start with the marvellous books *et al.* [Purves 2004, Kandel 2000, Rolls 2002] and read the biophysics of neurons and the visual pathways (see also [Wohrer 2008, Grimbert 2008, Chemla 2010b, Reynaud 2011, Seriès 2002a]).

The brain is composed of an incredible amount of cells that process the inputs from the eyes and other sensory pathways. In this Thesis, we focus on the role of neurons, which will be more thoroughly introduced in the next chapter. Neurons are a particular type of cell whose membrane voltage potential fluctuates depending on the inputs they receive. If their somatic membrane potential exceeds a threshold, they produce an action potential, which is transmitted to another neuron through an axon. Indeed, neurons are connected to other neurons and this is a very important aspect of the phenomenology.

Definition 1.0.1 (Action potential). *The action potential, or spike, is a self-regenerating wave of electrical activity that propagates from its point of initiation*

at the cell body (called the axon hillock, see figure 2.2) to the terminus of the axon where synaptic contacts are made. It constitutes the basis of the information code[1] *used in the brain.*

Given a neuron, we can study what type of stimulus will induce a change in its voltage potential. Note that a particular neuron is likely to feel the stimulus after it has been "processed" by many other neurons. This motivates the following definition.

Definition 1.0.2 (Receptive field). *The receptive field (RF) of a neuron is the region in sensory space (e.g., the body surface, or a specialized structure such as the retina) within which a specific stimulus elicits an action potential response.*

The receptive field of neurons is usually subdivided in subregions ON (resp. OFF) which are excitatory (resp. inhibitory) in that they increase (resp. decrease) the action potential response.

1.1 The visual pathway in the primates

We recall some of the basic layout of visual pathways in primates. When data is not available for the primates, we use data for other animals and stress that the results may not be true for primates.

1.1.1 The eye and the retina

The first element of the vision pathway (see figure 1.1 Left) is the eye, but more importantly from a neuronal viewpoint, the retina. The retina is the network that covers the back of the eye ball. It is composed of 5 cells types, stacked in the order that light is received: ganglion cells - amacrine cells - bipolar cells - horizontal cells and the photoreceptors. Due to the connections in and between upper layers, light scatters through the network before reaching the photoreceptors. These photoreceptors further subdivide into two main categories[2]:

- The cones, which are located in the fovea[3] and are in charge of the diurnal vision. There are roughly 4.5 million in the human retina. The foveola region is the central region in the fovea: it has the highest density of cones and is avascular in order to maintain a high visual acuity. Hence, the foveola is dependent upon the resources coming from the underlying choroid and pigment epithelium for oxygenation and metabolic sustenance.

- The rods, which are mainly located in the peripheral region, outside the fovea. They are photoreceptors for the nocturnal vision and their number is roughly 90 million. During diurnal vision, their response saturates, *i.e.* they are not sensitive to changes in light.

[1] which is still unknown
[2] named because of their shape
[3] part of the retina mainly composed of cones

Upon photon scattering, the photoreceptors membrane hyperpolarizes and the changes in the membrane potentials are transmitted through the network to the ganglion cells (GC). The ganglion cells are the only cells in the retina which produce action potentials. The axons, roughly 1.2 million, are packed into the optic nerve which sends information to the thalamus relay, also called the lateral geniculate nucleus (LGN). However, unlike a camera, the output from the GCs is influenced

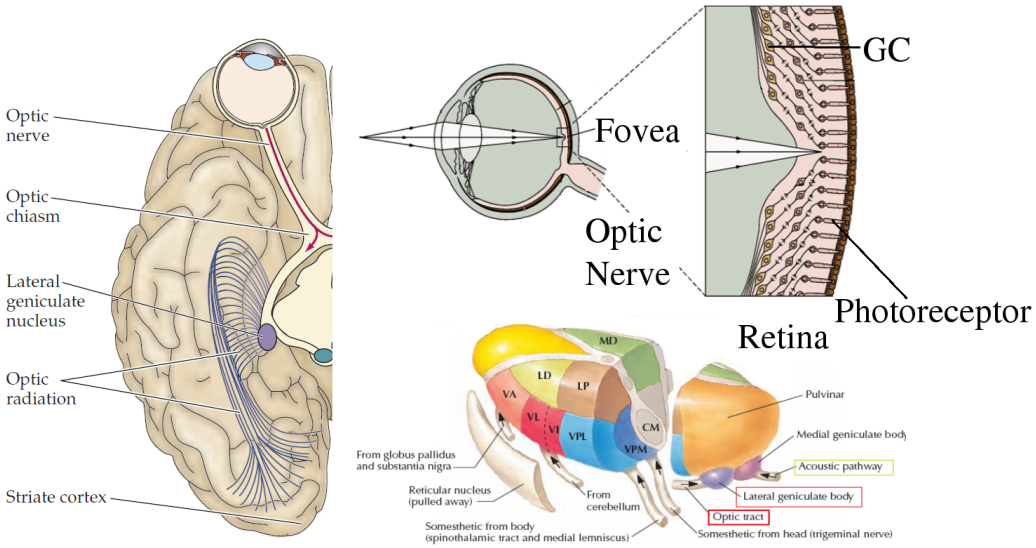

Figure 1.1: Left: the 4 main elements of the visual pathway. Right: the eye and the retina. The fovea is zoomed in on to show the GCs and the photoreceptors. Bottom: the thalamus and the LGN with the optic nerve coming in. Figures modified from [Purves 2004, Kandel 2000, Felten 2010].

by the network made of the cells we have listed above. The RFs of most ganglion cells display a characteristic, roughly circular center-surround architecture where the center is excitatory (resp. inhibitory) and the surround is inhibitory (resp. excitatory), see figure 1.2. Moreover, the ON/OFF subregions are usually associated with particular wavelengths of light. Hence, the GCs act as local spatial contrast detectors. On the other hand, the temporal responses of the GCs subdivide in two broad categories: *tonic* and *phasic* (see [Gouras 1968]). Tonic cells, also called P-cells, respond to light stimuli in a steady maintained manner and their RF centers are extremely small. These cell axons terminate in the parvocellular layer of the LGN and form the beginning of the parvocellular pathway. The phasic cells, also called M-cells, are selective for temporal changes in the stimulus. They form the beginning of the magnocellular pathway and their axons contact the magnocellular layers of the LGN. Hence, we could think of the retina, as a first approximation, as a spatiotemporal contrast detector. Indeed, transmitting the same information constantly is useless, it is changes in the information flow that are important. For

a general discussion of the retina, see [Wohrer 2008].

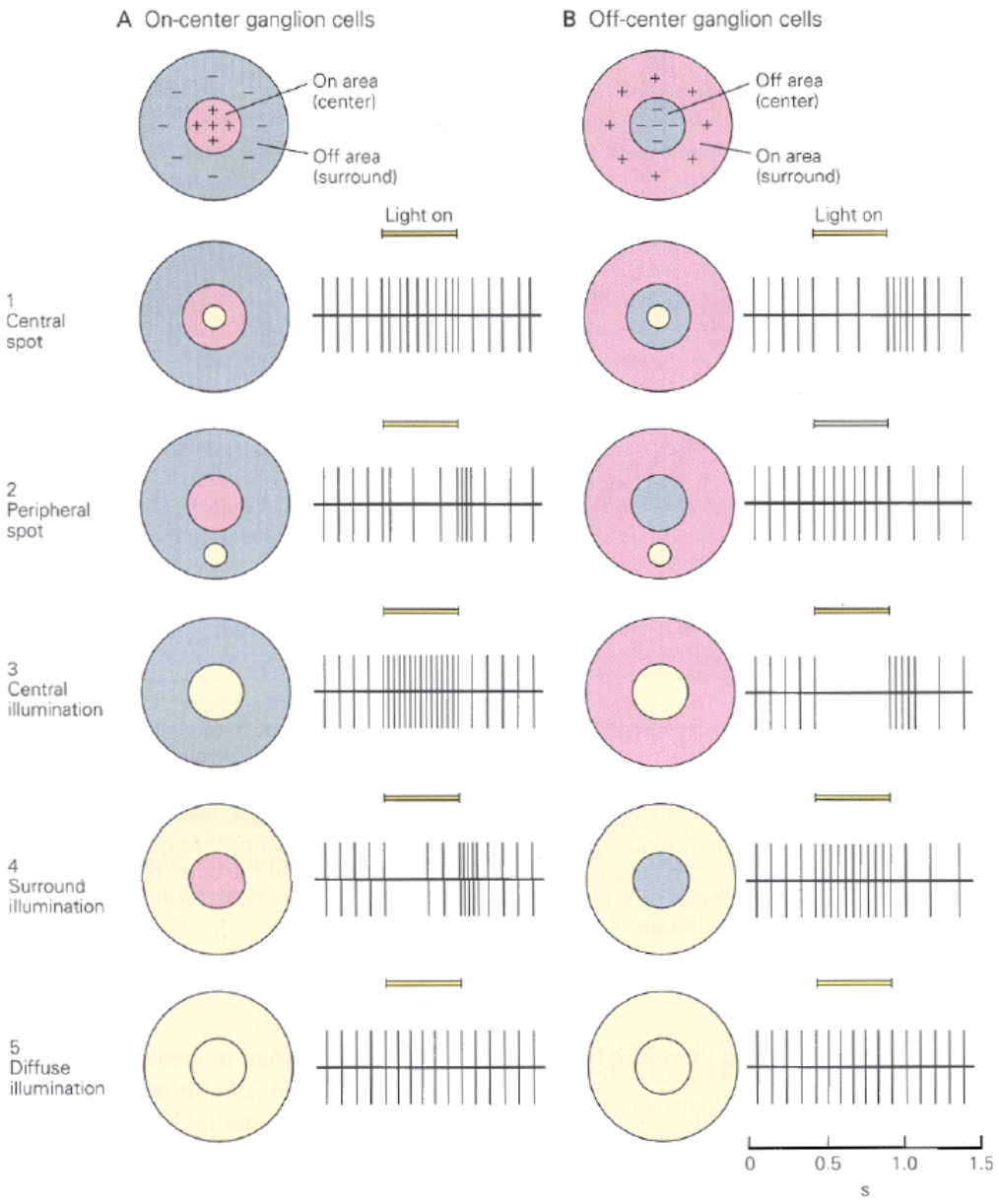

Figure 1.2: Responses of the retinal ganglion cells whose receptive field is shown in the top row. The yellow area indicates which region of the receptive field is stimulated (time scale is in seconds). From [Kandel 2000].

1.1.2 The lateral geniculate nucleus (LGN)

The thalamus is the entrance portal for all sensory information passed to the cortex (see figure 1.1) but it is more than just a relay. The LGN, the part of the thalamus concerned with vision, is composed of roughly 125 million of neurons and only 10% of its inputs come from the retina. It is a layered structure and each of the 6 layers receives input from GCs from *one* eye and from one visual hemisphere (see figure 1.11). Also, the retinal P-cells and M-cells projections are segregated in the LGN: each type sends projections to specific layers in the LGN, respectively the parvocellular layers and the magnocellular layers (see figure 1.11). Finally, the LGN features the *retinotopy* property as does the primary visual area (see below). The retinotopy in the LGN is the fact that two adjacent points in the visual field are processed by LGN cells located next to one another in the same layer. If we travel perpendicular to the layers, we find neurons that process the same part of the visual field, but seen by each retina and through the responses of the P/M-cells. Hence, it is as if there was a spatio-temporal decoupling of the stimulus in the 3D shape of the LGN.

The neurons in the LGN are separated[4] in two broad categories: the *relay* cells (excitatory) and the interneurons (inhibitory). Most of the GCs contact the relay cells which inherit of their RF, *i.e.* they are roughly circular with center-surround organization. The relay cells also receive input from the visual cortex but this feedback must be seen as modulatory because its inactivation has few effects on the RF of the relay cells. Finally, the relay cells are found to spike in two firing modes: the *tonic* firing mode and the *bursting* firing mode. Some evidence exists (reviewed in [Sherman 1996, Sherman 2001]) suggesting that the cortex promotes the firing mode *via* direct inputs to the relay cells and promotes bursting firing *via* indirect input (*i.e.* via reticular and possibly interneurons) to the relay cells. For a more precise account of the LGN properties, see [Sherman 1996].

1.1.3 The visual cortex

The cortex is a folded sheet of width 2cm known as the grey matter. It contains the somas of the neurons. The white matter is made of the myelinated[5] axons of the grey matter. The cortex shares many features of the LGN. It is a layered structure, 6 layers that have been identified by [Brodmann 1909], which is also retinotopically organised (see figure 1.11 where the retinotopy is shown). The mapping between the visual field and the cortical coordinates is approximatively log-polar (see [Schwartz 1977]). From the LGN, the information is transmitted to the visual cortex located at the back of the head (see figure 1.1), mostly to the primary visual area V1.

[4] More precisely, they are separated by the use of a specific neurotransmitter: glutamate for the relay cells and GABA for the interneurons.

[5] Some axons are entoured of myeline which increases the propagations speed of actions potentials.

Where does the information go after V1? There are roughly thirty other visual areas, all smaller than V1, for example V2, V4, MT, MST... (see [Felleman 1991, DeYoe 1996]) that are different one from one another in architecture, connectivity or functional properties. As a general principle, as we ascend the hierarchical architecture of visual areas, the RF of neurons is larger and the neurons are selective for stimuli that increase in complexity. For example, the area MT, which receives direct input from V1, has neurons selective for direction of motion and depth (see [DeAngelis 1999, Born 2005]). Hence, it is as if the local processing of information precedes the processing of global properties. This is not completely true as most higher order area send feedback projections, for example MT send connections back to V1 which itself connects back to the LGN.

Let us consider V1 more precisely. From the studies of Hubel and Wiesel (see [Hubel 1962, Hubel 1968]) of extracellular recording of single cells responses to simple stimuli of anaesthetised cats, the authors characterised two families of neurons in V1: the simple and the complex cells. The RF of the simple cells is more elongated than the RF of the LGN cells which accounts for their selectivity for the orientation of the stimulus. It is also comprised of ON/OFF subregions (see figure 1.7). It has been shown that these cells better respond to bars than to spots. Moreover, given a stimulus, one can predict the cell response from the RF. On the other hand, the complex cells are not so well characterised by their RF despite being responsive to which eye is stimulated, the orientation, the spatial frequency of the stimulus and other properties. Among all possible orientations of the stimulus, one yields the maximum cell response, we call it the *preferred orientation* (see figure 1.10 below). For moving bars or drifting gratings, 30% of V1 cells are selective for the direction of motion (see [Geisler 2001]). In this case, we can define the *preferred direction of motion*. However, these neurons have a greater sensitivity to orientation than direction of motion.

Based on the retinotopy property, it is interesting to compare the preferred stimulus of V1 cells and see how it is spatially organised in the cortex. This was first studied in the 50s by Mouncastle and Hubel and Wiesel.

1.1.4 Selectivity and maps

Following [Mountcastle 1957], Hubel and Wiesel also showed that V1 is spatially organised in columns where every neuron in each layer responds to the same stimulus property. More precisely, by studying different cells located in the same column perpendicular to the cortex surface, Hubel and Wiesel in [Hubel 1962, Hubel 1965, Hubel 1977] showed that the preferred orientation of these cells is the same. However, when moving the electrode parallel to the surface, the preferred orientation of cells, if it exists, changes gradually. A similar columnar organization exists for eye preference, spatial frequency preference, orientation preference, direction of motion preference... The point-by-point sampling with microelectrodes of cells preferences, performed by Hubel and Wiesel, has since been supplemented by the optical imaging method of intrinsic signals (see

[Blasdel 1986a, Grinvald 1986]), which reveals that the orientation preference map is composed of pinwheel-like structures as shown in figure 1.3 for the tree shrew visual cortex. A similar structure has been shown for the macaque primary visual cortex (see [Blasdel 1986a] and figure 10.1) and the cat visual cortex (see [Bonhoeffer 1991]). In figure 1.3 B, the colour indicates the preferred orientation of neurons in the underlying column. This figure was obtained by combining the cortical responses for different orientation stimulus as shown in figure 1.3 A. The striking feature, already found by Huber and Wiesel, is the existence of particular points called pinwheels (see figure 1.3 C Right) where all orientations are represented. Between these pinwheels, there are linear zones where the local orientation preference has not radial organization (see figure 1.3 C Left).

Due to the low spatial precision of the optical imaging technique $50\mu m$ (see [Meister 2001]), a study of the pinwheel structure at the neuron scale was not possible. However, it was shown by Ohki *et al.* in [Ohki 2005, Ohki 2006], by using calcium imaging techniques, that the fine-scale structure of the pinwheel centres is independent of the depth in the cortex. Hence the pinwheel points are not an averaging artefact from the imaging technique but are functional correlates of the spatial organization of the cortex.

In addition to the pinwheel structure, there are ocular preference domains, in effect large bands, that shows to which stimulated eye the columns are more responsive. This property comes from the connections from the LGN[6] which projects each eye pathway in a segregated manner (see [Blasdel 1992b, Blasdel 1992a, Blasdel 1986a]). The two maps of orientation preference and ocular preference can be superposed as in figure 1.4 from [Hubener 1997] (in the cat), it becomes clear that both systems are spatially related: many iso-orientation lines cross the borders between ocular dominance columns close to right angles, and the pinwheel-centers are preferentially located in the middle of the ocular dominance columns (see [Obermayer 1993] and figure 1.4 for the cat, a similar figure is found in [Hubener 1997] for the monkey). It seems a general principle that the primary visual cortex is organized in modules corresponding to each part (left or right) of the visual field, where evenly possible orientation is represented along with ocular dominance. This is what Hubel and Wiesel called the *hypercolumn* (see [Hubel 1962, Hubel 1977]). The module periodicity is usually in the millimetre range. Moreover, the columnar organization implies that all feature maps are "superimposed" on the 2D cortical sheet.

Remark 1.In the cat primary visual cortex, the preferred direction of movement maps have been compared to the orientation map in [Swindale 2003]. These maps are respectively obtained with static and drifting gratings. It appears that the vertical (for example) preferred orientation zones (the blue zones in figure 1.3 B) are subdivided in two zones of opposed preferred direction of movement and this direction of movement is horizontal, i.e. perpendicular to the preferred orientation.

[6] where the eye pathways are separated

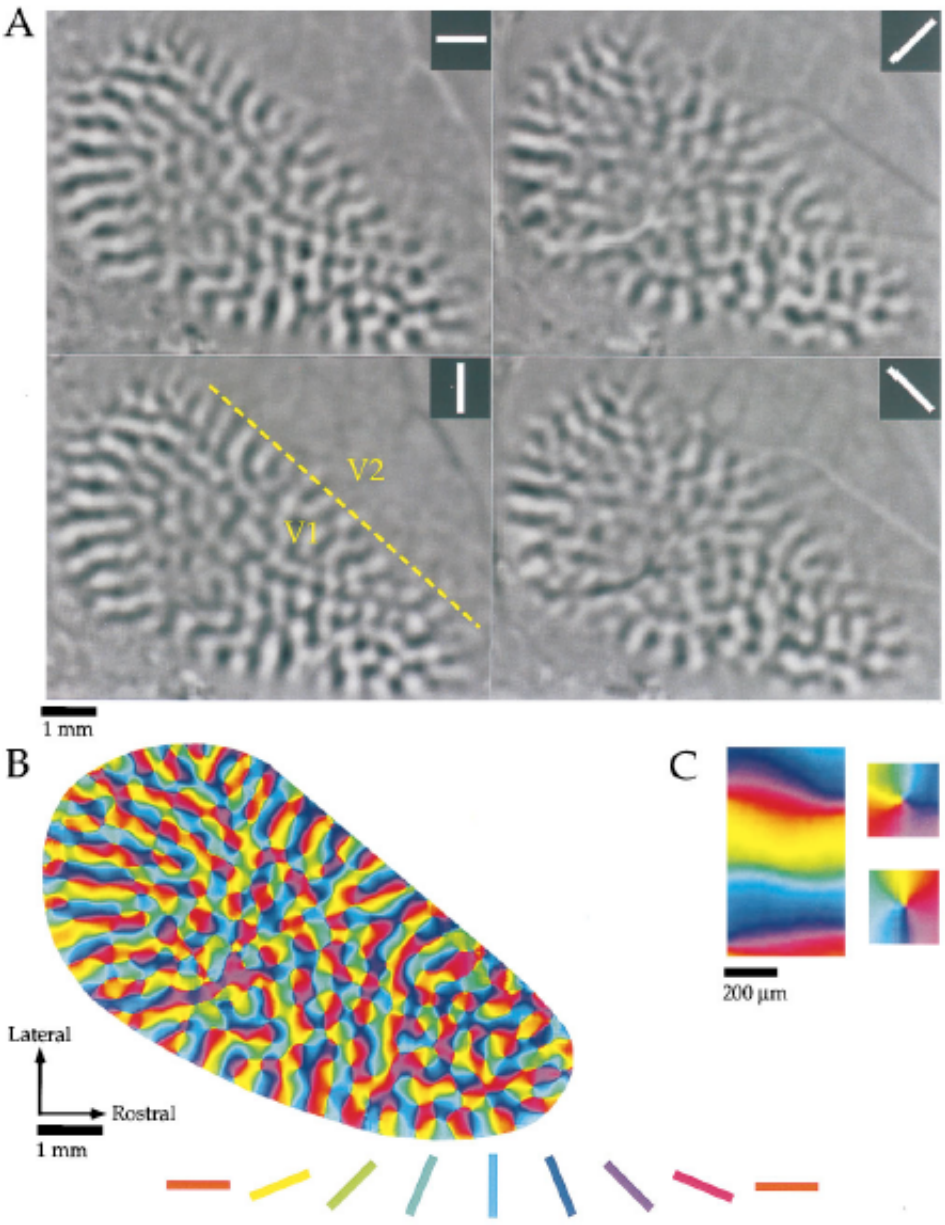

Figure 1.3: Optical imaging of intrinsic signals in tree shrew visual cortex. A) Difference images obtained for four stimulus angles (0^0, 45^0, 90^0, 135^0, shown in inset of each panel) from one animal. Black areas of each panel indicate areas of cortex that were preferentially activated by a given stimulus, and light grey areas indicate areas that were active during presentation of the orthogonal angle. The dashed line in the 90^0 panel indicates the approximate location of the V1/V2 border. B) Orientation preference map obtained by vector summation of data obtained for each angle. Orientation preference of each location is colour-coded according to the key shown below. C) Common features of the orientation preference maps. Portions of the orientation preference map shown in B have been enlarged to demonstrate that the orientation preference maps contained both linear zones (left) and pinwheel arrangements (right). From [Bosking 1997] for the tree shrew.

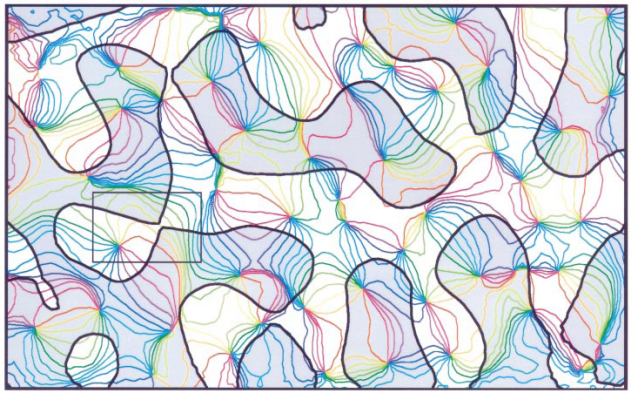

Figure 1.4: Relationship between ocular dominance and orientation maps. The coloured iso-orientation lines were derived from the orientation preference map. All points on lines with a given colour prefer the same orientation. The contours of the ocular dominance columns were obtained from the ocular dominance map of the same cortical region, using an objective automated procedure; grey denotes contralateral eye dominance. From [Hubener 1997] for the cat.

As a last example of a map, we show from [Diogo 2003], redrawn in figure 1.5, the motion selectivity map of the visual area MT in monkeys which has been obtained using micro-electrodes arrays. This area is thought to (see [Born 2005, Masson 2010, Tlapale 2011]) be implicated in the processing of movement. It is highly connected with V1 (forward and feedback connections) and its cells are mainly tuned for a direction of movement and speed.

The figure 1.5 illustrates the dependency of the maps on stimulus (Left of figure 1.5 is for drifting grating, Right for a moving dot). A pinwheel[7] point is shown as a white square and the linear zones are shown as in the orientation maps. Note that it is difficult to obtain these maps because the MT area is not easy to access in the macaque.

Finally, we would like to mention that adaptation shapes the feature maps. Prolonged synaptic activation leads to a decrease in the strength of cortical activation. Hence, by showing prolonged (2 minutes) stimuli, one grating of fixed orientation to cats, the neurons which belong to the same orientation column adapt and are less responsive. The authors in [Dragoi 2000a, Dragoi 2001] show how the initial orientation map is altered by adaptation (see figure 1.6). In particular, the response of adapted neurons near pinwheels is more affected than those in the linear zone; see [Dragoi 2001]. This is very important from an information processing viewpoint. It means that the network adjusts its response to the stimulus and even the orientation preferences of the cells change. Coupled to the micro-saccades of the eyes, it suggests several interesting extensions to the rather static approach to visual information processing that we have adopted in this Thesis; see [Schummers 2002].

[7] In this case the definition of the pinwheel point is a bit different, see [Diogo 2003]

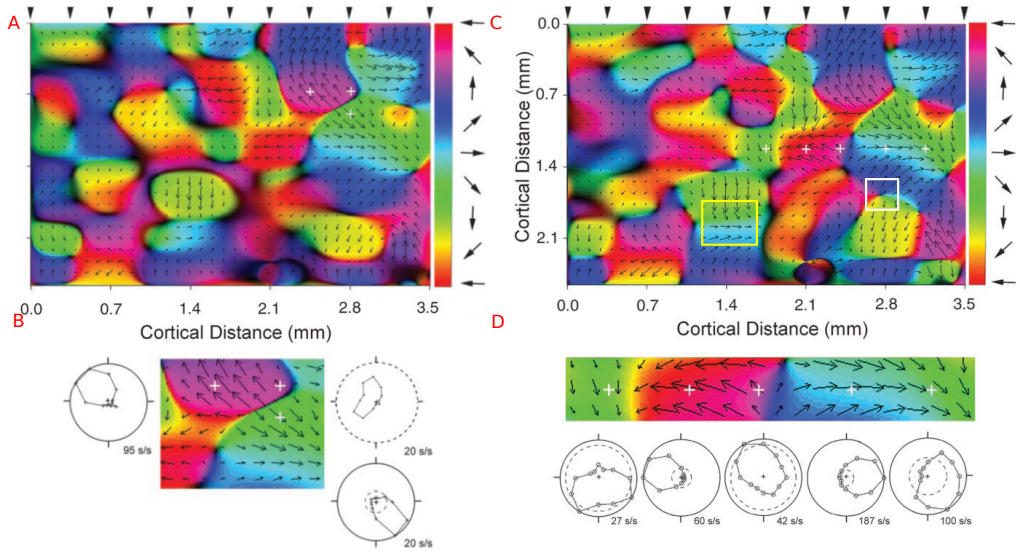

Figure 1.5: A: Colour-coded composite map of the two-dimensional surface of area MT, which represents the preferred direction for a drifting grating. B: same but for a moving dot stimulus. Colour code for preferred direction of motion appears along the right margin of each map. Arrows overlaid on the colour map are a sub-sampled vector description of local directional preference where relative length reflects the strength of selectivity. Dark regions of the colour-coded map indicate areas for which measurements were deemed unreliable. The white crosshairs indicate the locations of recording sites. C/D: Directional tuning curves obtained at these sites are illustrated at the bottom. Firing rate tuning curves are illustrated in polar format. Spike rates (s/s) correspond to the scale of the outer circle in each plot. Broken circles indicate spontaneous activity level. From [Diogo 2003] for the monkey.

Remark 2.It also suggests that the preference maps are dynamical and are influenced by the history of the stimuli. It would be interesting to analyse the concepts of maps in the formalism of dynamical systems.

1.2 Connections

We now focus on the connections between the LGN and the cortex and on intracortical connections.

1.2.1 Thalamo-cortical connections

The primary visual cortex has been anatomically subdivided in 6 layers. The LGN makes most of its connections to layer 4 which is further subdivided into four sublay-

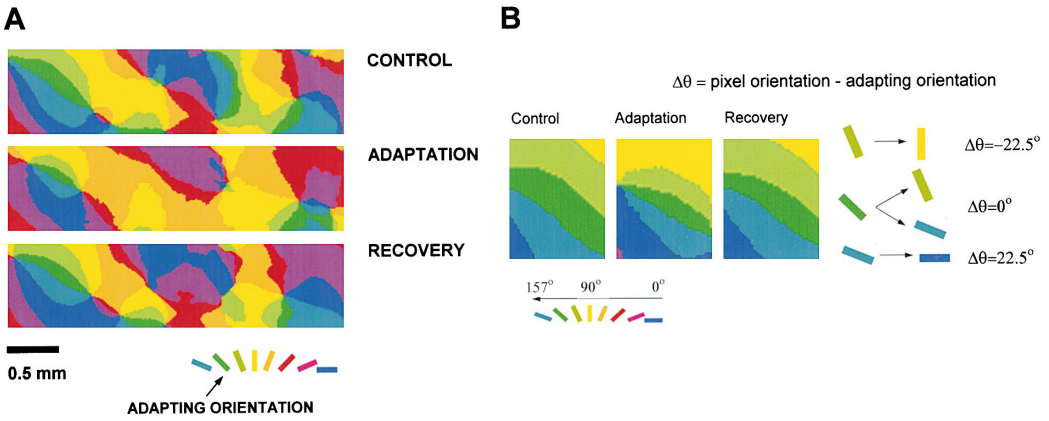

Figure 1.6: A) Composite maps of orientation angle obtained during control, adaptation, and recovery conditions. To obtain these composite maps, the response at each pixel to the eight single-stimulus orientations (including both directions of motion) were summed vectorially and the resultant angle of preferred orientation is displayed in pseudo-colour according to the key at bottom. Adapting orientation is coded dark green. B) Magnified portion from A), showing the postadaptation repulsive shift in orientation and the recovery from adaptation. Depending on the difference between pixel orientation and that of the adapting stimulus, orientation domains exhibit repulsive shift toward neighbouring orientations: for $\Delta\theta = -22.5^o$ (light green) most pixels shift toward the "yellow" domain; for $\Delta\theta = 0^o$ (dark green) many pixels are unchanged while others shift either toward the "light green" or "light blue" domain; for $\Delta\theta = 22.5^o$ (light blue) most pixels shift toward the "dark blue" domain. From [Dragoi 2000a] for the cat.

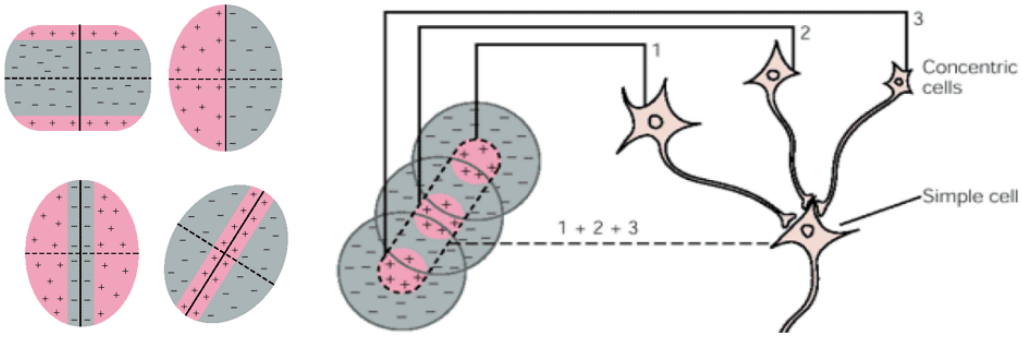

Figure 1.7: Left: examples of RFs of simple cells in V1. Right: illustration of the Hubel and Wiesel models which gives elongated RF to V1 simple cells from circular RF of the LGN. From [Kandel 2000].

ers $4A$, $4B$, $4C\alpha$, $4C\beta$. The M-cells axons terminate in layer $4C\alpha$ while the P-cells axons make contact in layer $4C\beta$. Hence, the two pathways are still segregated when they enter the primary visual cortex (see [Lund 1988, Lund 2003a, Solomon 2002]) and the connections are only excitatory (see [Perkel 1986]). It should be noted that there is a third pathway, called the koniocellular pathway that links cells between the LGN layers directly to superficial layers of cortex within the cytochrome oxidase (CO) blobs[8].

The question of how V1 simple cells acquire orientation selectivity from the LGN cells[9] has been addressed in the studies of Hubel and Wiesel (see also section 1.3). Hubel and Wiesel hypothesised (see below and figure 1.7) that a V1 simple cell receives many inputs from LGN cells and the sum of the RFs of these LGN cells is roughly the RF of the simple cell. This has been demonstrated[10] for the cat in a recent paper [Jin 2011]. In this paper, the authors experimentally computed the thalamic population receptive field of the ON and OFF inputs to a V1 simple cells of preferred orientation θ. The sum of the (circular) RF of the population thalamic RF gives an elongated RF in V1 that provides an accurate prediction of the preferred orientation θ (see also [Reid 1995]).

The area V1 also sends feedback to the LGN mainly from its layer 6. These connections are called cortico-fugal. An interesting question is to know how the ON and OFF zones of simple cells in V1 are spatially aligned with the ON and OFF center LGN cells they influence. For the cat, it has been shown in [Murphy 1996, Wang 2006] that in general, feedback axons contact LGN cells lying in a line either parallel to, or perpendicular to, the axis of the orientation preference of the parent layer 6 cell (see figure 1.8). This was measured by studying the change of the balance

[8] These blobs are cortical functional compartments revealed by CO, a mitochrondrial enzyme.
[9] with no orientation preference
[10] The results reported in this paper calls for more experiments to be sure that they do not depend on the place of the recorded V1 simple cell inside the pinwheel network.

between the bursting/tonic firing modes of the LGN cells (see section 1.1.2). Note that there is a phase reversal of the feedback influence with respect to the ascending connections, which we now explain. Indeed, the ascending connections connect LGN cells with ON center area in their RF to V1 simple cells with ON center area in their RF. The feedback connections show a different pattern. Indeed an ON-center V1 cell sends direct feedback to OFF-center LGN cells and feedback to ON-centers LGN cells only via an inhibitory interneuron. The "phase" is said to be *aligned* when ON-center cells are connected to ON-center cells and is said *reversed* when ON-center cells are connected to OFF-center cells. Moreover, LGN cells arranged on a line send axons to a V1 simple cell whose RF is elongated along the same line but the V1 cell sends feedback connections to LGN cells either aligned, or perpendicular to the V1 cell RF. The authors call this scheme of the feedback connectivity a *reverse Hubel and Wiesel scheme* (see figure 1.7 for the usual Hubel and Wiesel schema) in feedback from V1 to LGN.

1.2.2 Intra-cortical connections in V1

We now focus on the intra-cortical connections. We will not look at the detailed connectivity between the layers (see for example [Salin 1995, Nowak 1997, Thomson 2002, Thomson 2003, Markram 2004, Markram 2006, Thomson 2007] and also [Grimbert 2008, Chemla 2010b]). Let us first mention that the term *horizontal* connectivity is used for the intra-cortical connections between columns, parallel to the cortical surface, whereas the *vertical* connectivity is used for intra-column connections. The thalamo-cortical connections that we have described in section 1.2.1 provide a very small percentage of the inputs in layer 4: 95% of these inputs are made of recurrent connections, *i.e.* intracortical connections (see [Douglas 1995]).

The *local* excitatory/inhibitory connections are *homogeneous*, *i.e.* the pattern of connections is the same over the cortex. At a given cortical location $\mathbf{r}$, the contacted neurons are located in a disc of radius which is of the order of $0.5 - 1mm$ (see [Malach 1993, Angelucci 2002] for the primate, [Das 1999, Mariño 2005] for the cat and [Fitzpatrick 1996] for the tree shrew) and they are uniformly distributed in this disc. In [Das 1999], it is concluded that the synaptic efficacy of these connections decreases with the distance of projection. This particular organization of local connectivity together with the structure of orientation maps (as in figure 1.3) implies that these connections play a different role depending on the place of the neurons in the pinwheel map (see [Shelley 2002, Mariño 2005, Nauhaus 2008]). Indeed, the homogeneous connections provide a uniform sampling of the neighbouring neurons. In the linear zones, the neurons "see" mainly neurons with the same orientation preference, whereas near pinwheels the neurons can "see" all orientations.

Concerning the *long-range* connections, it has been demonstrated that they are mainly made by excitatory neurons in layers 2/3, 4B, 4Cα, 5/6 of macaque area V1 in [Rockland 1983, Malach 1993, Yoshioka 1996]. These projections are patchy rather than homogeneous, axons ramify and make extensive terminal branches only at particular discrete locations across the cortex. In particular, the long-range con-

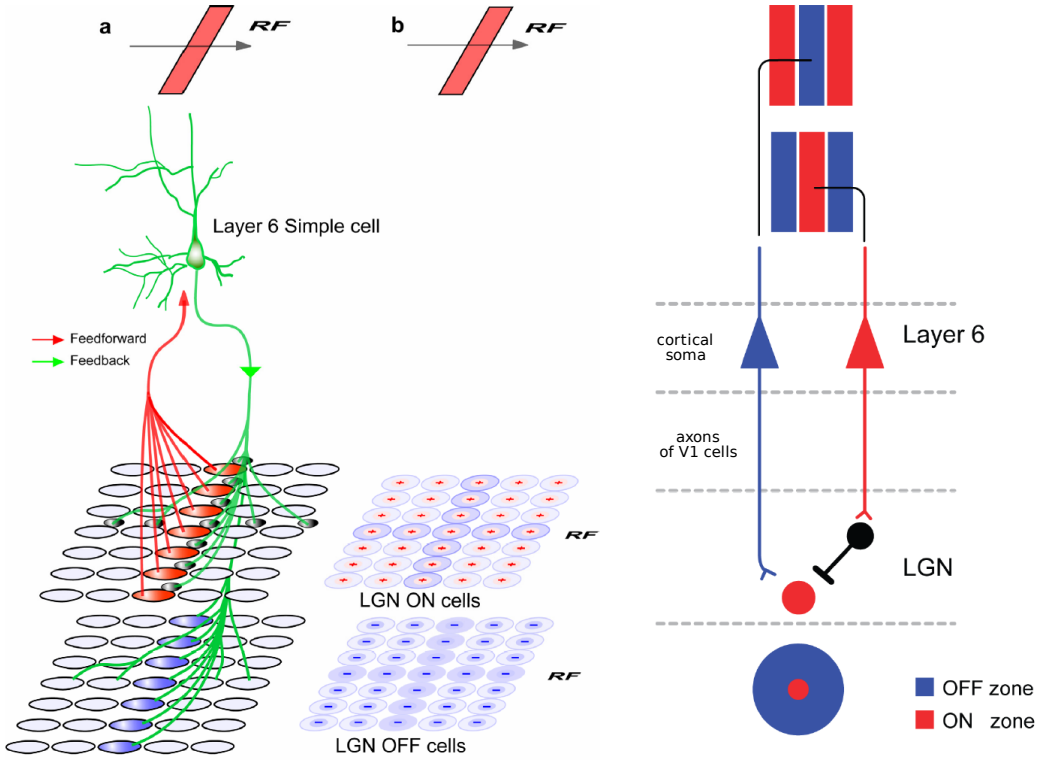

Figure 1.8: Left: a) Arrangement for the phase aligned connections via inhibitory interneurons (drawn in black) and direct phase reversed connections to relay cells. b) Receptive field types associated with phase aligned and phase reversed connections. Cortical cell is shown as having an ON center. LGN cells with "+" centers are ON center and "-" centers are OFF center. Right: the diagram shows the pattern of feedback made by two layer 6 cells to an ON- center LGN relay cell. The receptive field of one feedback cell matches that of the LGN cell, in that it has a central ON sub-region (red cell). The other has a central OFF sub-region (blue cell). All three receptive fields are centred on the same point in visual space. The cell with the matched field contacts the LGN cell through an inhibitory inter neuron (black). Conversely, the cell with the mismatched field makes direct excitatory contact. Modified from [Wang 2006] for the cat.

nections preferentially link cortical domains of similar orientation preference $\pm 30^o$ (see [Malach 1993, Yoshioka 1996, Stettler 2002, Lund 2003a]). The anisotropy ratio is the extent of long/short axis of the ellipse which contains all the long-range connections. In [Angelucci 2002], it is found that the mean anisotropy ratio is 1.56 (see white ellipses in figure 1.9). The anisotropy of horizontal connections in macaques follows from the anisotropy of the visual field representation in V1 (*cf.* retinotopy and log-polar map. Recall that there is a cortical magnification of the fovea.), *i.e.* it is not correlated to a feature like orientation. In other words, if we

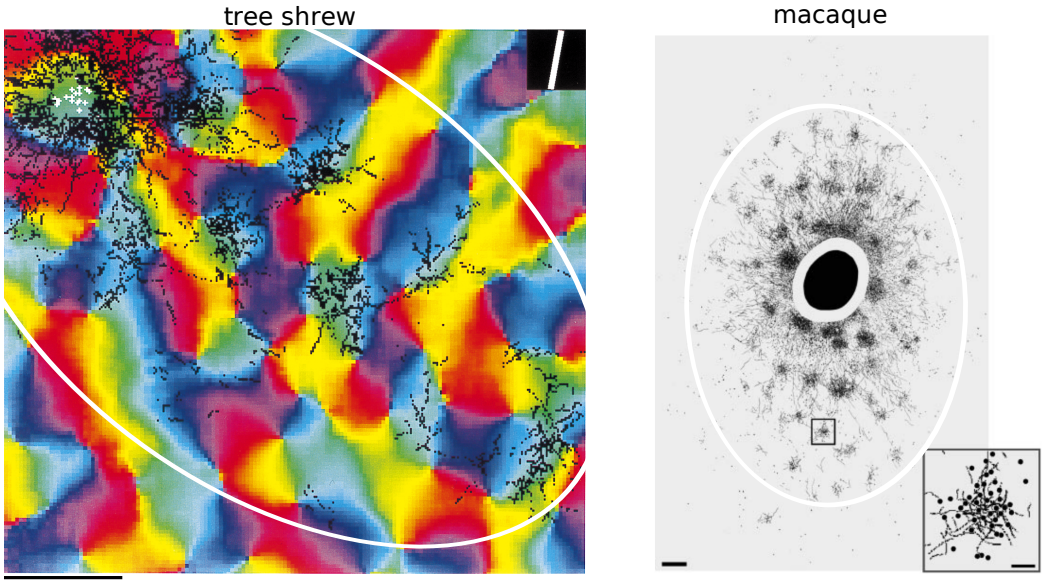

Figure 1.9: Left: Synaptic bouton distributions after an injection of biocytin shown over orientation preference maps for the tree shrew. The injection site has a preferred orientation of 80^o. The boutons are localized along the axis of preferred orientation of the marked cells. From [Bosking 1997]. The synaptic bouton is the presynaptic terminal at the synapse. Right: patchy horizontal connections in layers 2/3 of macaque area V1. *Small square*, labeled patch shown at higher power in the *inset*. Scale bar, $500\mu m$. *Inset*, High-power drawing of patch in the small square, showing labeled fibers and somata (dots), indicating reciprocity of connections. Scale bar, $100\mu m$. From [Angelucci 2002]. The white ellipses are meant to show the anisotropy of the connections.

drew[11] figure 1.9 Right in visual field coordinates, the patches would appear to lie in a disc and not in an ellipse. Finally, these long-range connections are modulatory, *i.e.* they cannot elicit a spike in the contacted neuron although they can modulate its membrane potential.

Remark 3. On the other hand, it has been shown for the tree shrew that the patchy long-range connections have an anisotropy axis aligned with the axis of preferred orientation (see [Fitzpatrick 1996, Bosking 1997] and figure 1.9 Left). Hence, the long-range connections implement a principle of good continuation unlike in the monkey.

To finish, we would like to emphasize the difference between anatomy and function. Feature preferences are found by using stimuli, *i.e.* by puting the network to work. However, there are no anatomical clues about orientation, spatial frequency... columns. At best, there are clues for an organization into functional columns in the macaque area V1 (see [Lund 2003a] and figure 1.9). Also the feature selectivity

[11] It is specific to macaques.

does not dictate a columnar organization. One of the best examples is the rat with well-defined orientation selective neurons mixed spatially in a salt-and-pepper way without columnar match in preferred orientation whereas its barrel cortex, which processes its whisker movements, is organised in columns.

See [Voges 2010, Chavane 2011] for a review about patchy connections and long-range connections.

1.3 A closer look at orientation selectivity

The problem of orientation selectivity is central to the neuroscience community; most likely because it is a simple phenomenon, easily reproducible, that takes place at the boundary between the thalamus and the cortex. In effect, the orientation selectivity properties lie in the relative contributions of the afferent inputs and recurrent computations (see [Ferster 2000, Martin 2002] and also [Monier 2002]). Whether the orientation selectivity stems from LGN inputs or cortical computation is still a matter of debate. More theoretically, this question is related to how much the cortex is influenced by its sensory inputs.

1.3.1 Biological facts

We have seen that V1 simple cells are orientation selective and that V1 is spatially organised in a pinwheel network. However, the V1 simple cells in cats share an additional and remarkable property which is linked to their tuning curves properties.

Definition 1.3.1 (Tuning curve). *The tuning curve is the response (firing rate, membrane potential) of a neuron or a population of neurons to a stimulus as function of the stimulus parameter(s) (orientation, spatial frequency...).*

In [Sclar 1982], the authors showed how the firing rate tuning curves of V1 simple cells in cats depend on the stimulus contrast[12]. In particular, the response at the preferred orientation increases with the exponential of the contrast but the orientation selectivity, related to the width of the firing rate tuning curve, is contrast invariant (see figure 1.10). Moreover, the maximum response is an increasing function of the contrast but it saturates below the maximum firing rate of the simple cell (see [Albrecht 1982, Levitt 1997]) and in some cases, it hypersaturates, *i.e.* declines with very high contrast levels (see [Levitt 1997]). Hence, the saturation effect comes from a network property: it is an important clue for the operating regime of the cortex because it normalizes the signal at the cortical level.

For the macaques, the picture is less clear. For now, contrast invariance has not been firmly established and a recent study by Nowak *et al.* in [Nowak 2009] shows that contrast adaptation is implicated in the contrast invariance of tuning curves width for the marmoset monkey. In particular, they showed that the tuning curves are not contrast invariant when the stimulus is presented for 0.2s. For the rest of

[12]For a drifting grating stimulus $S(\mathbf{x}, t) = S_0(1 + C\cos(t - \mathbf{k}\cdot\mathbf{x}))$, the contrast is given by the pre-factor C. The orientation is given by the angle of the vector $\mathbf{k}$.

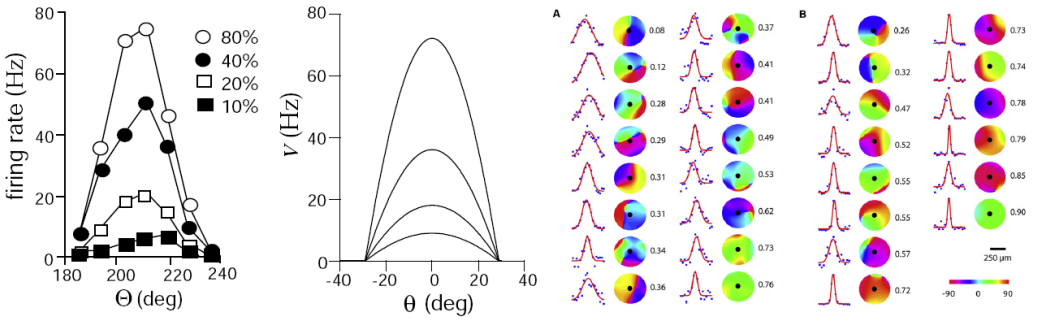

Figure 1.10: Left: typical tuning curves of a cat V1 simple cell as a function of the contrast of drifting gratings. From [Sclar 1982]. Also shown is the idealisation of the result on the left. Right: Examples of orientation tuning curves and their location within the orientation map are shown for a monkey (A) and a cat (B). They are ranked in order of increasing values of the local homogeneity index (shown near each local orientation map). From [Nauhaus 2008].

this section, we will focus on the cat biology, especially on the contrast invariance of tuning curve widths in cats because adaptation is not seen to play a role.

Moreover, it has been shown that the firing rate tuning properties depend on the spatial localisation of the simple cell in the orientation map for monkeys and cats (see [Nauhaus 2008]). In particular, it appears (see figure 1.10 Right) that tuning width decreases with increasing values of the local homogeneity index, which is an indication of the neighbouring preferred orientations. Note that this result is in contradiction with the studies in [Schummers 2002, Mariño 2005] which report a firing rate tuning curve that is invariant across the cortex[13]. It is supposed in [Nauhaus 2008] that the discrepancy comes from the coarse sampling of the orientation tuning curves at 22.5^o steps used in [Schummers 2002, Mariño 2005] given the range of tuning widths seen in cat $\Delta\theta = 5^o - 20^o$.

1.3.2 Two classes of models

In order to account for this contrast invariance property, two classes of models have emerged that emphasize the role of the LGN afferent inputs, also called the *feedforward models*, or the role of the recurrent connections in the cortex, also called the *recurrent models*.

The original feedforward model dates back to Hubel and Wiesel's work. The model consists of two processing stages. The first is a linear summation of inputs from LGN cells whose receptive fields are arranged in rows as in figure 1.7. The second stage is the nonlinear filtering of the summed inputs by the spike threshold.

[13]These studies also demonstrate that the tuning width of subthreshold membrane potential in cat, is broader near pinwheels than in iso-orientation domains.

To have an output, *i.e.* to be above threshold, the net excitation[14] must be larger than the net inhibition[15] and these net contributions are increasing functions of the contrast[16]. Unfortunately, after thresholding, the width is also an increasing function of the contrast, this is called the *iceberg effect* (see [Rose 1974]). The model has then been modified in [Troyer 1998] to account for contrast invariance by using orientation dependent inhibition in order to compensate for the net activation. However it is not supported by biology. Recently, a new version of the feedforward model as been proposed in [Finn 2007] (see also [Carandini 2007]). It features contrast-gain control, additive noise, and a firing threshold to account for the contrast invariance of selectivity.

The other type of models that have been used to account for the contrast invariance of tuning width is the recurrent models (see [Ben-Yishai 1995, Somers 1995, Hansel 1997, Douglas 1995, Carandini 1997, Shelley 2002, Kang 2003]). These models are motivated by the fact that most of synaptic inputs of layer 4 neurons are recurrent connections. Hence, the model assumes that the thalamic inputs are weakly tuned and the tuning is sharpened by the cortical computations. These recurrent models are further subdivided in two classes, those that make explicit use of a feature dependent connectivity (see [Ben-Yishai 1995, Somers 1995, Hansel 1997, Douglas 1995, Carandini 1997]) and the one that are based on the local connections we have described in section 1.2.2 (see [Shelley 2002, Kang 2003]). However, it is important to note that the latter class of models do not work in the same regime as the first which operate near a static bifurcation (see chapter 3).

1.4 Conclusion

In this chapter we have reviewed the basic material about the visual pathways in mammals. I gave in to the temptation to provide more information than will actually be used in the sequel, but hope that the reader is amazed, as much as I am, by the fine structure/properties of the retina, the LGN and the cortex. For convenience, we have collected the principal information in figure 1.11.

In particular, the focus was on the tuning properties of V1 simple cells in cats. We will come back to the recurrent models in chapter 3 and in part IV. The point we want to make is that by using simple network models with few parameters and by trying to account for well-established biological facts, we can constrain a lot the possible parameters values. The resulting network with those equiped parameters is likely to feature new behaviours that will be the basis of interesting predictions that could be tested experimentally.

[14] sum of the ON subregion responses
[15] sum of the OFF subregion responses
[16] from retinal and thalamic cells properties.

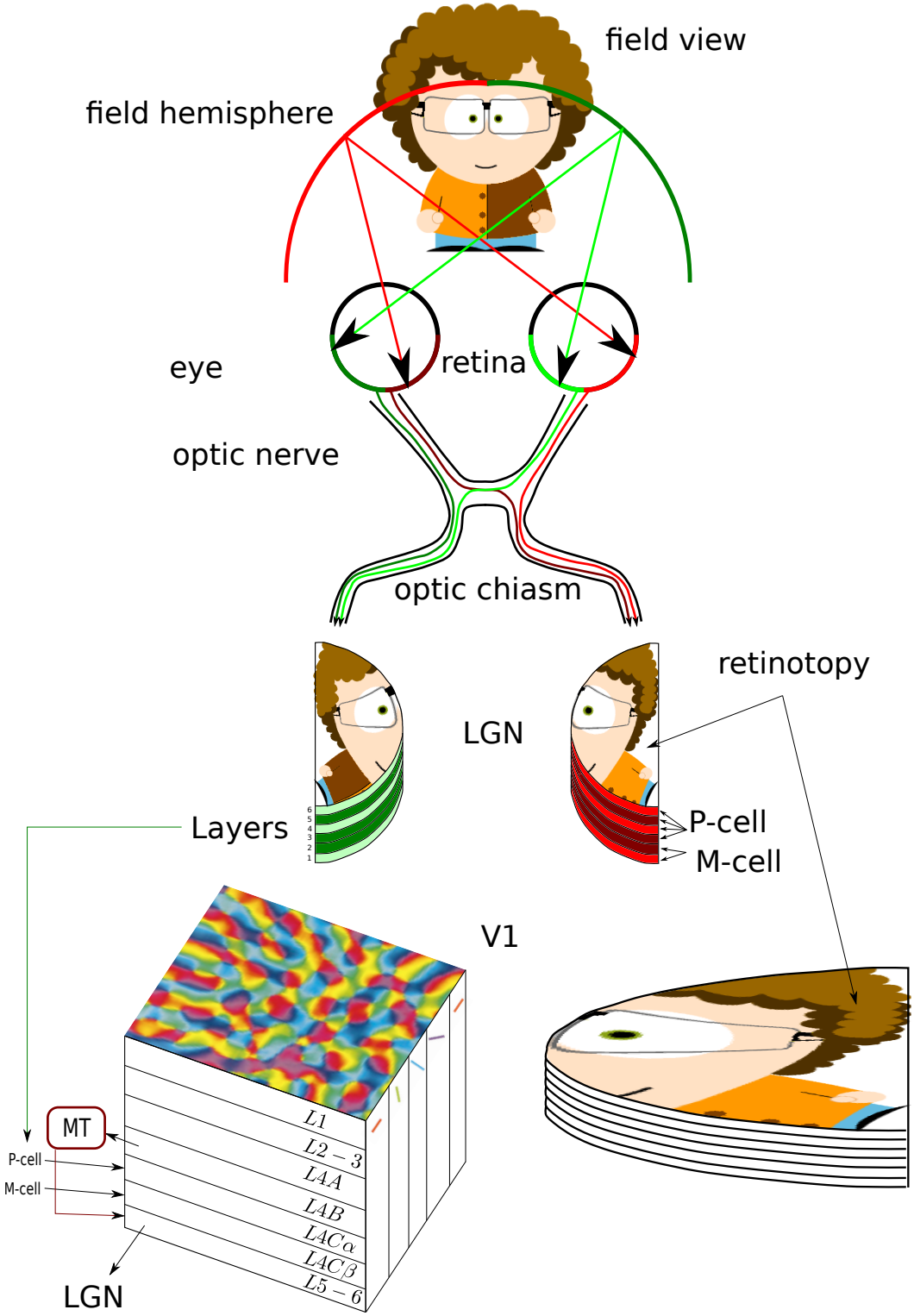

Figure 1.11: Schematic representation of the visual pathway. Note the retinotopic representation and the magnification of the fovea. Each LGN has 6 layers which project to V1. For V1, we have represented the orientation and the retinotopy maps.

Chapter 2

The neural fields model

Contents

In this chapter, we present the neural field (NF) model. It first appeared in the 50's (see [Beurle 1956]) but the theory really took off in the 70's with the work of Wilson and Cowan [Wilson 1972, Wilson 1973] and Amari [Amari 1977]. This model is a continuous network of interacting populations which are distributed over the cortex. The spiking activity is approximated by the mean firing rate. Compared to spiking neural networks, the NF model presents the advantage of having less parameters, hence, is simpler to analyse. The NF equations are heuristically derived (see below). A huge effort of researching is put in finding mean field equations that are the limit equations, when the number of neurons tends to infinity, of equations of spiking neural networks. The mean field equations have not yet been linked to the NF equations.

The disadvantages of the neural field model lie in their main modelling assumptions. They cannot cope with the spike timing and spike correlation effects. These effects are at the basis of important intrinsic mechanisms of adaptation and learning. We would like to point out that these mechanisms have been incorporated at the mesoscopic level using heuristic arguments. For example, the effects of synaptic depression/facilitation have been introduced in the NF formalism in [Tsodyks 1998] and further studied in [Kilpatrick 2010a, Kilpatrick 2010b]. The effects of spike frequency adaptation, which are neuronal effects and not synaptic effects, have been studied in [Curtu 2004, Coombes 2003, Coombes 2005a]. For a review on neural field models, see [Ermentrout 1998, Coombes 2005b].

2.1 A brief account for the flow neuronal activity

2.1.1 Introduction

The goal of this section is not to give a detailed account of the neurons biophysics and models (see for example [Tuckwell 1988, Dayan 2001a, Purves 2004, Koch 2005, Izhikevich 2007, Felten 2010, Sterratt 2011]). Rather, we would like to recall some basic properties of the neural activity that are needed for the derivation of the NF model.

The neurons are composed of four main components: the dendritic tree, the soma, the axon which is linked to the soma at the axon hillock and the pre-synaptic terminals (see figure 2.2). The neurons are connected with synapses which are the interface between the afferent axon and the targeted neuron. There are two kind of synapse, the chemical and the electrical (also called gap junctions). We will not consider the electrical synapses in this Thesis (see [Steyn-Ross 2007] for more information). When the somatic potential across the membrane reaches a threshold, a sequence of action potentials (also called spikes) is produced at the axon hillock. This sequence is then transmitted, without alteration, to the axon terminals where the synapses with the targeted neuron are located.

When a spike arrives at a synapse, it triggers the release of neurotransmitter in the synaptic cleft. These neurotransmitters bind to specific receptors on the post-synaptic neuron. The binding causes ion channels to open (or close), thus changing the ability of ions to flow through the post-synaptic membrane. Hence, the binding of neurotransmitters alters the conductance of the post-synaptic membrane. Let us consider a spike that arrives at $t = 0$ at the synapse, then we write:

$$I_{syn}(t) = g_{syn}(t)(V(t) - E_{syn}) \tag{2.1}$$

where g_{syn} is the conductance of the post-synaptic membrane, I_{syn} is the post-synaptic electrical current, V is the voltage across the post-synaptic membrane[1] and E_{syn} is the reversal potential of the ion channels that mediate the synaptic current. Three waveforms of synaptic conductance are commonly used in the literature

$$\begin{array}{rcl} g_{syn}(t) & = & \bar{g}_{syn} e^{-t/\tau} H(t) \\ g_{syn}(t) & = & \bar{g}_{syn} \frac{t}{\tau} e^{-t/\tau} H(t) \\ g_{syn}(t) & = & \bar{g}_{syn} \frac{\tau_{raise}\tau_{decay}}{\tau_{raise}-\tau_{decay}} \left(e^{-t/\tau_{raise}} - e^{-t/\tau_{decay}} \right) H(t) \end{array} \tag{2.2}$$

where H is the Heaviside function. The waveforms, respectively called the exponential decay, the alpha function and the dual exponential, are shown in figure 2.1. The characteristics of the synapses are contained in the constants $\bar{g}_{syn}, \tau \cdots$

In order to know the time evolution of the post-synaptic potential V, which will be written PSP below, another equation is required. It is usually of the form:

$$\tau_v \frac{dPSP}{dt} = \psi(PSP) + I_{syn} \tag{2.3}$$

[1] also called the post-synaptic potential and written PSP below.

where ψ is a nonlinear function of the potential PSP. We need to solve (2.3) in order to know the post-synaptic potential waveform PSP caused by the incoming pre-synaptic spike at the synapse. However, this is not easily done and we assume a particular waveform PSP in the next sections 2.2.1 and 2.2.2.

Remark 4. If the decay of the synapse is very fast, then the decay of the post-synaptic membrane potential PSP is dominated by the passive decay of the post-synaptic cell membrane. On the other hand, if the synapse is long-lasting, then the decay of the post-synaptic membrane potential PSP is dominated by the synaptic time constant.

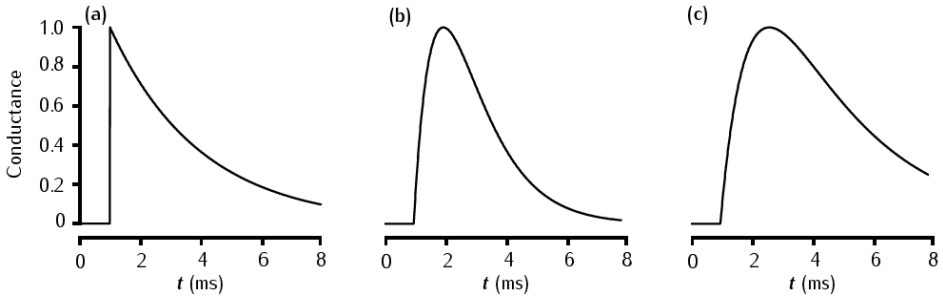

Figure 2.1: Three waveforms of synaptic conductance: a) exponential decay with $\tau = 3ms$, b) alpha function with $\tau = 1ms$ and c) dual exponential with $\tau_{raise} = 3ms$ and $\tau_{decay} = 1ms$. From [Sterratt 2011].

If we connect two neurons with a single synapse described by (2.1), we can study under what conditions a spike produced in the first neuron will trigger the production of a spike in the second neuron. If the dendrite processing is neglected, it can be shown that the synapses introduce an *effective delay* D in the production of the spike by the second neuron (see [Fourcaud-Trocme 2003, Roxin 2005, Roxin 2011]). This is because of the action potential initiation dynamics in Hodgkin-Huxley-type neurons. This dynamics is neglected in the NF model but, following [Roxin 2005], we introduce an effective delay D in the NF model. Indeed, the authors show that such a delay is necessary for the firing rate models where the spike initiation dynamics is neglected, to reproduce behaviours found in spiking neurons networks.

They are other sources of delays in the transmission of the neuronal activity like the propagation delays d which arise because of the finite velocity of spikes along axons. To roughly take into account the dendritic processing, we could also introduce another effective delay.

2.1.2 Propagation of activity between two neurons

We have described the basic biophysics of an isolated neuron in the last section. Let us now recall, in a very schematic way, the path of information from one neuron j to another one i. When a spike arrives at a synapse $s_{ij;k}$, depicted by A1 in figure 2.2, it produces a post-synaptic potential $PSP_{ij;k}$ as we describe in the previous section. We drop the index of the synapse k between neuron i and j for convenience. This

potential is then filtered by the dendritic tree (A1-A2) and the effective potential felt by the soma is a temporally shifted and attenuated version of the original PSP_{ij}. Hence, depending on where the input comes to the dendrite, the potential felt by the soma can be quite different. If the somatic membrane potential V_i is above

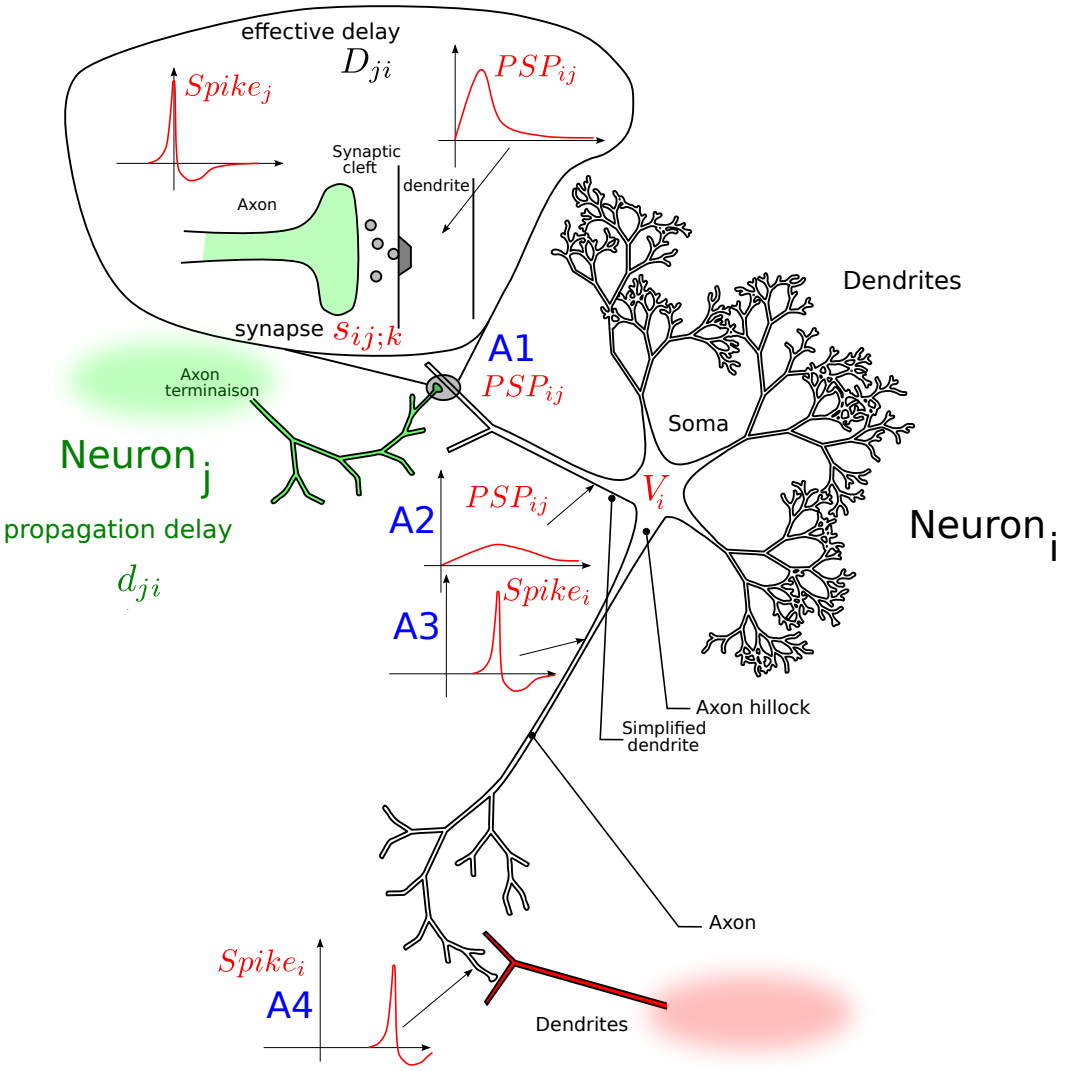

Figure 2.2: Schematic drawing of the membrane potentials during the transmission of a spike from a neuron i to a neuron j. The soma has the membrane potential V_i and produces spikes at a rate $\nu_i = S_i(V_i)$, where S_i is a nonlinear function defined below. Adapted from [Ermentrout 2009] and N.Rougier's drawing

a threshold, then a spike is produced at the axon hillock (see A3). This spike is transmitted along the axon, without attenuation, until it reaches another synapse (see A4). The delay it takes for a spike to go from the axon hillock to the synapse is written d_{ji}.

In the NF model, we suppose that the dendrite is punctual and we neglect the effects of nonlinear spatial filtering that are produced by the dendritic tree (see [Coombes 2003, Venkov 2008] for a NF model of dendrite). We also assume that there is a single synapse to simplify the notations. We can compensate for this assumption by assuming that more spikes come to the synapse between i and j. In particular, we neglect the propagation delays in the dendritic tree although they could be easily introduced, in a heuristic way, in our final equations (2.12). On the other hand, we have seen above that this synapse introduces an effective delay D_{ji}. Hence, the total delay between the production of the spikes in each neuron is $\tau_{ji} \equiv D_{ji} + d_{ji}$.

2.2 The local models

We consider p interacting populations of neurons such as those shown in figure 2.3. The figure is inspired by the work of Alex Thomson [Thomson 2003] and Wolfgang Maass [Haeusler 2007]. It shows six populations of neurons. Red indicates excitation, blue inhibition. The thickness of the arrows pertains to the strength of the interaction. The six populations are located in layers 2/3, 4 and 5 of the neo-cortex.

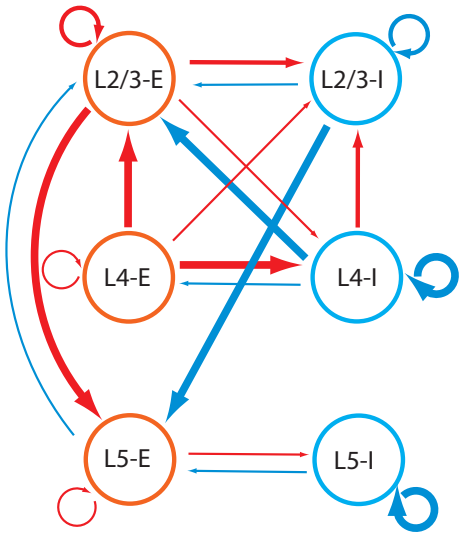

Figure 2.3: A model with six interacting neural populations.

The following derivation follows closely that of Ermentrout [Ermentrout 1998]. We consider that each neural population i is described by its average (somatic) membrane potential $V_i(t)$ or by its average instantaneous firing rate $\nu_i(t)$, the relation between the two quantities being of the form $\nu_i(t) = S_i(V_i(t))$ [Gerstner 2002, Dayan 2001a], where S_i is sigmoidal

$$S_i(x) = \frac{S_{im}}{1 + e^{-\sigma_i(x-\theta_i)}}, \tag{2.4}$$

σ_i is the nonlinear gain and θ_i is the threshold. The threshold determines the minimum somatic potential that triggers the initiation of a spike at the axon hillock. The shape of the sigmoidal function is shown in figure 2.4 for the values of the parameters $\theta_i = 0$ and $\sigma_i = 0.5, 1, 10$. When $\sigma_i \to \infty$, S_i/S_{im} converges to the Heaviside function $H(v - \theta_i)$ defined by

$$H(v-\theta_i) = \begin{cases} 0 & \text{if} \quad v < \theta_i \\ 1 & \text{otherwise} \end{cases} .$$

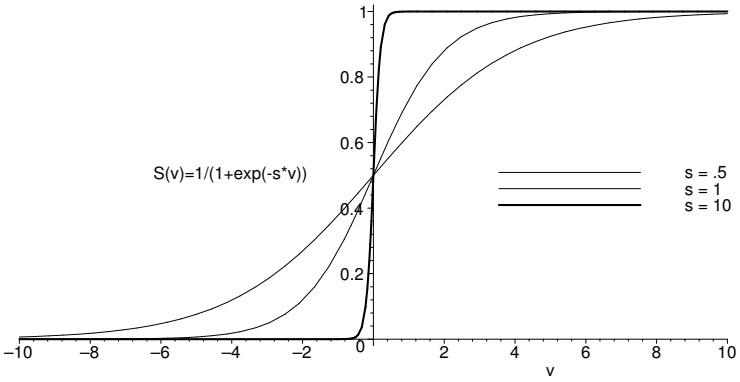

Figure 2.4: Three examples of sigmoidal functions for different values of the parameter σ_i and $\theta_i = 0$, see text.

Neurons in population j are connected to neurons in population i. A single action potential from neurons in population j is seen as a post-synaptic potential $t \to PSP_{ij}(t-s)$ by neurons in population i, where s is the time of the spike hitting the synapse and t the time after the spike.

Assuming that the spikes contributions sum linearly, the average membrane potential of population i due to action potentials of population j is

$$V_i(t) = \sum_k PSP_{ij}(t - t_k - D_{ji}),$$

where the sum is taken over the arrival times, at the synapse between the neurons j and i, of the spikes produced by the neurons in population j. Recall that the effective delay D_{ji} is the time interval between the spike time arrival at the synapse and the maximum of the postsynaptic membrane potential of neuron i. These spikes have been produced at time $t_k - d_{ji}$ by the neuron j. The number of spikes arriving between t and $t + dt$ is $\nu_j(t - d_{ji})dt$. Therefore we have

$$V_i(t) \quad = \quad \sum_j \int_{t_0}^{t} PSP_{ij}(t - s - D_{ji})\nu_j(s - d_{ji})\, ds \tag{2.5}$$

or, equivalently

$$\nu_i(t) = S_i \left(\sum_j \int_{t_0}^{t} PSP_{ij}(t - s - D_{ji})\nu_j(s - d_{ji})\ ds \right) \tag{2.6}$$

The model as described above is not well defined as we see at $t = t_0$ that we have set the potentials all to be 0. Since one often takes $t_0 \to -\infty$, this is not a big problem. The PSP_{ij} can depend on several variables in order to account for adaptation, learning... There are two main simplifying assumptions that appear in the literature [Ermentrout 1998, Pinto 1996] and produce two different models that we describe below. Note that the previous equations are integral equations. It would simplify the analysis if we could write them as differential equations. This is possible if PSP_{ij} are sums of exponentials and powers as we suppose below.

Note that we are not able to solve analytically (2.3) to obtain the post-synaptic membrane potential PSP. This would allow to plug the expression of PSP in (2.5) and obtain a system of equations for V_i. This is why we assume a simple shape for PSP_{ij} in the following two sections and discuss in section 2.2.3 under what conditions our simple expression for PSP_{ij} is relevant.

2.2.1 The voltage-based model

The assumption, [Hopfield 1984], is that the post-synaptic potential has the same shape no matter which pre-synaptic population caused it, the sign and amplitude may vary though. This leads to the relation

$$PSP_{ij}(t) = w_{ij} PSP_i(t).$$

If $w_{ij} > 0$ the population j excites population i whereas it inhibits it when $w_{ij} < 0$. The shape of synaptic response PSP_i is often approximated by a simple exponential decay $PSP_i(t) = k_i e^{-t/\tau_i} H(t)$, or equivalently that

$$\tau_i \frac{dPSP_i(t)}{dt} + PSP_i(t) = k_i \delta(t). \tag{2.7}$$

We end up with the following system of delayed differential equations.

Lemma 2.2.1. *Equation (2.5) implies that*

$$\tau_i \frac{dV_i(t)}{dt} + V_i(t) = \sum_j w_{ij} S_j(V_j(t - \tau_{ji})) + I^i_{\text{ext}}(t). \tag{2.8}$$

Proof. We compute

$$\tau_i \frac{d}{dt} V_i(t) = \sum_j \Big[\tau_i PSP_{ij}(-D_{ji}) \nu_j(t - d_{ji}) + w_{ij} \int_0^t \left(-PSP_i(t - s - D_{ji}) + k_j \delta_{t-s-D_{ji}} \right) \nu_j(s - d_{ji}) ds \Big]$$

As $PSP_{ij}(t) = 0$ if $t < 0$, the first term vanishes and we find:

$$\tau_i \frac{d}{dt} V_i(t) = -V_i(t) + \sum_j w_{ij} k_j \nu_j(t - \tau_{ji})$$

which concludes the proof. □

Equation (2.8) describes the dynamic behaviour of a population. We have incorporated the constant k_i in the weights w_{ij} and added an external current $I_{\text{ext}}(t)$ to model the non-local connections[2] of population i.

Since the decay is governed by the membrane properties of the post-synaptic cell, τ_i is legitimately called the membrane time constant.

However, the approximation PSP_i introduces a discontinuity at $t = 0$ and ignores the characteristic delay peak as seen in figure 2.1. A better choice is to use

$$PSP_i(t) = k_i \left(e^{-t/\tau_{i;1}} - e^{-t/\tau_{i;2}} \right) H(t)$$

where $\tau_{i;1}, \tau_{i;2}$ are the time constants of the synaptic response. With this choice of PSP_i, we find, up to a rescaling of w_{ij}, the equations

$$\tau_{i;1}\tau_{i;2}\frac{d^2V_i(t)}{dt^2} + (\tau_{i;1} + \tau_{i;2})\frac{dV_i(t)}{dt} + V_i(t) = \sum_j w_{ij}S_j(V_j(t - \tau_{ji})) + I^i_{\text{ext}}(t), \quad (2.9)$$

We will not consider the equations (2.9) except in part III where we show briefly how the delays impact the second-order time dynamics. In chapter 3, we are interested in stationary solutions of the NF models and they are the same for (2.8) and (2.9).

We introduce the $p \times p$ matrices $\mathbf{J}$ such that $J_{ij} = w_{ij}/\tau_i$, and the function $\mathbf{S}$, $\mathbb{R}^p \to \mathbb{R}^p$ such that $\mathbf{S}(\mathbf{x})$ is the vector of coordinates $S_i(x_i)$, if $x = (x_1, \cdots, x_p)$. We rewrite (2.8) in vector form and obtain the following system of n delayed differential equations

$$\dot{\mathbf{V}}(t) + \mathbf{L}\mathbf{V}(t) = \mathbf{J}\,\mathbf{S}(\mathbf{V}_t) + \mathbf{I}_{\text{ext}}(t), \quad (2.10)$$

where $\mathbf{L}$ is the diagonal matrix $\mathbf{L} = \text{diag}(1/\tau_i)$ and $\mathbf{V}_t$ is a compact notation for the delayed terms $V_j(t - \tau_{ji})$ (which will be introduced in part III).

2.2.2 The activity-based model

The assumption is that the shape of a PSP depends only on the nature of the pre-synaptic cell, that is

$$PSP_{ij}(t) = w_{ij}PSP_j(t).$$

As above, we suppose that $PSP_i(t)$ satisfies the differential equation (2.7) and define the time-averaged firing rate to be

$$A_j(t) = \int_{t_0}^{t} PSP_j(t - s)\nu_j(s)\,ds.$$

A similar derivation as in lemma 2.2.1 yields the following set of p delayed differential equations under the assumption that $t_0 \to -\infty$. Hence, the derivation

[2] for example with the thalamus

of the activity-based equations is not rigorous but rather heuristic.

$$\tau_i \frac{dA_i(t)}{dt} + A_i(t) = S_i \left(\sum_j w_{ij} A_j(t - \tau_{ji}) + I^i_{\text{ext}}(t) \right) \quad i = 1, \cdots, p.$$

We include the k_is in the sigmoids S_i and rewrite this in vector form:

$$\dot{\mathbf{A}}(t) + \mathbf{L}\mathbf{A}(t) = \mathbf{S}(\mathbf{J} \cdot \mathbf{A}_t + \mathbf{I}_{\text{ext}}(t)), \tag{2.11}$$

Note that the true firing rate is the right-hand side of (2.11). $\mathbf{A}$ is also called, in the literature, the *synaptic drive* (see [Pinto 1996]). Since the τ_i depend on the pre-synaptic time constants, they are related to the synaptic decay and not to the post-synaptic membrane time constant.

2.2.3 Relationship between the two formulations

We have derived two NF models in the last two sections. Based on remark 4, if the synapses are fast, the dominant time constant is the membrane time constant: the voltage-based model is more appropriate. On the other hand, if the membrane time constant is small, the dominant time constant is the synaptic decay time: the activity-based model is more appropriate.

If we suppose that $\mathbf{I}_{\text{ext}}$ is stationary, and assume that the delays τ_{ji} are zero and $\mathbf{L}$ is scalar $\mathbf{L} = l \cdot \text{Id}$, then the voltage-based model can be derived from the activity based model the change of variables $\mathbf{V}(t) = \mathbf{J} \cdot \mathbf{A}(t) + \mathbf{I}_{\text{ext}}$. Also the stationary points of each model are mapped by the change of variables $\mathbf{A} = \mathbf{S}(\mathbf{V})$.

2.2.4 The continuum models

We now combine these local models to form a continuum of neural fields, *e.g.*, in the case of a model of a significant part Ω of the cortex. We consider a subset Ω of $\mathbb{R}^d$, $d = 1, 2, 3$ which we assume to be connected and compact, *i.e.* closed and bounded. This encompasses several cases of interest.

When $d = 1$ we deal with one-dimensional sets of neural fields. Even though this appears to be of limited biological interest, this is one of the most widely studied cases because of its relative mathematical simplicity and because of the insights one can gain of the more realistic situations.

When $d = 2$ we discuss properties of two-dimensional sets of neural fields. This is perhaps more interesting from a biological point of view since Ω can be viewed as a piece of cortex where the third dimension, its thickness, is neglected. This case has received by far less attention than the previous one, probably because of the increased computational difficulty.

Finally $d = 3$ allows us to discuss properties of volumes of neural fields, *e.g.* cortical sheets where their thickness is taken into account [Kandel 2000, Chalupa 2004].

We note $\mathbf{V}(\mathbf{r}, t)$ (respectively $\mathbf{A}(\mathbf{r}, t)$) the p-dimensional state vector at the point $\mathbf{r}$ of the continuum. We introduce the $p \times p$ matrix function $\mathbf{J}(\mathbf{r}, \mathbf{r}')$ which describes

how the neural mass at point $\mathbf{r}'$ influences that at point $\mathbf{r}$. We call $\mathbf{J}$ the connectivity matrix function.

More precisely, $J_{ij}(\mathbf{r}, \mathbf{r}')$ describes how population j at point $\mathbf{r}'$ influences population i at point $\mathbf{r}$.

Equation (2.10) can now be extended to

$$\frac{d}{dr}\mathbf{V}(\mathbf{r},t) = -\mathbf{L}\mathbf{V}(\mathbf{r},t) + \int_\Omega \mathbf{J}(\mathbf{r},\mathbf{r}')\mathbf{S}(\mathbf{V}(\mathbf{r}', t - \boldsymbol{\tau}(\mathbf{r},\mathbf{r}')))\, d\mathbf{r}' + \mathbf{I}_{\text{ext}}(\mathbf{r},t), \tag{2.12}$$

and equation (2.11) to

$$\frac{d}{dr}\mathbf{A}(\mathbf{r},t) = -\mathbf{L}\mathbf{A}(\mathbf{r},t) + \mathbf{S}\left(\int_\Omega \mathbf{J}(\mathbf{r},\mathbf{r}')\mathbf{A}(\mathbf{r}', t - \boldsymbol{\tau}(\mathbf{r},\mathbf{r}'))\, d\mathbf{r}' + \mathbf{I}_{\text{ext}}(\mathbf{r},t)\right). \tag{2.13}$$

The quantity $\boldsymbol{\tau}(\mathbf{r},\mathbf{r}')$ is the total delay for the processing of the information, from populations located at $\mathbf{r}'$ to populations located at $\mathbf{r}$ (see next section 2.2.5).

As before, we shall write the above equations in a condensed way:

$$\begin{aligned} \dot{\mathbf{V}}(t) &= -\mathbf{L}\mathbf{V}(t) + \mathbf{J}\cdot\mathbf{S}(\mathbf{V}_t) + \mathbf{I}_{\text{ext}}(t), \\ \dot{\mathbf{A}}(t) &= -\mathbf{L}\mathbf{A}(t) + \mathbf{S}(\mathbf{J}\cdot\mathbf{A}_t + \mathbf{I}_{\text{ext}}(t)). \end{aligned} \tag{2.14}$$

A significant amount of work has been devoted to this or closely related problems, starting perhaps with the pioneering work of Wilson and Cowan [Wilson 1973]. A fairly recent review of this work, and much more, can be found in a paper by Coombes [Coombes 2005b]. Amari [Amari 1977] investigated the problem in the case $d = p = 1$ when the sigmoid function is approximated by a Heaviside function and the connectivity function has a "Mexican-hat shape". He proved the existence of stable localised stationary solutions in this case. His work has been extended to different firing-rate and connectivity functions [Gutkin 2000, Laing 2002, Laing 2003b, Rubin 2004, Guo 2005b, Guo 2005a].

The case $p = 1$, $d = 2$ has been considered by several authors including [Pinto 2001a, Pinto 2001b] for general firing-rate functions and Gaussian-like connectivity functions, and [Blomquist 2005] when the firing-rate functions are approximated by Heaviside functions.

Extending these analysis to two- or three-dimensional continuum is difficult because of the increase in the degrees of freedom in the choice of the connectivity function. The case $p = 2$, $d = 1$ has been studied in [Werner 2001, Bressloff 2005a] when the firing-rate functions are approximated by Heaviside functions and the connectivity function is circularly symmetric while the case $p = 2$, $d = 2$ is mentioned as difficult in [Doubrovinski 2005].

To be complete, let us point out that equations of the type of (2.12) and (2.13) without delays have been studied in pure mathematics, see [Hazewinkel 2001]. They are of the Hammerstein type [Hammerstein 1930, Tricomi 1985]. This type of equations has received some recent attention, see [Appell 2006], and progress have been made toward a better understanding of their solutions.

2.2.5 The propagation-delay function

Following the derivation in section 2.1.2, we call $\boldsymbol{\tau}(\mathbf{r}, \mathbf{r}')$ the total delay for the processing of the information, from populations located at $\mathbf{r}'$ to populations located at $\mathbf{r}$. What is the space dependent delay function $\boldsymbol{\tau}(\mathbf{r}, \mathbf{r}')$ in the cortex? Our analysis is built upon the recent paper [Budd 2010]. It is concluded that if a neuron located at $\mathbf{r}$ is connected to another neuron located at $\mathbf{r}'$, the path length of this connection is very close to $\|\mathbf{r} - \mathbf{r}'\|_2$, the Euclidean distance. In other words, axons are straight lines. This is true if the two neurons are at most $2mm$ apart but we will assume it is also true for long range connections. Our analysis carries through for more general delay functions. Moreover, we have seen in section 2.1.1 that constant delays have to be introduced in order to take into account the finite integration time of action potentials by synapses ans post-synaptic neurons. Hence, we choose the following delay function:

$$\tau_{ij}(\mathbf{r}, \mathbf{r}') = D_{ij} + c_{ij} \left\|\mathbf{r} - \mathbf{r}'\right\|_2 \;\; i, j = 1, \cdots, p \tag{2.15}$$

where c_{ij} is the inverse of the propagation speed along axons between populations j and i. The conduction speeds of the intra-cortical connections are in the range $0.1 - 1m/s$ (see [Nunez 1995]) while the conductions speed for inter-cortical connections are around $1 - 10m/s$.

2.3 The Mexican hat model

In order to develop some intuition for NF models and to prepare the ground for chapter 6 and part IV, we briefly analyse a simple, two-populations, model.

Let us consider two populations of excitatory/inhibitory neurons of the neocortex spread over a cortex (see [Stetter 2000, Pinto 2001b, Kang 2003]). We write the NF equations (2.12) as

$$\begin{array}{rcl} \left(\tau_E \frac{d}{dt} + 1\right) V_E & = & J_{EE} \cdot S_E(V_E) - J_{EI} \cdot S_I(V_I) + I_E \\ \left(\tau_I \frac{d}{dt} + 1\right) V_I & = & J_{IE} \cdot S_E(V_E) + I_I \end{array} \tag{2.16}$$

For simplicity, we neglect the recurrent inhibition J_{II} and we suppose that the connections J_{ij} are modelled with gaussian functions. We also assume that time constant of inhibition is smaller than that of excitation ([McCormick 1985]). Hence, we suppose that the inhibitory activity is stationary at the time scale of the excitation τ_E. This gives a single equation for the excitation:

$$\left(\tau_E \frac{d}{dt} + 1\right) V_E = J_{EE} \cdot S_E(V_E) - J_{EI} \cdot S_I\Big(J_{IE} \cdot S_E(V_E) + I_I\Big) + I_E \tag{2.17}$$

This equation can be further simplified. Let us assume that the inhibition is recruited, *i.e.* the inhibition membrane potential is above threshold: $V_I > \theta_I$. The inhibitory neurons can sustain high firing rate (see [McCormick 1985]), their activity

does not saturate. This means that V_I is in the linear part of the sigmoid S_I, *i.e.* $S_I(V_I) \approx \alpha V_I$ for some positive $\alpha > 0$ being the gain of the sigmoid S_I. It gives:

$$\begin{aligned} \left(\tau_E \tfrac{d}{dt} + 1\right) V_E &= \Big(J_{EE} - \alpha J_{EI} \cdot J_{IE}\Big) \cdot S_E(V_E) + I_E - \alpha J_{EI} \cdot I_I \\ &\equiv J \cdot S_E(V_E) + I \end{aligned} \quad . \tag{2.18}$$

For example, if the connectivities $J_{ij}(\mathbf{r}, \mathbf{r}') = e^{-\|\mathbf{r}-\mathbf{r}'\|_2^2/2\sigma^2}$ are gaussians with the same spatial extension σ, then $J_{EI} \cdot J_{IE}$ is a gaussian of spatial extension 2σ. Hence in effect, J is a *difference-of-Gaussians* (DoG) connectivity. It is also called the *Mexican hat* connectivity when $\alpha < 1$. Note that the effective connectivity J

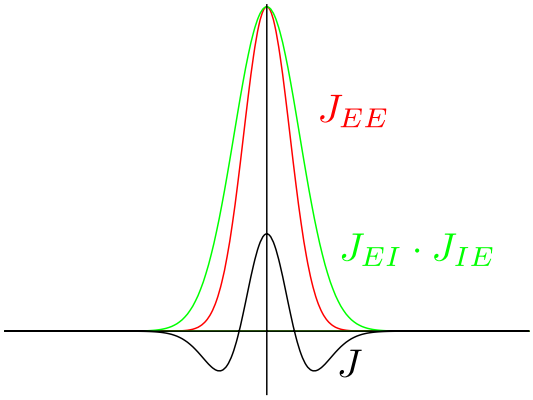

Figure 2.5: Plot of the effective connectivity $J(\cdot)$ for $\sigma = 1$ and $\alpha = 0.8$ on a 1d cortex.

has never been directly observed in biology because it features local excitation and lateral inhibition. Indeed, what is commonly observed is local excitation/inhibition and long-range excitation (see for example [Mariño 2005]).

We can have an intuition about the action of the DoG. Let us assume that we look at the stationary activity V_E^f, *i.e.* $\dot{V}_E^f = 0$. Then we find:

$$V_E^f = J \cdot S_E(V_E^f) + I = J \cdot S_E\Big(J \cdot S_E(V_E^f) + I\Big) + I$$

If the input I is strong compared is strong compared to the recurrent activity V_E^f, we can write:

$$V_E^f \approx I + J \cdot S_E(I)$$

Hence, V_E^f is linked to $J \cdot S_E(I)$. It is straightforward to see that the effect of applying a mexican hat J to an external input $S_E(I)$ is to localise (*i.e.* to regroup) the activity spread in space. Hence, given a stationary input, this type of connectivity favours a stationary activity V_E^f. This is called the *winner-take-all* mechanisms, well known from the signal processing community.

On the contrary, the inverted-mexican hat connectivity[3], favours the spread of activity in the tail of the connectivity. Hence, given a stationary input, this type of connectivity favours a dynamical activity.

Obviously, more quantitative work is needed to validate this first intuition. We will come back to these two types of connectivities in chapter 6.

[3] which is a mexican hat connectivity multiplied by -1

Part II

Stationary cortical states

Chapter 3

General properties of the stationary states

Contents

We have derived the delayed neural fields equations in the previous chapter. The solutions of these equations represent the state of activity of these populations when submitted to inputs form neighbouring brain aeras. In this chapter we study the dependency of the stationary solutions of the neural fields equations with respect to the nonlinear gain and the contrast of the external inputs. This is done by

using degree theory and bifurcation theory. The joint use of these two theories allows us to make new detailed predictions about the global and local behaviours of the solutions. We also provide a generic finite dimensional approximation of these equations which allows us to study in great details two models. The first model is a neural mass model of a cortical hypercolumn of orientation sensitive neurons, the Ring Model [Ben-Yishai 1995, Hansel 1997]. The second model is a general neural field model where the spatial connectivity is described by heterogeneous Gaussian-like functions.

3.1 Introduction

Neural or cortical fields are continuous assemblies of mesoscopic models, also called neural masses, of neural populations that are essential in the modeling of macroscopic parts of the brain.

They were first studied by Wilson and Cowan, Amari [Wilson 1973, Amari 1977] and play an important role in the design of the models of the visual cortex such as those proposed by Bressloff [Bressloff 2001b]. Neural fields describe the mean activity of neural populations by nonlinear integro-differential equations. The solutions of these equations represent the state of activity of these populations either in isolation, one talks about intrinsic activity, or when submitted to inputs from neighbouring brain areas. Understanding the properties of these solutions is therefore important for advancing our understanding of how the brain encodes and processes its internal and external inputs.

Among these solutions, the persistent states (or stationary solutions) are important for at least two reasons. First, in the case of autonomous systems, looking for persistent states helps to understand the dynamics because they are an easy way to divide the phase space into smaller components. If one makes the further assumption that the connectivity function is symmetric (see the review by [Ermentrout 1998]), the dynamics is described by heteroclinic orbits connecting the stationary solutions. Second, they are thought to be good models of the memory holding tasks on the time scale of the second, as demonstrated by experimentalists on primates [Colby 1995, Funahashi 1989, Miller 1996].

There are four major ingredients that occur in the mathematical description of these equations. First, the domain Ω of integration (typically a piece of cortex) which is of dimension d and can be bounded or unbounded, second, the type of the nonlinearity (sigmoidal, Heaviside), third, the type of the connectivity function that appears in the integral (homogeneous,*i.e.* translation invariant, or heterogeneous), and fourth, the number p of neuronal populations that are modeled.

Working with an unbounded domain Ω is not biologically relevant and also raises some mathematical difficulties. We work with a bounded Ω. Besides its biological relevance, this hypothesis is **crucial** for our mathematical analysis: it implies that there is at least one persistent state for any set of parameter values and provides bounds for these persistent states.

The nonlinearity in the neural field equations is most of the time chosen to be a Heaviside function which leads to several mathematical difficulties, one of them being the difficulty to apply a normal form theory. It is easier, as in [Faugeras 2009], to use smooth nonlinear functions instead to study the persistent states. Only a few papers use sigmoidal functions, e.g., [Atay 2005, Venkov 2007], or an alpha function[1], [Laing 2003a]. Moreover, Pinto and Ermentrout have shown how to extend results obtained with Heaviside functions to results holding for smooth sigmoids using singular perturbation theory [Pinto 2001a], while in [Kishimoto 1979, Ermentrout 1993] fixed points theorems are used to prove results for sigmoids. Let us also mention the fact that some perturbative results for smooth sigmoids have been obtained in the case of weakly interacting pulses [Bressloff 2006] and inhomogeneous travelling waves [Bressloff 2001a, Kilpatrick 2008]. In this chapter we make the assumption that the nonlinearity is a sigmoid function, *i.e.* infinitely differentiable.

Regarding the connectivity function we only assume that it is square integrable. Hence it can be heterogeneous, *i.e.* not translation invariant unlike what is often assumed in the literature. Despite the fact that they are rarely considered, networks with heterogenous weights have been studied in previous publications [Jirsa 2000, Qubbaj 2007, Bressloff 2001a, Bressloff 2003, Kilpatrick 2008, Rubin 2004]. Our work provides a firmer mathematical setting and generalizes these attempts.

Surprisingly, there are few papers dealing with the persistent states. Their authors use two main methods: Turing patterns (or bifurcation theory) and reduction to ODEs and PDEs.

The first method is used in almost every paper, *e.g.* [Atay 2005, Coombes 2004, Blomquist 2005, Venkov 2007], very often in the case of a translation invariant connectivity function (hence a convolution kernel), and leads to the description of a large amount of solutions and behaviours thereof such as traveling waves, breathers, persistent states, etc... that depend on special relations between the spatial frequency k and the temporal frequency, ω. We generalize this approach as follows: we do not worry about the spatial structure of the cortical states (i.e. the solutions, indexed by the spatial frequency k in these previous studies) but think instead of a cortical state as a point in a (functional) vector space. We can then elegantly and economically study how this point trajectory varies (and eventually bifurcates) when the relevant parameters in the neural field equations vary. By doing so we are able to harvest a lot of results that do not depend upon the translation invariant assumption, but of course also hold in this case.

The second method is to reduce the search for the persistent states to the problem of finding homoclinic orbits for some ODEs [Laing 2002] when $\Omega = \mathbb{R}$ and $p = 1$, or of finding of homoclinic orbits for some PDEs [Laing 2003a] if and only if $\Omega = \mathbb{R}^2$. The obvious advantage of these approaches is that one can use finite-dimensional tools such as those described in [Kuznetsov 1998, Guckenheimer 1983], or PDE methods, such as those described for example in [Kielhöfer 2003], for the

[1] $e^{-1/v^2}H(v)$, H the Heaviside function.

bifurcation analysis. When successful, these approaches allow to compute the persistent states independently of their stability and to compute their number as a function of the strength of the connections.

In [Faugeras 2009], an analysis of the neural fields equations defined over a finite part of the cortex is performed from two different viewpoints, theoretical and numerical. The same article concludes that the dynamics is "boring" (every initial condition converged to a single persistent state) if the nonlinear gain was small. For example the system could not exhibit oscillatory behaviours. More importantly this paper do not produce a method for computing more than one, or even all the persistent states when the system featured several such states.

In this chapter, we relax the hypothesis leading to the uniqueness of the persistent state and try to understand the structure of the set, noted $\mathcal{B}$, of stationary solutions as the parameters[2] vary over large ranges of values, thereby departing from a purely local analysis. The local structure of the set $\mathcal{B}$ is described using bifurcation theory (see [Kuznetsov 1998, Guckenheimer 1983, Kielhöfer 2003, Haragus 2010]) whereas degree theory helps to understand its global structure. This latter theory can predict the existence of stationary solutions that cannot be obtained using only bifurcation theory. In order to compute numerically these persistent states, we use a multiparameter continuation scheme that allows to compute non-connected branches[3] of persistent states that would otherwise be unattainable.

In order to perform our numerical experiments we consider a very general method for approximating the connectivity kernels, the Pincherle-Goursat kernels method [Tricomi 1985], which allows to reduce exactly the dynamics to a system of ODEs whose dimension is directly related to the level of approximation and can be arbitrarily large, if needed. Hence our choice to use infinite dimensional techniques to the integral equation is guided by the fact that it offers a simple, albeit abstract, conceptual framework in which the behaviours of interest to us can be described in a clean and dimension-independent manner. When it comes to numerical experiments, we use the system of ODEs provided by the Pincherle-Goursat kernels.

The chapter is organized as follows. In section 3.2 we introduce the functional analysis framework that allows us to study the neural field equations as a Cauchy problem in a functional space and to derive a number of useful properties of the solutions of these equations. In section 3.3 we combine the results of the previous section with a bifurcation study in order to obtain more information about the set $\mathcal{B}$ of solutions. A numerical scheme is proposed to compute the structure of this set. In section 3.4 we show how to reduce the neural field equations to a set of ODEs through the use of the Pincherle-Goursat kernels. In section 3.5 we study in detail a neural mass model that reduces exactly to a finite set of ODEs, the Ring Model. In section 3.6, we compute the stationary solutions for a model featuring two populations of neurons on a two-dimensional cortex sheet connected

[2] We use the nonlinear gain and the contrast of the external inputs but our analysis applies to other parameters.

[3] A branch is a one-dimensional set of stationary solutions obtained by varying one parameter.

by heterogenous Gaussian-like functions: it allows us to provide salient examples of the predictions obtained in sections 3.2 and 3.3. In section 3.7 we discuss the biological and numerical validity of two of our main hypotheses, the fact that the cortex has a finite size and the use of a smooth sigmoid instead of a Heaviside function. We conclude in section 3.8.

3.2 General framework

In this section, we precise a bit more the notations introduced in the previous chapter. The voltage-based model without delays is written:

$$\begin{cases} \dot{\mathbf{V}}(\mathbf{r},t) &= -\mathbf{L}\cdot\mathbf{V}(\mathbf{r},t) + [\mathbf{J}(t)\cdot\mathbf{S}(\boldsymbol{\sigma}(\mathbf{V}(t)-\boldsymbol{\theta}))](\mathbf{r}) + \mathbf{I}_{ext}(\mathbf{r},t) \quad t>0 \\ \mathbf{V}(\cdot,0) &= \mathbf{V}_0(\cdot) \end{cases} \tag{3.1}$$

This equation is an initial value problem that describes the time variation of the p-dimensional vector function $\mathbf{V}$ defined on Ω, starting from the initial condition $\mathbf{V}_0$, a function defined on Ω. At each time $t \geq 0$ $\mathbf{V}$ belongs to some functional space, in effect a Hilbert space $\mathcal{F}$, that we describe in the next section. We now discuss the various quantities that appear in (3.1). We suppose that Ω is an open bounded subset of $\mathbb{R}^d$.

$\mathbf{J}(t)$ is a linear operator from $\mathcal{F}$ to itself defined by:

$$[\mathbf{J}(t)\cdot\mathbf{V}(t)](\mathbf{r}) = \int_\Omega \mathbf{J}(\mathbf{r},\mathbf{r}',t)\mathbf{V}(\mathbf{r}',t)\,d\mathbf{r}', \tag{3.2}$$

where $\mathbf{J}(\mathbf{r},\mathbf{r}',t)$ is a $p\times p$ matrix that describes the "strength" of the connections. We also describe in the next section the functional space to which $\mathbf{J}(t)$ belongs and the conditions it must satisfy in order for the equation (3.1) to be well-defined. The external current input, $\mathbf{I}_{ext}(\cdot,t)$, is in $\mathcal{F}$ for all $t\geq 0$. The function $\mathbf{S}:\mathbb{R}^p\to\mathbb{R}^p$ is defined by $\mathbf{S}(x) = [S(x_1),\cdots,S(x_p)]^T$, where $S:\mathbb{R}\to(0,1)$ is the normalized sigmoid function of equation

$$S(z) = \frac{1}{1+e^{-z}}. \tag{3.3}$$

It is infinitely differentiable on $\mathbb{R}^p$ and all its derivatives $S^{(q)}(x)$, $q=1,2,\cdots$ are bounded. For all integer $q\geq 1$ we note $\mathbf{S}^{(q)}(x)$ the $p\times p$ diagonal matrix $\mathrm{diag}(S^{(q)}(x_1),\cdots,S^{(q)}(x_p))$. Because of the form of the function $\mathbf{S}$, the qth order derivative of $\mathbf{S}$ at $x\in\mathbb{R}^p$ is the multilinear function defined by

$$D^q\mathbf{S}(x)\cdot(y_1,\cdots,y_q) = \mathbf{S}^{(q)}(x)\cdot(y_1\cdots y_q), \quad y_i\in\mathbb{R}^p, i=1,\cdots,q \tag{3.4}$$

where $y_1\cdots y_q$ is the component pointwise product of the q vectors $y_1,\cdots,y_q$ of $\mathbb{R}^p$,*i.e.* the vector of $\mathbb{R}^p$ whose kth coordinate, $k=1,\cdots,p$ is equal to the product of the q kth coordinates of each vector y_i, $i=1,\cdots,q$.

$\boldsymbol{\sigma}$ is the $p\times p$ diagonal matrix $\mathrm{diag}(\sigma_1,\cdots,\sigma_p)$, $\sigma_i\geq 0$, $i=1,\cdots,p$ that determines the nonlinear gain of each of the p sigmoids at the origin.

$\boldsymbol{\theta}$ is a p-dimensional vector that determines the threshold of each of the p sigmoids.

The diagonal $p \times p$ matrix $\mathbf{L}$ is equal to $\mathrm{diag}(\frac{1}{\tau_1}, \cdots, \frac{1}{\tau_p})$, where the positive numbers τ_i, $i = 1, \cdots, p$ determine the exponential decrease dynamics of each neural population.

We shall also write the activity-based model which leads to the following initial value problem:

$$\begin{cases} \dot{\mathbf{A}}(\mathbf{r},t) &= -\mathbf{L}_a \cdot \mathbf{A}(\mathbf{r},t) + \mathbf{S}\left(\boldsymbol{\sigma}\left([\mathbf{J}(t)\cdot\mathbf{A}](\mathbf{r},t) + \mathbf{I}_{ext}(\mathbf{r},t)\right)\right) \quad t>0 \\ \mathbf{A}(\cdot,0) &= \mathbf{A}_0(\cdot) \end{cases} \tag{3.5}$$

We let $\mathbf{L}_a = \mathrm{diag}(\alpha_1, \cdots, \alpha_p)$.

The two problems (3.1) and (3.5) are closely related. In particular there is a one to one correspondence between their equilibria, as recalled below for the Ring Model of section 3.5, which is an activity-based model.

3.2.1 The Cauchy problem

In this section we prove that equation (3.1) is well-posed and provide some properties of its solutions. We rewrite it as a Cauchy Problem, *i.e.* as an ordinary differential equation on the Hilbert space $\mathcal{F} \equiv \mathrm{L}^2(\Omega, \mathbb{R}^{\mathrm{p}})$ endowed with the inner product

$$\langle \mathbf{V}^{(1)}, \mathbf{V}^{(2)} \rangle_{\mathcal{F}} = \sum_{i=1}^{p} \int_{\Omega} d\mathbf{r} \mathbf{V}_i^{(1)}(\mathbf{r}) \mathbf{V}_i^{(2)}(\mathbf{r}).$$

This turns out to be convenient for the upcoming computations. Let us also define $\mathcal{G} \equiv \mathrm{L}^\infty(\Omega, \mathbb{R}^{\mathrm{p}}) \subset \mathcal{F}$. Then we can rewrite (3.1) in a compact form:

$$\begin{cases} \frac{d\mathbf{V}}{dt} &= -\mathbf{L}\cdot\mathbf{V} + \mathbf{R}(t,\mathbf{V}) \quad t>0 \\ \mathbf{V}(0) &= \mathbf{V}_0 \in \mathcal{F} \end{cases} \tag{3.6}$$

The nonlinear operator $\mathbf{R}$ is defined by

$$\mathbf{R}(t,\mathbf{V}) = \mathbf{J}(t)\cdot\mathbf{S}(\boldsymbol{\sigma}(\mathbf{V}-\boldsymbol{\theta})) + \mathbf{I}_{ext}(t) \tag{3.7}$$

Proposition A.2.1 shows that $\mathbf{R}(t,\cdot) : \mathcal{F} \to \mathcal{F}$ for all $t > 0$. We have the further properties:

Lemma 3.2.1. *If $\mathbf{J} \in \mathrm{L}^\infty(\Omega^2, \mathbb{R}^{\mathrm{p}\times\mathrm{p}})$, then $\mathbf{R}$ satisfies the following properties:*

- $\mathbf{R}(t,\cdot) \in C^1(\mathcal{F},\mathcal{F})$ *and its differential is given by* $D\mathbf{R}(t,\mathbf{V}_0) = \mathbf{J}(t)D\mathbf{S}(\boldsymbol{\sigma}(\mathbf{V}_0-\boldsymbol{\theta}))\boldsymbol{\sigma}$ *for all* $\mathbf{V}_0$ *in* $\mathcal{F}$.
- $\forall q \in \mathbb{N}$, $\mathbf{R}(t,\cdot) \in C^q(\mathcal{G},\mathcal{G})$ *and its pth differential is:* $D^q\mathbf{R}(t,\mathbf{V}_0) = \mathbf{J}(t)\mathbf{S}^{(q)}(\boldsymbol{\sigma}(\mathbf{V}_0-\boldsymbol{\theta}))\boldsymbol{\sigma}^q$ *for all* $\mathbf{V}_0$ *in* $\mathcal{F}$.
- $\|\mathbf{R}(t,\mathbf{U}_1) - \mathbf{R}(t,\mathbf{U}_2)\|_{\mathcal{F}} \leq \sigma_m \|\mathbf{J}(t)\|_{\mathcal{F}} \|\mathbf{U}_1 - \mathbf{U}_2\|_{\mathcal{F}}$ *for all* $t > 0$ *and for all* $\mathbf{U}_1$, $\mathbf{U}_2$ *in* $\mathcal{F}$ *where* $\sigma_m = \max_i \sigma_i$.

- $\mathbf{R}(t,\cdot)$ *is a compact operator on* $\mathcal{F}$ *for all* $t>0$.

Proof. It is easy to see from the definition (3.7) of $\mathbf{R}$ that, if it exists, $D^q\mathbf{R}(t,\mathbf{V}_0)[\mathbf{U}_1,\cdots,\mathbf{U}_q]=\mathbf{J}(t)\cdot\left(\mathbf{S}^{(q)}(\boldsymbol{\sigma}(\mathbf{V}_0-\boldsymbol{\theta}))\boldsymbol{\sigma}^q\cdot(\mathbf{U}_1\cdots\mathbf{U}_q)\right)$. The notation $\mathbf{U}_1\cdots\mathbf{U}_q$ is the same as in the definition of $D^q\mathbf{S}$ in equation (3.4), *i.e.* the component pointwise product of the q functions $\mathbf{U}_1,\cdots,\mathbf{U}_q$ of $\mathcal{G}$. The first property follows from $\mathbf{J}\in\mathrm{L}^\infty(\Omega^2,\mathbb{R}^{\mathrm{p}})$ and from the proposition A.2.1. The q-multilinear operator $D^q\mathbf{R}(t,\mathbf{V}_0)$ is well-defined because, $\mathbf{U}_1\cdots\mathbf{U}_q$ is in $\mathcal{G}$. It is easy to show that the q-multilinear operator $D^q\mathbf{R}(t,\mathbf{V}_0)$ is continuous on $\mathcal{G}$:

$$\begin{aligned}\|D^q\mathbf{R}(t,\mathbf{V}_0)\cdot(\mathbf{U}_1\cdots\mathbf{U}_q)\|_{\mathcal{G}}&\\ \leq|\Omega|\left\|\mathbf{J}(t)\mathbf{S}^{(q)}(\boldsymbol{\sigma}(\mathbf{V}_0-\boldsymbol{\theta}))\boldsymbol{\sigma}^q\right\|_{\mathrm{L}^\infty(\Omega^2,\mathbb{R}^{\mathrm{p}\times\mathrm{p}})}&\|\mathbf{U}_1\cdots\mathbf{U}_q\|_{\mathcal{G}}\\ \leq K\prod_i\|\mathbf{U}_i\|_{\mathcal{G}}&\end{aligned}$$

for some positive constant K because $\mathcal{G}$ is a Banach algebra. It follows that $D^q\mathbf{R}$ is continuous and $\mathbf{R}(t,\cdot)\in C^q(\mathcal{G},\mathcal{G})$. This proves the second property. The third and fourth property were proved in [Faugeras 2009]. □

It is now routine to apply the Cauchy-Lipschitz theorem to obtain the next proposition as in [Faugeras 2009]:

Proposition 3.2.2. *If the following two hypotheses are satisfied:*

1. *The connectivity function* $\mathbf{J}$ *is in* $C(\mathbb{R}^+;\mathrm{L}^\infty(\Omega^2,\mathbb{R}^{\mathrm{p}}))$ *and is bounded,* $|||\mathbf{J}(t)|||_{\mathcal{F}}\leq J$, $t\geq 0$,
2. *the external current* $\mathbf{I}_{\mathrm{ext}}$ *is in* $C(\mathbb{R}^+;\mathcal{F})$,

then for any function $\mathbf{V}_0$ *in* $\mathcal{F}$ *there is a unique solution* $\mathbf{V}$, *defined on* $\mathbb{R}^+$ *and continuously differentiable, of the initial value problem* (3.1).

This solution depends upon $3p$ parameters, the slopes $\boldsymbol{\sigma}$, the thresholds $\boldsymbol{\theta}$ and the diagonal matrix $\mathbf{L}$.

Even if we have made progress in the formulation of the neural field equations, it still remains the unsatisfactory possibility that the membrane potential becomes unbounded as $t\to\infty$. However this is not the case as shown in the next proposition:

Proposition 3.2.3. *If the external current is bounded in time* $\|\mathbf{I}_{\mathrm{ext}}(t)\|_{\mathcal{F}}\leq I_{\mathrm{ext}}$, *for all* $t\geq 0$, *then the solution of equation* (3.6) *is bounded for each initial condition* $\mathbf{V}_0\in\mathcal{F}$.

Proof. Let us define $f:\mathbb{R}\times\mathcal{F}\to\mathbb{R}^+$ as

$$f(t,\mathbf{V})\stackrel{\text{def}}{=}\langle-\mathbf{L}\cdot\mathbf{V}+\mathbf{J}(t)\cdot\mathbf{S}(\boldsymbol{\sigma}(\mathbf{V}-\boldsymbol{\theta}))+\mathbf{I}_{ext}(t),\mathbf{V}\rangle_{\mathcal{F}}=\frac{1}{2}\frac{d\|\mathbf{V}\|_{\mathcal{F}}^2}{dt}.$$

We note $\tau_{max}=\max_{i=1\cdots,p}\tau_i$ and notice that

$$f(t,\mathbf{V})\leq-\frac{1}{\tau_{max}}\|\mathbf{V}\|_{\mathcal{F}}^2+(J+I_{ext})\|\mathbf{V}\|_{\mathcal{F}}.$$

Thus, if $\|\mathbf{V}\|_{\mathcal{F}} \geq 2\tau_{max}(J + I_{ext}) \stackrel{\text{def}}{=} R$, $f(t, \mathbf{V}) \leq -2\tau_{max}(J + I_{ext})^2 \stackrel{\text{def}}{=} -\delta < 0$.

Let us show that the open ball of $\mathcal{F}$ of center 0 and radius R, B_R, is stable under the dynamics of equation (3.1). We know that $\mathbf{V}(t)$ is defined for all $t \geq 0$s and that $f < 0$ on ∂B_R, the boundary of B_R. We consider three cases for the initial condition $\mathbf{V}_0$.

If $\mathbf{V}_0 \in B_R$ and set $\tau = \sup\left\{t \,|\, \forall s \in [0, t], \mathbf{V}(s) \in \overline{B}_R\right\}$. Suppose that $\tau \in \mathbb{R}$, then $\mathbf{V}(\tau)$ is defined and belongs to $\overline{B}_R$, the closure of B_R, because $\overline{B}_R$ is closed, in effect to ∂B_R. We also have $\frac{d}{dt}\|\mathbf{V}\|^2_{\mathcal{F}}|_{t=\tau} = f(\tau, \mathbf{V}(\tau)) \leq -\delta < 0$ because $\mathbf{V}(\tau) \in \partial B_R$. Thus we deduce that for $\varepsilon > 0$ and small enough, $\mathbf{V}(\tau + \varepsilon) \in \overline{B}_R$ which contradicts the definition of τ. Thus $\tau \notin \mathbb{R}$ and $\overline{B}_R$ is stable.

Because $f < 0$ on ∂B_R, $\mathbf{V}_0 \in \partial B_R$ implies that $\forall t > 0, \quad \mathbf{V}(t) \in B_R$.

Finally we consider the case $\mathbf{V}_0 \in \complement\overline{B}_R$. Suppose that $\forall t > 0, \ \mathbf{V}(t) \notin \bar{B}_R$, then $\forall t > 0, \ \frac{d}{dt}\|\mathbf{V}\|^2_{\mathcal{F}} \leq -2\delta$, thus $\|\mathbf{V}(t)\|_{\mathcal{F}}$ is monotonically decreasing and reaches the value of R in finite time when $\mathbf{V}(t)$ reaches ∂B_R. This contradicts our assumption. Thus $\exists \tau > 0 \,|\, \mathbf{V}(\tau) \in B_R$. □

Corollary 3.2.4. *If $\mathbf{V}_0 \notin B_R$ and $T = \inf\{t > 0 | \mathbf{V}(t) \notin B_R\}$. Then*

$$T \leq \frac{\|\mathbf{V}_0\|^2_{\mathcal{F}} - R^2}{2\delta}$$

This proposition shows that $\overline{B}_R$ is an attracting set and that it suffices to study the dynamics within this set to understand the long time behavior of the solutions of the Neural Fields Equations. This attracting set contains the stationary solutions of (3.1), we devote the next section to their study. We quote a result from [Faugeras 2009] concerning their stability:

Proposition 3.2.5. *If the condition*

$$\sigma_m \rho(\mathbf{J}_s) < 1,$$

where holds, then every stationary solution of (3.1) is globally asymptotically stable. $\sigma_m = \max \sigma_i$, $\mathbf{J}_s$ is the symmetric part $(\mathbf{J} + \mathbf{J}^*)/2$ of the operator $\mathbf{J}$, and $\rho(\mathbf{J}_s)$ its spectral radius. We define σ_L to be $\rho(\mathbf{J}_s)^{-1}$.

Similar results hold for the activity-based model (3.5). We end this section by quoting [Hopfield 1984] which gives the local dynamics in a simple case.

Proposition 3.2.6. *If the operator J is symmetric, $p = 1$, and J, I_{ext} are constant in time, then there is no homoclinic orbit nor non-constant periodic orbit for (3.1).*

Proof. Write $A = S(V)$ and $E = -\frac{1}{2}\langle A, J \cdot A + 2I_{ext}\rangle_{\mathcal{F}} + \int d\mathbf{r} \int_0^{A(\mathbf{r})} S^{-1}(a)da$ is a bounded function. Using the symmetries of J:

$$\begin{aligned}\frac{dE}{dt} &= -\left\langle \frac{dA}{dt}, I_{ext} + J \cdot A \right\rangle + \int d\mathbf{r} \frac{dA}{dt} V = \left\langle \frac{dA}{dt}, -I_{ext} - J \cdot A + V \right\rangle \\ &= -\left\langle \frac{dA}{dt}, \frac{dV}{dt} \right\rangle = -\left\langle \frac{dV}{dt} S'(V), \frac{dV}{dt} \right\rangle = -\int d\mathbf{r} S'(V(\mathbf{r})) \left(\frac{dV(\mathbf{r})}{dt}\right)^2 \leq 0\end{aligned}$$

It follows that there is no homoclinic orbit nor non-constant periodic orbit since $E(V)$ is decreasing on the trajectories. Since E is bounded, its reaches its minimuma which satisfy $\nabla E(V^f) = 0$ *i.e.* $I + J \cdot S(V^f) = V^f$, the trajectories are heteroclinic orbits. □

3.2.2 Global properties of the set of persistent states

We look at the equilibrium states of (3.1), when $\mathbf{I}_{ext}$ and $\mathbf{J}$ do not depend upon the time. Our goal is to estimate their number and, if possible, to compute them numerically, for a given set of parameters. It is quite demanding to do it at a given point in the parameter space except in some very special cases[4]. We note that when $\boldsymbol{\sigma} = 0$ (or $\mathbf{J} = 0$), the stationary equation is trivially solved. Hence, we can think of deforming this trivial solution to a solution when $\boldsymbol{\sigma} \neq 0, \mathbf{J} \neq 0$. This raises a number of questions. Does such a "manifold" of solutions exist *i.e.* can we link the trivial solution to a solution for any given set of parameters? If yes, are there any other solutions? How do these "manifolds" look globally? These questions concern global properties of the set of solutions (existence of branches, existence of intersection points, connectedness...) and are difficult to answer. We provide some partial answers in the remainder of the chapter.

Before going deeper in the analysis, we need to simplify the parameter space. The equilibria $\mathbf{V}^f_\lambda$, independent of time, are solutions of

$$0 = -\mathbf{L} \cdot \mathbf{V}^f_\lambda + \mathbf{J} \cdot \mathbf{S}(\boldsymbol{\sigma}(\mathbf{V}^f_\lambda - \boldsymbol{\theta})) + \mathbf{I}_{\text{ext}},$$

Note that we have written the dependency of these solutions on an arbitrary parameter λ which is not necessarily scalar. We redefine $\mathbf{J}$ as $\mathbf{L}^{-1}\mathbf{J}$, $\mathbf{V}$ as $\mathbf{V} - \boldsymbol{\theta}$ and $\mathbf{I}_{ext}$ as $\mathbf{L}^{-1} \cdot \mathbf{I}_{ext} - \boldsymbol{\theta}$ and restrict our study to:

$$0 = -\mathbf{V}^f_\lambda + \mathbf{J} \cdot \mathbf{S}(\boldsymbol{\sigma}\mathbf{V}^f_\lambda) + \mathbf{I}_{\text{ext}} \tag{3.8}$$

Still, equation (3.8) contains many parameters such as the ones describing $\mathbf{J}$ and $\mathbf{I}_{\text{ext}}$, or the nonlinear gains $\boldsymbol{\sigma}$. Which parameters λ to choose for the continuation method: $\boldsymbol{\sigma}$ or $\mathbf{J}$? We decide to fix $\mathbf{J}$ and control $\boldsymbol{\sigma}$ for two reasons:

- the stationary solutions are bounded for $\boldsymbol{\sigma} \in \mathbb{R}^p_+$, see proposition 3.2.7 1, this is not the case when $\|\mathbf{J}\|_{\mathrm{L}^2(\Omega^2, \mathbb{R}^{\mathrm{P}\times\mathrm{P}})} \to \infty$.
- previous studies usually use a Heaviside nonlinearity which is formally equivalent to our nonlinearity when $\boldsymbol{\sigma}$'='∞, varying $\boldsymbol{\sigma}$ can thus bridge the gap with previous approaches.

As a matter of fact, the techniques we are about to expose are applicable to any set of parameters with minor modifications. Hence, we now focus on the influence

[4] When the nonlinearity $\mathbf{J} \cdot \mathbf{S}(\boldsymbol{\sigma}(\mathbf{V}^f_\lambda - \boldsymbol{\theta}))$ is small compared to the linear part $\mathbf{L} \cdot \mathbf{V}^f_\sigma$, we know there exists a unique solution and how to compute it. This was shown in [Faugeras 2009].

of the nonlinear gains $\boldsymbol{\sigma}$ on the solutions of (3.1). We make the assumption that they are all equal to σ, $\boldsymbol{\sigma} = \sigma \mathrm{Id}_p$, $\sigma \geq 0$. where Id_p is the $p \times p$ identity matrix. The equation becomes

$$0 = -\mathbf{V}_\sigma^f + \mathbf{J} \cdot \mathbf{S}(\sigma \mathbf{V}_\sigma^f) + \mathbf{I}_{\text{ext}} \stackrel{\text{def}}{=} -F(\mathbf{V}_\sigma^f, \sigma) \tag{3.9}$$

It is clear that when $\boldsymbol{\sigma} = 0$, the stationary equation is trivially solved by

$$\mathbf{V}_0^f \stackrel{\text{def}}{=} \mathbf{J} \cdot \mathbf{S}(0) + \mathbf{I}_{\text{ext}} = \frac{1}{2} \mathbf{J} \cdot \mathbf{1} + \mathbf{I}_{\text{ext}},$$

where $\mathbf{1}$ is the p-dimensional vector with all coordinates equal to 1. Let $\mathcal{B}_\sigma$ be the set of solutions of equation (3.9) for a given nonlinear gain σ:

$$\mathcal{B}_\sigma = \{\mathbf{V} \,|\, F(\mathbf{V}, \sigma) = 0\}$$

We next provide some properties of the sets $\mathcal{B}_\sigma$.

Proposition 3.2.7.

1. *The persistent states satisfy the following inequality*

$$\left\| \mathbf{V}_\sigma^f - \mathbf{V}_0^f \right\|_{\mathcal{F}} \leq \|\mathbf{J}\|_{\mathcal{F}} \sqrt{p|\Omega| S_0\left(\frac{\sigma^2 B_1^2}{p|\Omega|}\right)}, \text{ where } B_1 \stackrel{\text{def}}{=} \sqrt{p|\Omega|}\, \|\mathbf{J}\|_{\mathcal{F}} + \|\mathbf{I}_{\text{ext}}\|_{\mathcal{F}},$$

   $S_0 : \mathbb{R} \to \mathbb{R}$ is the "shifted" sigmoid defined by $S_0(x) = S(x) - S(0)$ and the constant B_1 is defined in proposition A.6.2 of appendix A.6.

2. *If the condition*

$$\sigma \|\mathbf{J}\|_{\mathcal{F}} < 1 \tag{3.10}$$

   is satisfied, then $\#\mathcal{B}_\sigma = 1$. We define σ^* to be $\|\mathbf{J}\|_{\mathcal{F}}^{-1}$.

3. *$\forall \sigma \in \mathbb{R}^+$, $\mathcal{B}_\sigma \neq \emptyset$,*

4. *If the number of non critical solutions[5] in $\mathcal{B}_\sigma$ is finite, then it must be odd.*

5. *Let $0 \leq a < b$ be two reals, and consider the set $\mathcal{B} = \cup_{\sigma \in [a,b]} (\mathcal{B}_\sigma \times \{\sigma\})$. Then $\mathcal{B}$ contains a connected component $\mathcal{C}$ which intersects $\mathcal{B}_a \times \{a\}$ and $\mathcal{B}_b \times \{b\}$.*

6. *If $\mathbf{I}_{ext} = \varepsilon \mathbf{I}_{ext}^{(0)}$ with $\mathbf{I}_{ext}^{(0)} \neq 0$ a.e. and $\varepsilon > 0$ is called the contrast, then $\forall \sigma > 0$, $\#\mathcal{B}_\sigma = 1$ for ε large enough.*

Proof.

1. From lemma A.6.1 in appendix A.6 we have $S_0(\sigma V_{\sigma i}^f)^2 \leq S_0(\sigma^2 (V_{\sigma i}^f)^2)$, $i = 1, \cdots, p$. Therefore

$$\sum_{i=1}^p S_0(\sigma V_{\sigma i}^f)^2 \leq \sum_{i=1}^p S_0(\sigma^2 (V_{\sigma i}^f)^2) \leq p S_0\left(\frac{\sigma^2}{p} \sum_{i=1}^p (V_{\sigma i}^f)^2\right).$$

[5] *i.e.* solutions where the jacobian is not singular.

The second inequality comes from Jensen's and the fact that $S_0(\cdot)$ is concave in $\mathbb{R}^+$. It then follows, using again Jensen's inequality and the fact that $\mathbf{S}_0$ is monotonously increasing, that

$$\left\|\mathbf{S}_0(\sigma\mathbf{V}_\sigma^f)\right\|_{\mathcal{F}}^2 \leq p|\Omega|S_0\left(\frac{\sigma^2}{p|\Omega|}\left\|\mathbf{V}_\sigma^f\right\|_{\mathcal{F}}^2\right)$$

Now

$$\left\|\mathbf{V}_\sigma^f - \mathbf{V}_0^f\right\|_{\mathcal{F}}^2 = \left\|\mathbf{J}\cdot\mathbf{S}_0(\sigma\mathbf{V}_\sigma^f)\right\|_{\mathcal{F}}^2 \leq |||\mathbf{J}|||_{\mathcal{F}}^2\left\|\mathbf{S}_0(\sigma\mathbf{V}_\sigma^f)\right\|_{\mathcal{F}}^2$$

The inequality then follows from proposition A.6.2.

2. Use the Picard Theorem. As shown in figure 3.2, this imposes that $\sigma^* \leq \sigma_L$. Indeed, as $\rho(\mathbf{J}_s) \leq |||\mathbf{J}_s|||$ and $|||\mathbf{J}_s||| = |||\mathbf{J}|||$, and $|||\mathbf{J}||| \leq \|\mathbf{J}\|_{\mathcal{F}}$, we have $\sigma^* = \|\mathbf{J}\|_{\mathcal{F}}^{-1} \leq \sigma_L = \rho(\mathbf{J}_s)^{-1}$.

3. The first property is that it is non empty: in [Faugeras 2009] we proved that persistent states always existed in $\mathbf{L}^2(\Omega, \mathbb{R}^p)$ for all positive values of σ.

4. If $\mathcal{B}_\sigma$ has a finite number of non critical solutions, we can assume that these points are non critical. Then according to the Leray-Schauder degree theory sketched in appendix A.3 we have

$$\deg_{\mathrm{LS}}(F(\mathbf{V},\sigma), B_r, 0) = \sum_{\mathbf{V}_\sigma^f \in \mathcal{B}_\sigma} \mathrm{sign}\ \det{}_{\mathrm{F}}(D_V F(\mathbf{V}_\sigma^f, \sigma), B_r, 0) = \sum_{\mathbf{V}_\sigma^f \in \mathcal{B}_\sigma} \mathrm{sign}\ \det{}_{\mathrm{F}}(\mathrm{Id} - \sigma\mathbf{J}D\mathbf{S}(\sigma\mathbf{V}_\sigma^f)), \quad (3.11)$$

where $r = 2B_1$, B_1 is defined in proposition A.6.2 in appendix A.6 and $\det_{\mathrm{F}}$ is the Fredholm determinant (see appendix C.1.2). We prove in corollary A.3.2 in appendix A.3 that the first term is equal to 1. Suppose now that $\mathcal{B}_\sigma$ contains an even number of points, say $2k$ among which l correspond to a negative sign and hence $2k - l$ to a positive sign. The sum that appears in the last term is equal to $2k - 2l$, hence even. Hence $\mathcal{B}_\sigma$ must possess an odd number of points.

5. The proof uses the Leray-Schauder theorem, see appendix A.3. We apply the theorem to the function $F : \mathcal{F} \times J \to \mathcal{F}$ which is of the form $\mathrm{Id} + m$, with $m(\cdot) = -\mathbf{R}$. Because m is compact on $\mathcal{F} \times J$ (see proof in [Faugeras 2008]), $\mathcal{B}_a \times \{a\}$ bounded, and there exists an open bounded neighbourhood $\mathcal{U}_a$ of $\mathcal{B}_a$ such that $\deg_{\mathrm{LS}}(F(\cdot, a), \mathcal{U}_a, 0) \neq 0$ (corollary A.3.2 in appendix A.3), the conclusion follows since the connected component cannot be unbounded, $\mathcal{B}$ being bounded.

6. Let us write $\mathbf{V}_\sigma^f = \varepsilon\mathbf{I}_{ext}^{(0)} + \tilde{\mathbf{V}}_\sigma^f$, then $\tilde{\mathbf{V}}_\sigma^f = \mathbf{J}\cdot\mathbf{S}(\sigma\tilde{\mathbf{V}}_\sigma^f + \varepsilon\mathbf{I}_{ext}^{(0)})$. We know that this last equation has always a (bounded) solution. Hence, any solution $\mathbf{V}_\sigma^f$

satisfies $\mathbf{V}_\sigma^f \overset{\varepsilon\to\infty}{\sim} \mathbf{I}_{ext}$. As $\mathbf{I}_{ext}^{(0)} \neq 0$ *a.e.*, the operator $\mathbf{J}D\mathbf{S}(\sigma\tilde{\mathbf{V}}_\sigma^f + \varepsilon\mathbf{I}_{ext}^{(0)}) \overset{\varepsilon\to\infty}{\to} 0$ in $\mathcal{L}(\mathcal{F})$ and $\det_{\mathrm{F}}(\mathrm{Id} - \mathbf{J}D\mathbf{S}(\sigma\tilde{\mathbf{V}}_\sigma^f + \varepsilon\mathbf{I}_{ext}^{(0)})) = 1$ for ε large enough. By using (3.11) and $\deg_{\mathrm{F}}(F(\mathbf{V},\sigma), B_r, 0) = 1$, we conclude that there is a unique stationary state for the contrast large enough.

□

Point 4 is not true at bifurcation points where the jacobian is singular.

Point 6 in the proposition shows that, if the external input $\mathbf{I}_{ext}$ is strong, the network "follows" it.

This proposition answers some of the previous questions at the beginning of the section. For any positive value of σ, there is always at least one persistent state and we can find a way to connect the trivial solution $\mathbf{V}_0^f$ to a persistent state corresponding to an arbitrary value of the parameter σ. We return to this connection later and also see that not all the solutions in $\mathcal{B}_\sigma$ are in the connected component of $(\mathbf{V}_0^f, 0)$ in $\mathcal{F}\times\mathbb{R}_+$.

Regarding the connection $\mathcal{C}$ between $\mathbf{V}_0^f$ and $\mathbf{V}$, proposition 3.2.7 does not give us any indication on its regularity but we have the following corollary.

Corollary 3.2.8. *Let a and b be as in proposition 3.2.7. For all $\varepsilon > 0$ there exists a finite sequence $(\mathbf{V}_1,\sigma_1)$, …, $(\mathbf{V}_n,\sigma_n)$ of points of $\mathcal{C}$ such that $\|\mathbf{V}_i - \mathbf{V}_{i+1}\|_{\mathcal{F}} \leq \varepsilon$ for $i = 1,\cdots,n-1$ and $\sigma_1 = a$, $\sigma_n = b$.*

Proof. $\mathcal{C}$ is connected for any topology equivalent to the product topology of $\mathcal{F}\times[a,\,b]$, e.g. for the metric defined by $d((\mathbf{V}_1,\sigma_1),(\mathbf{V}_2,\sigma_2)) = \|\mathbf{V}_1 - \mathbf{V}_2\|_{\mathcal{F}} + |\sigma_1 - \sigma_2|$. Since it is connected for this metric, it is also well-chained [Choquet 1969], and the conclusion follows. □

In fact, except at points where the Jacobian of F is non-invertible (such points like B in figure 3.1 are potential bifurcation points, see definition A.0.1), the implicit functions theorem tells that $\sigma \to (\mathbf{V}_\sigma^f, \sigma)$ is differentiable. Hence in effect proposition 3.2.7.5 imposes strong constraints on the set $\mathcal{B}_\sigma$ as shown in figure 3.1. The horizontal axis represents the parameter σ, the vertical axis the space $\mathcal{F}$ where the solutions of (3.9) live. The curves represent possible solutions as functions of σ. The configurations in the lefthand part of the figure are forbidden by proposition 3.2.7 5 while those on the righthand side are allowed, the green curve being an example of a continuous curve $s \to (\mathbf{V}_{\sigma(s)}^f, \sigma(s))$ from $[0,1]$ to $\mathcal{F}\times[a,b]$.

Proposition 3.2.7 5 gives a very interesting general (non-local) property of the set of solutions. But it is non-constructive, for example it does not tell us which branch to chose at point B in figure 3.1 and we need to compute all the branches to know the path to $\sigma = b$. Hopefully such branching points as B are very rare and one only sees turning points rather than branching points (such as the one at σ_1 in figure 3.2, left): (almost) any perturbation will indeed destroy such branching points (see figure 3.2 right). Hence, if one continues the trivial solution (obtained

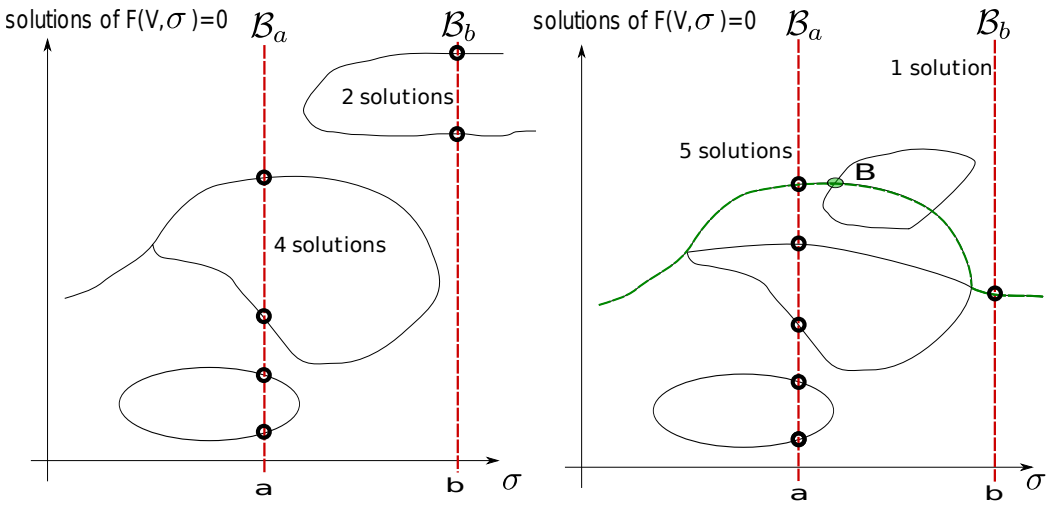

Figure 3.1: In the lefthand part of the figure, there is no connected curve of solutions in $[a, b]$: this is forbidden by proposition 3.2.7.5 which states that we must be in the situation shown in the righthand part of the figure, where the green curve connects $\mathcal{B}_a \times \{a\}$ and $\mathcal{B}_b \times \{b\}$, see text.

for $\sigma = 0$), one will typically find a curve like the green one in figure 3.2 Right. This may lead to the wrong conclusion that for σ big enough there is only one stationary solution instead of three. The problem is to find a way to compute, if it exists, the second, red, curve which is not connected to the green curve, hence not attainable by σ-continuation.

An idea, directly suggested by the above picture is to restore the branching points by perturbation. Among all possible perturbations, we choose one of the simplest, *i.e.* we vary the amplitude of the external input $\mathbf{I}_{\text{ext}}$. Hence, similar to proposition 3.2.7 6, we define the external current $\mathbf{I}_{\text{ext}}$ to be $\varepsilon\mathbf{I}_{\text{ext}}$ where the contrast ε satisfies $0 \leq \varepsilon \leq 1$. This is suggested by the work of experimentalists who usually provide neural responses as functions of the contrast. Note that some non-generic external input may not break the branching points (see section 3.3.2).

The conclusion is that if we only want one solution for $\sigma \neq 0$, we can use a σ-continuation of the trivial solution, but if we want more than one (or the maximum number of) solutions for $\sigma \neq 0$, then we have to perform at least a (σ, ε)-continuation of the trivial solution.

Remark 5. An interesting question is to predict how close to σ_L the smallest value of σ where a "turning point" occurs can be.

However, performing this (σ, ε)-continuation of the trivial solution is bound to generate a large amount of data. In order to help us to make sense of it, it is useful to have a priori information about the structure of the set $(\mathbf{V}^f_{\sigma,\varepsilon}, \sigma, \varepsilon)$. The idea is, again, to think of this set as a deformation of an easier to compute set of stationary solutions. This is done in the next section.

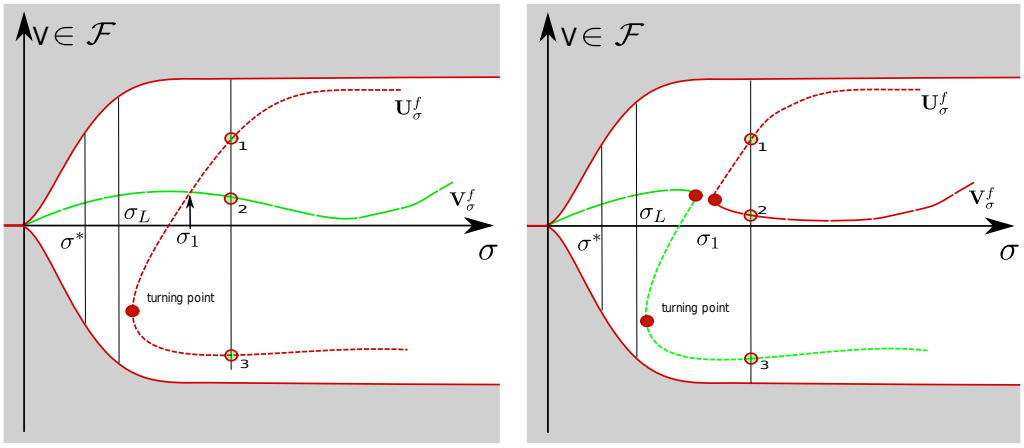

Figure 3.2: The white zone is the domain of existence of $\mathbf{V}^f$. The grey zone is excluded thanks to proposition 3.2.7.1. Left: non generic situation, a transcritical bifurcation occurs at σ_1. Right: same as left with a small perturbation (for example a small change of the external input $\mathbf{I}_{\text{ext}}$), the transcritical bifurcation has opened up. σ_L is defined in proposition 3.2.5 and σ^* in proposition 3.2.7.

Remark 6.It is highly possible that this (σ, ε)-continuation scheme still misses some solutions. One possibility is to introduce a third parameter, but the continuation may become quickly numerically untractable.

3.3 Exploring the set of persistent states

We exploit the fact that in the neural field equation (3.9) the ratio between the external current $\mathbf{I}_{ext}$ and $\mathbf{J}$ is not fixed a priori. Hence when studying the NFE, one would rather look at

$$-\mathbf{V} + \mathbf{J} \cdot \mathbf{S}(\sigma\mathbf{V}) + \varepsilon\mathbf{I}_{\text{ext}} = 0 \tag{3.12}$$

where $\varepsilon \geq 0$ allows to vary the respective weights of $\mathbf{I}_{ext}$ and $\mathbf{J}$. The persistent states now depend upon the pair (σ, ε) *i.e.* $\mathbf{V}^f_{\sigma,\varepsilon}$. The idea is to infer the persistent states of (3.12) from those, $\mathbf{V}^f_{\sigma,0}$ of

$$-\mathbf{V} + \mathbf{J} \cdot \mathbf{S}(\sigma\mathbf{V}) = 0 \tag{3.13}$$

We further simplify the problem by considering

$$-\mathbf{V} + \mathbf{J} \cdot \mathbf{S}_0(\sigma\mathbf{V}) + \mu\mathbf{J} \cdot \mathbf{S}(0) = 0, \tag{3.14}$$

where $\mathbf{S}_0$ is defined in proposition 3.2.7. We recover equation (3.13) when $\mu = 1$. The advantage is that when $\mu = 0$, we can say a great deal about the persistent states.

3.3.1 A simpler case

This simpler case reduces to the study of the previous equation when $\mu = 0$:

$$-\mathbf{V} + \mathbf{J} \cdot \mathbf{S}_0(\sigma\mathbf{V}) = 0 \tag{3.15}$$

In other words, we infer the persistent states of (3.12) from those, $\mathbf{V}_{\sigma,\varepsilon=0,\mu=0}$ of equation (3.15). This case has been studied a lot by several authors [Ermentrout 1998, Coombes 2005b, Bressloff 2005a] when a constant current $\mathbf{I}_{ext}$ is applied, which amounts to changing the threshold $\boldsymbol{\theta}$ in $\mathbf{S}$. $\mathbf{V} = 0$ is a trivial persistent state for (3.15). Recall that a necessary condition for the equation $F(\mathbf{V}, \sigma) = 0$ to bifurcate at the solution $(\mathbf{V}^f_\sigma, \sigma)$ is that $D_V F(\mathbf{V}^f_\sigma, \sigma)$ is non-invertible. This jacobian at $\mathbf{V}^f_\sigma = 0$ is given by:

$$\mathbf{L}_\sigma = -\mathrm{Id} + \sigma\mathbf{J}D\mathbf{S}_0(0) = -\mathrm{Id} + \frac{\sigma}{4}\mathbf{J} \tag{3.16}$$

The operator $\mathbf{L}_\sigma$ satisfies the following properties.

Proposition 3.3.1.

1. *$\mathbf{L}_\sigma$ is a continuous operator which belongs $\mathcal{L}(\mathcal{G}, \mathcal{F})$*
2. *The spectrum of $\mathbf{L}_\sigma$ is discrete and the eigenvalues have finite algebraic multiplicity.*
3. *If $\mathbf{J} \in \mathrm{L}^\infty(\Omega^2, \mathbb{R}^{\mathrm{p}\times\mathrm{p}})$ then $\left\|(i\omega\mathrm{Id} - \mathbf{L}_\sigma)^{-1}\right\|_{\mathcal{L}(\mathcal{F})} \leq \frac{2}{|\omega|}$ and $\left\|(i\omega I - \mathbf{L}_\sigma)^{-1}\right\|_{\mathcal{L}(\mathcal{G})} \leq \frac{2}{|\omega|}$ for ω large enough.*

Proof.

1. The first property is proved in proposition A.2.1.
2. Because $\mathbf{J}$ is a compact operator (see lemma 3.2.1), the kernel of $-\mathrm{Id} + \frac{\sigma}{4}\mathbf{J}$ is of finite dimension. Also the generalized eigenspace is finite-dimensional (see [Brezis 1983]), this gives the second property.
3. We now prove the last property. $|||i\omega I - \mathbf{L}_\sigma|||_{\mathcal{F}} \geq |\omega| - |||\mathbf{L}_\sigma|||_{\mathcal{F}} \geq \frac{|\omega|}{2}$ for ω large enough. Then $\left\|(i\omega\mathrm{Id} - \mathbf{L}_\sigma)^{-1}\right\|_{\mathcal{L}(\mathcal{F})} \leq \frac{2}{|\omega|}$ for ω large enough. From $\mathbf{J} \in \mathrm{L}^\infty(\Omega^2, \mathbb{R}^{\mathrm{p}})$, it follows that $R(\mathbf{J}) \subset \mathcal{G}$ and $\mathbf{L}_\sigma : \mathcal{G} \to \mathcal{G}$. It is straightforward to see that $\mathbf{L}_\sigma$ is continuous on $\mathcal{G}$. Hence, we can apply the same kind argument as above to obtain $\left\|(i\omega\mathrm{Id} - \mathbf{L}_\sigma)^{-1}\right\|_{\mathcal{L}(\mathcal{G})} \leq \frac{2}{|\omega|}$ for ω large enough.

□

Remark 7. In the next chapter, we will prove and apply the center manifold theorem in the case where space-dependent delays are taken into account. In this chapter, we don't need such a powerful result to compute the stationary solutions, the Lyapunov-Schmidt method is sufficient. Nevertheless, we wish to show how to

apply the center manifold theorem[6] *of [Haragus 2010] to the non-delayed neural field equations. We first rewrite* $\dot{\mathbf{V}} = -\mathbf{V} + \mathbf{J}\cdot\mathbf{S}_0(\sigma\mathbf{V})$ *as* $\dot{\mathbf{V}} = \mathbf{L}_{\sigma_n} + \mathbf{R}(\mathbf{V},\sigma)$ *with* $\mathbf{R}(\mathbf{V},\sigma) = (\mathbf{L}_\sigma - \mathbf{L}_{\sigma_n})\mathbf{V} + \mathbf{G}(\mathbf{V},\sigma)$ *and* $\mathbf{G}(\mathbf{V},\sigma)$ *is the second order Taylor integral remainder term in* $\mathbf{V}$*. We choose a semilinear formulation with* $\mathcal{X} = \mathcal{F}$, $\mathcal{Y} = \mathcal{Z} = \mathcal{G}$*. Then* $\mathbf{L}_{\sigma_n} \in \mathcal{L}(\mathcal{Z},\mathcal{X})$ *(see proposition 3.3.1) and* $\forall q \geq 0$, $\mathbf{R} \in C^q(\mathcal{Z}\times\mathbb{R},\mathcal{Y})$ *(see lemma 3.2.1). The other properties necessary to the use of the center manifold theorem (see therorem A.1.1) have been demonstrated in proposition 3.3.1.*

We can therefore state that the values of the parameter σ that determine the *possible* bifurcation points are:

$$\sigma_n = \frac{4}{\Re\lambda_n},\ n = 1,\ 2, \cdots \tag{3.17}$$

where λ_n is an eigenvalue of the compact operator $\mathbf{J}$. We assume in the sequel that $\sigma_1 \leq \sigma_2 \leq \cdots$. We will assume that the first $k \geq 1$ (k is arbitrary) eigenvalues are simple because this class of operators is dense in the set of compact operators set (see appendix A.4). We denote by e_n (respectively by e_n^*) the eigenvector of $\mathbf{J}$ (respectively of the ajoint operator $\mathbf{J}^*$) for the eigenvalue λ_n which satisfies:

$$\langle e_n^*, e_n\rangle_{\mathcal{F}} = 1.$$

Let us define $\chi_q^{(n)} \equiv \langle e_n^*, G_q(e_n,\sigma_n)\rangle_{\mathcal{F}}$, $G_q(e_n,\sigma_n) = \frac{1}{q!}D^q\mathbf{R}(\mathbf{0},\sigma_n)[e_n\cdots e_n] = \frac{\sigma_n^q}{q!}s_q\mathbf{J}\cdot(e_n\cdots e_n)$ and $S_0^{(q)}(0) \stackrel{\text{def}}{=} s_q$.

Lemma 3.3.2. *If* $\lambda_n \in \mathbb{R}$ *is a simple eigenvalue of* $\mathbf{J} \in \mathrm{L}^\infty(\Omega^2,\mathbb{R}^{\mathrm{p}\times\mathrm{p}})$ *and* $\chi_3^{(n)} \neq 0$*, then in a neighbourhood of* $(\mathbf{V}_\sigma^f = 0, \sigma_n)$*, all the non trivial stationary solutions of (3.15) are given by* $\mathbf{V}_\sigma^f = x(\sigma)e_n + o(x)$ *where* $x(\sigma) \in \mathbb{R}$ *solves*

$$\begin{array}{rcl} 0 & = & (-1+\sigma\lambda_n/4)x + \chi_3^{(n)}x^3 + O(x^5) \\ & = & \frac{\sigma-\sigma_n}{\sigma_n}x + \chi_3^{(n)}x^3 + O(x^5) \end{array} \tag{3.18}$$

Proof. We wish to apply the Lyapunov-Schmidt method (see [Golubitsky 1984, Golubitsky 1988, Kielhöfer 2003]). As $\mathbf{J} \in \mathrm{L}^\infty(\Omega^2,\mathbb{R}^{\mathrm{p}\times\mathrm{p}})$, it follows that the stationary solutions $\mathbf{V}_\sigma^f$ belongs to $\mathrm{L}^\infty(\Omega,\mathbb{R}^{\mathrm{p}})$. We write $\mathbf{V} = xe_n + \mathbf{W}$ with $\langle e_n^*, \mathbf{W}\rangle_{\mathcal{F}} = 0$ for $\mathbf{V} \in \mathcal{F}$. We can define the projection P on $\mathcal{F}$ as $P\mathbf{V} = \mathbf{W}$. $\mathbf{V} \to \mathbf{J}\mathbf{S}_0(\sigma\mathbf{V})$ is smooth on $\mathrm{L}^\infty(\Omega,\mathbb{R}^{\mathrm{p}})$ so we can compute its Taylor expansion. By using the projector P, we decompose the equation $\mathbf{V} = \mathbf{J}\mathbf{S}_0(\sigma\mathbf{V})$:

$$\begin{array}{rcl} 0 & = & \left(1 - \frac{\sigma\lambda_n}{4}\right)x + \frac{\sigma}{48}\langle e_n^*, \mathbf{J}(xe_n+\mathbf{W})^3\rangle_{\mathcal{F}} + h.o.t. \\ 0 & = & \left(\mathrm{Id} - \frac{\sigma\lambda_n}{4}\mathbf{J}\right)\mathbf{W} + \frac{\sigma}{48}P\mathbf{J}(xe_n+\mathbf{W})^3 + h.o.t. \end{array} \tag{3.19}$$

We solve the second equation with the implicit functions theorem by noting that $\mathrm{Id} - \frac{\sigma\lambda_n}{4}\mathbf{J}$ is invertible on $\{e_n^*\}^\perp$. We find:

$$\mathbf{W} = -\frac{\sigma}{48}\left(\mathrm{Id} - \frac{\sigma\lambda_n}{4}\mathbf{J}\right)^{-1} P\mathbf{J}(x^3e_n^3) + O(x^5)$$

[6] recalled in appendix A.1.1

which is replaced in the first equation to give:

$$0 = (-1 + \sigma\lambda_n/4)x + \chi_3^{(n)} x^3 + O(x^5).$$

□

We solve (3.18) for σ close to σ_n to find the structure of the bifurcated branches, *i.e.* the nontrivial solutions. By parity, $S_0^{(q)}(0) \overset{\text{def}}{=} s_q \neq 0$ if and only if q is odd. Hence, the parity of q tells that we have a Pitchfork bifurcation at σ_n. In particular, the bifurcated branch is given by

$$\mathbf{V}_\sigma^f = x(\sigma)e_n + o(x),$$

with $x(\sigma)$ solution of (3.18). Thus the bifurcation portrait is a set of branches $\mathcal{C}_n$ emanating at points (at least for $n \leq k$) $(0, \sigma_n)$ for $\sigma_n \in \mathbb{R}$. Depending on the sign of $\chi_q^{(n)}$ in (3.18), the Pitchfork branch is oriented toward $\sigma < \sigma_n$ (resp. $\sigma > \sigma_n$) if $\chi_q^{(n)} > 0$ (resp. $\chi_q^{(n)} < 0$). Let us note e_n^q the vector $\underbrace{e_n \cdots e_n}_{q \text{ times}}$. We have

$$\chi_q^{(n)} = \frac{\sigma_n^q s_q}{q!} \langle \mathbf{J} \cdot e_n^q, e_n^* \rangle_{\mathcal{F}} = \frac{\sigma_n^q s_q}{q!} \langle e_n^q, \mathbf{J}^* \cdot e_n^* \rangle_{\mathcal{F}} = \frac{\sigma_n^{q-1} s_q}{q! s_1} \langle e_n^q, e_n^* \rangle_{\mathcal{F}}$$

Thus, we have found local branches of stationary solutions and continue them globally in order to obtain the global branches named $\mathcal{C}_n$. An interesting question, yet unsolved, is to know whether the branches $\mathcal{C}_n$ are connected. Some results exist in this direction in the line of those of Rabinowitz (see [Rabinowitz 1971, Kielhöfer 2003]) but do not provide much insight in the general case ($d > 1, p > 1$...). However, they can be used to derive some properties of the first branch $\mathcal{C}_1$.

Proposition 3.3.3 (Turning point property). *If $\sigma_1 \in \mathbb{R}$ and $\chi_q^{(1)} > 0$, then $\exists \sigma_T < \sigma_1$ such that $\forall \sigma \in (\sigma_T, \sigma_1)$, (3.15) has at least 3 solutions and $\sigma_T = \min\{\sigma | (\mathbf{V}^f, \sigma) \in \mathcal{C}_1\}$.*

Proof. Let $\mathcal{C}_1$ be the connected component in $\bar{B}$ where $B = \{(\mathbf{V}, \sigma) | \mathbf{V} \neq \mathbf{0}$, $(\mathbf{V}, \sigma)$ satisfies (3.15)$\}$ to which $(\mathbf{0}, \sigma_1)$ belongs. Then (see [Ma 2005]) $\mathcal{C}_1$ is unbounded in $\mathcal{F} \times \mathbb{R}_+$ or contains a point $(\mathbf{0}, \sigma_n)$, $n > 1$. In either case, $\mathcal{C}_1$ exists until $\sigma = \sigma_2$. (If σ_2 does not exist, the same result shows that $\mathcal{C}_1$ is unbounded). We assume that σ_2 exists, it does not alter the results.The proof when σ_2 does not exist requires minor changes.

$\tilde{\mathcal{C}} = \bar{\mathcal{C}_1} \cap (\mathcal{F} \times [\sigma^*, \ \sigma_2])$ is closed and bounded (because every solution $\mathbf{V}_\sigma^f$ is bounded in $\mathcal{F}$). Let us show that $\tilde{\mathcal{C}}$ is compact in $\mathcal{F} \times [0, \ \sigma_2]$. Consider a sequence $(\mathbf{V}_n, s_n)$ in $\tilde{\mathcal{C}}$. As s_n is bounded, we can assume it is convergent. We also have $\mathbf{V}_n = \mathbf{J} \cdot \mathbf{S}_0(s_n \mathbf{V}_n)$. As $(\mathbf{V}, \sigma) \to \mathbf{J} \cdot \mathbf{S}_0(\sigma \mathbf{V})$ is a compact operator, there exists a subsequence $(\mathbf{V}_{\phi(n)}, s_{\phi(n)})$ such that $\mathbf{J} \cdot \mathbf{S}_0(s_{\phi(n)} \mathbf{V}_{\phi(n)})$ is convergent, hence $\mathbf{V}_{\phi(n)}$ is converging. We have proved that $\tilde{\mathcal{C}}$ is compact. Hence $\Pi_{\mathbb{R}^+}(\tilde{\mathcal{C}})$ is a compact subset of $\mathbb{R}^+$. Then $\inf \Pi_{\mathbb{R}^+}(\tilde{\mathcal{C}})$ is a *min* written $\sigma_T \in \Pi_{\mathbb{R}^+}(\tilde{\mathcal{C}})$. As it is an inf, there exists a sequence s_n associated to a $\mathbf{V}_n \in \Pi_{\mathbb{R}^+}^{-1}(s_n)$ in $\tilde{\mathcal{C}}$ such that $s_n \to \sigma_T$. But as $\tilde{\mathcal{C}}$ is

compact, we can assume that $\mathbf{V}_n \to \mathbf{V}_T$. Then $(\mathbf{V}_T, \sigma_T) \in \mathcal{C}$ is called a *turning point*[7].

So we have proved that $\sigma_T \leq \sigma_1$. But in the case q odd with $\chi_q^{(n)} > 0$, $\mathcal{C}_1$ exists for $\sigma < \sigma_1$ and $\sigma_T < \sigma_1$.

Now, $\forall \sigma \in (\sigma_T, \sigma_1)$, $\exists (\mathbf{V}_\sigma^f, \sigma) \in \mathcal{C}_1 \setminus \{(\mathbf{0}, \sigma)\}$ because $\mathcal{C}_1$ intersects $\{\mathbf{0}\} \times \mathbb{R}_+$ only at bifurcation points $(\mathbf{0}, \sigma_n)$ located 'after' σ_1. Then because of proposition 3.2.7 part 4, there are at least three solutions. □

Remark 8.If the sigmoidal function had satisfied $S^{(2)}(0) \neq 0$, we would have seen transcritical bifurcations and the previous proposition still holds in this case.

Remark 9.If we were able to prove that the branches do not intersect, the previous proposition would apply to all branches $\mathcal{C}_n$ satisfying the required conditions but see section 3.6.

Even if we do not deal with the dynamics, we can say a little using [Haragus 2010, Kuznetsov 1998]. At every bifurcation point, the center manifold at $\mathbf{V} = 0$ (see theorem A.1.1) is one-dimensional while the dimension of the unstable manifold increases as σ crosses values corresponding to transcritical points. Hence for large σs, we can have a large unstable manifold. Note that every value of σ is biologically plausible because the locally (around $\mathbf{V} = 0$) exponentially divergent dynamic is bounded (see proposition 3.2.3), which can make the "global" dynamics very intricate. In effect, when σ grows to infinity, the sigmoid tends to a Heaviside function which acts as a threshold.

We now study a particular case where the structure of the nontrivial solutions is almost entirely understood.

3.3.1.1 The case $d = 1, p = 1$

We suppose *here* that $d = p = 1$ and the connectivity operator $\mathbf{J}$ is symmetric with simple eigenvalues σ_n and corresponding eigenfunctions e_n. In this case, we can use the results of Rabinowitz (see [Rabinowitz 1971]). The Taylor formula allows to write $\mathbf{S}_0(x) = xh(x)$ with $h > 0$, this is required in order to apply [Rabinowitz 1971]. Then from [Rabinowitz 1971], it follows that the bifurcated branches (Pitchforks or transcritical)[8] $\mathcal{C}_n$ are unbounded and are characterized by the number of simple zeros in $\mathring{\Omega}$ of their elements ; namely $\forall\ (\mathbf{V}^f, \sigma) \in \mathcal{C}_n$, $\mathbf{V}^f$ has exactly $n-1$ simple zeros in $\mathring{\Omega}$. As a consequence, the branches $\mathcal{C}_n$ do not intersect.

If we were able to prove that all the stationary solutions are connected to the zero solution, we would have completely characterized $\mathcal{B}$. Nevertheless, we still have collected a lot of information.

Remark 10.The study of the simpler case is very important for the numerics. Indeed, it allows analytical predictions. When one performs the $(\sigma, \mu, \varepsilon)$-continuation, one should look at the section of solutions $(\sigma, \mu = 0, \varepsilon = 0)$ and compare to the

[7]Not in the sense of [Kuznetsov 1998], here it denotes a local extremum in the parameter along the curve of solutions.

[8]In this case, they are connected components in $C^1(\Omega, \mathbb{R}) \times \mathbb{R}_+$ rather than in $\mathcal{F} \times \mathbb{R}_+$.

predictions of the simpler case to see if we did not miss any solution (that may happen when the system has some symmetries).

3.3.2 Returning to the original equation

The overall picture that emerges from the previous section is interesting despite the fact that some of its features are hard to justify from the biological viewpoint: no external input, rate function $\mathbf{S}_0$ possibly negative. The reason is that it gives clues about the set of persistent states when $\varepsilon \neq 0$ and provides a way to compute them numerically. Starting with the trivial solution $\mathbf{V}_0^f$ of (3.13) when the slope parameter σ is null, we can perform a numerical continuation (see [Kuznetsov 1998, Guckenheimer 1983, Allgower 2003]) with respect to the two parameters σ, ε.

When $\varepsilon \neq 0$, the only[9] bifurcations that are possibly unaltered are the turning points. The transcritical/Pitchfork bifurcations will be "opened" as described below. We are still able to predict the stability near the points $(\mathbf{0}, \sigma_n)$. Let us write $\bar{I} = \langle \mu \mathbf{J} \cdot \mathbf{S}(0) + \varepsilon \mathbf{I}_{ext}, e_n^* \rangle_{\mathcal{F}}$ and suppose that $\mathbf{I}_{ext} \in \mathrm{L}^\infty(\Omega^2, \mathbb{R}^p)$. By using the Lyapunov-Schmidt reduction (see [Golubitsky 1984, Golubitsky 1988, Kielhöfer 2003]) with external input, we find the following equation:

$$0 = (-1 + \frac{\sigma \lambda_n}{4})x + \chi_3^{(n)} x^3 + \bar{I} + O(x^3(\mu^2 + \varepsilon^2 + x^2)) \tag{3.20}$$

Solving the polynomial equation (3.20) allows us to describe different opening scenarios depending on the sign of $\bar{I}$. This is shown on figure 3.3. The case of σ_1 is a little bit special according to proposition 3.3.3 and is shown in the righthand part of figure 3.3. Note that if $\bar{I} = 0$, a non generic situation, the Pitchfork bifurcations are not opened by the addition of the external current.

Remark 11. When the first eigenvalue generates a subcritical Pitchfork branch, proposition 3.3.3 says that a turning point must occurs on this branch: there are in effect two turning points on this branch. Still we have a local description and it would be interesting to have more global results for example concerning the behavior of these turning points when (σ, ε) varies.

3.4 Reduction to a finite dimensional analysis

Neural field models are one of the possible generalizations of standard neural networks considered as discrete sets of connected neurons. They can be characterized by two limit processes. First, we let the total number of neurons grow to infinity so that each node of the network represents an ideally infinite number of neurons, in practice a large number of such neurons belonging to different populations, in effect a neural mass. Second, we assume that these neural masses form a continuous neural material and let the connectivity graph of the neural network become

[9] if the equations are G-equivariant for a symmetry group G, some Pitchfork bifurcation may also be unaltered (see definition A.0.2 and chapter 9).

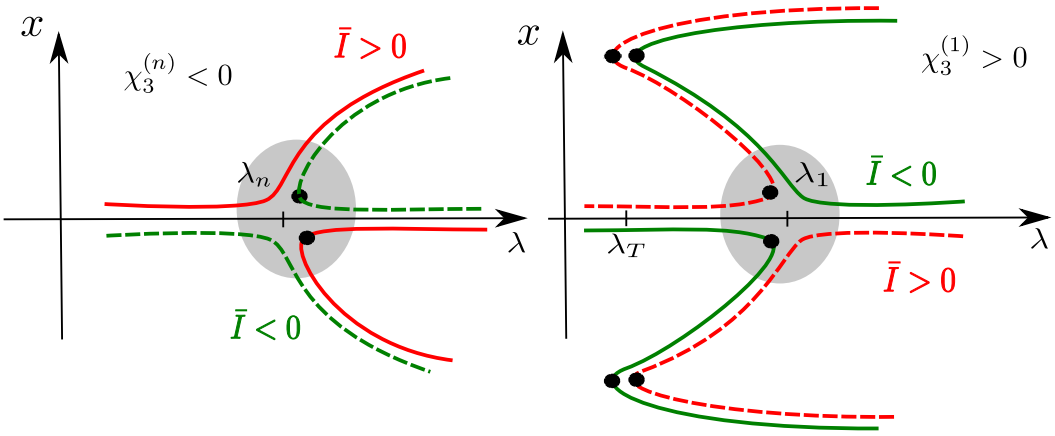

Figure 3.3: Opening of the Pitchfork bifurcation at the first (right) and nth ($n > 1$, left) eigenvalue. Black dots indicate saddle nodes. Note that there are three such points, see proposition 3.3.3, for the first eigenvalue. Note that the branch may have a more intricate shape than the one shown. The gray ellipses represent the part of the phase space which is explained by bifurcation theory.

continuous. The graph connectivity matrix then turns into a continuous function of the spatial coordinates. One would think that after passing twice to the limit the resulting system would be infinite-dimensional. However, the dimensionality of the neural field models depends essentially upon the linear operator $\mathbf{J}$ representing the connectivity function. If this linear operator has a finite-dimensional range, we show below that the corresponding neural field model is finite-dimensional and is equivalent to a finite set of ordinary differential equations. Moreover, even if this condition is not met, we also show that we can always approximate the operator as accurately as desired by a finite-dimensional range operator and reduce the neural field model to a finite set of ordinary differential equations.

3.4.1 The Pincherle-Goursat Kernels

In our numerical studies, we use connectivity functions that are such that the corresponding linear operators of $\mathcal{F}$ have finite rank, *i.e.* their range is a finite dimensional subspace of $\mathcal{F}$. This is without loss of generality because of the following theorem (see, e.g. [Brezis 1983]):

Theorem 3.4.1. *The subspace $\mathcal{R}_f(\mathcal{F})$ of finite-dimensional range linear operators of $\mathcal{F}$ is dense in $\mathcal{H}$, the set of linear compact operators of $\mathcal{F}$.*

In the area of integral equations, these operators are called Pincherle-Goursat kernels [Tricomi 1985], in short PG-kernels. They are defined as follows

Definition 3.4.2 (Pincherle-Goursat Kernels). *The connectivity kernel $\mathbf{J}(\mathbf{r}, \mathbf{r}')$ is a PG-kernel if*

$$\mathbf{J}(\mathbf{r}, \mathbf{r}') = \sum_{k=1}^{N} X_k(\mathbf{r}) \otimes Y_k(\mathbf{r}')$$

where X_k, Y_k, $k = 1 \cdots N$ *are two sets of* N *linearly independent elements of* $\mathcal{F}$, *and* $X_k(\mathbf{r}) \otimes Y_k(\mathbf{r}')$ *is the rank 1* $p \times p$ *matrix* $X_k(\mathbf{r}) Y_k^T(\mathbf{r}')$.
We have

$$\mathbf{J} \cdot \mathbf{U} = \sum_k X_k \langle Y_k, \mathbf{U} \rangle_{\mathcal{F}}.$$

Thus $\mathbf{J} \cdot \mathbf{U} \in \mathrm{Span}(X_1, \cdots, X_N)$ which we denote by $R(\mathbf{J})$.

3.4.2 Persistent state equation for PG-kernels

We now cast the problem of the computation of the solutions of equation (3.9) into the PG-kernel framework:

$$\mathbf{V} - \mathbf{I}_{\mathrm{ext}} = \mathbf{J} \cdot \mathbf{S}(\sigma \mathbf{V})$$

Since $\mathbf{V} - \mathbf{I}_{\mathrm{ext}} \in R(\mathbf{J})$, we can write $\mathbf{V} - \mathbf{I}_{\mathrm{ext}} = \sum_k v_k X_k$, and note $v = (v_k)_{k=1 \cdots N}$.
The persistent state equation reads:

$$v_k = \left\langle Y_k, \mathbf{S}\left(\sigma\left(\sum_k v_k X_k + \mathbf{I}_{\mathrm{ext}}\right)\right)\right\rangle_{\mathcal{F}} \quad k = 1, \cdots, N \tag{3.21}$$

This is a set of N nonlinear equations in the N unknowns $v_1, \cdots, v_N$ which can be solved numerically using classical methods.

3.4.3 Reduction to a finite number of ordinary differential equations

In this section, we reduce equation (3.1) (when $\mathbf{J}$ is independent of t) to a system of ODEs. We write $\mathbf{I}$ instead of $\mathbf{I}_{\mathrm{ext}}$ for simplicity.

We note $R(\mathbf{J})^\perp$ the orthogonal complement of $R(\mathbf{J})$ in $\mathcal{F}$ with respect to the inner-product $\langle , \rangle_{\mathcal{F}}$:

$$\mathcal{F} = R(\mathbf{J}) \oplus R(\mathbf{J})^\perp.$$

We write

$$\mathbf{V} = \mathbf{V}^{\parallel} + \mathbf{V}^{\perp},$$

where $\mathbf{V}^{\parallel}$ (resp. $\mathbf{V}^{\perp}$) is the orthogonal projection of $\mathbf{V}$ on $R(\mathbf{J})$ (resp. $R(\mathbf{J})^\perp$). We have a similar decomposition for the external current $\mathbf{I}$

$$\mathbf{I} = \mathbf{I}^{\parallel} + \mathbf{I}^{\perp}$$

We now decompose $R(\mathbf{J})$ as a Cartesian product of p finite dimensional subspaces of $\mathrm{L}^2(\Omega, \mathbb{R})$. Because

$$\mathbf{J}_{ij}(\mathbf{r}, \mathbf{r}') = \sum_{k=1}^{N} X_k^i(\mathbf{r}) Y_k^j(\mathbf{r}') \quad i, j = 1, \cdots, p,$$

the membrane potentials V_i for each of the p populations, $i = 1, \cdots, p$ of $\mathbf{V}$ satisfy

$$\dot{V}_i + \frac{1}{\tau_i} V_i = \sum_{k=1}^{N} \langle Y_k, \mathbf{S}(\sigma \mathbf{V}) \rangle_{\mathcal{F}} X_k^i + I_i \quad i = 1, \cdots, p$$

Let us consider the p finite dimensional subspaces E_i, $i = 1, \cdots, p$ of $\mathrm{L}^2(\Omega, \mathbb{R})$, where each E_i is generated by the N elements X_k^i, $k = 1, \cdots, N$. We note $E_i^\perp$ the orthogonal complement of E_i in $\mathrm{L}^2(\Omega, \mathbb{R})$. This induces a decomposition of $\mathcal{F}$ as the direct sum of the cartesian product $\prod_{i=1}^p E_i = R(\mathbf{J})$ and its orthogonal complement $\prod_{i=1}^p E_i^\perp = R(\mathbf{J})^\perp$. We write $V_i = V_i^{\|} + V_i^\perp$ as well as $I_i = I_i^{\|} + I_i^\perp$. We then have

$$\begin{cases} \dot{V}_i^{\|} + \frac{1}{\tau_i} V_i^{\|} = \sum_{k=1}^N \langle Y_k, \mathbf{S}(\sigma \mathbf{V}) \rangle_{\mathcal{F}} X_k^i + I_i^{\|} \\ \dot{V}_i^\perp + \frac{1}{\tau_i} V_i^\perp = I_i^\perp \end{cases} \quad i = 1, \cdots, p \tag{3.22}$$

Considering the canonical basis e_i, $i = 1, \cdots, p$, of $\mathbb{R}^p$, we define

$$\mathbf{V}^{\|} = \sum_{i=1}^p V_i^{\|} e_i \quad \mathbf{I}^{\|} = \sum_{i=1}^p I_i^{\|} e_i$$
$$\mathbf{V}^\perp = \sum_{i=1}^p V_i^\perp e_i \quad \mathbf{I}^\perp = \sum_{i=1}^p I_i^\perp e_i$$

We obtain the pN-dimensional non-autonomous system of ODEs:

$$\begin{cases} \dot{\mathbf{V}}^{\|} + \mathbf{L} \cdot \mathbf{V}^{\|} = \mathbf{J} \cdot \mathbf{S}(\sigma \mathbf{V}) + \mathbf{I}^{\|} \\ \dot{\mathbf{V}}^\perp + \mathbf{L} \cdot \mathbf{V}^\perp = \mathbf{I}^\perp \end{cases} \tag{3.23}$$

Remark 12. *If $\mathbf{I}^\perp$ is stationary then $\mathbf{V}^\perp$ converges to $\mathbf{L}^{-1}\mathbf{I}^\perp$.*

3.5 One population of orientation tuned neurons: the Ring Model

As an application of the previous results, we study the Ring Model of orientation tuning introduced by Hansel and Sompolinski (see [Hansel 1997, Shriki 2003, Ermentrout 1998, Dayan 2001a, Bressloff 2000, Bressloff 2001b]), after the work of Ben-Yishai (see [Ben-Yishai 1995]). It is a model of a hypercolumn in primary visual cortex. It can be written as:

$$\tau \dot{A}(x,t) = -A(x,t) + S\left(\sigma\left(\int_{-\pi/2}^{\pi/2} J(x-y)A(y,t)dy/\pi + \varepsilon I(x) - \theta\right)\right)$$

Some authors, [Bressloff 2000, Bressloff 2001b], chose J to be a difference of Gaussians. On the other hand, Ben-Yishai, in [Ben-Yishai 1995], started with a network of excitatory/inhibitory spiking neurons and derived a meanfield approximation of this network yielding the activity response described by the following equations:

$$\begin{cases} J(x) = J_0 + J_1 \cos(\alpha(y - x)) \\ I(x) = 1 - \beta + \beta \cos(\alpha(x - x_0)) \end{cases} \tag{3.24}$$

$\alpha = 2$, $0 \leq \beta \leq 1$ and the threshold $\theta = 1$ in the above cited papers. We can, up to a rescaling of the previous equation, make the assumption

$$J_0 = \varepsilon_0 \in \{-1, 1\}$$

Being an activity model and not a voltage model in the terminology of [Ermentrout 1998, Faugeras 2008] it is not directly amenable to our analysis. We can either extend this analysis to activity models as shown in appendix A.5 or do the following. We rewrite the previous equation as

$$\tau \dot{A} = -A + S(\sigma(J \cdot A + \varepsilon I - \theta)),$$

and perform the change of variable $V = J \cdot A + \varepsilon I - \theta$. This leads to the following equations

$$\begin{cases} \tau \dot{V}(x,t) = -V(x,t) + \int_{-\pi/2}^{\pi/2} [J_0 + J_1 \cos(\alpha(y-x))]\, S(\sigma V(y,t)) dy/\pi + \varepsilon I(x) - \theta \\ I(x) = 1 - \beta + \beta \cos(\alpha(x - x_0)) \end{cases} \tag{3.25}$$

We are now in the case of the model studied in this chapter with $p = 1$, $d = 1$ and $\Omega = (-\pi/2, \pi/2)$.

The nonlinearity is often chosen to be a Heaviside function, or, as in [Ben-Yishai 1995], a piecewise linear approximation of the sigmoid, or, as in [Ermentrout 1998, Dayan 2001a, Bressloff 2000], a true sigmoidal function. J_1 can take any sign and I is an external current coming from the LGN. J_0 is most of the time negative (see [Ben-Yishai 1995, Dayan 2001a, Bressloff 2000, Bressloff 2001b]) but can be positive as well (see [Bressloff 2001b]): the J_is can be thought of as the first Fourier coefficients of J, J_0, being its mean value.

For example, in [Dayan 2001a], we find $J_0 = -7.3$, $J_1 = 11$, $\beta = 0.1$, $\theta = 0$ which are taken from [Ben-Yishai 1995] except for $\theta = 1$. The nonlinear gain is assumed to be $\sigma = 1$. Using the previous rescaling, it becomes $J_0 = -1$, $J_1 = 1.5$, $\sigma = 7.3/s_1 = 29.2$ and $\theta \to \theta/7.3$ which gives $\theta \approx 0.1$ in the case of [Ben-Yishai 1995] and $\theta = 0$ in [Dayan 2001a].

The goal of this section is not to derive the whole bifurcation diagram of the Ring Model but rather to show how the stationary solutions are organized and to give clues about the dynamics in a given range of parameters. This study is helpful because some large scale models of V1 (see for example the work of Bressloff *et al.* [Bressloff 2001b]) use the Ring Model for the hypercolumns or can be mapped onto the Ring Model equations (see [Blumenfeld 2006, Carandini 1997] and Part IV). We will see that, depending on the nonlinear gain, there may exist many stationary solutions, which are all acceptable responses of the network for a given input of the LGN. Thus these local orientation detectors may behave less trivially than they were initially made for.

Moreover, the next section will show the importance of the symmetries in the model. Indeed, for $\alpha = 2$, the model is translation invariant if Ω has periodic boundary conditions. It implies that whenever there is a stationary solution, all its translated versions will also be stationary solutions. This is not very straightforward to handle numerically. Hence we chose to 'break' this symmetry by chosing $\alpha \neq 2$ and study the corresponding system. We will come back later in chapter 9 to the Ring Model in the case $\alpha = 2$ by using a change of variable to cope with the symmetries. Finally, the present study, will show how the stationary solutions evolve as functions of the nonlinear gain σ and the contrast ε.

3.5.1 Mapping the Ring Model to the PG-kernel formalism

Expanding the cosine in the previous equation, and denoting by $\cos_\alpha$ (respectively $\sin_\alpha$) the function $x \to \cos(\alpha x)$ (respectively $x \to \sin(\alpha x)$), we find that, depending on the sign of J_i, ($\varepsilon_i = sign(J_i), i = 0, 1$):

$$J = \varepsilon_0 1\otimes 1 + \varepsilon_1\sqrt{|J_1|}\cos_\alpha \otimes \sqrt{|J_1|}\cos_\alpha + \varepsilon_1\sqrt{|J_1|}\sin_\alpha \otimes \sqrt{|J_1|}\sin_\alpha \overset{\text{def}}{=} \sum_{i=0}^{2} \varepsilon_i X_i \otimes X_i,$$

This formulation has the advantage of preserving the symmetries of J. With the notations of the previous section, we have $I^\perp = 0$, and

$$\tau \dot{V}^\parallel = -V^\parallel + J \cdot S(\sigma(V^\parallel + V_0^\perp e^{-t/\tau})) + \varepsilon I^\parallel - \theta$$

where

$$V^\parallel(x,t) = v_1(t) + v_2(t)\sqrt{|J_1|}\cos_\alpha x + v_3(t)\sqrt{|J_1|}\sin_\alpha x, \tag{3.26}$$

i.e. the model is three-dimensional. Note that the previous equation is equivalent to (3.25). Similarly we have

$$I = I^\parallel = 1 - \beta + \frac{\beta \cos_\alpha x_0}{\sqrt{|J_1|}} \overbrace{\sqrt{|J_1|}\cos_\alpha x}^{X_1} + \frac{\beta \sin_\alpha x_0}{\sqrt{|J_1|}} \overbrace{\sqrt{|J_1|}\sin_\alpha x}^{X_2} \tag{3.27}$$

As $V^\perp(t) \to 0$, we restrict the study to the case $V^\perp = 0$ even if we lose some of the 'real' dynamics by doing so. This is motivated by the fact that the dynamics is made of heteroclinic orbits (as we will see in a moment) between persistent states belonging to the vector space $V^\perp = 0$. Hence, using this simplification, we are led to study the following 3D system:

$$\begin{cases} \tau \dot{v}_1 = -v_1 + \varepsilon_0 \langle S(\sigma V), 1\rangle + \varepsilon I_1^\parallel - \theta \\ \tau \dot{v}_2 = -v_2 + \varepsilon_1\sqrt{|J_1|}\langle S(\sigma V), \cos_\alpha\rangle + \varepsilon I_2^\parallel \\ \tau \dot{v}_3 = -v_3 + \varepsilon_1\sqrt{|J_1|}\langle S(\sigma V), \sin_\alpha\rangle + \varepsilon I_3^\parallel \end{cases} \tag{3.28}$$

where $\langle f, g\rangle = \int_{-\pi/2}^{\pi/2} f(x)g(x)\frac{dx}{\pi}$, V is given by equation (3.26) and $I_i^\parallel$, $i = 1, 2, 3$ is given by equation (3.27). Note that the basis (X_0, X_1, X_2) is not orthogonal for

this inner product. We note $\mathbf{v}$ the 3D vector:

$$\mathbf{v} = (v_1,\ v_2,\ v_3).$$

Remark 13.In the numerical applications, the integrals in (3.28) have to be computed with precision ortherwise some spurious solutions may appear (data not shown). In practice, we compute the 1D integrals with (ALGLIB), a simple to use C++ librairy.

The system enjoys the symmetries described by the following lemma.

Lemma 3.5.1. *When $I_3^{\|} = 0$, if $\mathbf{v} = (v_1\ v_2\ v_3)$ is a solution, then so is $(v_1\ v_2\ -v_3)$. The plane $v_3 = 0$ is invariant by the dynamics.*

Proof. This is a consequence of the fact that $\sin_\alpha$ is an odd function while $\cos_\alpha$ is an even function. □

It is easy to see that

$$E(\mathbf{v}) = -\frac{\langle \mathbf{v}, \mathbf{v}\rangle}{2} + \frac{1}{\sigma}\int_{-\pi/2}^{\pi/2} \bar{S}(\sigma v_1 \varepsilon_0 + \sigma v_2 \varepsilon_1 \sqrt{|J_1|}\cos_\alpha x + \sigma v_3 \varepsilon_1 \sqrt{|J_1|}\sin_\alpha x)\frac{dx}{\pi} + \left\langle \varepsilon I^{\|} - \vec{\theta}, \mathbf{v}\right\rangle,$$

where $\bar{S}$ is a primitive of S and $\vec{\theta} = (\theta, 0, 0)$, is an energy function for the dynamics,*i.e.* $\tau\dot{\mathbf{v}} = \nabla E(\mathbf{v})$. Consequently, even for I non spatially homogenous, there are no non-constant periodic trajectories nor homoclinic orbits[10]. Moreover, all bounded trajectories are stationary solutions or trajectories converging to stationary solutions. Having proven that all trajectories are bounded for the neural field equations in proposition 3.2.3, we have characterized the dynamics. It remains to compute the stationary solutions and their attraction basins.

Remark 14.We can generalize these facts to PG-kernels of the type $\mathbf{J} = \sum_{k=0}^{N} \varepsilon_k X_k \otimes X_k$ by choosing $E(\mathbf{v}) = -\frac{\langle \mathbf{v}, \mathbf{L}\mathbf{v}\rangle}{2} + \frac{1}{\sigma}\sum_{i=1}^{p}\int_\Omega \bar{S}(\sum_{k=0}^{N}\sigma\varepsilon_k v_k X_k^i(\mathbf{r}))\,d\mathbf{r} + \langle \mathbf{I}, \mathbf{v}\rangle$

3.5.2 Finding the persistent states

In order to characterize the set $\mathcal{B}$ of stationary solutions, we apply the scheme of section 3.3.1. Hence we study the following equation

$$V = J \cdot S_0(\sigma V) + \varepsilon I^{\|} + \mu(-\theta + J \cdot S(0))$$

with the nonlinearity being the *odd* function: $S_0(x) = \frac{1}{1+e^{-x}} - \frac{1}{2}$. Note that $J\cdot S(0) = \frac{1}{2}(\varepsilon_0 + J_1 \frac{2sin_\alpha(\pi/2)}{\alpha\pi} cos_\alpha) = \frac{1}{2}\varepsilon_0 + \varepsilon_1\sqrt{|J_1|}\frac{sin_\alpha(\pi/2)}{\alpha\pi}X_1$. This gives:

$$\begin{cases} v_1 = \varepsilon_0 \langle S_0(\sigma V), 1\rangle + \varepsilon I_1^{\|} + \mu(-\theta + \frac{\varepsilon_0}{2}) \\ v_2 = \varepsilon_1\sqrt{|J_1|}\langle S_0(\sigma V), \cos_\alpha\rangle + \varepsilon I_2^{\|} + \mu\varepsilon_1\sqrt{|J_1|}\frac{sin_\alpha(\pi/2)}{\alpha\pi} \\ v_3 = \varepsilon_1\sqrt{|J_1|}\langle S_0(\sigma V), \sin_\alpha\rangle + \varepsilon I_3^{\|} \end{cases} \tag{3.29}$$

[10] This follows from the time derivative of the energy E.

3.5.2.1 The simpler case $\mu = \varepsilon = 0$

This corresponds to finding the persistent states when $\mu = \varepsilon = 0$ ensuring that $\mathbf{v} = 0$ is a solution. For the sake of simplicity, we reduce the study to the case $\alpha \neq 2$ which breaks the translation symmetry so that we do not get involved with equivariant bifurcation theory (see chapter 9 for a study of the Ring Model with the symmetries.). The Jacobian at $\mathbf{v} = 0$ is given by (using some symmetries):

$$-\mathrm{Id}_{3\times 3} + \sigma s_1 \mathbf{K},$$

where $s_1 = S_0^{(1)}(0) = \frac{1}{4}$ and the matrix $\mathbf{K}$ is equal to

$$\mathbf{K} = \begin{bmatrix} \varepsilon_0 & \varepsilon_0\sqrt{|J_1|}\,\langle 1, \cos_\alpha\rangle & 0 \\ \varepsilon_1\sqrt{|J_1|}\,\langle 1, \cos_\alpha\rangle & J_1\,\langle 1, \cos_\alpha^2\rangle & 0 \\ 0 & 0 & J_1\,\langle 1, \sin_\alpha^2\rangle \end{bmatrix}$$

$\mathbf{K}$ has in general (for $\alpha \approx 2$) three real eigenvalues. We note σ_1 the eigenvalue of $\mathbf{K}$ corresponding to the eigenvector $(0, 0, 1)$, σ_2 and σ_3 the two eigenvalues ot its upper left-hand 2×2 submatrix. The values, noted σ_i, $i = 1, 2, 3$, corresponding to potential[11] bifurcations are equal to $4/\sigma_i$. The signs of the σ_is give the number of bifurcated branches (recall that $\sigma > 0$). Because $s_2 = S_0^{(2)}(0) = 0$ and $s_3 = S_0^{(3)}(0) = -1/8 \neq 0$, all branches are Pitchfork branches (see section.3.3.1) whose third order term is $\chi_3^{(i)} = \sigma_i^2 \frac{s_3}{6s_1} \langle e_i^3, e_i^* \rangle_{\mathcal{F}} = \sigma_i^2 \frac{s_3}{6s_1} \|e_i^2\|_{\mathcal{F}}^2 < 0$. Indeed, as J is self adjoint, we find: $e_i^* = e_i$. Hence these branches are directed toward $\sigma > \sigma_i$. This is summarized in table 3.1. The eigenvectors e_i, $i = 1, 2, 3$, of the Jacobian of (3.28)

ε_0 \ ε_1	-1	1
-1	0	2
1	1	3

Table 3.1: Number of bifurcated Pitchfork branches from $(0, \sigma)$ depending on the values of ε_0, ε_1. The value of α in (3.25) is close to 2.

at $\mathbf{v} = 0$ are given by:

$$e_1 = \sin_\alpha, \quad e_{2,3} = a_{2,3} + b_{2,3}\cos_\alpha$$

We reduce the number of possibilities by assuming, from now on, that $J_1 > 0$. It turns out that in this case $\sigma_2 < 0$ and there are only two possibilities to consider: $\sigma_1 < \sigma_3$ for $\alpha > 2$ and $\sigma_3 < \sigma_1$ for $\alpha < 2$. This gives the relative position of the different bifurcated branches, noted P_i, $i = 1, 3$. Once we have found the bifurcation point, we can numerically compute the bifurcated branches for all positive values of σ using a continuation method (we used the pseudo-arc length method as described

[11] The upcoming nonlinear analysis will show that they are indeed bifurcation points.

for example in [Sala 2004, Kuznetsov 1998]). From our numerical experiments, we conjecture that in the case $\varepsilon_0 = -1$ and $\varepsilon_1 = 1$, P_1 and P_3 satisfy the following properties

1. P_1 lies on the v_3-axis.
2. P_3 lies in the plane of equation $v_3 = 0$.
3. P_1 and P_3 do not intersect.

Remark 15. We can reverse the orientation of the Pitchforks by choosing a non-linearity such that $s_3 > 0$, the bifurcation diagram would be more complex: more saddle node points would appear because of proposition 3.3.3. It is the fact that $s_2 = 0$ for the sigmoid which produces Pitchfork branches. Another choice of non-linearity, for example $S(x) = \frac{1}{1+exp(-x+\varepsilon)}$, would produce transcritical branches.

Figure 3.4 shows a typical example corresponding to the values of the parameters that are found in the largest number of published articles. We come back to this choice in section 3.5.4. The left part of the figure shows the three components of the persistent states as functions of σ. For P_1 there is only one non-zero component, v_3, in blue. For P_3 there are two non-zero components, v_1 shown in red and v_2 shown in green. The right part of the figure shows another representation of P_1 and P_3 as curves parametrized by σ in the (v_1, v_2, v_3) space. P_3 is clearly in the (v_1, v_2) plane while P_1 is along the v_3-axis. The color at each point of the curves represents the value of σ according to the color scale shown on the right.

In detail we have

$\sigma_3 < \sigma < \sigma_1$ When σ goes through σ_3, the 0-solution loses its stability and becomes a saddle. There are three persistent states, 0 (unstable node) and two persistent states located on the Pitchfork branch P_3, both stable. The corresponding dynamics is shown in the left part of figure 3.4.

$\sigma_1 < \sigma$ When σ goes through σ_1, the 0-solution loses its stability along the v_3-axis. There are two new persistent states located on the Pitchfork branch P_1, both are unstable nodes (the unstable manifold is one-dimensional). The corresponding dynamics is also shown in the left part of figure 3.4.

There are at most 5 stationary solutions.

Remark 16. In the case $J_0 = 1$ and $\varepsilon_1 = 1$, there is another Pitchfork branch, see table 3.1. For σ big enough, $\mathbf{v} = 0$ becomes an unstable node and there are 7 stationary solutions instead of 5 for the case $J_0 = -1$

3.5.2.2 The case $\mu = 1,\ \varepsilon \neq 0$

We are now halfway from our scheme completion. To have an idea of the persistent states at low contrast (*i.e.* $\varepsilon \approx 0$), we need to know the persistent states for: $\sigma, \mu = 1, \varepsilon = 0$, that is we need to know the solutions of

$$V_\sigma^f = J \cdot S(\sigma V_\sigma^f) - \theta$$

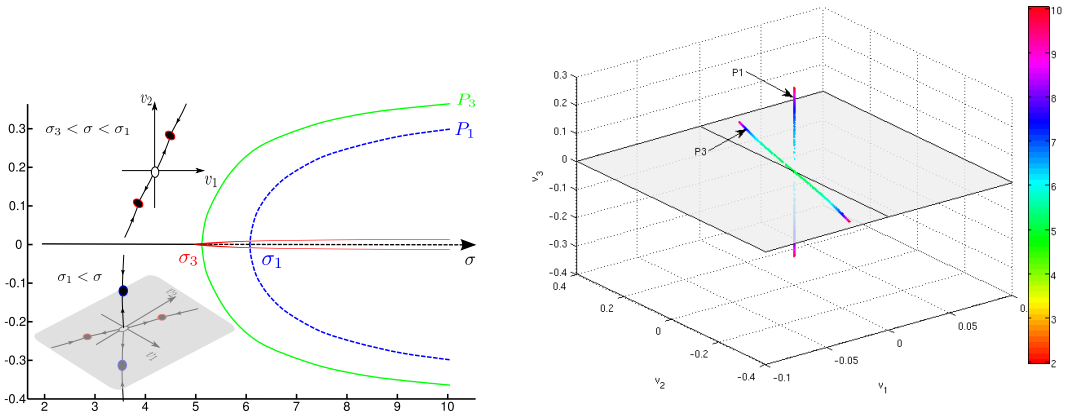

Figure 3.4: Left: Plot of the bifurcation diagram for $\alpha = 2.2$. It shows the two Pitchfork branches P_1 and P_3. For each branch, we have only plotted the non-zero coordinates with $v_1 = red$, $v_2 = green$ for P_3 and $v_3 = blue$ for P_1. We have also plotted the dynamics in two and three dimensions according to the values of the nonlinear gain σ. Right: Plot of the equilibrium points. The color encodes the value of the nonlinear gain σ (see text). $J_0 = -1$, $J_1 = 1.5$, $\mu = 0$, $\varepsilon = 0$, $\alpha = 2.2$

Following our program, we numerically compute the persistent states when the nonlinear gain σ and μ both vary. As described in section 3.2.2 we expect many of the previous bifurcations to disappear thereby breaking some of the connectivity of the sets $\mathcal{B}_\sigma$ which can actually be (partially) recovered by considering the sets $\mathcal{B}_{\sigma,\mu}$ This was done using the library TRILINOS (see [Sala 2004] and the website) using a multiparameter continuation.

We show an example of this continuation in figure 3.5 Left where we display the v_2 component of the persistent states as a function (sometimes multivalued) of σ and μ. A cross-section of this set by the plane of equation $\mu = 0$ (shown as semi-transparent in the figure) yields a curve identical to the one shown in green figure 3.4 Left. The figure nicely shows how the first Pitchfork bifurcation branch P_3 opens up when μ becomes non zero: this gives the connected component of $\mathbf{V}_\sigma^f$ which is linearly stable.

$$\begin{cases} 0 = v_1 - \varepsilon_0 \langle S_0(\sigma V), 1\rangle + \mu(-\theta + \frac{\varepsilon_0}{2}) \\ 0 = v_2 - \varepsilon_1 \sqrt{|J_1|}\, \langle S_0(\sigma V), \cos_\alpha\rangle + \mu\varepsilon_1 \sqrt{|J_1|}\, \frac{sin_\alpha(\pi/2)}{\alpha\pi} \\ 0 = v_3 - \varepsilon_1 \sqrt{|J_1|}\, \langle S_0(\sigma V), \sin_\alpha\rangle \end{cases} \tag{3.30}$$

However, as can be seen from 3.5 Right, non-zero values of μ do not break the Pitchfork P_1. It is easy to qualitatively understand why, even though a full mathematical proof is more difficult to come up with: μ does not affect the third equation which produces the Pitchfork P_1. We can prove it locally for μ near 0 using the implicit function theorem. We are looking for a point $(v_1(\mu), v_2(\mu), 0)$ at

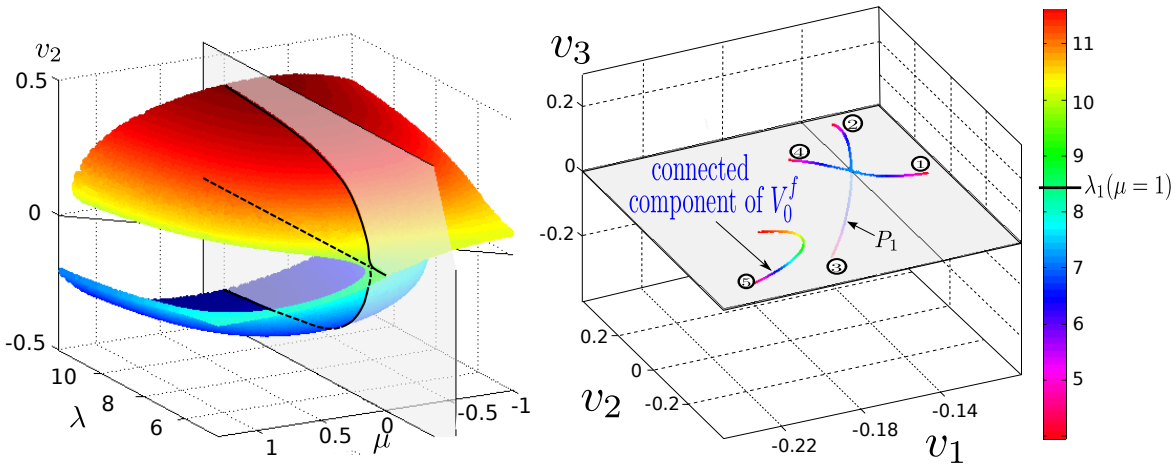

Figure 3.5: Left: The v_2 component of the 2-parameters continuation (σ, μ). Right: Plot of the equilibrium points. The color encodes the value of the nonlinear gain σ. Parameters are $J_0 = -1,\ J_1 = 1.5,\ \mu = 1,\ \varepsilon = 0,\ \alpha = 2.2,\ \theta = 0.1$.

which a Pitchfork occurs for $\sigma = \sigma_1(\mu)$. Let us consider

$$H(v_1, v_2, \sigma; \mu) = \begin{bmatrix} v_1 - \varepsilon_0 \langle S_0(\sigma V), 1\rangle + \mu(-\theta + \frac{\varepsilon_0}{2}) \\ v_2 - \varepsilon_1\sqrt{J_1}\,\langle S_0(\sigma V), \cos_\alpha\rangle + \mu\varepsilon_1\sqrt{|J_1|}\frac{sin_\alpha(\pi/2)}{\alpha\pi} \\ 1 - \sigma J_1 \left\langle DS_0(\sigma v_1 X_0 + \sigma v_2 X_1), sin_\alpha^2 \right\rangle \end{bmatrix} \tag{3.31}$$

where the last component of $H(v_1, v_2, \sigma; \mu)$ is the partial derivative with respect to v_3 of the third equation in (3.30). It is easy to see that $H(0, 0, \sigma_1; 0) = [0\ 0\ 0]$. The Jacobian of H w.r.t. (v_1, v_2, σ) at $(0, 0, \sigma_1, 0)$ is (because $S^{(2)}(0) = 0$):

$$\begin{bmatrix} -1 + \sigma_1 s_1 \varepsilon_0 & \sigma_1 s_1 \varepsilon_1 \sqrt{|J_1|}\,\langle 1, \cos_\alpha\rangle & 0 \\ \sigma_1 s_1 \varepsilon_0 \sqrt{|J_1|}\,\langle 1, \cos_\alpha\rangle & -1 + \sigma_1 s_1 J_1 \left\langle 1, \cos_\alpha^2 \right\rangle & 0 \\ 0 & 0 & -s_1 J_1 \left\langle 1, \sin_\alpha^2 \right\rangle \end{bmatrix}$$

It is invertible, hence there exists a unique solution defined locally for $\mu \geq 0$ satisfying $H(v_1(\mu), v_2(\mu), \sigma_1(\mu); \mu) = 0$: we have found a bifurcated point. Moreover, as $\chi_1^{(3)}(\mu = 0) \neq 0$, it will remains so for small μ: the Pitchfork P_1 is not affected by μ. For large values of μ we have to rely on numerical simulations.

Now, because of lemma 3.5.1, the solutions (v_1, v_2) corresponding to $v_3 \neq 0$ (*i.e.* lying on the Pitchfork branch) are the same for v_3 and $-v_3$ which gives the branch 2-3 in figure 3.6. Hence, when $\mu \neq 0$, we still have the Pitchfork P_1 and the branch (located in $v_3 = 0$) arising from the opening of P_3. This gives the diagram shown in figure 3.6 for the three components of $\mathbf{v}$. The left part of the figure shows the case $\mu = 0.2$ while the right part shows te case $\mu = 1$, the one we are interested in. Each triplet of (red,green,blue) curves represents the variation of (v_1, v_2, v_3) as a function of the parameter σ. They are labeled by integers between 1 and 5.

This diagram is a bit misleading because if we count the *red* components, there are four of them for $\sigma > \sigma_1$ which gives an even number of solutions (in contradiction

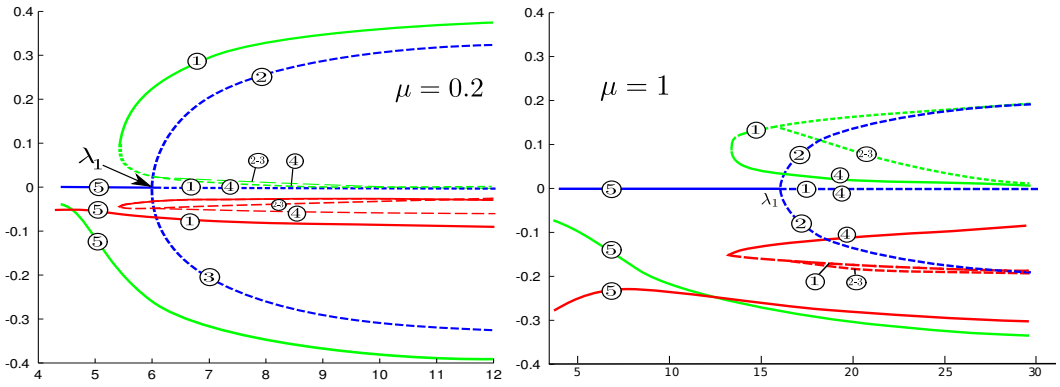

Figure 3.6: Plot of the three components $(v_1, v_2, v_3) = (red, green, blue)$ as functions of the nonlinear gain σ for the following values of the parameters: $J_0 = -1$, $J_1 = 1.5$, $\mu = 1$, $\varepsilon = 0$, $\alpha = 2.2$, $\theta = 0.1$. Remember that the nonlinear gain of the model has to be around $\sigma = 29$ in order to be compatible with previous work. The numbers label the different solutions, any solution is made of 3 components (v_1, v_2, v_3), hence requires three labels. The label $2-3$ indicates that the solutions 2 and 3 shares one common component.

with proposition 3.2.7). In fact by doing so we miss the symmetry $v_3 \leftrightarrow -v_3$ and the corresponding solutions. It is easier to look at figure 3.5 Right to count the stationary solutions.

From section 3.3.1, it follows that the connected branch of V_0^f is stable as well as the branch P_1. The only unstable branch comes from the opening of P_3 and is shown in figure 3.5 Right.

Remark 17.Figure 3.5 shows an example where our scheme allows to detect another branch of solutions which is not connected to the connected component of the trivial solution.

Figure 3.6 also tells us which branches will appear when the contrast ε becomes positive: this will be a perturbation of figure 3.5. Except in the case $x_0 = 0$ (see equation (3.25)), the Pitchfork P_1 will open up, giving two new connected components in addition to the connected component of $\mathbf{V}_0^f$.

To illustrate further these ideas we have plotted in figures 3.7, 3.8 and 3.9 all the persistent states (i.e. the functions $A^f(x) = S(V^f(x))$ for $-90^\circ \leq x \leq 90^\circ$) for various values of the nonlinear gain σ, and the contrast ε. In detail we have $\varepsilon I(x) = \varepsilon(1 - 0.1 + 0.1\cos_\alpha(x - 0.1))$, $\alpha = 2.2$, $J_0 = -1$, $J_1 = 1.5$, and $\mu = 1$. Unstable solutions are shown in dotted line, stable solutions in continuous lines. The width of the continuous lines is proportional to the smallest magnitude of the (negative) eigenvalues of the Jacobian of the system for this solution. We show in appendix A.7 that this magnitude is a lower bound of the size of the corresponding attraction basin. The external current $I(x)$ is plotted as a red continuous line in figures 3.8 and 3.9.

Figures 3.7 and 3.8 correspond to the cases $\varepsilon = 0$ (no input current) and $\varepsilon =$

0.05, respectively. In each figure the three subfigures correspond, from left to right, to the increasing values 14, 20, and 29 of the nonlinear gain σ. In the case of figure 3.7 the number and the stability of the solutions can be predicted directly from the righthand side of figure 3.6 while for figure 3.8 this can be achieved from a perturbation of the same figure. Note that, except for the unstable solution peaking at $x = 0°$, the effect of increasing the nonlinear gain of the sigmoid is to increase the amplitude of the solutions, as can be seen from an examination of the branches labelled 4 in the righthand side of figure 3.6.

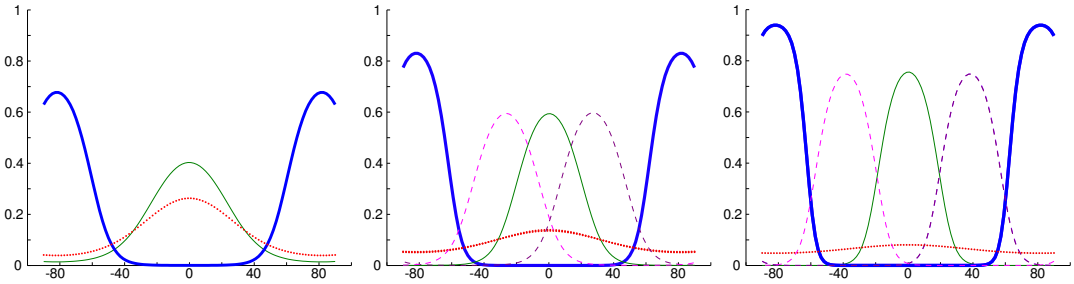

Figure 3.7: Stationary solutions for the Ring Model with no input current ($\varepsilon = 0.0$) for three values of the nonlinear gain parameter σ. From left to right $\sigma = 14$, 20, 29. For $\sigma = 14$ there are three solutions, two stable (shown in continuous line) and one unstable (shown in dotted line). For $\sigma = 20$ and $\sigma = 29$ there are five solutions, two stable, and three unstable, see text.

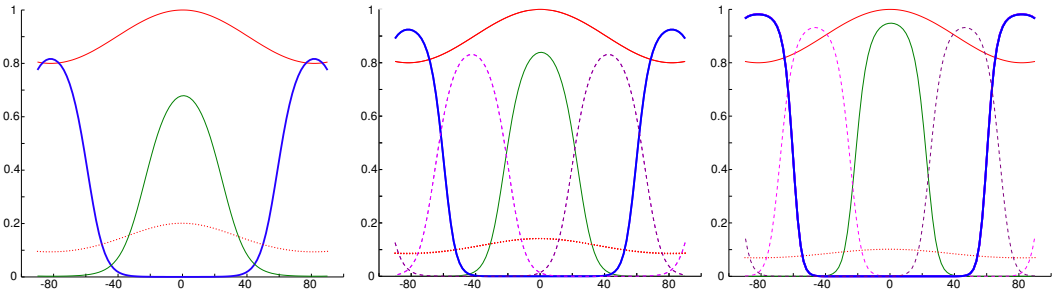

Figure 3.8: Stationary solutions for the Ring Model with an input current corresponding to the contrast $\varepsilon = 0.05$ for three values of the nonlinear gain parameter σ. From left to right $\sigma = 14$, 20, 29. In all the cases there are at most five solutions, two of them stable (shown in continuous lines), and three (one for $\sigma = 14$) unstable (shown in dotted line), see text.

Figure 3.9 corresponds to an even higher current than in figure 3.8,*i.e.* the contrast ε is equal to 0.1. In this case we only show the stationary solutions for the values 20 and 29 of the nonlinear gain parameter because there is little difference between the cases $\sigma = 14$ and $\sigma = 20$. We note that the effect of increasing the nonlinear gain is the same as in figure 3.8 and that for a given nonlinear gain, the effect of increasing the contrast ε is also to increase the amplitude of the solutions,

except for the unstable solution peaking at $x = 0°$. The labels of the five solutions shown in the righthand part of the figure are the same as in figure 3.6. The reader should have no problem to transfer them to the solutions plotted in figures 3.7 and 3.8.

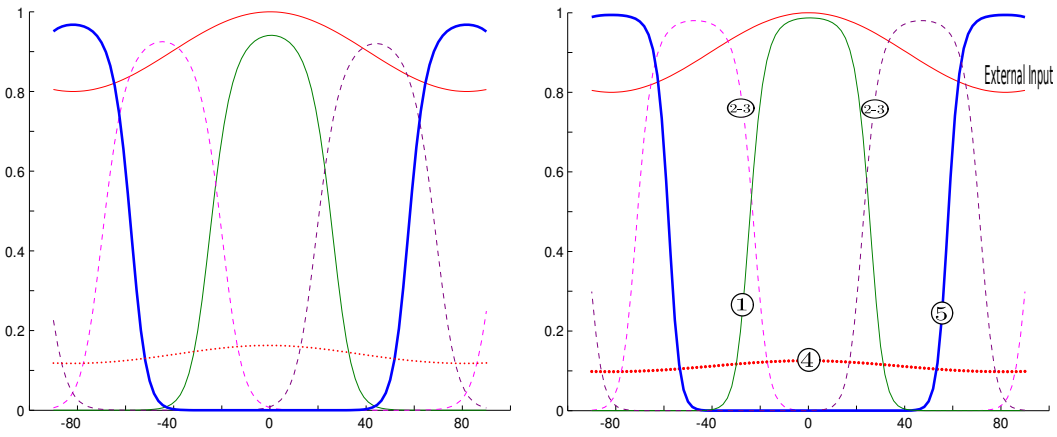

Figure 3.9: Stationary solutions for the Ring Model with an input current corresponding to the contrast $\varepsilon = 0.1$ for two values of the nonlinear gain parameter σ. From left to right $\sigma = 20, 29$. In both cases there are five solutions, two of them stable (shown in continuous lines), and three unstable (shown in dotted line), see text.

3.5.3 A closer inspection of contrast dependency and the broken symmetry

The previous numerical/theoretical analysis has shown a very interesting point: it predicts two orthogonal stable stationary states. It means that when an hypercolumn is presented (let us say) an horizontal drifting grating, *i.e.* $x_0 = 0$ in (3.24), the hypercolumn can interpret this stimulus as being vertical (see figure 3.9). However, we know from prop 3.2.7 that there is a unique stationary state for a large enough contrast ε, this state will correspond to a horizontal state. The question we wish to examine is how much contrast is needed to destroy the *illusory* vertical stationary state which is not related to the stimulus orientation? We will come back in chapter 9 to a precise definition of the illusions states and the illusory states. For now, we just call an illusory state, a state which is not related to the stimulus orientation.

Our analysis have been confined to the case $\alpha > 2$ up until now. It is straightforward to make a similar study for $\alpha < 2$. The main point to notice is that the Pitchfork P_1 would happen before the Pitchfork P_3 (see figure 3.4). Hence, the stable cortical states would be the solutions labelled $2 - 3$ in figure 3.9, *i.e.* cortical states correspond to a drifting grating oriented at $\pm 45^o$. These states have no relation with the horizontal input for $x_0 = 0$.

We will see that all these illusory persistent states are 'artefacts' coming from the hypothesis $\alpha \neq 2$. This hypothesis implies that the network is not anymore

translation invariant: it has a preference. We have seen that, depending on the case $\alpha \lessgtr 2$ and on the nonlinear gain σ, the network prefers horizontal/vertical drifting gratings. The following study will show that contrasts ε of the order the asymmetry $|\alpha - 2|$ destroy the illusory persistent states.

We use the Lyapunov-Schmidt reduction (see [Golubitsky 1984, Golubitsky 1988, Kielhöfer 2003]) to study the effect of the anisotropy. Hence, our analysis will work for constrasts/asymmetries small (*i.e.* close to 0). For larger values, one has to rely on numerical computations as we did in the previous section.

Let us consider the case $\alpha = 2, \mu = 1, \varepsilon = 0$. For any nonlinear gain there is a constant (in space) solution[12] $\mathbf{v} = (v_0, 0, 0)$. We will see in chapter 9 that there is always a nonlinear gain σ_c for which the network (at $\alpha = 2, \mu = 1, \varepsilon = 0$) displays a Pitchfork bifurcation. We summarize the results in the next proposition.

Proposition 3.5.2. *Let us consider the parameters $\nu = (\sigma, \alpha, \varepsilon) \in \mathbb{R}^3$ and the bifurcation point $\nu_c = (\sigma_c, 2, 0)$. If we write $\mathbf{V} = v_0 + x_1 \cos_2 x + x_2 \sin_2$, then the equation (around the bifurcation point ν_c) reads*

$$\begin{cases} 0 &= x_1 \left(\delta\sigma + \delta\alpha + \chi_3(x_1^2 + x_2^2)\right) + \varepsilon I_1 \\ 0 &= x_2 \left(\delta\sigma - \delta\alpha + \chi_3(x_1^2 + x_2^2)\right) + \varepsilon I_2 \end{cases} \tag{3.32}$$

with $I = \beta \cos_2(x_0)$, $I_2 = \beta \sin_2(x_0)$, $\sigma = \sigma_c + \frac{2}{s_1 J_1}\delta\sigma$, $\alpha = 2 + \frac{4}{s_1 J_1}\delta\alpha$ and $s_1 = DS(\sigma_c v_0(\sigma_c))$.

Proof.

Let us write $\mathbf{L}_\nu$ the linearised r.h.s. of (3.25) for a given triplet ν around the stationary point $\mathbf{V}^f = v_0(\sigma_c)$, $\mathbf{V} \equiv \mathbf{V}^f + \mathbf{U}$ and $\mathbf{L} \equiv \mathbf{L}_{\nu_c}$. The kernel of $\mathbf{L}$ is spanned by $\cos_2, \sin_2$ and we write $\mathbf{P}_c = \langle \cdot, \cos_2 \rangle \cos_2 \frac{2}{\pi} + \langle \cdot, \sin_2 \rangle \sin_2 \frac{2}{\pi}$ the projection on the kernel. The equation to solve is $0 = F(\mathbf{U}, \nu) \equiv -\mathbf{U} + \mathbf{J}(\alpha) \cdot \big(\mathbf{S}(\sigma\mathbf{V}^f + \sigma\mathbf{U}) - \mathbf{S}(\sigma\mathbf{V}^f)\big) + \varepsilon \mathbf{I}_{ext}(\alpha)$. We compute the equation satisfied by (x_1, x_2) using the Lyapunov-Schmidt reduction. The method is similar to the one used in the proof of lemma 3.3.2 except that there are symmetries and the number of unknowns is 2. The same procedure gives the linear part $x_1\delta\sigma, x_2\delta\sigma$ and the terms corresponding to the external input $\varepsilon I_1, \varepsilon I_2$. We compute in chapter 9 the nonlinear part of the "reduced" equation and show that it yields the terms $\chi_3(x_1^2 + x_2^2)x$ and $\chi_3(x_1^2 + x_2^2)y$ for each component x_1, x_2. The coefficient χ_3 depends on the threshold θ, the critical gain σ_c and $v_0(\sigma_c)$.

It remains to compute the terms in the "reduced" equations corresponding to the parameter α. There are the linear terms $p_i \times (\alpha - 2)$ in each equation. The coefficient p_1 (for example) satisfies $p_1 = \langle \frac{2}{\pi} cos_2, \partial_\alpha F(0; \sigma_c, 2, 0) \rangle = 0$ where the first equality is given in [Golubitsky 1984][chapter VII.1.d]. We find $p_1 = p_2 = 0$. The next terms are $q_{ij} x_j (\alpha - 2)$ for the equation $i = 1, 2$. From [Golubitsky 1984][chapter

[12] This is a consequence of prop 3.2.7 applied to the equation for v_0.

VII.1.d], we find

$$q_{11} = \langle \frac{2}{\pi} cos_2, \partial_\alpha \mathbf{L}_\nu \cdot \cos_2 - D^2_{\mathbf{U}} F(0;\sigma_c,2,0)[\cos_2, \mathbf{L}^{-1}(\mathrm{Id} - \mathbf{P}_c)\partial_\alpha F(0;\sigma_c,2,0)]\rangle$$
$$= \langle \frac{2}{\pi} cos_2, \partial_\alpha \mathbf{L}_\nu \cdot \cos_2 \rangle$$

We write $\alpha = 2 + \frac{4}{s_1 J_1}\delta\alpha$ with $s_1 = DS(\sigma_c v_0(\sigma_c))$. From $\mathbf{P}_c(\partial_\alpha \mathbf{L})_{\nu_c}|_{\mathcal{X}_c} = s_1 \frac{J_1}{4}\begin{bmatrix} 1 & 0 \\ 0 & -1 \end{bmatrix}$, we conclude the proof of the proposition. □

We use this proposition to understand the effect of the different parameters. Let us assume that the external input is horizontal, *i.e.* $I_2 = 0$. For $\theta = 0$, we find (see chapter 9) that $\chi_3 < 0$. Up to a rescaling of (x_1, x_2, ε), we can assume that $\chi_3 = -1$. A little algebra shows that the stationary solutions of (3.32) are given by:

$$(S_1) : \begin{cases} x_1^3 - (\delta\sigma + \delta\alpha)x_1 - \varepsilon I_1 = 0 \\ x_2 = 0 \end{cases}$$

and

$$(S_2) : \begin{cases} x_1 = -\frac{\varepsilon I_1}{2\delta\alpha} \\ (2x_2)^2 = 4(\delta\sigma + \delta\alpha) - \left(\frac{\varepsilon I_1}{\delta\alpha}\right)^2 \end{cases}$$

We are ready to study more carefully what stationary states can be produced depending on the different parameters. Let us start with the case we have been studying until now and assume the network is at the edge of the bifurcation: $\nu \approx \nu_c$.

Case $\delta\alpha > 0$: we know that the solutions (S_2) correspond to the Pitchfork P_1 because x_1 and x_2 are non-zero. We are not interested in these solutions. The illusory persistent state comes from the first group of solutions S_1. The stationary states are solutions of a polynomial equation of third degree. There are real solutions i.i.f. $\Delta \equiv -4(\delta\sigma + \delta\alpha)^3 + 27(\varepsilon I_1)^2 \leq 0$. Hence, if $\delta\alpha, \delta\sigma$ are fixed, for constrasts of order $\delta\alpha^{3/2}$, only one solution remains.

Case $\delta\alpha < 0$: we know that the second set of solutions (S_2) produces the illusory stationary states. It is easy to show that for constrasts of order $|\delta\alpha|^{3/2}$, only one solution remains.

3.5.4 Discussion

There are two reasons why we presented this example. First, it is a nice simple model to which the formalism of this chapter easily applies and allows us to push the analysis far enough to grasp an almost complete understanding of its persistent states and a somewhat detailed understanding of its dynamics. Second, it conveys information for models of V1 that is likely to be biologically relevant. For example, as the nonlinear gain σ of the sigmoid is increased, many new stationary states appear whose stability evolves with σ. One of these solutions is "dramatic" for the

purpose of orientation detection: even if the LGN input orientation peaks around the angle $x_0 = 0$, the Ring Model can produce a stable cortical state (or a percept) corresponding to an angle of $\pi/2$!

However these solutions may be destabilized/destroyed by adding lateral spatial connections in a spatially organized network of Ring Models; it remains an area of future investigations. As far as we know, only Bressloff and co-workers looked at this problem (see [Bressloff 2002a, Bressloff 2001b]) in the case $\alpha = 2$ but they did not show cortical responses incompatible with the stimulus.

In an analysis using the Lyapunov-Schmidt reduction, we were able to understand, in a small region of the parameter space, the impact of the asymmetries $|\alpha-2|$ on the network behaviour. Basically, for contrasts of the order of the anisotropies $|\alpha - 2|$, the illusory states are destroyed. We will come back on the impact of asymmetries in chapter 10.

It should be noted that neural mass models are very often written with a Heaviside function for the nonlinearity which, as mentioned previously, is the limit case: $H(x) = \lim_{\sigma\to\infty} S(\sigma x)$.

We also made the assumption $\alpha \neq 2$ in the previous analysis. It remains to know how much of the preceding holds in the case $\alpha = 2$. More generally, what would remain if one were to choose a difference of Gaussians as a connectivity function over a cortex $\Omega = (-\pi/2, \pi/2)$. This will be done in chapter 9 where we provide a way to handle the symmetries numerically.

Chapter 9 will also provide a complete understanding of the effects of all the parameters. We will see that in order for the Ring Model to account for biological data, one must give specific values to its parameters. In other works, the model is completely specified by experiments.

3.6 Two populations of spatially organized neurons

We apply the previous theoretical analysis to a system we started to analyse in [Faugeras 2009]. In the somewhat reduced form we consider here, it consists of two populations ($p = 2$), one excitatory, one inhibitory, distributed over a flat ($d = 2$) cortex of rectangular shape[13] $\Omega = [-1,\ 1] \times [-0.95,\ 0.95]$. The connectivity matrix kernel writes:

$$\mathbf{J}(\mathbf{r}, \mathbf{r}') = \begin{bmatrix} aG_{11}(\mathbf{r} - \mathbf{r}') & -bG_{12}(\mathbf{r} - \mathbf{r}') \\ bG_{12}(\mathbf{r} - \mathbf{r}') & -cG_{22}(\mathbf{r} - \mathbf{r}') \end{bmatrix} \tag{3.33}$$

where $G_{ij}(\mathbf{r}) = e^{-\frac{\|\mathbf{r}\|^2}{2\sigma_{ij}}}$, $i, j = 1, 2$ are two-dimensional Gaussian functions and a, b, $c > 0$ characterize the strength of the connections. We also assume $\mathbf{I}_{ext} = 0$. The parameter μ controlling the translation of the sigmoid (see (3.14)) is therefore the only parameter, outside σ, that we vary from 0 to 1. We also chose (notice that

[13] Such choice is motivated by the requirement to break the maximum number of symmetries which otherwise could make the numerical continuation process more difficult.

$s_2 \neq 0$):

$$S(x) = \frac{1}{1+e^{-x+\theta}}, \quad \theta = 1.3$$

In [Faugeras 2009], we were able to compute the stationary solutions $\mathbf{V}^f_{\sigma,\mu=1}$ when the slope σ is small (*i.e.* $\sigma < \sigma^*$) using the Nystrom (see for example [Kress 1999]) method. We know, from the previous analysis, that if we perform a continuation of these solutions with respect to σ, we are bound to miss quite a few of them. Therefore we perform a two-parameter continuation with respect to the pair (σ, μ) in order to recover more stationary solutions.

Biologically speaking, no systematic investigation has been performed to test the validity of the translation invariance of the connectivity function. Hence a roughly translation invariant (called heterogeneous in [Ermentrout 1980]) is not less biologically relevant. This is where the PG-kernels are useful: they provide an easy way to approximate the convolution operation as well as an effective representation of the connectivity (see section 3.4).

There are three reasons why we think this example is interesting:

- We want to show how to deal with heterogeneous kernels. In particular, we will impose a null connectivity $\mathbf{J}$ on the cortex boundary $\partial\Omega$.
- We want to show an example of application of proposition 3.3.3.
- More importantly, we want to show how the results of section 3.3.1.1 may change in the two-dimensional case.

We also want to give a non trivial example of the existence of a branch of solutions not connected to the trivial solution $\mathbf{V}^f_0$. We did not find a model which showed this behaviour while featuring the three points above. Notice that we gave an example of our method showing how to compute some non connected components in the previous example 3.5.

As in the previous case, we are not interested in obtaining the complete bifurcation diagram of the system but rather in giving numerical examples of the previously enumerated points.

3.6.1 Approximation of J

Let us write

$$e^{-\|\mathbf{r}-\mathbf{r}'\|^2/2} = e^{-\|\mathbf{r}\|^2/2} e^{-\|\mathbf{r}'\|^2/2} e^{\langle \mathbf{r},\mathbf{r}'\rangle} \approx e^{-\|\mathbf{r}\|^2/2} e^{-\|\mathbf{r}'\|^2/2} \left(1 + \langle \mathbf{r},\mathbf{r}'\rangle + \frac{1}{2}\langle \mathbf{r},\mathbf{r}'\rangle^2 + ...\right)$$

We notice two important facts:

- $1 + \langle \mathbf{r},\mathbf{r}'\rangle + \frac{1}{2}\langle \mathbf{r},\mathbf{r}'\rangle^2 + ...$ is a polynomial in the components of $\mathbf{r}$ and $\mathbf{r}'$, hence a PG-kernel.

- $e^{-a\|\mathbf{r}\|^2/2} = e^{-ar_1^2/2}e^{-ar_2^2/2}$ has a bell-shape which we approximate with the function $B_a(\mathbf{r}) \equiv \left(1-r_1^2\right)^{a/2}\left(0.95^2-r_2^2\right)^{a/2}$. This choice is also motivated by the fact that $e^{-a\|\mathbf{r}\|^2/2}$ tends to zero at the edges of the infinite cortex that is usually considered in the literature. We preserve this property with our finite cortex since $B_a = 0$ on the boundary $\partial\Omega$ of Ω. Any other positive bell shaped function would be appropriate.

Putting these two facts together, we end-up with the following approximation of a Gaussian convolution kernel with a PG-kernel.

$$J_{ij}(\mathbf{r},\mathbf{r}') = B_{a_{ij}/2}(\mathbf{r})B_{a_{ij}/2}(\mathbf{r}')P_{ij}(\mathbf{r},\mathbf{r}'), \quad i,\, j = 1,\, 2 \tag{3.34}$$

where $\mathbf{P}$ is a 2×2 matrix with polynomial entries in $\mathbf{r}$ and $\mathbf{r}'$. It is easy to see that this type of connectivity (3.34) is a PG-kernel. The smaller the degree of the polynomials P_{ij}, the smaller is the number of unknowns v_i in (3.21). Hence, if one wants a small number of variables, one should try to approximate e^x on $[-2,2]$ with polynomials. This could be done using the series $\sum_{k=0}^{N}\frac{x^k}{k!} \overset{N\to\infty}{\to} e^x$ or the best polynomials interpolation given by the Chebyshev Equioscillation Theorem.

There is the disadvantage that the integrals in (3.21) must be computed accurately using some numerical library.

An other alternative is to discretize Ω and compute the integrals of the integral kernels with a fixed quadrature rule, this may be cheaper computationally but it produces a lot of unknowns.

In the following numerical study, we chose the second alternative, *i.e.* we discretize Ω with $n = 15$ points on each axis which gives $15^2\cdot 2 = 450$ unknowns. Hence, we do not use the PG-kernels approximation and use the connectivity given by:

$$J_{ij}(\mathbf{r},\mathbf{r}') = B_{a_{ij}/2}(\mathbf{r})B_{a_{ij}/2}(\mathbf{r}')e^{a_{ij}\langle\mathbf{r},\mathbf{r}'\rangle}, \quad i,\, j = 1,\, 2 \tag{3.35}$$

We use the library TRILINOS (see [Sala 2004] for the website) for the multiparameter continuation. The vectors/matrices, in the program, are coded using the library EPETRA which is a parallel implementation of the linear algebra operations. Finally, the code is run on 8 processors.

3.6.2 Numerical experiments

In this numerical experiment we have $a_{11} = a_{22} = 3$, $a_{12} = a_{21} = 2$, $a = 20, b = 21, c = 25.5$ and $\mathbf{L} = 0.2\cdot\mathrm{Id}$. Each of the 450 variables is a function of the parameters σ, μ. We represent in figure 3.10 the 2-norm of the 450-dimensional vector $\mathbf{V}^f$ as a function of the slope parameter σ for $\mu = 0$. We find numerically the first 5 bifurcation points σ_i, $i = 1\cdots 5$ for $\sigma \in [0,\ 12]$. Depending on the symmetries of the eigenvectors of $\mathbf{J}$ and its adjoint $\mathbf{J}^*$, the different bifurcation points are Pitchfork or Transcritical bifurcations.

In figure 3.10 (case $\mu = 0$), we see three Pitchforks branches at σ_2, σ_3, σ_4 and two Transcritical branch at σ_1 and σ_5. According to proposition 3.3.3, a

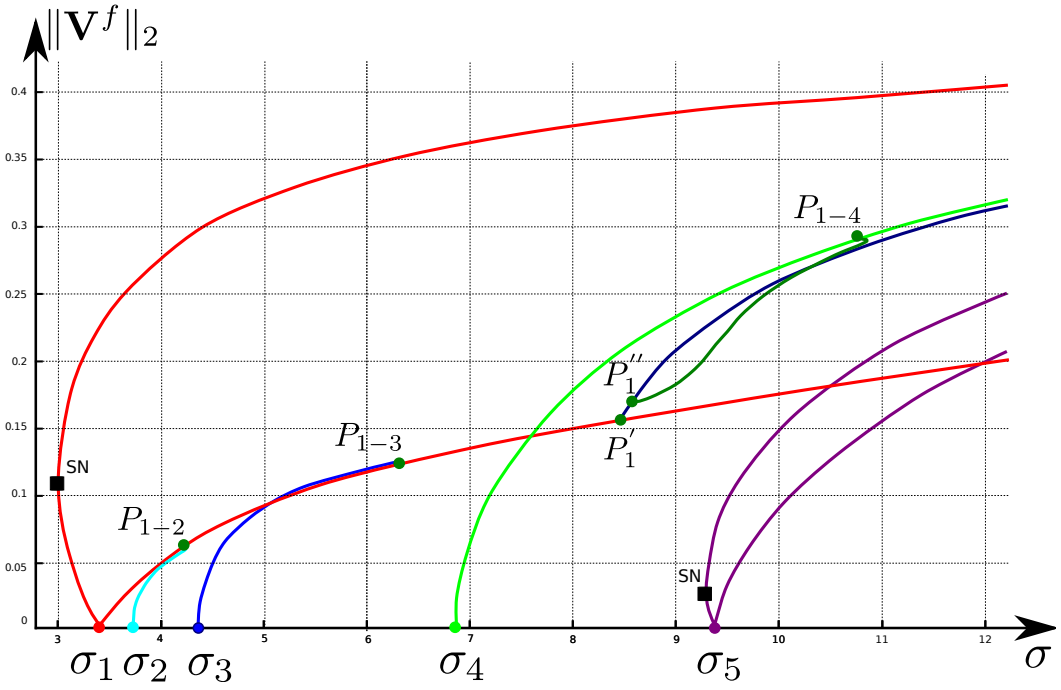

Figure 3.10: Plot of the 2-norm $\|\cdot\|_2$ of the 450-dimensional vector $\mathbf{V}^f$ as a function of the slope parameter σ for $\mu = 0$. Some intersection points are labelled. Notice that $\mathbf{V}^f = 0$ is solution for all values of σ. Each dot shows the intersection between two branches. SN stands for saddle-node.

saddle-node (noted SN in the figure) must appear on the Transcritical branches (see section 3.3.1).

It seems that all the bifurcation points (except σ_5 for $\sigma \in [0,\ 12]$) are connected to the first bifurcation point σ_1 by bifurcated branches. The intersections between the different branches are indicated by green dots in figure 3.10. The bifurcated branch from $(0, \sigma_1)$ displays secondary $P_1^{'}$ and tertiary bifurcation points $P_1^{''}$ by which it connects to the bifurcation point $(0, \sigma_4)$. We had some difficulties to find such an 'extreme' example but it seems, based on our numerical experiments, that it is deeply rooted in the fact that the connectivity is null on the cortex boundary $\partial\Omega$. Indeed, this property is also true for the stationary solutions and it seems to constrain the nodal structure of the stationary solutions: we have not been able to find properties of the nodal structure. When the connectivity has symmetries, some topological equivariant tools have been developed (see for example [Ize 2003, Balanov 2006]) which are closely related to the results we presented in section 3.3.1.1. We have not pushed forward in this direction.

Thus, this example shows, at least numerically, that the Rabinowitz conclusions in section 3.3.1.1 are specific to the one-dimensional case.

We plot, in figure 3.11, the stationary membrane potential V_1^f of the first population for different values of σ along the branch connecting P_{1-3} to $(0, \sigma_3)$. It shows how the symmetry of the state, which has the symmetries of a rectangle, change along the branch until the point σ_3 which only displays the reflexion symmetry.

Remark 18. We have chosen the parameters a, b, c such that the first three eigenvalues have zero imaginary parts. Numerically, most of the other eigenvalues $\sigma_{\mathbf{n}}$ have non-zero imaginary part leading to Hopf bifurcations. Other stationary bifurcation may appear for large slope values (i.e. $\sigma > 12$).

3.7 Discussion

In this section we briefly discuss two important aspects of the neural fields model with respect to the biology.

3.7.1 Is the cortex really finite?

An important aspect of our work is to assume that the domain Ω is bounded. As pointed out in the introduction this has the effect of simplifying somewhat the functional analysis of the problem. Since we can then rely essentially on the fact that the operator defined by the connectivity function is compact, hence also its Frechet derivative. The spectrum of this derivative is therefore at most countable, 0 being an accumulation point. The inverses of its positive eigenvalues (multiplied by 4, see equation (3.17)) determine the possible points of bifurcation of the steady-state solution with respect to the parameter σ. They accumulate at $+\infty$ but will in general have values smaller than the range of values biologically relevant. Assuming in the worst case that each of these values corresponds to a bifurcation, if they

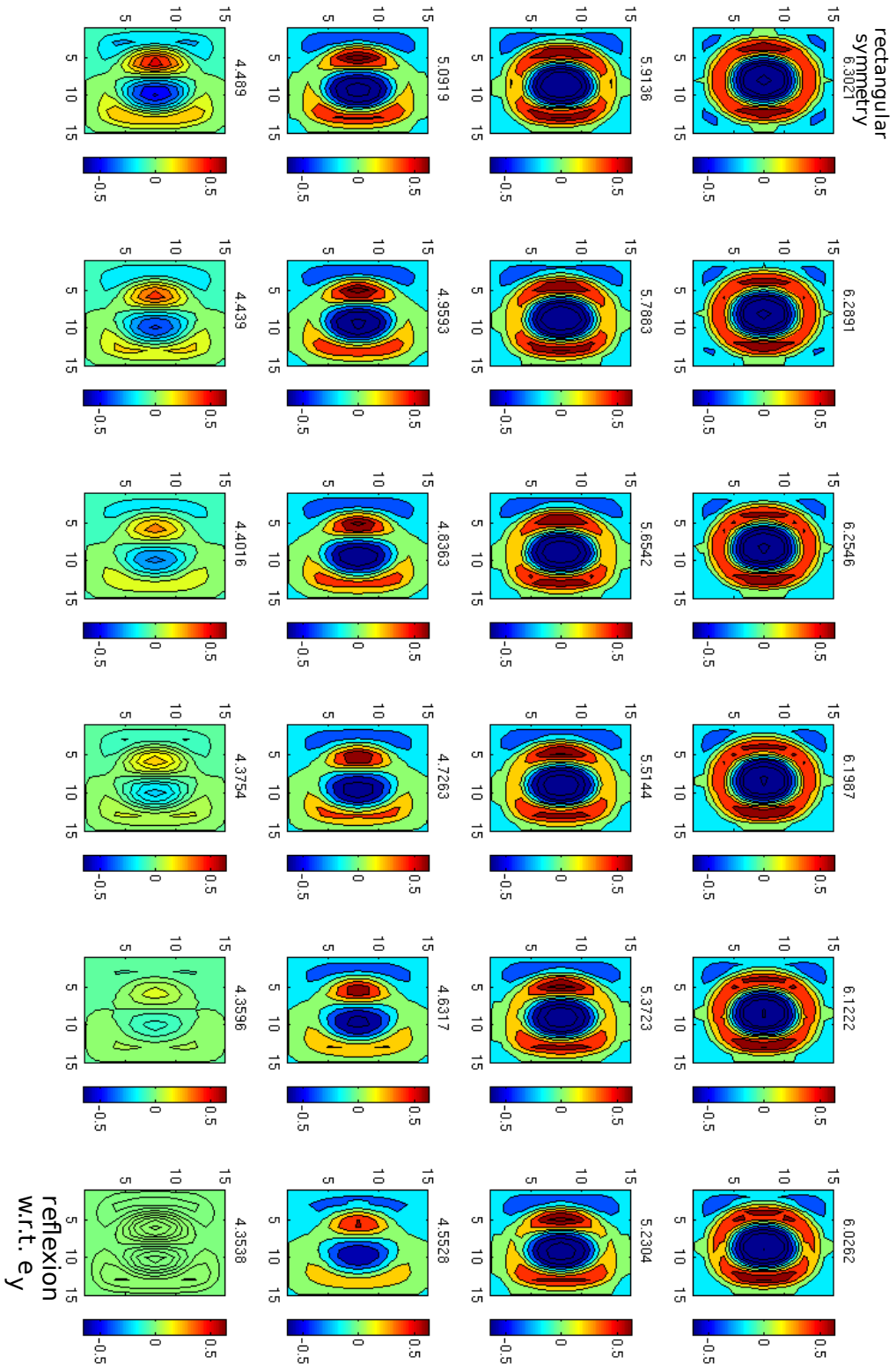

Figure 3.11: Plot of the first component V_1^f of the solution $\mathbf{V}^f = (V_1^f, V_2^f)$ along the branch connecting P_{1-3} to σ_3 in figure 3.10. The nonlinear gain is indicated on top of each sub-figure. This figure shows how the symmetry of the bifurcated solution evolves along the branch from the point P_{1-3} with the symmetry group of a rectangle to the point σ_3 with just the symmetry reflexion w.r.t. e_y.

are very close to each other the task of the numerical continuation program will become extremely difficult. This situation occurs when the spread of the connectivity function **J** is very small with respect to the size of the domain Ω, making the finite size assumption questionable from the practical viewpoint. In order to get a feeling for the domain of applicability of our theory we have done the following experiment. Assume that the domain Ω is 1D, and of length a. Assume further that the local interaction is described by a Gaussian with zero mean and variance σ^2 normalized in such a way that its integral on the interval $[-a/2, a/2]$ is equal to 1. The eigenvalues σ_n of **J** can be computed analytically as the Fourier coefficients of the function **J**. As it was just mentioned, they accumulate at 0 since **J** is compact. What is important is the separation of their inverses (the σ_ns). For a ratio σ/a equal to 10% the first 10 positive σ_ns are given by

n	1	2	3	4	5
	1.000	1.218	2.202	5.909	23.530
n	6	7	8	9	10
	139	1220	15785	337734	2629893

If we decrease the ratio to 5% these numbers become

n	1	2	3	4	5
	1.000	1.051	1.218	1.559	2.202
n	6	7	8	9	10
	3.4341	5.909	11.224	23.530	54.445

and if we decrease the ratio to 1%:

n	1	2	3	4	5
	1.0000	1.0020	1.0079	1.0179	1.0321
n	6	7	8	9	10
	1.0506	1.0736	1.1015	1.1347	1.1734

We conclude from this numerical experiment that our methods are applicable in a straightforward fashion for ratios roughly above 2-3%.

Now, what does the biology tell us about the ratio σ/a? In the cat area 17 (analogue to V1 in humans), it is commonly agreed that excitatory connections can span as much as 8mm whereas inhibitory are limited to 3mm for an area which is roughly 25x20mm, hence a ratio between 12% and 32%. In humans, less data is available but Bressloff et al. in [Bressloff 2001b] use a lateral connectivity function spanning 10mm for an area V1 with area 144x96mm, hence a ratio of roughly 7%. In both species we are well in the range of separations of the eigenvalues that poses no numerical problems to the continuation methods.

3.7.2 How steep should the sigmoid be?

When the nonlinear gain σ of the sigmoid in the model increases without bound, the sigmoid converges toward the Heaviside function. As shown in the chapter, when

σ increases, we predict the appearance of a variety of new stationary solutions of the neural field equations. From the biological viewpoint one observes hard thresholds at the level of single neurons f-I curves [Izhikevich 2000], the curves that relate the external current to the firing rate. At the population level, the one described by the neural field equations, these hard thresholds are smoothed over by the effect of population averaging. Our mathematical analysis can provide an answer to the question of how steep is a sigmoid from a biological perspective. The answer is related, in the case of the Ring Model, to the connection between the nonlinear gain σ and the connectivity function $\mathbf{J}$. As shown in equation (3.24) the relevant parameter is the product $\sigma|J_0|$ which is constrained by a) the fact that it must be larger than the first bifurcation value in order for the model to produce tuning curves, and b) that it must be smaller than the value for which the tuning curves saturate, hence do not vary with the contrast anymore, in contradiction with biological measurements. For each application of the neural field equations this is how the biology enters the mathematics to constrain the model parameter values.

3.8 Conclusion

In this chapter, we have pursued the analysis, started in [Faugeras 2008, Faugeras 2009], of a special type of integro-differential equation that appears in neural field and neural mass models where we are interested in approximating mesoscopic and macroscopic ensembles of neurons by continuous descriptions.

In effect, these equations depend upon a number of biological or experimental parameters such as the nonlinear gain σ of the nonlinearity, the connectivity matrix $\mathbf{J}$, or the input $\mathbf{I}$. These parameters vary in general in neural populations because of such processes as plasticity and learning. It is therefore important to understand how the solutions of these equations vary when these parameters change. To this end, we used two theories: the degree theory and the bifurcation theory. The degree theory describes the general behaviour of the cortical states as the parameters vary. On the other hand, the bifurcation theory describes the precise local behaviours of the cortical states as the parameters vary.

We believe that a good model should exhibit bounded membrane potentials which requires to take a bounded nonlinearity (as opposed to some papers, see for example [Ben-Yishai 1995]). The degree theory yields the powerful estimate that the number of persistent states has to be odd, hence it predicts an additional persistent state in the neighbourhood of subcritical Pitchfork/transcritical bifurcation points. This extra point is invisible to bifurcation theory, which is a local theory (this was conjectured numerically in [Ermentrout 1980]). The extra point may change drastically the dynamics and shows that local analysis is not sufficient for the study of the neural field equations.

We have focused on the description of the stationary solutions of the neural equations when varying the nonlinear gain, and tried to compute numerically the additional persistent state given by the degree theory for arbitrary external current

and connectivity. As the set of stationary solutions may not be connected, we used a multiparameter continuation scheme in order to compute non-connected branches of solutions and were able to show examples of these (see section 3.5). Whether these different branches of solutions intersect or are unbounded is still unknown in the general case. However, the scalar case for a one-dimensional cortex ($p = 1,\ d = 1, \mathbf{I}_{ext} = 0$) is almost completely solved (see section.3.3.1.1): we still don't know if isolas may exist. This point has never been mentioned in the literature to our knowledge. The question of whether we have computed all the solutions by using our multiparameter scheme is unfortunately still open.

To summarize, we have found new stationary solutions that were not predicted before. This suggests that the analysis of neural field models of the visual system should be re-examined.

Part III

Delayed neural field equations

Chapter 4

Theoretical properties

Contents

4.1 Introduction

The Hodgkin-Huxley equations [Hodgkin 1952] provide an accurate and mathematically tractable description of the behavior of an individual neuron in isolation, which later formed the foundation for mesoscopic descriptions of neural networks where the fine properties of the neurons do not play a fundamental role. The neural field models [Wilson 1973, Amari 1977, Coombes 2005b], which describe the firing rate evolution of spatially extended populations of neurons have been used successfully to model the rat barrel cortex [Pinto 1996] and

the visual cortex [Ben-Yishai 1995, Markounikau 2010]. More specifically, neural field models have been used to study both stationary and oscillatory behaviors; in both regimes the connectivity between neurons dictates the possible cortical states (see [Ermentrout 1979] for the oscillatory regime). The stationary regime has been used to describe neural hallucinations as spontaneous cortical activity [Bressloff 2000, Bressloff 2001b]. The computation of the stationary cortical states and their stability is now well documented [Ermentrout 1980, Bressloff 2000, Bressloff 2001b, Coombes 2005b, Faugeras 2008, Veltz 2010]. An immediate question is how this stability is altered when delays are introduced. There are a limited number of studies for which delays are taken into account but only constant delays are considered in non spatially extended populations [Bélair 1994, Bélair 1996, Coombes 2009, Shayer 2000, Wu 2001]. Here, we use bifurcation theory to study both stationary and oscillatory behaviors in a spatially extended system with space dependent delays.

Moving from a description of neural activity by ordinary differential equations (ODEs) to delay differential equations (DDEs) requires significantly more complex mathematical and numerical tools, mainly due to the fact that the phase space becomes infinite dimensional [Wu 1998, Hale 1993, Diekmann 1995, Shampine 2001]. This explains the small number of studies of mesoscopic models with delays. Indeed, whenever possible, one should try to find a description of the biophysical behavior with ordinary differential equations. In the case of constant delay across all populations there is no significant increase in mathematical difficulty, however, in the case of propagation (spatially dependent) delays, there is no way to give an accurate description of the dynamics with a reduction to ODEs. However, it would be advantageous to use equations that intrinsically contain finite propagation speeds (like the wave equation) instead of neural field equations. When the spatial connectivity is homogeneous, one can find a partial differential equation which approximates the delayed neural field equations [Coombes 2007]; a major advantage of this approach is the speed-up in the numerical computation. However this advantage has been recently superseded by the algorithm in [Hutt 2010] where the authors take advantage of the convolutional structure of the homogeneous connectivities to efficiently compute the solutions of delayed neural field equations (DNFEs). All in all, no simplification exists for general connectivities which suggests that a description of propagation delays with delay differential equations is still satisfactory.

In the quest to approximate networks of spiking neurons by neural field equations, it has recently been shown that constant delays must be incorporated in the mesoscopic description in order to produce oscillations — traveling waves or standing waves — observed in spiking neural networks [Roxin 2005, Roxin 2011]. These constant delays take into account the finite integration time of the pre-synaptic action potentials by synapses. On the other hand, the space dependent delays coming from the finite velocity of action potentials propagating along axons are thought to play an important role in the long range connections observed in the visual cortex ([Bressloff 2003, Lund 2003a]).

The linear stability of stationary cortical states of delayed neural field equations

was studied in [Atay 2005, Atay 2006, Bressloff 2008, Coombes 2007, Hutt 2009, Hutt 2008, Jirsa 2000, Bojak 2010] and some delay dependent/independent bounds of stability were given in [Atay 2005, Atay 2006, Hutt 2006, Hutt 2008, Veltz 2011b]. Due largely to the fact that the eigenvalue problem is infinite dimensional, the computation of the stability has been confined to some very particular cases [Venkov 2007, Bressloff 2008]. Hence, little is known about the impact of (space dependent) delays on the stability of equilibria. Due to the high computational cost (even for one dimensional cortices with homogeneous connectivities), an in-depth analysis of the values of delays and connectivity properties giving rise to oscillatory behavior has yet to be produced. Despite this limitation, the nonlinear stability has been studied in two papers [Roxin 2011, Venkov 2007]. The first reference gives, by means of a numerical investigation of the eigenvalue problem, an almost complete description of the linear stability for constant delays; we show that it can be done analytically in the most general case. Notice that the nonlinear analysis is done using weakly nonlinear analysis. The second reference [Venkov 2007] applies the weakly nonlinear analysis techniques to produce simplified equations from which the stability is studied. They were able to compute the normal form of the Hopf bifurcation for different neural field models including neuronal adaptation. From a mathematical point of view, the method produces nonlinear partial differential equations for the reduced equation which are not so straightforward to study in practice; the authors consider infinite cortices, modeled in effect as the real line. By looking at bounded cortices (as in [Roxin 2011]), we show that our method produces ordinary differential equations whose normal forms are well-documented [Guckenheimer 1983, Kuznetsov 1998, Haragus 2010].

The main drawback in the use of the weakly nonlinear expansion is that convergence of the dynamics to those of the reduced equation has not been proven. We decide to apply center manifold and normal form theory in order to get around this difficulty; hence, we look for such an appropriate version of the theory that can be applied to DNFEs. The development of bifurcation theory for delayed functional differential equations was begun in [Hale 1993, Chapter 10], where the authors give a center manifold equation for finite dimensional delay equations where the neuronal activity is a vector and not a function of space as in the neural field equations. This work was later pushed further by Faria and co-authors in [Faria 1995]. Later, they extended their own work to the infinite-dimensional case for the class of equations that can be decomposed into a linear delay independent term and a nonlinear delay dependent term. One restriction, that the linear operator representing the delay independent terms can generate a compact C^0-semigroup [Faria 2001, Faria 2002], is not satisfied in our case and, therefore, we need to prove a center manifold result for our equations. We could prove a center manifold theorem as in [Faria 2002] but we find it more convenient to use the tools developed by Haragus and Iooss [Haragus 2010]. In contrast with [Hale 1993, Faria 2002], we choose a Hilbert space for the state space, which simplifies the computation of the spectral projectors and normal forms. In this way, we only have to identify a bifurcation point in the spectrum and then directly apply the corresponding normal forms from [Haragus 2010].

Our last comment concerns the importance of computing some particular normal forms. Many of the neural field models operate near a static bifurcation point and the bifurcation can be changed into a Fold-Hopf bifurcation point or a Bogdanov-Takens bifurcation point by the introduction of delays [Ben-Yishai 1995, Bressloff 2001b]. This has only been studied for point neurons in [Campbell 2008], which motivates further the need to compute these bifurcation points in order to understand the effect of the delays.

The chapter has the following structure. In section 4.3, we explain the mathematical setting to study the DNFEs. In section 4.4, we study the linearized equation around an equilibrium: we show how to compute the spectrum of the linearized operator and we also give the formula to compute the spectral projector. In section 4.5, we give bounds for the asymptotic stability of stationary cortical states. Finally, in section 4.6, we derive the center manifold theorem and the reduced equation, and give the general normal forms for the transcritical/pitchfork bifurcations.

The reader who is not interested in the mathematical details can go directly to section 4.4.1.1 for the study computation of the Hopf bifurcation curves where efficient techniques are proposed.

4.2 The neural field model

In this chapter, we consider the most general neural fields models that are studied in this Thesis, namely the delayed neural fields equations. They have been introduced in chapter 2 and satisfy

$$\begin{cases} \left(\frac{d}{dt}+l_i\right)V_i(t,\mathbf{r}) &= \sum_{j=1}^{p}\int_\Omega J_{ij}(\mathbf{r},\bar{\mathbf{r}})S\left[\sigma_j V_j\left(t-\tau_{ij}(\mathbf{r},\bar{\mathbf{r}}),\bar{\mathbf{r}}\right)-h_j\right]d\bar{\mathbf{r}} \\ & \qquad + \quad I_{ext,i}(\mathbf{r},t), \quad t\geq 0,\ 1\leq i,\ j\leq p \\ V_i(t,\mathbf{r}) &= \phi_i(t,\mathbf{r}), \quad t\in[-T,\ 0] \end{cases} \tag{4.1}$$

Recall that Ω is an open **bounded** set of $\mathbb{R}^p$. There are the nonlinear gains σ_i and the thresholds h_i. In particular, the delay function is given by the following formula:

$$\tau_{ij}(\mathbf{r},\bar{\mathbf{r}}) = D_{ij} + c_{ij}\left\|\mathbf{r}-\bar{\mathbf{r}}\right\|_2.$$

If the labels are not specified, it means that the delays are the same for every population:

$$\tau_{ij}(\mathbf{r},\bar{\mathbf{r}}) = D + \left\|\mathbf{r}-\bar{\mathbf{r}}\right\|_2.$$

4.3 Mathematical framework and notations

In the first part of this Thesis, we have considered neural field equations without delays. We have rewritten these equations as an abstract Cauchy problem in the space $\mathcal{F} = \mathrm{L}^2(\Omega,\mathbb{R}^\mathrm{p})$. Then, we have used the classical Cauchy-Lipschitz theorem (see proposition 3.2.2) to show existence and uniqueness of the solutions to the Cauchy problem. In order to be able to study delayed neural field equations, we

need to change the phase space $\mathrm{L}^2(\Omega, \mathbb{R}^p)$. Indeed, in order to give a meaning

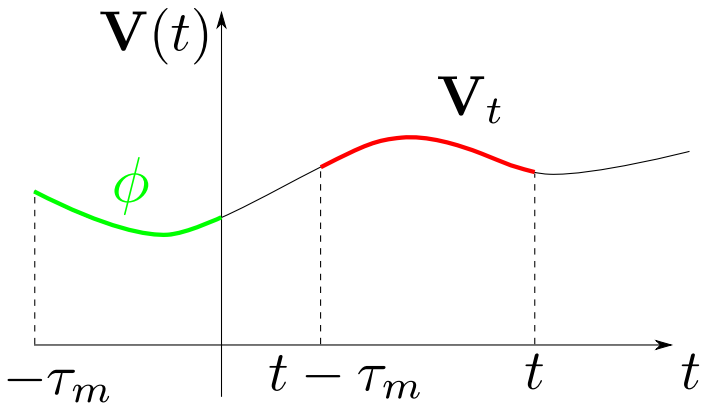

Figure 4.1: The history segment (reproduced from [Bátkai 2005]).

to (4.1), or at least to compute its right-hand side, we need to know the function $t \to \mathbf{V}(t, \cdot)$ on a time interval of length equal to

$$\tau_m \equiv \max_{1 \leq i,\, j \leq p,\ (\mathbf{r}, \bar{\mathbf{r}}) \in \overline{\Omega}^2} \tau_{ij}(\mathbf{r}, \bar{\mathbf{r}})$$

whereas for (3.1), only the membrane potential $\mathbf{V}(t, \cdot)$ at time t is necessary. The phase space of the equation (4.1) consists of spatio-temporal functions $\theta \to \mathbf{V}(t + \theta, \mathbf{r})$ where $\theta \in [-\tau_m, 0]$. This suggests the introduction of the following, classical, notation: $\mathbf{V}_t$ is the *history segment* $\mathbf{V}_t(\theta) = \mathbf{V}(t + \theta)$ with $\theta \in [-\tau_m, 0]$. In a way, delay differential equations are evolution equations for time-window vectors $\mathbf{V}_t$ (see figure 4.1). Hence, the phase space, also called the *history space*, is made of functions $\mathbf{V}_t$ from $[-\tau_m, 0]$ to $\mathcal{F}$. We have to specify the regularity of these functions. Intuitively, given an initial history function ϕ, (4.1) tells how the end of the history segment $\mathbf{V}_t(0) = \mathbf{V}(t)$ evolves but not how the whole segment $\mathbf{V}_t$ evolves. Let us start by rewriting (4.1) in a compact way using the notation for history segments:

$$\begin{cases} \dot{\mathbf{V}}(t) = -\mathbf{L}_0 \mathbf{V}(t) + \mathbf{L}_1 \mathbf{S}(\mathbf{V}_t) + \mathbf{I}_{ext}(t) \\ \mathbf{V}_0 = \psi \end{cases} \tag{4.2}$$

where $\mathbf{L}_1 : \phi \to \int_\Omega \mathbf{J}(\cdot, \bar{\mathbf{r}}) \phi(-\boldsymbol{\tau}(\cdot, \bar{\mathbf{r}}), \bar{\mathbf{r}}) d\bar{\mathbf{r}}$ and $\mathbf{S}(x) = [S(\sigma_1 x_1 - h_1), \cdots, S(\sigma_p x_p - h_p)]$. The sigmoid S has been defined in chapter 2. From a modeling viewpoint, it is natural to consider the space of continuous functions

$$\mathcal{C} \equiv C^0([-\tau_m, 0], \mathcal{F})$$

as the history space. The space $\mathcal{C}$ is convenient for proving existence and uniqueness of solutions of (4.2) but not for the study of the eigenspaces. Indeed, it is easier to work in a Hilbert space to take advantage of the scalar product properties.

Moreover, the ultimate goal of this chapter is to derive a normal form theory for the delayed neural field equations. This requires to write (4.2) as an abstract Cauchy problem:

$$\begin{cases} \dot{u} = \mathbf{A}u + \mathbf{R}(u) \\ \mathbf{A} \in \mathcal{L}(\mathcal{Z}, \mathcal{X}), \quad \mathbf{R} \in C^k(\mathcal{Z}, \mathcal{Y}),\ k \geq 2 \\ \mathcal{Z} \subset \mathcal{Y} \subset \mathcal{X} \quad \mathcal{Z}, \mathcal{Y}, \mathcal{X} \text{ Banach spaces,} \end{cases} \tag{4.3}$$

This is a differential equation for u which belongs to the history space $\mathcal{X}$. Hence u is a history segment. It is not possible to write a Cauchy problem for (4.2) with $\mathcal{X} = \mathcal{C}$, although one can find such a formulation with $\mathcal{X} = \mathcal{F} \times \mathcal{C}$ in [Faria 1995, Faria 2001]. Indeed, if we try to write a Cauchy problem $\dot{u} = \mathbf{A}_{\mathcal{C}} u$ for (4.2) in the linear case with $\mathbf{I}_{ext} = 0$ and $\mathbf{S}(x) = x$, we find (see [Hale 1993, Faria 1995, Wu 1996, Arino 2006]) that $\mathbf{A}_{\mathcal{C}}\phi = \frac{d}{d\theta}\phi$ and $\mathbf{A}_{\mathcal{C}}$[1] is defined[2] on $\mathcal{Z} = \left\{\phi \in C^1([-\tau_m, 0], \mathcal{F}) \mid \dot{\phi}(0) = -\mathbf{L}_0\phi(0) + \mathbf{L}_1\phi\right\}$. Hence the action of $\mathbf{A}_{\mathcal{C}}$ is independent of (4.2), it is a derivation, and equation (4.2) only enters in the definition of the domain $\mathcal{Z}$ of $\mathbf{A}_{\mathcal{C}}$. If we vary some parameters, for example in the definition of $\mathbf{L}_1$, $\mathcal{Z}$ changes and we are not able to apply the bifurcation tools from [Haragus 2010]. Extending the space from $\mathcal{X} = \mathcal{C}$ to $\mathcal{X} = \mathcal{F} \times \mathcal{C}$ solves this problem as shown in [Faria 1995].

Hence, we have seen that working in $\mathcal{X} = \mathcal{C}$ do not allow to apply the normal form theory. This is why we have to work in $\mathcal{X} = \mathcal{F} \times \mathcal{C}$.

However, in order to compute normal forms, we need to be able to compute projections. This task is easy to do in a Hilbert space by using the scalar product. This motivates the choice of the larger Hilbert space

$$\mathcal{X} = \mathcal{F} \times \mathrm{L}^2([-\tau_{\mathrm{m}}, 0], \mathcal{F})$$

for the *history space* for which a general expression of the spectral projectors is known. In order to write (4.2) as a Cauchy problem (4.3), we need to give the spaces $\mathcal{Y}, \mathcal{Z}$. This will be done later in section 4.6

The structure of our study is the following. We first prove existence and uniqueness of solutions of (4.2) in $\mathcal{C}$ but not in $\mathcal{X}$, we also give a bounded attractor set for these solutions in section 4.3.2. Recall that by doing so, we do not solve a Cauchy problem. Then, we study (4.2), linearized around an equilibrium $\mathbf{V}^f$, in the space $\mathcal{X}$. In particular, we give an estimate of the norm of the solutions of the linearized equation on $\mathcal{X}$ with the spectrum of $\mathbf{A}$ in section 4.4.1. Then, we use this estimate to prove the 'principle of linear stability', which states that the stability of the zero solution of the linearized equation in $\mathcal{X}$ implies the stability of $\mathbf{V}^f$ in $\mathcal{C}$. We also give conditions on the connectivity function $\mathbf{J}$ and the delay function $\boldsymbol{\tau}$ for which $\mathbf{V}^f$ is asymptotically stable in section 4.5.4. Then, we restate (4.2) as an abstract

[1] we add the subscript to avoid confusions
[2] *i.e.* has a domain $D(\mathbf{A}) = \mathcal{Z}$

Cauchy problem (4.3) for which we give a center manifold theorem in section 4.6. Hence, the least regular history segments for which we study (4.2) belong to $\mathcal{C}$. If we want to say more than asymptotic stability, for example, characterize the center manifold, then we have to restrict the study to more regular history segments in $\mathcal{Z}^{(q)} = \mathrm{L}^{\mathrm{q}}(\Omega, \mathbb{R}^{\mathrm{p}}) \times \mathrm{W}^{1,\mathrm{q}}(-\tau_{\mathrm{m}}, 0; \mathrm{L}^{\mathrm{q}}(\Omega, \mathbb{R}^{\mathrm{p}}))$.

4.3.1 Solutions of the nonlinear problem

We look at the existence of solutions of

$$\begin{cases} \dot{\mathbf{V}}(t) = -\mathbf{L}_0\mathbf{V}(t) + \mathbf{L}_1\mathbf{S}(\mathbf{V}_t) + \mathbf{I}_{ext}(t) \\ \mathbf{V}_0 = \phi \in \mathcal{C} \end{cases} \tag{4.4}$$

in the space $\mathcal{C}$ with $\|\phi\|_{\mathcal{C}} = \sup_{t\in[-\tau_m,0]} \|\phi(t)\|_{\mathcal{F}}$, which is the history space associated to equation (4.4). The proof is made of two parts. First we find a *mild* solution, *i.e.* a solution of the integral equation associated to (4.4). Then we prove that the *mild* solution is differentiable in time. This is the method used in [Travis 1974, Wu 1996, Arino 2006].

Proposition 4.3.1. *If the following assumptions are satisfied:*

1. $\mathbf{J} \in \mathrm{L}^2(\Omega^2, \mathbb{R}^{\mathrm{p}\times\mathrm{p}})$
2. *the external current* $\mathbf{I}_{ext} \in C^0(\mathbb{R}, \mathcal{F})$
3. $\boldsymbol{\tau} \in C^0(\bar{\Omega}^2, \mathbb{R}_+^{p\times p})$, $\max_{i,j,\ (\mathbf{r},\bar{\mathbf{r}})\in\bar{\Omega}^2} \tau_{ij}(\mathbf{r},\bar{\mathbf{r}}) = \tau_m < \infty$,

Then for any initial condition, $\phi \in \mathcal{C}$, there exists a unique solution $\mathbf{V} \in C^1(0,\infty;\mathcal{F}) \cap C^0(-\tau_m,\infty;\mathcal{F})$ to (4.4).

Proof. The mapping $f(t,\phi) = -\mathbf{L}_0\phi(0) + \mathbf{L}_1\mathbf{S}(\phi) + \mathbf{I}_{ext}(t)$ is the right-hand side of (4.4) and $f(t,\cdot) \in C^0(\mathcal{C},\mathcal{F})$. Indeed, $\mathbf{S}(\phi) \in \mathcal{F}$ because $\mathbf{S}$ is bounded and Ω is also bounded. It is easy to check that $f(t,\cdot)$ is Lipschitz continuous on $\mathcal{C}$ because the linear operator

$$\begin{cases} \mathbf{L}_1 : \mathcal{C} \longrightarrow \mathcal{F} \\ \boldsymbol{\phi} \to \int_\Omega \mathbf{J}(\cdot,\bar{\mathbf{r}})\boldsymbol{\phi}(\bar{\mathbf{r}}, -\boldsymbol{\tau}(\cdot,\bar{\mathbf{r}}))d\bar{\mathbf{r}} \end{cases}$$

is continuous with $|||\mathbf{L}_1||| \le \|\mathbf{J}\|_{\mathbf{L}^2(\Omega^2,\mathbb{R}^{p\times p})}$. If we write $\mathbf{T}_0(t) = e^{-\mathbf{L}_0 t}$, we find that $|||\mathbf{T}_0(t)|||_{\mathcal{C}} \le e^{\omega t}$ with $\omega = -\min_i l_i$. Using the variation of constant formula, (4.4) is equivalent to:

$$\begin{cases} \mathbf{V}(t) = \mathbf{T}_0(t)\phi(0) + \int_0^t \mathbf{T}_0(t-s)f(s,\mathbf{V}_s)ds \quad t \ge 0 \\ \mathbf{V}_0 = \phi \end{cases} \tag{4.5}$$

We apply [Wu 1996, theorem 2.1.1.] to find the unique solution $\mathbf{V} \in C^0([0,\infty],\mathcal{C})$ to the previous equation. As $t \to \mathbf{V}(t) \in C^0([-\tau_m,\infty],\mathcal{F})$, we apply lemma 2.1. in [Hale 1993] stating that $t \to \mathbf{V}_t$ is in $C^0([0,\infty],\mathcal{C})$. Hence $t \to f(t,\mathbf{V}_t) \in C^0([0,\infty],\mathcal{F})$. This implies that $t \to \int_0^t \mathbf{T}(t-s)f(s,\mathbf{V}_s)ds$ is in $C^1([0,\infty],\mathcal{F})$, *idem* for $t \to \mathbf{T}(t)\phi(0)$. We have shown that $\mathbf{V} \in C^1([0,\infty),\mathcal{F}) \cap C^0([-\tau_m,\infty),\mathcal{F})$. □

4.3.2 Boundedness of solutions in $\mathcal{C}$

A valid model of neural network should only feature bounded membrane potentials. We find a bounded attracting set in the spirit of our previous work with non-delayed neural mass equations. The proof is almost the same as in proposition 3.2.3 but some care has to be taken because of the delays.

Theorem 4.3.2. *All the trajectories of the equation (4.4) are ultimately bounded by the same constant R (see the proof) if $I \equiv \max_{t\in\mathbb{R}^+} \|\mathbf{I}_{ext}(t)\|_{\mathcal{F}} < \infty$.*

Proof. Let us define $f : \mathbb{R} \times \mathcal{C} \to \mathbb{R}^+$ by

$$f(t, \mathbf{V}_t) \overset{\text{def}}{=} \langle -\mathbf{L}_0\mathbf{V}_t(0) + \mathbf{L}_1\mathbf{S}(\mathbf{V}_t) + \mathbf{I}_{ext}(t), \mathbf{V}(t)\rangle_{\mathcal{F}} = \frac{1}{2}\frac{d\|\mathbf{V}\|^2_{\mathcal{F}}}{dt}.$$

We note $l = \min_{i=1\cdots p} l_i$ and from lemma B.2.1:

$$f(t, \mathbf{V}_t) \leq -l\|\mathbf{V}(t)\|^2_{\mathcal{F}} + (\sqrt{p|\Omega|} \cdot |||\mathbf{J}|||_{\mathcal{F}} + I)\|\mathbf{V}(t)\|_{\mathcal{F}}.$$

Thus, if $\|\mathbf{V}(t)\|_{\mathcal{F}} \geq 2\frac{\sqrt{p|\Omega|}\cdot|||\mathbf{J}|||_{\mathcal{F}}+I}{l} \overset{\text{def}}{=} R$, $f(t, \mathbf{V}_t) \leq -\frac{lR^2}{2} \overset{\text{def}}{=} -\delta < 0$.

Let us show that the open ball of $\mathcal{F}$ of center 0 and radius R, B_R, is stable under the dynamics of equation (4.4). We know that $\mathbf{V}(t)$ is defined for all $t \geq 0$s and that $f < 0$ on ∂B_R, the boundary of B_R. We consider three cases for the initial condition $\mathbf{V}_0$.

If $\|\mathbf{V}_0\|_{\mathcal{C}} < R$ and set $T = \sup\left\{t \,|\, \forall s \in [0, t], \mathbf{V}(s) \in \overline{B}_R\right\}$. Suppose that $T \in \mathbb{R}$, then $\mathbf{V}(T)$ is defined and belongs to $\overline{B}_R$, the closure of B_R, because $\overline{B}_R$ is closed, in effect to ∂B_R. We also have $\frac{d}{dt}\|\mathbf{V}\|^2_{\mathcal{F}}|_{t=T} = f(T, \mathbf{V}_T) \leq -\delta < 0$ because $\mathbf{V}(T) \in \partial B_R$. Thus we deduce that for $\varepsilon > 0$ and small enough, $\mathbf{V}(T + \varepsilon) \in \overline{B}_R$ which contradicts the definition of T. Thus $T \notin \mathbb{R}$ and $\overline{B}_R$ is stable.

Because $f < 0$ on ∂B_R, $\mathbf{V}(0) \in \partial B_R$ implies that $\forall t > 0,\ \ \mathbf{V}(t) \in B_R$.

Finally we consider the case $\mathbf{V}_0 \in \complement\overline{B}_R$. Suppose that $\forall t > 0,\ \mathbf{V}(t) \notin \bar{B}_R$, then $\forall t > 0,\ \frac{d}{dt}\|\mathbf{V}\|^2_{\mathcal{F}} \leq -2\delta$, thus $\|\mathbf{V}(t)\|_{\mathcal{F}}$ is monotonically decreasing and reaches the value of R in finite time when $\mathbf{V}(t)$ reaches ∂B_R. This contradicts our assumption. Thus $\exists T > 0 \,|\, \mathbf{V}(T) \in B_R$. □

4.4 Linear analysis

In the Introduction, we have emphasized the need for the study of the stability of stationary cortical states. Let us consider an equilibrium $\mathbf{V}^f$ which has been computed for example with tools from [Ermentrout 1980, Bressloff 2000, Bressloff 2001b, Coombes 2005b, Veltz 2010] or in part II. We recall that this equilibrium needs not be constant in space. How stable to perturbations is this cortical state? This is generally studied by looking at a perturbation of the form $\mathbf{U} = \mathbf{V} - \mathbf{V}^f$ and studying the linearized equation satisfied by $\mathbf{U}$:

$$\begin{cases} \dot{\mathbf{U}}(t) = -\mathbf{L}_0\mathbf{U}(t) + \tilde{\mathbf{L}}_1\mathbf{U}_t \equiv \mathbf{L}\mathbf{U}_t \\ \mathbf{U}_0 = \phi \in \mathcal{C} \end{cases} \tag{4.6}$$

where $\tilde{\mathbf{L}}_1 : \phi \to \int_\Omega \mathbf{J}(\cdot,\bar{\mathbf{r}}) D\mathbf{S}(\mathbf{V}^f(\bar{\mathbf{r}}))\phi(\bar{\mathbf{r}}, -\boldsymbol{\tau}(\cdot,\bar{\mathbf{r}}))\, d\bar{\mathbf{r}}$ (this operator will be more properly defined in section 4.4.1). Looking for exponential perturbations like $\mathbf{U}(t,\mathbf{r}) = e^{\lambda t}\mathbf{U}(\mathbf{r})$ in (4.6), we find that $\mathbf{U}$ solves the eigenvalue problem

$$(\lambda \mathrm{Id} + \mathbf{L}_0)\,\mathbf{U} = \mathbf{J}(\lambda)\mathbf{U} \tag{4.7}$$

where $\mathbf{J}(\lambda)$ is the compact operator (being a Hilbert-Schmidt operator)

$$\begin{cases} \mathbf{J}(\lambda) : \mathcal{F} \longrightarrow \mathcal{F} \\ \mathbf{U} \to \int_\Omega \mathbf{J}(\cdot,\bar{\mathbf{r}}) D\mathbf{S}(\mathbf{V}^f(\bar{\mathbf{r}})) e^{-\lambda\boldsymbol{\tau}(\cdot,\bar{\mathbf{r}})}\mathbf{U}(\bar{\mathbf{r}})\, d\bar{\mathbf{r}} \end{cases} \tag{4.8}$$

A stationary state is linearly stable if any solution $(\lambda, \mathbf{U})$ of (4.7) satisfies $\Re\lambda < 0$. Notice that because of the delays, the eigenvalue λ appears in a nonlinear way in the right-hand side of (4.7). The eigenproblem without delays would have been:

$$(\lambda \mathrm{Id} + \mathbf{L}_0)\,\mathbf{U} = \mathbf{J}(0)\mathbf{U}$$

The difficulty of the linear stability analysis lies in this complicated transcendental eigenvalue equation (4.7) for which we show an elegant solution in the next section. But before solving the eigenvalue equation, we make our qualitative explanation of the stability mathematically rigorous in the next section. Then we compute a spectral projector and find a decomposition of the history space $\mathcal{X}$ according to the generalized eigenspaces in order to prepare the application, to the neural field equations, of the center manifold theorem given in [Haragus 2010].

4.4.1 Semigroup properties from the spectral study

As we have explained earlier, we look at the equation (4.6) in the larger space $\mathcal{X} = \mathcal{F} \times \mathrm{L}^2(-\tau_\mathrm{m}, 0; \mathcal{F})$ with

$$\left\langle \begin{bmatrix} x \\ \phi \end{bmatrix}, \begin{bmatrix} y \\ \psi \end{bmatrix} \right\rangle_{\mathcal{X}} = \langle x, y\rangle_{\mathcal{F}} + \int_{-\tau_m}^{0} \langle \phi(s), \psi(s)\rangle_{\mathcal{F}}\, ds$$

We note π_1, π_2 the canonical projections of $\mathcal{X}$ on $\mathcal{F}$ and $\mathrm{L}^2(-\tau_\mathrm{m}, 0; \mathcal{F})$: $\pi_1 \begin{bmatrix} x \\ \phi \end{bmatrix} = x$, $\pi_2 \begin{bmatrix} x \\ \phi \end{bmatrix} = \phi$. The choice of $\mathcal{X}$ is motivated by the fact that $\mathcal{X}$ is a Hilbert space which simplifies the computation of the spectral projector. This is especially useful when one wants to compute normal forms as we do later. Indeed, in order to compute the spectral projectors for delay differential equations, [Hale 1993, Faria 1995, Arino 2006] introduced a quantity called the *bilinear product*. However, this quantity is difficult to extend to the case where $\mathcal{F}$ is a Banach space (see [Arino 2006]) whereas it appears naturally in the Hilbert space setting. Next, we rewrite the problem (4.6) in the space $\mathcal{X}$. Note that we need to define

two functions for the initial condition of (4.9) because $\phi(0)$ has no meaning for $\phi \in \mathrm{L}^2(-\tau_m, 0; \mathcal{F})$. Hence we write:

$$\begin{cases} \dot{\mathbf{U}}(t) = -\mathbf{L}_0\mathbf{U}(t) + \tilde{\mathbf{L}}_1\mathbf{U}_t \equiv \mathbf{L}\mathbf{U}_t \\ \mathbf{U}_0 = \phi \in \mathrm{L}^2(-\tau_\mathrm{m}, 0; \mathcal{F}),\ \mathbf{U}(0) = \mathrm{x} \in \mathcal{F} \end{cases} \tag{4.9}$$

where the linear operator $\tilde{\mathbf{L}}_1$ is given by

$$\begin{cases} \tilde{\mathbf{L}}_1 : W^{1,2}(-\tau_m, 0; \mathcal{F}) \longrightarrow \mathcal{F} \\ \phi \to \int\limits_\Omega \mathbf{J}(\cdot, \bar{\mathbf{r}}) D\mathbf{S}(\mathbf{V}^f(\bar{\mathbf{r}}))\phi(\bar{\mathbf{r}}, -\boldsymbol{\tau}(\cdot, \bar{\mathbf{r}}))\, d\bar{\mathbf{r}} \end{cases}$$

and $W^{1,2}(-\tau_m, 0; \mathcal{F})$ is the Sobolev space of functions with values in $\mathcal{F}$. This operator is continuous because of lemma[3] B.3.1.

Remark 19. *In this section, we have used the space* $\mathrm{L}^2(-\tau_\mathrm{m}, 0; \mathcal{F})$ *(resp.* $\mathrm{W}^{1,2}(-\tau_\mathrm{m}, 0; \mathcal{F})$*) of vector valued square integrable functions (resp. vector valued functions of the Sobolev space) without definition. More precisely, the Lebesgue-Bochner space*[4] $\mathrm{L}^\mathrm{p}(-\tau_\mathrm{m}, 0; \mathcal{F})$, $1 \leq \mathrm{p} < \infty$ *is made of the set of all equivalence classes of measurable functions*[5] $\phi : [-\tau_m, 0] \to \mathcal{F}$ *such that* $\|\phi\|_p \equiv \left(\int_{-\tau_m}^0 \|\phi(\theta)\|_{\mathcal{F}}^p\, d\theta\right)^{\frac{1}{p}} < \infty$. *We define the Sobolev space*[6] *as follow:* $\mathrm{W}^{1,\mathrm{p}}(-\tau_\mathrm{m}, 0; \mathcal{F}) \equiv \left\{\phi \in \mathrm{L}^\mathrm{p}(-\tau_\mathrm{m}, 0; \mathcal{F}) \mid \exists \psi \in \mathrm{L}^\mathrm{p}(-\tau_\mathrm{m}, 0; \mathcal{F}) \text{ such that } \phi(\theta) = \phi(-\tau_\mathrm{m}) + \int_{-\tau_\mathrm{m}}^\theta \psi(\mathrm{s})\mathrm{ds}\right\}$. *Then* $\frac{d}{d\theta}\phi = \psi$ *for* $\psi \in \mathrm{W}^{1,\mathrm{p}}(-\tau_\mathrm{m}, 0; \mathcal{F})$ *and* $\|\phi\|_{1,p} \equiv \|\phi\|_p + \left\|\frac{d}{d\theta}\phi\right\|_p$.

Note that $\mathbf{L}_0$ is defined on $\mathrm{L}^2(-\tau_\mathrm{m}, 0; \mathcal{F})$ whereas $\tilde{\mathbf{L}}_1$ is defined on $W^{1,2}(-\tau_m, 0; \mathcal{F})$. We call a classical solution of (4.9) a function $\mathbf{U} \in C^0([-\tau_m, \infty), \mathcal{F}) \cap C^1([0, \infty), \mathcal{F})$ such that $\mathbf{U}_t \in W^{1,2}(-\tau_m, 0; \mathcal{F})$ and $\mathbf{U}$ satisfies (4.9). To study (4.9), let us introduce the abstract Cauchy problem

$$\begin{cases} \dot{u} = \mathbf{A}u \\ u(0) = u_0 \in \mathcal{X} \end{cases} \tag{4.10}$$

where

$$\mathbf{A} \equiv \begin{bmatrix} -\mathbf{L}_0 & \tilde{\mathbf{L}}_1 \\ 0 & \frac{d}{d\theta} \end{bmatrix} \tag{4.11}$$

with domain

$$D(\mathbf{A}) = \left\{ \begin{bmatrix} x \\ \phi \end{bmatrix} \in \mathcal{F} \times W^{1,2}(-\tau_m, 0; \mathcal{F}),\ \phi(0) = x \right\}.$$

[3] Modulo the change of variable $\mathbf{J}D\mathbf{S} \to \mathbf{J}$.

[4] it is a Banach space

[5] such that $\theta \to \|\phi(\theta)\|_{\mathcal{F}}$ is integrable and $\int_{-\tau_m}^0 \|\phi(\theta)\|_{\mathcal{F}}\, d\theta < \infty$. It is called Bochner integrable (see for example [Yosida 1980, Dunford 1988]).

[6] it is a Banach space

From [Bátkai 2005], it is known that (4.9) and (4.10) are equivalent: every integral/classical solution of (4.9) is a mild/strong solution of (4.10) and conversely. This allows to apply the semigroup theory to (4.10) in order to study (4.9). More precisely, following [Bátkai 2005][theorem 4.23] (see also [Engel 2001, Arino 2006, Hale 1993, Wu 1996, Diekmann 1995] in a different functional setting), $\mathbf{A}$ generates a strongly continuous semigroup $(\mathbf{T}(t))_{t\geq 0}$ on $\mathcal{X}$ for which $\mathbf{A}$ is the infinitesimal generator. Every solution of (4.10) is given by $\mathbf{T}(t)u_0$: if $u_0 \in D(\mathbf{A})$, then $\mathbf{T}(t)u_0$ is a strong solution of (4.10). Hence, any solution $\mathbf{U}$ of (4.9) is given by $\mathbf{U}(t) = \pi_1 \mathbf{T}(t)u_0$.

Let us turn to the study of the spectral properties: we want to find an estimate of $\|\mathbf{U}(t)\|_{\mathcal{F}}$ with the spectrum $\Sigma(\mathbf{A})$ of $\mathbf{A}$, *i.e.* to link estimates of the semigroup $\mathbf{T}$ to the spectrum of $\mathbf{A}$. This is usually achieved using the Spectral Mapping Theorem (see [Engel 2001, Bátkai 2005] and theorem B.1.4). Recall (see [Wu 1998, Hale 1993, Engel 2001, Bátkai 2005, Veltz 2011b]) that λ is in the spectrum $\Sigma(\mathbf{A})$ of $\mathbf{A}$ if and only if the operator

$$\Delta(\lambda) \equiv \lambda \mathrm{Id} + \mathbf{L}_0 - \mathbf{J}(\lambda) \in \mathcal{L}(\mathcal{F}, \mathcal{F}) \tag{4.12}$$

is not invertible and that u is an eigenvector of $\mathbf{A}$ if and only if $u(\theta, \mathbf{r}) = \begin{bmatrix} \mathbf{U}(\mathbf{r}) \\ e^{\lambda\theta}\mathbf{U}(\mathbf{r}) \end{bmatrix}$ with $\mathbf{U} \in \ker \Delta(\lambda)$. Hence the *characteristic values* (also written CV, see definition B.1.10) of $\lambda \to \Delta(\lambda)$ are the eigenvalues of $\mathbf{A}$, they are solutions of (4.7). We denote the set of eigenvalues by $\Sigma_p(\mathbf{A})$, the point spectrum. In order to characterize the spectrum $\Sigma(\mathbf{A})$, we find it convenient to split it into the essential spectrum $\Sigma_{ess}(\mathbf{A})$ and the point spectrum. As we intend to use the theory of Kato in [Kato 1995] to study the spectrum, we chose the definition[7] of Kato for the essential spectrum, *i.e.* $\Sigma_{ess}(\mathbf{A}) \equiv \{\lambda \in \mathbb{C} | \lambda \mathrm{Id} - \mathbf{A} \text{ is not semi-Fredholm}\}$. This definition is different from the one adopted in [Engel 2001, Bátkai 2005] which is $\Sigma_{ess,\ Engel}(\mathbf{A}) \equiv \{\lambda \in \mathbb{C} | \lambda \mathrm{Id} - \mathbf{A} \text{ is not Fredholm}\}$. We state a useful lemma which links the spectral properties of $\mathbf{A}$ to the spectral properties of $-\mathbf{L}_0 + \mathbf{J}(\lambda) \in \mathcal{L}(\mathcal{F}, \mathcal{F})$.

Lemma 4.4.1. $\lambda \in \Sigma_{ess}(\mathbf{A}) \Leftrightarrow \lambda \in \Sigma_{ess}(-\mathbf{L}_0 + \mathbf{J}(\lambda))$

Proof. Straightforward adaptation of [Bátkai 2005, lemma 3.20] where it is shown that $\lambda \in \Sigma_{ess,\ Engel}(\mathbf{A}) \Leftrightarrow \lambda \in \Sigma_{ess,\ Engel}(-\mathbf{L}_0 + \mathbf{J}(\lambda))$ □

Let us summarize the properties of the spectrum $\Sigma(\mathbf{A})$ of $\mathbf{A}$:

Lemma 4.4.2. $\mathbf{A}$ *satisfies the following properties:*

1. *its essential spectrum is:* $\Sigma_{ess}(\mathbf{A}) = \Sigma(-\mathbf{L}_0)$
2. $\Sigma(\mathbf{A})$ *is at most countable.*
3. $\Sigma(\mathbf{A}) = \Sigma(-\mathbf{L}_0) \cup CV$. *These sets are possibly non-disjoint.*

[7] see definitions B.1.7 and B.1.8

4. *For* $\lambda \in \Sigma(\mathbf{A}) \setminus \Sigma(-\mathbf{L}_0)$, λ *is an isolated eigenvalue and the generalized eigenspace* $E_\lambda(\mathbf{A}) \equiv \cup_k \ker(\lambda \mathrm{Id} - \mathbf{A})^k$ *is finite dimensional. Hence* $\Sigma(\mathbf{A}) \setminus \Sigma(-\mathbf{L}_0) \subset \Sigma_p(\mathbf{A})$.

5. *Card* $\Sigma(\mathbf{A}) \cap \{\lambda \in \mathbb{C},\ \Re\lambda > -l\} < \infty$ *where* $l = \min_i l_i$.

Proof.

1. From lemma 4.4.1 $\lambda \in \Sigma_{ess}(\mathbf{A}) \Leftrightarrow \lambda \in \Sigma_{ess}(-\mathbf{L}_0 + \mathbf{J}(\lambda))$. Then, we apply [Kato 1995, Theorem IV.5.26]. It shows that the essential spectrum does not change under compact perturbation. As $\mathbf{J}(\lambda) \in \mathcal{L}(\mathcal{F})$ is compact, we find $\Sigma_{ess}(-\mathbf{L}_0 + \mathbf{J}(\lambda)) = \Sigma_{ess}(-\mathbf{L}_0)$. Let us show that $\Sigma_{ess}(-\mathbf{L}_0) = \Sigma(-\mathbf{L}_0)$. The assertion "$\subset$" is trivial. Now if $\lambda \in \Sigma(-\mathbf{L}_0)$, for example $\lambda = -l_1$, then $\lambda\mathrm{Id} + \mathbf{L}_0 = diag(0, -l_1 + l_2, ...)$. Then $\mathcal{R}(\lambda\mathrm{Id} + \mathbf{L}_0)$ is closed and $\mathrm{L}^2(\Omega, \mathbb{R}) \times \{0\} \times ... \times \{0\} \subset \mathcal{N}(\lambda\mathrm{Id} + \mathbf{L}_0)$. Hence $dim\mathcal{N}(\lambda\mathrm{Id} + \mathbf{L}_0) = \infty$. Also $\mathcal{R}(\lambda\mathrm{Id} + \mathbf{L}_0) = \{0\} \times \mathrm{L}^2(\Omega, \mathbb{R}^{\mathrm{p}-1})$, hence $codim\mathcal{R}(\lambda\mathrm{Id} + \mathbf{L}_0) = \infty$. Hence, according to definition B.1.9, $\lambda \in \Sigma_{ess}(-\mathbf{L}_0)$.

2-4. The assertions 2-4 are direct consequences of [Kato 1995, Theorem IV.5.33].

5. If $\lambda = \rho + i\omega \in \Sigma(\mathbf{A})$ and $\rho > -l$, then λ is a CV *i.e.* $\mathcal{N}(\mathrm{Id} - (\lambda\mathrm{Id} + \mathbf{L}_0)^{-1}\mathbf{J}(\lambda)) \neq \emptyset$ stating that $1 \in \Sigma_p((\lambda\mathrm{Id} + \mathbf{L}_0)^{-1}\mathbf{J}(\lambda))$. But $|||(\lambda\mathrm{Id} + \mathbf{L}_0)^{-1}\mathbf{J}(\lambda)|||_{\mathcal{F}} \leq |||(\lambda\mathrm{Id} + \mathbf{L}_0)^{-1}|||_{\mathcal{F}} \cdot |||\mathbf{J}(\lambda)|||_{\mathcal{F}} \leq \frac{1}{\sqrt{\omega^2 + (\rho+l)^2}}|||\mathbf{J}(\lambda)|||_{\mathcal{F}} \leq \frac{1}{2}$ for λ big enough since $|||\mathbf{J}(\lambda)|||_{\mathcal{F}}$ is bounded. Hence, for λ large enough $1 \notin \Sigma_p((\lambda\mathrm{Id} + \mathbf{L}_0)^{-1}\mathbf{J}(\lambda))$, which holds by the spectral radius inequality. This relationship states that the CVs λ satisfying $\Re\lambda > -l$ are located in a bounded set of the right part of $\mathbb{C}$; given that the elements of $\Sigma(\mathbf{A}) \setminus \Sigma(-\mathbf{L}_0)$ are isolated, there are a finite number of them.

□

As an example, Figure 4.2 shows the first 200 eigenvalues computed for a very simple one-dimensional model. We notice that they accumulate at $\lambda = -1$ which is the essential spectrum. These eigenvalues have been computed using the method in [Jarlebring 2010], a very efficient method for computing the CVs which is described in the next chapter. We have shown that the CVs are almost all, *i.e.* except for possibly a finite number of them, located on the left part of the complex plane. This indicates that the unstable manifold is always finite dimensional for the models we are considering here. The last result of this section is devoted to the regularity of the semigroup and an estimate of its operator norm. This is useful in order to prove stability results.

Lemma 4.4.3. *If* $\mathbf{J} \in \mathrm{L}^\infty(\Omega^2, \mathbb{R}^{\mathrm{p}})$, *then the semigroup* $(\mathbf{T}(t))_{t\geq 0}$ *on* $\mathcal{X}$ *satisfies the following properties:*

1. $(\mathbf{T}(t))_{t\geq 0}$ *is norm continuous*[8] *on* $\mathcal{X}$ *for* $t > \tau_m$.

[8] see definition B.1.3

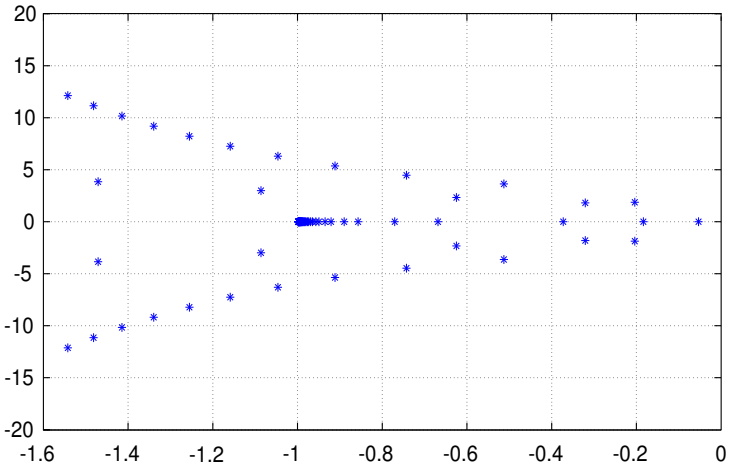

Figure 4.2: Plot of the first 200 eigenvalues of $\mathbf{A}$ in the scalar case ($p = 1,\ d = 1$) and $\mathbf{L}_0 = \mathrm{Id},\ J(x) = -1 + 1.5\cos(2x)$. The delay function $\tau(x)$ is the π periodic saw-like function shown in figure 5.2. Notice that the eigenvalues accumulate at $\lambda = -1$.

2. *Let us define*[9] $\varepsilon \equiv \max(-l, \varepsilon_p)$, $\varepsilon_p \equiv \max \Re\left(\Sigma(\mathbf{A}) \cap \{\lambda \in \mathbb{C},\ \Re\lambda > -l\}\right)$ *and* $l = \min_i l_i$. *If* $\varepsilon < 0$, *then* $\exists M \geq 1$ *such that* $|||\mathbf{T}(t)|||_{\mathcal{X}^{(2)}} \leq Me^{\varepsilon t/2},\ \forall t \geq 0$.

Proof.

1. This is consequence of lemma B.3 and [Bátkai 2005, prop.4.3].

2. We use the result in [Engel 2001, chapter 4, theorem 3.10 and corollary 3.12] for eventually norm continuous semigroups (see definition B.1.3 in appendix B.1) recalled in theorem B.1.4 which links the growth bound of the semigroup to the spectrum of $\mathbf{A}$:

$$\inf\left\{w \in \mathbb{R} : \exists M_w \geq 1 \text{ such that } |||\mathbf{T}(t)|||_{\mathcal{X}} \leq M_w e^{wt},\ \forall t \geq 0\right\} = \sup \Re\Sigma(\mathbf{A}). \tag{4.13}$$

From[10] lemma B.3.2 and [Bátkai 2005][proposition 4.3], the semigroup $(\mathbf{T}(t))$ is eventually norm continuous so we can apply theorem B.1.4. From the previous lemma 4.4.2, we conclude the proof.

□

This lemma states that the asymptotic stability of $\mathbf{U} = 0$ in (4.9) is equivalent to the condition:

$$\max \Re\left(\Sigma(\mathbf{A}) \cap \{\lambda \in \mathbb{C},\ \Re\lambda > -l\}\right) < 0$$

The fact that $\mathbf{V}^f$ is asymptotically stable in $\mathcal{C}$ under the same condition will be examined in section 4.5. Computing the eigenvalues of $\mathbf{A}$ is a difficult task in general.

[9] where we set $\max \emptyset \equiv -\infty$.

[10] Modulo the change of variable $\mathbf{J}D\mathbf{S} \to \mathbf{J}$.

In the next two sections, we present two analytical formulas for the Hopf bifurcation curves in the parameter plane (D, c) (see section 4.2). The main argument for these formulae is that we can estimate the rightmost eigenvalue in some cases. We will come back to the general numerical computation of the eigenvalues in the next chapter.

4.4.1.1 Hopf curve in the case of constant delays $c = 0$

We restrict our study to the case where $D_{ij} = D, l_i = l, c = 0$. This case has been studied in [Roxin 2005, Roxin 2011] where the authors show that constant delays have to be introduced in neural field equations in order to explain oscillatory patterns seen in spiking networks. Notice that in this case, the eigenvalue problem reads

$$(\lambda + l)\,\mathbf{U} = e^{\lambda D}\mathbf{J}(0)\mathbf{U} \tag{4.14}$$

If we write $J_n,\ n \in \mathbb{N}$, the eigenvalues of $\mathbf{J}(0)$, then the previous equation becomes $\lambda + l = e^{-\lambda D} J_n$ which is solved using the different branches W_k of the Lambert[11] function (see [Corless 1996], it is tabulated in *Matlab* and *Maple*) by:

$$\lambda_{k,n} = \frac{1}{D} W_k\left(De^{lD}J_n\right) - l,\ k \in \mathbb{Z},\ n \in \mathbb{N} \tag{4.15}$$

This expression was not reported in [Roxin 2005, Roxin 2011] whereas it makes the linear analysis entirely analytical. The main result of this section is:

Proposition 4.4.4. *The following statements are true:*

1. $0 \in \Sigma(\mathbf{A})$ *if and only if* $\exists n \mid l = J_n$, *this condition does not depend on* D.
2. *The rightmost characteristic value belongs to the sub-sequence* $(\lambda_{0,n})_n$.
3. *A necessary and sufficient condition for the rightmost characteristic value of* $\mathbf{A}$ *to be purely imaginary and nonzero is the existence of an integer* n_0 *such that* $l \leq |J_{n_0}|$ *and* $\arccos\left(\frac{l}{|J_n|}\right) \leq |\arg J_n|$. *In this case the corresponding critical delay* D_{n_0} *and the eigenvalue* $i\omega_{n_0}$ *satisfy:*

$$lD_{n_0} = \frac{1}{\sqrt{\left(\frac{|J_{n_0}|}{l}\right)^2 - 1}}\left(|\arg J_{n_0}| - \arccos\left(\frac{l}{|J_{n_0}|}\right)\right), \quad \omega_{n_0} = l\sqrt{\left(\frac{|J_{n_0}|}{l}\right)^2 - 1}$$

Proof.

1. Set $\lambda = 0$ in (4.7) in order to obtain the result.
2. We first quote a result (see [Shinozaki 2007]): if we define $BC = \left\{z \in \mathbb{C}, \Re z \leq -e^{-1}, \Im z = 0\right\}$, then:

$$\max_k \Re W_k(z) = \begin{cases} \Re W_0(z),\ z \notin BC \\ \Re W_0(z) = \Re W_{-1}(z),\ z \in BC \end{cases} \tag{4.16}$$

[11] It is any function W such that $W(z)e^{W(z)} = z,\ z \in \mathbb{C}$.

In the latter case, there are two rightmost roots corresponding to W_0 and W_{-1}, one of which serves as the critical root for stability because $\Re W_0(z) = \Re W_{-1}(z)$. We solve the characteristic equation $\lambda + l = e^{-\lambda D} J_n$ with the help of the Lambert function: $\lambda_{k,n} = \frac{1}{D} W_k\left[De^{lD}J_n\right] - l = l\left(\frac{W_k\left[De^{lD}J_n\right]}{lD} - 1\right)$. According to (4.16), the rightmost characteristic value corresponds to $k = 0$. We look for conditions such that $\lambda_{0,n}$ is purely imaginary. Write $X = lDe^{lD}$, *i.e.* $lD = W_0(X)$, then $\lambda_{0,n} = l\left(\frac{W_0[XJ_n/l]}{W_0(X)} - 1\right)$ and look for X such that $\lambda_{0,n}$ is purely imaginary. From lemma B.4.1, there is a unique solution $X_0 = W_0(lD)$ such that $W_0(X_0) = \Re W_0\left(X_0 J_n\right)$ if and only if $l \leq |J_n|$ and $\arccos\left(\frac{l}{|J_n|}\right) \leq |\arg J_n|$. Then $lD_n = \frac{1}{\sqrt{|J_n/l|^2 - 1}}\left(|\arg J_n| - \arccos\left(\frac{l}{|J|}\right)\right)$ and $\omega_n = l\sqrt{\left(\frac{|J_n|}{l}\right)^2 - 1}$

□

In the case the eigenvalue J_n is real, we find that the condition for the existence of a critical delay D_n is $J_n \leq -l$. The critical delay is then given by

$$lD_n = \frac{1}{\sqrt{\left(\frac{|J_n|}{l}\right)^2 - 1}}\left(\pi - \arccos\left(\frac{l}{|J_n|}\right)\right)$$

Also, from the above expression, if $J_p < J_n \leq -l$, then $D_p < D_n$.

Similar expressions were found for a network of neurons on a ring in [Campbell 2005]. This proposition provides some biological insights: if we analyze a network without delays, we can only make it oscillate (through a Hopf mechanism) if the inhibition is strong enough, that is $J_n \leq -l$ for some n. This result, together with the bifurcation analysis exposed in [Roxin 2011], gives a fairly complete overview of what can happen in neural field equations with constant delays.

Remark 20.Note that for a homogeneous[12] *connectivity and a space constant equilibrium* $\mathbf{V}^f$*, the* J_n *are given by the Fourier transform of the connectivity.*

Remark 21.These results are straightforward to generalize for more general intrinsic dynamics like $\left(\frac{d}{dt} + l_i\right)^2$.

4.4.1.2 Hopf curve in the case of space dependent delays

We now turn to the main result of this section. As in the previous section, we assume $D_{ij} = D, l_i = l$ but this time $c \neq 0$. This problem has been studied in [Coombes 2007, Venkov 2007, Bressloff 2008]. Our approach is the following: instead of looking for parameters which produce purely imaginary eigenvalues $\lambda = i\omega$, we plug $\lambda = i\omega$ into (4.7) and vary ω. This provides naturally a parametrization of the Hopf curve. Hence, we do not need to look for this curve in the parameter plane, we are already there. Notice that it works for general delay functions τ. In

[12] *i.e.* convolutional

practice the following result gives the rightmost Hopf curves in the parameter plane (D, c) (see also [Veltz 2011a]):

Proposition 4.4.5. *Suppose that the spectrum of* $-l \cdot \mathrm{Id} + \mathbf{J}(0)$ *has negative real part. Consider the integral operator*[13] $\mathbf{J}(z)$ *whose kernel is given by* $J_{qr}(\mathbf{r}, \bar{\mathbf{r}}) DS(V_r^f(\bar{\mathbf{r}})) e^{-z\|\mathbf{r}-\bar{\mathbf{r}}\|_2}$, $z \in \mathbb{C}$, $q, r = 1 \cdots p$. *Then* $\mathbf{J}(iy)$, $y > 0$ *is a Hilbert Schmidt operator on* $\mathrm{L}^2(\Omega, \mathbb{C}^p)$ *whose spectrum* $\Sigma(\mathbf{J}(iy))$ *is indexed*[14] *by decreasing modulus:* $|J_0(iy)| \geq |J_1(iy)| \cdots$.

Let us define the curves $\mathcal{C}_n$ *for* $n \in \mathbb{N}$*:*

$$\mathcal{C}_n : \left[il\sqrt{|J_n(iy)/l|^2 - 1}, D_n(y), \frac{y}{l\sqrt{|J_n(iy)/l|^2 - 1}} \right], \ iy \in \mathcal{E}_n \tag{4.17}$$

where $lD_n(y) = \frac{1}{\sqrt{|J_n(iy)/l|^2 - 1}} \left(|\arg(J_n(iy))| - \arccos\left(\frac{l}{|J_n(iy)|}\right)\right)$ *and*

$$iy \in \mathcal{E}_n = \Big\{ iy \in i\mathbb{R}_+ \mid \Im J_n(iy) > 0, \ l \leq |J_n(iy)| \text{ and } \arccos\left(\frac{l}{|J_n(iy)|}\right) \leq |\arg(J_n(iy))| \Big\}.$$

1. *A necessary and sufficient condition for a rightmost characteristic value of* $\mathbf{A}$ *to be purely imaginary and nonzero is the existence of an integer* n_0 *such that* $(i\omega_0, D, c)$ *belongs to the curve* $\mathcal{C}_{n_0}$. *In this case,* $i\omega_0$ *is a rightmost characteristic value of* $\mathbf{A}$.

2. *If we look for solutions* $(i\omega, D, c)$ *with* $c \leq c_\infty$, *then the sets* $\mathcal{E}_n$ *are bounded by* $y \leq c_\infty \|\mathbf{J}(0)\|_2$. c_∞ *is an arbitrary upper bound on the inverse velocity.*

3. *The set* $\mathcal{E}_n$ *is empty if* $nl > \|\mathbf{J}(0)\|_2^2$. *Hence, there are at most* $\lfloor \|\mathbf{J}(0)\|_2^2 / l \rfloor$ *curves* $\mathcal{C}_n$.

Proof. We start as in the proof of lemma 4.4.4 but the characteristic equation is a bit different $\lambda + l = e^{-\lambda D} J_n(c\lambda)$. We solve it with the help of the Lambert function:

$$\lambda_{k,n} = \frac{1}{D} W_k\left[De^{lD} J_n(c\lambda_{k,n}) \right] - l = l\left(\frac{W_k\left[De^{lD} J_n(c\lambda_{k,n}) \right]}{lD} - 1 \right).$$

1. According to (4.16), the rightmost characteristic values correspond to $k = 0$. We look for conditions such that $\lambda_{0,n}$ is purely imaginary. Write $X = lDe^{lD}$, then $\lambda_{0,n} = l\left(\frac{W_0\left[XJ_n(c\lambda_{k,n})/l \right]}{W_0(X)} - 1 \right)$. For a given

$$iy \in \mathcal{E}_n = \Big\{ iy \in i\mathbb{R}_+ \mid \Im J_n(iy) > 0, \ l \leq |J_n(iy)| \text{ and } \arccos\left(\frac{l}{|J_n(iy)|}\right) \leq |\arg(J_n(iy))| \Big\},$$

[13] It has been defined in (4.8).

[14] if two different eigenvalues have the same modulus, we chose am arbitrary labeling

there is a unique $X_0(y) = lD(y)e^{lD(y)}$ such that $W_0(X_0(y)) = \Re W_0\left(X_0(y)J_n(y)\right)$ (see lemma B.4.1). Then $\frac{1}{D(y)}W_0\left(lD(y)e^{lD(y)}J_n(y)\right) - l = iz \in i\mathbb{R}_+$ where $z = l\sqrt{|J_n(iy)/l|^2 - 1}$. Then choose $c = y/z > 0$: it gives a solution $(y, D(y), y/z)$ to the characteristic equation parametrized by y, $iy \in \mathcal{E}_n$.

2. If $iy \in \mathcal{E}_n$, we can find a solution $(i\omega, D, c)$ of the characteristic equation and $y = c\omega$. It remains to show that $|\omega| \leq \|\mathbf{J}(0)\|_2$. We have $i\omega + l = e^{-i\omega D}J_n(ic\omega)$ hence: $|\omega| = |\Im(e^{-i\omega D}J_n(ic\omega))| \leq |e^{-i\omega D}J_n(ic\omega)| = |J_n(ic\omega)| \leq \|\mathbf{J}(ic\omega)\|_2 \leq \|\mathbf{J}(0)\|_2$.

3. As $\mathbf{J}(z)$ is a Hilbert-Schmidt operator, we have $\sum_{q=0}^{\infty} |J_q(iy)|^2 \leq \|\mathbf{J}(iy)\|_2^2$. It gives for all $q \geq 0$: $q|J_q(iy)|^2 \leq \|\mathbf{J}(iy)\|_2^2 \leq \|\mathbf{J}(0)\|_2^2$. If $\|\mathbf{J}(0)\|_2^2 < n$, then $\frac{\|\mathbf{J}(0)\|_2^2}{n} < 1$ and $|J_n(iy)|^2 \leq \frac{\|\mathbf{J}(0)\|_2^2}{n} < 1$ for all $y \in \mathbb{R}$ which implies that $\mathcal{E}_n = \emptyset$.

□

We will examine the numerical usefulness of this proposition in the next chapter.

4.4.2 Generalized eigenspaces

Let us now compute the generalized eigenspaces of $\mathbf{A}$ (see [Hale 1993, Arino 2006, Wu 1996, Diekmann 1995]). The proof of the next proposition closely follows [Hale 1993] although it has to be adapted to our functional setting. A *generalized eigenvector* $\phi \neq 0$ is a vector which satisfies $(\lambda\mathrm{Id} - \mathbf{A})^k\phi = 0$ for some integer k. The generalized eigenspace is then defined by $E_\lambda(\mathbf{A}) = \cup_{i=1}^{\infty} \ker(\lambda\mathrm{Id} - \mathbf{A})^i$. A convenient way to characterize these spaces is the notion of Jordan chain (see definition B.1.10). Briefly, a Jordan chain $(\phi_1, \cdots, \phi_m) \in \mathcal{X}^{m+1}$ of *length* m is an ordered set of vectors such that $\phi_1 \neq 0$ and:

$$(\lambda\mathrm{Id} - \mathbf{A})\phi_1 = 0, \tag{4.18}$$

$$(\lambda\mathrm{Id} - \mathbf{A})\phi_{i+1} = \phi_i, \ 1 \leq i \leq m-1. \tag{4.19}$$

Hence, ϕ_i is in $\ker(\lambda\mathrm{Id} - \mathbf{A})^i$ and the first vector ϕ_1 is always an eigenvector. Note that this implies that the ϕ_i are linearly independent. Conversely, given a generalized eigenvector ϕ such that $(\lambda\mathrm{Id} - \mathbf{A})^m\phi = 0$, $(\lambda\mathrm{Id} - \mathbf{A})^{m-1}\phi \neq 0$, we can build a Jordan chain. Indeed, it is given (for example) by $\phi_m = \phi$, $\phi_{m-1} = (\lambda\mathrm{Id} - \mathbf{A})\phi_m \cdots$. Finally, the generalized eigenspace is spanned by a finite number of Jordan chains. This motivates their use for the linear analysis.

The definition B.1.10 of the Jordan chain that we use is different, although equivalent, but a bit more convenient for the proofs of the next two propositions.

Proposition 4.4.6. *For $\lambda_0 \in \Sigma(\mathbf{A}) \setminus \Sigma(-\mathbf{L}_0)$ and $\forall m \geq 1$,*

$$\ker\,(\lambda_0 \mathrm{Id} - \mathbf{A})^m = \left\{ \phi \in D(\mathbf{A}) \mid (\pi_2\phi)(\theta) = e^{\lambda_0\theta} \sum_{i=0}^{m-1} \frac{\theta^i}{i!} \mathbf{U}_{m-1-i} \right.$$

$$\left. \textit{where } (\mathbf{U}_0, \cdots, \mathbf{U}_{m-1}) \textit{ is a Jordan chain (see definition B.1.10) for } \Delta(\lambda_0) \right\}$$

Proof. Let us define the following operator: $\mathbf{A}_0\phi = \frac{d}{d\theta}\phi$ with domain $D(\mathbf{A}_0) = \left\{\phi \in W^{1,2}(-\tau_m, 0; \mathcal{F}) |\ \phi(0) = 0\right\}$ and the exponential function $\varepsilon_\lambda(\theta) = e^{\lambda\theta}$. From [Bátkai 2005][Lemma 3.20]:

$$\forall \lambda \quad \begin{bmatrix} \Delta(\lambda) & 0 \\ 0 & \lambda\mathrm{Id} - \mathbf{A}_0 \end{bmatrix} = \mathbf{F}(\lambda)(\lambda\mathrm{Id} - \mathbf{A})\mathbf{E}(\lambda) \tag{4.20}$$

where $\mathbf{F}(\lambda) = \begin{bmatrix} \mathrm{Id} & \mathbf{L}_1 R(\lambda, \mathbf{A}_0) \\ 0 & \mathrm{Id} \end{bmatrix} \in \mathcal{L}(\mathcal{X})$ and $\mathbf{E}(\lambda) = \begin{bmatrix} \mathrm{Id} & 0 \\ \varepsilon_\lambda \otimes \mathrm{Id} & \mathrm{Id} \end{bmatrix} \in \mathcal{L}(\mathcal{X})$ are invertible operators with $(\varepsilon_\lambda \otimes \mathrm{Id})x \equiv \varepsilon_\lambda x \in \mathrm{L}^2([-\tau_\mathrm{m}, 0], \mathcal{F})$ and $R(\lambda, \mathbf{A}_0)$ is the resolvent of $\mathbf{A}_0$. We first prove that the Jordan chains of $\lambda Id - \mathbf{A}$ at $\lambda = \lambda_0$ are in one-to-one correspondence with the Jordan chains of $\Delta(\lambda)$ at $\lambda = \lambda_0$ if $\ker \Delta(\lambda_0) \neq \emptyset$. From (4.20) and the fact that $\Sigma(\mathbf{A}_0) = \emptyset$ (see next section), it implies that the null spaces $\ker \Delta(\lambda_0)$ and $\ker(\lambda\mathrm{Id} - \mathbf{A})$ are isomorphic, it suffices to show that there is a one-to-one correspondence between the Jordan chains of length $k, k \geq 1$ of $\lambda\mathrm{Id} - \mathbf{A}$ and Δ at λ_0.

Indeed, if $\alpha(\lambda)$ is a root function for $\lambda Id - \mathbf{A}$ at $\lambda = \lambda_0$, then $\pi_1\mathbf{E}(\lambda)^{-1}\alpha(\lambda)$ is a root function for $\Delta(\lambda)$ at $\lambda = \lambda_0$ and if $\alpha(\lambda)$ is a root function of $\Delta(\lambda)$ at $\lambda = \lambda_0$, we find that $\mathbf{E}(\lambda)\begin{bmatrix} \alpha(\lambda) \\ 0 \end{bmatrix}$ is a root function for $\lambda Id - \mathbf{A}$ at $\lambda = \lambda_0$. In particular $\ker(\lambda_0 Id - \mathbf{A})^m$ is in one-to-one correspondence with the Jordan chains of length m of $\Delta(\lambda)$ at $\lambda = \lambda_0$. Hence the Jordan chains of $\lambda\mathrm{Id} - \mathbf{A}$ and $\Delta(\lambda)$ have the same length.

Now, take a Jordan chain $(\mathbf{U}_0, \cdots, \mathbf{U}_{m-1})$ for $\Delta(\lambda_0)$ and form the root function $\alpha(\lambda) = \sum_{i=0}^{m-1} (\lambda - \lambda_0)^i \mathbf{U}_i$. Then, $\mathbf{E}(\lambda)\begin{bmatrix} \alpha(\lambda) \\ 0 \end{bmatrix} = \begin{bmatrix} \alpha(\lambda) \\ e^{\lambda\cdot}\alpha(\lambda) \end{bmatrix} \equiv \sum_{i=0}^{m-1} (\lambda - \lambda_0)^i \mathbf{V}_i$ is a root function for $\lambda Id - \mathbf{A}$ at $\lambda = \lambda_0$. The Taylor expansion in λ at λ_0 of $e^{\lambda\theta}\alpha(\lambda)$ is given by $\sum_{i=0}^{m-1} (\lambda - \lambda_0)^i \left(\sum_{l=0}^{i} \frac{\theta^i}{i!} \mathbf{U}_{i-l} e^{\lambda_0\theta} \right)$. This gives $\mathbf{V}_i(\theta) = \sum_{l=0}^{i} \frac{\theta^i}{i!} \mathbf{U}_{i-l} e^{\lambda_0\theta}$ and $\mathbf{V}_{m-1} \in \ker(\lambda\mathrm{Id} - \mathbf{A})^m$ which concludes the proof. □

A characterization of the Jordan chains of $\Delta(\lambda)$ is obtained from lemma B.1.12.

Given $\lambda \in \Sigma_p(\mathbf{A})$ and the finite dimensional generalized eigenspace $E_\lambda(\mathbf{A}) = \cup_{i=1}^{\infty} \ker(\lambda\mathrm{Id} - \mathbf{A})^i$, we want to find a spectral projector P_λ on $E_\lambda(\mathbf{A})$ which commutes with $\mathbf{A}$. As $\mathcal{X}$ is a Hilbert space and $\mathbf{A}$ is densely defined, we can define the adjoint $\mathbf{A}^*$ of $\mathbf{A}$, then $\bar{\lambda} \in \Sigma_p(\mathbf{A}^*)$ and $dim E_\lambda(\mathbf{A}) = dim E_{\bar{\lambda}}(\mathbf{A}^*) \equiv m_\lambda$. Thus, if

$(\phi_1, \cdots, \phi_m)$ is a basis of $E_\lambda(\mathbf{A})$ and $(\phi_1^*, \cdots, \phi_m^*)$ is a basis of $E_{\bar{\lambda}}(\mathbf{A}^*)$ such that $\langle \phi_i^*, \phi_j \rangle_{\mathcal{X}} = \delta_{ij}$, a spectral projector is given by:

$$\forall u \in \mathcal{X}, \quad P_\lambda u \equiv \sum_{i=1}^{m} \langle \phi_i^*, u \rangle_{\mathcal{X}} \phi_i \tag{4.21}$$

Notice that P_λ commutes with $\mathbf{A}$. Although the expression of $\mathbf{A}^*$ is not needed in what follows, we give it in proposition B.5.1.

4.4.3 Spectral projector on generalized eigenspaces

In order to derive the center manifold theorem in section 4.6, we need to know how to project any vector of the state space $\mathcal{X}$ onto the generalized eigenspaces computed in section 4.4.1. The expression (4.21) of the spectral projector P_λ for an eigenvalue λ is impractical as it requires to compute the generalized eigenspace of the adjoint operator. We show in this section that the inner products $\langle \phi_i^*, u \rangle_{\mathcal{X}}$, required to give P_λ, can be computed without explicitly computing $\mathbf{A}^*$. By following closely the proof of [Hale 1993, Theorem VII.5.1] adapted in order to fit to our functional setting by using the tools of [Bátkai 2005], we are able to prove proposition 4.4.10. This proposition is the basis of the upcoming computation of the normal forms.

Let us define the operator $\mathbf{A}_0$ on $\mathrm{L}^2(-\tau_\mathrm{m}, 0; \mathcal{F})$ by $\mathbf{A}_0 \phi = \frac{d}{d\theta}\phi$ with domain $D(\mathbf{A}_0) = \left\{ \phi \in W^{1,2}(-\tau_m, 0; \mathcal{F}) |\ \phi(0) = 0 \right\}$. The resolvent of $\mathbf{A}_0$ is easily found using a variation-of-constants formula:

$$\left[R(\lambda, \mathbf{A}_0)\phi \right](\theta) = \int_\theta^0 e^{\lambda(s-\theta)} \phi(s) ds$$

Notice that $\Sigma(\mathbf{A}_0) = \emptyset$. An integration-by-parts gives the adjoint of $R(\lambda, \mathbf{A}_0)$

$$\left[R(\lambda, \mathbf{A}_0)^* \phi \right](\theta) = \int_{-\tau_m}^\theta e^{-\bar{\lambda}(s-\theta)} \phi(s) ds$$

The next lemma is used in the proof of proposition 4.4.10.

Lemma 4.4.7. *if* $\mathbf{F}(\lambda) = \begin{bmatrix} \mathrm{Id} & \mathbf{L}_1 R(\lambda, \mathbf{A}_0) \\ 0 & \mathrm{Id} \end{bmatrix} \in \mathcal{L}(\mathcal{X})$, *then we have*

$$\mathbf{F}(\lambda)^* = \begin{bmatrix} \mathrm{Id} & 0 \\ \mathbf{J}[\cdot]^* - \bar{\lambda} R(\lambda, \mathbf{A}_0)^* \mathbf{J}[\cdot]^* & \mathrm{Id} \end{bmatrix}$$

where $\mathbf{J}[s]^*$ *is the adjoint in* $\mathcal{F}$ *of* $\mathbf{J}[s]$ *(see lemma B.3.1 for a definition of* $\mathbf{J}[s]$*).*

Proof. Let us compute the following scalar product:

$$\langle \begin{bmatrix} y \\ \psi \end{bmatrix}, \mathbf{F}(\lambda) \begin{bmatrix} x \\ \phi \end{bmatrix} \rangle_{\mathcal{X}} = \langle y, x \rangle_{\mathcal{F}} + \int_{-\tau_m}^{0} \langle \psi(s), \phi(s) \rangle_{\mathcal{F}} ds + \langle y, \mathbf{L}_1 R(\lambda, \mathbf{A}_0)\phi \rangle_{\mathcal{F}}$$

$$= \langle y, x \rangle_{\mathcal{F}} + \int_{-\tau_m}^{0} \langle \psi(s), \phi(s) \rangle_{\mathcal{F}} ds + \langle y, \mathbf{J}\left[R(\lambda, \mathbf{A}_0)\phi\right](0) \rangle_{\mathcal{F}} - \int_{-\tau_m}^{0} \langle y, \mathbf{J}[s] \frac{d}{ds}\left[R(\lambda, \mathbf{A}_0)\phi\right](s) ds \rangle_{\mathcal{F}}$$

$$= \langle y, x \rangle_{\mathcal{F}} + \int_{-\tau_m}^{0} \langle \psi(s), \phi(s) \rangle_{\mathcal{F}} ds - \int_{-\tau_m}^{0} \langle \mathbf{J}[s]^* y, \left[\mathbf{A}_0 R(\lambda, \mathbf{A}_0)\phi\right](s) ds \rangle_{\mathcal{F}}$$

$$= \langle y, x \rangle_{\mathcal{F}} + \int_{-\tau_m}^{0} \langle \psi(s), \phi(s) \rangle_{\mathcal{F}} ds - \int_{-\tau_m}^{0} \langle \mathbf{J}[s]^* y, \left[-\phi + \lambda R(\lambda, \mathbf{A}_0)\phi\right](s) ds \rangle_{\mathcal{F}}$$

$$= \langle y, x \rangle_{\mathcal{F}} + \int_{-\tau_m}^{0} \langle \psi(s) + \mathbf{J}[s]^* y, \phi(s) \rangle_{\mathcal{F}} ds - \int_{-\tau_m}^{0} \langle \bar{\lambda} R(\lambda, \mathbf{A}_0)^* \mathbf{J}[s]^* y, \phi(s) \rangle_{\mathcal{F}} ds$$

The identification of the adjoint is now straightforward. □

Using the previous lemma, the proof of the next proposition is very close to the one of proposition 4.4.6. It consists in showing that the generalized eigenvectors of $\mathbf{A}^*$ are closely related to the Jordan chains of $\lambda \to \Delta(\lambda)^*$. Let us first define $\mathbf{F}^T$ on $D(\mathbf{A})$ by:

$$\mathbf{F}^T \begin{bmatrix} x \\ \phi \end{bmatrix} \equiv \begin{bmatrix} x \\ \mathbf{J}^*[\theta]\phi(0) - \int_{-\tau_m}^{\theta} \mathbf{J}[s]^* \frac{d}{ds}\left[\phi(s-\theta)\right] ds \end{bmatrix}$$

Before stating the main result of this section, let us define the following bilinear product:

Definition 4.4.8. *The bilinear product $\langle\langle \psi, u \rangle\rangle$ for $\psi, u \in \mathcal{X}$ reads:*

$$\langle\langle \psi, u \rangle\rangle \equiv \langle \pi_1\psi, \pi_1 u \rangle_{\mathcal{F}} + \int_{\Omega^2} d\mathbf{r} d\bar{\mathbf{r}} \sum_{ij} \int_{-\tau_{ij}(\mathbf{r},\bar{\mathbf{r}})}^{0} (\pi_2\psi)_i(\mathbf{r}, -s - \tau_{ij}(\mathbf{r},\bar{\mathbf{r}})) \tilde{J}_{ij}(\mathbf{r},\bar{\mathbf{r}}) (\pi_2 u)_j(\bar{\mathbf{r}}, s) ds$$

where

$$\tilde{\mathbf{J}} \equiv \mathbf{J}(0).$$

This is written:

$$\langle \pi_1\psi, \pi_1 u \rangle_{\mathcal{F}} + \int_{\Omega^2} d\mathbf{r} d\bar{\mathbf{r}} \int_{-\boldsymbol{\tau}(\mathbf{r},\bar{\mathbf{r}})}^{0} \left\langle (\pi_2\psi)(\mathbf{r}, -s - \boldsymbol{\tau}(\mathbf{r},\bar{\mathbf{r}})), \tilde{\mathbf{J}}(\mathbf{r},\bar{\mathbf{r}})(\pi_2 u)(\bar{\mathbf{r}}, s) \right\rangle_{\mathbb{R}^p} ds.$$

It is straightforward to check that:

Lemma 4.4.9. *The bilinear product $\langle\langle , \rangle\rangle$ is symmetric if $\tilde{J}_{ij}(\mathbf{r},\bar{\mathbf{r}}) = \tilde{J}_{ji}(\bar{\mathbf{r}},\mathbf{r})$ and $\tau_{ij}(\mathbf{r},\bar{\mathbf{r}}) = \tau_{ji}(\bar{\mathbf{r}},\mathbf{r})$.*

Using the bilinear product, we find an expression of the spectral projector P_λ.

Proposition 4.4.10.

1. *For $\bar{\lambda}_0 \in \Sigma(\mathbf{A}^*) \setminus \Sigma(-\mathbf{L}_0^*)$ and $\forall m \geq 1$, we have as in proposition 4.4.6:*

$$\ker\left(\bar{\lambda}_0 \mathrm{Id} - \mathbf{A}^*\right)^m = \left\{ \mathbf{F}^T\psi, \psi \in D(\mathbf{A}) \mid (\pi_2\psi)(\theta) = e^{\bar{\lambda}_0\theta} \sum_{i=0}^{m-1} \frac{\theta^i}{i!} \mathbf{U}^*_{m-1-i} \right.$$

where $(\mathbf{U}_0^*, \cdots, \mathbf{U}_{m-1}^*)$ *is a Jordan chain (see definition B.1.10) for* $\Delta(\bar{\lambda}_0)^*$ $\Big\}$

2. *For* $\lambda_0 \in \Sigma(\mathbf{A}) \setminus \Sigma(-\mathbf{L}_0)$, *choose a basis* $(\phi_i)_{i=1\cdots m_{\lambda_0}}$ *(resp.*$(\phi_i^*)_{i=1\cdots m_{\lambda_0}}$*) of* $E_{\lambda_0}(\mathbf{A})$ *as in proposition 4.4.6 (resp.* $E_{\bar{\lambda}_0}(\mathbf{A}^*)$*) such that* $\langle \phi_i^*, \phi_j \rangle_{\mathcal{X}} = \delta_{ij}$. *Then,* $\forall i \leq m_{\lambda_0}$, *there are* $\psi_i \in D(\mathbf{A})$ *as above such that* $\forall u \in \mathcal{X}$:

$$\langle \phi_i^*, u \rangle_{\mathcal{X}} = \langle\langle \psi_i, u \rangle\rangle$$

where $(\pi_2 \psi_i)(\theta) = e^{\bar{\lambda}_0 \theta} \sum_{r=0}^{m_i - 1} \frac{\theta^r}{r!} \mathbf{U}_{i;m_i-1-r}^*$. *Then, the projector* P_{λ_0} *is given by:*

$$\forall u \in \mathcal{X}, \quad P_{\lambda_0} u = \sum_{i=1}^{m_{\lambda_0}} \langle\langle \psi_i, u \rangle\rangle \phi_i$$

Proof. From [Bátkai 2005][Lemma 3.20]: $\begin{bmatrix} \Delta(\lambda) & 0 \\ 0 & \lambda \mathrm{Id} - \mathbf{A}_0 \end{bmatrix} = \mathbf{F}(\lambda)(\lambda \mathrm{Id} - \mathbf{A}) \mathbf{E}(\lambda)$ with $\mathbf{F}(\lambda) = \begin{bmatrix} \mathrm{Id} & \mathbf{L}_1 R(\lambda, \mathbf{A}_0) \\ 0 & \mathrm{Id} \end{bmatrix} \in \mathcal{L}(\mathcal{X})$ and $\mathbf{E}(\lambda) = \begin{bmatrix} \mathrm{Id} & 0 \\ \varepsilon_\lambda \otimes \mathrm{Id} & \mathrm{Id} \end{bmatrix} \in \mathcal{L}(\mathcal{X})$, we find:

$$\begin{bmatrix} \Delta(\lambda)^* & 0 \\ 0 & (\lambda \mathrm{Id} - \mathbf{A}_0)^* \end{bmatrix} = \mathbf{E}(\lambda)^* (\bar{\lambda} \mathrm{Id} - \mathbf{A}^*) \mathbf{F}(\lambda)^* \tag{4.22}$$

Proof of 1.

Similarly to the proof of proposition 4.4.6, the Jordan chains of $\bar{\lambda}\mathrm{Id} - \mathbf{A}^*$ at $\bar{\lambda} = \bar{\lambda}_0$ are in one-to-one correspondence with the Jordan chains of $\Delta(\lambda)^*$ at $\bar{\lambda} = \bar{\lambda}_0$. The proof reduces to finding the Jordan chains ϕ^* of $\mathbf{A}^*$. Take a Jordan chain $(\mathbf{U}_0, \cdots, \mathbf{U}_{m-1})$ of $\Delta(\lambda)^*$ at $\bar{\lambda} = \bar{\lambda}_0$, then from (4.22), $\mathbf{F}(\lambda)^* \begin{bmatrix} \alpha^*(\bar{\lambda}) \\ 0 \end{bmatrix}$ is a root function for $\mathbf{A}^*$ where $\alpha^*(\bar{\lambda}) = \sum_{i=0}^{m-1} (\bar{\lambda} - \bar{\lambda}_0)^i \mathbf{U}_i$. Computing $\pi_2 \mathbf{F}(\lambda)^* \begin{bmatrix} \alpha^*(\bar{\lambda}) \\ 0 \end{bmatrix}$ using lemma 4.4.7, we find up to orders $O((\bar{\lambda} - \bar{\lambda}_0)^m)$:

$$\mathbf{J}^*(\theta)\alpha^*(\bar{\lambda}) - \int_{-\tau_m}^{\theta} \bar{\lambda} e^{-\bar{\lambda}(\theta - s)} \mathbf{J}[s]^* \alpha^*(\bar{\lambda}) ds =$$

$$\mathbf{J}^*(\theta)\alpha^*(\bar{\lambda}) - \int_{-\tau_m}^{\theta} \mathbf{J}[s]^* \frac{d}{ds} \left[e^{-\bar{\lambda}(\theta - s)} \alpha(\bar{\lambda}) \right] ds =$$

$$\sum_{l=0}^{m-1} (\bar{\lambda} - \bar{\lambda}_0)^l \left\{ \mathbf{J}^*(\theta) \mathbf{U}_l - \int_{-\tau_m}^{\theta} \mathbf{J}[s]^* \frac{d}{ds} \left[e^{\bar{\lambda}_0 (s - \theta)} \sum_{j=0}^{l} \mathbf{U}_{l-j} \frac{(s-\theta)^j}{j!} \right] \right\} ds$$

Hence, we find that

$$\mathbf{F}(\lambda)^* \begin{bmatrix} \alpha^*(\bar{\lambda}) \\ 0 \end{bmatrix} = \sum_{l=0}^{m-1} (\bar{\lambda} - \bar{\lambda}_0)^l \mathbf{F}^T \psi_l$$

where $\psi_l = \begin{bmatrix} \mathbf{U}_l^* \\ e^{\bar{\lambda}_0\theta} \sum_{j=0}^{l} \mathbf{U}_{l-j}^* \frac{\theta^j}{j!} \end{bmatrix} \in D(\mathbf{A})$. We have found that the generalized eigenvectors of $\mathbf{A}^*$ are given by the $\mathbf{F}^T\psi_l$.

Proof of 2.

Let ϕ^* be a generalized eigenvector of $\mathbf{A}$. According to 1., we can write $\phi^* = \mathbf{F}^T \begin{bmatrix} x \\ \phi \end{bmatrix}$. For the computation of the projector P_λ, we need to compute the scalar product $\langle u, \phi^* \rangle_{\mathcal{X}}$.

$$\begin{aligned}
\langle u, \phi^* \rangle_{\mathcal{X}} = \langle \begin{bmatrix} y \\ \psi \end{bmatrix}, \mathbf{F}^T \begin{bmatrix} x \\ \phi \end{bmatrix} \rangle_{\mathcal{X}} &\equiv \langle y, x \rangle_{\mathcal{F}} + \int_{-\tau_m}^{0} d\theta \langle \psi(\theta), \mathbf{J}[\theta]^* \phi(0) \rangle_{\mathcal{F}} \\
&\quad - \int_{-\tau_m}^{0} d\theta \int_{-\tau_m}^{\theta} ds \langle \psi(\theta), \mathbf{J}[s]^* \frac{d}{ds} [\phi(s-\theta)] \rangle \\
&= \langle y, x \rangle_{\mathcal{F}} + \int_{-\tau_m}^{0} d\theta \langle \psi(\theta), \mathbf{J}[\theta]^* \phi(0) \rangle_{\mathcal{F}} \\
- \int_{-\tau_m}^{0} d\theta \int_{\Omega^2} d\mathbf{r} d\bar{\mathbf{r}} \int_{-\tau_m}^{\theta} ds \langle \psi(\mathbf{r}, \theta), \mathbf{J}^*(\mathbf{r}, \bar{\mathbf{r}})^* \dot{\phi}(\bar{\mathbf{r}}, s-\theta) \rangle_{\mathbb{R}^p} H(s + \boldsymbol{\tau}(\mathbf{r}, \bar{\mathbf{r}})) \\
&= \langle y, x \rangle_{\mathcal{F}} + \int_{-\tau_m}^{0} d\theta \langle \psi(\theta), \mathbf{J}[\theta]^* \phi(0) \rangle_{\mathcal{F}} \\
- \sum_{ij} \int_{\Omega^2} d\mathbf{r} \tilde{J}_{ij}(\mathbf{r}, \bar{\mathbf{r}}) d\bar{\mathbf{r}} \int_{-\tau_m}^{0} d\theta \int_{-\tau_m}^{\theta} ds \ \psi_j(\mathbf{r}, \theta) \dot{\phi}_i(\bar{\mathbf{r}}, s-\theta) H(s + \tau_{ij}(\mathbf{r}, \bar{\mathbf{r}})) \\
&= \langle y, x \rangle_{\mathcal{F}} + \int_{-\tau_m}^{0} d\theta \langle \psi(\theta), \mathbf{J}[\theta]^* \phi(0) \rangle_{\mathcal{F}} \\
- \sum_{ij} \int_{\Omega^2} d\mathbf{r} \tilde{J}_{ij}(\mathbf{r}, \bar{\mathbf{r}}) d\bar{\mathbf{r}} \int_{-\tau_{ij}(\mathbf{r}, \bar{\mathbf{r}})}^{0} d\theta \int_{-\tau_{ij}(\mathbf{r}, \bar{\mathbf{r}})}^{\theta} ds \ \psi_j(\mathbf{r}, \theta) \dot{\phi}_i(\bar{\mathbf{r}}, s-\theta) \\
= \langle y, x \rangle_{\mathcal{F}} + \sum_{ij} \int_{\Omega^2} d\mathbf{r} \tilde{J}_{ij}(\mathbf{r}, \bar{\mathbf{r}}) d\bar{\mathbf{r}} \int_{-\tau_{ij}(\mathbf{r}, \bar{\mathbf{r}})}^{0} ds \ \psi_j(\mathbf{r}, \theta) \phi_i(\bar{\mathbf{r}}, s - \tau_{ij}(\mathbf{r}, \bar{\mathbf{r}})) \quad (4.23)
\end{aligned}$$

where H is the Heaviside function. The last line equals the definition of $\langle\langle \begin{bmatrix} x \\ \phi \end{bmatrix}, u \rangle\rangle$. The proof is complete. □

We have found an analytical expression for the spectral projector P_λ. We can use this result to obtain a decomposition (see [Yosida 1980] p228) of the history space for the eigenvalue $\lambda \in \Sigma_p(\mathbf{A})$ of algebraic multiplicity m_λ:

$$\mathcal{X} = \ker(\lambda \mathrm{Id} - \mathbf{A})^{m_\lambda} \oplus \mathrm{Im}(\lambda \mathrm{Id} - \mathbf{A})^{m_\lambda} = E_\lambda(\mathbf{A}) \oplus \mathrm{Im}(\lambda \mathrm{Id} - \mathbf{A})^{m_\lambda}, \quad (4.24)$$

the last equality comes from $\ker(\lambda \mathrm{Id} - \mathbf{A})^{m_\lambda} = E_\lambda(\mathbf{A})$. From the general formula $\ker(\bar{\lambda} \mathrm{Id} - \mathbf{A}^*)^{m_\lambda} = (\mathrm{Im}(\lambda \mathrm{Id} - \mathbf{A})^{m_\lambda})^\perp$, we obtain that $\mathrm{Im}(\lambda \mathrm{Id} - \mathbf{A})^{m_\lambda} = \{\phi \in \mathcal{X} \mid \forall \psi \in E_{\bar{\lambda}}(\mathbf{A}^*),\ \langle \psi, \phi \rangle_{\mathcal{X}} = 0\}$.

4.4.4 Phase space decomposition

We end the section on linear analysis with a decomposition of the history space according to the eigenvalues of the infinitesimal generator $\mathbf{A}$. This will be useful for the derivation of the center manifold theorem in section 4.6. Let us write a splitting of the spectrum of $\mathbf{A}$ according to the real part of the eigenvalues[15]:

$$\Sigma_u \equiv \Sigma(\mathbf{A}) \cap \mathbb{C}_+,\ \Sigma_c \equiv \Sigma_p(\mathbf{A}) \cap i\mathbb{R},\ \Sigma_s \equiv \Sigma(\mathbf{A}) \cap \mathbb{C}_-$$

It was shown in lemma 4.4.2 that: $\forall a > \min_i l_i,\ Card\Sigma(\mathbf{A}) \cap (a, +\infty)_{\mathbb{C}} < \infty$. Hence, we can find a spectral gap $\gamma > 0$ such that

$$\max \Re\Sigma_s < -\gamma,\ \min \Re\Sigma_u > \gamma$$

As Σ_c and Σ_u are finite and included in the point spectrum $\Sigma_p(\mathbf{A})$ of $\mathbf{A}$, we can use (4.24) to obtain a decomposition of $\mathcal{X}$ according to the splitting of the spectrum:

$$\mathcal{X} = \mathcal{X}_u \oplus \mathcal{X}_c \oplus \mathcal{X}_s$$

where the spaces $\mathcal{X}_u, \mathcal{X}_c, \mathcal{X}_s$ are invariant by $\mathbf{A}$ and $\mathbf{T}(t)$ for all $t \geq 0$. For example, the center part, $\mathcal{X}_c = \bigoplus_{\lambda \in \Sigma_c} E_\lambda(\mathbf{A})$. We write $P_c = \sum_{\lambda \in \Sigma_c} P_\lambda, P_u = \sum_{\lambda \in \Sigma_u} P_\lambda$ the spectral projectors on $\mathcal{X}_c, \mathcal{X}_u$ and $P_s = \mathrm{Id} - P_c - P_u$. We also write $\mathbf{A}_u, \mathbf{A}_c, \mathbf{A}_s$ (resp. $\mathbf{T}_u, \mathbf{T}_c, \mathbf{T}_s$) the restriction of $\mathbf{A}$ (resp. $\mathbf{T}$) to the different subspaces. Notice that $\Sigma(\mathbf{A}_i) = \Sigma_i,\ i = u, c, s$. The spectral mapping theorem (see [Engel 2001] and theorem B.1.4) gives:

$$|||\mathbf{T}_s(t)|||_{\mathcal{X}} \leq Me^{-\gamma t},\ t \geq 0$$

where M is a constant. As $\mathcal{X}_u$ is finite dimensional, there is a matrix such that $\mathbf{T}_u(t) = e^{tA_u}$ (see for example [Engel 2001]). Thus, $\mathbf{T}_u$ can be extended to a group such that:

$$|||\mathbf{T}_u(t)|||_{\mathcal{X}} \leq Me^{-\gamma|t|},\ t \leq 0$$

Finally, we define the hyperbolic projector $P_h = P_u + P_s$ and associated operators $\mathbf{A}_h = \mathbf{A}P_h$ and $\mathbf{T}_h = \mathbf{T}P_h$.

4.5 Stability results in $\mathcal{C}$

When studying a dynamical system, a good starting point is to look for invariant sets. Theorem 4.3.2 provides such an invariant set but it is a very large one, not sufficient to convey a good understanding of the system. Other invariant sets (included in the previous one) are stationary points. Notice that delayed and non-delayed equations share exactly the same stationary solutions. We can therefore make good use of the harvest of results that are available about these persistent states which we note $\mathbf{V}^f$. Note that in most papers dealing with persistent states,

[15] We have written $\mathbb{C}_- = \{z \in \mathbb{C} \mid \Re z < 0\}$ and $\mathbb{C}_+ = \{z \in \mathbb{C} \mid \Re z > 0\}$.

the authors compute one of them and are satisfied with the study of the local dynamics around this particular stationary solution. Very few authors (we are aware only of [Ermentrout 1980, Veltz 2010]) address the problem of the computation of the whole set of persistent states. Despite these efforts they have yet been unable to get a complete grasp of the global dynamics. To summarize, in order to understand the impact of the propagation delays on the solutions of the neural field equations, it is necessary to know all their stationary solutions and the dynamics in the region where these stationary solutions lie. Unfortunately such knowledge is currently not available. Hence we must be content with studying the local dynamics around *each* persistent state (computed for example with the tools of [Veltz 2010]) with and without propagation delays. This is already, we think, a significant step forward toward understanding delayed neural field equations.
From now on we note $\mathbf{V}^f$ a persistent state of (4.1) and study its stability. Note that the existence of a stationary solution requires the external current $\mathbf{I}_{ext}$ in (4.2) to be time constant.
We can identify at least three ways to do this:

1. to derive a Lyapunov functional,
2. to use a fixed point approach,
3. to determine the spectrum of the infinitesimal generator associated to the linearized equation.

Previous results concerning stability bounds in delayed neural mass equations are "absolute" results that do not involve the delays: they provide a sufficient condition, independent of the delays, for the stability of the fixed point (see [Atay 2005, Atay 2006, Hutt 2008, Hutt 2006]). The bound they find is similar to our second bound in proposition 4.5.7. They "proved" it by showing that if the condition was satisfied, the eigenvalues of the infinitesimal generator of the semi-group of the linearized equation had negative real parts. This is not sufficient because a more complete analysis of the spectrum (e.g., the essential part) is necessary as shown below in order to prove that the semi-group is exponentially bounded. In our case we prove this assertion in the case of a bounded cortex (see section 4.5.1).

These authors also provide a delay-dependent sufficient condition to guarantee that no oscillatory instabilities can appear, i.e., they give a condition that forbids the existence of solutions of the form $e^{i(\mathbf{k}\cdot\mathbf{r}+\omega t)}$. However, this result does not give any information regarding stability of the stationary solution.

We use the second method cited above, the fixed point method, to prove a more general result which takes into account the delay terms. We also use both the second and the third method above, the spectral method, to *prove* the delay-independent bound from [Atay 2005, Atay 2006, Hutt 2008, Hutt 2006]. We then evaluate the conservativeness of these two sufficient conditions. Note that the delay-independent bound has been correctly derived in [Faye 2010] using the first method, the Lyapunov method. It might be of interest to explore its potential to derive a delay-dependent bound.

For convenience, we recall the linearized equation we are interested in here:

$$\begin{cases} \dot{\mathbf{U}}(t) = -\mathbf{L}_0\mathbf{U}(t) + \tilde{\mathbf{L}}_1\mathbf{U}_t \equiv \mathbf{L}\mathbf{U}_t \\ \mathbf{U}_0 = \phi \in \mathcal{C} \end{cases} \tag{4.25}$$

4.5.1 Stability results in $\mathcal{C}$ from the characteristic values

There are two steps in proving the (asymptotic) stability of an equilibrium. First we show that if the eigenvalues, solutions of (4.7), satisfy $\Re\lambda < 0$, then any solution of (4.25) is exponentially decaying to $\mathbf{U} = 0$ in $\mathcal{C}$. Then, we show[16] that any initial condition $\mathbf{V}_0 \in \mathcal{C}$ close enough[17] to $\mathbf{V}^f$ converges to $\mathbf{V}^f$ for the equation (4.1). Using the spectrum computed in lemma 4.4.2 and the formula in lemma 4.4.3, we can state the asymptotic stability of the linear equation (4.9):

Corollary 4.5.1 (Linear stability). *The zero solution of (4.25) is asymptotically stable in $\mathcal{C}$ if and only if* $\max \Re\left(\Sigma(\mathbf{A}) \cap \{\lambda \in \mathbb{C},\ \Re\lambda > -l\}\right) < 0$.

We conclude by showing that the computation of the characteristic values of $\mathbf{A}$ is enough to state the stability of the stationary solution $\mathbf{V}^f$.

Corollary 4.5.2. *Let us assume that* $\mathbf{J} \in \mathrm{L}^\infty(\Omega^2, \mathbb{R}^{\mathrm{p}\times\mathrm{p}})$. *If* $\max \Re\left(\Sigma(\mathbf{A}) \cap \{\lambda \in \mathbb{C},\ \Re\lambda > -l\}\right) < 0$, *then the persistent solution $\mathbf{V}^f$ of (4.4) is asymptotically stable in $\mathcal{C}$.*

Proof. We write $\mathbf{U}(t) = \mathbf{V}(t) - \mathbf{V}^f$ for $\mathbf{V}(t)$ solution of (4.4) in $\mathcal{C}$, we write (4.4) as $\dot{\mathbf{U}}(t) = -\mathbf{L}_0\mathbf{U}(t) + \tilde{\mathbf{L}}_1\mathbf{U}_t + G(\mathbf{U}_t)$. The function G is in $C^1(\mathcal{C}, \mathcal{F})$ and satisfies $G(0) = 0$, $DG(0) = 0$ and $\|G(\mathbf{U}_t)\|_{\mathcal{F}} = O(\|\mathbf{U}_t\|^2_{\mathcal{C}})$. Let us write $\|G(\mathbf{U}_t)\|_{\mathcal{F}} \leq K_G\|\mathbf{U}_t\|^2_{\mathcal{C}}$ and $\omega = \max(-l, \varepsilon_p) < 0$ where $\varepsilon_p \equiv \max \Re\left(\Sigma(\mathbf{A}) \cap \{\lambda \in \mathbb{C},\ \Re\lambda > -l\}\right)$. Then lemma 4.4.3 gives $|||\mathbf{T}(t)|||_{\mathcal{X}} \leq Me^{\omega t}$ with $M \geq 1$. Let us define the function $f : t \to G(\mathbf{U}_t) \in C^0(\mathbb{R}_+, \mathcal{F})$, then $\mathbf{U}(t)$ solves the linear inhomogeneous problem:

$$\begin{cases} \dot{\mathbf{U}}(t) = -\mathbf{L}_0\mathbf{U}(t) + \tilde{\mathbf{L}}_1\mathbf{U}_t + f(t) \\ \mathbf{U}_0 \in \mathcal{C} \end{cases}$$

From the proof of proposition B.7.4, $v : t \to \int_0^t \mathbf{T}(t-s)\begin{bmatrix} f(s) \\ 0 \end{bmatrix} ds \in C^1(\mathbb{R}^+, \mathcal{X})$ and from [Pazy 1983][theorem 2.4], v is a strong solution of $\dot{u} = \mathbf{A}u + \begin{bmatrix} f(t) \\ 0 \end{bmatrix}$, $u(0) = 0$. Hence, $\mathbf{U}(t) - \pi_1 v$ solves the homogeneous linear problem with initial condition $\mathbf{U}_0$ which is also solved by $\pi_1\mathbf{T}(t)u(0)$. In particular, we have $\mathbf{U}(t) = \pi_1 u(t)$ with $u(t) \equiv v(t) + \mathbf{T}(t)u(0)$ (it is a mild solution).

The proof is now an adaptation of [Wu 1996][theorem 4.1]. We choose R such that $K_G R < \frac{|\omega|e^{\omega\tau_m}}{2M}$. We want to show that the set $B_R = \left\{ \begin{bmatrix} \phi(0) \\ \phi \end{bmatrix}, \phi \in \mathcal{C},\ \|\phi\|_{\mathcal{C}} < R \right\}$ is invariant by the dynamics if $\|\mathbf{U}_0\|_{\mathcal{C}} < \frac{R}{2M(1+\tau_m)}$.

[16] We also have to show that this solution stays in a neighborhood of $\mathbf{V}^f$ in $\mathcal{C}$.
[17] in $\mathcal{C}$

By way of contradiction, if there exists $t_1 > 0$ so that $\|\mathbf{U}_{t_1}\|_{\mathcal{C}} = R$ and $\|\mathbf{U}_t\|_{\mathcal{C}} < R$ for $t \in [0, t_1)$. Then we find $\|\mathbf{U}(t_1)\|_{\mathcal{F}} = R$ and:

$$R = \|\mathbf{U}(t_1)\|_{\mathcal{F}} \leq \|u(t_1)\|_{\mathcal{X}} < M \overbrace{e^{\omega t_1}}^{\leq 1} \frac{R}{2M} + \int_0^{t_1} M e^{\omega(t_1-s)} K_G \|\mathbf{U}_s\|_{\mathcal{C}}^2 \, ds$$
$$< \frac{R}{2} + M\frac{K_G R}{|\omega|} R \leq R$$

a contradiction to the choice of t_1. If $\|\mathbf{U}_0\|_{\mathcal{C}} < \frac{R}{2M(1+\tau_m)}$, we have shown that $\|\mathbf{U}_t\|_{\mathcal{C}} < R$ for all $t \geq 0$. Therefore $\forall \theta \in [-\tau_m, 0]$ such that $t + \theta > 0$:

$$\|\mathbf{U}(t+\theta)\|_{\mathcal{F}} \leq \|u(t+\theta)\|_{\mathcal{X}}$$
$$\leq M e^{\omega t + |\omega|\tau_m} \|u(0)\|_{\mathcal{X}} + M K_G R \int_0^t e^{\omega(t-s)+|\omega|\tau_m} \|\mathbf{U}_s\|_{\mathcal{C}} \, ds$$

which gives:

$$\|\mathbf{U}_t\|_{\mathcal{C}} \leq M e^{\omega t + |\omega|\tau_m} \|u(0)\|_{\mathcal{X}} + M K_G R \int_0^t e^{\omega(t-s)+|\omega|\tau_m} \|\mathbf{U}_s\|_{\mathcal{C}} \, ds.$$

By using Gronwall inequality, we find:

$$\|\mathbf{U}_t\|_{\mathcal{C}} \leq M e^{|\omega|\tau_m} \|u(0)\|_{\mathcal{X}} e^{(\omega + M K_G R e^{|\omega|\tau_m})t} \leq M e^{|\omega|\tau_m} \|u(0)\|_{\mathcal{X}} e^{\omega t/2}$$

which shows that $\|\mathbf{U}_t\|_{\mathcal{C}} \to 0$ as $t \to \infty$. □

Remark 22. There is correspondence between the continuous functions of $C^0(\mathbb{R}, \mathcal{F})$ and the continuous functions with values in $\mathcal{X}$. Indeed, given a continuous function $f \in C^0(\mathbb{R}, \mathcal{F})$, we build a continuous function $t \to \begin{bmatrix} f(t) \\ f_t \end{bmatrix} \in \mathcal{X}$. Hence the history segment $\begin{bmatrix} f(t) \\ 0 \end{bmatrix}$ represents a Dirac function $X_0 f(t)$: $(X_0 f(t))(\theta) = \begin{cases} 0 & \text{if} \quad \theta < 0 \\ f(t) & \text{if} \quad \theta = 0 \end{cases}$, which does not belong to $\mathcal{C}$. If we had worked in $\mathcal{C}$ and built a semigroup $\mathbf{T}_{\mathcal{C}}(t) : \mathcal{C} \to \mathcal{C}$, we could not have used the variation-of-constant formula in the previous proof, because it relies on the quantity $\mathbf{T}_{\mathcal{C}}(t-s) X_0 f(s)$ which has no meaning because $X_0 f(s) \notin \mathcal{C}$. This is why we chose to work in $\mathcal{X}$ for the study of the semigroup $\mathbf{T}(t)$.

Finally, we can use the CVs to derive a sufficient stability result.

Proposition 4.5.3. *If $\|\mathbf{J} \cdot DS(\mathbf{V}^f)\|_{\mathbf{L}^2(\Omega^2, \mathbb{R}^{p\times p})} < \min_i l_i$ then $\mathbf{V}^f$ is asymptotically stable for (4.4).*

Proof. Suppose that a CV λ of positive real part exists, this gives a vector in the Kernel of $\Delta(\lambda)$. Using straightforward estimates, it implies that $\min_i l_i \leq \|\mathbf{J} \cdot DS(\mathbf{V}^f)\|_{\mathbf{L}^2(\Omega^2, \mathbb{R}^{p\times p})}$, a contradiction. □

4.5.2 Generalization of the model

In the description of our model, we have pointed out a possible generalization. It concerns the linear response of the populations, *i.e.*, the left-hand side $\left(\frac{d}{dt}+l_i\right)$ of (4.1). It can be replaced by a polynomial in $\frac{d}{dt}$, namely $P_i\left(\frac{d}{dt}\right)$, where the zeros of the polynomials P_i have negative real parts. Indeed, in this case, when $\mathbf{J}$ is small, the network is stable. We obtain a diagonal matrix $\mathbf{P}\left(\frac{d}{dt}\right)$ such that $\mathbf{P}(0)=\mathbf{L}_0$ and change the initial condition (as in the theory of ODEs) while the history space becomes $(\mathcal{C}([-\tau_m,0],\mathcal{F}))^{d_s}\simeq\mathcal{C}([-\tau_m,0],\mathcal{F}^{d_s})$ where $d_s=\max_i degP_i$. Having all this in mind equation (4.1) writes

$$\begin{cases} P_i\left(\frac{d}{dt}\right)V_i(t,\mathbf{r}) &= \sum_{j=1}^{p}\int_\Omega J_{ij}(\mathbf{r},\bar{\mathbf{r}})S[\sigma_j V_j\Big(t-\tau_{ij}(\mathbf{r},\bar{\mathbf{r}}),\bar{\mathbf{r}}\Big)-\theta_j]d\bar{\mathbf{r}}+I_{ext,i}(\mathbf{r},t), \\ & \qquad t\geq 0,\ 1\leq i\leq p \\ V_i^{(k)}(t,\mathbf{r}) &= \phi_{i,k}(t,\mathbf{r})\in\mathcal{C},\quad t\in[-\tau_m,\ 0],\quad k=0\cdots d_s \end{cases} \tag{4.26}$$

Introducing the classical variable $\mathcal{V}(t)\equiv[\mathbf{V}(t),\mathbf{V}'(t),\cdots,\mathbf{V}^{(d_s)}(t)]$, we rewrite (4.26) as

$$\dot{\mathcal{V}}(t)=-\mathcal{L}_0\mathcal{V}(t)+\mathcal{L}_1\mathcal{S}(\mathcal{V}_t)+\mathcal{I}_{ext} \tag{4.27}$$

where $-\mathcal{L}_0$ is the Vandermonde matrix (we put a minus sign in order to have a formulation very close to (4.1)) associated to $\mathbf{P}$ and $(\mathcal{L}_1)_{k,l=1\cdots d_s}=(\delta_{k=d_s,l=1}\mathbf{L}_1)_{k,l=1\cdots d_s}$, $\mathcal{I}_{ext}=[0,\cdots,\mathbf{I}_{ext}]$, $\mathcal{S}(\mathcal{V})=[\mathbf{S}(\mathbf{V}(t)),\cdots,\mathbf{S}(\mathbf{V}^{(d_s)})]$. It appears that equation (4.27) has the same structure as (4.1): $\mathcal{L}_0,\mathcal{L}_1$, are bounded linear operators on $C^0([-\tau_m,0],\mathcal{F}^{d_s})=\mathcal{C}^{d_s}$; we can conclude that there is a unique solution $\mathcal{V}$ to (4.26) in $\mathcal{C}^{d_s}$. Using similar tools as in section 4.4.1, the linearized equation around a persistent states yields a strongly continuous semigroup $\mathcal{T}(t)$ which is eventually continuous. Hence the stability is given by the sign of $\max\Re\Sigma(\mathcal{A})$ where $\mathcal{A}$ is the infinitesimal generator of $\mathcal{T}(t)$. It is then routine to show that

$$\lambda\in\Sigma(\mathcal{A})\Leftrightarrow\Delta(\lambda)\equiv\mathbf{P}(\lambda)-\mathbf{J}(\lambda)\text{ non invertible}$$

This indicates that the essential spectrum $\Sigma_{ess}(\mathcal{A})$ of $\mathcal{A}$ is equal to $\cup_i Root\,(P_i)$ which is located in the left side of the complex plane. Thus the point spectrum is enough to characterize the linear stability:

Proposition 4.5.4. *If* $\max\Re\Sigma_p(\mathcal{A})<0$ *the persistent solution* $\mathbf{V}^f$ *of (4.26) is asymptotically stable in* $\mathcal{C}^{d_s}$.

Using the same proof as in [Atay 2005], one can prove that $\max\Re\Sigma(\mathcal{A})<0$ provided that $\|\mathbf{J}\cdot DS(\mathbf{V}^f)\|_{\mathbf{L}^2(\Omega^2,\mathbb{R}^{p\times p})}<\min_{k\in\mathbb{N},\omega\in\mathbb{R}}|P_k(i\omega)|$.

Proposition 4.5.5. *If* $\|\mathbf{J}\cdot DS(\mathbf{V}^f)\|_{\mathbf{L}^2(\Omega^2,\mathbb{R}^{p\times p})}<\min_{k\in\mathbb{N},\omega\in\mathbb{R}}|P_k(i\omega)|$ *then* $\mathbf{V}^f$ *is asymptotically stable in* $\mathcal{C}^{d_s}$.

4.5.3 Principle of the linear stability analysis via fixed point theory in $\mathcal{C}$

The idea behind this method (see [Burton 2006]) is to write (4.6) as an integral equation. This integral equation is then interpreted as a fixed point problem. We already

know that this problem has a unique solution in $C^0(\mathbb{R}_+, \mathcal{C})$. However, by looking at the definition of the (Lyapunov) stability, we can express the stability as the existence of a solution of the fixed point problem in a smaller space $\mathcal{S} \subset C^0(\mathbb{R}_+, \mathcal{C})$. The existence of a solution in $\mathcal{S}$ gives the unique solution in $C^0(\mathbb{R}_+, \mathcal{C})$. Hence, the method is to provide conditions for the fixed point problem to have a solution in $\mathcal{S}$; in the two cases presented below, we use the Picard fixed point theorem to obtain these conditions. Usually this method gives conditions on the averaged quantities arising in (4.6) whereas a Lyapunov method would give conditions on the sign of the same quantities. There is no method to be preferred, rather both of them should be applied to obtain the best bounds.

In order to be able to derive our bounds, we make the further assumption that there exists a $\beta > 0$ such that:

$$\left\| \frac{1}{\boldsymbol{\tau}^\beta} \right\|_{\mathbf{L}^2(\Omega^2, \mathbb{R}^{p\times p})} < \infty.$$

Note that the notation $\frac{1}{\boldsymbol{\tau}^\beta}$ represents the matrix of elements $1/\tau_{ij}^\beta$. Finally we use the notation $\tilde{\mathbf{J}}$ for the integral operator on $\mathcal{F}$ with kernel $\mathbf{J}_{ij}(\mathbf{r}, \bar{\mathbf{r}}) DS(\mathbf{V}_j^f(\bar{\mathbf{r}}))$, *i.e.*

$$\tilde{\mathbf{J}}_{ij}(\mathbf{r}, \bar{\mathbf{r}}) \equiv \mathbf{J}_{ij}(0) = \mathbf{J}_{ij}(\mathbf{r}, \bar{\mathbf{r}}) DS(\mathbf{V}_j^f(\bar{\mathbf{r}})). \tag{4.28}$$

Remark 23.For example, in the 2D one-population case for $\tau(\mathbf{r}, \bar{\mathbf{r}}) = c\|\mathbf{r} - \bar{\mathbf{r}}\|_2$, we have $0 \leq \beta < 1$.

We rewrite (4.6) in two different integral forms to which we apply the fixed point method. The first integral form is obtained by a straightforward use of the variation-of-parameters formula. It reads

$$\begin{cases} (\mathbf{P}_1\mathbf{U})(t) &= \phi(t), \quad t \in [-\tau_m, 0] \\ (\mathbf{P}_1\mathbf{U})(t) &= e^{-\mathbf{L}_0 t}\phi(0) + \int_0^t e^{-\mathbf{L}_0(t-s)}(\tilde{\mathbf{L}}_1\mathbf{U}_s)\, ds, \quad t \geq 0 \end{cases} \tag{4.29}$$

The second integral form is less obvious. Let us define

$$\mathbf{Z}(\mathbf{r}, t) = \int_\Omega d\bar{\mathbf{r}} \tilde{\mathbf{J}}(\mathbf{r}, \bar{\mathbf{r}}) \int_{t-\boldsymbol{\tau}(\mathbf{r},\bar{\mathbf{r}})}^t ds\, \mathbf{U}(\bar{\mathbf{r}}, s),$$

Note the slight abuse of notation, namely $\left(\tilde{\mathbf{J}}(\mathbf{r}, \bar{\mathbf{r}}) \int_{t-\boldsymbol{\tau}(\mathbf{r},\bar{\mathbf{r}})}^t ds \mathbf{U}(\bar{\mathbf{r}}, s)\right)_i = \sum_j \tilde{\mathbf{J}}_{ij}(\mathbf{r}, \bar{\mathbf{r}}) \int_{t-\boldsymbol{\tau}_{ij}(\mathbf{r},\bar{\mathbf{r}})}^t ds \mathbf{U}_j(\bar{\mathbf{r}}, s)$.

Lemma B.6.1 in appendix yields the upper-bound

$$\|\mathbf{Z}(t)\|_{\mathcal{F}} \leq \tau_m{}^{\frac{3}{2}+\beta} \left\| \frac{\tilde{\mathbf{J}}}{\boldsymbol{\tau}^\beta} \right\|_{\mathbf{L}^2(\Omega^2, \mathbb{R}^{p\times p})} \sup_{s\in[t-\tau_m, t]} \|\mathbf{U}(s)\|_{\mathcal{F}}$$

where $\frac{\tilde{\mathbf{J}}}{\boldsymbol{\tau}^\beta}$ represents the matrix of elements $\frac{\tilde{J}_{ij}}{\tau_{ij}^\beta}$. This shows that $\forall t,\ \mathbf{Z}(t) \in \mathcal{F}$. Hence we propose the second integral form:

$$\begin{cases} (\mathbf{P}_2\mathbf{U})(t) &= \phi(t), \quad t \in [-\tau_m, 0] \\ (\mathbf{P}_2\mathbf{U})(t) &= e^{(\tilde{\mathbf{J}}-\mathbf{L}_0)t}\mathbf{U}(0) - \mathbf{Z}(t) + e^{(\tilde{\mathbf{J}}-\mathbf{L}_0)t}\mathbf{Z}(0) - \int_0^t ds(\tilde{\mathbf{J}}-\mathbf{L}_0)e^{(\tilde{\mathbf{J}}-\mathbf{L}_0)(t-s)}\mathbf{Z}(s), \quad t \geq 0 \end{cases} \tag{4.30}$$

We have the following lemma.

Lemma 4.5.6. *The formulation* (4.30) *is equivalent to (4.6).*

Proof. The idea is to write the linearized equation as:

$$\begin{cases} \frac{d}{dt}\mathbf{U} &= (-\mathbf{L}_0 + \tilde{\mathbf{J}})\mathbf{U} - \frac{d}{dt}\mathbf{Z}(t) \\ \mathbf{U}_0 &= \phi \end{cases} \tag{4.31}$$

By the variation-of-parameters formula we have:

$$\mathbf{U}(t) = e^{(\tilde{\mathbf{J}}-\mathbf{L}_0)t}\mathbf{U}(0) - \int_0^t e^{(\tilde{\mathbf{J}}-\mathbf{L}_0)(t-s)}\frac{d}{ds}\mathbf{Z}(s)\,ds.$$

We then use an integration by parts:

$$\int_0^t e^{(\tilde{\mathbf{J}}-\mathbf{L}_0)(t-s)}\frac{d}{ds}\mathbf{Z}(s)\,ds = \mathbf{Z}(t) - e^{(\tilde{\mathbf{J}}-\mathbf{L}_0)t}\mathbf{Z}(0) + \int_0^t (\tilde{\mathbf{J}}-\mathbf{L}_0)e^{(\tilde{\mathbf{J}}-\mathbf{L}_0)(t-s)}\mathbf{Z}(s)\,ds$$

which allows us to conclude. □

Using the two integral formulations of (4.6) we obtain sufficient conditions of stability, as stated in the following proposition:

Proposition 4.5.7. *If one of the following two conditions is satisfied:*

1. $\max \Re\Sigma(\tilde{\mathbf{J}} - \mathbf{L}_0) < 0$ *and there exist* $\alpha < 1,\ \beta > 0$ *such that*

$$\tau_m^{\frac{3}{2}+\beta} \left\| \frac{\tilde{\mathbf{J}}}{\boldsymbol{\tau}^\beta} \right\|_{\mathbf{L}^2(\Omega^2, \mathbb{R}^{p\times p})} \left(1 + \sup_{t\geq 0} \int_0^t ds |||(\tilde{\mathbf{J}}-\mathbf{L}_0)e^{(\tilde{\mathbf{J}}-\mathbf{L}_0)(t-s)}|||_{\mathcal{F}}\right) \leq \alpha.$$

2. $\|\tilde{\mathbf{J}}\|_{\mathbf{L}^2(\Omega^2, \mathbb{R}^{p\times p})} < \min_i l_i.$

then $\mathbf{V}^f$ *is asymptotically stable for (4.4), hence in* $\mathcal{C}$.

Proof. We start with the first condition. The problem (4.6) is equivalent to solving the fixed point equation $\mathbf{U} = \mathbf{P}_2\mathbf{U}$ for an initial condition $\phi \in \mathcal{C}$. Let us define the Banach space $\mathcal{B} = C^0([-\tau_m, \infty), \mathcal{F})$ with the supremum norm written $\|\cdot\|_{\infty,\mathcal{F}}$, as well as

$$\mathcal{S}_\phi = \left\{\psi \in \mathcal{B},\ \psi|_{[-\tau_m,0]} = \phi \text{ and } \psi \to 0 \text{ as } t \to \infty\right\}$$

$\mathcal{S}_\phi$ is a complete space because it is closed in the complete space $\mathcal{B}$. We define $\mathbf{P}_2$ on $\mathcal{S}_\phi$. For all $\psi \in \mathcal{S}_\phi$ we have $\mathbf{P}_2\psi \in \mathcal{B}$ and $(\mathbf{P}_2\psi)(0) = \phi(0)$. We want to show that $\mathbf{P}_2\mathcal{S}_\phi \subset \mathcal{S}_\phi$. We prove two properties.

1. $\mathbf{P}_2\psi$ tends to zero at infinity.

Choose $\psi \in \mathcal{S}_\phi$.

Using corollary B.6.1, we have $\mathbf{Z}(t) \to 0$ as $t \to \infty$.

Let $0 < T < t$, we also have

$$\left\| \int_0^t (\tilde{\mathbf{J}} - \mathbf{L}_0) e^{(\tilde{\mathbf{J}}-\mathbf{L}_0)(t-s)} \mathbf{Z}(s) \right\|_{\mathcal{F}} \leq$$
$$\left\| \int_0^T (\tilde{\mathbf{J}} - \mathbf{L}_0) e^{(\tilde{\mathbf{J}}-\mathbf{L}_0)(t-s)} \mathbf{Z}(s) ds \right\|_{\mathcal{F}} + \left\| \int_T^t (\tilde{\mathbf{J}} - \mathbf{L}_0) e^{(\tilde{\mathbf{J}}-\mathbf{L}_0)(t-s)} \mathbf{Z}(s) ds \right\|_{\mathcal{F}}$$

For the first term we write:

$$\left\| \int_0^T (\tilde{\mathbf{J}} - \mathbf{L}_0) e^{(\tilde{\mathbf{J}}-\mathbf{L}_0)(t-s)} \mathbf{Z}(s)\, ds \right\|_{\mathcal{F}} \leq \int_0^T \left\| (\tilde{\mathbf{J}} - \mathbf{L}_0) e^{(\tilde{\mathbf{J}}-\mathbf{L}_0)(t-s)} \mathbf{Z}(s) \right\|_{\mathcal{F}} ds \leq$$
$$\left\| \left\| e^{(\tilde{\mathbf{J}}-\mathbf{L}_0)(t-T)} \right\| \right\|_{\mathcal{F}} \cdot \int_0^T |\!|\!| (\tilde{\mathbf{J}} - \mathbf{L}_0) e^{(\tilde{\mathbf{J}}-\mathbf{L}_0)(T-s)} |\!|\!|_{\mathcal{F}} \cdot \|\mathbf{Z}(s)\|_{\mathcal{F}} ds \leq$$
$$\tau_m{}^{\frac{3}{2}+\beta} \left\| \frac{\tilde{\mathbf{J}}}{\boldsymbol{\tau}^\beta} \right\|_{\mathbf{L}^2(\Omega^2, \mathbb{R}^{p\times p})} \cdot \left\| \left\| e^{(\tilde{\mathbf{J}}-\mathbf{L}_0)(t-T)} \right\| \right\|_{\mathcal{F}} \cdot \int_0^T \left\| \left\| (\tilde{\mathbf{J}} - \mathbf{L}_0) e^{(\tilde{\mathbf{J}}-\mathbf{L}_0)(T-s)} \right\| \right\|_{\mathcal{F}} ds \cdot \|\psi\|_{\infty,\mathcal{F}}$$
$$\leq \alpha \left\| \left\| e^{(\tilde{\mathbf{J}}-\mathbf{L}_0)(t-T)} \right\| \right\|_{\mathcal{F}} \cdot \|\psi\|_{\infty,\mathcal{F}}$$

Similarly, for the second term we write

$$\left\| \int_T^t (\tilde{\mathbf{J}} - \mathbf{L}_0) e^{(\tilde{\mathbf{J}}-\mathbf{L}_0)(t-s)} \mathbf{Z}(s) ds \right\|_{\mathcal{F}} \leq$$
$$\tau_m{}^{\frac{3}{2}+\beta} \left\| \frac{\tilde{\mathbf{J}}}{\boldsymbol{\tau}^\beta} \right\|_{\mathbf{L}^2(\Omega^2, \mathbb{R}^{p\times p})} \cdot \int_T^t \left\| \left\| (\tilde{\mathbf{J}} - \mathbf{L}_0) e^{(\tilde{\mathbf{J}}-\mathbf{L}_0)(t-s)} \right\| \right\|_{\mathcal{F}} ds \cdot \sup_{s\in[T-\tau_m,\infty)} \|\psi(s)\|_{\mathcal{F}} \leq$$
$$\alpha \sup_{s\in[T-\tau_m,\infty)} \|\psi(s)\|_{\mathcal{F}}$$

Now for a given $\varepsilon > 0$ we choose T large enough so that $\alpha \sup_{s\in[T-\tau_m,\infty)} \|\psi(s)\|_{\mathcal{F}} < \varepsilon/2$. For such a T we choose t^* large enough so that $\alpha \left\| \left\| e^{(\tilde{\mathbf{J}}-\mathbf{L}_0)(t-T)} \right\| \right\|_{\mathcal{F}} \cdot \|\psi\|_{\infty,\mathcal{F}} < \varepsilon/2$ for $t > t^*$. Putting all this together, for all $t > t^*$:

$$\left\| \int_0^t (\tilde{\mathbf{J}} - \mathbf{L}_0) e^{(\tilde{\mathbf{J}}-\mathbf{L}_0)(t-s)} \mathbf{Z}(s) ds \right\|_{\mathcal{F}} \leq \varepsilon.$$

From (4.30), it follows that $\mathbf{P}_2\psi \to 0$ when $t \to \infty$.

Since $\mathbf{P}_2\psi$ is continuous and has a limit when $t \to \infty$ it is bounded and therefore $\mathbf{P}_2 : \mathcal{S}_\phi \to \mathcal{S}_\phi$.

2. $\mathbf{P}_2$ is contracting on $\mathcal{S}_\phi$

Using (4.30) for all $\psi_1, \psi_2 \in \mathcal{S}_\phi$ we have

$$\begin{aligned}
&\|(\mathbf{P}_2\psi_1)(t) - (\mathbf{P}_2\psi_2)(t)\|_{\mathcal{F}} \leq \\
&\quad \|\mathbf{Z}_1(t) - \mathbf{Z}_2(t)\|_{\mathcal{F}} + \left\| \int_0^t ds(\tilde{\mathbf{J}} - \mathbf{L}_0) e^{(\tilde{\mathbf{J}}-\mathbf{L}_0)(t-s)} (\mathbf{Z}_1(s) - \mathbf{Z}_2(s)) \right\|_{\mathcal{F}} \leq \\
&\qquad \tau_m{}^{\frac{3}{2}+\beta} \left\| \frac{\tilde{\mathbf{J}}}{\boldsymbol{\tau}^\beta} \right\|_{\mathbf{L}^2(\Omega^2, \mathbb{R}^{p\times p})} \|\psi_1 - \psi_2\|_{\infty,\mathcal{F}} + \\
&\tau_m{}^{\frac{3}{2}+\beta} \left\| \frac{\tilde{\mathbf{J}}}{\boldsymbol{\tau}^\beta} \right\|_{\mathbf{L}^2(\Omega^2, \mathbb{R}^{p\times p})} \|\psi_1 - \psi_2\|_{\infty,\mathcal{F}} \int_0^t ds \left\| \left\| (\tilde{\mathbf{J}} - \mathbf{L}_0) e^{(\tilde{\mathbf{J}}-\mathbf{L}_0)(s-t)} \right\| \right\|_{\mathcal{F}} \\
&\qquad\qquad \leq \alpha \|\psi_1 - \psi_2\|_{\infty,\mathcal{F}}
\end{aligned}$$

We conclude from Picard theorem that the operator $\mathbf{P}_2$ has a unique fixed point in $\mathcal{S}_\phi$.

There remains to link this fixed point to the definition of stability and first show that

$$\forall \varepsilon > 0 \ \exists \delta \text{ such that } \|\phi\|_{\mathcal{C}} \leq \delta \text{ implies } \|\mathbf{U}(t,\phi)\|_{\mathcal{C}} < \varepsilon, \quad t \geq 0,$$

where $\mathbf{U}(t,\phi)$ is the solution of (4.25) with initial condition $\phi \in \mathcal{C}$.

Let us choose $\varepsilon > 0$ and $M \geq 1$ such that $\left\| \left\| e^{(\tilde{\mathbf{J}}-\mathbf{L}_0)t} \right\| \right\|_{\mathcal{F}} \leq M$. M exists because, by hypoThesis, $\max \Re\Sigma(\tilde{\mathbf{J}} - \mathbf{L}_0) < 0$. We then choose $\delta < \varepsilon$ satisfying

$$M \left(1 + \tau_m{}^{\frac{3}{2}+\beta} \left\| \frac{\tilde{\mathbf{J}}}{\boldsymbol{\tau}^\beta} \right\|_{\mathbf{L}^2(\Omega^2, \mathbb{R}^{p\times p})} \right) \delta < \varepsilon(1-\alpha), \tag{4.32}$$

and $\phi \in \mathcal{C}$ such that $\|\phi\|_{\mathcal{C}} \leq \delta$. Next define

$$\mathcal{S}_{\phi,\varepsilon} = \left\{ \psi \in \mathcal{B}, \|\psi\|_{\infty,\mathcal{F}} \leq \varepsilon, \ \psi|_{[-\tau_m,0]} = \phi \text{ and } \psi \to 0 \text{ as } t \to \infty \right\} \subset \mathcal{S}_\phi$$

We already know that $\mathbf{P}_2$ is a contraction on $\mathcal{S}_{\phi,\varepsilon}$ (which is a complete space because it is closed in the complete space $\mathcal{S}_\phi$). The last thing to check is $\mathbf{P}_2\mathcal{S}_{\phi,\varepsilon} \subset$

$\mathcal{S}_{\phi,\varepsilon}$, that is $\forall\psi \in \mathcal{S}_{\phi,\varepsilon}$, $\|\mathbf{P}_2\psi\|_{\infty,\mathcal{F}} < \varepsilon$. Using lemma B.6.1 in appendix B.6.1:

$$\|(\mathbf{P}_2\psi)(t)\|_{\mathcal{F}} \leq M\delta + \|\mathbf{Z}(t)\|_{\mathcal{F}} + \left\|e^{(\tilde{\mathbf{J}}-\mathbf{L}_0)t}\mathbf{Z}(0)\right\|_{\mathcal{F}} + \left\|\int_0^t (\tilde{\mathbf{J}}-\mathbf{L}_0)e^{(\tilde{\mathbf{J}}-\mathbf{L}_0)(t-s)}\mathbf{Z}(s)\,ds\right\|_{\mathcal{F}}$$

$$\leq M\delta + \|\mathbf{Z}(t)\|_{\mathcal{F}} + M\|\mathbf{Z}(0)\|_{\mathcal{F}} + \|\mathbf{Z}\|_{\infty,\mathcal{F}} \int_0^t \left|\left|\left|(\tilde{\mathbf{J}}-\mathbf{L}_0)e^{(\tilde{\mathbf{J}}-\mathbf{L}_0)(t-s)}\right|\right|\right|_{\mathcal{F}} ds$$

$$\leq M\delta + \tau_m{}^{\frac{3}{2}+\beta}\left\|\frac{\tilde{\mathbf{J}}}{\boldsymbol{\tau}^\beta}\right\|_{\mathbf{L}^2(\Omega^2,\mathbb{R}^{p\times p})} \|\psi_t\|_{\mathcal{C}} + M\tau_m{}^{\frac{3}{2}+\beta}\left\|\frac{\tilde{\mathbf{J}}}{\boldsymbol{\tau}^\beta}\right\|_{\mathbf{L}^2(\Omega^2,\mathbb{R}^{p\times p})}\delta +$$

$$\sup_{s\in(0,t)}\|\psi_s\|_{\mathcal{C}} \int_0^t \left|\left|\left|(\tilde{\mathbf{J}}-\mathbf{L}_0)e^{(\tilde{\mathbf{J}}-\mathbf{L}_0)(t-s)}\right|\right|\right|_{\mathcal{F}} ds \leq$$

$$M\delta + \alpha\varepsilon + M\tau_m{}^{\frac{3}{2}+\beta}\left\|\frac{\tilde{\mathbf{J}}}{\boldsymbol{\tau}^\beta}\right\|_{\mathbf{L}^2(\Omega^2,\mathbb{R}^{p\times p})}\delta$$

$$= M\left(1 + \tau_m{}^{\frac{3}{2}+\beta}\left\|\frac{\tilde{\mathbf{J}}}{\boldsymbol{\tau}^\beta}\right\|_{\mathbf{L}^2(\Omega^2,\mathbb{R}^{p\times p})}\right)\delta + \alpha\varepsilon < \varepsilon$$

Thus $\mathbf{P}_2$ has a unique fixed point $\mathbf{U}^{\phi,\varepsilon}$ in $\mathcal{S}_{\phi,\varepsilon}$ $\forall\phi,\varepsilon$ which is the solution of the linear delayed differential equation *i.e.*

$$\forall\varepsilon, \exists\delta < \varepsilon \text{ (from (4.32))}, \mid \forall\phi \in \mathcal{C},\ \|\phi\| \leq \delta \Rightarrow \forall t > 0, \|\mathbf{U}^{\phi,\varepsilon}\|_{\infty,\mathcal{F}} \leq \varepsilon \text{ and } \mathbf{U}^{\phi,\varepsilon}(t) \to 0 \text{ in } \mathcal{F}$$

As $\mathbf{U}^{\phi,\varepsilon}(t) \to 0$ in $\mathcal{F}$ implies $\mathbf{U}_t^{\phi,\varepsilon} \to 0$ in $\mathcal{C}$, we have proved the asymptotic stability for the linearized equation.

The proof of the second property is straightforward. If 0 is asymptotically stable for (4.6) all the CV are negative and corollary 4.5.2 indicates that $\mathbf{V}^f$ is asymptotically stable for (4.4).

The second condition says that $\mathbf{P}_1\psi = e^{-\mathbf{L}_0 t}\phi(0) + \int_0^t e^{-\mathbf{L}_0(t-s)}(\tilde{\mathbf{L}}_1\psi)(s)ds$ is a contraction because

$\|(\mathbf{P}_1\psi_1)(t) - (\mathbf{P}_1\psi_2)(t)\|_{\mathcal{F}} \leq \frac{|||\tilde{\mathbf{J}}|||_{\mathcal{F}}}{\min_i l_i}\|\psi_1 - \psi_2\|_{\infty,\mathcal{F}}$.

The asymptotic stability follows using the same arguments as in the case of $\mathbf{P}_2$.

□

We next simplify the first condition of the previous proposition to make it more amenable to numerics.

Corollary 4.5.8. *Suppose that* $\forall t \geq 0,\ |||e^{(\tilde{\mathbf{J}}-\mathbf{L}_0)t}|||_{\mathcal{F}} \leq M_\varepsilon e^{-t\varepsilon}$ *with* $\varepsilon > 0$.

If there exist $\alpha < 1,\ \beta > 0$ *such that*

$\tau_m^{\frac{3}{2}+\beta}\left\|\frac{\tilde{\mathbf{J}}}{\boldsymbol{\tau}^\beta}\right\|_{\mathbf{L}^2(\Omega^2,\mathbb{R}^{p\times p})}\left(1 + \frac{M_\varepsilon}{\varepsilon}\left\|\tilde{\mathbf{J}} - \mathbf{L}_0\right\|_{\mathbf{L}^2(\Omega^2,\mathbb{R}^{p\times p})}\right) \leq \alpha$, *then* $\mathbf{V}^f$ *is asymptotically stable.*

Proof. This corollary follows immediately from the following upper-bound of the integral $\int_0^t |||e^{(\tilde{\mathbf{J}}-\mathbf{L}_0)(t-s)}|||_{\mathcal{F}}\, ds \leq M_\varepsilon \frac{1-e^{-\varepsilon t}}{\varepsilon} \leq \frac{M_\varepsilon}{\varepsilon}$. Then if there exists $\alpha < 1,\ \beta > 0$ such that $\tau_m^{\frac{3}{2}+\beta} \left\| \frac{\tilde{\mathbf{J}}}{\boldsymbol{\tau}^\beta} \right\|_{\mathbf{L}^2(\Omega^2,\mathbb{R}^{p\times p})} \left(1 + \frac{M_\varepsilon}{\varepsilon} \left\| \tilde{\mathbf{J}} - \mathbf{L}_0 \right\|_{\mathbf{L}^2(\Omega^2,\mathbb{R}^{p\times p})}\right) \leq \alpha$, it implies that the condition 1. in proposition 4.5.7 is satisfied, from which the asymptotic stability of $\mathbf{V}^f$ follows. □

Notice that $\varepsilon > 0$ is equivalent to $\max \Re\Sigma(-\mathbf{L}_0 + \tilde{\mathbf{J}}) < 0$. The previous corollary is useful in at least the following cases:

- If $\tilde{\mathbf{J}} - \mathbf{L}_0$ is diagonalizable, with associated eigenvalues/eigenvectors: $\lambda_n \in \mathbb{C}, e_n \in \mathcal{F}$, then $\tilde{\mathbf{J}} - \mathbf{L}_0 = \sum_n e^{\lambda_n t} e_n \otimes e_n$ and $|||e^{(\tilde{\mathbf{J}}-\mathbf{L}_0)t}|||_{\mathcal{F}} \leq e^{-t \max\limits_n \lambda_n} = e^{t \max \Re\Sigma(-\mathbf{L}_0+\tilde{\mathbf{J}})}$.
- If $\mathbf{L}_0 = l_0 \mathrm{Id}$ and the range of $\tilde{\mathbf{J}}$ is finite dimensional: $\tilde{\mathbf{J}}(\mathbf{r},\mathbf{r}') = \sum\limits_{k,l=1}^{N} J_{kl} e_k(\mathbf{r}) \otimes e_l(\mathbf{r}')$ where $(e_k)_{k\in\mathbb{N}}$ is an orthonormal basis of $\mathcal{F}$, then $e^{(\tilde{\mathbf{J}}-\mathbf{L}_0)t} = e^{-l_0 \cdot \mathrm{Id} \cdot t} e^{\tilde{\mathbf{J}}t}$ and $|||e^{(\tilde{\mathbf{J}}-\mathbf{L}_0)t}|||_{\mathcal{F}} \leq e^{-l_0 t} |||e^{\tilde{\mathbf{J}}t}|||_{\mathcal{F}}$. Let us write $J = (J_{kl})_{k,l=1\cdots N}$ the matrix associated to $\tilde{\mathbf{J}}$ (see above). Then $e^{\tilde{\mathbf{J}}t}$ is also a compact operator with finite range and $|||e^{\tilde{\mathbf{J}}t}|||_{\mathcal{F}} \leq \left\| e^{\tilde{\mathbf{J}}t} \right\|_{\mathbf{L}^2(\Omega^2,\mathbb{R}^{p\times p})} = \sqrt{Tr(e^{(\tilde{\mathbf{J}}+\tilde{\mathbf{J}}^*)t})} = \left(\sum\limits_{\lambda \in \Sigma(\tilde{\mathbf{J}}+\tilde{\mathbf{J}}^*)} e^{\lambda t} \right)^{1/2} \leq \sqrt{N} e^{\max \Re\Sigma(\tilde{\mathbf{J}})t}$. Finally, it gives $|||e^{(\tilde{\mathbf{J}}-\mathbf{L}_0)t}|||_{\mathcal{F}} \leq \sqrt{N} e^{t \max \Re\Sigma(-\mathbf{L}_0+\tilde{\mathbf{J}})}$.
- If $\tilde{\mathbf{J}} - \mathbf{L}_0$ is self-adjoint, then it is diagonalizable and we can chose $\varepsilon = \max \Re\Sigma(-\mathbf{L}_0 + \tilde{\mathbf{J}})$, $M_\varepsilon = 1$.

Remark 24. *If we suppose that we have higher order time derivatives as in section 4.5.2, we can write the linearized equation as*

$$\dot{\mathcal{U}}(t) = -\mathcal{L}_0 \mathcal{U}(t) + \tilde{\mathcal{L}}_1 \mathcal{U}_t \tag{4.33}$$

Suppose that $\mathcal{L}_0$ is diagonalizable then $|||e^{-\mathcal{L}_0 t}|||_{(\mathcal{F})^{d_s}} \leq e^{-\min \Re\Sigma(\mathcal{L}_0)t}$ where $\|\mathcal{U}\|_{(\mathcal{F})^{d_s}} \equiv \sum\limits_{k=1}^{d_s} \|\mathcal{U}_k\|_{\mathcal{F}}$ and $-\min \Re\Sigma(\mathcal{L}_0) = \max\limits_k \Re Root(P_k)$. Also notice that $\tilde{\mathcal{J}} = \tilde{\mathcal{L}}_1|_{\mathcal{F}}$, $|||\mathcal{L}_1|||_{(\mathcal{C})^{d_s}} \leq |||\mathbf{L}_1|||_{\mathcal{C}}$. Then using the same functionals as in the proof of proposition 4.5.7, we can find two bounds for the stability of a stationary state $\mathbf{V}^f$:

- *Suppose that $\max \Re\Sigma(\tilde{\mathcal{J}} - \mathcal{L}_0) < 0$ i.e. $\mathbf{V}^f$ is stable for the non-delayed equation where $(\tilde{\mathcal{J}})_{k,l=1\cdots d_s} = (\delta_{k=d_s,l=1}\tilde{\mathbf{J}})_{k,l=1\cdots d_s}$. If there exist $\alpha < 1,\ \beta > 0$ such that $\tau_m^{\frac{3}{2}+\beta} \left\| \frac{\tilde{\mathbf{J}}}{\boldsymbol{\tau}^\beta} \right\|_{\mathbf{L}^2(\Omega^2,\mathbb{R}^{p\times p})} \left(1 + \sup\limits_{t\geq 0} \int\limits_0^t ds |||(\mathcal{L}_0 + \tilde{\mathcal{J}})e^{(\mathcal{L}_0+\tilde{\mathcal{J}})(t-s)}|||_{(\mathcal{F})^{d_s}}\right) \leq \alpha$.*

- $\|\tilde{\mathbf{J}}\|_{\mathbf{L}^2(\Omega^2,\mathbb{R}^{p\times p})} < \max_k \Re Root(P_k)$.

To conclude, we have found an easy-to-compute formula for the stability of the persistent state $\mathbf{V}^f$. It can indeed be cumbersome to compute the CVs of neural field equations for different parameters in order to find the region of stability whereas the evaluation of the conditions in Corollary 4.5.8 is very easy numerically.

The conditions in proposition 4.5.7 and corollary 4.5.8 define a set of parameters for which $\mathbf{V}^f$ is stable in $\mathcal{C}$. Notice that these conditions are only sufficient conditions: if they are violated, $\mathbf{V}^f$ may still remain stable. In order to find out whether the persistent state is destabilized we have to look at the characteristic values.

Condition 1 in proposition 4.5.7 indicates that if $\mathbf{V}^f$ is a stable point for the non-delayed equation (see [Faugeras 2009]) it is also stable for the delayed-equation. Thus, according to this condition, it is not possible to destabilize a stable persistent state by the introduction of small delays, which is indeed meaningful from the biological viewpoint. Moreover this condition gives an indication of the amount of delay one can introduce without changing the stability.

Condition 2 is not very useful as it is independent of the delays: no matter what they are, the stable point $\mathbf{V}^f$ will remain stable. Also, if this condition is satisfied there is a unique stationary solution (see [Faugeras 2009]) and the dynamics is trivial, i.e. converging to the unique stationary point.

4.5.4 Summary of the different stability bounds

The next proposition summarizes the results we have obtained in proposition 4.5.7 and corollary 4.5.8 for the stability of a stationary solution.

Proposition 4.5.9. *If one of the following conditions is satisfied:*

1. *There exist* $\varepsilon > 0$ *such that* $|||e^{-(\tilde{\mathbf{J}}-\mathbf{L}_0)t}|||_{\mathcal{F}} \leq M_\varepsilon e^{-\varepsilon t}$ *and* $\alpha < 1$, $\beta > 0$ *such that*
$$\tau_m^{\frac{3}{2}+\beta} \left\| \frac{\tilde{\mathbf{J}}}{\boldsymbol{\tau}^\beta} \right\|_{L^2(\Omega^2,\mathbb{R}^{p\times p})} \left(1 + \frac{M_\varepsilon}{\varepsilon} \left\| \tilde{\mathbf{J}} - \mathbf{L}_0 \right\|_{\mathbf{L}^2(\Omega^2,\mathbb{R}^{p\times p})}\right) \leq \alpha,$$
2. $\|\tilde{\mathbf{J}}\|_{\mathbf{L}^2(\Omega^2,\mathbb{R}^{p\times p})} < \min_i l_i$

then $\mathbf{V}^f$ *is asymptotically stable for (4.4).*

The only general results known so far for the stability of the stationary solutions are those of Atay and Hutt (see for example [Atay 2005]): they found a bound similar to condition 2 in proposition 4.5.9 by using the CVs, but no proof of stability was given. Their condition involves the L^1-norm of the connectivity function $\mathbf{J}$ and it was derived using the CVs in the same way as we did in the previous section. Thus our contribution with respect to condition 2 is that, once it is satisfied, the stationary solution is asymptotically stable: up until now this was numerically inferred on the basis of the CVs. We have *proved* it in two ways, first by using the CVs, and second by using the fixed point method.

Condition 1 is of interest, because it allows one to find the minimal propagation delay that does not destabilize. Notice that this bound, though very easy to compute, overestimates the minimal speed.

As mentioned above, the bounds in condition 1 are sufficient conditions for the stability of the stationary state $\mathbf{V}^f$. In order to evaluate the conservativeness of these bounds, we need to compare them to the stability predicted by the CVs. This is done in chapter 6 on one specific example.

4.6 Center manifold reduction

Let us recall what we have done so far. We have considered a stationary cortical state $\mathbf{V}^f$ of the delayed neural field equations (4.1). We have shown how to compute the punctual spectrum Σ_p of the linearized equation and have proved that the equilibria $\mathbf{V}^f$ is asymptotically stable if and only if all elements in the spectrum have negative real parts. In the case where some eigenvalue has positive real part the local dynamics around $\mathbf{V}^f$ is exponentially divergent. In particular, we have a good understanding of the dynamics as long as $\Sigma_c \equiv \Sigma_p(\mathbf{A}) \cap i\mathbb{R} = \emptyset$.

In the case where $\Sigma_c \neq \emptyset$, our program is to study the nonlinear dynamics of (4.1), using the tools of [Haragus 2010]. We find a manifold, called the *center manifold*, which is invariant by the dynamics of (4.1) and which is (exponentially) attractive if $\Sigma_u(\mathbf{A}) = \emptyset$. From lemma 4.4.2, the center part $\mathcal{X}_c$ of the history space is finite dimensional. As it has the same dimension as the center manifold, it follows that the center manifold is also finite dimensional. Hence, when studying the neural field equations with a non empty *center part*, we can restrict the study to the center manifold, which produces the local non trivial dynamics: it gives a finite dimensional system without approximation. A *bifurcation* is said to occur when the center part changes.

The study of the center manifold theorem in infinite dimension has led to some 'optimal' requirements to make the theorem work. The first is to write the dynamical system as an abstract Cauchy problem a bit more specific than (4.3). More precisely, we need to find three Banach spaces $\mathcal{Z} \hookrightarrow \mathcal{Y} \hookrightarrow \mathcal{X}$ with continuous embeddings such that

$$\frac{d}{dt}u = \mathbf{A}u + \mathbf{R}(u) \tag{4.34}$$

where $\mathbf{A}$ is a continuous linear operator in $\mathcal{L}(\mathcal{Z}, \mathcal{X})$ and $\mathbf{R} \in C^k(\mathcal{V}, \mathcal{Y})$, $k \geq 2$, is a nonlinear function defined on a neighborhood $\mathcal{V} \subset \mathcal{Z}$ of 0 satisfying $\mathbf{R}(0) = 0$ and $D\mathbf{R}(0) = 0$. Then the spectrum of the linear operator $\mathbf{A}$ needs to have a spectral decomposition with finite dimensional central part $\mathcal{X}_c$ and a spectral gap γ as in section 4.4.4. This gives a finite dimensional center manifold and well defined convergence/divergence rates to/from the center manifold. Finally, the linear system

$$\frac{d}{dt}u = \mathbf{A}u + f(t)$$

has to feature exponentially bounded solutions for $t \in \mathbb{R}$ for some exponentially bounded function f defined on $\mathbb{R}$. This will be explained more precisely below. This last property is needed to give some regularity to the center manifold (it has the same regularity as $\mathbf{R}$) and also to prove its existence. Note that in the "simple" version of the Center Manifold theorem that we give in appendix A.1, the fourth condition implies that the above linear system can be solved. We check the conditions in the next subsections.

We prove the center manifold theorem for delayed neural field equations in theorem 4.6.3. Then, we consider the problem of establishing the normal forms of several important static and dynamic bifurcations. The (classical) idea being that a) these normal forms are the same for all systems satisfying the same non-degeneracy conditions and the same conditions on the spectrum and b) if we understand their dynamics we will understand that of (4.2) (see, e.g. [Guckenheimer 1983, Kuznetsov 1998, Haragus 2010]).

4.6.1 Formulation as a Cauchy problem

We start by writing (4.2) as in (4.34). We choose a stationary cortical state $\mathbf{V}^f$ and $\mathbf{A}$ as in (4.11). Let us consider a parameter μ, for example it can be the nonlinear gain σ, the constant delay D or the pair (σ, c): we assume that $\mu \in \mathbb{R}^{m_{par}}$, m_{par} being the number of parameters. Notice that the equilibrium $\mathbf{V}^f$ may depend on μ. It is such that when $\mu = \mu_c$, then the punctual spectrum contains purely imaginary eigenvalues. We write the equation (4.4) for a perturbation $\mathbf{U}$ of $\mathbf{V}^f$ where $\mathbf{V}(t) = \mathbf{V}^f + \mathbf{U}(t)$:

$$\dot{\mathbf{U}}(t) = -\mathbf{L}_0\mathbf{U}(t) + \mathbf{L}_1(\mu) \cdot \Big(\mathbf{S}(\mathbf{U}_t + \mathbf{V}^f) - \mathbf{S}(\mathbf{V}^f)\Big) \tag{4.35}$$

Using a Taylor expansion with integral remainder (we have also made the dependency of $\mathbf{V}^f$ on the parameter μ implicit), we find:

$$\begin{aligned} -\mathbf{L}_0\mathbf{U}(t) + \mathbf{L}_1(\mu) \cdot \Big(\mathbf{S}(\mathbf{U}_t + \mathbf{V}^f) - \mathbf{S}(\mathbf{V}^f)\Big) = \\ (-\mathbf{L}_0 + \mathbf{L}_1(\mu)) \cdot \mathbf{U}_t + \mathbf{L}_1(\mu) \cdot \int_0^1 (1-s)\mathbf{S}^{(2)}(\mathbf{V}^f + s\mathbf{U}_t)\mathbf{U}_t^2 ds \\ \equiv \mathbf{L}(\mu)\mathbf{U}_t + \mathbf{L}_1(\mu)\mathbf{G}(\mathbf{U}) \end{aligned} \tag{4.36}$$

In order to use [Haragus 2010, Theorem II.3.3], *i.e.* the parameter dependent center manifold, we write the previous equation:

$$\mathbf{L}(\mu)\mathbf{U}_t + \mathbf{L}_1(\mu)\mathbf{G}(\mathbf{U}) = \mathbf{L}(\mu_c)\mathbf{U}_t + (\mathbf{L}_1(\mu)\mathbf{G}(\mathbf{U}) + (\mathbf{L}(\mu) - \mathbf{L}(\mu_c))\mathbf{U}_t)$$

We take a classical solution $\mathbf{U}(t)$ of (4.35), *i.e.* a function $\mathbf{U} \in C^0([-\tau_m, \infty), \mathcal{F}) \cap C^1([0, \infty), \mathcal{F})$ such that $\mathbf{U}_t \in W^{1,2}(-\tau_m, 0; \mathcal{F})$ and $\mathbf{U}$ satisfies (4.35). The history

segment $u(t) \equiv \begin{bmatrix} \mathbf{U}(t) \\ \mathbf{U}_t \end{bmatrix}$ satisfies:

$$\begin{cases} \dot{u}(t) = \mathbf{A}u(t) + \mathbf{R}(u(t), \mu) \\ u(0) \in \mathcal{X} \end{cases} \quad \text{with} \quad \mathbf{R}(u, \mu) = \begin{bmatrix} \mathbf{L}_1(\mu)(\mathbf{G}(\pi_2(u)) + (\mathbf{L}(\mu) - \mathbf{L}(\mu_c))\pi_2(u) \\ 0 \end{bmatrix} \tag{4.37}$$

and $\mathbf{A}$ is given by (4.11). It follows that $\mathbf{R}(0, \mu_c) = 0$, $D\mathbf{R}(0, \mu_c) = 0$. Indeed, we have removed the linear terms in the definition of $\mathbf{R}$. This is the Cauchy problem to which we will apply the Center Manifold Theorem. In order to apply this theorem, we need more regularity for $\mathbf{R}$. This is classically obtained by restricting the space. Thus, we define three Banach spaces for any integer $2 \leq q < \infty$. The "older" history space $\mathcal{X}$ corresponds to the case $q = 2$. Note that the spaces (for example) $\mathcal{X}^{(q)}$ are subsets of one another for deacreasing qs.

$$\begin{cases} \mathcal{X}^{(q)} \equiv \mathrm{L}^{\mathrm{q}} \times \mathrm{L}^{\mathrm{q}}(-\tau_{\mathrm{m}}, 0; \mathrm{L}^{\mathrm{q}}), \\ \mathcal{Y}^{(q)} \equiv \mathrm{L}^{\mathrm{q}} \times \mathrm{L}^{\mathrm{q}}(-\tau_{\mathrm{m}}, 0; \mathrm{L}^{\mathrm{q}}), \\ \mathcal{Z}^{(q)} \equiv \left\{ u \in \mathrm{L}^{\mathrm{q}} \times \mathrm{W}^{1,\mathrm{q}}(-\tau_{\mathrm{m}}, 0; \mathrm{L}^{\mathrm{q}}) \mid \pi_1 \mathrm{u} = (\pi_2 \mathrm{u})(0) \right\} \end{cases} \tag{4.38}$$

where $\mathrm{L}^{\mathrm{q}} \equiv \mathrm{L}^{\mathrm{q}}(\Omega, \mathbb{R}^{\mathrm{p}})$ and

$$\begin{array}{lcl} \|\phi\|_{\mathrm{L}^{\mathrm{q}}(-\tau_{\mathrm{m}}, 0; \mathrm{L}^{\mathrm{q}})} & = & \left(\int_{-\tau_m}^{0} \|\phi(\theta)\|_{\mathrm{L}^{\mathrm{q}}}^{q} \, d\theta \right)^{\frac{1}{q}} \\ \|\phi\|_{\mathrm{W}^{1,\mathrm{q}}(-\tau_{\mathrm{m}}, 0; \mathrm{L}^{\mathrm{q}})} & = & \|\phi\|_{\mathrm{L}^{\mathrm{q}}(-\tau_{\mathrm{m}}, 0; \mathrm{L}^{\mathrm{q}})} + \left\| \frac{d}{d\theta}\phi \right\|_{\mathrm{L}^{\mathrm{q}}(-\tau_{\mathrm{m}}, 0; \mathrm{L}^{\mathrm{q}})}. \end{array} \tag{4.39}$$

We write $\mathbf{A}_{(q)}$ the linear operator given by (4.11) with domain $D(\mathbf{A}_{(q)}) = \mathcal{Z}^{(q)}$. Then, the regularity of the nonlinear term $\mathbf{R}$ is given by the following lemma:

Lemma 4.6.1. *For all integer $2 \leq q < \infty$,*

$$\begin{array}{rcl} \mathbf{A}_{(q)} & \in & \mathcal{L}(\mathcal{Z}^{(q)}, \mathcal{X}^{(q)}), \\ \mathbf{R} & \in & \mathcal{C}^{q-1}(\mathcal{Z}^{(q)} \times \mathbb{R}^{m_{par}}, \mathcal{Y}^{(q)}). \end{array}$$

and

$$D_u^q \mathbf{R}(u_0, \mu)[u_1, \cdots, u_q] = \begin{bmatrix} \mathbf{L}_1(\mu)\mathbf{S}^{(q)}(\mathbf{V}^f)\pi_2(u_1 \cdots u_q) \\ 0 \end{bmatrix}, \text{ for } u_0 = \begin{bmatrix} \mathbf{V}^f \\ \mathbf{V}^f \end{bmatrix}$$

where $u_1 \cdots u_p$ is the component-wise product of the functions u_i. We also define condensed notations for $\mathbf{R}_q(u_0, \mu_0) \equiv \frac{1}{q!} D_u^q \mathbf{R}(u_0, \mu_0)$ and $\mathbf{R}_{ql}(u_0, \mu_0) \equiv \frac{1}{q!l!} \frac{\partial^{q+l}}{\partial^q u \partial^l \mu} \mathbf{R}(u_0, \mu_0)$.

Proof.

Case of $\mathbf{A}_{(q)}$. We use the continuous embeddings $W^{1,q}(-\tau_m, 0; \mathrm{L}^{\mathrm{q}}(\Omega, \mathbb{R}^{\mathrm{p}})) \hookrightarrow \mathrm{C}^0(-\tau_{\mathrm{m}}, 0; \mathrm{L}^{\mathrm{q}}(\Omega, \mathbb{R}^{\mathrm{p}}))$ and $\mathrm{L}^{\mathrm{q}} \hookrightarrow \mathrm{L}^1$. From lemma B.7.1:

$$\begin{aligned} &\|\mathbf{L}_1 \pi_2(u)\|_{\mathrm{L}^{\mathrm{q}}} \leq \|\mathbf{L}_1 \pi_2(u)\|_{\mathrm{L}^{\mathrm{q}}} = O\left(\|\pi_2(u)\|_{C^0(-\tau_m, 0; \mathrm{L}^1)} \right) \\ &= O\left(\|\pi_2(u)\|_{\mathrm{W}^{1,\mathrm{q}}(-\tau_{\mathrm{m}}, 0; \mathrm{L}^1)} \right) = O\left(\|\pi_2(u)\|_{\mathrm{W}^{1,\mathrm{q}}(-\tau_{\mathrm{m}}, 0; \mathrm{L}^{\mathrm{q}})} \right) = O\left(\|u\|_{\mathcal{Z}^{(q)}} \right). \end{aligned}$$

It follows that $\left\| \mathbf{A}_{(q)} u \right\|_{\mathcal{X}^{(q)}} = O\left(\|u\|_{\mathcal{Z}^{(q)}} \right)$ which proves that $\mathbf{A}_{(q)}$ is continuous.

Case of R. Let us ignore for simplicity the dependence on the parameter μ. It is easy to see from the definition (4.35) of $\mathbf{R}$ that, if it exists, $\pi_1 D^q\mathbf{R}(u_0)[u_1,\cdots,u_q] = \mathbf{L}_1\mathbf{S}^{(q)}(\mathbf{V}^f)\pi_2(u_1\cdots u_q)$ while $\pi_2 D^q\mathbf{R}(u_0) = 0$. The notation $u_1\cdots u_q$ is the component-wise product of the q functions $u_1,\cdots,u_q$ in $\mathcal{Z}^{(q)}$.

We write $\phi_i \equiv \pi_2 u_i$. As $W^{1,q}(-\tau_m,0;\mathrm{L^q}) \subset \mathrm{C}^0(-\tau_\mathrm{m},0;\mathrm{L}^1)$, we find, from the generalized Hölder's inequality, that $\forall\theta\ \phi_1(\theta)\cdots\phi_q(\theta)$ is in L^1 and

$$\|\phi_1\cdots\phi_q\|_{C^0(-\tau_m,0;\mathrm{L}^1)} \le \prod_{i=1}^{q}\|\phi_i\|_{C^0(-\tau_m,0;\mathrm{L^q})}\,.$$

From lemma B.7.1, it follows that $D^q\mathbf{R}(u_0)$ exists is continuous:

$$\begin{aligned}\|D^q\mathbf{R}(u_0)[u_1,\cdots,u_q]\|_{\mathcal{Y}^{(q)}} &= \|\mathbf{L}_1(\phi_1\cdots\phi_q)\|_{\mathrm{L^q}} \le \\ |||\mathbf{L}_1|||\cdot\|(\phi_1\cdots\phi_q)\|_{C^0(-\tau_m,0;\mathrm{L}^1)} &\le |||\mathbf{L}_1|||\cdot\prod_{i=1}^{q}\|\phi_i\|_{C^0(-\tau_m,0;\mathrm{L^q})} \\ \le K|||\mathbf{L}_1|||\cdot\prod_{i=1}^{q}\|\phi_i\|_{W^{1,q}(-\tau_m,0;\mathrm{L^q})} &\le K|||\mathbf{L}_1|||\cdot\prod_{i=1}^{q}\|u_i\|_{\mathcal{Z}^{(q)}}\end{aligned}$$

for some constant K. Note that we have used the continuous embedding $W^{1,q}(-\tau_m,0;\mathrm{L^q}(\Omega,\mathbb{R}^\mathrm{p}) \hookrightarrow \mathrm{C}^0(-\tau_\mathrm{m},0;\mathrm{L^q}(\Omega,\mathbb{R}^\mathrm{p}))$. To prove that $\mathbf{R} \in \mathcal{C}^q(\mathcal{Z}^{(q+1)}\times\mathbb{R}^{m_{par}},\mathcal{Y}^{(q+1)})$, we first notice that the above expression for $D^q\mathbf{R}(u_0)$ exists and is well defined because $\mathcal{Y}^{(q+1)}\hookrightarrow\mathcal{Y}^{(q)}$ and $\mathcal{Z}^{(q+1)}\hookrightarrow\mathcal{Z}^{(q)}$. Using the Taylor expansion with integral remainder at order q of $\mathbf{S}$, it is easy to find a power expansion of $\pi_1\mathbf{R}(u)$ up to order q with remainder

$$\frac{1}{q!}\mathbf{L}_1(\mu)\cdot\int_0^1(1-s)^q\mathbf{S}^{(q+1)}(\mathbf{V}^f+s\mathbf{U}_t)\mathbf{U}_t^{q+1}ds.$$

Using, the previous estimation, this remainder is of order $\|u\|^{q+1}_{\mathcal{Z}^{(q+1)}}$ and we can conclude that $\mathbf{R}$ is $\mathcal{C}^q$.

□

Hence we have the quasi-linear formulation (4.40) of the nonlinear problem (4.1):

$$\begin{cases}\mathbf{A}\in\mathcal{L}(\mathcal{Z}^{(q)},\mathcal{X}^{(q)}) \text{ continuous}\\ \mathbf{R}(\cdot,\mu)\in C^{q-1}(\mathcal{Z}^{(q)},\mathcal{Y}^{(q)}),\ \forall q\ge 2\\ \mathcal{Y}^{(q)}=\mathcal{X}^{(q)}\end{cases}\tag{4.40}$$

with continuous embeddings: $\mathcal{Z}^{(q)}\hookrightarrow\mathcal{Y}^{(q)}\hookrightarrow\mathcal{X}^{(q)}$. We refer the reader to section 4.4.4 for notations that are heavily used in the sequel.

It is easy to see that $\Sigma(\mathbf{A}_{(q)}) = \Sigma(\mathbf{A})$ if $\mathbf{J}\in\mathrm{L}^\infty(\Omega^2,\mathbb{R}^{\mathrm{p}\times\mathrm{p}})$ and that the eigenvectors are the same for the two operators. Also P_λ commutes with $\mathbf{A}_{(q)}$. Indeed, we can check that $\mathbf{A}_{(q)}P_\lambda = \lambda P_\lambda$ on $D(\mathbf{A}_{(q)})$. Moreover, $\langle u^*_\lambda, \mathbf{A}_{(q)}\phi\rangle_{\mathcal{X}^{(2)}} =$

$\langle u_\lambda^*, \mathbf{A}_2\phi\rangle_{\mathcal{X}^{(2)}} = \lambda\langle u_\lambda^*, \phi\rangle_{\mathcal{X}^{(2)}}$ because $\mathbf{A}_{(q)} = \mathbf{A}_2$ on $\mathcal{X}^{(q)}$. This last equality shows $P_\lambda \mathbf{A}_{(q)} = \lambda P_\lambda$ and we have found that P_λ commutes with $\mathbf{A}_{(q)}$. As a consequence, P_λ is the spectral projector of all the operators $\mathbf{A}_{(q)}$.

From the continuity[18] of $\mathbf{L}_1 \in \mathcal{L}(\mathrm{W}^{1,\mathrm{q}}(-\tau_\mathrm{m}, 0; \mathrm{L}^\mathrm{q}), \mathrm{L}^\mathrm{q})$ and from [Bátkai 2005][theorem II.3.23], $\mathbf{A}_{(q)}$ generates a strongly continuous semigroup $(\mathbf{T}_{(q)}(t))$ on $\mathcal{X}^{(q)}$. Lemma B.3.2, [Bátkai 2005][proposition 4.3] and theorem B.1.4 imply[19] that $(\mathbf{T}_{(q)}(t))$ satisfies the spectral mapping theorem and that the bounds for the hyperbolic projections found in section 4.4.4 in the case $q = 2$ are true for all integer $2 \leq q < \infty$.

We shall drop the index $^{(q)}$ even if all the spaces depend on the integer q from now on.

4.6.2 Solution of the inhomogeneous problem

Here, we prove the last condition (see the next proposition 4.6.2) for the application of the center manifold theorem. This condition is more general[20] than the fourth condition given in appendix A.1. This proposition is not easy to prove in general and the proof is usually done using the sufficient conditions given in [Haragus 2010] *i.e.* the norm of the resolvent $(i\omega - \mathbf{A})^{-1}$ has to be bounded by some power of $\frac{1}{|\omega|}$. This implies[21] that the spectrum of $\mathbf{A}$ is included in a cone centered on the real axis, the operator satisfying this condition are called *sectorial*. The spectrum does not satisfy this property in the general case. Indeed, by applying (4.15), we see that the spectrum is rather included in a cone with exponential boundary. Hence the resolvent $(i\omega - \mathbf{A})^{-1}$ is not bounded by some power of $\frac{1}{|\omega|}$ in our case. This is why we have to prove proposition 4.6.2 directly. Notice that the authors in [Iooss 2000] also prove a similar result for 'advance-delay' scalar differential equations with a method that is different from the one we describe in the present section. Let us comment a bit about the difficulties raised in proposition 4.6.2. We start with a definition for a given Banach space $\mathcal{E}$:

$$C^0_\eta(\mathbb{R}, \mathcal{E}) \equiv \left\{ \phi \in C^0(\mathbb{R}, \mathcal{E}), \|\phi\|_{C^0_\eta} \equiv \sup_{t\in\mathbb{R}} e^{-\eta|t|}\|\phi(t)\|_\mathcal{E} < \infty \right\}.$$

Let us define the hyperbolic projection of $\mathcal{Y}, \mathcal{Z}$ by $\mathcal{Y}_h \equiv P_h\mathcal{Y}$, $\mathcal{Z}_h \equiv P_h\mathcal{Z}$. We have to build a solution of (4.41) in $C^0_\eta(\mathbb{R}, \mathcal{Z}_h)$ which is linearly and continuously depending on $F \in C^0_\eta(\mathbb{R}, \mathcal{Y}_h)$. This solution $u = \mathbf{K}\cdot F$ is built using a variation-of-constants formula which uses a convolution of the semigroup $\mathbf{T}$ and F. The linear operator $\mathbf{K}$ is the operator that gives the unique solution of (4.41) given the term F. There are two main things to prove:

[18] it results from lemma B.3.1

[19] Modulo the change of variable $\mathbf{J}D\mathbf{S} \to \mathbf{J}$.

[20] the version of the theorem in appendix A.1 is simple but too restrictive for its application to the delayed systems.

[21] We thank G.Iooss for pointing out this fact.

- $u(t) \in \mathcal{Z}_h$ with $F(t) \in \mathcal{Y}_h$.
- $\|u(t)\|_{\mathcal{Z}}$ is exponentially bounded on $\mathbb{R}$.

However, from the proof of the center manifold theorem in [Haragus 2010], it can be noted that the linear operator $\mathbf{K}$ is always applied to vectors like $P_h\mathbf{R}(v)$, $P_hD\mathbf{R}(v)\cdots$ for some vector v. Given the particular shape of these vectors[22] $P_h\begin{bmatrix}\star\\0\end{bmatrix}$, we have to solve (4.41) for functions F that belong to a distinct subspace of $\mathcal{Y}$, *i.e.* the space $P_h\left(\mathrm{L}^q\times\{0\}\right)$. This is done in the next proposition.

We are now in position to prove the main result of the section:

Proposition 4.6.2. *Define for all integer $2 \le q < \infty$, $\mathcal{Y}_h = P_h\mathcal{Y}$, $\mathcal{Z}_h = P_h\mathcal{Z}$. For any $\eta \in [0,\gamma]$ and for any function $F = P_h\begin{bmatrix}f\\0\end{bmatrix} \in C^0_\eta(\mathbb{R},\mathcal{Y}_h)$, the problem*

$$\dot{u} = \mathbf{A}u + F(t) \tag{4.41}$$

has a unique solution $u = \mathbf{K}_hF \in C^0_\eta(\mathbb{R},\mathcal{Z}_h)$ and

$$|||\mathbf{K}_h|||_{\mathcal{L}(C^0_\eta(\mathbb{R},\mathcal{Y}_h),C^0_\eta(\mathbb{R},\mathcal{Z}_h))} \le C(\eta)$$

with $C \in C^0([0,\gamma],\mathbb{R})$.

Proof. Note that there is no initial condition in (4.41) because the solution is required to be defined on $\mathbb{R}$ for f given.

Let us prove uniqueness. If $f \equiv 0$ then any solution is given by $u(t) = \mathbf{T}(t)u(0)$ where $u(0) \in \mathcal{Z}_h$. To ensure that $\|u(t)\|_{\mathcal{X}} = O(e^{\eta|t|})$ as $t \to \infty$ requires that $u(0) \in \mathcal{Z}_s$ but in that case $e^{-\eta|t|}\|u(t)\|_{\mathcal{X}}$ is unbounded as $t \to -\infty$ unless $u(0) = 0$. Hence the only solution when $f = 0$ is $u_h = 0$. This proves uniqueness of the solution.

Let us prove existence. Write

$$(\mathbf{K}_hF)(t) \equiv \int_{-\infty}^{t}\mathbf{T}_s(t-r)F(r)dr - \int_{t}^{\infty}\mathbf{T}_u(t-r)F(r)dr$$

The second term $u_u(t) \equiv -\int_t^\infty \mathbf{T}_u(t-r)F(r)dr$ will not be considered in this proof. Indeed, as $\mathbf{T}_u(t)$ has a finite dimensional range, it is straightforward to prove that $u_u(t)$ fulfills all the properties stated in the proposition. Rather, we will focus on the study of $u_s(t) \equiv \int_{-\infty}^t \mathbf{T}_u(t-r)F(r)dr$ as it is much more difficult to show that it yields a solution of the inhomogeneous problem.

The first difficulty arises from the statement that $u_s(t) \in \mathcal{Z}$, *i.e.* the convolution of F by $\mathbf{T}_s$ yields a vector in the domain of $\mathbf{A}$. This is solved in two steps. First, we study in lemma B.7.2 the general properties of $\mathbf{T}(t)\begin{bmatrix}x\\0\end{bmatrix}$. Then, we use a variation-of-constants formula in lemma B.7.2 to compute $\mathbf{T}(t)$ by a perturbation result. Then, proposition B.7.4 in appendix shows that:

[22] see the definition of $\mathbf{R}$ in (4.37).

- $u_s \in C^0_\eta(\mathbb{R}, \mathcal{Z})$ and $\|u_s\|_{C^0_\eta(\mathbb{R},\mathcal{Z})} \leq K(\eta)\|f\|_{C^0_\eta(\mathbb{R},\mathcal{Y})}$ with $\eta \to K(\eta)$ positive continuous,
- $u_s \in C^1(\mathbb{R}, \mathcal{X})$,
- u_s satisfies $\dot{u}_s = \mathbf{A}u_s + P_s \begin{bmatrix} f \\ 0 \end{bmatrix}$ on $\mathcal{X}$, *i.e.* is a classical solution.

This concludes the proof of the proposition. □

4.6.3 Center manifold and reduced equation

We are now in a position to state the center manifold for an integer q sufficiently large to ensure the regularity of $\mathbf{R}$ required by a series expansion for example. Note that we drop the index $^{(q)}$ of the different spaces.

Theorem 4.6.3 (Center manifold for delayed neural field equations). *Let us write $\mathcal{X}_c$ the vector space of generalized eigenvectors of $\mathbf{A}$ with zero real part. As it is finite dimensional, we can write $\mathcal{X} = \mathcal{X}_c \oplus \mathcal{X}_h$ where $\mathcal{X}_h$ is the hyperbolic part of the history space. Then, there exist a neighborhood $\mathcal{O} = \mathcal{O}_u \times \mathcal{O}_\mu$ of $(0,0)$ in $\mathcal{X} \times \mathbb{R}^{m_{par}}$, a mapping $\Psi \in C^q(\mathcal{X}_c \times \mathbb{R}^{m_{par}}; \mathcal{Z}_h)$ with $\Psi(0,0) = 0$, $D\Psi(0,0) = 0$ and a manifold $\mathcal{M}(\mu) = \{u_c + \Psi(u_c, \mu), u_c \in \mathcal{X}_c\}$ for $\mu \in \mathcal{O}_\mu$ such that:*

1. *$\mathcal{M}(\mu)$ is locally invariant, i.e., if u is a solution of (4.37) satisfying $u(0) \in \mathcal{M}(\mu) \cap \mathcal{O}_u$ and $u(t) \in \mathcal{O}_u$ for all $t \in [0,T]$, then $u(t) \in \mathcal{M}(\mu)$ for all $t \in [0,T]$.*
2. *$\mathcal{M}(\mu)$ contains the set of bounded solutions of (4.37) staying in $\mathcal{O}_u$ for all $t \in \mathbb{R}$, i.e. if u is a solution of (4.37) satisfying for all $t \in \mathbb{R}$, $u(t) \in \mathcal{O}_u$, then $u(0) \in \mathcal{M}(\mu)$.*
3. *(Parabolic case) if $\Sigma_u(\mathbf{A}) = \emptyset$, then $\mathcal{M}(\mu)$ is locally attracting, i.e. if u is a solution of (4.37) satisfying $u(0) \in \mathcal{O}_u$ and $u(t) \in \mathcal{O}_u$ for all $t > 0$, then there exists $v(0) \in \mathcal{M}(\mu) \cap \mathcal{O}_u$ and $\tilde{\gamma} > 0$ such that*

$$u(t) = v(t) + O(e^{-\tilde{\gamma}t}) \text{ as } t \to \infty$$

where v is a solution of (4.37) with initial condition $v(0)$.

Proof.

1-2 Having written our nonlinear problem as (4.40), in order to apply [Haragus 2010, theorem II.2.9] we have to check several hypotheses. The first is to check the existence of a spectral decomposition with positive spectral gap γ where the central part $\mathbf{A}_c \equiv \mathbf{A}|_{\mathcal{X}_c}$ has only a finite number of eigenvalues with finite algebraic multiplicities, this was proved in section 4.4.4 (see also the end of section 4.6.1). Finally we have to check an hypothesis regarding the existence of solutions with exponential divergence at $t = \pm\infty$: this was done in proposition 4.6.2. As a consequence, we can apply [Haragus 2010, Theorem II.2.9] and obtain the theorem.

3 This is a consequence of [Haragus 2010, Theorem II.3.23] which requires several conditions to be checked. These conditions are very similar to the ones for 1-2. They are given and checked in appendix B.7.3.

□

From [Haragus 2010, Corollary 2.12], consider a solution u of (4.37) which belongs to $\mathcal{M}(\mu)$ for $t \in \mathbb{R}$, then $u = u_c + \Psi(u_c, \mu)$ with $u_c \in \mathcal{X}_c$ and u_c satisfies

$$\frac{du_c}{dt} = \mathbf{A}u_c + P_c\mathbf{R}\left(u_c + \Psi(u_c, \mu), \mu\right) \tag{4.42}$$

where the projector P_c is defined by the Dunford formula. It is known (see [Kato 1995, theorem III.6.17]) that the projector given by the Dunford formula is the unique spectral projector that commutes with $\mathbf{A}$. Hence, we have the expression from section 4.4.4, $P_c = \sum_{\lambda \in \Sigma_c(\mathbf{A})} P_\lambda$ with P_λ given in proposition 4.4.10.

Let us derive a simpler equation for u_c. Write $u_c = \sum_{i=1}^{dim\mathcal{X}_c} z_i\phi_i$ where z_i are complex numbers and ϕ_i, $i = 1, \cdots, dim\mathcal{X}_c$ is a basis of $\mathcal{X}_c$ (see proposition 4.4.6). We want to write ordinary differential equations for the coordinates z_i. As $\mathcal{X}_c$ is invariant by $\mathbf{A}$, there is a matrix A_c of size $dim\mathcal{X}_c$ such that: $\mathbf{A}u_c = \sum_{i=1}^{dim\mathcal{X}_c} (A_c z)_i\phi_i$ with $z = (z_1, \cdots, z_{dim\mathcal{X}_c})$. To find equations for the z_i, we need to project (4.42) on each generalized eigenvector ϕ_i. Hence, let us consider a family of vectors ψ_i as in proposition 4.4.10, then $\langle\langle \psi_i, u_c\rangle\rangle = z_i$ and $\langle\langle \psi_i, \mathbf{R}\left(u_c + \Psi(u_c, \mu), \mu\right)\rangle\rangle = \langle \pi_1\psi_i, \pi_1\mathbf{R}\left(u_c + \Psi(u_c, \mu), \mu\right)\rangle_{\mathcal{F}}$ (see proposition 4.4.10 for the bilinear product). We use these expressions together with (4.42) to find the reduced equations:

$$\boxed{\dot{z}_i = (A_c z)_i + \langle \pi_1\psi_i, \pi_1\mathbf{R}\left(u_c + \Psi(u_c, \mu), \mu\right)\rangle_{\mathcal{F}}} \tag{4.43}$$

This equation was given in [Hale 1993, Faria 1995, Wu 1996] in a different functional setting when $\mathbf{L}_0$ generates a compact semigroup.

We have mentioned in the introduction that most of the neural field models are used close to a stationary bifurcation. This bifurcation can be changed by the introduction of the delays producing either a purely imaginary eigenvalue or changing the algebraic multiplicity of the static eigenvalue. As we have seen in section 4.4.1.2, no general criterion is known for the appearance of a purely imaginary eigenvalue. However such a criterion exists for the algebraic multiplicity and allows to test very easily if a Bogdanov-Takens can emerge from the initial static bifurcation. This is done in the next lemma:

Lemma 4.6.4. *Let us consider a stationary cortical state $\mathbf{V}^f$ of (4.1) and the (time) constant function $\phi = \begin{bmatrix} e_1 \\ e_1 \end{bmatrix}$ in the one-dimensional kernel of $\mathbf{A}$ where $e_1 \in \mathcal{F}$. We write $\psi = \begin{bmatrix} e_1^* \\ e_1^* \end{bmatrix}$ the constant vector in $\ker \mathbf{A}^*$ with $\langle e_1^*, e_1\rangle_{\mathcal{F}} = 1$. The algebraic multiplicity of the zero eigenvalue is at least two if and only if*

$$0 = \langle\langle \psi, \phi\rangle\rangle = 1 + \langle e_1^*, \mathbf{J}D\mathbf{S}(\mathbf{V}^f)\boldsymbol{\tau}e_1\rangle_{\mathcal{F}}$$

Proof. We use proposition 4.4.6) to express $\ker \mathbf{A}^2$:

$$\ker \mathbf{A}^2 = \{V + \theta U,\ (U, V) \text{ is a Jordan chain for } \Delta(0)\}$$

is two-dimensional. By the lemma B.1.12, we have $\Delta(0)U = 0,\ \Delta'(0)U + \Delta(0)V = 0$ which gives $\begin{bmatrix} U \\ U \end{bmatrix} \in \ker \mathbf{A}$ and $U = e_1$. From the Fredholm alternative, $\ker \mathbf{A}^2$ is larger than $\ker \mathbf{A}$ if and only if $\langle e_1^*, \Delta'(0)e_1 \rangle_{\mathcal{F}} = 0$. From (4.12): $\Delta'(0) = \mathrm{Id} + \mathbf{J}D\mathbf{S}(\mathbf{V}^f)\boldsymbol{\tau}$. Therefore $\langle e_1^*, \Delta'(0)e_1 \rangle_{\mathcal{F}} = 1 + \langle e_1^*, \mathbf{J}D\mathbf{S}(\mathbf{V}^f)\boldsymbol{\tau} e_1 \rangle_{\mathcal{F}}$. Notice that this last quantity is equal to $\langle\langle \psi, \phi \rangle\rangle$. The lemma is proved. □

4.6.4 Normal form of the Pitchfork bifurcation

As we have mentioned in the Introduction, many of the neural field models operate near a static bifurcation point (see for example [Ben-Yishai 1995, Bressloff 2001b]), it is thus interesting to see how this can be altered by the introduction of delays. We will treat the case of the pitchfork bifurcation (see [Kuznetsov 1998, Haragus 2010]), the case of the transcritical bifurcation is very similar. We look at the quantitative modification of the reduced equation (in the non-delayed case) from the introduction of delays. Recall that we consider an equilibrium $\mathbf{V}^f$ and that we write an equation for $\mathbf{U} = \mathbf{V} - \mathbf{V}^f$. Let us consider the nonlinear gain $\sigma \in \mathbb{R}$ as a bifurcation parameter. Suppose that e_1 (resp. e_1^*) is in the one-dimensional kernel of $\Delta(0) = -\mathbf{L}_0 + \mathbf{J}(0)$ (resp. $\Delta(0)^* = -\mathbf{L}_0 + \mathbf{J}(0)^*$) at $\sigma = \sigma_c$. Suppose that the reduced equation[23] for the non-delayed neural mass equation near $\sigma = \sigma_c$ with $\mathbf{V} = \mathbf{V}^f + xe_1 + o(x)$ reads (see also lemma 3.3.2):

$$\dot{x} = \frac{\sigma - \sigma_c}{\sigma_c} x + \chi_q x^q + o(x^q)$$

for some $\chi_q \neq 0$. What happens if we introduce space-dependent delays? If the delays are small, we expect the eigenvalues of $\mathbf{A}$ to be close to the spectrum of the non-delayed linearized equation, thus yielding again a Pitchfork or a Transcritical bifurcation. Notice that e_1 is in the kernel of $\Delta(0)$, hence $0 \in \Sigma_p(\mathbf{A})$. Let us write $\phi = \begin{bmatrix} e_1 \\ e_1 \end{bmatrix} \in \ker \mathbf{A}$, from proposition 4.4.10, we find that $\psi = \beta \begin{bmatrix} e_1^* \\ e_1^* \end{bmatrix} \in \ker \mathbf{A}^*$ with $\beta \in \mathbb{R}$. It is normalized such that $\langle\langle \psi, \phi \rangle\rangle = 1$. Some algebra shows that $\langle\langle \psi, \phi \rangle\rangle = \beta + \beta \langle \mathbf{J}D\mathbf{S}\boldsymbol{\tau} e_1, e_1^* \rangle_{\mathcal{F}}$ where $\mathbf{J}D\mathbf{S}\boldsymbol{\tau}$ is the integral operator on $\mathcal{F}$ with kernel[24] $\mathbf{J}(\mathbf{r}, \mathbf{r}')DS(\mathbf{V}^f(\mathbf{r}'))\boldsymbol{\tau}(\mathbf{r}, \mathbf{r}')$. The normalization condition requires:

$$\beta^{-1} = 1 + \langle \mathbf{J}D\mathbf{S}\boldsymbol{\tau} e_1, e_1^* \rangle_{\mathcal{F}} \neq 0$$

Notice that $\beta^{-1} \neq 0$ is equivalent to saying that 0 is a simple eigenvalue of $\mathbf{A}$ (see [Hale 1993, Faria 2001] and lemma 4.6.4). Then $u_c = x\phi + \Psi(x\phi, \sigma)$ and $A_c = 0$

[23] resulting from the application of the center manifold theorem for example

[24] It is a component-wise product.

because $\mathbf{A}\phi = 0$. Hence, the reduced equation (3.18) reads:

$$\dot{x} = \langle \pi_1\psi, \pi_1\mathbf{R}(u_c + \Psi(u_c,\sigma),\sigma)\rangle_{\mathcal{F}} = \beta\langle e_1^*, \pi_1\mathbf{R}(u_c + \Psi(u_c,\sigma),\sigma)\rangle_{\mathcal{F}} \quad (4.44)$$

From appendix A.1, $\Psi(u_c,\sigma) = o(|x|)$ which gives[25] $\mathbf{R}(u_c+\Psi(u_c,\sigma),\sigma) = \mathbf{R}(u_c,\sigma)+$ *h.o.t.*. By using (4.37), the reduced equation (4.44) is now:

$$\begin{aligned} \dot{x}/\beta &= \langle e_1^*, \pi_1\mathbf{R}(u_c,\sigma)\rangle_{\mathcal{F}} + h.o.t. = \tfrac{\sigma-\sigma_c}{\sigma_c}x + \langle e_1^*, G(xe_n)\rangle_{\mathcal{F}} + h.o.t. \\ &= \tfrac{\sigma-\sigma_c}{\sigma_c}x + \chi_q x^q + o(x^q), \end{aligned} \quad (4.45)$$

from the definition of χ_q in lemma 3.3.2 and (4.36). Thus, introducing delays only results in a rescaling of time. This analysis holds as long as the only eigenvalue at σ_c is the simple 0 eigenvalue. Notice that another eigenvalue may approach the imaginary axis by increasing the delays (decreasing the propagation speed), if it is purely imaginary, it would lead to a Fold-Hopf bifurcation scenario, if it is 0, it would lead to a Bogdanov-Takens bifurcation scenario.

4.7 Conclusion

In this chapter, we have developed a theoretical framework for the study of neural field equations with space dependent delays. This has allowed us to prove the existence, uniqueness and the boundedness of the solutions to these equations for continuous history segments in $\mathcal{C}$. But this is the least one can expect from a theoretical framework.

Hence, we have then studied the stability of the stationary solutions of these equations and have proved that the characteristic values are sufficient to characterize the asymptotic stability of the stationary states in $\mathcal{C}$. This was done using the semigroups theory (see [Engel 2001]). By using a Hilbert space $\mathcal{X}$ for the history space, we are able, by combining ideas from [Hale 1993] and [Bátkai 2005], to find a closed form formula for the spectral projector. This formula leads naturally to the introduction of the bilinear product, a quantity introduced in [Hale 1993] which is difficult to generalize from DDEs with values in $\mathbb{R}^n$ to DDEs with values in a Banach space (see [Arino 2006]).

However the numerical computation of the characteristic values is very difficult in the general case. This is why we have looked for simple conditions on the connectivity/delay functions ensuring the asymptotic stability of the stationary states.

By formulating the stability of the stationary solutions as a fixed point problem we have found delay-dependent sufficient conditions. This is a powerful method which is less used than the Lyapunov method. Compared to the Lyapunov method, it presents the advantage of requiring conditions on the average connectivity function rather than on its sign. These conditions involve all the parameters in the delayed neural field equations, the connectivity function, the nonlinear gain and the delay function. Albeit seemingly very conservative, they are useful in order to

[25] h.o.t. means higher order terms.

avoid the numerically intensive computation of the CV. They can be applied prior to the characteristic values computation, to get a rough idea of the impact of the delays on the network under study.

Then, we gave an analytical expression for the Hopf bifurcation curves, allowing for the study of heterogeneous connectivities in Nd-cortices at low computational cost. This is a great achievement as it allows to study, in detail and at low computational cost, different connectivities. It is also absolutely necessary for the numerical study with the normal forms. Indeed, the locus of the bifurcation point have to be known with great precision. If not, we need to compensate this loss of precision with higher order terms in the normal forms which is a difficult task.

Moreover, this analytical formula gives the following biological insight: given a network without delays, if one wants to make the network oscillate (through a Hopf mechanism), then inhibition must be sufficiently strong. The formula for the Hopf curve introduces the following 'paradox': even if it is simple to compute the Hopf bifurcation curves, it is difficult to forecast their very intricate structure; we could not find a criterion predicting the shape of these curves *a priori*. This is important because it would allow for the prediction, without computations, of the changes to various cortical models by the introduction of space-dependent delays. Nevertheless, our analytical formula can allow this study.

Later, we proved a center manifold theorem for the delayed neural field equations. This is not a straightforward task as the usual estimate tools for sectorial operators do no apply. We used the more powerful tools of the semigroups theory as exposed in [Engel 2001, Bátkai 2005]. Hence we combined ideas from [Haragus 2010] and [Engel 2001, Bátkai 2005] to prove a center manifold theorem. This being done, we can apply[26] a "generic" normal form theory as in [Haragus 2010] and not a specific one as in [Faria 1995]. It appears that the computation of normal forms of the delayed neural field equations is not more difficult than for the non-delayed equations. Formalism by itself is not our ultimate goal. We want to show how the delays shape the dynamics qualitatively. Hence, after the proof of the center manifold, we showed how a Pitchfork bifurcation is altered by the introduction of delays. This is important because most of the neural field models operate near a stationary bifurcation: the Pitchfork is unaltered (it is only scaled in time) if the delays are smaller than a given bound. For larger delays, the Pitchfork bifurcation may degenerate into a Bogdanov-Takens bifurcation or a Fold-Hopf bifurcation. This introduces the computation of more normal forms in the next chapter. But before this, we need to be able to compute the bifurcation diagrams accurately. This is done in the following chapter.

[26] This will be done in chapter 5.

Chapter 5

Numerical and symbolic tools

Contents

This chapter collects results concerning the numerical computation of the eigenelements of the operator $\mathbf{A}$ defined in chapter 4. Depending on the shape of the operator $\mathbf{L}_0$, two methods can be used. More precisely, if $\mathbf{L}_0 = l\mathrm{Id}$ for some $l > 0$, then we can use the formulas in proposition 4.4.5 which yield a fast and precise computation of the Hopf bifurcation curves. When the condition $\mathbf{L}_0 = l\mathrm{Id}$ is not satisfied, no analytical formula is known and the computation of the Hopf bifurcation curves relies on the numerical computation of the eigenvalues. This is done in section 5.1.

At the end of the previous chapter 4, we proved a center manifold theorem and gave the reduced equation that is a finite dimensional system of ordinary differential equations. In the section 5.2 of the present chapter, we push forward the analysis by applying a normal form theory and computing the normal forms of the main bifurcations that appear in the next study of delayed neural fields equations in chapter 6.

5.1 Numerical computations

In this section, we show how to solve the delayed differential equations (4.1) and how to compute the spectrum of $\mathbf{A}$. This is essential for the study of the delay neural fields that is done in chapter 6.

5.1.1 Evolution equation

In this thesis, we have not studied how to compute a numerical solution of (4.1). In particular, we have not given a numerical scheme to compute the time-dependent solution. Note that we have not focused on this point but we shall explain our

method. It relies on a space discretization of Ω in order to form a system of N_Ω scalar delay differential equations:

$$\begin{aligned}\dot{\mathbf{V}}(t,\mathbf{r}_i) &= -\mathbf{L}_0\mathbf{V}(t,\mathbf{r}_i) + \mathbf{I}^{ext}(\mathbf{r}_i,t) + \\ &\quad \sum_{j=0}^{N_\Omega} w_j\ \mathbf{J}(\mathbf{r}_i,\mathbf{r}_j)\mathbf{S}(\mathbf{V}(t-\tau(\mathbf{r}_i,\mathbf{r}_j),\mathbf{r}_j)), \quad \forall i = 1\cdots N_\Omega\end{aligned} \tag{5.1}$$

where the $(w_j)_{j=1\cdots N_\Omega}$ is the weight associated to some numerical integration scheme. More precisely, we use a trapezoidal rule to approximate the integrals and use the Matlab routine `dde23` to solve the system (5.1). This scheme has been described in [Hutt 2003, Venkov 2008]. For homogeneous networks, one can take advantage of the convolutional structure to compute more efficiently the right-hand side of (5.1) using Fourier transforms (see for example [Hutt 2010] for a recent reference).

5.1.2 Spectrum computation

This section shows how to compute the (rightmost) eigenvalues of the linear operator $\mathbf{A} = \begin{bmatrix} -\mathbf{L}_0 & \mathbf{L}_1 \\ 0 & \frac{d}{d\theta} \end{bmatrix}$ with domain $D(\mathbf{A}) = \left\{ \begin{bmatrix} x \\ \phi \end{bmatrix} \in \mathcal{F} \times W^{1,2}(-\tau_m, 0; \mathcal{F}),\ \phi(0) = x \right\}$. From section 4.4.1, we know that the eigen-elements are given by $u(\theta,\mathbf{r}) = \begin{bmatrix} \mathbf{U}(\mathbf{r}) \\ e^{\lambda\theta}\mathbf{U}(\mathbf{r}) \end{bmatrix}$ where $\mathbf{U} \in \mathcal{F}$ is solution of $\Delta(\lambda)\mathbf{U} = 0$ and $\lambda \notin \Sigma(-\mathbf{L}_0)$. Basically, we reduce the delayed neural field equations to a system of scalar delay different equations by sampling the space Ω and apply generic tools for finding the eigenvalues of this set of equation. We use the toolbox TraceDDE, [Breda 2009], a very efficient method for computing the eigenvalues. The library has recently been improved in [Jarlebring 2010], allowing a much faster computation of the eigenvalues: this is the scheme we have been using in [Veltz 2011b]. Notice that, even with this scheme, it is difficult, in practice, to explore many pairs $(\tau, \mathbf{J})$ in order to know what are the possible spatio-temporal behaviors depending on the parameters.

In the next section, we study more thoroughly how to compute the eigenvalues, in particular, we give a bound for the error made when computing the eigenvalues with the discretized space instead of Ω rather than with the 'true' delayed neural field equations. Because of the particular structure of the equations, involving Fredholm operators on Hilbert space, we are able to generalize the method in [Breda 2006] to prove the convergence of the approximated eigenvalues to the 'true' eigenvalues.

5.1.2.1 General case

We start by showing an analytical function whose zeros are the eigenvalues.

Lemma 5.1.1. *Define* $\mathbf{J}_0(\lambda) \equiv (\lambda\mathrm{Id} + \mathbf{L}_0)^{-1}\mathbf{J}(\lambda)$ *on* $B \equiv (-\min_i l_i, \infty)_{\mathbb{C}} \subset \mathbb{C}$ *and the function*

$$d(\lambda) \equiv \det{}_{\mathrm{F}}\left(\mathrm{Id} - \mathbf{J}_0(\lambda)\right)$$

where $\det_F$ *is the Fredholm determinant (see property C.1.2). Then the zeros of* d *are the eigenvalues of* $\mathbf{A}$ *and* d *is analytical on* B.

Proof. The Fredholm determinant is defined for trace-class operators (see [Grothendieck 1956, Simon 2010]). From the definition C.1.1, it is easy to see that $\mathbf{J}(\lambda)$ is trace-class on $\mathcal{F}$ so is $\mathbf{J}_0(\lambda)$. Hence, d is well defined (see proposition C.1.2). Also $\lambda \to \mathbf{J}_0(\lambda)$ is analytical on B. As $\mathbf{K} \to \det_F(\mathrm{Id} - \mathbf{K})$ is analytical on the space of trace-class operators (see [Grothendieck 1956, Simon 2010]), it follows that d is analytical on B. The fact that the zeros of d are the eigenvalues of $\mathbf{A}$ is a direct consequence of the property $\mathrm{Id} - \mathbf{K}$ invertible if and only if $\det_F(\mathrm{Id} - \mathbf{K}) \neq 0$. □

Let us consider an eigenvalue λ, then there is a function $\phi \in C^1(-\tau_m, 0; \mathcal{F})$ such that:

$$\begin{cases} -\mathbf{L}_0\phi(0) + \mathbf{L}_1\phi = \lambda\phi(0) \\ \frac{d}{d\theta}\phi = \lambda\phi \end{cases} \tag{5.2}$$

Next, we build a finite dimensional approximation of (5.2). Let us consider an orthonormal basis $(e_n)_n$ of $\mathcal{F}$. For $N_\Omega \in \mathbb{N}$, $\mathcal{F}_{N_\Omega}$ is the finite dimensional subspace $Span(e_0, \cdots, e_{N_\Omega})$ of $\mathcal{F}$. We use these spaces to define the projector

$$P_{N_\Omega} : \begin{cases} \mathcal{F} \to \mathcal{F}_{N_\Omega} \\ \mathbf{U} \to \sum_{i=0}^{N_\Omega} \langle \mathbf{U}, e_i \rangle_{\mathcal{F}} e_i \end{cases}$$

and the approximation

$$\mathbf{L}_{1,N_\Omega} \equiv P_{N_\Omega}\mathbf{L}_1 : \mathcal{F} \to \mathcal{F}_{N_\Omega}.$$

The theorem of Parseval-Bessel gives:

$$\varepsilon_{N_\Omega} \equiv |||\mathrm{Id} - P_{N_\Omega}||| \overset{N_\Omega \mathcal{F} \to \infty}{\to} 0.$$

Let us consider the time discretization $\Theta_{N_t} = \{-\tau_m = \theta_{N_t} < \theta_{N_t-1} < \cdots < \theta_0 = 0\}$ of $[-\tau_m, 0]$ of length $N_t + 1$ where

$$\theta_i \equiv \frac{\tau_m}{2}\left[1 - \cos\left(\frac{N_t - i}{N_t}\pi\right)\right].$$

This particular discretization is motivated by the approximation result in lemma 5.1.2. We start with an approximation of the exponential function on $[-\tau_m, 0]$. Because of the general shape of the eigenvectors: $e^{\lambda\theta}\mathbf{U}$. For $\mathbf{U} \in \mathcal{F}$, we define the family of polynomials $P_{N_t+1}(\theta; \mathbf{U}, \lambda)$ in the variable θ with coefficients in $\mathcal{F}$, of degree smaller than N_t, such that:

$$\begin{cases} \frac{d}{d\theta}\left(P_{N_t+1}(\theta_i; \mathbf{U}, \lambda)\right) = \lambda P_{N_t+1}(\theta_i; \mathbf{U}, \lambda), \quad i = 1 \cdots N_t \\ P_{N_t+1}(\theta_0; \mathbf{U}, \lambda) = \mathbf{U} \end{cases} \tag{5.3}$$

From [Breda 2006, lemma 7], we have:

Lemma 5.1.2. *Let $\lambda^* \in \mathbb{C}$ and $\rho_0 > 0$. There exists $N_t^0 \in \mathbb{N}$ such that for all $N_t > N_t^0$, $\lambda \in B(\lambda^*, \rho_0)$, the disc of center λ^* and radius ρ_0, and $\mathbf{U} \in \mathcal{F}$, the polynomial $P_{N_t+1}(\cdot; \mathbf{U}, \lambda)$ exists and is unique. Moreover:*

$$\max_{\theta \in [-\tau_m, 0]} \left\| P_{N_t+1}(\theta; \mathbf{U}, \lambda) - e^{\lambda\theta}\mathbf{U} \right\|_{\mathcal{F}} \leq \frac{C_1}{\sqrt{N_t}} \left(\frac{C_0}{N_t} \right)^{N_t} \|\mathbf{U}\|_{\mathcal{F}}$$

with $C_0 = \tau_m(|\lambda^*| + \rho_0)e$ and $C_1 = C_1(\lambda^*, \rho_0)$ is independent of N_t.

This allows to define an approximation of (5.2) by using a time-polynomial approximation of the eigenvector ϕ, *i.e.* $\phi \approx P_{N_t+1}(\cdot; \mathbf{U}, \lambda)$. Hence we write:

$$\begin{array}{rcl} \mathbf{U} & = & (\lambda \mathrm{Id} + \mathbf{L}_0)^{-1} \mathbf{L}_{1,N_\Omega} P_{N_t+1}(\cdot; \mathbf{U}, \lambda) \\ & \equiv & \mathbf{J}_{0,N_\Omega,N_t}(\lambda)\mathbf{U} \end{array} \tag{5.4}$$

We define the approximated characteristic values λ and eigenvectors $\mathbf{U}$ as the solutions of (5.4). In particular, the characteristic values are zeros of the analytical function d_{N_Ω,N_t} defined on $B \subset \mathbb{C} \setminus \Sigma(-\mathbf{L}_0)$ by:

$$\begin{array}{rcl} d_{N_\Omega,N_t}(\lambda) & = & \det_F(\mathrm{Id} - \mathbf{J}_{0,N_\Omega,N_t}(\lambda)) \\ & \underset{regular\ det.}{=} & \det(\mathrm{Id}_{\mathcal{F}_{N_\Omega}} - \mathbf{J}_{0,N_\Omega,N_t}(\lambda)|_{\mathcal{F}_{N_\Omega}}) \end{array} \tag{5.5}$$

We wish to build a finite dimensional approximation of the linear operator $\mathbf{A}$ whose eigen-elements are the approximated eigen-elements we just defined. Let us define $\mathrm{Pol}_{\mathrm{N}_\Omega,\mathrm{N_t}}$ to be the space of polynomials of degree less than N_t with coefficients in $\mathcal{F}_{N_\Omega}$. This allows to define an approximation of the space $\mathcal{X}$ by $\mathcal{X}_{N_\Omega,N_t} \equiv \mathcal{F}_{N_\Omega} \times \mathrm{Pol}_{\mathrm{N}_\Omega,\mathrm{N_t}}$. Each polynomial of $\mathrm{Pol}_{\mathrm{N}_\Omega,\mathrm{N_t}}$ is written $\mathcal{P}_{N_t+1}x$ which is the unique polynomial of degree less than N_t such that $(\mathcal{P}_{N_t+1}x)(\theta_i) = x_i$, $i = 0 \cdots N_t$ and $x \equiv (x_i)_{i=0\cdots N_t} \in \mathcal{F}_{N_\Omega}^{N_t+1}$. We can now define $\mathbf{A}_{N_\Omega,N_t}$ on the elements $\begin{bmatrix} \mathbf{U} \\ \mathcal{P}_{N_t+1}x \end{bmatrix} \in \mathcal{X}_{N_\Omega,N_t}$ satisfying $x_0 = \mathbf{U}$. If we write $\begin{bmatrix} \mathbf{V} \\ \mathcal{P}_{N_t+1}y \end{bmatrix} = \mathbf{A}_{N_\Omega,N_t} \begin{bmatrix} \mathbf{U} \\ \mathcal{P}_{N_t+1}x \end{bmatrix}$, then we have:

$$\begin{cases} \mathbf{V} \equiv -\mathbf{L}_0\mathbf{U} + \mathbf{L}_{1,N_\Omega}(\mathcal{P}_{N_t+1}x) \\ y_i \equiv \frac{d}{d\theta}(\mathcal{P}_{N_t+1}x)|_{\theta=\theta_i},\ i = 0 \cdots N_t \end{cases} \tag{5.6}$$

It is straightforward to check that the eigenvectors of $\mathbf{A}_{N_\Omega,N_t}$ are given by the functions $P_{N_t+1}\mathbf{U}$ with $\mathbf{U}$ solution of (5.4). The next lemma shows that the two analytical functions d and d_{N_Ω,N_t} are very close on every bounded open set of $B \subset \mathbb{C} \setminus \Sigma(-\mathbf{L}_0)$.

Lemma 5.1.3. *Let $\lambda^* \in \mathbb{C}$ and $\rho_0 > 0$. There exits $N_t^0 \in \mathbb{N}$ such that for all $N_t > N_t^0$ and $\lambda \in B(\lambda^*, \rho_0)$, we have:*

$$|d(\lambda) - d_{N_\Omega,N_t}(\lambda)| \leq C_3 \left(\varepsilon_{N_\Omega} + \frac{C_1}{\sqrt{N_t}} \left(\frac{C_0}{N_t} \right)^{N_t} \right)$$

with $C_3 = C_3(\lambda^*, \rho_0)$ independent of N_Ω, N_t.

Proof. For all $\mathbf{U} \in \mathcal{F}$, we have

$$\begin{aligned}\|\mathbf{J}_0(\lambda)\mathbf{U} - \mathbf{J}_{0,N_\Omega,N_t}(\lambda)\mathbf{U}\|_{\mathcal{F}} &\leq |||(\lambda\mathrm{Id}+\mathbf{L}_0)^{-1}|||\cdot\|\mathbf{L}_1\cdot\varepsilon_\lambda\mathbf{U} - \mathbf{L}_{1,N_\Omega}\cdot P_{N_t+1}(\theta;\mathbf{U},\lambda)\|_{\mathcal{F}} \\ &\leq |||(\lambda\mathrm{Id}+\mathbf{L}_0)^{-1}||| \\ &\left(\|\mathbf{L}_1\cdot\varepsilon_\lambda\mathbf{U} - \mathbf{L}_{1,N_\Omega}\varepsilon_\lambda\mathbf{U}\|_{\mathcal{F}} + \|\mathbf{L}_{1,N_\Omega}\cdot\varepsilon_\lambda\mathbf{U} - \mathbf{L}_{1,N_\Omega}\cdot P_{N_t+1}(\theta;\mathbf{U},\lambda)\|_{\mathcal{F}}\right) \\ &\leq C\left(\varepsilon_{N_\Omega}|||\mathbf{L}_1||| + \sup_{N_\Omega}|||\mathbf{L}_{1,N_\Omega}|||\frac{C_1}{\sqrt{N_t}}\left(\frac{C_0}{N_t}\right)^{N_t}\right)\|\mathbf{U}\|_{\mathcal{F}} \\ &\leq C_3\left(\varepsilon_{N_\Omega} + \frac{C_1}{\sqrt{N_t}}\left(\frac{C_0}{N_t}\right)^{N_t}\right)\|\mathbf{U}\|_{\mathcal{F}} \quad (5.7)\end{aligned}$$

with $C_3 = \sup_{\lambda\in B(\lambda^*,\rho_0)} |||(\lambda\mathrm{Id}+\mathbf{L}_0)^{-1}|||\cdot\max(|||\mathbf{L}_1|||, \sup_{N_\Omega}|||\mathbf{L}_{1,N_\Omega}|||)$. Since the derivative of $\mathbf{K} \to \det_F(\mathrm{Id}-\mathbf{K})$ is continuous on trace-class operators, the assertion follows easily. □

We are in a position to state the main result of this section which is adapted from [Breda 2009]:

Theorem 5.1.4. *Let $\lambda^* \in \mathbb{C}$ zero of d with multiplicity ν. There exits $C, \rho_1 > 0$ such that if $\rho_{N_\Omega,N_t} < \rho_1$ with $\rho_{N_\Omega,N_t} \equiv \left(\frac{C_3}{C}\right)^{1/\nu}\left(\varepsilon_{N_\Omega} + \frac{C_1}{\sqrt{N_t}}\left(\frac{C_0}{N_t}\right)^{N_t}\right)^{1/\nu}$, then d_{N_Ω,N_t} has ν zeros, counted with multiplicities, such that*

$$\max_{i=1\cdots\nu}|\lambda^* - \lambda_i| \leq \rho_{N_\Omega,N_t}$$

Proof. From [Breda 2009, lemma 4], there exists $C, \rho_1 > 0$ such that $\forall\lambda \in B(\lambda^*,\rho_1)\setminus\lambda^*$ we have $|d(\lambda)| > C|\lambda-\lambda^*|^\nu$. Since $\rho_{N_\Omega,N_t} \equiv \left(\frac{C_3}{C}\right)^{1/\nu}\left(\varepsilon_{N_\Omega} + \frac{C_1}{\sqrt{N_t}}\left(\frac{C_0}{N_t}\right)^{N_t}\right)^{1/\nu} < \rho_1$, we have for $|\lambda-\lambda^*| = \rho_{N_\Omega,N_t}^{1/\nu}/C$

$$|d(\lambda) - d_{N_\Omega,N_t}(\lambda)| \leq \rho_{N_\Omega,N_t} = C|\lambda-\lambda^*|^\nu < |d(\lambda)|$$

Hence, from Rouché's theorem [Conway 1978, 7, section 5, theorem 3.8], d and d_{N_Ω,N_t} have the same number of zeros counted with their multiplicities in $B(\lambda^*,\rho_{N_\Omega,N_t})$. □

Let us sum up the way we compute the eigenvalues of $\mathbf{A}$. They are approximated by the zeros of d_{N_Ω,N_t} (see theorem 5.1.4). Hence, to approximate the characteristic values of $\mathbf{A}$, we need to compute the zeros of d_{N_Ω,N_t} which are the eigenvalues of the finite dimensional operator $\mathbf{A}_{N_\Omega,N_t}$. To do this, we write $\mathbf{A}_{N_\Omega,N_t}$ in a basis of $\mathcal{X}_{N_\Omega,N_t}$ to find a matrix of size $(N_t+1)(N_\Omega+1)$ to which we can apply functions like `eigs` in *Matlab*©. This is what is done in the package TraceDDE, [Breda 2009], which takes advantage of the very fast convergence rate in $O\left(N_t^{-N_t}\right)$ of the approximated eigenvalues λ_i for N_Ω fixed. The main problem of this method is that it requires to compute eigenvalues of huge matrices. For a 2D cortex with a rough spatial discretization $N_\Omega = 100^2, N_t = 100$, it gives already $N_\Omega N_t = 10^6$ lines for the

matrix $\mathbf{A}_{N_\Omega,N_t}$. Given that we need to find bifurcation points, *i.e.* that we need to compute the eigenvalues of $\mathbf{A}_{N_\Omega,N_t}$ for many parameters, the method is not very practical.

However, thanks to the special way $\mathbf{A}_{N_\Omega,N_t}$ changes shape when one varies the time discretization of Θ_{N_t}, [Jarlebring 2010] gives a factorization of $\mathbf{A}_{N_\Omega,N_t}$, which allows a much faster computation of the eigenvalues. Based on an Arnoldi method, the authors in [Jarlebring 2010] show how to compute the rightmost eigenvalues of $\mathbf{A}_{N_\Omega,N_t}$ by using matrices of size only $N_\Omega \times N_\Omega$. This is the scheme we have been using in the most general cases, *i.e.*, when we cannot apply the result of the next section.

5.1.2.2 Hopf curve in the case of space dependent delays

In this section, we show how to use proposition 4.4.5 to compute numerically the Hopf curves with space dependent delays. This proposition implies that if we want to compute the curves for $c \leq c_\infty$, we need to compute the eigenvalues $J_n(y)$ of the integral operator $\mathbf{J}(iy)$ whose kernel is given by $J_{qr}(\mathbf{r},\bar{\mathbf{r}})DS(V_r^f(\bar{\mathbf{r}}))e^{-iy\|\mathbf{r}-\bar{\mathbf{r}}\|_2}$, $z \in \mathbb{C}$, $q,r = 1\cdots p$, for $y \leq c_\infty \|J(0)\|_2$ and $n \leq \|\mathbf{J}(0)\|_2$. It also implies that we do not miss any Hopf curves in the interval $c \in [0, c_\infty]$ if we respect the bounds given in the proposition. Recall that the numerical computation of the Hopf bifurcation curve, for general delay functions τ_{ij}, requires to find the eigenvalues of a matrix A_N of size N_tN_Ω and that we have to look for the bifurcation curve in the parameter plane. In our case, the computation of the eigenvalues of $\mathbf{J}(iy)$ for a given y requires to find the eigenvalues of a matrix of size N_Ω and, with the formulas in proposition 4.4.5, we directly have the bifurcation curve.

Moreover, the numerical error made in the computation of the eigenvalues $J_n(iy)$ of the integral operator $\mathbf{J}(iy)$ is only function of the space discretization which itself corresponds to a numerical integration scheme. For example, with a trapezoidal rule, we know *a priori* the error made by computing the eigenvalues of the discretized integral kernel $\mathbf{J}(iy)$, *i.e.* we know that the exact eigenvalue $J_n(iy)$ is within a ball of center $J_{n,N_\Omega}(iy)$ (the nth eigenvalue of the approximated operator $\mathbf{J}_{N_\Omega}(iy)$) and radius ε given by the trapezoidal rule (for example). We can use this ball to plot around each curve $\mathcal{C}_n$, described in proposition 4.4.5, a neighborhood where the exact curve belongs: it allows to first look at the curves at a low resolution and refine where more resolution is needed.

We use this in figure 5.1. In order to evaluate the efficiency of the scheme, we compute the eigenvalues for a convolutional network for which the eigenvalues of the operator $\mathbf{J}(iy)$ are known analytically. More precisely, we consider a scalar network with $\Omega = [-\pi/2, \pi/2]$, $\tau(x,y) = D + c|x-y|_\pi$, $l = 1$, $J(x,x') = -(0.5 + 2.1\cos(2x - 2x'))\frac{2}{\pi}$, $S(x) = \frac{1}{1+e^{-x}} - \frac{1}{2}$. The equation is linearized around the stationary state $V^f = 0$. The delay function is π-periodic and is shown in 5.2. From these properties, the eigenvalues of $\mathbf{J}(iy)$ are given by the

Fourier coefficients:

$$J_n^{(2)}(y) \equiv \int_0^{\pi} J(x) e^{-iy|x|_\pi} \cos(nx) dx, \quad n \in \mathbb{N}. \tag{5.8}$$

These eigenvalues are not ordered as the $J_n(y)$, that is why they have a different name. Nevertheless, if we use the coefficients $J_n^{(2)}$ to draw the curves of proposition 4.4.5, the only numerical error we make lies in the discretization of the interval $[0,\ c_\infty \|\mathbf{J}(0)\|_2]$ for y which parametrizes the Hopf curve. These 'exact' curves are plotted with continuous lines in figure 5.1. On the other hand, we can 'forget' about the convolutional structure of the linear operators $\mathbf{J}(iy)$ and compute their eigenvalues using a spatial discretization. For a given space discretization $N_\Omega = 100$ of space and $N_y = 250$ for $[0,\ c_\infty \|\mathbf{J}(0)\|_2]$, we show the points defining the curves $\mathcal{C}_n$ in figure 5.1 with stars. Notice how close they lie to the 'exact' curves. The color of these stars labels the index n in the Hopf curves $\mathcal{C}_n$ in proposition 4.4.5. Each star is surrounded by an ellipse (see above) which shows where the exact point (c, D) of the corresponding curve $\mathcal{C}_n$ lies. Note how these ellipses are bigger for larger delays.

In the previous numerical example, we have used the Rectangle rule to approximate the integrals.

The bifurcation curves in figure 5.1 indicate that 'simple' convolutional systems may produce a wealth of interesting behaviors. Indeed, when two Hopf curves intersect, they give birth to a Hopf-Hopf bifurcation point with rich dynamics (see [Guckenheimer 1983, Kuznetsov 1998] for example). This is more thoroughly studied in chapter 6 after we derive the main normal forms associated to the bifurcation points in the next section.

5.2 Symbolic computation of some normal forms

In the previous chapter, we have shown how to reduce the dynamics of the delayed neural field equations to a finite dimensional region of the history space called the center manifold. In particular, we gave a *reduced equation* (4.43), in effect, finite dimensional ordinary differential equations, which describe the dynamics on the center manifold. This is obtained by the bifurcation theory.

Among all the different reduced equations, some of them produce the same dynamics up to a change of variable. Normal form theory aims at finding a polynomial change of variable which "simplifies" the reduced equation by removing the maximum number of terms at every order of its Taylor expansion. Once simplified, the truncation[1], at order k, of the Taylor expansion of the reduced equation is a polynomial vector field which is called the *normal form*. In most of the cases, the truncation of the Taylor expansion of the reduced equation do not change the dynamics. If the reduced equation satisfies some properties, such as its linear part has a one dimensional null space, for example, in addition to some non-degeneracy conditions then, the simplified polynomial vector field has

[1] *i.e.* it gives a polynomial of degree k.

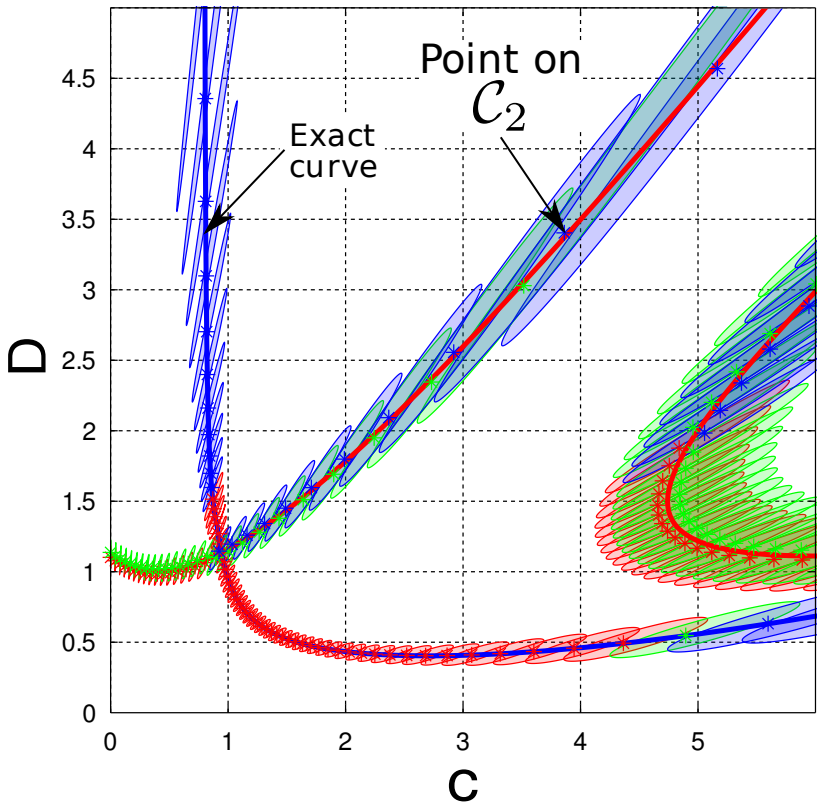

Figure 5.1: Plot of the Hopf curves for $\Omega = [-\pi/2, \pi/2]$, $\tau(x, y) = D + c|x - y|_\pi$, $l = 1$, $J(x, x') = -(0.5 + 2.1\cos(2x - 2x'))\frac{2}{\pi}$, $S(x) = \frac{1}{1+e^{-x}} - \frac{1}{2}$. We show in continuous lines (blue for $n = 0$ in (5.8) and red for $n = 1$ in (5.8), the index n is not the same used in proposition 4.4.5) the exact curves. The stars are computed from a discretization $\mathbf{J}_{N_\Omega}(iy)$ with $N_\Omega = 100$. The elliptic curves surround the regions where the exact point (c, D) lies (see text). Note how they compare with the continuous solutions. The color of each star and its surrounding ellipse labels the index n of the curve $\mathcal{C}_n$ as in proposition 4.4.5. We have: red for $n = 0$, green for $n = 1$ and blue for $n = 2$.

always the same monomials. These conditions are listed in [Guckenheimer 1983, Golubitsky 1984, Golubitsky 1988, Kuznetsov 1998, Haragus 2010] as well as the corresponding normal forms. Moreover, these references also contain the study of the dynamical system associated to the normal form. Hence, there are two steps in finding the normal form:

- compute the Taylor expansion of the reduced equation,
- recognize which conditions are satisfied by the reduced equation and use the tabulated formulas in [Guckenheimer 1983, Golubitsky 1984, Golubitsky 1988, Kuznetsov 1998, Haragus 2010] to extract the full dynamics of the delayed neural field equations on the center manifold.

If the normal form is not tabulated, then we need to compute the change of variable. This is lengthy because we need to compute the center manifold correction Ψ and then the polynomial change of variable. In fact, we can find the normal form directly without computing the center manifold correction Ψ as explained in [Haragus 2010]. More specifically, from the Cauchy problem

$$\frac{du}{dt} = \mathbf{A}u + \mathbf{R}(u, \mu),$$

we build a reduced equation (4.43) for $u_c \in \mathcal{X}_c$ with the center manifold correction Ψ:

$$u = u_c + \Psi(u_c, \mu), \quad \Psi(u_c, \mu) \in \mathcal{Z}_h.$$

This reduced equation is

$$\frac{du_c}{dt} = \mathbf{A}u_c + P_c\mathbf{R}\left(u_c + \Psi(u_c, \mu), \mu\right).$$

Then, we apply a change of variable to u_c

$$u_c = v_0 + \Phi_\mu(v_0), \quad v_0 \in \mathcal{X}_c$$

to bring the reduced equation to a normal form given by:

$$\frac{dv_0}{dt} = \mathbf{A}|_{\mathcal{X}_c}v_0 + \mathbf{N}_\mu(v_0) + \rho(v_0, \mu),$$

where $\mathbf{N}_\mu$ is a polynomial of some degree p such that $\mathbf{N}_0(0) = 0$, $D_v\mathbf{N}_0(0) = 0$ and $\rho(v_0, \mu) = o(\|v_0\|^p)$. The general shape of $\mathbf{N}$ can be guessed from symmetries for example (see [Golubitsky 1984, Golubitsky 1988, Haragus 2010]). This nonlinear function Φ_μ is solution of a nonlinear equation which is given in [Haragus 2010]. Finally, we can combine the center manifold correction and the change of variable in one formula:

$$u = v_0 + \tilde{\Psi}(v_0, \mu), \quad \tilde{\Psi}(v_0, \mu) \equiv \Phi_\mu(v_0) + \Psi(v_0 + \Phi_\mu(v_0), \mu) \in \mathcal{Z}$$

The nonlinear function $\tilde{\Psi}$ is solution (see [Haragus 2010, III.4.1]) of the next equations:

$$\begin{cases} D_{v_0}\tilde{\Psi}(v_0,\mu)\mathbf{A}|_{\mathcal{X}_c}v_0 - \mathbf{A}\tilde{\Psi}(v_0,\mu) + \mathbf{N}_\mu(v_0) = \mathbf{Q}(v_0) \\ \mathbf{Q}(v_0) \equiv \Pi_p\left[\mathbf{R}(v_0+\tilde{\Psi}(v_0,\mu),\mu) - D_{v_0}\tilde{\Psi}(v_0,\mu)\mathbf{N}_\mu(v_0)\right] \end{cases} \tag{5.9}$$

where Π_p is the operator which takes the first $p+1$ terms in the Taylor expansion in the variable v_0.

To sum up, when the normal form is not tabulated, then we need to solve (5.9) to find the normal form. In the following section, we will use tabulated formulas for the Pitchfork normal form and the Hopf normal form. The normal form of the Fold-Hopf bifurcation and the Hopf-Hopf bifurcation with symmetries is not tabulated and we have to solve (5.9). To this hand, we write a *Maple*© that helps us in this task.

5.2.1 Maple program for computing the normal form $\mathbf{N}_\mu$

In order to know which dynamics can be produced by the delayed neural fields equations, we need to compute the coefficients of the polynomial $\mathbf{N}_\mu$ as functions of the parameters that appear in the neural field model. Let us write the Taylor expansion of $\mathbf{R}$ for a given p:

$$\mathbf{R}(u) = \sum_{2\leq q+l\leq p} \mathbf{R}_{ql}[u^{(q)},\mu^{(l)}] + o\left(\|u\|^p\right),\ \mathbf{R}_{01} = 0 \tag{5.10}$$

with $\mathbf{R}_q$ defined in lemma 4.6.1, $u^{(q)} \equiv (u,\cdots,u) \in \mathcal{Z}_h^q$ and $\mu^{(l)} \equiv (\mu,\cdots,\mu) \in (\mathbb{R}^{m_{par}})^l$.

From symmetry arguments, the general shape of $\mathbf{N}_\mu$ can usually be guessed. For example, in the case of the Hopf bifurcation with O(2)-symmetry truncated at order 3, it is known from [Chossat 2000, Haragus 2010] that the normal form looks like (5.16):

$$\mathbf{N}_\mu = \begin{bmatrix} A(b_1|A|^2 + c_1|B|^2) \\ B(b_1|B|^2 + c_1|A|^2) \end{bmatrix} \tag{5.11}$$

with $v_0 = A\phi_0 + B\phi_1 + c.c.$ (complex conjugate). Note that this normal form has no second order term and that only particular monomials are present. It remains to compute the coefficients b_1, c_1 of this normal form in terms of the parameters of the reduced equation. To this hand, we plug (5.11) in (5.9). Then, we Taylor expand $\tilde{\Psi}$:

$$\tilde{\Psi}(v_0,\mu) = \sum_{m,p,q,r,s} A^p\bar{A}^q B^r \bar{B}^s \mu^m \Psi_{pqrsm},\ \Psi_{pqrsm} \in \mathcal{Y}$$

and collect the monomials in (5.9). This gives the equations satisfied by the Ψ_{pqrsm} and by the coefficients of the normal form b_1, c_1. This operation can easily be done with a Maple program. Let us assume that the eigenvalues are $\pm i\omega_H$ and the (complex) eigenvectors are $\zeta_1, \zeta_2, \overline{\zeta}_1, \overline{\zeta}_2$.

```
 > restart; with(linalg); assume(x, real); assume(omega, real);
> # A1=conjugate(A), B1=conjugate(B)
```

```
> v0 := A*zeta1+B*zeta2+A1*conjugate(zeta1)+B1*conjugate(zeta2);
> TildePsi := sum(sum(sum(sum(sum(Psi[q1, q2, l1, l2, r]*A^q1*A1^q2*B^l1*B1^l2
*x^(q1+q2+l1+l2)*mu^r, q1=0..3), q2=0..3), l1=0..3), l2=0..3), r=0..1):
> u := v0+TildePsi;
> N := (a1*mu*A+(b1*A*A)*A1+c1*B*B1*A)*zeta1
      +(a1*mu*B+(b1*B*B)*B1+c1*A*A1*B)*zeta2
      +conjugate(zeta1)
*(conjugate(a1)*mu*A1+(conjugate(b1)*A1*A1)*A+conjugate(c1)*B1*B*A1)
      +conjugate(zeta2)
*(conjugate(a1)*mu*B1+(conjugate(b1)*B1*B1)*B+conjugate(c1)*A1*A*B1);
```

Then we formally write a Taylor expansion of the neural field equations where `R2(mu)` represents the second differential $\mathbf{R}_2$ for example. As the variable `A` is already used, we write `L0(0)` for $\mathbf{A}$. The name of the different variables has been chosen to make it easy the mapping with (5.9).

```
> R := (v, mu)->L0(mu)+L1(mu)*v+R2(mu)*v*v+R3(mu)*v*v*v;
> DTildePsiL0v0 := I*(diff(TildePsi, B))*B*omega-I*B1*omega*(diff(TildePsi, B1))+
            I*(diff(TildePsi, A))*A*omega-I*A1*omega*(diff(TildePsi, A1));
> DTildePsiN := (diff(TildePsi, A))*(a1*mu*A+(b1*A*A)*A1+c1*B*B1*A)
          +(diff(TildePsi,A1))
*(conjugate(a1)*mu*A1+(conjugate(b1)*A1*A1)*A+conjugate(c1)*B1*B*A1)
          +(diff(tPhi2, B))*(a1*mu*B+(b1*B*B)*B1+c1*A*A1*B)+(diff(TildePsi, B1))
*(c*conjugate(a1)*mu*B1+(conjugate(b1)*B1*B1)*B+conjugate(c1)*A1*A*B1);
> eq := DTildePsiL0v0-L0(0)*TildePsi+N-(R(u,mu)-DTildePsiN);

> # For example, the equation for the coefficient of A*A is given
by:
> subs(A=0,A1=0,B=0,B1=0,x=1,mu=0,L1(mu)=0,diff(eq, A, A));
```

$$4 * I * Psi[2,0,0,0,0] * omega - 2 * L0(0) * Psi[2,0,0,0,0] - 2 * R2(0) * Zeta1^2$$

which gives the equation

$$(2i\omega_H - \mathbf{A})\Psi_{20000} = \mathbf{R}_{20}(\phi_1, \phi_1)$$

used in lemma 5.2.1 (see this lemma for the notations).

5.2.2 Normal forms for 1D convolutional neural fields

The nonlinear analysis with the normal forms requires the computation of the coefficients of the normal forms: this can be done without assuming a particular shape of the connectivity. What we would like to do here, is not to study a very realistic model (but see chapter 11), but to understand how the space-dependent delays impact the dynamics of simple models. Indeed, little is known on the relative roles of constant delays and space dependent delays on the cortical dynamics. The study of simple models can provide a hint about the importance of propagation delays

in the cortex. To this hand, having a small number of parameters is a necessity. A simple way to lower the number of parameters is to impose symmetries to the model: for example, it requires one parameter (*i.e.* the spatial extension) to describe a rotation invariant 2D connectivity with a Gaussian whereas it would require more parameters not to have such a symmetrical connectivity. However, there is a price to pay for having less parameters by assuming symmetries: the normal forms are more complex and not always tabulated. Nevertheless, we will study models with symmetries.

Hence, we assume that the connectivity is convolutional, also called *homogeneous* and that the cortex features periodic boundary conditions. The eigenvectors of the connectivity are the Fourier modes, *i.e.* the cosine and sine functions. We could do the case of a 3D cortex[2] but in this case, this numerical computation of the solutions of (4.1) would be quite long. Thus, we study neural fields on a one-dimensional cortex $\Omega = (-\frac{\pi}{2}, \frac{\pi}{2})$ with periodic boundary conditions. The connectivity function is *homogeneous* $J(x, y) = J(x - y)$ with J even, but otherwise unspecified. In chapter 6, we specialize this function to a Mexican hat to push the study one step further. We also assume the same for the delay function (the saw-function in figure 5.2)

$$\tau(x, y) = D + c|x - y|_\pi \equiv \tau(x - y)$$

in order to respect the topology of the network. Under these conditions, it can be shown that constant equilibria exist if the external input I_{ext} is constant in space. We restrict our analysis to functions (membrane potentials) which are π-periodic, hence: $\mathcal{F} = \mathrm{L}^2_\pi(\Omega, \mathbf{R})$. This kind of networks have been used in [Hansel 1997, Ben-Yishai 1995, Roxin 2005, Roxin 2011] and found useful to model cortical hypercolumns or to reproduce behaviors of spiking neural networks with rate models.

Remark 25. In the following, we use the notations $\cos_n(x) = \cos(2nx)$, $\sin_n(x) = \sin(2nx)$ *and* $e_n(x) = e^{2inx}$. *Also* $(f)_n \equiv \int_\Omega f \cos_n$ *written* f_n *when possible. It is useful to note that if* J *is even, then* $J \cdot e_n = (J)_n \, e_n$.

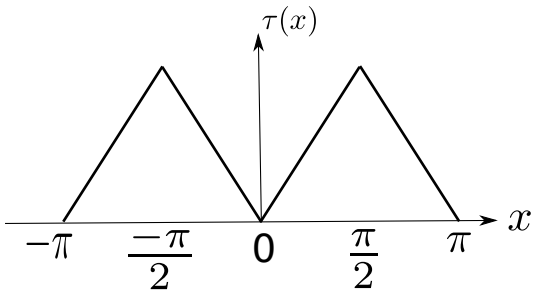

Figure 5.2: Plot of the periodic delay function, the saw-function.

[2]The computation of the normal forms is not more difficult.

Let us rewrite the neural field equations in this somewhat simpler framework:

$$\begin{cases} \left(\frac{d}{dt}+l\right)V(x,t) = \int_\Omega J(x-y)S_0[\sigma V(y,t-\tau(x-y))]dy + I_{ext}, \quad t \geq 0 \\ V_0 = \phi \in C^1(-\tau_m, 0; \mathrm{L}^\infty) \end{cases} \tag{5.12}$$

with the centered sigmoid given by $S_0(x) = S(x-h)-S(-h)$ and h is the threshold. We suppose that $l = 1$, $I_{ext} = 0$. By construction, $V^f = 0$ is a stationary solution. Let us also write $s_i = S_0^{(i)}(0)$.

Recall that (5.12) has a Lyapunov functional when $\tau = 0$ and that all trajectories are bounded. The trajectories of the non-delayed form of (5.12) are heteroclinic orbits and there are no non-constant periodic orbits. Here, we are not interested in the global dynamics of (5.12), rather we are looking at the local dynamics near the trivial solution $V^f = 0$ at bifurcation points.

Our assumptions have introduced symmetries that will make the computation of the normal forms a bit more involved. It requires some basic tools of equivariant bifurcation theory which can be found for example in [Golubitsky 1988, Chossat 2000, Haragus 2010]. Notice that (5.12) is G-equivariant (see definition A.0.2) with respect to the following action[3]:

$$(R_\gamma \cdot V)(x) = V(\gamma + x)$$
$$(S \cdot V)(x) = V(-x)$$

The fact that (5.12) commutes with the translations R_γ follows from J being homogeneous. Also the equivariance w.r.t. the reflection S comes from J being an even function.

The linearisation of (5.12) around the stationary solution $V = 0$ reads:

$$\frac{d}{dt}V(x,t) = -V(x,t) + \sigma s_1 \int_\Omega J(x-y)V(y,t-\tau(x-y))dy \tag{5.13}$$

The solutions of this linear equation are $e^{\lambda t}\sin_n$ or $e^{\lambda t}\cos_n$. Also, we can give the expression of $\Delta(\lambda)$ (see (4.12))

$$\Delta(\lambda) = \lambda \mathrm{Id} + 1 - \sigma s_1 J e^{-\lambda\tau}$$

where $Je^{-\lambda\tau}$ is the homogeneous integral operator with kernel $J(x)e^{-\lambda\tau(x)}$. The null vectors of $\Delta(\lambda)$ are $\cos_n, \sin_n$ and using complex coordinates, we find that

$$\Delta(\lambda)e^{2inx} = \left(\lambda + 1 - \sigma s_1 \left(Je^{-\lambda\tau}\right)_n\right) e^{2inx}$$

where $\left(Je^{-\lambda\tau}\right)_n$ have been defined in remark 25. Hence, the characteristic values are solution of

$$\lambda + 1 - \sigma s_1 \left(Je^{-\lambda\tau}\right)_n = 0.$$

[3] where G is the group generated by the two elements $\langle R_\gamma, S\rangle$ and is isomorphic to $O(2)$, see chapter 9 for more details.

Also, the null space of $\Delta(\lambda)$ for a characteristic value λ is made of $\cos_n, \sin_n$: it is two-dimensional if $n \neq 0$ and one-dimensional otherwise.

We will now compute the normal forms of some bifurcation points that will appear in chapter 6. In order to do this, we will use the fact that (5.12) is $O(2)$-equivariant. It turns out that this simplifies the computation of the normal forms. This is best achieved by using complex coordinates for the eigenvectors. Formally, this leads to the extension of the real history space to the complex space $\mathcal{X}_{\mathbb{C}} \equiv \mathcal{X} \oplus i\mathcal{X}$ and to a change from a scalar product on $\mathcal{X}$ to a sesquilinear form on $\mathcal{X}_{\mathbb{C}}$: $\langle \psi, \phi \rangle_{\mathcal{X}_{\mathbb{C}}} = \langle \overline{\psi}, \phi \rangle_{\mathcal{X}}$ where $\overline{\psi}$ is the complex conjugate of ϕ. Whenever there is no confusion, we shall write, by abuse of notation, $\langle \psi, \phi \rangle_{\mathcal{X}}$ for $\langle \psi, \phi \rangle_{\mathcal{X}_{\mathbb{C}}}$. For example, the spectral projector formula in prop 4.4.10 is now formally:

$$\forall u \in \mathcal{X}_{\mathbb{C}}, \quad P_{\lambda_0} u = \sum_{i=1}^{m_{\lambda_0}} \langle \langle \overline{\psi}_i, u \rangle \rangle \phi_i.$$

We wish to make an important remark on which parameters we are allowed to use in theorem 4.6.3. The nonlinearity must be regular enough with respect to these parameters and this can be an issue for the parameters c and D for two reasons. The first reason is that the state space is changing and the second is the lack of regularity of $\mathbf{R}$. In the case where only one of these parameters is non-zero, then we can rescale time and use theorem 4.6.3. For example, if $D = 0$, then[4] the time rescaling $t \to t/c$ yields

$$\frac{d}{dt} V(x,t) = c \left(-V(x,t) + \sigma s_1 \int_\Omega J(x-y) S(V(y, t - |x-y|_\pi)) dy \right)$$

and the right-hand side is regular in c. Note that the history space is fixed as the maximum time delay is $\tau_m = \pi$. This shows that we can't take the pair (c, D) as parameters. In the following, we compute the normal forms truncated at order 3: the coefficients of the nonlinear terms do not depend on the parameters, only the linear terms in the voltage variable V do. Hence, at order 3, if we are interested in other parameters, we only have to compute linear terms.

5.2.2.1 The Pitchfork bifurcation

We start with the simplest of all the bifurcations, the bifurcation parameter is the nonlinear gain σ. We took a first look at it in section 4.6.4 in the general case. Suppose that $\cos_n$, $\sin_n$ with $n \neq 0$, are in the null-space of $\Delta(0) = \mathrm{Id} - \sigma s_1 J$ at the value $\sigma_P = \frac{1}{s_1 J_n}$ of σ at the Pitchfork bifurcation, *i.e.* $0 \in \Sigma_P(\mathbf{A})$. If we write $v_0 = z\phi + c.c.$ (complex conjugate) with $z \in \mathbb{C}$ and $\phi \equiv \begin{bmatrix} e_n \\ e_n \end{bmatrix}$, in the non-delayed case, the normal form is (see [Golubitsky 1988, Curtu 2004, Roxin 2011]):

$$\dot{z} = \frac{\tilde{\sigma}}{\sigma_P} z + \chi_n z |z|^2 + o(z^3)$$

[4] The case $c = 0$ is analogue.

with $\sigma = \sigma_P + \tilde{\sigma}$ and $\chi_n = \sigma_P^3 J_n \left[\frac{s_3}{2} + \sigma_P s_2^2 \left(\frac{J_0}{1-J_0/J_n} + \frac{J_{2n}}{2(1-J_{2n}/J_n)}\right)\right]$. From section 4.6.4, the normal form in the delayed case is

$$\dot{z}/\bar{\beta} = \frac{\tilde{\sigma}}{\sigma_P} z + \chi_n z|z|^2 + o(z^3)$$

with (see above for the explanation about the complex conjugate):

$$\bar{\beta}^{-1} = \pi\left(1 + \sigma_P s_1 (J\tau)_n\right) \neq 0 \tag{5.14}$$

which shows that β is real. Recall that we have defined $(J\tau)_n = \int J\tau \cos_n$ in remark 25.

5.2.2.2 The O(2)-Hopf bifurcation

It is known that in the non-delay case ($\tau = 0$), the network (5.12) does not support periodic solutions; this is not the case with delays. Suppose that there is a simple eigenvalue $i\omega_H \in \Sigma_P(\mathbf{A})$ and $n \neq 0$ (but see below) when the parameters (D, c) are equal to (D_H, c_H). We write τ_H the delay function $D_H + c_H|c|_\pi$. Then a Hopf bifurcation with $O(2)$ symmetry. This bifurcation is described in [Golubitsky 1985, Haragus 2010]. By definition, we have $\Delta(i\omega_H)e_n = 0$ and the eigenvectors of $\mathbf{A}$ read: $\phi_1 = \begin{bmatrix} e_n \\ e^{i\omega_H\theta} e_n \end{bmatrix}$, $\phi_2 = \begin{bmatrix} e_{-n} \\ e^{i\omega_H\theta} e_{-n} \end{bmatrix}$. They satisfy:

$$R_\gamma \phi_1 = e^{in\gamma}\phi_1,\ R_\gamma \phi_2 = e^{-in\gamma}\phi_2,\ S\phi_1 = \phi_2,\ S\phi_2 = \phi_1.$$

Clearly, $\{\overline{\phi_1}, \overline{\phi_2}\}$ are the eigenvectors associated with $-i\omega_H$. By using proposition 4.4.10, we find: $\psi_1 = \beta_1 \begin{bmatrix} e_n \\ e^{-i\omega_H\theta} e_n \end{bmatrix}$, $\psi_2 = \beta_2 \begin{bmatrix} e_{-n} \\ e^{-i\omega_H\theta} e_{-n} \end{bmatrix}$. It is straightforward to check that $\langle\langle \psi_i, \phi_j \rangle\rangle = \delta_{ij}$ provided that[5]

$$\bar{\beta}_1^{-1} \overset{by\ parity}{=} \bar{\beta}_2^{-1} = \pi + \pi s_1 \sigma_H (J\tau_H e^{-i\omega_H\tau_H})_n \tag{5.15}$$

Let us assume that c is the free parameter[6] while σ is held constant at σ_H.

Remark 26. Recall from section 5.2.2 that the normal form (5.16) with parameter c is only valid for $D = 0$ even if the nonlinear coefficients β, γ does not depend on c at order 3. If we use the slope σ as the varying parameter with $c \neq 0, D \neq 0$, the coefficients β, γ have the same general expression.

In the coordinates system: $v_0 = z_1\phi_1 + z_2\phi_2 + c.c.$ with $z_i \in \mathbb{C}$, it is known that the normal form (see [Chossat 2000, Haragus 2010]) for the O(2)-Hopf is:

$$\begin{cases} \frac{dz_1}{dt} = z_1(i\omega_H + \alpha\frac{c-c_H}{c_H} + \beta|z_1|^2 + \gamma|z_2|^2) \\ \frac{dz_1}{dt} = z_2(i\omega_H + \alpha\frac{c-c_H}{c_H} + \beta|z_2|^2 + \gamma|z_1|^2) \end{cases} \tag{5.16}$$

[5] Recall that $(J\tau_H e^{-i\omega_H\tau_H})_n \equiv \int J\tau_H e^{-i\omega_H\tau_H} \cos_n$.

[6] If we chose D instead of c, it only changes the linear term $\alpha(c - c_H)$ in the normal form.

Lemma 5.2.1. *The coefficients are given by:*

$$\begin{cases} \alpha = i\omega_H \pi \overline{\beta_1} \\ \beta = \pi \overline{\beta_1} \frac{i\omega_H+1}{s_1} \sigma_H^2 \left[\frac{s_3}{2} + \sigma_H s_2^2 \left(\frac{J_0}{1-\sigma_H s_1 J_0} + \frac{(Je^{-2i\omega_H \tau_H})_{2n}}{2(2i\omega_H + 1 - \sigma_H s_1 (Je^{-2i\omega_H \tau_H})_{2n})} \right) \right] \\ \gamma = \pi \overline{\beta_1} \frac{i\omega_H+1}{s_1} \sigma_H^2 \left[s_3 + \sigma_H s_2^2 \left(\frac{J_0}{1-\sigma_H s_1 J_0} + \frac{J_{2n}}{1-\sigma_H s_1 J_{2n}} + \frac{(Je^{-2i\omega_H \tau_H})_0}{2i\omega_H + 1 - \sigma_H s_1 (Je^{-2i\omega_H \tau_H})_0} \right) \right] \end{cases}$$

Proof. See lemma C.2.1. □

Using polar coordinates $z_i = \rho_i e^{i\theta_i}$, the equations for ρ_i do not depend on θ_i and the dynamics is characterized by a planar system in (ρ_1, ρ_2). The phase diagram of this planar system is shown below, taken from [Haragus 2010, Chap.3.3.2]. The two equilibria $(0, \rho_1^f)$, $(\rho_0^f, 0)$ correspond to *traveling waves* while the equilib-

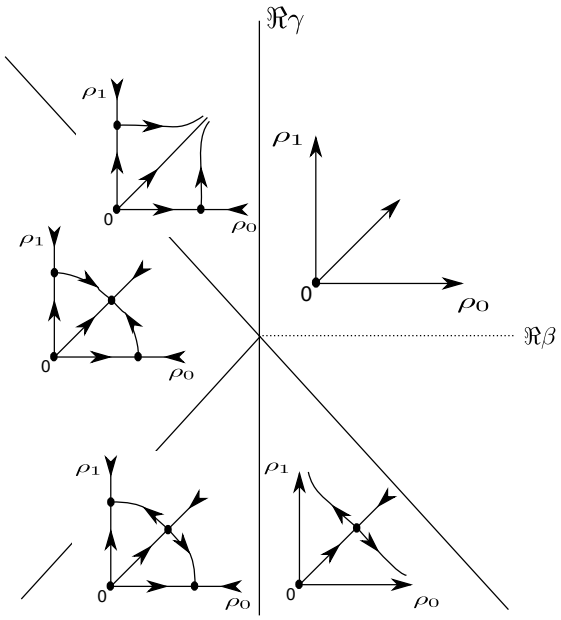

Figure 5.3: Phase portraits in the (ρ_0, ρ_1) plane of the equations for (ρ_0, ρ_1), for $\Re\alpha(c - c_H) > 0$.

rium (ρ_0^f, ρ_0^f) corresponds to a *standing wave*. Indeed, the standing wave solution is $2\rho_0^f \Re(e^{i\omega_H t} e^{2inx} + e^{i\omega_H t} e^{-2inx}) = 4\rho_0^f \cos(\omega_H t)\cos(2nx)$ and the traveling wave solution is $2\rho_0^f \Re(e^{i\omega_H t} e^{2inx}) = 2\rho_0^f \cos(\omega_H t + 2nx)$. Thus, the dynamics at the Hopf bifurcation point is fairly simple.

Remark 27.

If $n = 0$, following the same procedure, we find the normal form:

$$\frac{dz}{dt} = z(i\omega_H + \alpha\tilde{c} + \beta|z|^2)$$

Indeed, as in [Haragus 2010], we have:

$$\begin{cases} \alpha = \langle \phi_1^*, \mathbf{R}_{11}(\phi_1) + 2\mathbf{R}_{20}(\phi_1, \Psi_{001})\rangle_{\mathcal{X}} \\ \beta = \langle \phi_1^*, 2\mathbf{R}_{20}(\phi_1, \Psi_{110}) + 2\mathbf{R}_{20}(\bar{\phi}_1, \Psi_{200}) + 3\mathbf{R}_{30}(\phi_1, \phi_1, \overline{\phi_1})\rangle_{\mathcal{X}} \\ \Psi_{001} = -\mathbf{A}^{-1}\mathbf{R}_{01} = 0 \\ \Psi_{200} = (2i\omega_H - \mathbf{A})^{-1}\mathbf{R}_{20}(\phi_1, \phi_1) \\ \Psi_{110} = -2\mathbf{A}^{-1}\mathbf{R}_{20}(\phi_1, \overline{\phi_1}) \end{cases}$$

which gives:

$$\begin{cases} \alpha = \frac{i\omega_H}{c_H}\pi\overline{\beta_1} \\ \beta = \pi\overline{\beta_1}\frac{i\omega_H+1}{s_1}\sigma_H^2\left[\frac{s_3}{2} + \sigma_H s_2^2\left(\frac{J_0}{1-\sigma_H s_1 J_0} + \frac{(Je^{-2i\omega_H\tau_H})_0}{2(2i\omega_H+1-\sigma_H s_1(Je^{-2i\omega_H\tau_H})_0)}\right)\right] \end{cases}$$

a closed form expression for α, β.

5.2.2.3 The Fold-Hopf normal form

The other possible bifurcation that can happen on the line $\sigma = \sigma_P$, defined in section 5.2.2.1, is the occurrence of a purely imaginary eigenvalue $i\omega_{FH}$, which gives a Fold-Hopf bifurcation for a particular value of the delays. This bifurcation can be produced by the intersection of a Hopf curve and the Pitchfork curve in the parameters plane. We note σ_{FH} the value $\sigma_P = \frac{1}{s_1 J_n}$. We restrict the study to the case where the eigenvector associated with the eigenvalue $i\omega_{FH}$ is the 0-mode e_0 and suppose that the eigenvector for the eigenvalue 0 is in the n-mode with $n \neq 0$, it is called the $0 : n$ steady-state/Hopf mode interaction[7]. This is a simple case as well as the case $n : 0$. The difficult case, which we shall not study, is the case $n : p$ with n, p non zero.

In our case, we find two eigenvectors:

$$\phi_1 = \begin{bmatrix} e_n \\ e_n \end{bmatrix},\ \phi_2 = \begin{bmatrix} e_0 \\ e^{i\omega_{FH}\theta}e_0 \end{bmatrix},\ \psi_1 = \beta_1\phi_1,\ \psi_2 = \beta_2\begin{bmatrix} e_0 \\ e^{-i\omega_{FH}\theta}e_0 \end{bmatrix}$$

with $\bar{\beta}_1^{-1} = \pi + \pi\sigma_{FH}s_1(J\tau)_n \in \mathbb{R}$, $\bar{\beta}_2^{-1} = \pi + \pi\sigma_{FH}s_1(J\tau e^{-i\omega_H\tau})_0$. The coordinates are $v_0 = z_1\phi_1 + z_2\phi_2 + c.c.$ with $z_1, z_2 \in \mathbb{C}$. This normal form is not listed in [Haragus 2010], but from the $O(2)$-equivariance, it is known (see [Golubitsky 1988]) that the normal form does not contain any second order terms, hence it writes:

$$\begin{cases} \dot{z}_1 &= (a_1 + b_1|z_1|^2 + c_1|z_2|^2)z_1 \\ \dot{z}_2 &= (i\omega_{FH} + a_2 + b_2|z_2|^2 + c_2|z_1|^2)z_2 \end{cases} \tag{5.17}$$

where the complex coefficients $b_k, c_k,\ k = 1, 2$ are given in lemma C.2.2. In the case of a null threshold $h = 0$, we have $s_2 = 0$ and we find the simpler expressions:

$$b_1 = \pi\bar{\beta}_1\frac{\sigma_{FH}^2 s_3}{2s_1},\ c_1 = \pi\bar{\beta}_1\frac{\sigma_{FH}^2 s_3}{s_1},\ b_2 = \pi\bar{\beta}_2\frac{\sigma_{FH}^2 s_3}{2s_1}(1+i\omega_{FH}),\ c_2 = \pi\bar{\beta}_2\frac{\sigma_{FH}^2 s_3}{s_1}(1+i\omega_{FH})$$

[7] see [Golubitsky 1988] for example.

The choice of the varying parameters only affects the expression of the coefficients a_k: we will show how to compute them as functions of the parameters $\mu = (\sigma, c)$ (see the first remark in section 5.2.2.2). In the expression of $\mathbf{R}$ in (4.37), these coefficients come from $(\mathbf{L}(\mu) - \mathbf{L}(\mu_c))\phi$ which can be approximated by $(\mu - \mu_c)(\partial_\mu \mathbf{L})\phi$ close to the bifurcation point. Let us write $\sigma = \sigma_{FH} + \tilde{\sigma}$, $c = c_{FH} + \tilde{c}$, then we compute the expression of the linear terms on the center part $\mathcal{X}_c = Span\{\phi_1, \phi_2\}$:

Lemma 5.2.2. *The expression*[8] *of the linear terms on the center part reads:*

$$(\mu - \mu_c)(\partial_\mu \mathbf{L})\,(z_1\phi_1 + z_2\phi_2) = z_1\left(\frac{\tilde{\sigma}}{\sigma_{FH}}\right)e_n + z_2\left((1 + i\omega_{FH})\frac{\tilde{\sigma}}{\sigma_{FH}} + i\omega_{FH}\frac{\tilde{c}}{c_{FH}}\right)e_0.$$

It gives:

$$\begin{cases} a_1 = \langle \phi_1^*, (\partial_\mu \mathbf{L})\phi_1\rangle_{\mathcal{X}} = \pi\bar{\beta}_1 \frac{\tilde{\sigma}}{\sigma_{FH}} \\ a_2 = \langle \phi_2^*, (\partial_\mu \mathbf{L})\phi_2\rangle_{\mathcal{X}} = \pi\bar{\beta}_2\Big((1 + i\omega_{FH})\frac{\tilde{\sigma}}{\sigma_{FH}} + i\omega_{FH}\frac{\tilde{c}}{c_{FH}}\Big). \end{cases}$$

Proof. We follow the proof of lemma C.2.1. As one of the varying parameter is c, we shall rescale the time by c. It is easy to show that the normalisation factors β_1, β_2 are the same in the rescaled/not-rescaled case. In this case, the eigenvector e_n solves:

$$(i\tilde{\omega}_{FH} + c_{FH})e_0 = c_{FH}s_1\sigma_{FH}\int J(\cdot - y)e^{-i\tilde{\omega}_{FH}|\cdot - y|_\pi}e_0(y)dy$$

and we find that $\tilde{\omega}_{FH} = c_{FH}\omega_{FH}$. From $\left[\frac{\partial}{\partial\sigma}\mathbf{L}(\mu)\right]_{FH}\phi = c_{FH}s_1\int_\Omega dy J(\cdot - y)\phi(y, -|\cdot - y|_\pi)$ we find

$$\left[\frac{\partial}{\partial\sigma}\mathbf{L}(\mu)\right]_{FH} e_n = \frac{c_{FH}}{\sigma_{FH}}e_n, \quad \left[\frac{\partial}{\partial\sigma}\mathbf{L}(\mu)\right]_{FH}(e^{i\omega_{FH}\theta}e_0) = c_{FH}\frac{1 + i\omega_{FH}}{\sigma_{FH}}e_0$$

We have $\left[\frac{\partial}{\partial c}\mathbf{L}(\mu)\right]_{FH}\phi = -\phi + \sigma_{FH}s_1\int_\Omega dy J(\cdot - y)\phi(y, -|\cdot - y|_\pi)$, which gives:

$$\left[\frac{\partial}{\partial c}\mathbf{L}(\mu)\right]_{FH} e_n = 0, \quad \left[\frac{\partial}{\partial c}\mathbf{L}(\mu)\right]_{FH}(e^{i\omega_{FH}\theta}e_0) = i\omega_{FH}e_0$$

If we go back to the original equation by using $ct \to t$ and combine these formulas, we obtain the lemma. □

Using polar coordinates $z_1 = Pe^{i\phi_P}$, $z_2 = He^{i\phi_H}$, the variables decouple and we obtain a planar system for the amplitudes:

$$\begin{cases} \dot{P} &= (a_1 + b_1P^2 + c_1H^2)P \\ \dot{H} &= (\Re a_2 + \Re b_2H^2 + \Re c_2P^2)H \end{cases} \tag{5.18}$$

[8] This is an abuse of notation as $\mathbf{L}(\mu)$ is not differentiable *w.r.t.* c without the time rescaling.

The only fixed points of this system are (see [Guckenheimer 1983, Chapter 7.5]): $O_P = (0, \sqrt{\frac{-\Re a_2}{\Re b_2}})$, $O_H = (\sqrt{\frac{-a_1}{b_1}}, 0)$ and $O_{FH} = (\sqrt{-\frac{a_1\Re b_2 - c_1\Re a_2}{\Delta}}, \sqrt{-\frac{\Re a_2 b_1 - \Re c_2 a_1}{\Delta}})$ where $\Delta = b_1\Re b_2 - c_1\Re c_2$.

The equilibria of (5.18) on the P-axis are also equilibria of (5.17), while the equilibria not on the P-axis are periodic orbits[9] of (5.17). Periodic solutions in the plane (P, H) are quasi-periodic[10] solutions of (5.17) with two basic periods $2\pi/\omega_0, 2\pi/\omega_{FH}$ which form an invariant two-torus (see [Guckenheimer 1983, chapter 7.5, page 400]). Hence, the 3 points O_P, O_H, O_{FH} respectively correspond, to a stationary solution, to a uniformly oscillating solution and to a superposition of the two previous solutions. Another interesting point is the possibility of appearance of an invariant torus for (5.17) which is explained by the existence of a Hopf bifurcation for (5.18) around $O_{FH} = (P_s, H_s)$. No Hopf bifurcation can occur around O_P, O_H, however, it is possible around $O_{FH} = (P_s, H_s)$ (see [Langford 1980]) when $\Delta > 0$, $b_1\Re(b_2) < 0$. The different phase diagrams of (5.18) are listed in [Guckenheimer 1983, chapter 7]. We only show in figure 5.4 the phase diagram Ib from [Guckenheimer 1983, chapter 7.5, page 401]. This diagram will be used in chapter 6. It features (in red) bi-stability between the stationary solution O_P and the uniformly oscillating solution O_H. The mixed-mode O_{FH} solution is never stable.

5.2.2.4 The Hopf-Hopf normal form

As we shall see in the next chapter 6, the Hopf curves computed with prop.4.4.5 may intersect (see for example figure 5.1). This intersection may involve two different Fourier modes. To keep the computations manageable, we assume that the intersection happens between the 0-mode and the n-mode where $n > 0$: this is called the $0 : n$ Hopf-Hopf mode interaction. This case was investigated in [Roxin 2011] for constant delays. From proposition 4.4.4, it is easy to see that the Hopf-Hopf bifurcation is possible for constant delays if and only if the connectivity has two Fourier modes which are equal: $J_0 = J_n$. With propagation delays, we see in figure 5.1 that this is not the case. Let us write $i\omega_0$, $i\omega_n$, the purely imaginary eigenvalues at the Hopf-Hopf point. The normal form of this bifurcation is different depending on whether or not $\frac{\omega_0}{\omega_n} \in \mathbb{Q}$ (see for example [Golubitsky 1988, Haragus 2010]). It is impossible to check this hypothesis with the expressions in proposition 4.4.5. We will assume[11] that $\frac{\omega_0}{\omega_n} \notin \mathbb{Q}$. Indeed, in this case the nonlinear terms of the normal form are very similar to those of the Folf-Hopf normal form that we have analyzed in the previous section. The expression of the eigenvectors is the same as for the

[9] because we have $v_0 = 2\Re(Pe^{2inx+i\phi_P} + He^{i\omega_{FH}t+i\phi_H})$

[10] because we have $v_0 = 2\Re(P\cos(\omega_0 t)e^{2inx+i\phi_P} + H\sin(\omega_0 t)e^{i\omega_{FH}t+i\phi_H})$

[11] Another strategy is to study the case $\frac{\omega_0}{\omega_n} \notin \mathbb{Q}$ by considering the closest rational number $\frac{r}{s}$ to $\frac{\omega_0}{\omega_n}$ which has the smallest sum $r + s$, and then taking a detuning parameter $\delta = s\omega_0 - r\omega_n$ which is added to the varying parameters. Hence, it amounts to study the case $\frac{\omega_0}{\omega_n} \notin \mathbb{Q}$ as a perturbation of the rational case.

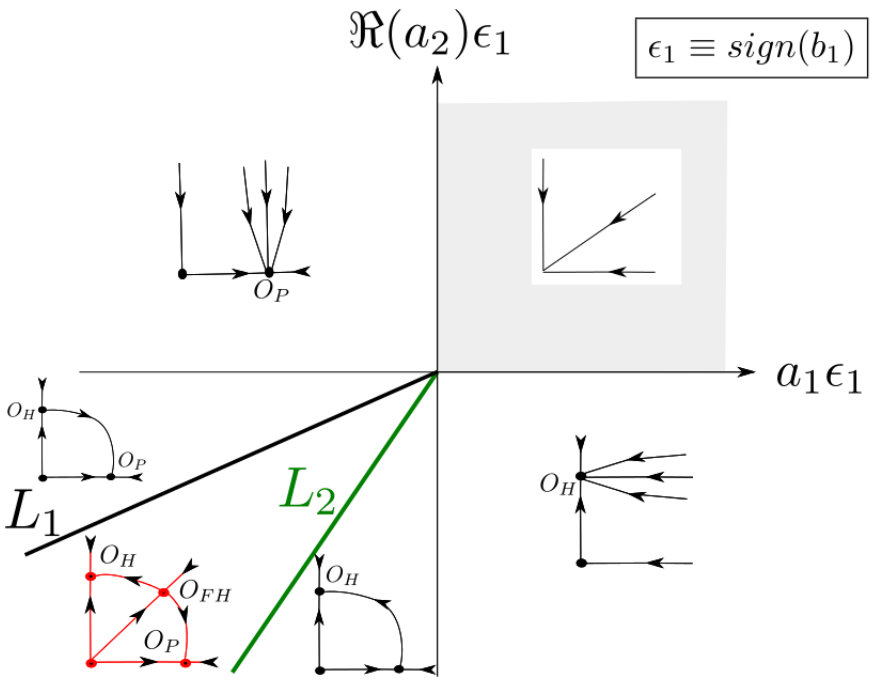

Figure 5.4: $\varepsilon_1 \equiv sign(b_1)$, L_1 : $\Re a_2\varepsilon_1 = \frac{|\Re b_2|}{c_1}a_1$, L_2 : $\Re a_2\varepsilon_1 = \frac{\Re c_2}{|b_1|}a_1$. Phase diagram *Ib* in [Guckenheimer 1983, chapter 7.5, page 401] with time reversal, *i.e.* in the terminology of [Guckenheimer 1983], it corresponds to the phase diagram Ib for which time has been reversed. We plot here the resulting diagram. In each domain, the small phase diagram gives the corresponding dynamics for the equations (5.18) in the plane (P, H). Note that the diagrams are a bit different from [Guckenheimer 1983, chapter 7.5, page 401] because we applied the inverse scaling of [Guckenheimer 1983, chapter 7.5, page 397].

O(2)-Hopf, hence

$$\phi_0 = \begin{bmatrix} e_0 \\ e^{i\omega_0\theta}e_0 \end{bmatrix},\ \phi_1 = \begin{bmatrix} e_n \\ e^{i\omega_1\theta}e_n \end{bmatrix},\ \phi_2 = \begin{bmatrix} e_{-n} \\ e^{i\omega_1\theta}e_{-n} \end{bmatrix},$$

and the associated vectors for the spectral projector are:

$$\psi_0 = \beta_0 \begin{bmatrix} e_0 \\ e^{-i\omega_0\theta}e_0 \end{bmatrix},\ \psi_1 = \beta_1 \begin{bmatrix} e_n \\ e^{-i\omega_1\theta}e_n \end{bmatrix},\ \psi_2 = \beta_2 \begin{bmatrix} e_{-n} \\ e^{-i\omega_1\theta}e_{-n} \end{bmatrix}$$

where $k = 0, 1, 2$ and the normalization factors satisfy $\bar{\beta}_k^{-1} = \pi + \pi s_1 \sigma_{HH}(J\tau_{HH}e^{-i\omega_k\tau_H})_{|n_k|}$ with $(n_0, n_1, n_2) = (0, n, -n)$. The coordinates on the center part are $v_0 = z_0\phi_0 + z_1\phi_1 + z_2\phi_2 + c.c.$ and, from [Golubitsky 1988], the normal form is:

$$\begin{cases} \dot{z}_0 = z_0\left(i\omega_0 + a_0 + b_0|z_0|^2 + c_0|z_1|^2 + d_0|z_2|^2\right) \\ \dot{z}_1 = z_1\left(i\omega_1 + a_1 + b_1|z_0|^2 + c_1|z_1|^2 + d_1|z_2|^2\right) \\ \dot{z}_2 = z_2\left(i\omega_1 + a_1 + b_1|z_0|^2 + d_1|z_1|^2 + c_1|z_2|^2\right) \end{cases} \tag{5.19}$$

The expressions for the coefficients b_k, c_k, d_k are given in lemma C.2.3, they are simple if the threshold h is zero:

$$b_0/\pi\bar{\beta}_0 = \frac{\sigma_{FH}^3 s_3}{2}(Je^{-i\omega_0\tau})_0,\ c_0/\pi\bar{\beta}_0 = \sigma_{FH}^3 s_3(Je^{-i\omega_0\tau})_0,\ d_0 = c_0$$

$$b_1/\pi\bar{\beta}_1 = \sigma_{FH}^3 s_3(Je^{-i\omega_1\tau})_n,\ c_1/\pi\bar{\beta}_1 = \frac{\sigma_{FH}^3 s_3}{2}(Je^{-i\omega_1\tau})_n,\ d_1/\pi\bar{\beta}_1 = \frac{\sigma_{FH}^3 s_3}{2}(Je^{-i\omega_1\tau})_n.$$

Notice that in the general case, $c_0 = d_0$ and the coefficients c_1, d_1 are the same as the coefficients β, γ in the O(2)-Hopf normal form (see lemma C.2.3). As before, the choice of the two varying parameters only affects the coefficients a_k. We will show how to compute the a_ks in the case $\mu = (\sigma, c)$ (see the first remark in section 5.2.2.2). Like for the Fold-Hopf bifurcation, let us write the linear part: $(\mu - \mu_c)(\partial_\mu \mathbf{L})$ and $\sigma = \sigma_{HH} + \tilde{D},\ c = c_{HH} + \tilde{c}$. The next lemma gives the expression of the linear on the center part $\mathcal{X}_c = Span\{\phi_0, \phi_1, \phi_2\}$:

Lemma 5.2.3. *The operator $\partial_\mu \mathbf{L}$ is diagonal in the base (ϕ_0, ϕ_1, ϕ_2) and*

$$\begin{aligned} a_0/\pi\bar{\beta}_0 &= (1 + i\omega_0)\frac{\tilde{\sigma}}{\sigma_{HH}} + i\omega_0\frac{\tilde{c}}{c_{HH}} \\ a_1/\pi\bar{\beta}_1 &= (1 + i\omega_1)\frac{\tilde{\sigma}}{\sigma_{HH}} + i\omega_1\frac{\tilde{c}}{c_{HH}} \end{aligned} \tag{5.20}$$

Proof. It is almost the same as the proof of lemma 5.2.2. □

Let us note that each space $\{z_0 = 0\}$ or $\{z_1 = z_2 = 0\}$ is invariant under the dynamics of (5.19): the dynamics is the same as in the Hopf case in the n or 0-mode. However, compared to the Hopf bifurcation case, this normal form can generate superpositions of oscillatory behaviors like $(z_0(t), z_1(t), 0)$ or $(z_0(t), z_1(t), z_1(t))$ for example. If we use polar coordinates $z_k = \rho_k e^{i\theta_k}$, we find (like for the Hopf or the Fold-Hopf bifurcation) that the equations in ρ and θ are decoupled and we end up with a 3D real system of ordinary differential equations for the amplitudes ρ_i, see

[Golubitsky 1988]. Notice that the equations for $(\rho_0, \rho_1, \rho_2 = 0)$ are the same as (5.18) in the Fold-Hopf bifurcation:

$$\begin{cases} \dot{\rho}_0 = \rho_0(\Re a_0 + \Re b_0 \rho_0^2 + \Re c_0 \rho_1^2) \\ \dot{\rho}_1 = \rho_1(\Re a_1 + \Re b_1 \rho_0^2 + \Re c_1 \rho_1^2). \end{cases} \tag{5.21}$$

Thus we expect the same kind of solutions: 2 oscillatory solutions, a mixed mode solution, and possibly, the 2-torus solution resulting from a Hopf bifurcation around the mixed mode solution. We will not push further the study of the 3D-system for the amplitude equations, this will be the subject of future work.

5.3 Conclusion

In this chapter, we have prepared the application of the tools developed in chapter 4 for the numerical study that will be performed in the next chapter 6. In particular, we have given two ways of computing the bifurcation curves depending on the form of the network under study. One is an analytical formula and the other is a numerical method for which the error has been bounded by a function of the space/time discretization. In the second case, the convergence of the approximated eigenvalue to the real value is very fast, it goes as $O(\varepsilon_{N_\Omega} + N_t^{-N_t - 1/2})$ where N_t is the discretization in time. This shows that the main part of the error comes from the space discretization N_Ω.

We have also computed normals forms and given their qualitative dynamics. This will simplify their use in the next chapter. Concerning the normal forms, a lot more can be done. We have computed the Fold-Hopf normal form for the $0 : n$ mode interaction. The "only" interesting feature of this mode interaction is the existence of an invariant torus. More interesting dynamics is expected for the interaction of two non zero modes. However we shall see that this mode interaction do not appear in our models (see next chapter and chapter 11).

Similarly, we have started the study of the Hopf-Hopf normal form for the $0 : n$ mode interaction and we have looked at a particular subspace of the dynamics. The full dynamics is much richer and deserve more investigations. As for the Fold-Hopf normal form, more sophisticated dynamics is expected for the interaction of two non zero modes and we will see, in section 6.1, that these points do occur quite often in the bifurcation diagrams.

Hence, our study is far from being complete but it is sufficient for the upcoming analysis of the models.

Chapter 6

Application to the study of different connectivities on a ring

Contents

We make good use of the results obtained in chapter 4 and Chapter 5 to deepen our understanding of 1D delayed neural fields with homogeneous connectivity functions and periodic boundary conditions. We started their study in chapter 5. We use this class of examples to get a feeling of the conservativeness of the bounds derived in chapter 4 and to push further the analysis of the bifurcations and dynamics they create.

6.1 Bifurcation analysis of two delayed neural field equations

We arrive at the last sections of this part concerning the study of the space-dependent delays: by using the formulas of section 4.4.1.2 for the Hopf curves together with the computation of the normal forms in section 5.2, we are in a position to analyse, in great detail, the most simple connectivity functions that have appeared in the literature. This is a great achievement because the relative role of constant delays/propagation delays has never been studied and it appears that the dynamics are fairly rich.

More precisely, we first study a connectivity function which is laterally excitatory and locally inhibitory, the so-called *inverted Mexican-hat* (see [Venkov 2007, Hutt 2008]). This connectivity is motivated by the fact (stereotyped) that inhibition is localized and long-range connections are mainly excitatory in the mammal visual cortex (see [Lund 2003a]). By construction, this type of connectivity favours the spread of activity. We then study the opposite connectivity, the *Mexican-hat*, which favours stationary activity: this connectivity has been mainly used as a functional connectivity in some feature domain (see [Ben-Yishai 1995, Bressloff 2000, Bressloff 2001b] and also part IV).

In both cases, we start with spatially extended connectivities given by two Fourier modes. To describe more localized connectivities requires more Fourier modes, and in this case we expect an increase in the number of bifurcations.

For convenience, we recall the model. More details are given in section 5.2.2.

$$\begin{cases} \left(\frac{d}{dt}+l\right)V(x,t) = \int_\Omega J(x-y)S_0[\sigma V(y,t-\tau(x-y))]dy, \quad t\geq 0 \\ V_0 = \phi \in C^1(-\tau_m, 0; \mathrm{L}^\infty) \end{cases} \tag{6.1}$$

6.1.1 Inverted Mexican-hat connectivity

This is the case where $J(x) = -(0.5 + J_1 \cos_2)\frac{2}{\pi}$.

We chose $J_1 = 2.1$ in order to have local inhibition and lateral excitation (see figure 6.1). Let us first note, that because the two Fourier modes of the connectivity are negative, no static bifurcation can occur; this is not generally true for *inverted Mexican-hat* connectivities because, for localized connectivities, more Fourier modes are non-zero and some are possibly positive. In our case, we can nevertheless restrict ourselves to searching for oscillatory behaviours. We start with constant delays and then extend the analysis to include space dependent delays.

According to lemma 4.4.4, an equivariant Hopf bifurcation happens for some constant delay D_n in the Fourier mode n if the connectivity has negative eigenmodes. Using the same lemma, we find that it is the mode $n = 1$ that first bifurcates for $c = 0$ when varying D. We plot the constant critical delay D_1 as function of the nonlinear gain σ in figure 6.1 Right: if the nonlinear gain σ is small, *i.e.* if the network is linear, then it is not possible to generate oscillations because $D_1 \to \infty$ as $s_1 J_1 \sigma \to 1$.

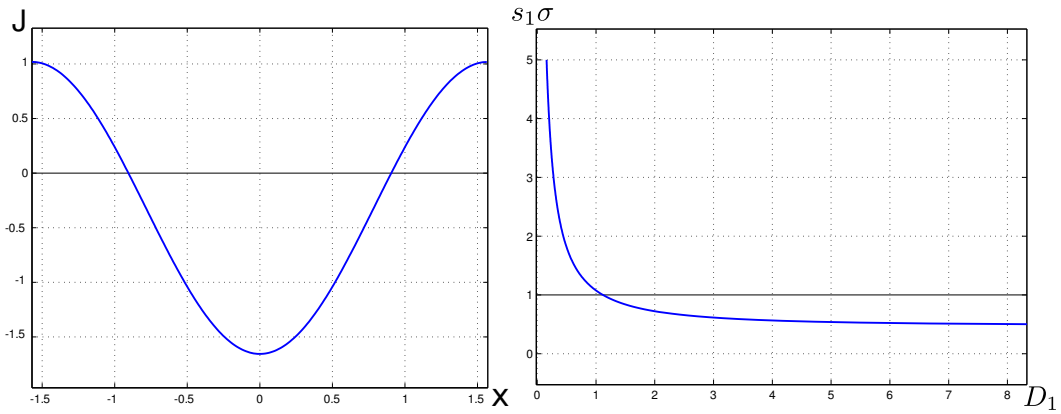

Figure 6.1: Left: connectivity used in the examples of this section ($J_1 = 2.1$). Right: plot of the critical constant delay D_1 (for the mode $n = 1$) as function of the nonlinear gain σ.

Moreover, if the threshold is null, $h = 0$, the coefficients of the Hopf normal form (5.16) simplify[1]: $\pi\beta_1 = (1+D-i\omega D)^{-1}$, $\Re\alpha = \frac{\omega^2}{(1+D)^2+\omega^2 D^2} > 0$ and $\Re\beta = \Re\gamma/2 =$

[1] after a little algebra.

$\frac{\sigma_H^2 s_3}{2s_1}\frac{1+D+D\omega^2}{(1+D)^2+\omega^2 D^2} < 0$, which implies that the Hopf is supercritical. Depending on the initial condition (see figure 5.3), it can produce travelling waves (stable) or standing waves (unstable) (see figure 6.2). The fact that the Hopf is supercritical and produces stable travelling waves was also proved[2] in [Roxin 2011].

We now investigate the case of space dependent delays.

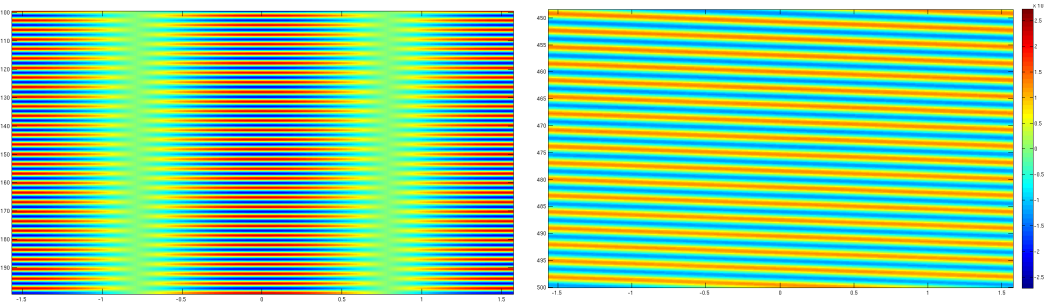

Figure 6.2: Left: standing wave, Right: travelling wave. Parameters: $s_1\sigma = 1, c = 0$, $D = 1.14$ (Left) and $D \approx 1.12$ (Right). The space discretization is $N = 300$.

If we introduce propagation delays (*i.e.* $c > 0$), we expect changes in the bifurcation diagram. We know from proposition 4.5.9 that if the nonlinear gain is too small, oscillations are impossible. Hence, we expect a strong dependency of the Hopf curves on the nonlinear gain. This is shown in figures 6.3 and 6.4

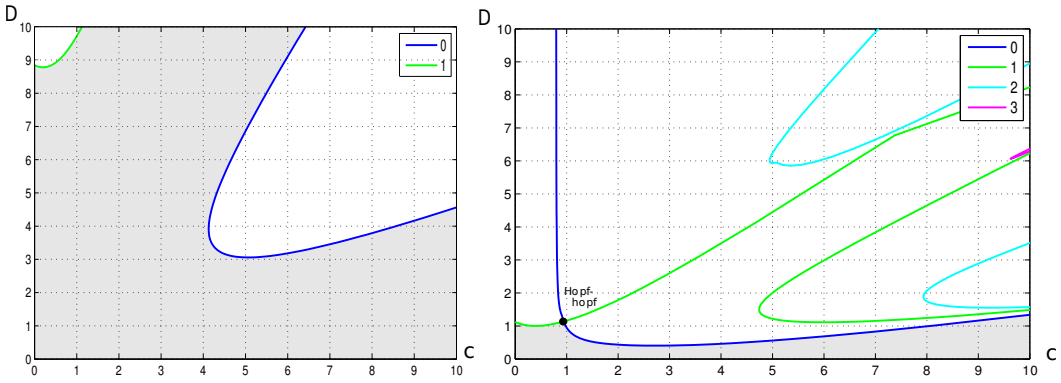

Figure 6.3: Plot of the Hopf curves in the (c, D) plane for $s_1\sigma = 0.5$ (left) and $s_1\sigma = 1$ (right). The different Hopf curves are labelled with the corresponding Fourier mode. The grey part is where the stationary state $V^f = 0$ is asymptotically stable.

where $s_1\sigma = 0.5$ in the left panel and $s_1\sigma = 1$ in the right panel. There are three interesting features that come out of these figures:

1. No Hopf curve crosses the c-axis for $s_1\sigma < 2$: it is impossible to produce oscillations with only propagation delays in this network. This is shown up

[2] for a different varying parameter.

to $s_1\sigma < 1.3$, but further numerical investigations have led to this conclusion (data not shown). For $s_1\sigma > 2$, the Hopf curve for the 0-mode crosses the c-axis, more Hopf curves do this as σ is increased. We could not find a criterion to predict when a Hopf curve crosses the c-axis.

2. The accumulation of the Hopf curves around $c \approx 10$ (see figure 6.4 Left): for small changes in the constant delays, a lot of eigenvalues cross the imaginary axis. Very sophisticated dynamics should happen in this parameter region.

3. The number of intersections between Hopf curves, shown with black dots (in particular in figure 6.4 Left). These intersection points are Hopf-Hopf bifurcation points where the dynamics can lead to complicated behaviours (see [Guckenheimer 1983, Kuznetsov 1998]). We have not studied these bifurcation points in detail.

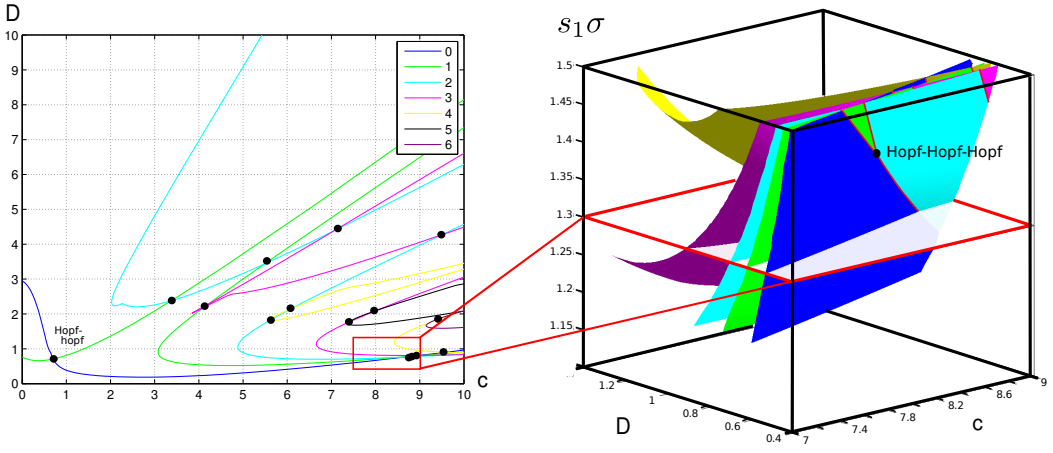

Figure 6.4: Left: plot of the Hopf curves in the (c, D) plane for $s_1\sigma = 1.3$. Right: plot of the Hopf surfaces in the (c, D, σ) space for a particular region which is shown in the 2D bifurcation plot. The Hopf-Hopf curves, intersection of two Hopf surfaces are shown in red. Finally, two Hopf-Hopf curves intersect at a Hopf-Hopf-Hopf bifurcation point.

Let us go back to figure 6.3 where we have plotted the Hopf curves for $s_1\sigma = 1$; the grey part is the parameter region where the stationary solution $V^f = 0$ is asymptotically stable. For small propagation delays $c \approx 0$, by increasing the constant delay D, it is the 1-mode that first bifurcates and we find solutions like those shown in figure 6.2. For larger values of c, it is the 0-mode that first bifurcates, hence giving a non-equivariant hopf bifurcation; a plot of the oscillatory uniform solution is shown in figure 6.9 Right. Thus, we find the rather surprising fact that even if the connectivity does not have a sufficiently negative eigenmode (*i.e.* $s_1\sigma J_0 = -1$), Hopf bifurcations may still appear due to the intricate interaction between the connectivity and the propagation delay functions. Hopf bifurcation can also happen in modes that are not present in the connectivity as shown in figure 6.4:

for example there is a Hopf curve in the 2-mode whereas the connectivity has no 2-mode. We have not been able to find a simple criterion to predict the appearance of an oscillatory solution as we did for constant delays in section 4.4.1.1.

Let us say a few words about the Hopf-Hopf bifurcation points: based on the normal form study in section 5.2.2.4, we have looked at the Hopf-Hopf bifurcation point (the one with the smallest c) between the 0-mode and the 1-mode under the non-resonant assumption $\frac{\omega_0}{\omega_n} \notin \mathbb{Q}$. We have computed the phase diagram of the reduced amplitude equations (5.21) for $s_1\sigma = 1$ and for $s_1\sigma = 1.3$ as listed in [Guckenheimer 1983, Chapter 7.5] when the threshold h is varied. If h is close to zero, then the phase diagram of (5.21) is Ib (with time reversal as shown in figure 5.4). In all cases, the mixed-mode solution is unstable and the two-torus does not appear: no new behaviour emerges and the dynamics is that of the Hopf bifurcation. In order to look for 3-torus and other solutions, it would be necessary to study the full 3D system as opposed to (5.21). This is the subject of future work.

Remark 28.In the computation of the Hopf-Hopf bifurcation points, we have looked at a rational approximation $\frac{r}{s}$ *of* $\frac{\omega_p}{\omega_n}$ *with smallest sum* $r+s$*. We always found a sum* $r+s$ *strictly greater than* 5 *which suggests that the bifurcations Hopf-Hopf belong to the weakly resonant case (see [Haragus 2010, Chapter III.4.5]).*

Finally, for $(c, D, s_1\sigma) \approx (8.06, 0.6, 1.412)$, we find an intersection between three Hopf curves in the Fourier modes $0, 1, 3$. It is difficult to see this interaction in the 2D bifurcation planes. This is why we show in figure 6.4 Right a selected region of the 3D parameter space (c, D, σ) with the plot of the Hopf surfaces[3]. This intersection is a Hopf-Hopf-Hopf bifurcation point which we have not studied.

6.1.2 Mexican-hat connectivity

This is the case where $J(x) = (-1 + J_1 \cos(2x))\frac{2}{\pi}$.

As explained before, the Mexican-hat connectivity is often used to produce stationary solutions through a static bifurcation. We want to look at the possible intersection of the Pitchfork line with a Hopf curve. We write the connectivity $J(x) = (J_0 + J_1 cos(2x))\frac{2}{\pi}$ with $J_0 = -1$ and $J_1 \in (1, 2)$ in order to generate locally excitatory connections. It follows that there is a Pitchfork line $\sigma_P = \frac{1}{s_1 J_1}$ which is shown in the bifurcation diagram in figure 6.5 Left labelled as (P). Two time-evolutions are also shown in figure 6.5 Right in the neighbourhood of the Pitchfork bifurcation. The x-axis of the bifurcation diagram in figure 6.5 Left is c: we will see that the diagram stays qualitatively the same if we use the constant delays D instead.

Let us first consider the case of constant delays $c = 0$. We know from proposition 4.4.4 that there is only one Hopf curve (for the Fourier mode $n = 0$) in the plane (σ, D), its analytical expression was also given. Recall that a necessary and sufficient condition for the existence of a critical delay D_0 is $2s_1\sigma J_0 \leq -1$ *i.e.* $\sigma > \frac{1}{2s_1}$: the Hopf curve intersects the Pitchfork curve at the Fold-Hopf bifurcation

[3] given by proposition 4.4.5.

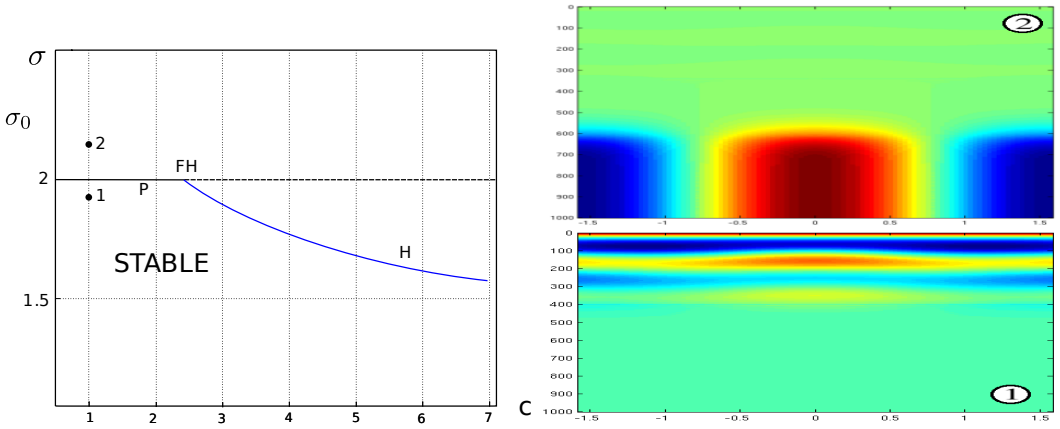

Figure 6.5: Left : bifurcation diagram in the plane (c, σ), P is the Pitchfork line, H is the Hopf curve. Right : Time evolution corresponding to the points labelled 1 and 2 in the bifurcation diagram on the left. We used $J_1 = 1.5$.

point if $2\frac{|J_0|}{J_1} > 1$. This Hopf bifurcation cannot generate travelling waves or standing waves because it happens in the 0-mode[4]. This is also true at the Fold-Hopf bifurcation point as we will see below.

We plot in figure 6.6 the coefficients of the Fold-Hopf normal form[5] as function of (J_1, h) in (recall that h is the threshold). The phase diagram is characterized in [Guckenheimer 1983, Chapter 7.5, page 401]. We are particularly interested in the appearance of the quasi-periodic solution described in section 5.2.2.3 because it is a striking behaviour compared to the dynamics produced by the Hopf bifurcation. Recall that this solution produces an invariant two-torus and its existence is conditioned by the conditions $\Delta > 0, b_1\Re(c_2) < 0$. We plot the sign of Δ as function of (J_1, h) in figure 6.6 Left, we also found that $b_1\Re(c_2) > 0$ for all parameters $h, J_1 \in [0,\ 2]$ and this indicates that the doubly periodic solution does not exist in our network.

The interesting solution, which does not appear in the other bifurcations discussed so far, is the Mixed-Mode solution (associated to the point O_{FH} in section 5.2.2.3). This solution is a superposition of the static bifurcated state and the oscillatory solution: $V(x,t) = v_1\cos(2x) + v_2\cos(\omega_{FH}t)$, for some v_1, v_2. The Mixed-Mode solution exists when $\Delta \neq 0$. More precisely, we find that in the region where $\Delta > 0$ (resp. $\Delta < 0$), the system has the phase diagram Ia (resp. Ib) in [Guckenheimer 1983, Chapter 7.5], modulo a time reversal[6]. It is then straightforward to select parameters and see the Mixed-Mode solution, shown in figure 6.6.

For $J_1 > 1$, *i.e.* in the Mexican-hat case, the solution is found to be unstable. Thanks to the computation of the normal form, we numerically observe this (unstable) solution, see figure 6.6 Right.

[4] it has no spatial structure whereas this is required in order to "see" waves
[5] they are given in section 5.2.2.3.
[6] It is shown that the diagrams Ia and Ib are very similar.

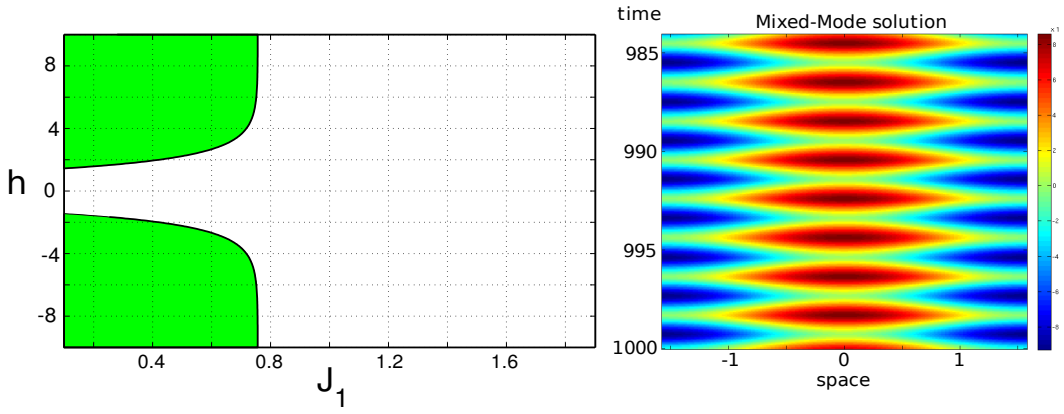

Figure 6.6: Left: Sign of Δ as a function of (J_1, h). Green means positive. Right: example of a (unstable) Mixed-Mode solution for $J_1 = 1.5, h = 1, \sigma - \sigma_{FH} \approx 0.0127, D - D_{FH} \approx -0.0027, N = 200$.

The other interesting feature of the phase diagram for $J_1 > 1$ is the bi-stability between the stationary solution $v_1 cos(2x)$ and the oscillating solution $v_2 cos(\omega_{FH} t)$, which are both stable for particular values of the couple (σ, D), as shown in figure 5.4 Red. The cortical state V can switch from a stationary state to an oscillatory state (and vice-versa) upon application of the correct external stimulation I_{ext}.

To sum up, the bifurcation portrait is composed of a Pitchfork line, a Hopf curve in the $0-$mode and a Fold-Hopf point. The phase diagram is the same for all $J_1 > 1, -2 \leq h \leq 2$, it is the one of figure 5.4.

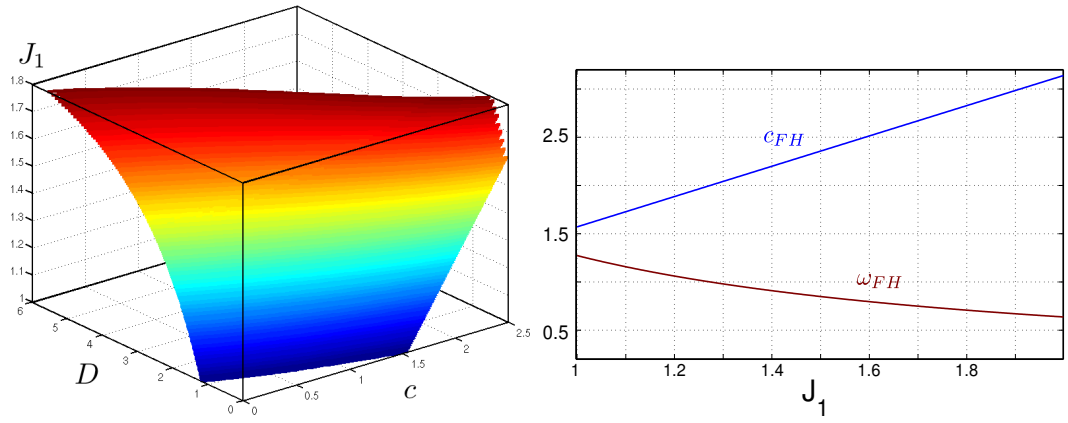

Figure 6.7: Left: Fold-Hopf bifurcation surface in the parameter space (c, D, J_1). Right: plot of c_{FH} (blue) and ω_{FH} (red) as function of J_1 where $D = 0$, *i.e.* the case of purely propagation delays.

We now consider the case of propagation delays. We want to know if the previous instabilities remain and what are the critical values of the constant delays/propagation delays. Using the proposition 4.4.5, we compute the Hopf curves in the parameter plane (D, c) for each Fourier coefficient J_1 (not shown). It appears

that for $c \leq 10$, only the Hopf curve in the 0-mode appears, which is very similar to the case of purely constant delays, *i.e.* $c = 0$. Note that unlike the previous case of the *inverted Mexican-hat*, we can destabilize the equilibrium $V^f = 0$ with purely propagation delays (see figure 6.7 Right). We also find that the Hopf curve and the Pitchfork line intersect in a Fold-Hopf bifurcation point for all $J_1 \in [1,\ 2)$. Hence we have computed the Fold-Hopf surface in the space (c, D, J_1), see figure 6.7 Right. Using the normal form given in section 5.2.2.3, we can compute the phase diagram [7] of the Fold-Hopf bifurcation point in the space (c, D, J_1) for different thresholds $h \in [-2,\ 2]$. We find that it is the same as for constant delays, *i.e.* *Ib* (see figure 5.4). Hence compared with the constant delay case, no new behaviour appears.

To conclude, for the *Mexican-hat* connectivity considered in this section, the bifurcation diagram is quite simple: there is a Pitchfork line and a Hopf curve in the mode $n = 0$. When these two curves intersect at a Fold-Hopf point, it can produce two different phase diagrams that have been completely characterized (see figure 5.4). In particular, we found that the doubly periodic solution cannot occur and that bi-stability between an oscillatory solution and a stationary solution exists in a limited region of the parameter space.

6.2 Numerical evaluation of the bounds in section 4.5.4

We consider the connectivity function $J(x) = (-1 + 1.5\cos(2x))\frac{2}{\pi}$ in (5.12). The bifurcation diagram with respect to the parameters (c, σ) is shown in figure 6.8. It is computed in section 6.1.2. The two bounds derived in section 4.5.4 are also shown, they are labelled Bound. 1 and Bound. 2. The delay-dependent bound is computed using the fact that $\tilde{J} \equiv DS(0)J = s_1 J$ is self-adjoint. Under the Pitchfork bifurcation curve, labelled (P), and the Hopf bifurcation curve, labelled (H), the stationary state $V^f = 0$ is stable. This region of stability is larger than the one delimited by the two bounds, shown in grey in figure 6.8. Hence, it is found that the bounds are very conservative.

The first bound gives the minimal velocity $1/c$ below which the stationary state might be unstable, in this case, even for smaller speed, the state is stable as long as (c, σ) is below the bifurcation curves. Notice that in the parameter domain defined by the two curves labelled Bound.1. and Bound.2. in figure 6.8, the dynamic is very simple: it is characterized by a unique and asymptotically stable stationary state, $V^f = 0$.

In figure 6.9, we show the dynamics for different parameters corresponding to the points labelled 1, 2 and 3 in figure 6.8 for a random (in space) and constant (in time) initial condition ϕ. When the parameter values are below the curves (P) and (H), the dynamics converges to the stable stationary state $V^f = 0$. Along the Pitchfork line labelled (P) in figure 6.8, there is a static bifurcation leading to the birth of new stable stationary states, this is shown in the middle part of figure 6.9. The Hopf curve labelled (H) in figure 6.8 indicates the transition to oscillatory

[7] recall that it does only depend on the nonlinear terms.

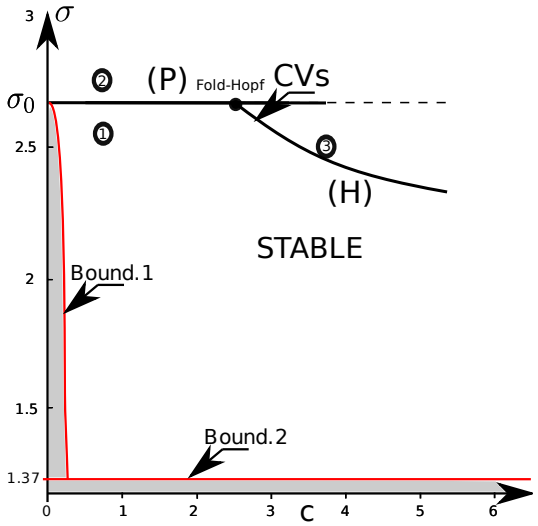

Figure 6.8: Plot of the CVs in the plane (c, σ), the line labelled (P) is the pitchfork line, the line labelled (H) is the Hopf curve. The two bounds of proposition 4.5.9 are also shown. Parameters are: $L_0 = \mathrm{Id}$, $J(x) = s_1(-1+1.5\cos(2x))\frac{2}{\pi}, \beta = \frac{1}{4}$, $s_1 = \frac{1}{4}$. The labels 1, 2, 3, indicate approximate positions in the parameter space (c, σ) at which the trajectories shown in Figure 6.9 are computed. The grey region is the stability region of $V^f = 0$ given by the bounds 1 and 2.

behaviours as one can see in the right-hand part of figure 6.9.

These numerical simulations reveal that the Lyapunov function derived in [Enculescu 2007] is likely to be incorrect. Indeed, if such a function existed, as its value decreases along trajectories, it must be constant on any periodic orbit which is not possible. However the third plot in figure 6.9 strongly suggests that we have found an oscillatory trajectory produced by a Hopf bifurcation (this is proved in section 6.1.2): this oscillatory trajectory converges to a periodic orbit which contradicts the existence of a Lyapunov functional such as the one proposed in [Enculescu 2007] .

Let us comment on the tightness of the delay-dependent bound: as shown in proposition 4.5.7, this bound involves the maximum delay value τ_m and the norm $\left\| \frac{\tilde{\mathbf{J}}}{\boldsymbol{\tau}^\beta} \right\|_{\mathbf{L}^2(\Omega^2, \mathbb{R}^{p\times p})}$, hence the specific shape of the delay function, *i.e.* $\tau(\mathbf{r}, \bar{\mathbf{r}}) = c\|\mathbf{r} - \bar{\mathbf{r}}\|_2$, is not completely taken into account in the bound. We can imagine many different delay functions with the same values for τ_m and $\left\| \frac{\tilde{\mathbf{J}}}{\boldsymbol{\tau}^\beta} \right\|_{\mathbf{L}^2(\Omega^2, \mathbb{R}^{p\times p})}$ that will cause possibly large changes to the dynamical portrait. For example, in the previous example, the singularity $\sigma = \sigma_0$, corresponding to the fact that $0 \in \Sigma_p(\mathbf{A})$, is independent of the details of the shape of the delay function: however for specific delay functions, the multiplicity of this eigenvalue could change as in the Bogdanov-Takens bifurcation which involves changes in the dynamical portrait compared to the Pitchfork bifurcation. Similarly, an additional purely imaginary eigenvalue could emerge (as for $c \approx 2.5$ in the numerical example) leading to a

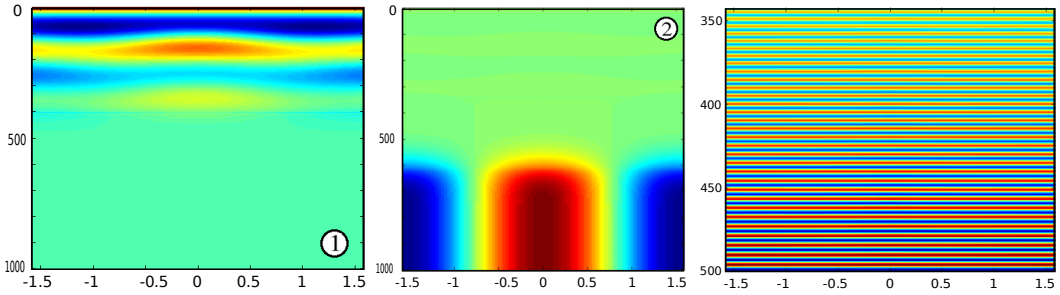

Figure 6.9: Plot of the solution of (5.12) for different parameters corresponding to the points shown as 1, 2 and 3 in the right-hand part of figure 6.8 for a random (in space) and constant (in time) initial condition, see text. The horizontal axis corresponds to space, the range is $\left(-\frac{\pi}{2}, \frac{\pi}{2}\right)$. The vertical axis represents time.

Fold-Hopf bifurcation. These instabilities depend on the expression of the delay function (and the connectivity function as well). These reasons "explain" why the bound in proposition 4.5.7 is not very tight.

6.3 Conclusion

In this chapter, we have applied the tools developed in part III to a simple 1D neural fields model with homogeneous connectivity and periodic boundary conditions. This choice of application is motivated by the fact that the eigenvectors of the operator $\mathbf{A}$ are analytically known. Hence, we can compute the normal forms analytically and look at the dependency of the dynamics on the different parameters. We will do the same for 2D a neural fields model in chapter 11 although we will not study in detail the normal forms.

Unsurprisingly, the bounds computed in section 6.2 are very conservative but compared to the whole bifurcation study, they are much faster to compute. They should be used in a first attempt to understand a delayed neural fields model, in order to evaluate the importance of the delays in the model.

Despite the simplicity of the models we chose to study as an application of the normal form theory, we found interesting bifurcation diagrams, especially for the inverted Mexican hat connectivity. The bifurcations we have studied, in particular the codim 2 Fold-Hopf and Hopf-Hopf bifurcations, did not produce sophisticated dynamics. This is to be expected because we have only considered mode interactions between the trivial $0-$mode and another mode. Much more sophisticated dynamics is expected for a mode interaction between two non constant modes. In particular, it could be interesting to study more thoroughly the Hopf-Hopf bifurcation point, the codim 3 bifurcation Hopf-Hopf-Hopf and see if this codim 3 bifurcation appears generically for more general connectivities.

As a conclusion, this chapter calls for several extensions. For example, we have

started to study the "simple" case of n : 0-Hopf/Hopf mode interaction, *i.e.* when the Hopf mode is zero. A more detailed analysis of this bifurcation point is needed. The more general n : p-Hopf/Hopf mode interaction occurs in the bifurcation diagram (see figure 6.4) of the inverted Mexican-hat connectivity, it has not been considered in this chapter. Note that the complete study of these Hopf/Hopf mode interactions would require an entire chapter. This is the subject of future work.

Chapter 7

The Deco-Roland model of long-range apparent motion perception

Contents

This chapter is devoted to the study of a recent model [Deco 2010] by Deco *et al.* of the long-range apparent motion percept. We are able to describe with closed form formulas, the impact of all the parameters in the model whereas the authors in [Deco 2010] had to rely on numerical simulations. In order to achieve this, we use the tools developed in chapter 5. We also show how to incorporate intracortical propagation delays and give the relationship between the apparent speed and the contrast of the stimulus. This model is a good example of the application of all the tools developed in this Thesis.

7.1 Introduction

Apparent motion (AM) is the illusory perception of real motion created when two spatially distinct stationary visual objects are presented in alternating sequence. It has been used for a long time by the movies maker companies and this perception has been known for more than a century (see [Exner 1875, Wertheimer 1912, Adelson 1985]). There are two kind of AMs:

- the short-range apparent motion where the distance between the two consecutive objects is less than two degrees of visual angle,
- the long-range apparent motion where the distance between the two consecutive objects is larger than two degrees of visual angle (see [Kolers 1964, Newsome 1986, Seriès 2002b, Fregnac 2010]).

The long-range AM is present even when stimulus locations are separated by distances that are many times the size of receptive fields of direction selective neurons in V1. Also, V1 is activated in locations that are not directly stimulated by the individual stimuli but correspond to locations on the perceived illusory motion path (see for example [Muckli 2002]). Therefore, communications between V1 and high order visual areas, like MT, are expected for the perception of long-range AM (see [Newsome 1986, Merchant 2004, Zhuo 2003, Hupé 2001]).

In [Deco 2010], based on experiments made in the *anaesthetized ferret* (see [Roland 2006, Ahmed 2008]), the authors describe a possible mechanism for long-range AM. An elicited activity in area 17/18, similar to the V1 area in macaques, is sent through divergent feedforward connections[1] to the high order area 19/21, similar to the MT area in macaques, where the cortical activity spreads in space. Upon application of the second stimulus, a short-range AM activity is induced in the area 19/21 which is sent to 17/18 by the divergent feedback connections. Note that the loop 17/18→19/21→17/18 is fast and the activity in the area 17/18 can travel faster though this loop than by intra-cortical connections alone. The model in [Deco 2010] is simple in that it does not have a lot of parameters. The main idea is to design a network slow enough to sustain a cortical activity during the inter-stimulus interval such that this long lasting activity interacts with the afferent input corresponding to the second stimulus. As we will see in section 7.3, this is achieved by bringing the network close to a static bifurcation.

We start by recalling the model of [Deco 2010] in section 7.2. Then we explain in section 7.3 how to tune correctly the parameters to make the model work. This study is made analytically, unlike [Deco 2010]. In section 7.4, we show the effect of the different parameters on the properties of the long-range AM. In particular, we show how the inter-cortical communication delays impact the AM. Then, in section 7.5, we extend the model by incorporating intra-cortical propagation delays and we study analytically their effects. In section 7.6, we show that the delays cannot produce time oscillations: this is necessary to check in view of the results of chapter 4. Finally, in section 7.7, we give the relationship between the apparent speed and the contrast of the two stimulations.

7.2 Neural field model

We study the dynamical interactions of the visual area 17/18 and 19/21 borders. We suppose that each cortical area is spread over one-dimensional cortices $\Omega_{17/18}, \Omega_{19/21}$, hence we assume that $\Omega_{17/18}$, $\Omega_{19/21} = [-\pi, \pi]$. We also assume, to make the computations easier, that there are periodic conditions in each cortical part $\Omega_{17/18}, \Omega_{19/21}$. We work in cortical coordinates, hence a distance of 1 in $\Omega_{17/18}$ corresponds to a distance of 1 in $\Omega_{19/21}$. The use of neural field equations is motivated by their restricted number of parameters. We index by 1 the quantities related to $\Omega_{17/18}$, by 2 the quantities related to $\Omega_{19/21}$ and write the following ac-

[1] which are retinotopically organized

tivity based model. In the case considered here, the external input is time constant and the two populations share the same intrinsic time constant τ. Hence, the activity and voltage based models are equivalent. We chose the activity based model to stick with [Deco 2010] even if this choice is arbitrary (but see at the end of the conclusion).

$$\begin{aligned}
\tau\tfrac{dA^{(1)}(x,t)}{dt} + A^{(1)}(x,t) = S\Big[& \int_{-\pi}^{\pi} J^{(1)}(x-y)A^{(1)}(y,t)dy \\
& + f^b \int_{-\pi}^{\pi} W^{(2)}(x-y)A^{(2)}(y,t-\tau_2)dy + I^{ext}(x)\Big] \\
\tau\tfrac{dA^{(2)}(x,t)}{dt} + A^{(2)}(x,t) = S\Big[& \int_{-\pi}^{\pi} J^{(2)}(x-y)A^{(2)}(y,t)dy \\
& + \int_{-\pi}^{\pi} W^{(1)}(x-y)A^{(1)}(y,t-\tau_1)dy\Big].
\end{aligned} \tag{7.1}$$

The intra cortical connections $J^{(1)}, J^{(2)}$ in each area are locally excitatory and laterally inhibitory. Even if this in not in agreement with the biology, it is an assumption that avoid the use of excitatory/inhibitory populations in each area thereby doubling the number of equations and of parameters (see section 2.3). We also assume, as in [Deco 2010], that the spread of the intra-cortical connections in 19/21 is two times the value of the spread of the intra-cortical connections in 17/18. The feedforward connections $W^{(1)}$ from 17/18 to 19/21 are excitatory, the same is assumed for the feedback connections $f^b W^{(2)}$ from 19/21 to 17/18. In order to further simplify the model, we assume that $W^{(1)} = W^{(2)}$:

$$\begin{cases}
J^{(1)}(x) = \frac{2\pi}{\lambda_1}\left(-J_0 + J_2 e^{-\frac{|x|}{\lambda_1}}\right), \\
J^{(2)}(x) = \frac{2\pi}{\lambda_2}\left(-J_0 + J_2 e^{-\frac{|x|}{\lambda_2}}\right), \ \lambda_2 = 2\lambda_1 \\
W^{(1)} = W^{(2)} = \frac{2\pi}{\alpha} e^{-\frac{|x|}{\alpha}}
\end{cases} \tag{7.2}$$

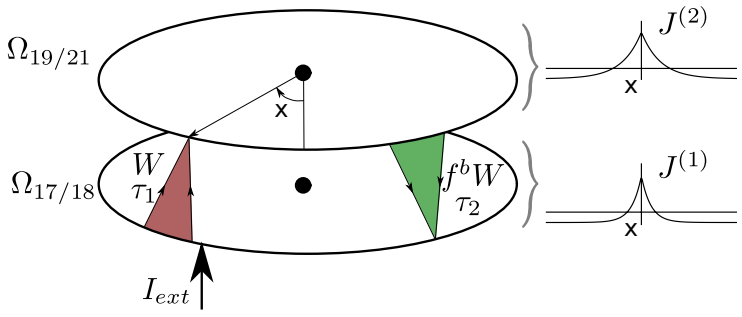

Figure 7.1: The network architecture. The two interacting fields are indicated by the ellipses. The feedforward connections are plotted in red, the feedback connections are in green. The intra-cortical connectivities $J^{(1)}, J^{(2)}$ are also shown in the right part of the figure.

We take, as in [Deco 2010], a delay of $\tau_1 = 4ms$ for the feedforward connections and a delay of $\tau_2 = 8ms$ for the feedback connections. The time constant of each population is assumed to be $\tau = 10ms$. Finally, only the area 17/19 border receives an external input from the LGN. Hence, the area 19/21 only sees the stimulation through the area 17/18. The external input is

$$I_{ext}(x) = \varepsilon \left(1 - \beta + \beta e^{-\frac{(x-x_0)^2}{\mu}} \right) \tag{7.3}$$

where ε is the contrast, β is the anisotropy, μ is the spread of the sensorial input and x_0 is the position at which the external stimulus is presented.

The transfer function is $S(x) = \frac{1}{1+e^{-\sigma x+h}} - \frac{1}{1+e^h}$ where σ is the nonlinear gain and h is the threshold. Compared to the choice of a semi-linear function as in [Deco 2010], our choice has the advantage of the regularity which allows the use of normal form theory. In our case, there is the disadvantage that $S(x) < 0$ if $x < 0$ but note that it does not reduce the generality of our study as we are looking for a mechanism and not for precise values of the membrane potentials $A^{(1)}, A^{(2)}$. Hence, the network has the *trivial* stationary solution $(A^{(1)}, A^{(2)}) = (0, 0)$.

Remark 29. The numerical applications use the following set of parameters $\lambda_2 = 2\lambda_1 = 0.6,\ \alpha = 0.4,\ \tau_1 = 4ms, \tau_2 = 8ms,\ \tau = 10ms, J_0 = 0.2,\ J_2 = 0.9, f^b = 0.16,\ \theta = 0,\ \lambda = 0.192.$

7.3 Parameter tuning

Let us recall the experimental setup. A stimulus is presented at position x_1 which elicits a stationary cortical response. Then, the stimulation is switched off for an inter-stimulus interval Δt (of the order of several $100ms$) after which a stimulus is presented at position x_2. The apparent motion comes from the interaction of the cortical activity at time $t = \Delta t$ with the new incoming stimulation at position x_2 (see also [Jancke 2004, Bringuier 1999] for a similar argument in the cat and the macaque). Hence, during the interval Δt, the cortical activity must not return to the trivial resting state. This suggests that the network has slow dynamics, indeed the inter-stimulus interval Δt is much larger than the intrinsic decay time τ of the populations $\Delta t >> \tau$. As a consequence, the trivial state must be slow to reach and thus, the Jacobian of (7.1) at the trivial state should be close to singular, *i.e.* have a zero eigenvalue. We conclude that the network must be working at the edge of a static bifurcation.

We look for the (bifurcation) curves[2] in the plane (J_2, f^b) where the trivial stationary state produces a static bifurcation. Finding these curves with the communication delays τ_1, τ_2 is not an easy task[3]. Hence, we start by assuming that these delays are null $\tau_1 = \tau_2 = 0$. We will see in the next section 7.4 the impact,

[2] there are many of them.
[3] at least analytically.

on the network behaviour, of the introduction of communication delays. The computation of the bifurcation curves is done in appendix D. The result is that these curves are parabolas noted P_n. They are plotted in figure 7.2.

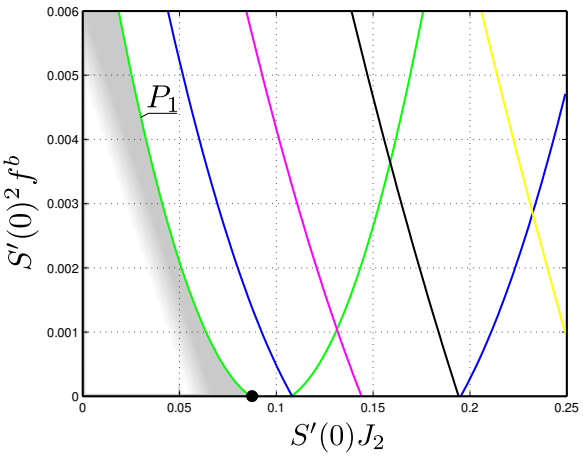

Figure 7.2: plot of the bifurcation curves P_n given in appendix D. The grey region is the working range of the model where it produces AM . The intersection between the first parabola P_1 and the J_2-axis is marked with a black dot. $S'(0) > 0$ is the derivative of the nonlinear function S at 0.

For parameters (J_2, f^b) that lie above one of the parabolas P_n, the network produces non-trivial spontaneous activity (*i.e.* when the contrast ε of the external input equal to zero $\varepsilon = 0$). This is not the working range of the model because no spontaneous activity is seen in the experimental data (see [Deco 2010, Ahmed 2008]). Hence, the parameters must be adjusted such that (J_2, f^b) lies just under the first parabola which is written P_1 in figure 7.2. The grey region in figure 7.2 is the working range of the network. Notice that there is a small region near the black dot where the AM could be produced by the network without feedback $f^b = 0$ from the area 19/21.

7.4 Effect of communication delays and feedback

Let us start with the discussion about the feedback. From the expression of the eigenvalues given in appendix D, it can be shown that a decrease of the feedback to zero increases the speed of the dynamics (except at the parameter point marked by a black dot in figure 7.2), the model cannot produce the AM anymore because it is too fast.

We have designed the model to work near a Pitchfork bifurcation[4] because the network is slow in this case. If we add small communication delays, we have shown

[4] in effect, a O(2)-Pitchfork bifurcation

in 5.2.2.1 that this amounts to rescale time near a Pitchfork bifurcation:

$$t \to \frac{t}{1 + S'(0)\hat{W}_1(f^b\tau_2 + \tau_1)}, \tag{7.4}$$

where $S'(0) > 0$ is the derivative of the nonlinear function S at 0 and $\hat{W}_1 \approx \frac{4\pi}{1+\alpha^2} \approx 4\pi$ (see appendix D). This time rescaling slows down the dynamics when adding the delays. Indeed, the convergence to the zero stationary states is proportional to $e^{-\frac{\beta_{1,+}t}{1+S'(0)\hat{W}_1(f^b\tau_2+\tau_1)}}$, for some positive coefficient[5] $\beta_{1,+} > 0$, instead of $e^{-\beta_{1,+}t}$: if we remove the delays, the dynamics are too fast to produce AM. Also, note that we can compensate small delays τ_i by strong feedback f^b in the previous formula (7.4). The simple formula (7.4) has the advantage, over numerical computation, to give the precise relationship between the dynamics and all the parameters. In particular, the precise value of f^b, τ_1, τ_2 is irrelevant, what matters is the quantity

$$f^b\tau_2 + \tau_1.$$

7.5 Effect of the intra-cortical propagation delays

If we consider intra-cortical propagation delays in each area, we can also use the result in section 7.4 to find the time rescaling near the Pitchfork bifurcation. The propagation delays are modelled by changing in (7.1) $\int_{-\pi}^{\pi} J^{(1)}(x-y)A^{(1)}(y,t)dy$ to $\int_{-\pi}^{\pi} J^{(1)}(x-y)A^{(1)}(y,t-\frac{1}{v_{propa}}|x-y|)dy$ and $\int_{-\pi}^{\pi} J^{(2)}(x-y)A^{(2)}(y,t)dy$ to $\int_{-\pi}^{\pi} J^{(2)}(x-y)A^{(2)}(y,t-\frac{1}{v_{propa}}|x-y|)dy$. Hence, we assume that the propagation speed v_{propa} is the same in each area. Then, we find that the time rescaling is now given by:

$$t \to \frac{t}{1 + S'(0)\hat{W}_1(f^b\tau_2 + \tau_1) + S'(0)\frac{D(\lambda_1)+D(\lambda_2)}{v_{propa}}}, \tag{7.5}$$

where $D(\lambda)$ is a function of λ which is given in appendix D. It is positive for $\lambda_1, \lambda_2 < 1$, hence the intra-cortical propagation delays favour production of the AM.

7.6 Study of oscillatory patterns

It is known that delays can produce time-oscillations[6] (see for example Part III). It is an unsatisfactory behaviour in the present model because it is not seen in the experiments. Hence, we investigate whether it is possible to produce time-oscillations by increasing the constant delays τ_i or by changing the intra-cortical propagation speed v_{propa}. There are basically two mechanisms to produce these

[5] given in appendix D. It is the largest eigenvalue of the linearised equations around $V = 0$.
[6] Not considered in [Deco 2010].

oscillations with delays near bifurcations: by the Bogdanov-Takens bifurcation or by the Hopf bifurcation.

From lemma 4.6.4, we see that the model cannot produce the Bogdanov-Takens bifurcation because $S'(0)\hat{W}_1(f^b\tau_2+\tau_1)+S'(0)\frac{D(\lambda_1)+D(\lambda_2)}{v_{propa}}>0$.

The case of the Hopf bifurcation is investigated in appendix D. The result is that a Hopf bifurcation is possible strictly above the parabola P_1 in the parameter plane (J_2, f^b). Hence, under the working assumption of the model, no time-oscillations patterns can be produced with the inter-cortical delays (τ_1, τ_2). We have not computed the Hopf bifurcation curves produced by the intra-cortical propagation delays in order to keep the present study short. It should be noted that the analytical formula in proposition 4.4.5 only applies when the two constant delays τ_i are zeros: $\tau_1=\tau_2=0$.

7.7 Study of the apparent speed/contrast relationship

Close to the bifurcation point where the model is working, we can predict cortical responses to stimuli. It is shown in appendix D that if the cortical response is modeled by $A^{(1)}(x,t)=A(x-\omega_0 t)$ for some function A peaked around 0, then we can estimate the speed ω_0. This is done in the case where the contrast ε is small. The result is

$$\omega_0 \propto \frac{\varepsilon\beta}{(1+S'(0)\hat{W}_1(f^b\tau_2+\tau_1))}$$

Hence, an increase of the contrast ε gives an increase of the apparent motion velocity. The same is true for a decrease of the delays τ_i. Note that the above formula is valid for $\varepsilon\beta << 1$.

7.8 Conclusion

In this chapter, we have studied analytically the model of Deco *et al.* of long-range AM. There are two main assumptions in this model:

- two areas 17/18 and 19/21 with divergent inter-connections are necessary for the perception of the long-range apparent motion,
- the network works near a static bifurcation.

The first assumption tells what is necessary for the model to reproduce the AM while the second hypothesis tells where (in the parameter domain) the model can produce the AM. The second assumption is necessary for the network to sustain a localized activity during the inter-stimulus interval which can interact with the upcoming afferent input from the second stimulus. The second assumption has very strong implications but we think that its major consequence lies in the normal form theory (see part III). Any system of ordinary differential equations, or model, with or without delays, which works close to a static bifurcation such as the one we have

studied here, can be simplified into two polynomials equations of degree three (see appendix D). For example, we could consider two excitatory/inhibitory populations in each cortical area in order to use more realistic connectivities than the one of the model, it would still produce the same system of two polynomials equations of degree three. This is apparent for example in (7.4), where we can compensate a decrease of a parameter by the increase of another one. In a way, the model is still over-parametrized.

This model can certainly be further generalized in at least three directions. The first is to apply the model to the macaque by using the specific (to macaques) parameters that we can infer from [Albright 1987].

The second is to incorporate the contrast saturation mechanism (see [Stetter 2000, Stetter 2002]). When the contrast of the stimulus is increased, the response of the network saturates. It is a property of the population and not of the neuron[7]. Therefore, it is not explained by the fact that the nonlinear transfer function S is bounded. Rather, it should come from the different properties of excitatory/inhibitory populations. At small contrasts, only the excitatory neurons are recruited whereas at high contrasts, the inhibitory neurons are recruited, which damps the overall network response. The primary visual cortex is known to exhibit contrast saturation. Hence, it would be interesting to make the Deco model account for contrast saturation.

Finally, the third extension is to change the form of the feedforward/feedback expressions. Indeed, it is implied by [Hupé 1998], that the feedback connections are only modulatory and that they modulate the firing rate of the targeted neurons, *i.e.* the response above threshold of the neurons. Hence, we would have to consider a feedback of the form $\int W^{(2)}(x-y)(C + A^{(2)}(y, t-\tau_1))A^{(1)}(y,t)dy$. Another choice of interaction amounts to modulate the afferent input from the LGN as in $I_{ext}(1 + CA^{(2)}(y, t-\tau_1))$ (see [Bayerl 2004, Sillito 2006]). In any case, these simple models are meant to give a hint of the working range and to express basic principles such as working close to a static bifurcation. We strongly believe that the tools developed in the two previous parts can help to further simplify their study.

[7] The characteristics of the neurons of a given population appears in the sigmoidal transfer function.

Part IV

Application to models study

Chapter 8

General Introduction

We arrive at the last part of the Thesis, the one concerned with the models. We wish to apply the tools developed in the two previous parts to rate models with an emphasis on biology. As a consequence, the style of writing changes: the mathematics are less detailed, the technical parts are put in appendix or referenced from the other chapters. The goal of this part is to use the mathematics we have developed to make predictions. In effect, we want to explore the biological implications of some parameter sets for the neural fields model. In particular, we will study three neural fields models that operate near a Pitchfork bifurcation. Note that we have already analysed this idea in section 3.5 and in chapter 7.

8.1 The mechanism of Ben-Yishai et al.

We focus essentially on the study of orientation selectivity, especially the property that the tuning width of V1 simple cells in cats is contrast invariant. We have already discussed in chapter 1 the two classes of models that have been developed to account for this property. Here, we analyse the class of recurrent models, *i.e.* the one that assumes that the LGN input provides a weakly tuned signal to the cortex. This signal is sharpened by recurrent intra-cortical connections. To be a bit more specific, let us consider a neural field model over a two-dimensional cortex (see chapter 2):

$$\tau \frac{d}{dt} V(\mathbf{x},t) = -V(\mathbf{x},t) + \int_\Omega J(\mathbf{x},\mathbf{y}) S\left[\sigma V(\mathbf{y},t)\right] d\mathbf{y} + \varepsilon I_{ext}(\mathbf{x},t) \tag{8.1}$$

where $V(\mathbf{x},t)$ is the membrane potential a location $\mathbf{x}$ at time t, τ is the intrinsic time constant of the neuronal population, $J(\mathbf{x},\mathbf{y})$ are the intra-cortical connections, S is the firing rate transfer function, σ is the nonlinear gain, $\varepsilon I_{ext}(\mathbf{x})$ is the LGN input at location $\mathbf{x}$ and ε is the contrast of the stimulus[1]. To agree with biology, the connectivity is chosen *homogeneous* in a first approximation, *i.e.* $J(\mathbf{x},\mathbf{y}) = J(\mathbf{x}-\mathbf{y})$. Note that this implies that we neglect the long-range connections[2]. As a consequence, for a space constant input[3], there exists a space-constant stationary membrane potential $V(\mathbf{x}) \equiv v_0$ for any set of parameters. Recall that, by definition, a stationary solution satisfies (see chapter 3 for more properties):

$$0 = -V(\mathbf{x}) + \int_\Omega J(\mathbf{x},\mathbf{y}) S\left[\sigma V(\mathbf{y})\right] d\mathbf{y} + \varepsilon I_{ext}(\mathbf{x}) \tag{8.2}$$

[1] To be correct, the ε constant is related in a monotone way to the stimulus contrast, but we assume that they are the same to simplify the study.

[2] but see chapter 11.

[3] in particular, it is true when there is no input

where the LGN input is stationary. The constant solution v_0 is usually called *untuned* because it has no particular spatial structure. From now on, we assume that there is only one population and that the connectivity J is effective (see section 2.3 for an explanation).

Let us assume that $I_{ext}^{\theta}(\mathbf{x})$ represents a grating oriented at θ, then the cortical response $V^{\theta,\varepsilon}(\mathbf{x})$ to this stimulus is a stable stationary solution of (8.2). It is not evident, and in fact it is not true in general, that there exists a unique stationary cortical response to this stimulus. Hence, at each location $\mathbf{x}$, we have a firing rate tuning curve (see definition 1.3.1) $TC_{\mathbf{x}}$ defined as

$$TC_{\mathbf{x}}(\theta,\varepsilon) = S\left[\sigma V^{\theta,\varepsilon}(\mathbf{x})\right].$$

We know from biology that, as a function of the orientation θ, the tuning curve is *unimodal*, *i.e.* has a unique maximum for a particular orientation $\theta(\mathbf{x})$ called the *preferred orientation*. Also, the tuning curve width at half-height is independent of the contrast ε. How can this be possible? At this stage, it is very important to note that the experimental tuning curves at each location $\mathbf{x}$ can be well approximated by $S(A + B\cos(\theta - \theta_0))$, θ_0 being the preferred angle of the simple cell, for some well chosen coefficients A, B. In the 90s, Ben-Yishai *et al.* discovered a mechanism (see [Ben-Yishai 1995]) that we shall describe. The main idea is to set the parameters such that the model works close to a static bifurcation point as we explain below. Imagine that for no stimulus, $\varepsilon = 0$, **the network can spontaneously produce a tuned stationary activity $V^f(\mathbf{x})$ that is very close to the experimental tuning curve**. The parameters have to be adjusted for this to happen, otherwise the spontaneous activity is the untuned one v_0. Moreover, if the nonlinear gain is small, the untuned activity is the only stationary solution. We decompose the tuned spontaneous activity into a constant activity v_0 and a tuned activity $v_1(\mathbf{x})$ of zero spatial mean:

$$V^f(\mathbf{x}) = v_0 + v_1(\mathbf{x}),$$

If we require that $S\left[\sigma(v_0 + v_1(\mathbf{x}))\right]$ looks like an experimental tuning curve, we are faced with the problem that there is no analogue of the stimulus orientation θ in the theoretical tuning curve $S\left[\sigma(v_0 + v_1(\mathbf{x}))\right]$. The network must therefore be able to spontaneously produce a continuum of tuned activities that are labelled for example by an angle θ, namely $V^{f,\theta}(\mathbf{x})$. As the orientation is an angle, it means that the set of spontaneous tuned activities must be homeomorphic to a circle. Now, we can go back to the tuning width invariance. What happens if we stimulate the network? In the recurrent models, the LGN input is assumed to be weakly tuned, *i.e.* we can write

$$I_{ext}^{\theta_{aff}}(\mathbf{x}) = I_0 + I_1^{\theta_{aff}}(\mathbf{x})$$

with a small tuned component $I_1^{\theta_{aff}}$ and where θ_{aff} is the stimulus orientation. What will be the network response to this stimulus? At small contrasts ε, according to (8.2), the cortical response will be a perturbation of the spontaneous activity, hence the dependency of the tuning properties of the response on the contrast will

be small. Also, the cortex will select among its spontaneous responses, the one that match the best the LGN input, *i.e.* it will try to select a θ that is consistent with θ_{aff}.

This mechanism raises four issues, two being mathematical, and two biological. The two mathematical questions are 1) can we adjust the parameters in order for (8.2) to produce tuned spontaneous solutions? and 2) can we make the number of solutions of (8.2) infinite? From a biological viewpoint, it seems unsatisfactory for the network to feature a high cortical activity when no inputs is present, it is a waste of energy. The first biological issue is how can we modify the above mechanism to remove the spontaneous activity? This will be done in chapter 9 where we show a solution that naturally introduce a *perception threshold*. This perception threshold is shared by the three models studied in this part of the Thesis although it will be only studied in the next chapter 9. The second biological issue regards the dependency of the tuning width on high contrasts. Again this will be only thoroughly studied in the next chapter, it is linked to the perception threshold.

It turns out that the second mathematical issue is solved as a consequence of the connectivity being invariant by a continuous group of symmetries like the translations or the rotations. Indeed, in this case, any translation (for example) of a spontaneous tuned activity is also a spontaneous tuned activity. Let us show how to solve the first mathematical issue using bifurcation theory. We consider the untuned activity v_0 solution of (8.2) as a function of the nonlinear gain σ (for example). As we vary the nonlinear gain, tuned solutions may exist for a particular value of the nonlinear gain σ_0 called a (static) *bifurcation point* (see definition A.0.1). That is, we can find a curve of solutions parametrized by σ $\sigma \to V^f_\sigma(\mathbf{x})$ which intersects the curve of untuned solutions, such that $V^f_{\sigma_0}(\mathbf{x}) = v_0(\sigma_0)$, the tuned solution is said to *bifurcate* at σ_0. How can this be detected? This happens when the linearised equation (8.3) of (8.1) around the untuned solution v_0 has non-zero time constant solutions.

$$\tau \frac{d}{dt} U(\mathbf{x},t) = -U(\mathbf{x},t) + \sigma_0 S'\left[\sigma_0 v(\sigma_0)\right] \int_\Omega J(\mathbf{x},\mathbf{y}) U(\mathbf{y},t) d\mathbf{y} \tag{8.3}$$

where S' is the differential of S. A time constant $U(\mathbf{x})$ solution of (8.3) satisfies

$$0 = -U(\mathbf{x}) + \sigma_0 S'\left[\sigma_0 v(\sigma_0)\right] \int_\Omega J(\mathbf{x},\mathbf{y}) U(\mathbf{y}) d\mathbf{y} \tag{8.4}$$

written

$$\frac{1}{\sigma_0 S'\left[\sigma_0 v(\sigma_0)\right]} U(\mathbf{x}) = \int_\Omega J(\mathbf{x},\mathbf{y}) U(\mathbf{y}) d\mathbf{y} \tag{8.5}$$

which is called an eigenvalue problem. Indeed, if a non-zero (also called non-trivial) solution exist, it is an eigenvector of the integral operation (think of the right-hand side as a matrix-vector product between J and U). The eigenvalues λ_n, $n \in \mathbb{N}$, and eigenvector $U_n(\mathbf{x})$ of J can be computed in advance, they satisfy

$$\lambda_n U_n(\mathbf{x}) = \int_\Omega J(\mathbf{x},\mathbf{y}) U_n(\mathbf{y},t) d\mathbf{y}. \tag{8.6}$$

The U_n are the only possible solutions of (8.3), hence the bifurcation point σ_0 must solve:

$$\frac{1}{\sigma_0 S'\left[\sigma_0 v(\sigma_0)\right]} = \lambda_n \tag{8.7}$$

for a particular value of the index n. Note that this equation has usually a finite number of solutions. We are now very close to solve the first mathematical issue. Indeed, let us say that we have detected a bifurcation point σ_0 corresponding to a time constant solution U_{n_0}. Then, for a nonlinear gain close to the bifurcation point σ_0, $\sigma \approx \sigma_0$, the spontaneous stationary solutions of (8.1) for $\varepsilon = 0$ are given[4] by

$$V^f(\mathbf{x}) = \begin{cases} v_0(\sigma_0) & \text{if } \sigma \approx \sigma_0 \\ v_0(\sigma_0) + f(\sigma - \sigma_0) U_{n_0}(\mathbf{x}) & \text{if } \sigma \geq \sigma_0 \end{cases} \tag{8.8}$$

for a particular function $f(\sigma - \sigma_0)$ which can be computed. Hence, the tuned component of the cortical activity is given by $f(\sigma - \sigma_0)U_{n_0}(\mathbf{x})$. We have identified the spontaneous activity if the nonlinear gain σ is close to σ_0: it is tuned only if $\sigma > \sigma_0$.

What happens if we present a stimulus? The LGN input will affect the spontaneous activity only if its tuned component $I_1(\mathbf{x})$ looks like[5] the tuned component U_{n_0} of the spontaneous activity.

To summarize, we require the spontaneous tuned activity $S\left[\sigma_0(v_0(\sigma_0) + f(\sigma - \sigma_0)U_{n_0}(\mathbf{x}))\right]$ to look like the experimental tuning curves. It implies to find the corresponding eigenvector $U_{n_0}(\mathbf{x})$ by an educated choice. This, in turn, sets the bifurcation point σ_0 according to (8.7) and the nonlinear gain $\sigma \approx \sigma_0$. Furthermore, the LGN input is assumed to be:

$$I_{ext}(\mathbf{x}) = I_0 + I_1 U_{n_0}(\mathbf{x}) + I_2(\mathbf{x}) \tag{8.9}$$

with I_1, I_2 small without further assumptions. Hence, the requirement of matching experimental tuning curves through a static bifurcation scenario basically sets the form of the external input and the connectivity (see chapter 10 for another derivation). As seen above, the parameters of the tuning curves will have a weak dependency on the external input contrast.

In the next chapters, we study in detail this mechanism and show that it features emergent behaviours that were not explicitly incorporated in the design of the model(s).

8.2 The three models

The Ring Model of orientation tuning is a bit different from the model we have considered in (8.1) in that it is not a model over the 2D cortex but over the orientation

[4] Note that other possibilities are possible, *i.e.* when the bifurcated solution exist for $\sigma < \sigma_0$ or also for $\sigma \approx \sigma_0$.

[5] To be more precise, they need to have a non-zero scalar product

domain. More precisely, it assumes that the activity is a function of the orientation θ and not a function of the cortical position $\mathbf{x}$ as in (8.1). Hence, the connectivity is defined between two orientations θ, $\bar{\theta}$. Almost no biological evidence supports the fact that the connectivity is only orientation dependent[6]. It should be understood as an *effective* connectivity as in the case where we suppose that the connectivity is locally excitatory and laterally inhibitory in contradiction with biological data (see section 2.3 for a derivation of the effective connectivity in the cortical space). The Ring Model is a model of hypercolumn (see figure 8.1) which assumes that all the neurons sharing the same preferred orientation, hence located on a polar ray (black line), have a similar cortical activity $A(\theta, t)$.

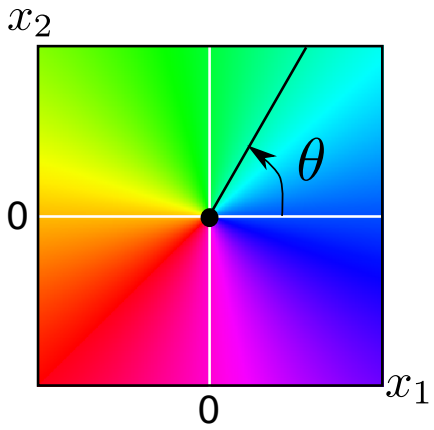

Figure 8.1: Representation of a hypercolumn centred on a pinwheel (black dot). The colour gives the preferred orientation of the cells located on the cortex at the point $\mathbf{x}$ of coordinates (x_1, x_2) (phase arbitrary): it only depends on the polar angle θ.

Let us show how we can derive a feature dependent, effective, connectivity. We start with one population $V(\mathbf{x}, t)$ spread over the hypercolumn with an effective connectivity $J(\|\mathbf{x} - \mathbf{y}\|_2)$ as explained in section 2.3. The spontaneous stationary activity solves:

$$\frac{d}{dt}V(\mathbf{x}, t) + V(\mathbf{x}, t) = \int_\Omega J(\|\mathbf{x} - \mathbf{y}\|_2) S\left[\sigma V(\mathbf{y}, t)\right] d\mathbf{y} \tag{8.10}$$

Next, we introduce the following quantities which are similar to weighted means of the membrane potential along polar rays:

$$\overline{V}(\theta, t) \equiv \int_0^1 r V(r, \theta, t) dr \tag{8.11}$$

where $\mathbf{x} = (r\cos\theta, r\sin\theta) \equiv (r, \theta)$. As we are working close to the pinwheel located

[6] More generally, we speak of a feature dependent connectivity when it depends on a feature like orientation, spatial phases, texture... This type of connectivity is difficult to support from a biological viewpoint. They are usually assumed to implement Gestalt principles.

at $\mathbf{x} = 0$, we consider the Taylor expansion of the connectivity[7]

$$J(\|\mathbf{x}-\mathbf{y}\|_2) = J_0 + J_1 \|\mathbf{x}-\mathbf{y}\|_2^2 + h.o.t. = J_0 + J_1 \left(r^2 + \bar{r}^2 - 2r\bar{r}\cos(\theta - \bar{\theta})\right) + h.o.t. \tag{8.12}$$

where we have used polar coordinates and $\mathbf{y} \equiv (\bar{r}, \bar{\theta})$. Then, we find:

$$\frac{d}{dt}V(\mathbf{x}) + V(\mathbf{x}) = (J_0 + r^2 J_1) \int_\Omega \bar{r} S\left[\sigma V(\bar{r}, \bar{\theta}, t)\right] d\bar{r}d\bar{\theta} + J_1 \int_\Omega \bar{r}^3 S\left[\sigma V(\bar{r}, \bar{\theta}, t)\right] d\bar{r}d\bar{\theta} - 2rJ_1 \int_\Omega \bar{r}^2 \cos(\theta - \bar{\theta}) S\left[\sigma V(\bar{r}, \bar{\theta})\right] d\bar{r}d\bar{\theta}.$$

As $r \to V(r, \theta)$ is assumed to be almost constant, we approximate $2\int_0^1 \bar{r} S\left[\sigma V(\bar{r}, \bar{\theta}, t)\right] d\bar{r} \approx 4\int_0^1 \bar{r}^3 S\left[\sigma V(\bar{r}, \bar{\theta}, t)\right] d\bar{r} \approx S(2\sigma\overline{V}(\bar{\theta}, t))$ By integrating the previous equation on polar rays, it gives:

$$\frac{d}{dt}\overline{V}(\theta, t) + \overline{V}(\theta, t) = \pi\left(\frac{J_0}{2} + \frac{J_1}{3} + \frac{J_1}{4}\right) \int_{-\pi}^{\pi} S(2\sigma\overline{V}(\theta, t))d\bar{\theta} - \frac{J_1}{3}\int_{-\pi}^{\pi} \cos(\theta - \bar{\theta}) S(2\sigma\overline{V}(\theta, t))d\bar{\theta}$$

Finally, by adding the LGN input, we find the equation:

$$\frac{d}{dt}\overline{V}(\theta, t) + \overline{V}(\theta, t) = \int_{-\pi}^{\pi} \left[\overline{J_0} + \overline{J_1}\cos(\theta - \bar{\theta})\right] S(2\sigma\overline{V}(\theta, t))d\bar{\theta} + I_{ext}(\theta, t). \tag{8.13}$$

where $\overline{J_0} = \pi\left(\frac{J_0}{2} + \frac{J_1}{3} + \frac{J_1}{4}\right)$, $\overline{J_1} = -\frac{J_1}{3}$. The external input is chosen according to (8.9), $I_{ext}(\theta, t) = \varepsilon(1 + \beta\cos(2(\theta - \theta_{aff}(t))))$. We have found an effective connectivity $\overline{J_0} + \overline{J_1}\cos(\theta - \bar{\theta})$ in the orientation domain for the weighted mean $\overline{V}$: this is the connectivity used in the Ring Model of a hypercolumn that will be studied in chapter 9. Note that we can apply the mechanism of Ben-Yishai *et al.* , described above, to (8.13) even if it has only one "spatial" dimension whereas we explained it for a 2D cortex. A variant of (8.13) exists:

$$\frac{d}{dt}\overline{A}(\theta, t) + \overline{A}(\theta, t) = S\left[2\sigma\left(\int_{-\pi}^{\pi} \left[\overline{J_0} + \overline{J_1}\cos(\theta - \bar{\theta})\right] \overline{A}(\theta, t))d\bar{\theta} + I_{ext}(\theta, t)\right)\right], \tag{8.14}$$

it is equivalent to (8.13) if I_{ext} is stationary. It can be derived using the same approximations from an activity based version of (8.10).

The main feature of the Ring Model is the presence of excitatory connections between similar preferred orientations and inhibitory ones between distinct orientations. Hence, given an orientation map $\theta(\mathbf{x})$ like in figure 1.3 Bottom, we can generalise (8.13) to a network of pinwheels encoded in an orientation map $\theta(\mathbf{x})$:

$$\frac{d}{dt}V(\mathbf{x}, t) + V(\mathbf{x}, t) = \int_{-\pi}^{\pi} \left[\overline{J_0} + \overline{J_1}\cos(\theta(\mathbf{x}) - \theta(\mathbf{y}))\right] S(2\sigma\overline{V}(\mathbf{y}, t))d\mathbf{y} + I_{ext}(\mathbf{x}, t). \tag{8.15}$$

[7] *h.o.t.* means higher order terms.

This is almost[8] the Blumenfeld *et al.* model that we will study in chapter 10, it will feature many of the Ring-Model properties.

Finally, one may wonder why we should consider (8.13) whereas we know that an homogeneous connectivity like $J(\mathbf{x}-\mathbf{y})$ is more biologically relevant. The reason is mainly mathematical: the two equations (8.13), (8.15) can be reduced exactly to three equations in three unknown functions of time, eliminating the variable θ, see chapter 9. Thus, these low dimensional systems can be thoroughly studied. Nevertheless, it is not clear that the approximations made at the beginning of this section work very well. This is why we will consider a more plausible V1 model in the last chapter 11 of this Thesis and see how the mechanism of section 8.1 applies. Moreover, this last approach will allow to study the influence of space-dependent delays, a much more difficult endeavour for (8.15). Finally, we will consider the long-range connections and how they impact the network behaviours.

[8] We will see in chapter 10 that the selectivity is also incorporated in the model.

Chapter 9

Illusory persistent states in the Ring Model of visual orientation selectivity

In this chapter, we study in detail the Ring Model equation (8.13). We investigate the mechanism explained in the previous chapter and characterize the dependency of the tuning curves on the different parameters. We consider more general connectivities than in (8.13) and study how they influence the tuning curves. Their computation is difficult because equation (8.13) has a lot of symmetries. Once it is completed, we study how the width of the tuning curves varies with the contrast. This dependency naturally introduces a perception threshold.

Contents

The Ring Model of orientation tuning is a dynamical model of a hypercolumn of visual area V1 in the human neocortex. It has been designed to account for the experimentally observed orientation tuning curves (see definition 1.3.1) by local, *i.e.*, cortico-cortical computations. The tuning curves are stationary, *i.e.* time independent, solutions of this dynamical model. One important assumption underlying the Ring Model is that the LGN input to V1 is weakly tuned to the retinal orientation and that it is the local computations in V1 that sharpen this tuning. Because the equations that describe the Ring Model have built-in symmetry properties in the synaptic weight distribution, the model in effect encodes an infinite number of tuning curves that are arbitrarily translated with respect to each other. By using the Orbit Space Reduction technique, we rewrite the model equations in canonical form as functions of polynomials that are invariant by the symmetries. This allows us to combine equivariant[1] bifurcation theory with an efficient numerical continuation method in order to compute the tuning curves of the Ring Model. Surprisingly some of these tuning curves are not tuned to the stimulus. We interpret them as neural illusory persistent states and show numerically how they can be induced by simple dynamical stimuli. These neural illusory persistent states are important biological predictions of the model. They correspond to a remarkable behaviour of the model as consequence of its working regime. This behaviour should be observed in any model with the same working range, in this sense, it is generic. We also show how our theoretical analysis allows to very simply specify the ranges of all the model parameters by comparing the model predictions with published experimental observations.

9.1 Introduction

9.1.1 Chronology

Since the discovery by Hubel and Wiesel [Hubel 1962] of the selective response of a single neuron to some orientations, a long-standing debate has taken place about the degree of cortical computation involved in this selectivity compared to the feedforward selectivity implied by the LGN projections. Cortical models [Somers 1995, Ben-Yishai 1995, Hansel 1997] have been used to show how this selectivity can be produced in a cortex with center-surround interactions in the orientation domain and to reproduce the interactions between contrast and orientation selectivity (see [Dean 1981, Sclar 1982, Skottun 1987, Alitto 2004]). In particular, they were designed so that their predictions agree with the fact that the amplitude of the tuning curves increases with contrast whereas their width remains constant.

The Ring Model of orientation tuning was introduced by Hansel and Sompolinski [Hansel 1997] and studied by several other scientists [Shriki 2003, Ermentrout 1998, Dayan 2001b, Bressloff 2000, Bressloff 2001b], after the seminal work of Ben-Yishai

[1] This is defined in section 9.1.4.

and colleagues [Ben-Yishai 1995], as a model of a hypercolumn in primary visual cortex. This rate model is a simplification of complex spiking networks models [Somers 1995, Douglas 1995, Carandini 1997] that were designed to make it easier to understand the role of several mesoscopic parameters.

9.1.2 Modelling with neural fields equations

The rate model assumes that the local orientation θ in the receptive fields of the neurons in the column, is encoded in their activity, or firing rate, noted $A(\theta, t)$. The interaction between the neurons is modeled by a function J of the orientation that represents how the activities corresponding to two different orientations reinforce or inhibit each other. This function is called the connectivity function of the model. With this in mind, the dynamics of the firing rate can be represented by the neural field equations, a slight generalization of (8.14). Note that the orientation domain spans $(-\pi/2, \pi/2)$ and not $(-\pi, \pi)$ as the direction domain.

$$\left\{ \begin{array}{rcl} \tau \dot{A}(\theta,t) & = & -A(\theta,t) + S\left[\sigma\left(\int_{-\pi/2}^{\pi/2} J(\theta-\bar{\theta})A(\bar{\theta},t))\frac{d\bar{\theta}}{\pi} + \varepsilon I_{ext}(\theta,t)\right)\right] \quad t>0 \\ A(\theta,0) & = & A_0(\theta) \end{array} \right. \tag{9.1}$$

τ defines the intrinsic dynamics of the population and I_{ext} is the input from the lateral geniculate nucleus (LGN) to the hypercolumn whose contrast is defined by the parameter ε, see figure 9.1. S is the sigmoidal function

$$S(x) = \frac{1}{1+e^{-x+T}},$$

σ is a parameter that determines the nonlinear gain of the sigmoid, T is a threshold that, together with σ, controls for which value the sigmoid takes the value $1/2$.

Remark 30. The convention in the literature is to take σT for the threshold instead of T. We found it mathematically more convenient to use our scaling, the scope of the analysis is not reduced because we also vary T as a parameter.

9.1.3 Parametrization of the external input and of the connectivity function

We have seen in chapter 8 how to build an effective connectivity that only depends on the angle θ. As a consequence of our derivation, the effective connectivity is periodic. From a biological point of vue, it is reasonable to assume that the cortex processes the different orientations equally: this is translated by the connectivity function $J(\theta)$ being π-periodic. Also, in the derivation of the effective connectivity $J(\theta)$ in the previous chapter, we used a first order Taylor expansion of $J(\|\mathbf{r}-\bar{\mathbf{r}}\|_2)$ in (8.12). If we had use a better Taylor approximation, it would have introduced powers of cosines $\cos(\theta-\bar{\theta})^k$ which can be transformed in cosines $\cos(p(\theta-\bar{\theta}))$ for some integer p. Thus, by using a better approximation than (8.12), it yields an

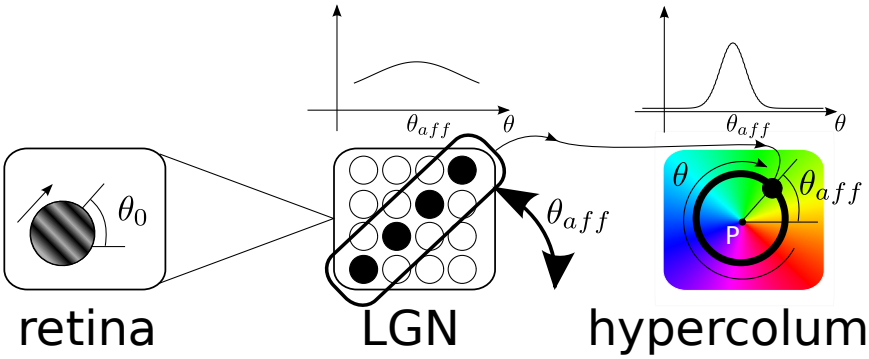

Figure 9.1: A simplified view of the visual path from the retina through the LGN to cortical area V1. The receptive field of the LGN cells feeding the hypercolumn of orientation of V1 contains a grating of orientation θ_0. This grating excites mostly the LGN cells that share this receptive field and are aligned in the direction θ_0; the tuning is broad, see the curve in the middle part of the figure. These LGN cells project onto the network of cells in the hypercolumn of orientation of V1 whose interactions, represented by the Ring Model, result in a sharpening of the tuning around the grating direction, see the curve in the righthand side of the figure. The hypercolumn is centered on a pinwheel P and the colour encodes the prefered orientation of the cells in the nearby columns.

effective connectivity as a sum of cosines $\cos(p(\theta - \bar{\theta}))$. Hence, we assume J is an even π-periodic function.

Several variants of this model have been studied in the literature, e.g., in [Bressloff 2000, Bressloff 2001b] J is a difference of Gaussians while in [Ben-Yishai 1995] the authors start with a network of excitatory/inhibitory spiking neurons and derive a mean field approximation of this network yielding a connectivity function J described by:

$$J(\theta) = J_0 + J_1 \cos(2\theta) \tag{9.2}$$

This is obtained by taking the first two Fourier modes of the periodic function J. The input I_{ext} from the LGN in response to a drifting grating (DG) has a similar shape

$$I_{ext}(\theta) = 1 - \beta + \beta \cos(2(\theta - \theta_{aff})). \tag{9.3}$$

As mentioned above, and as shown in figure 9.1, it is weakly tuned, *i.e.*, maximal, at $\theta = \theta_{aff}$ and it is the network, modeled by (9.1), that sharpens this tuning. The anisotropy $\beta > 0$ is a parameter that adjusts how weak the input is tuned.

Remark 31.Note that the general shape of I_{ext} does not matter much. Indeed, in the following study, we will approximate J by the truncation of its Fourier expansion. This naturally produces a PG-kernel (see definition 3.4.2). The network can then be described, without approximation for the stationary states, by ordinary differential equations (see section 3.4.2). In these equations, what only matters is

the projection of the external input I_{ext} on the cosine modes in the expression for J. This is why we can assume the shape (9.3) for the input:

$$I_{ext}(\theta) = \sum_{p=0}^{N} I_p \cos(2kp(\theta - \theta_{aff})). \tag{9.4}$$

where N is the number of Fourier modes in the truncation of the Fourier series of J.

The sigmoid S is often replaced by a Heaviside function, or, as in [Ben-Yishai 1995, Hansel 1997], by a piecewise linear approximation of the sigmoid which forbids the use of bifurcation theory because these approximations are not differentiable. Indeed, we have seen in the previous chapter that we need to study a linearized equation (8.3) which requires to differentiate the sigmoid. In [Ermentrout 1998, Dayan 2001b, Bressloff 2000] it is a true sigmoidal function.

The parameter J_1 is positive, an important property of the network that is necessary to produce the tuning curves. J_0 is most of the time negative [Ben-Yishai 1995, Dayan 2001b, Bressloff 2000, Bressloff 2001b] but can be positive as well [Bressloff 2001b]. For example, we find the following values:

Paper	J_0	J_1	β	T
[Dayan 2001b]	-7.3	11	0.1	0
[Ben-Yishai 1995]	-7.3	11	0.164	1

Rescaling the values of the parameters by $|J_0|$, we find:

Paper	J_0	J_1	β	T
[Dayan 2001b]	-1	1.5	0.1	0
[Ben-Yishai 1995]	-1	1.5	0.164	0.1

9.1.4 Symmetries of the cortical network

The symmetries of J play a prominent role in our upcoming analysis of the Ring Model. The reason for this is that, when the contrast ε is equal to 0, equation (9.1), is equivariant (see [Golubitsky 1984, Chossat 2000, Haragus 2010] and definition A.0.2), *i.e.* it has some nice properties with respect to the action of a certain group that we proceed to describe.

Let us consider the group of translations of $\mathbb{R}$ modulo 2π. An element T_γ, $\gamma \in [0,\ 2\pi)$ of this group[2] acts on the orientation θ by $T_\gamma \cdot \theta = \gamma/2 + \theta$ and on the activity function $A(\theta, t)$ by $T_\gamma \cdot A(\theta, t) = A(\gamma/2 + \theta, t)$. Similarly, we consider the reflection, noted R, such that $R \cdot \theta = -\theta$ and therefore $R \cdot A(\theta, t) = A(-\theta, t)$. G is the group generated by the T_γ, $\gamma \in [0,\ 2\pi)$ and R: $G \equiv \langle T_\gamma, R \rangle$. Observe that the elements of G further satisfy the following relations:

$$\begin{cases} T_{\gamma_1} T_{\gamma_2} = T_{\gamma_1+\gamma_2} & RT_\gamma = T_{-\gamma} R \quad \text{for all} \quad \gamma_1,\, \gamma_2,\, \gamma \in \mathbb{R}/2\pi\mathbb{Z} \\ T_0 = Id & R^2 = Id \end{cases}$$

[2] $\gamma \in [0,\ 2\pi]$ because 2π is equivalent to 0

the group G is, in effect, isomorphic to $O(2)$, the group of two-dimensional orthogonal transformations [Haragus 2010, Chapter 1].

Let us examine how this group acts on the equation (9.1). We can abstractly rewrite equation (9.1) as $\mathcal{F}(A) = 0$, where

$$\mathcal{F}(A) = \tau\dot{A}(\theta,t) + A(\theta,t) - S\left[\sigma\Big(\int_{-\pi/2}^{\pi/2} J(\theta-\bar{\theta})A(\bar{\theta},t))\frac{d\bar{\theta}}{\pi} + \varepsilon I_{ext}(\theta,t)\Big)\right].$$

In the case when there is no stimulus ($\varepsilon = 0$), it is useful to note that $\mathcal{F}$ commutes with T_γ because J is periodic and that $\mathcal{F}$ commutes with R because J is even. This reads [3]:

$$\text{when } \varepsilon = 0,\ \mathcal{F}(g\cdot A) = g\cdot\mathcal{F}(A),\ \forall g\in G$$

These two fundamental properties of the connectivity are directly translated into properties of the network. The fundamental consequence is that, because of these symmetries, the network is ready to process the different grating orientations equally.

We say that the model is G-*equivariant* when $\varepsilon = 0$ (see definition A.0.2). We will see in the next chapter what happens if the connectivity does not possess these symmetries.

What happens when there is a stimulus, *i.e.* when $\varepsilon > 0$? We already know the integral term in $\mathcal{F}$ is G-equivariant. Hence the equivariance of $\mathcal{F}$ when $\varepsilon > 0$ amounts[4] to the *invariance* of $g\cdot I_{ext} = I_{ext}$. What are the elements of G which leave I_{ext} invariant? The only possible invariance comes from I_{ext} in (9.4) being an even function of $\theta - \theta_{aff}$. It yields the invariance by the reflexion around the axis $\theta = \theta_{aff}$. Hence, if we define this reflexion by

$$\tilde{R} = T_{2\theta_{aff}} R T_{-2\theta_{aff}},$$

we find[5] that

$$\tilde{R}\cdot I_{ext} = I_{ext}.$$

Hence, when the input is switched on, the symmetry group of the model reduces to the subgroup $\mathbb{Z}_2$ of G with two elements generated by $\tilde{R}$. This phenomenon is called symmetry breaking. We call $\tilde{R}$ the *residual symmetry*.

[3] For example $T_\gamma\cdot\mathcal{F}(A) = \tau\dot{A}(\frac{\gamma}{2}+\theta,t) + A(\frac{\gamma}{2}+\theta,t) - S\left[\sigma\Big(\int_{-\pi/2}^{\pi/2} J(\frac{\gamma}{2}+\theta-\bar{\theta})A(\bar{\theta},t))\frac{d\bar{\theta}}{\pi}\Big)\right]$ and $\mathcal{F}(T_\gamma\cdot A) = \tau\dot{A}(\frac{\gamma}{2}+\theta,t) + A(\frac{\gamma}{2}+\theta,t) - S\left[\sigma\Big(\int_{-\pi/2}^{\pi/2} J(\theta-\bar{\theta})A(\frac{\gamma}{2}+\bar{\theta},t))\frac{d\bar{\theta}}{\pi}\Big)\right]$ are equal because A and J are π-periodic.

[4] Indeed, for example

$T_\gamma\cdot\mathcal{F}(A) = \tau\dot{A}(\frac{\gamma}{2}+\theta,t) + A(\frac{\gamma}{2}+\theta,t) - S\left[\sigma\Big(\int_{-\pi/2}^{\pi/2} J(\frac{\gamma}{2}+\theta-\bar{\theta})A(\bar{\theta},t))\frac{d\bar{\theta}}{\pi}\Big) + \varepsilon I_{ext}(\theta+\frac{\gamma}{2})\Big)\right]$

and

$\mathcal{F}(T_\gamma\cdot A) = \tau\dot{A}(\frac{\gamma}{2}+\theta,t) + A(\frac{\gamma}{2}+\theta,t) - S\left[\sigma\Big(\int_{-\pi/2}^{\pi/2} J(\theta-\bar{\theta})A(\frac{\gamma}{2}+\bar{\theta},t))\frac{d\bar{\theta}}{\pi} + \varepsilon I_{ext}(\theta)\Big)\right]$ are equal

if $T_\gamma\cdot I_{ext}(\theta) \equiv I_{ext}(\theta+\frac{\gamma}{2}) = I_{ext}(\theta)$.

[5] Indeed: $\tilde{R}\cdot I_{ext}(\theta) = I_{ext}(-\theta+2\theta_{aff}) = I_{ext}(\theta)$.

9.1.5 General properties of the network and plan of the study

For technical reasons we turn the activity model (9.1) into a voltage model as follows. We first rewrite equation (9.1) in a more compact and convenient functional form :

$$\tau \dot{A} = -A + S\left[\sigma(J \cdot A + \varepsilon I)\right].$$

J is now thought of as a linear (integral) operator acting on the function A as the periodic convolution $J \cdot A(\theta, t) = \int_{-\pi/2}^{\pi/2} J(\theta - \bar{\theta}) A(\bar{\theta}, t)) \frac{d\bar{\theta}}{\pi}$, see part II. We then perform the change of variable $V = J \cdot A + \varepsilon I$. Assuming that the input current is not a function of time, this leads to the following equation

$$\tau \dot{V} = -V + J \cdot S(\sigma V) + \varepsilon I \tag{9.5}$$

Note that this equation, as (9.1), is G-equivariant. It is worth noticing that the stationary solutions of (9.1) and (9.5) are in one to one correspondence. As a consequence we will work on (9.5) because it is mathematically more convenient.

The stationary solutions (some of them called tuning curves, see below and the section 9.5) of (9.1) (respectively of (9.5)) satisfy $\dot{A} = 0$ (respectively $\dot{V} = 0$). Characterizing and computing them for different values of the parameters is the first step toward understanding the dynamics of the solutions to these equations. Indeed, it is known (see propositions 3.2.3 and 3.2.6) that this type of equations only produces heteroclinic (linking two stationary solutions, or equilibria) orbits. This motivates further the study of the stationary solutions of (9.5). One of our goals is to show how the stationary solutions are organized and to give indications about the dynamics in a given range of parameters, corresponding to biologically plausible values. This is important by itself and because some large scale models of V1 (see for example the work of Bressloff *et al* [Bressloff 2001b]) including many hypercolumns represent them with the Ring Model. Therefore a good understanding of one hypercolumn paves the way to an understanding of a population thereof. We show that, depending on the nonlinear gain σ, there may exist many stationary solutions, which are all acceptable responses of the network to a given input from the LGN (at least for the model at hand). Thus, this local orientation tuning device may behave less trivially than what it was initially designed for. In effect, the existence of these stationary solutions, can make the local dynamics quite intricate when σ is large enough to support the existence of these extra solutions.

We will follow a method similar to the one developed in part II to compute the stationary states of (9.5). The method has been modified to take into account the symmetries of the Ring Model. The general idea is that the LGN input is weak and only modulates the network activity. Hence the cortical network (represented by the Ring Model) encodes the possible tuning curves within its connectivity function and when presented with a weak external input, produces small deviations of 'its' tuning curves. Our goal is to compute these tuning curves. However, because of the symmetries of the connectivity function J, the model in effect encodes an infinite

number of tuning curves, and this is an endless cause of numerical problems. Indeed we pointed out above that if the input current was null, equation (9.5) (respectively (9.1)) was G-equivariant. This implies that if $V(\theta)$ is a stationary solution of (9.5) for $\varepsilon = 0$, so are $V(\theta + \gamma)$, $\gamma \in \mathbb{R}$, and $V(-\theta)$. We show that by performing an appropriate change of variables, we can get rid of this redundancy, recover numerical accuracy, and make the model amenable to analysis.

Among the stationary solutions, two classes are especially important to us, we call them the *illusions* and the *illusory persistent states*. The illusions are stable stationary solutions that are unfaithful representations of the stimulus I_{ext}. The illusory persistent states are unstable stationary solutions that are unfaithful representations of the stimulus I_{ext} and such that the corresponding unstable eigenvalues (see below) are small compared to the intrinsic time constant τ in the Ring Model. Hence they seem persistent because, despite being unstable solutions, at the time scale τ, they look 'stable'. Finally a third class is that of the *tuning curves* which are unimodal, stable or unstable stationary solutions.

The structure of the study is the following. In section 9.2, we derive a finite set of ordinary differential equations which are equivalent to (9.1). However, this simplification is not enough for the numerical study because of the symmetries: if we know a tuned stationary cortical state, all its translated versions will also be tuned stationary states. As a computer cannot handle an infinity of such states, we use a change of variables that generalizes the polar coordinates and allows a numerical study by removing the redundancy in the equations coming from the symmetries. In section 9.3, we use the new formulation with the change of variables to find the stationary states of the network. This study predicts some characteristic dynamical responses that we discuss in section 9.4. They are based on illusory persistent states. Finally, in the Discussion section 9.5, we show that all the values of the parameters of the model are fixed by experimental data. We then study how the network behaves when the contrast ε of the stimulus is increased.

9.2 Reformulation of the problem and handling of the symmetries

In this section, we derive a number of finite dimensional equations equivalent to (9.5) which are further simplified using a change of variables to take care of the symmetries. These equations are solved numerically and their consequence are explored in the following section 9.3. As such, this section may be skipped in a first reading and the reader who is not interested in the mathematical details can go directly to section 9.3.

9.2.1 Turning the problem into a finite dimensional one

Problem (9.1) (respectively (9.5)) is infinite dimensional since the solutions are function of the orientation θ. By truncating the Fourier series of the connectivity

function J, we reduce the problem to a finite number of dimensions. We write

$$J(\theta) = J_0 + \sum_{p=1}^{N} J_p \ \cos(2p\theta) \tag{9.6}$$

where N is the number of Fourier modes that are appropriate to represent J. We will show how the choice of N affects the functional properties of the Ring Model. Notice that by varying N, we generate a family of models that approximate all previously published ones up to the desired accuracy. For example we can approximate a difference-of-Gaussians connectivity function (see figure 9.5 Left).

Remark 32.For convenience, we shall write $\cos_k$ *for the function* $\theta \to \cos(k\theta)$. *The same holds for* $\sin_k$.

It was shown in section 3.4 that this form of the connectivity function implies that the solutions to (9.5) can be written $V(\theta,t) = V^{\parallel}(\theta,t) + V^{\perp}(\theta,t)$, where $V^{\parallel}$ is a linear combination of the functions $\cos_{2p}$ and $\sin_{2p}$, $p = 0, \cdots, N$ and the function $V^{\perp}$ tends to $I^{\perp}$ exponentially fast when $t \to \infty$. The form of the external input (9.4) together with (9.6) imply that the stationary solutions satisfy $V^{\perp} = 0$. It follows that any stationary solution to (9.5) can be written

$$V(\theta) = v_0 + \sum_{p=1}^{N} \sqrt{|J_p|} \left[v_p^{(1)} \ \cos_{2p}(\theta) + v_p^{(2)} \ \sin_{2p}(\theta) \right],$$

where $v_0, v_p^{(1),(2)}$, $p = 1, \cdots, N$ are $2N+1$ reals. Solving (9.7) is therefore equivalent to finding these reals.

We can, up to a rescaling of σ in (9.1), assume that J_0 takes the values ± 1:

$$J_0 \stackrel{\text{def}}{=} \varepsilon_0 \in \{-1, 1\}.$$

Similarly we define $\varepsilon_k = \pm 1$ by

$$J_k = \varepsilon_k |J_k|, \ \varepsilon_k \in \{-1, 1\} \quad k = 1, \cdots, N$$

With all this in hands, the stationary solutions of (9.1) satisfy the equation:

$$V(\theta) = \int_{-\pi/2}^{\pi/2} \left[J_0 + \sum_{p=1}^{N} J_p \ \cos_{2p}(\theta - \bar{\theta}) \right] S\left[\sigma V(\bar{\theta}, t))\right] \frac{d\bar{\theta}}{\pi} + \varepsilon I_{ext}(\theta) \tag{9.7}$$

In the case of a general non stationary solution, $V^{\parallel}(\theta,t)$ is given by the same formula where the coefficients $v_p^{(1)}, v_p^{(2)}$ are now real functions of time. Under the assumption that $V^{\perp}$ is neglected, it is easy to obtain the system of ordinary differential equations that are satisfied by the functions $v_0, v_p^{(1),(2)}$. Using the complex values $z_k \stackrel{\text{def}}{=}$

$v_k^{(1)} + iv_k^{(2)}$, $k = 1, \cdots, N$ these equations read[6]:

$$\left\{\begin{array}{rcl} \tau\dot{v}_0 + v_0 & = & \varepsilon_0 \int\limits_{-\frac{\pi}{2}}^{\frac{\pi}{2}} S\left[\sigma v_0 + \sigma \sum\limits_{p=1}^{N} \sqrt{|J_p|} z_p e^{-2pi\bar{\theta}} + c.c.\right] \frac{d\bar{\theta}}{\pi} + \varepsilon\tilde{I}_0 \\ & \stackrel{\text{def}}{=} & B_0(v_0, \{z_p\}) + \varepsilon\tilde{I}_0 \\ \tau\dot{z}_k + z_k & = & \varepsilon_k\sqrt{|J_k|} \int\limits_{-\frac{\pi}{2}}^{\frac{\pi}{2}} S\left[\sigma v_0 + \sigma \sum\limits_{p=1}^{N} \sqrt{|J_p|} z_p e^{-2pi\bar{\theta}} + c.c.\right] e^{2ki\bar{\theta}} \frac{d\bar{\theta}}{\pi} + \varepsilon\tilde{I}_k \\ & \stackrel{\text{def}}{=} & B_k(v_0, \{z_p\}) + \varepsilon\tilde{I}_k \quad k = 1, \cdots, N \end{array}\right. \tag{9.8}$$

where $I_{ext}(\theta) \stackrel{\text{def}}{=} I_0 + \sum\limits_{k=1}^{N} \tilde{I}_k \sqrt{|J_k|} e^{2ik\theta}$ and $\tilde{I}_k = \frac{I_k e^{2ik\theta_{aff}}}{\sqrt{|J_k|}}$ (see (9.4)).
The coefficients $(v_0, \{z_p\})$ defining the stationary solutions satisfy the following equations:

$$\left\{\begin{array}{l} v_0 = B_0(v_0, \{z_p\}) + \varepsilon\tilde{I}_0 \\ z_k = B_k(v_0, \{z_p\}) + \varepsilon\tilde{I}_k \quad k = 1, \cdots, N \end{array}\right.$$

A solution $(v_0, \{z_p\})$ is said *tuned* if $z_p \neq 0$ for some p. The $N+1$ coefficients $(v_0, z_1, \cdots, z_N)$ are the coordinates of $V^{\parallel}$. In this coordinate system: the group G action defined in section 9.1.4 reads

$$\begin{array}{rcl} T_\gamma \cdot (v_0, z_1, z_2, \cdots, z_N) & = & (v_0, e^{2i\gamma} z_1, e^{4i\gamma} z_2, \cdots, e^{2iN\gamma} z_N) \quad \gamma \in \mathbb{R} \\ R \cdot (v_0, z_1, z_2, \cdots, z_N) & = & (v_0, \bar{z}_1, \bar{z}_2, \cdots, \bar{z}_N) \end{array}$$

and also

$$\tilde{R} \cdot (v_0, z_1, z_2, \cdots, z_N) = (v_0, e^{4i\theta_{aff}} \bar{z}_1, e^{8i\theta_{aff}} \bar{z}_2, \cdots, e^{4iN\theta_{aff}} \bar{z}_N).$$

As shown in the section 9.1.4, if V^f is a stationary solution of (9.8) for $\varepsilon = 0$, so is $g \cdot V^f$, $\forall g \in G$: there is an infinity of stationary solutions, possibly tuning curves, that are encoded by the network. However, when $\varepsilon \neq 0$, the symmetries are broken, (9.8) is only $\mathbb{Z}_2$-equivariant and the number of stationary solutions becomes finite.

In the next two sections we study the cases $N = 1$ and $N = 2$. In particular we give another system of coordinates for $V^{\parallel}$ that takes advantage of the symmetries and removes the redundancy in the equations (9.8). The second case $N = 2$ shows that adding more modes does not change the main results of the analysis.

9.2.2 Keeping only one mode in the connectivity J, $N = 1$

We consider the following connectivity function also used [Ben-Yishai 1995, Hansel 1997] for example:

$$J = \varepsilon_0 + J_1 \cos_2,\ J_1 > 0$$

[6] c.c. means complex conjugate.

Any stationary membrane potential is described by the two-dimensional vector (v_0, z_1). More precisely, the firing rate tuning curve reads:

$$TC_\phi(\theta) = S\left[\sigma v_0 + \sigma|z_1|\cos_2(\theta-\phi)\right].$$

From our previous analysis of the Ring Model symmetries, we know that the equations (9.8) are redundant when $\varepsilon = 0$. Indeed, it is easy to show that B_1 in (9.8) only depends on $\rho = |z_1|$, the phase $\arg z_1$ being arbitrary. This produces an infinity of tuned membrane potentials. Let us therefore use polar coordinates $z_1 = v_1 + iv_2 = \rho e^{2i\varphi}$, which yields to the following equations, assuming $\theta_{aff} = 0$:

$$\left\{\begin{array}{rcl} \tau\dot{v}_0 &=& -v_0 + B_0(v_0,\rho) + \varepsilon(1-\beta) \\ \tau\dot{\rho} &=& -\rho + \Re B_1(v_0,\rho) + \frac{\varepsilon\beta}{\sqrt{J_1}}\cos_2(\varphi) \\ 2\tau\rho\dot{\varphi} &=& -\sin_2(\varphi)\frac{\varepsilon\beta}{\sqrt{J_1}} \end{array}\right. \tag{9.9}$$

for the dynamics, and

$$\left\{\begin{array}{rcl} v_0 &=& B_0(v_0,\rho) + \varepsilon(1-\beta) \\ \rho &=& \Re B_1(v_0,\rho) + \frac{\varepsilon\beta}{\sqrt{J_1}}\cos_2(\varphi) \\ 0 &=& \sin_2(\varphi)\frac{\varepsilon\beta}{\sqrt{J_1}} \end{array}\right. \tag{9.10}$$

for the stationary solutions. The functions B_0 and $\Re B_1$ are given by:

$$\begin{array}{rcl} B_0(v_0,\rho) &=& \varepsilon_0 \int_{-\frac{\pi}{2}}^{\frac{\pi}{2}} S(\sigma(v_0 + \sqrt{J_1}\rho\ \cos_2\theta))\,\frac{d\theta}{\pi} \\ \Re B_1(v_0,\rho) &=& \varepsilon_k\sqrt{J_1}\int_{-\frac{\pi}{2}}^{\frac{\pi}{2}} S(\sigma(v_0 + \sqrt{J_1}\rho\ \cos_2\theta))\cos_2\theta\,\frac{d\theta}{\pi} \end{array}$$

Equations (9.9) do not produce the same dynamics as (9.8) because the change from Cartesian to polar coordinates is not a diffeomorphism, but they yield the same stationary membrane potentials. Indeed equations (9.10) are most useful for computing the tuning curves. In the following section 9.3.1, we use (9.10) which have only two unknowns (v_0, ρ) to look for the stationary states of (9.1): this is a great simplification compared to (9.1) without any numerical approximation.

9.2.3 Keeping two modes in the connectivity J, $N = 2$

We apply the same ideas as in the previous section when there are two cosine modes in the connectivity, *i.e.* we look for the solution (v_0, z_1, z_2) of (9.8). It turns out that finding the change of variables to remove the equivariance with respect to G is a lot more difficult. We write:

$$J = \varepsilon_0 + J_1\cos_2 + J_2\cos_4.$$

In order to agree with experimental facts (see chapter 1), the stable stationary solutions should be mainly unimodal, *i.e.* tuning curves. Compared to the previous

case, the fact that the second mode J_2 is nonzero could induce an "interaction" between the two modes leading to stable multimodal stationary solutions that are unwanted.

Following the analysis of section 9.2.1, we have to solve three coupled equations which are redundant because of the action of the symmetry group G which, in this case, reads

$$\begin{cases} T_\gamma \cdot (v_0, z_1, z_2) &= (v_0, e^{2i\gamma} z_1, e^{4i\gamma} z_2) \\ R \cdot (v_0, z_1, z_2) &= (v_0, \bar{z}_1, \bar{z}_2) \end{cases}$$

In order to eliminate the redundancy arising from this symmetry we used polar coordinates in the case $N = 1$. It is tempting to do the same with each complex variables z_1 and z_2 but it turns out to lead to a dead-end.

The main reason for this failure is numerical: we compute (see appendix E.2) the solutions of the nonlinear equations (9.8) using numerical continuation. This algorithm computes the solutions of (9.8) depending on a parameter, for example, the nonlinear gain σ. From two already known solutions V_1, V_2 for two values of the nonlinear gain $\sigma_1 < \sigma_2$, it computes a solution V_3 of (9.8) for a third value of the nonlinear gain $\sigma_3 > \sigma_2$. If σ_3 is close to σ_2, then the solution (V_3, σ_3) is roughly on the line linking (V_1, σ_1) and (V_2, σ_2) which gives an approximation of V_3. This is why this algorithm is called 'continuation' because it continues the path of solutions from known solutions. This scheme works well if the equations (9.8) are not too singular[7].

If we use polar coordinates as in the previous section: $z_1 = \rho_1 e^{2i\phi_1}$, $z_2 = \rho_2 e^{4i\phi_2}$, then, we find equations for the phases:

$$\dot{\phi}_i = F_i(v_0, \rho_1, \rho_2, \phi_1, \phi_2), \ i = 1, 2$$

Using the equivariance by the translations T_γ, we can show that the functions F_i only depend on the difference of the phases $\varphi_1 - \varphi_2$. It turns out that the other equations (for $\dot{v}_0, \dot{\rho}_1, \dot{\rho}_2$) also involve only $\varphi_1 - \varphi_2$. We were unable to find a simple relation between F_1 and F_2. As a consequence we end up with 5 equations in the 4 unknowns $v_0, \rho_1, \rho_2, \varphi_1 - \varphi_2$: this is inappropriate for numerical continuation because there are too many equations. We need to find a way to obtain 4 equations in 4 unknowns.

To reach this goal we turn to a general technique, the Orbit Space Reduction (see for example [Chossat 2000]), which provides the right change of coordinates through the use of what is called a Hilbert Basis[8]. A fundamental property is that any smooth equivariant function (as the B_i in (9.8)) can be expressed using the elements of the Hilbert Basis and their gradients. A Hilbert basis associated to the

[7] more precisely, if the linear part of (9.8) has, at worst, a one-dimensional kernel for some isolated values of the nonlinear gain.

[8] The ring $\mathcal{R}_G$ of $O(2)$-invariant polynomials is finitely generated as an $\mathbb{R}$-algebra, this goes back to Hilbert. A family $\pi_1, \cdots, \pi_s$ of generators of $\mathcal{R}_G$ is called a Hilbert Basis.

action of the group G ([Chossat 2000, page 205][Golubitsky 1988] is given by the three polynomials:

$$\pi_1 = z_1\bar{z}_1, \quad \pi_2 = z_2\bar{z}_2, \qquad \pi_3 = \Re\left(z_1^2\bar{z}_2\right)$$

which satisfy the constraints

$$\pi_1 \geq 0, \quad \pi_2 \geq 0, \quad \pi_3^2 \leq \pi_1^2\pi_2 \tag{9.11}$$

Our upcoming analysis uses the so-called Orbit Space, *i.e.* the subset of $\mathbb{R}^4$ of the four-tuples $(v_0, \vec{\pi})$, $\vec{\pi} = (\pi_1, \pi_2, \pi_3)$, that satisfy the inequalities (9.11). Using these coordinates, the firing rate tuning curves read:

$$TC(\theta) = S\left[\sigma\left(v_0 + \sqrt{\pi_1 J_1}\cos_2(\theta) + \sqrt{\pi_2|J_2|}\cos_4(\theta + \varphi_2 - \varphi_1)\right)\right] \tag{9.12}$$

where $z_1 = \sqrt{\pi_1}e^{2i\varphi_1}$, $z_2 = \sqrt{\pi_2}e^{4i\varphi_2}$, and $\pi_1\sqrt{\pi_2}\cos_4(\varphi_2 - \varphi_1) = \pi_3$.

From the definition of the polynomials π_i, it is possible to rewrite (9.8) in the case of interest here, *i.e.* $N = 2$, only in terms of $(v_0, \vec{\pi})$ (as we did in the previous section with the polar coordinates):

$$\begin{cases} \tau\dot{v}_0 = -v_0 + \tilde{B}_0(v_0, \vec{\pi}) \\ \tau\dot{\pi}_1 = 2a(v_0, \vec{\pi})\pi_1 + 2b(v_0, \vec{\pi})\pi_3 \\ \tau\dot{\pi}_2 = 2c(v_0, \vec{\pi})\pi_2 + 2d(v_0, \vec{\pi})\pi_3 \\ \tau\dot{\pi}_3 = \left[2a(v_0, \vec{\pi}) + c(v_0, \vec{\pi})\right]\pi_3 + 2c(v_0, \vec{\pi})\pi_1\pi_2 + d(v_0, \vec{\pi})\pi_1^2 \end{cases} \tag{9.13}$$

where the functions $\tilde{B}_0, a, b, c, d$ are computed in appendix E.1. It should be noted that $a(v_0, \vec{\pi}), b(v_0, \vec{\pi}), c(v_0, \vec{\pi}), d(v_0, \vec{\pi})$ are G-invariant functions[9]. the stationary states are given by:

$$\begin{cases} 0 = -v_0 + \tilde{B}_0(v_0, \vec{\pi}) \\ 0 = 2a(v_0, \vec{\pi})\pi_1 + 2b(v_0, \vec{\pi})\pi_3 \\ 0 = 2c(v_0, \vec{\pi})\pi_2 + 2d(v_0, \vec{\pi})\pi_3 \\ 0 = \left[2a(v_0, \vec{\pi}) + c(v_0, \vec{\pi})\right]\pi_3 + 2c(v_0, \vec{\pi})\pi_1\pi_2 + d(v_0, \vec{\pi})\pi_1^2 \end{cases} \tag{9.14}$$

We will solve these equations numerically in section 9.3.2 with the algorithm of numerical continuation that we sketched at the beginning of this section.

9.3 Tuning curves of the simplified equations

We use the equations (9.10) and (9.14) to find the stationary solutions in the cases $N = 1$ and $N = 2$. Some of these solutions correspond to neuronal illusory persistent states. We then show that adding more modes ($N \geq 2$) to the connectivity function does not change the results. Finally we design two different types of external stimuli for bringing the network to the illusory persistent states.

[9] *i.e.* $a(g \cdot (v_0, \vec{\pi})) = a(v_0, \vec{\pi})$...

9.3.1 Finding the tuning curves, case $N = 1$

To reiterate, the Ring Model is based on one main ingredient: at null contrast and for small values of the nonlinear gain σ, there is a unique stationary solution (v_0, z_1), which is not tuned, *i.e.* $z_1 \equiv \rho e^{2i\phi} = 0$. Indeed, this stationary solution has to satisfy $\rho^f = 0$ otherwise it would not be unique because of the group action. Thus, in order to produce tuning curves (that are tuned by definition), we need a solution to (9.10) satisfying $\rho^f \neq 0$. This means that we must investigate for which values of σ, if any, the ρ solution of (9.10) becomes nonzero, *i.e.* **bifurcates** (see also chapter 8).

9.3.1.1 Case of no stimulus, $\varepsilon = 0$

For no external input, the equations (9.10) are:

$$\begin{cases} v_0^f &= \varepsilon_0 B_0(v_0^f, \rho^f) \\ \rho^f &= \sqrt{J_1} B_1(v_0, \rho^f) \\ & \varphi^f \in \mathbb{R} \end{cases} \tag{9.15}$$

A tuned solution $\rho^f \neq 0$ arises when the Jacobian at $(v_0, \rho) = (v_0^f, 0)$ is singular (see (8.7) in chapter 8). This Jacobian is given by $diag(-1 + \sigma\varepsilon_0 S'(\sigma v_0), -1 + \sigma\frac{J_1}{2} S'(\sigma v_0))$. As we are interested in tuned solutions $\rho^f \neq 0$, we obtain the condition:

$$-1 + \sigma \frac{J_1}{2} S'(\sigma v_0) = 0.$$

Finally, the equations for the existence of a tuned stationary solution are:

$$\begin{cases} v_0^f &= \varepsilon_0 S(\sigma_0 v_0^f) \\ 1 &= \sigma_0 S'(\sigma_0 v_0^f)\frac{J_1}{2} \end{cases} \tag{9.16}$$

We show in appendix E.3 that there is always a unique pair $(v_0^f(\sigma_0), \sigma_0)$ which solves (9.16) when $\varepsilon_0 < 0$. Around σ_0: $v_0^f(\sigma) \approx v_0^f(\sigma_0)$ and the equations (9.15) reduce to the following:

$$0 = \frac{\sigma - \sigma_0}{\sigma_0}\rho^f + \chi_3 \, (\rho^f)^3 \tag{9.17}$$

The fact that the previous equation does not have a second order term is a consequence of the connectivity J being an even function. Equation (9.17) is the normal form of a Pitchfork bifurcation (see for example [Chossat 2000, Haragus 2010]). Depending on the sign of χ_3, two things can happen. If $\chi_3 < 0$, the Pitchfork is oriented towards the increasing σs otherwise it points towards the decreasing σs (see figure 9.2). In this latter case, it can be shown (see proposition 3.3.3) that the bifurcated branch has to 'turn around', which produces 2 additional TCs on each branch (see figure 9.2.Middle). It is possible to find a closed form for χ_3, this is done appendix E.5. The resulting function of J_1 and T is plotted in figure 9.2.Right.

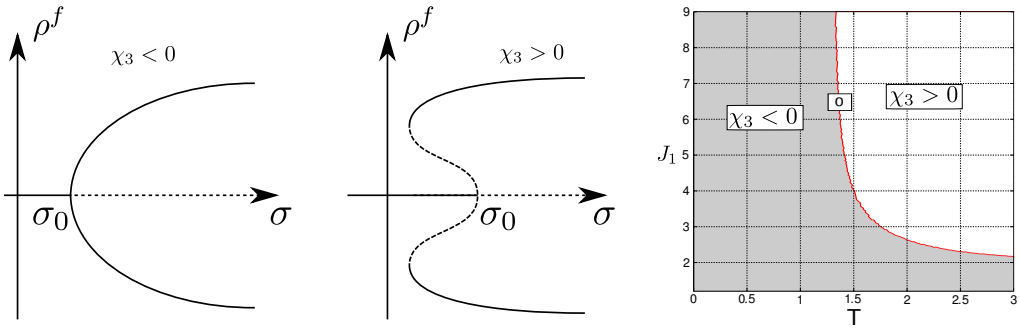

Figure 9.2: Middle: Plot of the solutions of (9.15) according to the sign of χ_3. The unstable solution are marked with dashed lines. Right: Plot of χ_3 as function of (J_1, T).

When $\rho^f \neq 0$, we obtain a continuum of stable tuning curves parametrized by an arbitrary phase angle φ, and noted TC_φ, which are given by:

$$TC_\varphi(\theta) = S\left[\sigma\left(v_0^f + \sqrt{J_1}\rho^f \cos_2(\theta - \varphi)\right)\right].$$

9.3.1.2 When there is a stimulus, $\varepsilon > 0$

The next step is to investigate what happens when we switch on the LGN drive, *i.e.* when $\varepsilon \neq 0$. The symmetry group of the equations (9.8) is reduced to the group $\mathbb{Z}_2$ (see section 9.1.4). Two important questions are 1) how many, if any, in the continuum of tuning curves remain solutions and 2) what is their stability? For very small $\varepsilon \neq 0$, switching on the LGN can be viewed as a perturbation of the nonlinear equations when $\varepsilon = 0$, as a consequence, we expect an opening of the Pitchfork as explained in section 3.3.2. We know from our previous analysis that these solutions satisfy:

$$\begin{cases} v_0^f = \varepsilon_0 B_0(v_0^f, \rho^f) + \varepsilon(1-\beta) \\ \rho^f = \sqrt{J_1} B_1(v_0^f, \rho^f) + \frac{\varepsilon\beta}{\sqrt{J_1}} \cos_2(\varphi^f) \\ 2\varphi^f = k\pi,\ k \in \mathbb{Z} \end{cases}$$

Considering the two cases k even and k odd we obtain:

$$\begin{cases} v_0^f = \varepsilon_0 B_0(v_0^f, \rho_e^f) + \varepsilon(1-\beta) \\ \rho_e^f = \sqrt{J_1} B_1(v_0^f, \rho_e^f) + \frac{\varepsilon\beta}{\sqrt{J_1}} \\ \varphi_e^f = k\pi,\ k \in \mathbb{Z} \end{cases} \quad \text{or} \quad \begin{cases} v_0^f = \varepsilon_0 B_0(v_0^f, \rho_o^f) + \varepsilon(1-\beta) \\ \rho_o^f = \sqrt{J_1} B_1(v_0^f, \rho_o^f) - \frac{\varepsilon\beta}{\sqrt{J_1}} \\ \varphi_o^f = (2k+1)\frac{\pi}{2},\ k \in \mathbb{Z} \end{cases}$$

Because $\rho \to B_0(v_0, \rho)$ is even and $\rho \to B_1(v_0, \rho)$ is odd, necessarily $\rho_e^f = -\rho_o^f$. Hence, these two systems of equations give exactly the same solutions $V^f(\theta)$:

$$V^f(\theta) = v_0^f \pm \rho_e^f \sqrt{J_1} \cos_2(\theta).$$

Also, each one the two solutions is invariant by the residual symmetry $\tilde{R}$, in particular there are not mapped one to another by $\tilde{R}$. Hence, the residual symmetry

plays no role in the existence of these solutions. If the contrast is high enough, proposition 3.2.7 gives that there is only one solutions V^f. It can be shown numerically (data not shown) that the two other solutions disappear in a saddle-node bifurcation for a high enough contrast.

We solve these equations for $(v_0,\, \rho_e)$ as functions of σ by using a continuation algorithm (see section 3.3.2), the results are shown in figure 9.3 Left in the case $\chi_3 < 0$.

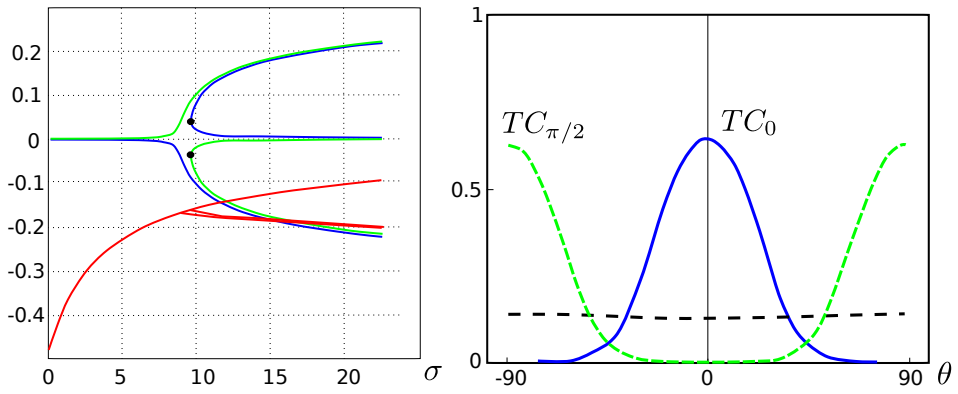

Figure 9.3: Left: Plot of the values of (v_0, ρ_e, ρ_o) shown in red, green, blue, respectively, as functions of σ for $\varepsilon = 0.01$, $T = 0$, $J_1 = 1.5$, $\beta = 0.1$. Notice the turning points labelled with black dots. Right: The tuning curves TC_0 and $TC_{\pi/2}$ for $\sigma = 15$, the other parameters are the same. Note that $\chi_3 < 0$ in this case.

The bifurcation diagram shown in figure 9.3 indicates that there are three stationary solutions for $\sigma > 10 \approx \sigma_0$. One, which turns out to be unstable, corresponding to a small value of ρ (thus it is untuned and, by definition, does not represent a tuning curve), and two which are tuning curves. The first of these tuning curves, noted TC_0, is maximum at $x = 0$ while the other, noted $TC_{\pi/2}$, is maximum at $\theta = \pi/2$. These two tuning curves are shown in figure 9.3 Right. Notice that the same is true in the case $\chi_3 > 0$ and $\sigma > \sigma_0$.

Let us now focus on the case $\chi_3 < 0$ (see section 9.5). The stability of the tuning curves is computed in appendix E.6. This analysis shows that TC_0 is stable although its stability along the v_2-axis is small in magnitude[10]. The other tuning curve $TC_{\pi/2}$ is stable along the v_1-axis but unstable[11] along the v_2-axis. In figure 9.4, we show the phase diagram of the dynamics in the plane (v_1, v_2) when $\varepsilon = 0$ and $\varepsilon > 0$. The stationary solutions are represented in red. In the case, $\varepsilon \neq 0$, the orbit linking $TC_{\pi/2}$ to TC_0 is very close to the circle of stationary solutions of the case $\varepsilon = 0$ and shows that the unstable tuning curve $TC_{\pi/2}$ dynamically transforms to TC_0 when a stimulus is applied (case $\varepsilon > 0$).

From the analysis in appendix E.6, if $\frac{\varepsilon\beta}{\rho^f\sqrt{J_1}} << \tau$, the unstable tuning curve $TC_{\pi/2}$ will appear to be persistent at the time scale defined by τ. When this

[10] For small positive values of the contrast ε it is equal to $-\frac{\varepsilon\beta}{\rho^f\sqrt{J_1}}$

[11] For small positive values of the contrast ε the unstable eigenvalue is equal to $\frac{\varepsilon\beta}{\rho^f\sqrt{J_1}}$.

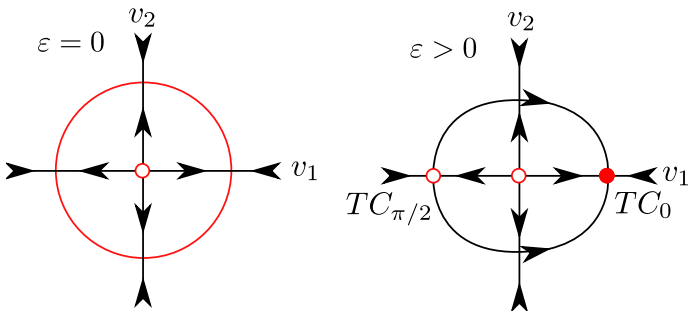

Figure 9.4: Left: phase diagram of the dynamics in the (v_1, v_2) plane when $\varepsilon = 0$ and $\varepsilon > 0$. The stationary solutions are represented in red. In the case $\varepsilon = 0$ there is an infinity of stable solutions represented by the large plain red circle. Small plain red disks represent stable tuning curves, small red circles represent unstable tuning curves. These diagrams are valid for $\sigma > \sigma_0$, ε small and $\chi_3 \lesseqgtr 0$. The arrows indicate the direction of the flow for some trajectories.

condition is satisfied we call the tuning curve $TC_{\pi/2}$ an illusory persistent state of the Ring Model, the 90 degrees illusion, since it corresponds to the fact that, even if the thalamic input is peaked at the zero degree orientation, the Ring Model may stay for a long time (compared to τ) in the neighbourhood of a state corresponding to a tuning curve peaking at 90 degrees! In other words, even if the thalamic input may "say" 0 degrees, the hypercolumn of orientation "says" 90 degrees (for some time).

Remark 33. The case $\chi_3 > 0$ does not correspond to a biological plausible behaviour of the network. Indeed, we will see in the discussion that the nonlinear gain σ must be less than σ_0. In this case, it can be shown that the contrast response function, i.e. the function $\max_\theta TC(\theta)$, as a function of the contrast ε is not continuous. This is not supported by biological data (see for example [Chalupa 2004]).

9.3.2 Finding the tuning curves, case $N = 2$

The previous results may seem to depend very much on the type of simple connectivity function that we have assumed so far. In fact this is not so. By adding one more mode to this function, we can better approximate, as shown in figure 9.5 an arbitrary Mexican-hat type of connectivity function which preserves the structure of the local excitation and the lateral inhibition.

9.3.2.1 Case of no stimulus, $\varepsilon = 0$

The tuning curves without input are now solutions of the nonlinear equations (9.14). For reasons that are detailed in the appendix E.2, we first look at the case where the sigmoid function S is zero at the origin, *i.e.* we formally replace S by $S_0(x) =$

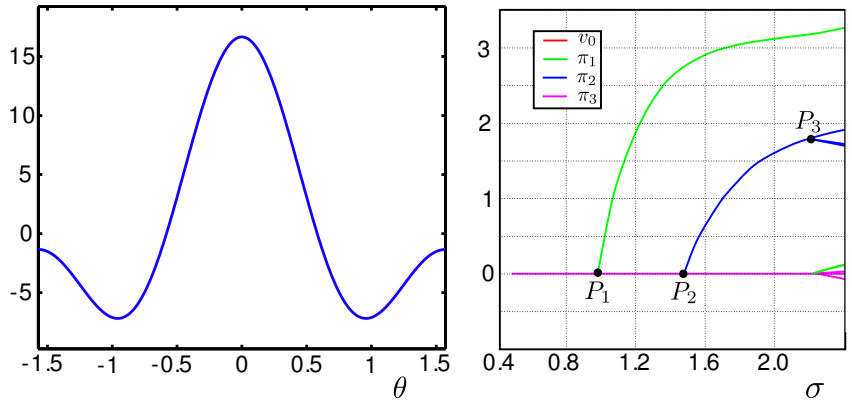

Figure 9.5: Left: Connectivity function used in the example described in the text. Right: Plot of the solutions obtained with the centered sigmoid S_0, see text, instead of S as functions of the nonlinear gain σ. Each solution is made of a 4-tuple (red, green,blue,violet). The parameter values are $J_0 = -1, J_1 = 9, J_2 = 6.66$, $T = 0$, $\varepsilon = 0$. The slightly 'wavy' aspect of the green branch from P_1 is a numerical artefact of the approximation of the centered sigmoid S_0 by polynomials, see the appendix E.1 for details. Note that, as expected because we are on the Orbit Space, the values of π_1 and π_2 are positive, see text. The discrepancy between the theoretical values of P_1, P_2 and the ones numerically obtained comes from our polynomial approximation of the sigmoid.

$S(x) - S(0)$. We see on the graph of solutions in the coordinates $(v_0, \vec{\pi})$ shown in figure 9.5 Right that there are two bifurcated[12] branches from the trivial solution $(v_0, \vec{\pi}) = 0$, at the points, noted P_1 and P_2, corresponding to the values $\sigma_1 < \sigma_2$ of the nonlinear gain. Considering again figure 9.5 Right, it motivates the following remarks:

1. The first bifurcated branch from P_1 reaches high values well before the one bifurcated from P_2.

2. The Orbit Space reduction procedure allows to compute numerically such secondary bifurcation points as P_3 which might produce stable solutions. These are undesirable from a biological viewpoint because they produce stable multimodal stationary solutions, hence not tuning curves.

The stability analysis shows that the branch bifurcating from P_1 is stable and corresponds to a continuum of stable tuning curves parametrized by the phase angle φ and given by:

$$\forall \varphi \quad TC^1_\varphi(\theta) = S_0 \left[\sigma \left(v_0^f + \sqrt{\pi_1^f J_1} \cos_2(\theta + \varphi) \right) \right]$$

[12] These are not regular bifurcations because we are working on the Orbit Space.

The same analysis shows that the branch bifurcating from P_2 (before P_3) is unstable and corresponds to a continuum of solutions:

$$\forall \varphi \quad TC^2_\varphi(\theta) = S_0\left[\sigma\left(v_0^f + \sqrt{\pi_2^f |J_2|}\cos_4(\theta+\varphi)\right)\right]$$

This shows that in order to have unimodal stable stationary solutions, hence tuning curves, it is necessary that $\sigma_1 < \sigma_2$ or equivalently $J_2 < J_1$ because the nonlinear gains which produce the Pitchforks are $S_0'(0)\sigma_i = \frac{2}{J_i}$, $i = 1, 2$. This formula explains the differences in the ranges of values of σ in figures 9.3 Left, 9.5 Right and 9.6. Moreover, since π_1^f quickly reaches high values when σ increases, $TC_0^1(0)$ is close to 1: the response does not depend upon the contrast ε of input from the LGN. *This implies that the working range of the nonlinear gain σ is close to the value σ_1.*

It is now possible to understand the diagram of solutions shown in figure 9.6 obtained with the regular sigmoid S as a deformation of the diagram shown in figure 9.5 Right. As in the case $N = 1$, the bifurcated branches will persist because we have shown in appendix E.3 that there is always a Pitchfork bifurcation for the regular nonlinearity S.

We again notice that the first branch bifurcating from P_1 (in green in figure 9.6) is quickly reaching high values and that the tuning curve is now asymmetric (this is much easier to see in the middle part of figure 9.7). This is because the π_2, π_3 components (in blue and magenta in figure 9.6) are not zero unlike in the case $N = 1$. The stable tuning curve corresponding to the first bifurcated branch is given by

$$TC(\theta) = S\left[\sigma\left(v_0^f + \sqrt{\pi_1^f J_1}\cos_2(\theta) + \underbrace{\sqrt{\pi_2^f |J_2|}}_{small}\cos_4(\theta+\varphi_2-\varphi_1)\right)\right] \tag{9.18}$$

where $z_1 = \sqrt{\pi_1}e^{2i\varphi_1}$, $z_2 = \sqrt{\pi_2}e^{4i\varphi_2}$, and $\pi_1\sqrt{\pi_2}\cos_4(\varphi_2-\varphi_1) = \pi_3$. Note that φ_1 and φ_2 are arbitrary which produces an infinity of tuning curves.

We have plotted in figure 9.7 examples of the tuning curves for three values of the nonlinear gain σ that are slightly larger than the values corresponding to the three bifurcation points P_1, P_2 and P_3 in figure 9.6. These tuning curves are obtained by reading from figure 9.6 the 4-tuple $(v_0, \vec{\pi})$. This yields, through the relation $\pi_1\sqrt{\pi_2}\cos_4(\varphi_2-\varphi_1) = \pi_3$, the value of $\varphi_2 - \varphi_1$ that is needed in equation (9.18). Notice the unstable multimodal tuning curves that appear once the stable tuning curve has saturated (right plot in figure 9.7). This is an indication that the nonlinear gain should not be too high, otherwise most responses of the network will be saturated.

9.3.2.2 When there is a stimulus, $\varepsilon > 0$

If we switch on the LGN, the contrast ε becomes nonzero. The external current is given by $I_{ext} = I_0 + I_1\sqrt{J_1}\cos_2 + I_2\sqrt{|J_2|}\cos_4$ (see section 9.2.1). If $I_1 I_2 \neq 0$, we expect a finite number of solutions because (9.8) does not commute with the

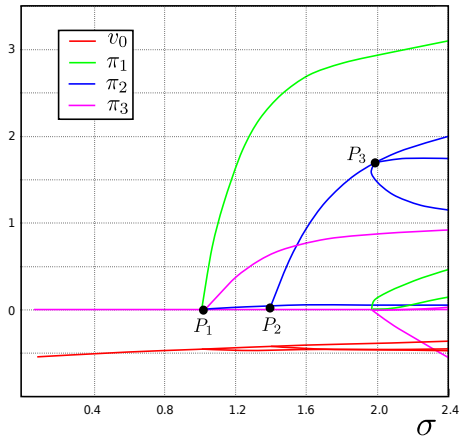

Figure 9.6: Plot of the solutions obtained with the regular sigmoid S as a function of the nonlinear gain σ. Case $J_0 = -1, J_1 = 9, J_2 = 6.66,\ T = 0\ \varepsilon = 0$.

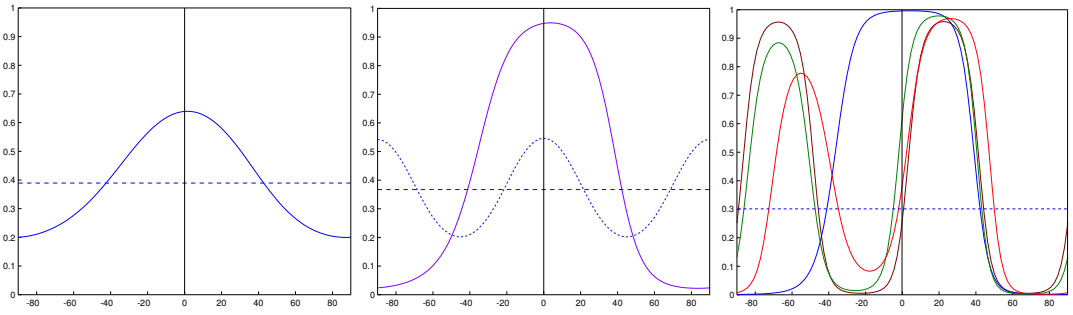

Figure 9.7: Tuning curves at nonlinear gains $\sigma = 1.04$ (left), $\sigma = 1.42$ (middle), and $\sigma = 2.32$ (right) when the input is equal to 0, see text. On the left and in the middle, stable tuning curves are shown in continuous line, unstable ones in dotted lines. Stability is not shown in the plot on the right, except for the null solution. The other parameters are the same as in figure 9.6.

symmetry group $O(2)$ anymore. More precisely, the same argument as in the case $N = 1$ shows that we can interpret (9.8) as a perturbation of (9.13) when ε is small. Hence, when the nonlinear gain σ is close to that of P_1 we have $z_2 \approx 0$ for ε small. Since the equations

$$\begin{cases} -v_0 + B_0(v_0, z_1, 0) + \varepsilon \tilde{I}_0 = 0 \\ -z_1 + B_1(v_0, z_1, 0) + \varepsilon \tilde{I}_1 = 0 \end{cases}$$

are the same as in the case $N = 1$ when $z_2 = 0$, they do not change much when $z_2 \approx 0$ and the 90 degrees illusory persistent state found in the previous section remains: there are two tuning curves, one peaking at the same value of the orientation as the external input I_{ext} and one translated by 90 degrees. This analysis is confirmed by the results of the numerical computations shown in figure 9.8 where we show the solutions of (9.8) for $N = 2$, $I_0 = 1 - \beta$, $\sqrt{J_1}\tilde{I}_1 = \beta$, $\sqrt{|J_2|}I\tilde{I}_2 = 0.1\beta$.

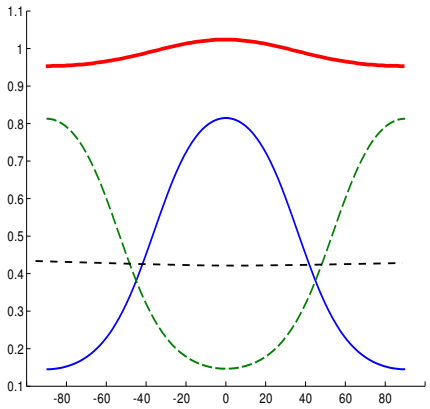

Figure 9.8: The tuning curves TC_0 and $TC_{\pi/2}$ for $\sigma = 1.04$, $\varepsilon = 0.01$, $x_0 = 0$, $T = 0$, $J_1 = 9$, $J_2 = 6.66$, $\beta = 0.05$ and $\tilde{I}_0 = 1 - \beta$, $\sqrt{J_1}\tilde{I}_1 = \beta$, $\sqrt{|J_2|}\tilde{I}_2 = 0.1\beta$. I_{ext} is plotted in red. Notice the unstable weakly tuned tuning curve shown in black and the unstable $TC_{\pi/2}$ in green.

9.3.3 Arbitrary number of modes in the connectivity function

We can perform the same computations using more modes, this will only bring in more stationary solutions. Because these stationary solutions only appear once the stable unimodal tuning curve has saturated, these high values for the nonlinear gain σ are biologically irrelevant. Notice also that the neuronal illusory persistent states found in the case $N = 1$, $J_1 > 0$ are still present for $N > 1$, $J_1 > 0$, as shown for example in figures 9.7 and 9.8. Indeed, as seen in the previous section, they only depend upon the fact that the network features a Pitchfork bifurcation at the point noted P_1 in figures 9.5 Right and 9.6 and this is always the case for any value of the number N of modes if the coefficients J_i satisfy the mild constraints we have described previously and that we summarize in the next section 9.4.

9.4 Dynamical 90 degrees illusory persistent state

In the last two sections, we found two cortical representations of the same external stimulus: TC_0, $TC_{\pi/2}$. An obvious set of questions is how can we bring a hypercolumn of orientation into each of these two states? Can we drive the cortical state to the illusory persistent state $TC_{\pi/2}$ using only the stimulus I_{ext}? We answer them positively in the next two sections.

9.4.0.1 Rotating the stimulus back and forth

Note that the tuning curve $TC_{\pi/2}$ is very close to the cortical response of the network to a vertical DG. We first present a horizontal DG to put the system in the TC_0 state. We then slowly rotate the DG to a vertical DG and stay there for some time Δt. The network follows the stimulus and its response is peaked at $\pi/2$, the longer Δt is, the closer to $TC_{\pi/2}$ the cortical state will be. We then suddenly change the stimulus back to a horizontal DG and since the responses of the network to vertical/horizontal DGs are very close, the cortical state will remain close to the state peaked at $\pi/2$, the one it is in just before the sudden change of the stimulus. As $TC_{\pi/2}$ and TC_0 have opposite transverse dynamical behaviour, we deduce that the cortical state will remain close to $TC_{\pi/2}$ at least for a time interval of the order of Δt. This is reminiscent of the after-effect illusion and can be confirmed by numerical simulation.

The resulting effect is shown in figure 9.9 when the time variation of the stimulus angle θ_{aff} of the stimulus in equation (9.3) is given by

$$\theta_{aff}(t) = \begin{cases} \frac{\pi}{2}\min(\frac{t}{2000}, 1) & \text{if } t \in [0, 2000]ms \\ \frac{\pi}{2} & \text{if } t \in [2000, 2e4]ms \\ 0 & \text{if } t > 2e4ms \end{cases}$$

This figure shows that after the system has been put in the state $TC_{\pi/2}$ for about 15s, it stays there for roughly the same amount of time. This is due to the fact that the eigenvalues corresponding to the stable and unstable states have the same magnitudes and opposite signs.

9.4.0.2 Using a mixture of the two stimuli

This second dynamical stimulus is very close in principle to the one presented in the previous section. Instead of rotating the DG, we change its contrast as follows. Let us note I_0^{DG} the horizontal DG and $I_{\pi/2}^{DG}$ the vertical one, the thalamic input to the hypercolumn of orientation takes the form

$$I_{ext}(t) = (1 - \psi(t))I_0^{DG} + \psi(t)I_{\pi/2}^{DG}$$

where $\psi(t)$ is the function shown in figure 9.10 satisfying $\psi(t_f) = 1$. We check numerically, using the dynamics given by equations (9.8), that the hypercolumn stays in the cortical state TC_0 (see figure 9.11) for roughly 10s after the stimulus

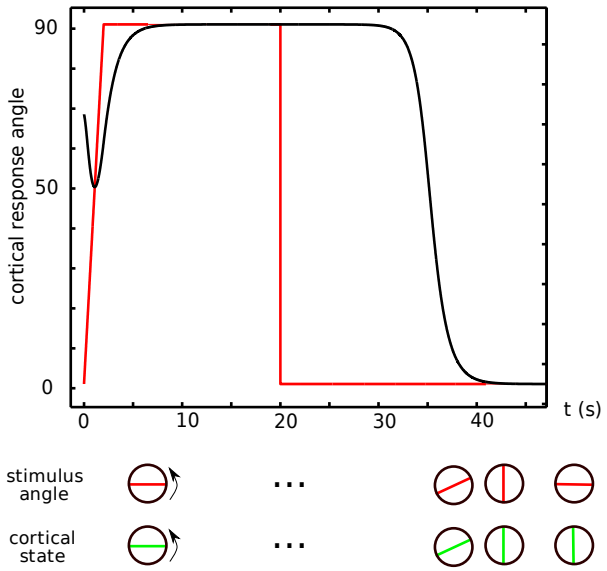

Figure 9.9: Plot of the stimulus angle θ_{aff} (in red) and the cortical angle response φ (in black), both as functions of time. Note that the stimulus drives the network into a state that is very close to its expected state when presented with a vertical DG and that it stays there even after the input has been switched to a horizontal DG. The parameters are the same as in figure 9.3. The time-scale parameter is $\tau = 10ms$.

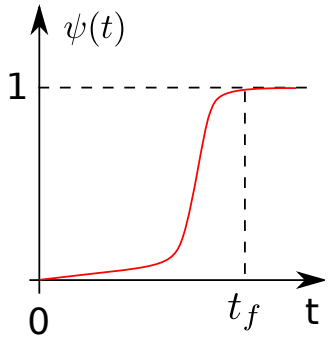

Figure 9.10: Plot of the function ψ allowing to vary the contrast of the thalamic input, see text.

changes from a horizontal DG to a vertical DG. Being an illusory persistent state, hence unstable, after these 10s the cortical state aligns itself with the stimulus.

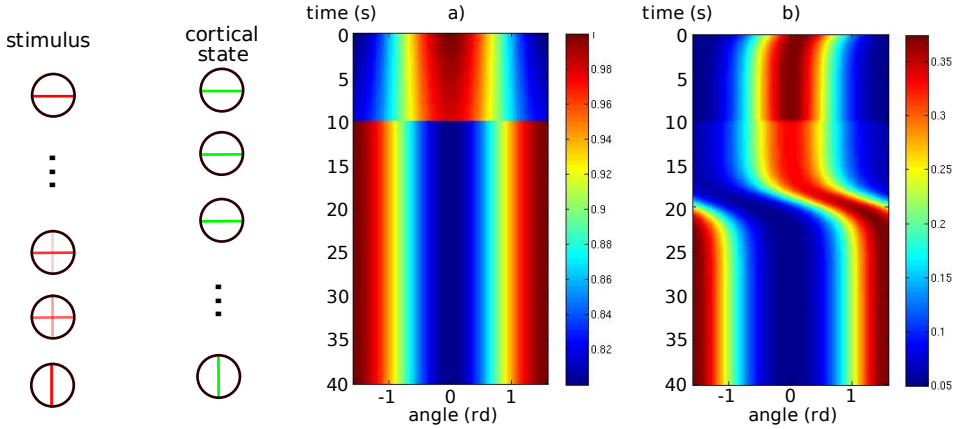

Figure 9.11: The vertical direction represents time (s), the horizontal one the orientation (rd). Left: Representation of the dynamical stimulus. a) spatio-temporal representation of I_{ext}. The stimulus starts as I_0^{DG} to become a mixture of I_0^{DG} and $I_{\pi/2}^{DG}$ and finishes as a pure $I_{\pi/2}^{DG}$. b) plot of the network response. It stays in the cortical state TC_0 before evolving to $TC_{\pi/2}$. The parameters are the same as in figures 9.3. The time-scale parameter is $\tau = 10ms$.

9.5 Discussion

In the previous technical sections, we have computed the tuning curves and shown how the network responded to stimuli. We will now tune the parameters to have TCs that are closer to experimental TCs. By doing so, we will constrain all the parameters. Hence, the working regime of the model will be imposed by experimental constraints. Then, we study the TC dependency on the stimulus contrast.

9.5.1 Parameter tuning

We provide a detailed account of the functional impact of the parameters T, σ, J_1 in the model. The influence of the external stimulus is analysed in the next subsection 9.5.2. It turns out that the combination of mathematical and biological constraints fixes their values. We first note that the requirement for stable unimodal responses, the tuning curves, is a very strong constraint. Indeed, it implies that the first Pitchfork bifurcation, that occurs when σ reaches σ_0, the first bifurcation point, must correspond to the first cosine mode, which requires

$$J_1 \geq 0, \quad J_1 > J_i \quad \forall i \neq 1$$

This in turn gives the range for the nonlinear gain σ: it should be large enough to produce tuning curves that are not saturated. If the tuning curves are saturated,

they do not vary with the input contrast ε anymore, in contradiction with the biological measurements. This fixes $\sigma \approx \sigma_0$. The next subsection 9.5.2 will show that necessarily[13]:

$$\sigma \precsim \sigma_0.$$

The next constraint comes from the width of the TCs whose experimental value (see chapter 1) is centered around 60^0. The width is defined from the values at which the tuning curve vanishes. As the TCs in our model do not vanish, in contrast to [Ben-Yishai 1995], our width is not well-defined. This is the reason why we prefer to use the width at half height whose value should therefore be roughly centered around 30^0. This width at half height, noted $\delta(\sigma, J_1, T)$, is a function of σ, J_1, T and can be computed analytically (see appendix E.4): for $\sigma < \sigma_0$, $\delta(\sigma, J_1, T) = 45^0$ because the cortical state is untuned, then the function $\sigma \to \delta(\sigma, J_1, T)$ appears (numerically) to increase toward a limit. For different pairs (J_1, T), we compute $\lim_{\sigma\to\infty} \delta(\sigma, J_1, T) = \delta_\infty(J_1, T)$. The result is shown in figure 9.12 Left, it does not depend on the threshold T. One can check that the widths at half height of the TCs in figures 9.3 and 9.7 are in agreement with the values of figure 9.12 Left. It follows that J_1 should be ≤ 2 in order to produce reasonable widths at half height for the TCs, *i.e.* widths at half-height around 30^0.

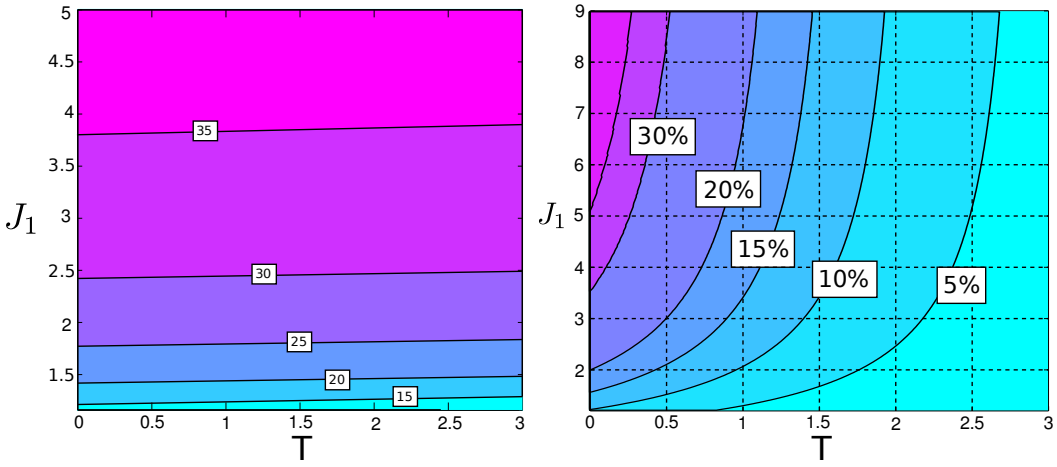

Figure 9.12: Left: Plot of $\frac{1}{2}\delta_\infty(J_1, T)$ as a function of (J_1, T). Right: plot of the spontaneous firing rate $S(\sigma_0 v_0^f(\sigma_0))$ which is also equal to $-v_0^f(\sigma_0)$.

The last constraint is the spontaneous firing rate (when $\varepsilon = 0$). As the network is working close to the Pitchfork bifurcation, the spontaneous firing rate is approximated by $S(\sigma_0 v_0^f(\sigma_0))$. We need to find this value for different pairs (J_1, T) which is done by solving (9.16) numerically. We chose this rate value to be between $5\% - 10\%$ which resulted in $T = 2$ (see figure 9.12 Right).

To conclude, the combination of mathematical and biological constraints leads to the choice $J_1 = 1.5,\ T = 2$ which yields $\sigma_0 \approx 40$.

[13] The following notation means below and close to σ_0.

Remark 34. *Numerically, we find that, for these values of the parameters,* $\chi_3 < 0$ *which produces a supercritical Pitchfork as shown in figure 9.2 Left. This is the reason why we only analysed this case in section 9.3.*

9.5.2 Perception threshold

Having set our parameters, we now discuss further the conditions for the appearance of tuning curves (*i.e.* stationary solutions such that $z_1 \neq 0$, $\sqrt{J_1}|z_1| >> \sqrt{|J_i|}|z_i|$, $i > 1$) when the external input is switched on: $\varepsilon > 0$. What condition on the external input must be satisfied in order to produce such stationary solutions whose width at half height varies slowly with the contrast ε? We consider only the case $N = 1$, because since the nonlinear gain σ is close to the Pitchfork bifurcation point σ_0, it does not restrict the generality of our discussion. We have seen (see figure 9.3 with the black dots indicating turning points) that if a tuning curve exists, there are two tuned cortical responses and one untuned. Moreover, for each contrast ε, there is a value $\sigma_c(\varepsilon)$ of the nonlinear gain σ below which the two tuning curves disappear, we call it a turning point[14]. When varying ε, we can look for the value of the nonlinear gain σ (if there is one) at which a turning point occurs: it is an indication that tuning curves do exist for higher nonlinear gains, but also, it is an indication that the illusory persistent state $TC_{\pi/2}$ can be produced by the network. The TRILINOS package we use in most our simulations features the numerical continuation of the locus of a turning point. As a result of this, starting with the turning point of figure 9.3, we were able to produce the locus $(\varepsilon, \sigma_c(\varepsilon))$ of the turning points in the plane (ε, σ) as shown in figure 9.13 Left. The blue curve starts at $(0, \sigma_c(0)) = (0, \sigma_0)$ and decreases to a minimum σ_{min}. Above the blue curve, the stable response of the network is a tuning curve. Note that in the region labeled `Stimulus driven`, there is a unique stationary solution given by the value of the external input. This parameter region is not in the operating range of the model, because the contrast of external input is too large. Indeed, in the case of large contrasts ε, the stimulus has too much weight compared to the cortical connections: it is as if the model were purely feedforward. In a similar fashion, below the dashed horizontal line labelled $\sigma = \sigma_{min}$, for any contrast ε there is a unique stationary solution which is poorly tuned (see figure 9.13 Right Top). This is not consistent with experimental findings and therefore this range of parameters does not belong either to the working range of the model. We conclude that we must have $\sigma > \sigma_{min}$.

Up until now, we have discussed the network behaviours with the contrast ε fixed in order to evaluate the most plausible value of the nonlinear gain. It is now time to simulate the network response, *i.e.* by fixing the value of the nonlinear gain σ and varying the contrast.

[14] It results from the opening of the Pitchfork bifurcation that exists when $\varepsilon = 0$, hence σ_c depends on ε and $\sigma_c(0) = \sigma_0$.

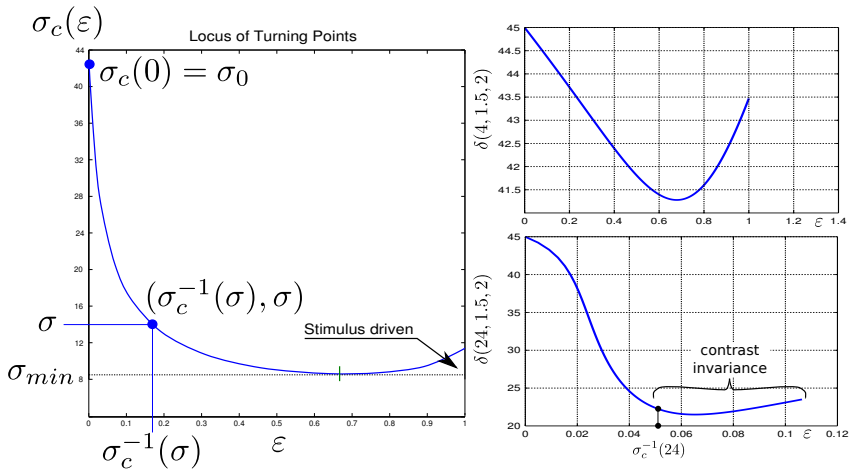

Figure 9.13: Left: Locus of the turning points as function of (ε, σ). The parameters are $J_1 = 1.5, T = 2$. Right: plot of the width at half height of the solutions for a nonlinear gain $\sigma = 4 < \sigma_{min}$ (top) and for $\sigma = 24 < \sigma_0 \approx 43$ (bottom). In both cases and in order to avoid saturation of the tuning curve, the width is plotted for contrast values such that the maximum firing rate is below 90%. Note that we have represented the perception threshold $\sigma_c^{-1}(24)$ with a black dot.

If the nonlinear gain is above the Pitchfork bifurcation point $\sigma > \sigma_0$, the cortical response for any contrast $\varepsilon \in [0,\ 1]$ is a tuning curve $V^f(\theta)$ whose tuning angle $\arg\max_\theta V^f(\theta)$ is randomly selected. Indeed, in this case, there is a continuum of tuning curves and the $\arg\max_\theta V^f(\theta)$ depends on the current state of the network. This is true even for null contrast. It is more biologically relevant that the network operates in the regime $\sigma < \sigma_0$, because otherwise the neurons would have a high firing rate (around 60% of their maximum firing rate, see figure 9.3) even though no stimulus is present, this is a waste of energy.

For $\sigma_{min} < \sigma < \sigma_0$, the situation is different. According to the blue curve in figure 9.13 Left, there exists a particular contrast $\sigma_c^{-1}(\sigma)$ for which a turning point occurs. More precisely, if the contrast is below this value, the network features a single cortical state which is poorly tuned. If the contrast is above this value, the network features three cortical states, two of which being tuned and aligned with the stimulus, the third one, poorly tuned, can be thought as a "remnant" of the cortical state when the contrast was not high enough to generate a tuned response. Hence, we may see this particular value $\sigma_c^{-1}(\sigma)$ of the contrast as a *perception threshold*: below this value, the network response is poorly tuned whereas it is tuned and in agreement with the stimulus if the contrast is above this value. It follows that the working range of the nonlinear gain is $\sigma \in (\sigma_{min}, \sigma_0)$.

Hence, it is natural to call the values $\sigma_c^{-1}(\sigma)$ for $\sigma \in (\sigma_{min}, \sigma_0)$, the perception thresholds. By definition, the perception threshold is null at the bifurcation point σ_0 and it becomes larger as the nonlinear gain of the network is set to a value close to σ_{min}. Hence, if the nonlinear gain is set to a value just below σ_0, the perception

threshold is tiny, even a small contrast will trigger a tuned response whereas for a smaller nonlinear gain, the tuning width becomes constant for contrasts above the perception threshold (see figure 9.13 Right Bottom).

The existence of the perception threshold in experiments can be studied through the dynamical stimulus of section 9.4. Indeed, *only* above the perception threshold, the network does feature the two tuned states (in particular the illusory persistent state) that are needed for the dynamical stimulus.

Also, intuitively, one may understand the threshold contrast $\sigma_c^{-1}(\sigma)$ as the boundary between a regime where the recurrent computations are not influenced by the stimulus and a regime where the recurrent computations are negligible compared to the LGN drive.

One may ask whether figure 9.13 is generic: under which conditions does the locus of the values $(\varepsilon, \sigma_c(\varepsilon))$ corresponding to a turning point have a shape like the one in figure 9.13, *i.e.* first decreasing when ε increases, reaching a local minimum σ_{min}, and increasing again? Using the implicit functions theorem, it can be shown that $\frac{\partial \sigma_c}{\partial \varepsilon}|_{\varepsilon=0} < 0$ when $J_0 < 0$, *i.e.* the curve is locally decreasing for increasing values of ε. Hence we conclude that the local behaviour around $(0, \sigma_c(0))$ in figure 9.13 is quite general in the case $J_0 < 0$. This analysis provides a tighter constraint on the nonlinear gain σ, it should be just below σ_c: $\sigma \lesssim \sigma_c$.

9.5.3 Illusory persistent states

The fact that the cortical network shows two states corresponding to perpendicular orientations in response to a single stimulus can also be put in resonance with some published models of the cortical primary visual area (see [Bressloff 2001b] for a spatial network of Ring Models). Indeed, in this study of planforms in relation to visual hallucinations, it may come as a surprise to the attentive reader that most of the stable planforms (in the cortical space) do not respect the good continuation principles of contours since adjacent hypercolumns show responses corresponding to orthogonal orientations (see for example the stable contoured rolls on a square lattice). However once we agree that, for a hypercolumn, two orthogonal states are closely related, this becomes perhaps less surprising.

We relate our formalism to previous studies of recurrent models of orientation selectivity by first noting that the 90 degrees illusory stationary solution was not reported in [Ben-Yishai 1995] although they share the same assumptions as ours.

In [Carandini 1997], the authors used a (voltage based) Ring Model in order to explain some of the features of the complicated spiking network of [Somers 1995]. Although they used the non-saturating nonlinearity $S(x) = \max(x, 0)$, they observed that narrowing the spatial extension of inhibition leads to multimodal responses which they interpreted as neuronal illusions. This can be understood within our formalism: decreasing the spatial extent of inhibition introduces more Fourier terms (possibly with high values) in the connectivity J and can produce stable multimodal responses to a unimodal stimulus (see section 9.3.2).

Under what conditions do the 90 degrees illusory persistent states survive in

a network of Ring Models? Can we find similar illusory persistent states in more sophisticated networks and which experiments could confirm/invalidate our predictions? We just discussed the matter of a network of Ring Models with the study of [Bressloff 2001b]. In [Blumenfeld 2006], the authors used a generalization of the Ring Model with a very similar connectivity to explain the spontaneous activity observed in optical imaging recordings. Although they identified the 90 degrees illusory persistent state, they did not explain how this additional cortical state could lead to a strongly history dependent cortical response. This is the subject of the next chapter.

Finally, despite its ability to reproduce several experimental facts, the Ring Model lacks some anatomical data support because it does not use realistic cortical circuitry. Note that we have provided some clues for the construction of an effective connectivity in the orientation domain from realistic cortical connections in chapter 8. Recently, Shelley *et al.* (see [Shelley 2002]) introduced a reduced system of a computationally intensive spiking neuron network model of a hypercolumn with realistic cortical circuitry. It could be interesting to look for neuronal illusions/illusory persistent states predicted by their model using the techniques developed in part II. In chapter 11, we introduce a V1 model that is very close to the rate model the Shelley *et al.* derived in [Shelley 2002] from their spiking network.

9.6 Conclusion

We have pushed further the study, started in part II, of the mathematical properties of the Ring Model of orientation tuning and of some of their biological implications. This was achieved by taking into consideration the rich symmetries of the network. The reduced equation (9.17) was already found in [Bressloff 2002a, Bressloff 2002b, Bressloff 2005b] where the authors used weakly nonlinear analysis (see also [Ermentrout 1998]) as well as the 'illusory' tuning curve. However, the dynamics were not used to make this 'illusory' tuning curve appear.

For the first time to our knowledge in the field of neural networks, we have introduced the Orbit Space Reduction technique to deal with translation invariant connectivity kernels. This allowed us to find a suitable change of coordinates in order to remove the redundancy introduced by the symmetries. This is a generic technique that can be applied to many other problems in neuroscience. Using this reduction, we have shown that the exact shape of the connectivity function did not matter much as long as the first mode, $\cos_2$, was the first to bifurcate, *i.e.* to produce tuned solutions.

Our study has allowed us to discover an (unstable) tuning curve encoded in the network that represents an orientation orthogonal to that of the LGN input. This neural illusory persistent state can be thought of as a ghost of the first Pitchfork bifurcation, itself coming from the fact that the connectivity is an even function.

We have shown that it was possible to drive a hypercolumn to the illusory state by adding some dynamics in the stimulus: this gave rise to two dynamical effects

showing the strongly history dependent behaviour of the cortical state, one relying on rotating the stimulus, the other relying on changing its contrast. This is a strong prediction of the model that could possibly be tested experimentally. However, this seems difficult given the fact that the Ring Model does not take into account the lateral spatial connectivity that is present in the visual cortex and allows different hypercolumns of orientation to interact with each other.

It would be interesting to see if and how the illusory persistent states are modified when adding lateral spatial connections in a spatially organized network of Ring Models. This will be done in the next two chapters.

Finally our approach leads to a close to complete understanding of the role of each parameter in the Ring Model: the shape of the connectivity function through the weights J_i, the threshold T, and the nonlinear gain σ.

Chapter 10

The model of V1 by Blumenfeld *et al.*

In this chapter, we study the second model proposed in chapter 8 as a generalization of the Ring Model studied in the previous chapter. Despite the fact that it is able to account for experimental data such as orientation/selectivity maps, the model studied in this chapter is very close to the Ring Model:

- it is formally equivalent to a three-dimensional model,
- it features the perception threshold...

Nature rarely features the kind of symmetries that are fundamental to the Ring Model. It is the goal of this chapter to explore how the mechanism explained in chapter 8 is affected if we relax the symmetry assumption.

Contents

The authors in [Blumenfeld 2006] used data from optical imaging (OI) signals (see [Grinvald 1986, Blasdel 1986b, Vanzetta 2008]), to build an activity based model of V1. Their model is a generalization of the Ring Model (see chapter 9) to which the tools developed in Part II apply well. In particular, it is a 3D-model based on experimental data, which was originally designed to account for the appearance of the orientation maps in the spontaneous activity (see [Kenet 2003]). As such, their model is required to work near a static bifurcation in order to produce spontaneous activity (see chapter 8). The network in [Blumenfeld 2006] deals with the orientation feature. We have already emphasized in section 9.1.4 that such a network should feature the translation invariance in the orientation space. However, it is difficult to design a network, based on experimental data, that enjoys this symmetry and the model in this chapter does not (see also section 3.5). We will

show that the asymmetries produce ambiguous cortical activity at small contrasts and that it is only for a high enough contrast that the network is able to respond in agreement with the input, *i.e.* there is a perception threshold as we studied thoroughly in the previous chapter. We are also interested to know if the predictions about the dynamics, made in the case of the Ring Model in chapter 9, are still valid. Finally, this study will draw our final conclusions concerning the impact of symmetries on the existence of illusions/illusory persistent states.

The chapter is structured as follows. In the Introduction, we recall the basics of the optical imaging techniques and how to model its signal. Then, we give in section 10.2, the model equation and show how to build the connectivity of the network. We reduce the full network to a 3D system in 10.4 and study the spontaneous and evoked activities in sections 10.5 and 10.6. Based on the working range of the model, we build a dynamical stimulus which produces a characteristic response in section 10.7. Conclusions are drawn in section 10.8.

10.1 Introduction

The model in [Blumenfeld 2006] was designed with the aim of reproducing the results of the optical imaging (OI, see chapter 1) study in Kenet *et al.* ([Kenet 2003]), where activity patterns, similar to orientation maps,[1] were observed in the absence of an external stimulus. Let us formalise a bit the experiment. Let $\phi_i \in \left[-\frac{\pi}{2}, \frac{\pi}{2}\right]$, $i = 1 \cdots p$ be the DG angles (equidistributed) presented to the animal (a cat or a macaque whose cortices produce orientation maps) and let $S_{\mathbf{x}}^{\phi_i}$ be the magnitude of the cortical response as seen from optical imaging signals, at location $\mathbf{x}$ evoked by orientation ϕ_i. Let us recall how we compute the orientation map, *i.e.* the map of preferred orientations by neurons at a given location $\mathbf{x}$. We first compute the 'Fourier' transform

$$z_{\mathbf{x}} \equiv r_{\mathbf{x}} e^{2i\theta_{\mathbf{x}}} = \frac{2}{p} \sum_{j=1}^{p} S_{\mathbf{x}}^{\phi_j} e^{2i\phi_j}.$$

Then, the preferred orientation map is given by the map $\theta_{\mathbf{x}}$ and the selectivity is given by $r_{\mathbf{x}}$. The selectivity $r_{\mathbf{x}}$ is the maximal response at location $\mathbf{x}$ for all possible stimulus orientations. Note that pinwheels in this representation are "black", *i.e.* $z_{\mathbf{x}} \approx 0$.

The function $\phi \to S_{\mathbf{x}}^{\phi}$ is called the tuning curve (see definition 1.3.1) at location $\mathbf{x}$. Notice that it is different from the tuning curve we have considered in the Ring Model in chapter 9. Indeed, the voltage-sensitive dye optical imaging signal corresponds to post-synaptic membrane potentials (see [Sharon 2002, Grinvald 2004, Faugeras 2007, Markounikau 2010] and also [Chemla 2010a] for a review) rather than firing rates: the spikes are too fast to make a contribution to the signal. Hence,

[1] Obtained for example with a drifting grating (DG) stimulus

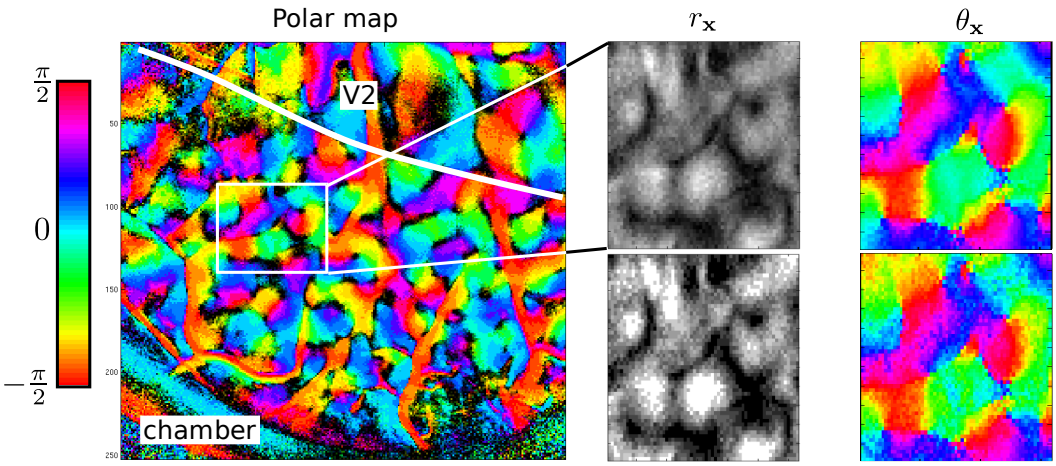

Figure 10.1: Left: plot of the polar map $z_{\mathbf{x}}$ of a part of the visual cortex in behaving macaques. The map displays the preferred orientation in colour superimposed to the selectivity (in grey). The white curve roughly delineates the boundary between V1 and V2 (which has larger orientation domains). The frontier of the opened skull is labelled "chamber". A part of the cortex is (numerically) selected (white rectangle of size 63×54) because it presents a small number of artefacts due to the presence of blood vessels (data not shown). The two figures on the top right are the selectivity map $r_{\mathbf{x}}$ and the preferred orientation map $\theta_{\mathbf{x}}$ of the selected rectangle. The two figures on the bottom right are the corrected maps to restore a rough uniform distribution of the values of $\theta_{\mathbf{x}}$ and a scaling of $r_{\mathbf{x}}$ (see text). Courtesy of A.Reynaud, I.Vanzetta and F.Chavane.

the tuning curves $S^\phi_{\mathbf{x}}$ correspond to membrane potentials tuning curves whereas we studied firing rate tuning curves in the previous chapter. This also suggests (see [Faugeras 2007]) the use of an activity based model (see chapter 2)

$$\dot{\mathbf{A}} = -\mathbf{A} + \mathbf{S}(\mathbf{J} \cdot \mathbf{A} + \mathbf{I}_{ext})$$

for the modelling of the membrane potential and the OI signal which is then assumed to be proportional to the total post-synaptic input $\mathbf{OI} = \mathbf{J} \cdot \mathbf{A} + \mathbf{I}_{ext}$. Here, $\mathbf{J} \cdot \mathbf{A}$ is the input due to recurrent connections and $\mathbf{I}_{ext}$ is the afferent input to the cortex: they are function of the cortical position $\mathbf{x}$. The spontaneous activity corresponds to the activity $\mathbf{A}$ when $\mathbf{I}_{ext} = 0$ whereas the evoked activity corresponds to the case when there a stimulus, *i.e.* $\mathbf{I}_{ext} \neq 0$. Note that the firing rate tuning curves at location $\mathbf{x}$ are modelled by a non-trivial (*i.e.* non constant) stationary state $\mathbf{A}(\mathbf{x})$ whereas membrane potential tuning curves, originated from the OI signal, are modelled by

$$\mathbf{OI} = \mathbf{J} \cdot \mathbf{A} + \mathbf{I}_{ext}. \tag{10.1}$$

10.2 Definition of the model parameters

Given the cortical responses $S^\phi_{\mathbf{x}}$ for different orientations ϕ, we would like to build a neural field model which produces spontaneous stationary signals $\mathbf{OI}_{spont} = \mathbf{J} \cdot \mathbf{A}$ (recall that in this case $\mathbf{I}_{ext} = 0$) similar to the signal $S^\phi_{\mathbf{x}}$ (see chapter 8 for this). The equation $\mathbf{OI}_{spont} = \mathbf{J} \cdot \mathbf{A}$ shows that the space of functions $S^\phi_{\mathbf{x}}$ for each orientation ϕ, is in the range of the integral operator $\mathbf{J}$. Given that this cortical activity is stationary, it suggests that the integral kernel $\mathbf{J}$ fixes this activity, *i.e.* $\forall \phi,\ S^\phi_{\mathbf{x}} \propto \mathbf{J} \cdot S^\phi_{\mathbf{x}}$. Hence, if one defines the space of tuning curves $\mathcal{E} \equiv \text{Span}\left\{\text{S}^\phi_{\mathbf{x}},\ \phi \in \left[-\frac{\pi}{2},\ \frac{\pi}{2}\right]\right\}$, then $\mathbf{J}$ acts as a projector on this space. It follows that we could choose the connectivity as

$$\mathbf{J}(\mathbf{x}, \mathbf{y}) = \int_{-\frac{\pi}{2}}^{\frac{\pi}{2}} S^\phi_{\mathbf{x}} S^\phi_{\mathbf{y}} d\phi. \tag{10.2}$$

The range of this operator is obviously included in the set of tuning curves $\mathcal{E}$. We could study the model with this connectivity but the different activities produced by the network is too large for a detailed analysis. Hence, we need to find a way to reduce the number of different possible activities. We can achieve this, as in [Blumenfeld 2006], by making the relationship between the cortical response $S^\phi_{\mathbf{x}}$ and the stimulus angle ϕ more explicit. Since the tuning curves tend to be unimodal and centred around the preferred orientation $\theta_{\mathbf{x}}$ (see for example [Benucci 2009]) at location $\mathbf{x}$, it seems reasonable to approximate $S^\phi_{\mathbf{x}}$ by

$$M^\phi_{\mathbf{x}} \equiv r_{\mathbf{x}} \cos(2\theta_{\mathbf{x}} - 2\phi) \approx S^\phi_{\mathbf{x}}. \tag{10.3}$$

In this case, equation (10.2) writes

$$\mathbf{J}(\mathbf{x}, \mathbf{y}) = r_{\mathbf{x}} r_{\mathbf{y}} \cos(2\theta_{\mathbf{x}} - 2\theta_{\mathbf{y}}) \frac{\pi}{2}. \tag{10.4}$$

We generalize it slightly by:

$$\mathbf{J}(\mathbf{x},\mathbf{y}) = J_0 + J_1 r_{\mathbf{x}} r_{\mathbf{y}} \cos(2\theta_{\mathbf{x}} - 2\theta_{\mathbf{y}}), \quad J_1 > 0. \tag{10.5}$$

Note that this connectivity connects locations with similar preferred orientations in a patchy manner because the regions of similar preferred orientations are clustered (see figure 10.1 and [Gilbert 1989, Bosking 1997, Kisvarday 1997]). Also, the strength of the connections is lower around pinwheels (because $r_{\mathbf{x}} \approx 0$) than in the inter-pinwheels region, also called linear zones. This is supported by [Yousef 2001] for the cat but it seems in contradiction with [Mariño 2005] (also for the cat). The connectivity (10.5) will be used in this chapter. It acts on the cortical activity $\mathbf{A}$ in the compact form:

$$\mathbf{J} \cdot \mathbf{A}(\mathbf{x}) = \int_{\Omega} \mathbf{J}(\mathbf{x},\mathbf{y}) \mathbf{A}(\mathbf{y},t) \frac{d\mathbf{y}}{|\Omega|},$$

where $|\Omega|$ is the area of the cortex Ω under study. Finally, the evolution of the cortical activity $\mathbf{A}$ is described by the standard rate equation

$$\tau \dot{\mathbf{A}} = -\mathbf{A} + \mathrm{Sig}\left[\sigma\left(\mathbf{J} \cdot \mathbf{A} + \mathbf{I}_{\mathrm{ext}}\right) - \mathrm{h}\right], \tag{10.6}$$

Sig is the sigmoid function $\mathrm{Sig(x)} = \frac{1}{1+\mathrm{e}^{-\mathrm{x}}}$, σ is the nonlinear gain and h is the threshold. We also define the firing rate function:

$$S(x) = Sig(x - h).$$

which allows to write (10.6):

$$\tau \dot{\mathbf{A}} = -\mathbf{A} + S\left[\sigma\left(\mathbf{J} \cdot \mathbf{A} + \mathbf{I}_{ext}\right)\right], \tag{10.7}$$

Remark 35. As in the previous chapter, the usual choice is to take σh for the threshold instead of h. We found it mathematically more convenient to use our scaling, the scope of the analysis is not reduced because we also vary h as a parameter.

The form of the connectivity $\mathbf{J}$ in (10.5) is a generalization of the connectivity (9.2) of the Ring Model but it also incorporates the selectivity map $r_{\mathbf{x}}$. Note that a similar model without selectivity has been studied in [Goldberg 2004]. In the following, we will consider an afferent input of the form

$$\mathbf{I}_{ext}(\mathbf{x}) = \varepsilon\left[1 + \beta r_{\mathbf{x}} \cos(2\theta_{\mathbf{x}} - 2\phi_{aff})\right], \tag{10.8}$$

where ε is the contrast and ϕ_{aff} is the stimulus orientation. Using the same reasoning as in section 9.1.3, we can show that this choice does not alter the generality of our study. For a time constant afferent input, (10.7) is formally equivalent, by the change of variables $\mathbf{A} \to \mathbf{J} \cdot \mathbf{A} + \mathbf{I}_{ext} = \mathbf{V}$ and $\mathbf{V} \to S(\sigma \mathbf{V}) = \mathbf{A}$ to a "formal" voltage based model:

$$\tau \dot{\mathbf{V}} = -\mathbf{V} + \mathbf{J} \cdot S\left(\sigma \mathbf{V}\right) + \mathbf{I}_{ext}. \tag{10.9}$$

This form is more convenient for the following study, this is why we will use (10.9) instead of (10.7).

Remark 36.In all the numerical experiments of this chapter, we use $J_0 = -1$, $J_1 = 1.5$, $h = 1$, $\beta = 0.1$. *This is motivated by the parameters values used in chapter 9 except for the threshold* h *which is equal to* 1 *here. In the last chapter, the value of* h *was constrained by the spontaneous firing rate. Here, the spontaneous membrane potential is not constrained by OI data as the "blank", i.e. the mean response of the OI signal, is removed from the OI signal to yield* $S^{\phi}_{\mathbf{x}}$.

From (10.1), we find that $\mathbf{OI} = \mathbf{V}$: this further motivates the use of the voltage-based representation. From the expressions of the connectivity (10.5) and the afferent input (10.8), we find that the stationary OI signals are scaled/shifted versions of the orientation maps, *i.e.* $\mathbf{OI} \propto A + Br_{\mathbf{x}}\cos(2\theta_{\mathbf{x}})$ for some constants A and B.

10.3 Symmetry/statistical properties of the connectivity J

For the upcoming computations, it is useful to assume that the selectivity map $r_{\mathbf{x}}$ is normalized to satisfy:

$$\int_{\Omega} r_{\mathbf{x}}^2 \frac{d\mathbf{x}}{|\Omega|} = 1,$$

which amounts to a rescaling of all the values $r_{\mathbf{x}}$. If the part of the cortex Ω under study is large enough, we can expect (see also section 9.1.4) that the distribution of preferred orientation $\theta_{\mathbf{x}}$ over the cortex Ω is almost uniform otherwise the processing of the afferent input $\mathbf{I}_{ext}$ by the cortex would favour an orientation over the others. Hence, given an experimental orientation map, we perform a statistical normalization of the data, as explained in [Blumenfeld 2006]. This is done in order to obtain a more uniform distribution for the preferred angles (see figure 10.1). Notice in figure 10.1 that it does not change much the maps $r_{\mathbf{x}}, \theta_{\mathbf{x}}$.

10.4 Simplification of the equations

We simplify the full equations (10.9) by using the particular form of the connectivity function $\mathbf{J}$ in (10.5). This yields a system of three equations which is easier to analyse as we show in the next sections. Following appendix A.5, we write $\mathbf{OI}(\mathbf{x},t) = \mathbf{V}(\mathbf{x},t) = v_0(t) + v_1(t)\sqrt{J_1}r_{\mathbf{x}}\cos(2\theta_{\mathbf{x}}) + v_2(t)\sqrt{J_1}r_{\mathbf{x}}\sin(2\theta_{\mathbf{x}})$ with $v_0, v_1, v_2 \in \mathbb{R}$ and obtain the equations:

$$\begin{cases} \tau\dot{v}_0 + v_0 &= J_0 \int\limits_{\Omega} S\left(\sigma V\right) \frac{d\mathbf{x}}{|\Omega|} + \varepsilon \\ \tau\dot{v}_1 + v_1 &= \sqrt{J_1} \int\limits_{\Omega} S\left(\sigma V\right) r_{\mathbf{x}} \cos(2\theta_{\mathbf{x}}) \frac{d\mathbf{x}}{|\Omega|} + \frac{\varepsilon\beta}{\sqrt{J_1}} \cos(2\phi_{aff}) \\ \tau\dot{v}_2 + v_2 &= \sqrt{J_1} \int\limits_{\Omega} S\left(\sigma V\right) r_{\mathbf{x}} \sin(2\theta_{\mathbf{x}}) \frac{d\mathbf{x}}{|\Omega|} + \frac{\varepsilon\beta}{\sqrt{J_1}} \sin(2\phi_{aff}) \end{cases} \tag{10.10}$$

Hence, we have reduced the original problem of solving (10.9) to the study of the 3D system (10.10). We need to find the triplets $\vec{v} \equiv (v_0, v_1, v_2)$ solutions of (10.10) in

order to identify the spontaneous/evoked cortical states. The spontaneous tuning curves are linked to the stationary solutions $\vec{v}^f$ for null contrast $\varepsilon = 0$, while the evoked tuning curves correspond to the case $\varepsilon \neq 0$. An *untuned* solution is a solution with $v_1 = v_2 = 0$ as opposed to a *tuned* solution. We would like to know when a tuned solution arises because it may correspond to an orientation map. We will see that spontaneous tuned activity is possible.

10.5 Study of the spontaneous activity

We start with the case with no stimulus, $\varepsilon = 0$. The analysis that follows is very similar to what we did in section 9.3.1 for the Ring Model of orientation tuning. The difficulty, here, is the absence of the network symmetries which helped us to build tuned activity in chapter 9. Hence, the problem at hand[2], is more related to the one we studied in section 3.5 where the symmetries were broken, than to the one in chapter 9. Let us recall the main results of section 3.5. If we consider the nonlinear gain σ as the bifurcation parameter, we can find up to 5 solutions to (10.10) when $\varepsilon = 0$ for a large enough nonlinear gain σ, 3 of which being stable.

It turns out that there are more than five spontaneous stationary states that emerge the experimental data shown in figure 10.1. The key to understand what happens here, is to "restore" the symmetries, it allows us to apply the study of chapter 9 and to interpret the results for (10.10) as a perturbation of the results in this chapter.

In order to make the link with the Ring Model more explicit, we change variables. We replace the spatial integration, *i.e.* the integration over $\mathbf{x}$, with an integration over the selectivity r and the preferred angle θ. As a result, we introduce a distribution function $P(r,\theta)$ such that $\frac{d\mathbf{x}}{|\Omega|} = P(r,\theta)drd\theta$. This is a formal change of variables between the cortical space and the space made of selectivity and preferred orientation (r,θ). Using this distribution[3], we can write (10.10) as:

$$\left\{\begin{array}{rcl} \tau\dot{v}_0 + v_0 &=& J_0 \int_0^R \int_{-\pi/2}^{\pi/2} S\left(\sigma V\right) P(r,\theta) dr d\theta \\ \tau\dot{v}_1 + v_1 &=& \sqrt{J_1} \int_0^R \int_{-\pi/2}^{\pi/2} S\left(\sigma V\right) r\cos(2\theta) P(r,\theta) dr d\theta \\ \tau\dot{v}_2 + v_2 &=& \sqrt{J_1} \int_0^R \int_{-\pi/2}^{\pi/2} S\left(\sigma V\right) r\sin(2\theta) P(r,\theta) dr d\theta \\ V &\equiv& v_0 + v_1\sqrt{J_1} r\cos(2\theta) + v_2\sqrt{J_1} r\sin(2\theta) \\ R &\equiv& \max_{\mathbf{x}\in\Omega} r_{\mathbf{x}}. \end{array}\right. \tag{10.11}$$

From section 10.3, we know that $P(r,\theta)$ can be written $\frac{1}{\pi}\widetilde{P}(r) + P_0(r,\theta)$, the *asymmetry* $P_0(r,\theta)$ being small. Indeed, the distribution of preferred orientations

[2] *i.e.* the one of finding the tuned solutions of (10.10)

[3] More precisely, we introduce the jacobian J_Φ of the map $\Phi : \mathbf{x} \to (r_{\mathbf{x}}, \theta_{\mathbf{x}})$ and it follows that $P(r,\theta) = \frac{|\det J_{\Phi^{-1}}|}{|\Omega|}$ where $J_{\Phi^{-1}}$ is the jacobian of the inverse map Φ^{-1}.

is almost uniform (see figure 10.2). It suggests to introduce a new problem rather than (10.11): let us consider the family of distributions $P_\alpha(r,\theta) = \frac{1}{\pi}\widetilde{P}(r) + \alpha P_0(r,\theta)$ and replace P in (10.11) by P_α. For $\alpha = 0$, we have a distribution of preferred orientations which is uniform whereas for $\alpha = 1$ we have the distribution obtained from the experimental data.

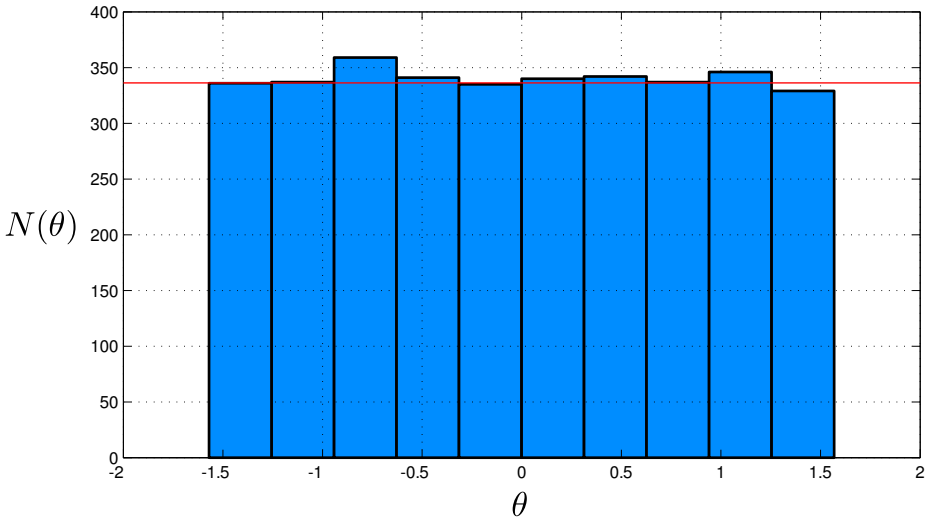

Figure 10.2: Distribution of the preferred orientations $\theta_{\mathbf{x}}$ for the experimental data shown in figure 10.1. The red line shows the level of uniform distribution if the orientations were equidistributed. The number $N(\theta)$ is related to the distribution $P(r,\theta)$ by $N(\theta) = \int_0^R P(r,\theta)dr \cdot N$ where $N = 3402$ is the number of points in the data and $R \equiv \max_{\mathbf{x}\in\Omega} r_{\mathbf{x}}$. The bin size is $\pi/10$.

In the case of the 'uniform' distribution (for $\alpha = 0$), it is easy to check that an untuned solution $\vec{v}^f(\sigma) = (v_0(\sigma), 0, 0)$ exists for all nonlinear gains σ. Using the result proved in appendix E.3, we know that from this untuned solution, a tuned solution emerges (or bifurcates) for a particular value of the nonlinear gain[4] σ_0. The precise value of σ_0 is not important. What is important is the value of σ compared to σ_0. How should we choose σ in order to see tuned spontaneous activity? The result is that if $\sigma > \sigma_0$, the network can produce spontaneous tuned stationary activity whereas it cannot for $\sigma < \sigma_0$. If we write $\rho^f = \sqrt{v_1^f + v_2^f}$, the situation is shown in figure 9.2 Left which shows the solution ρ^f as a function of the nonlinear gain σ. In particular, if $\sigma > \sigma_0$, there is a ring of tuned spontaneous activities given by $(v_0^f(\sigma), \rho^f(\sigma)\cos(\phi), \rho^f(\sigma)\sin(\phi))$ for ϕ arbitrary.

In the case of the experimental distribution (for $\alpha = 1$), we expect a perturbation of the diagram in figure 9.2 Left. The result[5] is shown in figure 10.3 where we plot

[4] which depends on the threshold h and the positive coefficient J_1

[5] It is possible to derive polynomial equations of degree three which approximate (10.11) for $\sigma \approx \sigma_0, \alpha \approx 0$ as we did in proposition 3.32. They would show that if $\alpha > 0$, the Pitchfork branch that appears at $\sigma = \sigma_0$ for $\alpha = 0$ is broken in 4 pieces when $\alpha > 0$ yielding 7 stationary solutions. A

the solutions (v_1^f, v_2^f) of (10.10) as functions of the nonlinear gain σ. We do not plot v_0^f because it is not necessary for knowing if the spontaneous activity is tuned or not. We see that if the nonlinear gain σ is above 4.5, there are 6 tuned activities and one untuned activity. Otherwise[6], there is only one stationary cortical state which is untuned, written $\mathbf{A}_0$.

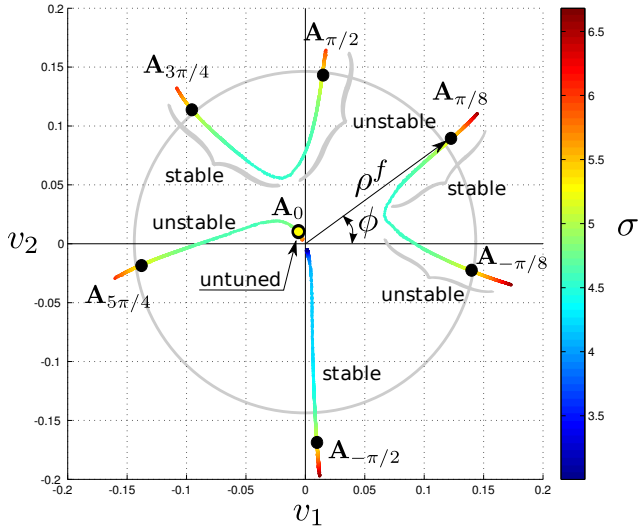

Figure 10.3: Plot of the stationary solutions (v_1^f, v_2^f) (v_0^f is not shown) of (10.10) as functions of the nonlinear gain σ in the case of no external input $\varepsilon = 0$. As σ reaches the value 4.5, 6 tuned cortical activities appear, beside the untuned one $\mathbf{A}_0$. We show the 7 solutions with large dots for $\sigma \approx 5.3$. The yellow disk corresponds to the untuned activity because it is close to the origin. The stability of the different branches of solutions is indicated. The grey circle shows that the solutions almost lie on a circle as in the case of the uniform distribution of preferred angles. The stability is computed numerically. Note that the polar angle ϕ of the vector (v_1^f, v_2^f) is twice the angle of the stimulus that produces the response $M_{\mathbf{x}}^{\phi/2}$ encoded by (v_0^f, v_1^f, v_2^f).

What does a stationary state $v^f = (v_0^f, v_1^f, v_2^f)$ represent? To answer this question, we write $v_1^f = \rho^f \cos(\phi)$ and $v_2^f = \rho^f \sin(\phi)$ (see figure 10.3) and compute

$$\begin{aligned} \mathbf{OI}(\mathbf{x}) = \mathbf{V}^f(\mathbf{x}) &= v_0^f + v_1^f \sqrt{J_1} r_{\mathbf{x}} \cos(2\theta_{\mathbf{x}}) + v_2^f \sqrt{J_1} r_{\mathbf{x}} \sin(2\theta_{\mathbf{x}}) \\ &= v_0^f + \sqrt{J_1} \rho^f r_{\mathbf{x}} \cos(2\theta_{\mathbf{x}} - \phi) \\ &= v_0^f + \sqrt{J_1} \rho^f M_{\mathbf{x}}^{\phi/2}. \end{aligned} \tag{10.12}$$

Hence $\mathbf{OI}(\mathbf{x})$ is a scaled-shifted version of $M_{\mathbf{x}}^{\phi/2}$ which is by definition (see (10.3)) the response of the cortex to a DG oriented at $\phi/2$. **Note that the polar angle**

perturbation of the O(2)-Pitchfork would yield $9 = 3 \cdot 3$ solutions at most according to the Bézout's theorem. Indeed, the theorem bounds the number of solutions by the product of the degree.

[6] *i.e.* if $\sigma \leq 4.5$

ϕ of the vector (v_1^f, v_2^f) is twice the angle of the stimulus that produces the response $M_{\mathbf{x}}^{\phi/2}$ encoded by (v_0^f, v_1^f, v_2^f).

Hence, the network spontaneously produces, for a sufficiently high nonlinear gain σ, three unstable tuned activities $\mathbf{A}_{\pi/2}, \mathbf{A}_{5\pi/4}, \mathbf{A}_{-\pi/4}$ oriented at $\frac{\pi}{4}, \frac{5\pi}{8}, -\frac{\pi}{8}$, three stable tuned activities $\mathbf{A}_{\pi/4}, \mathbf{A}_{-\pi/2}, \mathbf{A}_{3\pi/4}$ oriented at $\frac{\pi}{8}, -\frac{\pi}{4}, \frac{3\pi}{8}$ and one unstable untuned activities $\mathbf{A}_0$, see figure 10.3. Note that the stability of the solutions has been numerically obtained.

We plot the corresponding six OI signals (see (10.12)) in figure 10.4 for a nonlinear gain $\sigma = 5.3$. In line with the long-standing convention employed by experimentalists, we removed the DC component v_0, also called *blank* in the OI signals. Note that the OI signals in each column are phase reversed.

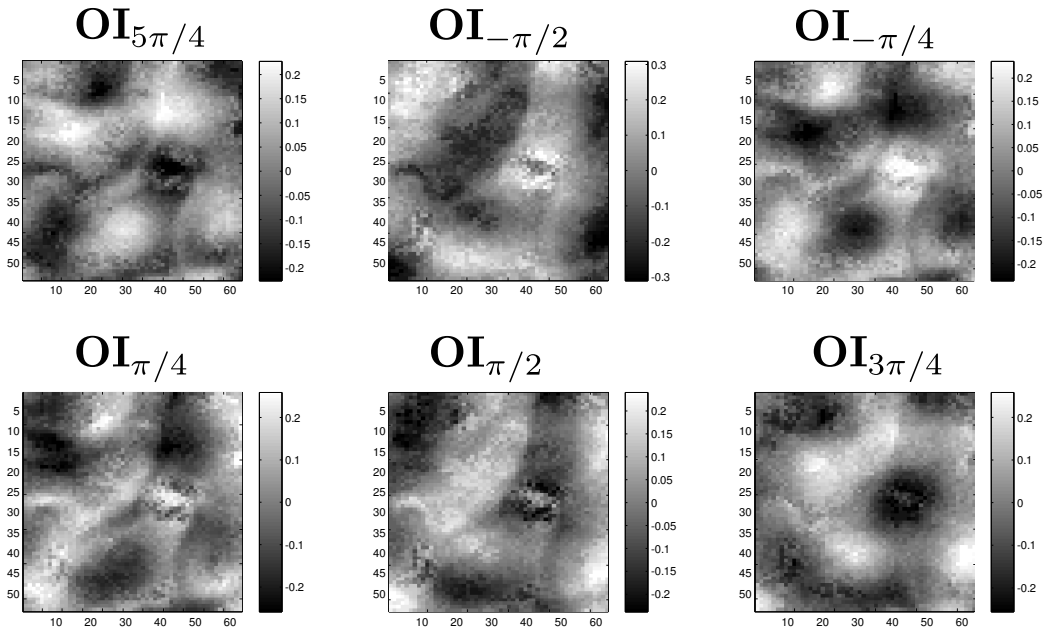

Figure 10.4: Plot of the spontaneous stationary **OI** signal associated to the stationary cortical states **A** found in figure 10.3 for a nonlinear gain $\sigma = 5.3$.

10.6 Study of the evoked activity

Having studied the spontaneous activity in the previous section, we now study what happens when the network is stimulated. We answer the question of how the different spontaneous cortical activities found in the previous section are modified by the afferent input. In particular, how can the network produce a response that is related to the stimulus orientation ϕ_{aff} despite its apparent preference for the orientations $\frac{\pi}{4}$, $\frac{3\pi}{4}$, $-\frac{\pi}{2}$? To answer these questions, we assume that the network works at the edge of the bifurcation we analysed in the previous section (see chapter 8). This means that we choose the nonlinear gain σ to be close to the bifurcation value $\sigma_0 \approx 4.5$ (see also chapter 9).

In the following numerical experiment, the afferent input is oblique, *i.e.* $\phi_{aff} = \pi/8$. It is a simple case because it is already aligned with one of the spontaneous cortical responses. However, one should note that this is not a great loss of generality because it is not aligned with the six others. Hence, we shall see how the tuned responses behave when the constrast is increased. The result is shown in figure 10.5.

Based on section 3.5 and chapter 9, if we switch on the afferent input, *i.e.* choose $\varepsilon > 0$, we expect two main phenomena to happen: 1) destruction of 4 tuned solutions when the contrast exceeds the asymmetry 2) persistence of a cortical state "orthogonal" to the stimulus angle for larger contrasts.

We start by discussing the results of figure 10.5. If the contrast is above 0.1, then the 4 tuned activities $\mathbf{A}_{\pm\pi/2}, \mathbf{A}_{-\pi/4}, \mathbf{A}_{3\pi/4}$ which are not aligned with the stimulus at $\phi = \frac{\pi}{4}$ are destroyed. More precisely, $\mathbf{A}_{3\pi/4}$ and $\mathbf{A}_{\pi/2}$ are destroyed[7] for contrasts $\varepsilon \approx 0.01$ while $\mathbf{A}_{-\pi/4}$ and $\mathbf{A}_{-\pi/2}$ are destroyed[8] for contrasts $\varepsilon \approx 0.1$. There remain two tuned solutions $\mathbf{A}_{\pi/4}$, $\mathbf{A}_{5\pi/4}$, the first one stable, *aligned* with the stimulus and the other, unstable, which is *perpendicular* to the stimulus orientation. For large contrasts (data not shown), the perpendicular solution $\mathbf{A}_{5\pi/4}$ disappears[9] together with $\mathbf{A}_0$ and it only remains the stable solution $\mathbf{A}_{\pi/4}$ (see section 9.5.2 for a detailed explanation). This agrees with 2).

With regard to the relationship between the asymmetry and the contrast for the existence of tuned solutions, we have not performed a detailed numerical analysis. Rather, we numerically observe that for contrasts ε of order the value of the asymmetry[10] $\max_{r,\theta} |P_0(r,\theta)| \approx 0.1055$, all cortical states which are not aligned with the stimulus are destroyed. This is in agreement with the results in section 3.5.3.

It should be noted that the existence of the perpendicular response, in the case of the symmetrical network ($\alpha = 0$), amounts to the symmetry $\theta \to -\theta$ in the synaptic weights $\mathbf{J}$. Hence, whenever the network is stimulated with a grating, 3 responses are possible. One is the untuned activity, the second is the response of the network (*i.e.* the one aligned with the stimulus) and the third is the perpendicular activity. A similar phenomenon happens here. In the numerical example shown in figure 10.5, the perpendicular activity is evidently $\mathbf{A}_{\frac{5\pi}{4}}$. However, as the experimental network is not symmetric, $\mathbf{A}_{\frac{\pi}{4}}$ and $\mathbf{A}_{\frac{5\pi}{4}}$ are not symmetric w.r.t. to the origin[11] in figure 10.5. In particular, these two states do not have the same amplitude: $\mathbf{A}_{\frac{5\pi}{4}}$ is closer to an untuned state than $\mathbf{A}_{\frac{\pi}{4}}$.

10.7 Design of a dynamical stimulus

In this section, we would like to construct a stimulus that puts the network in a state wich is not aligned with the stimulus like we did in chapter 9. This is a

[7] In effect, they disappear through a saddle-node bifurcation.
[8] idem.
[9] idem.
[10] numerically computed from the experimental data
[11] see figure 9.4 in the case of the Ring Model

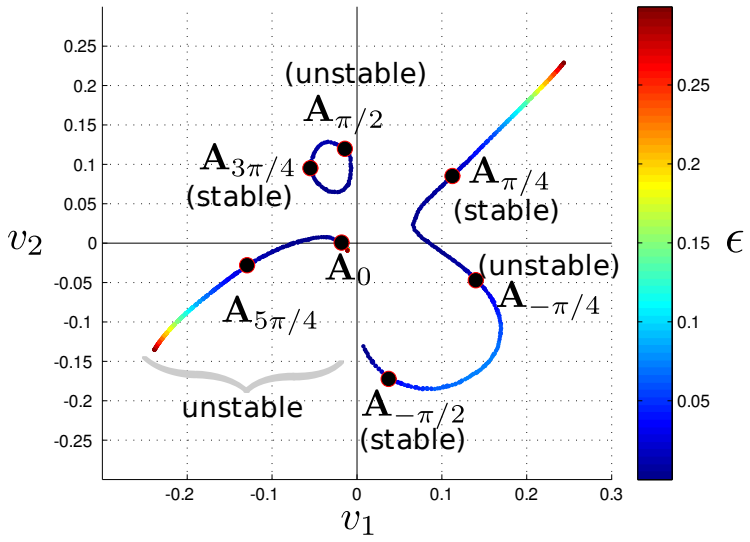

Figure 10.5: Plot of the stationary activities (v_1^f, v_2^f) (v_0^f is not shown) as functions of the contrast ε of the afferent input, for a stimulus orientation $\phi_{aff} = \frac{\pi}{8}$ and for a nonlinear gain σ very close to the critical gain $\sigma_0 = 4.5$ (see text). As ε reaches 0.1, only 3 evoked activities remain. We have indicated with large disks, as an example, the seven evoked activities obtained for $\varepsilon \approx 0.005$.

behaviour that was not explicitly incorporated in the design of the model.

In chapter 9, we have shown that when stimulated with a sequence of gratings respectively horizontal, vertical and then horizontal, the network response did not vary much: it was almost stationary. From its viewpoint, the two stimuli produce very similar cortical responses. We would like to derive the same dynamical stimulus for the experimental network. One should first note, that if the distribution of preferred angles is almost uniform, then the dynamical stimulus designed in chapter 9 also works. However, the slight asymmetries of the experimental network make the design of the dynamical stimulus more difficult and we have to rely on numerical computations. This makes the application of the dynamical stimulus idea to biological experiments more difficult.

In the previous section, we have studied the evoked activity and gained a good understanding of the states that the network produces spontaneously. We found that any[12] stimulus produces three activities[13]. Let us recall how the dynamical stimulus works. We know that $\mathbf{A}_{5\pi/4}$ is unstable when the stimulus angle is $\phi_{aff} = \frac{\pi}{8}$ and that $\mathbf{A}_{5\pi/4}$ is close to the stable cortical response to a stimulus oriented at $\phi_{aff} = \frac{5\pi}{4}$, we take advantage of this fact. We present a stimulus oriented at $\phi_{aff} = \frac{\pi}{8}$ which is called *horizontal* to make the analogy with section 9.4 more precise. In response to this stimulus, the cortical activity converges to the stable state $\mathbf{A}_{\pi/4}$. Then, we slowly rotate the stimulus angle from $\phi_{aff} = \frac{\pi}{8}$ to a *vertical*

[12] In effect, we have shown that the contrast must be higher than the asymmetry.
[13] possibly unstable.

one, *i.e.* $\phi_{aff} = \frac{5\pi}{8}$. It makes the cortical activity converges to $\mathbf{A}_{5\pi/4}$. We suddenly present again the *horizontal* stimulus. As the current cortical states $\mathbf{A}_{5\pi/4}$ is already very close to the stationary (unstable) cortical response to the *vertical* stimulus, the cortical response does not vary much and it takes a long time before the cortical activity moves to $\mathbf{A}_{\pi/8}$, *i.e.* the cortical response to a *horizontal* stimulus. The stimulus sequence is written *horizontal* $\overset{slow}{\longrightarrow}$ *vertical* $\overset{fast}{\longrightarrow}$ *horizontal*.

However, this scheme would not work as well as in the case of the Ring Model because of the asymmetry. This asymmetry gives different dependencies of the seven cortical response amplitudes (see figure 10.5) on the contrast. Hence, to improve the dynamical stimulus, we have to change the stimulus angle and also the contrast in the gratings sequence. The contrasts have to be more precisely adjusted in the case of large asymmetries. This was unnecessary in the case of the Ring Model.

Let us derive the condition to improve the above dynamical stimulus, *i.e.* to trap the cortex in the perpendicular state more efficiently. For convenience, we make the dependency on the contrast explicit. The first (horizontal) stimulus $\mathbf{I}_{ext}^{(1)}$ has orientation $\phi_{aff} = \frac{\pi}{8}$ and contrast ε_1. It produces the tuned responses $\mathbf{A}_{\pi/4}^{(1)}(\varepsilon_1), \mathbf{A}_{5\pi/4}^{(1)}(\varepsilon_1)$ respectively stable and unstable. The second (vertical) stimulus $\mathbf{I}_{ext}^{(2)}$ has orientation $\phi_{aff} = \frac{5\pi}{8}$ and contrast ε_2. It produces (data not shown) the tuned responses $\mathbf{A}_{\pi/4}^{(2)}(\varepsilon_2), \mathbf{A}_{5\pi/4}^{(2)}(\varepsilon_2)$ respectively unstable and stable. Hence, the dynamical stimulus works if

$$\mathbf{A}_{5\pi/4}^{(1)}(\varepsilon_1) \approx \mathbf{A}_{5\pi/4}^{(2)}(\varepsilon_2). \tag{10.13}$$

Having computed the stationary activities for the two stimuli as functions of the contrast (as in figure 10.5 for the *horizontal* stimulus $\mathbf{I}_{ext}^{(1)}$), it is straightforward, given a contrast ε_1, to find a second contrast ε_2 such that (10.13) is satisfied. This would trap more efficiently the network in the perpendicular state.

10.8 Conclusion

In this chapter, we have followed [Blumenfeld 2006] and built a neural field model that produces, as stationary activity, experimental orientation maps. We have shown in section 10.2 that the choice of the connectivity $\mathbf{J}$ was a direct consequence of the idea of cortical responses $S_{\mathbf{x}}^{\phi}$. We were then able to approximate the experimental orientation maps to produce a 3D network equivalent to (10.9).

This 3D network is formally similar to the Ring Model we studied in chapter 9. The resemblance is only formal as they do not model the same biology while they share a lot of mathematical properties (like being 3D, working near a Pitchfork bifurcation point, having very similar connectivity, a perception threshold...).

The Ring Model features a stationary spontaneous activity which is homeomorphic to a circle if the nonlinear gain is high enough[14]. Hence, it can produce an infinite number of stationary activities which are translations in the features space of

[14] We argued in section 3.7 that this is not the working range of the model.

each other. The model of this chapter only produces a discrete number of stationary spontaneous cortical states[15] which expresses the preference of the network for specific orientations stimuli. Hence, with an afferent input like (10.8), the spontaneous activity converges to one of these stationary cortical states. If we add a Brownian noise to the afferent input, then the structure of the noise will be transmitted to the cortical activity. Indeed, the network operating near a bifurcation, it is slow compared to the time-variations of the noise. For the modeling of the Kenet *et al.* experiment in [Kenet 2003] (see the beginning of section 10.1), it would predict that the statistics of appearance of orientation maps in the spontaneous activity reflect the noise properties and is very peaked around specific activities shown in figure 10.4 depending on the noise amplitude.

Compared to [Blumenfeld 2006], we have not supposed that the distribution of preferred orientations $\theta_{\mathbf{x}}$ was uniform. This has the consequence of creating orientation preferences (at roughly $\frac{\pi}{4}, \frac{3\pi}{4}, -\frac{\pi}{2}$ as shown in figure 10.3). We then studied how the network processed an arbitrary oriented stimulus. We saw that if the contrast was small, the response of the network was ambiguous. As soon as the contrast is high enough (above a perception threshold), this value of the threshold contrast being related to the asymmetry of the network, then the response is not ambiguous anymore, at least for stationary stimuli. However, if we switch alternatively between two perpendicular stimulus of well tuned contrasts, then the network response is stationary in time. This is a consequence of working near a Pitchfork bifurcation.

The connectivity given by (10.5) does not depend on the distance between the pre and postsynaptic locations as opposed to reported biological data (see [Gilbert 1989, Kisvarday 1997, Yousef 2001, Mariño 2005]).This can be modified by multiplying the connectivity (10.5) by a Gaussian $G_a(\mathbf{x}, \mathbf{y}) = e^{-\|\mathbf{x}-\mathbf{y}\|^2/2a^2}$ where a is the extent of lateral connections. We cannot use the reduced system (10.11) to study this new connectivity. However, the network could still be made work ingclose to a Pitchfork bifurcation. The specific nature of the connections only shapes the number of spontaneous/evoked stationary cortical states and we know it cannot be above 9 (see section 10.5). These states will be organized in a similar way as in figures 10.3 and 10.5. Also, the spatial structure of these spontaneous states will be very similar to the one shown in figure 10.4. Hence, the assumption that the system works close to a bifurcation is very strong and shapes completely the structure of the spontaneous/evoked activity. We will not further study this particular model but instead propose a new model of V1 which is much more driven by documented experimental data. The price to pay is that the numerics become very involved.

[15] up to 9 theoretically although we have obtained 7 with the experimental data of figure 10.1.

Chapter 11

A model of V1 without feature-based connectivity

In the last two chapters, we have applied the strategy proposed in chapter 8. We turn now to the last model studied in this Thesis. It is a model of interacting pinwheels with short-range connections that are feature-independent, each pinwheel working close to a Pitchfork bifurcation. This is a general principle that has been used in the models of Bressloff *et al.* (see for example [Bressloff 2001b]). We have arrived at a similar requirement from other considerations in chapter 8. In this chapter, we

- adjust the model parameters such that the mechanism of chapter 8 works
- study the influence of delays
- study the long-range connections.

In particular, we do not consider the problems of the width of the tuning curves and of the perception threshold because this is far more sophisticated than for the Ring Model. Indeed, the model of this chapter does not feature the symmetries of the Ring Model that allow "easy" computations.

Contents

11.1 Introduction

There are many models of V1/hypercolumn in the literature that have been introduced to account for biology. These models can be segregated in two categories: the spiking neural networks (to cite a few [Suarez 1995, Somers 1995, Somers 1998, Shelley 2002, Tao 2004, Rangan 2005, Haeusler 2007, Chemla 2010b]) and the rate models (for example [Ben-Yishai 1995, Carandini 1997, Dragoi 2000b, Bressloff 2000, Stetter 2000, Bressloff 2001b, Bressloff 2003, Kang 2003, Miikkulainen 2005, Blumenfeld 2006, Schwabe 2006, Baker 2009]). These models depend on a lot of parameters and it is rare, especially for the spiking network models, to find a study about the parameter tuning. In a caricature way, accounting for a few biological effects with thousands of independent parameters seems unreasonable. We think it is very important to make the choice of a parameter regime (*i.e.* a set of parameters) which implies predictions that are (or not) verified in the biology. This line of thinking have been more thoroughly applied to the rate models (see for example [Ben-Yishai 1995, Bressloff 2001b, Blumenfeld 2006]).

In the rate models community, the orientation selectivity have been mainly modelled by assuming a feature-dependent connectivity (see [Ben-Yishai 1995, Bressloff 2001b, Chossat 2009]), only a few studies, like [Ernst 2001, Kang 2003, Bressloff 2003, Baker 2009], use a more reasonable connectivity like we described in chapter 1, *i.e.* a connectivity that does not depend on the orientation (for example). Note that the paper [Kang 2003] does not consider the regime where the network is close to a stationary bifurcation.

Finally, in the rate model community, we are only aware of models (see the work of Bressloff *et al.*) of pinwheels interactions which assume a continuum of pinwheels spread over the cortex. This is not supported from a biological viewpoint. Also, the activity in the linear zones is neglected. Nevertheless, these models are often referenced for their spectacular ability to reproduce the contoured and non-contoured planforms (see also [Ermentrout 1979]) as reported by Kluver in [Kl"uver 1966]. In particular, the use of long range connections as shown in section 1.2.2 is critical for the model to produce contoured planforms. Note that the impact of space-dependent delays in these models have been studied in [Bressloff 2008] for the linear stability.

In this chapter, we consider a rate model with a connectivity that does not depend explicitly on the preferred orientation and respects the basic properties of the local connections (see section 1.2.2). We suppose that the populations are spread over a square lattice of hypercolumns, this choice is motivated by the analytical formulas it provides. This model has very few parameters and is tuned to operate in a similar regime than in the Ring Model, *i.e.* near a Pitchfork bifurcation. Then, we study what happens if we introduce long-range connections. Finally, we study how

the space-dependent delays impact the network behaviour. To our best knowledge, this is the only study, apart from [Bressloff 2008], about these effects with a rate model.

11.2 A rate model with one population

Let us recall why we do not want a feature-based connectivity (see also chapter 1). One of the most striking correlate of the orientation selectivity is the pinwheel columnar structure as shown in the experiments of Bosking *et al.* in [Bosking 1997]. This raises the question "Is the pinwheel structure encoded in the cortical connections?" An element of answer is given by [Lund 2003a] who concludes that the patchy lateral connections are the only clearly identifiable example of an anatomical column. Hence, in a dead cortex there is some evidence for a columnar organization and less for orientation selectivity or the pinwheel network. This indicates, that the connectivity should not depend on the orientation otherwise there should be some anatomical evidence for it. Let us note that the pinwheel structure is observed when an animal is shown highly contrasted full field drifting gratings[1], *i.e.* the network has to be activated. The other element of answer comes from the theoretical study in [Ernst 2001] of primary visual cortex at the very first stages of development. This model features a difference of Gaussians connectivity on a two-dimensional cortex that can generate pinwheels. Upon stimulation with drifting grating, the authors found a pinwheel network and the extent of the (produced) pinwheels lattice corresponds to the width of the connectivity. Hence, no feature-based connectivity between cortical neurons seems needed to account for the pinwheel structure. In particular, it seems unnecessary to introduce the pinwheel structure within the cortical connectivity.

To simplify the study, we will not consider two populations of excitatory/inhibitory spread over a 2D cortex. Indeed, such model requires too many parameters, for example in the definition of the connections between the two populations, the different nonlinear gains, the thresholds... Rather, we use the simplification exposed in section 2.3 and consider a single population. Hence, we consider the equation for the membrane potential $V(\mathbf{x},t)$ which depend only on the cortex position $\mathbf{x}$. This equation is:

$$\tau\frac{d}{dt}V(\mathbf{x},t) = -V(\mathbf{x},t) + \int_\Omega J(\mathbf{x},\mathbf{y})S\left[\sigma V(\mathbf{y},t)\right]d\mathbf{y} + I_{ext}(\mathbf{x}) \tag{11.1}$$

where Ω is a two-dimensional piece of cortex and $S(v) = \frac{1}{1+e^{-v+T}}$. **We suppose that Ω has periodic boundary conditions because this simplifies the computations of the spectral properties in (8.6) of the integral operator.** According to the biological properties of the connectivity seen in chapter 1, we shall decompose it as a sum of the local connectivity and the long-range connectivity:

$$J(\mathbf{x},\mathbf{y}) = J_{loc}(\mathbf{x}-\mathbf{y}) + \varepsilon_{LR}J_{LR}(\mathbf{x},\mathbf{y}).$$

[1] there are also orientation maps for local stimuli, see [Chavane 2011] for example.

As the long-range connectivity is modulatory, we assume that ε_{LR} is small. Hence, we start with the case where there are only local connections $\varepsilon_{LR} = 0$ in the next section. The long-range connections are introduced in section 11.6. The next three sections are devoted to the derivation of expressions for the connectivity function J_{loc} and the external input I_{ext}. For the input, this goes through the study of theoretical orientation maps $\theta(\mathbf{x})$ similar to the experimental ones that we studied in the previous chapter.

11.2.1 The expression of the local connectivity, J_{loc}

From [Lund 2003a, Mariño 2005], we know that the local connectivity is homogeneous in the cat and in the monkey:

$$J(\mathbf{x}, \mathbf{y}) = J_{loc}(\mathbf{x} - \mathbf{y}), \quad \|\mathbf{x} - \mathbf{y}\|_2 \leq 1 \tag{11.2}$$

If we suppose that the excitatory/inhibitory connections are modelled by Gaussians with identical width σ_{loc}, then the excitatory population features an *effective* connectivity given by a difference of Gaussians:

$$J_{loc}(\mathbf{x}) = ae^{-\frac{\|\mathbf{x}\|^2}{2\sigma_{loc}^2}} - e^{-\frac{\|\mathbf{x}\|^2}{4\sigma_{loc}^2}} \tag{11.3}$$

This local connectivity implies that there is always a space constant stationary activity $V(\mathbf{x}) = v_0$ for all parameters when there is no input I_{ext}. This activity solves:

$$v_0 = \hat{J}_0 S(\sigma v_0) \tag{11.4}$$

where $\hat{J}_0$ is the integral of J_{loc} over the cortex Ω.

11.2.2 The expression of the external input, I_{ext}

Here, we shall give an expression for I_{ext}. The optical imaging technique gives the preferred orientation (PO) map $\mathbf{x} \to \theta(\mathbf{x}) \in \left[-\frac{\pi}{2}, \frac{\pi}{2}\right]$ by a procedure that we described in section 10.1. The orientation map being computed with high contrast drifting gratings stimuli, we assume that the LGN drives the cortex and that the recurrent computations are negligible. Hence, for a given orientation stimulus θ_{aff} expressed by a particular form of I_{ext}, the membrane potential converges to a stationary solution V^f. Using equation (11.1), when $\|I_{ext}\|_2$ is large, we find that the stationary cortical state V^f is roughly[2] given by I_{ext} and is also the OI signal (see section 10.2). This stationary cortical state is used for the computation of the PO map. Hence, $I_{ext}(\mathbf{x})$ carries the information about $\theta(\mathbf{x})$. This motivates the expression

$$I_{ext}(\mathbf{x}) = f(\mathbf{x}, \theta(\mathbf{x}))$$

for some function f that has to be found. The rest of this section is devoted to finding f. We start with the case where there is a single pinwheel (like in figure 8.1) in the PO map.

[2] because S is bounded.

Around such a pinwheel, the preferred orientation is given by the polar angle θ (see figure 8.1): the LGN input only depends on this angle θ, *i.e.* $I_{ext}(\mathbf{x}) = f(\arg \mathbf{x})$ written $I(\mathbf{x}) = f(\theta)$. Moreover, f has to be a periodic function of θ because the preferred orientation is periodic around the pinwheel. Hence, by keeping the first Fourier modes of f, we can assume that

$$I_{ext}(\mathbf{x}) = A + B\cos(2\theta - 2\phi), \tag{11.5}$$

around the pinwheel for some arbitrary $A, B > 0$ and ϕ. For a given cortical location, $\theta = \phi$ gives the maximum response. Hence, we can interpret ϕ as the stimulus angle, written θ_{aff}, at location $\mathbf{x}$. Also, as the LGN input is supposed weakly tuned, we can fix $A = 1, B = \beta << 1$.

How can we generalise the above expression of I_{ext} for a network of pinwheels with the property that around each pinwheel, we have the same expression (11.5)? A solution is given by the expression

$$I_{ext}(\mathbf{x}) = 1 + \beta\cos(2\theta(\mathbf{x}) - 2\theta_{aff}(\mathbf{x})).$$

If we add a function I_0 of the space to localise the stimulus, we find (see also [Shelley 2002] for a different derivation):

$$I_{ext}(\mathbf{x}) = \varepsilon\left[1 + \beta\cos(2\theta(\mathbf{x}) - 2\theta_{aff}(\mathbf{x}))\right] I_0(\mathbf{x}) \tag{11.6}$$

where ε is the contrast and β is the (input) anisotropy. In the case of a full field stimulus, $I_0 = 1$ whereas for a local stimulus I_0 is a Gaussian, for example. In the model we consider here, the LGN gives a weakly tuned input which means that β is small. In order to proceed further, we need the expression of the PO map $\theta(\mathbf{x})$.

11.2.3 The pinwheel lattice

We now assume that the pinwheels are distributed on a planar lattice. This regularity makes it easier to apply the mechanism of chapter 8. Indeed, the tuned component of a full field grating stimulus

$$I_1^{\theta_{aff}}(\mathbf{x}) = \varepsilon\beta\cos(2\theta(\mathbf{x}) - 2\theta_{aff})$$

has to be approximated by an eigenvector of J_{loc} according to (8.9). We will see in section 11.3.2 that the eigenvectors of J_{loc} are given by $\cos(\mathbf{k}\cdot\mathbf{x})$, $\sin(\mathbf{k}\cdot\mathbf{x})$ where $\mathbf{k}$ is an arbitrary wavevector. Hence, the simpler $\theta(\mathbf{x})$, the easier the approximation of $I_1^{\theta_{aff}}(\mathbf{x})$ by eigenvectors is.

We describe a planar lattice $\mathcal{L}$ by two independent vectors $\mathbf{v}_1, \mathbf{v}_2$ and let

$$\mathcal{L} = \{2\pi n_1\mathbf{v}_1 + 2\pi n_2\mathbf{v}_2 \mid n_1, n_2 \in \mathbb{Z}\}.$$

We can distinguish three types of lattices depending on the angle ψ between the two basis vectors $\mathbf{v}_1, \mathbf{v}_2$: the *square* lattice ($\psi = \frac{\pi}{2}$), the rhombic lattice ($0 < \psi < \frac{\pi}{2}$, $\psi \neq \frac{\pi}{3}$) and the hexagonal lattice ($\psi = \frac{\pi}{3}$). To simplify the study, *i.e.* to reduce

the number of different cases, we assume that the pinwheels are distributed on a *square lattice*. The upcoming analysis could be easily extended to the rhombic lattice. The case of the hexagonal lattice is different, in particular, its larger number of symmetries changes the Pitchfork normal form expression (11.13) and its analysis in section 11.4.2.

We now show some particular PO maps $\theta(\mathbf{x})$ where the pinwheels are distributed over a square lattice. How can we build them? We have to find maps such that the preferred orientation around a pinwheel looks like figure 8.1. The tiled pinwheel map can be generated from a single $\pi \times \pi$ square hypercolumn like figure 8.1 by first generating a rectangle of size $2\pi \times \pi$ with a reflection along the vertical axis. From this rectangle, we then generate a $2\pi \times 2\pi$ square with a reflection along the horizontal axis. This periodic $2\pi \times 2\pi$ square tiles naturally without any transformation. We call N_p the number of tiles used to generate a PO map, hence $\Omega = [-N_p\pi,\ N_p\pi]$.

In figure 11.1 Left, we plot an example of PO map $\theta^{\mathbf{1}}$ and the procedure to make the $2\pi \times 2\pi$ square of 4 pinwheels is shown in white.

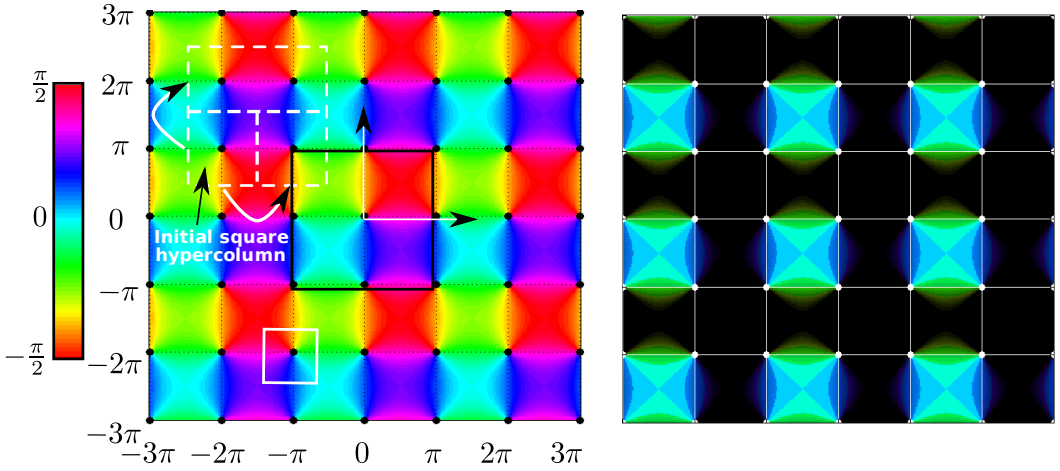

Figure 11.1: Left: Orientation map $\theta^{\mathbf{1}}$. Right: plot of $\cos(2\theta^{\mathbf{1}})$, the surface forms spots. Positive values are transparent whereas negative values are dark. The orientation map is seen by transparency. Note that $N_p = 3$.

How can we generate other maps? As the lattice inherits the properties of the initial square hypercolumn, given the initial square hypercolumn of the map $\theta^{\mathbf{1}}$ (see figure 11.1 Left), we can multiply it by -1 (modulo π) or add a constant (modulo π), it will produce a square hypercolumn like figure 8.1. Hence, we find that other PO maps are given by:

$$\theta = \pm\theta^{\mathbf{1}} + \theta_0\ [\pi]$$

where θ_0 is an arbitrary constant. We conjecture that we find all the square PO maps using this procedure starting from an initial square hypercolumn.

It is interesting to look at the tuned component of the input in the case of full field gratings. In figure 11.1 Right, we plot $\cos 2\theta^{\mathbf{1}}$: it is displayed as an alpha map on top of the underlying PO map $\theta^{\mathbf{1}}$, where transparency represents positive values of $\cos 2\theta^{\mathbf{1}}$ and dark represents negative values. We observe that $\cos 2\theta^{\mathbf{1}}$ generates *spots*. A shift of the PO map, similar to a rotation of a full field grating stimulus, would change the spots into *stripes* (see figure 11.2). Hence, by rotating the stimulus, the input patterns change from spots to stripes.

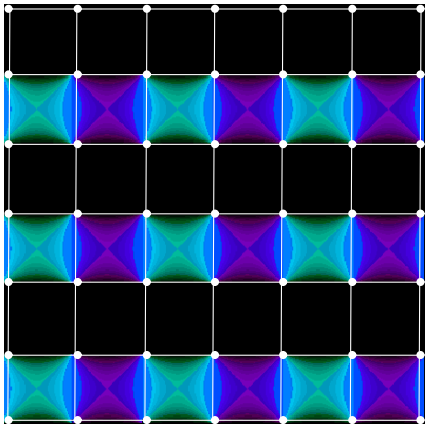

Figure 11.2: Plot of $\cos\left(2\theta^{\mathbf{1}} - 2\frac{\pi}{8}\right)$, the surface forms stripes. Positive values are transparent whereas negative values are dark. The orientation map is seen by transparency. Note that $N_p = 3$.

11.3 Basic properties of the network: local connectivity

We start by exploring the properties of the model that are solely due to the local connectivity.

11.3.1 Network symmetries

Let us write (11.1) as $\mathcal{F}(V) = 0$ with $\mathcal{F}(V) \equiv \dot{V} + V - J_{loc} \cdot S(\sigma V) - I_{ext}$. As in the case of the Ring Model in chapter 9, the symmetries of the model change if the stimulus is switched on ($\varepsilon \neq 0$) or not.

In the case where there is no stimulus ($\varepsilon = 0$), we find that $\mathcal{F}$ commutes with the translations:

$$\mathcal{F}(T_{\mathbf{t}} \cdot V) = T_{\mathbf{t}} \cdot \mathcal{F}(V) \text{ with } T_{\mathbf{t}} \cdot V(\mathbf{x}) \equiv V(\mathbf{x} + \mathbf{t}),$$

this is a consequence of J_{loc} being homogeneous and of the periodic boundary conditions imposed on Ω. Because of our assumptions, the group of spatial translations is isomorphic to the torus $\mathbb{T}^2 \equiv \mathbb{R}^2/(2N_p\pi\mathbb{Z})^2$. The model is also symmetric with respect to the transformations that leave the basic structure invariant. This is because

J_{loc} is rotation invariant and an even function. These transformations form the dihedral group $\mathbf{D}_4 = \langle R, S \rangle$ generated by R, S, a rotation and a reflection which act on the membrane potential as: $R{\cdot}V(x_1, x_2) = V(x_2, x_1)$ and $S{\cdot}V(x_1, x_2) = V(x_1, -x_2)$. The full symmetry group when $\varepsilon = 0$ is:

$$G_{loc} = \mathbf{D}_4 \ltimes \mathbb{T}^2. \tag{11.7}$$

The index *loc* is used to recall that the connectivity is the local connectivity. When the long-range connections are introduced in the model, the symmetries are changed, see section 11.6. Hence, we have shown that the model is G_{loc}-equivariant when $\varepsilon = 0$.

We now present a stimulus to the network, *i.e.* $\varepsilon > 0$. We have seen in section 9.1.4 that $\mathcal{F}$ commutes with a transformation if the input I_{ext} is invariant by the transformation. Hence, at most, the symmetry group of the model is G_{loc}. We are left to find the symmetries that leave the input invariant. When the LGN input I_{ext} is space constant, the model is G_{loc}-equivariant. We now focus on the case of full field gratings $I_0 = 1$. The input is not invariant under all the translations $T_{\mathbf{t}}$ but only those satisfying $\mathbf{t} = (2\pi n_1, 2\pi n_2)\,,\ n_i \in \mathbb{Z}$. This comes from the periodicity of the PO map θ which is obtained by tiling the basic $2\pi \times 2\pi$ square (see white dashed square in figure 11.1 Left). Hence the translations group is reduced from $\mathbb{T}^2$ to a discrete subgroup $\mathbb{Z}^2$. No further symmetries are found.

We end this section by looking at the symmetries of the PO map $\theta^{\mathbf{1}}$. They are "obvious" symmetries like the reflections along the vertical (resp. horizontal) axis of equation $x_1 = \pi/2$ (resp. $x_2 = \pi/2$). There are also transformations that do not leave $\theta^{\mathbf{1}}$ invariant, like the reflection, written $\bar{S}$, along the line $x_1 = x_2$ which change the sign of the map:

$$\theta^{\mathbf{1}}(\bar{S}\mathbf{x}) = -\theta^{\mathbf{1}}(\mathbf{x})\ [\pi].$$

Indeed the reflection S amounts to exchange the blue zones with the green zones. Finally, we have a nice transformation coming from the shift. If we add $\frac{\pi}{4}$ modulo π, to the map, it transfers the colour zones according to the chain blue→cyan→violet→red which amounts to rotate the entire map by an angle of $\frac{\pi}{2}$. Hence, if we write R_ϕ the rotation of angle ϕ, we find:

$$\theta^{\mathbf{1}}(R_{2\phi}\mathbf{x}) = \theta^{\mathbf{1}}(\mathbf{x}) + \phi\ [\pi], \quad \phi \in \frac{\pi}{4}\mathbb{Z}. \tag{11.8}$$

where R_ϕ is the rotation of angle ϕ. If we consider a general map $\theta^{\mathbf{2}} = \varepsilon_0\theta^{\mathbf{1}} + \theta_0$, $\varepsilon_0 = \pm 1$, we find:

$$\theta^{\mathbf{2}}(R_{2\phi}\mathbf{x}) = \theta^{\mathbf{2}}(\mathbf{x}) + \varepsilon_0\phi\ [\pi], \quad \phi \in \frac{\pi}{4}\mathbb{Z}. \tag{11.9}$$

This relation simply shows that $\theta(\mathbf{x})$ is affected in a counter-clockwise (resp. clockwise) way if the increasing values of θ are seen counter-clockwise (resp. clockwise) in the initial square hypercolumn.

11.3.2 Eigenvalue decomposition of the connectivity

In the mechanism described in chapter 8, we have seen that it was important to compute the eigen-elements (λ, U), satisfying (8.6), of the integral operator associated to the local connectivity J_{loc}. As we imposed periodic boundary conditions to the cortex Ω, the eigenvectors U are given by $\cos(\mathbf{k}\cdot\mathbf{x})$, $\sin(\mathbf{k}\cdot\mathbf{x})$ with the wavevector $\mathbf{k} = \left(\frac{k_1}{N_p}, \frac{k_2}{N_p}\right)$, $k_i \in \mathbb{Z}$. Then, the eigenvalues, noted $\hat{J}_{\mathbf{k}}$, read

$$\hat{J}_{\mathbf{k}} = \int_{\Omega} J_{loc}(\mathbf{y}) \cos(\mathbf{k}\cdot\mathbf{y}) d\mathbf{y}.$$

There is an analytical expression[3] for the $\hat{J}_{\mathbf{k}}$ but we choose a convenient approximation which is valid when N_p is large. In effect, we have:

$$\hat{J}_{\mathbf{k}} \approx 4\pi^2\sigma_{loc}^2 \left[a e^{-\sigma_{loc}^2 \|\mathbf{k}\|^2/2} - 2e^{-\sigma_{loc}^2\|\mathbf{k}\|^2} \right], \; N_p \to \infty$$

The eigenvalues indexed by the wavevector $\mathbf{k}$ may be the same for different $\mathbf{k}$. We find that the eigenvalue $\hat{J}_{(0,0)}$ is attained once, the eigenvalues $\hat{J}_{(k_1,0)}$ (resp. $\hat{J}_{(k_1,k_1)}$) are attained four times by the wavevectors $\mathbf{k} = (\pm k_1, 0), (0, \pm k_1)$ (resp. $\mathbf{k} = (\pm k_1, \pm k_1)$) and the eigenvalues $\hat{J}_{(k_1,k_2)}$ with $k_1, k_2 \neq 0$ are attained eight times[4]. This also gives the dimension of the eigenspace.

It is important to note that the largest eigenvalues are separated by a quantity of order $\frac{1}{N_p}$ [5] because the different wavevectors are separated by at most $\frac{1}{N_p}$. It implies that the bifurcation points, solution of (8.7), are very close.

11.3.3 A first look at the spontaneous activity

We would like to show some spontaneous cortical states that can be produced by the model and discuss their interpretation. We have seen in chapter 8 that the network features a constant (untuned) spontaneous activity v_0 when no stimulus is shown. What happens if we have pharmacologically modified the population properties like the threshold T or the nonlinear gain σ? For some value of the nonlinear gain (for example), the untuned activity may become unstable and tuned spontaneous activity may emerge. Close to a bifurcation point, this tuned activity would look like[6] $v_0 + U$ where U is an eigenvector for some wavevector $\mathbf{k}$. It is interesting to understand how this spontaneous activity may be interpreted. For example, we have seen that the spots or stripes of spatial extension π and centred on the linear zones should be interpreted as full field gratings.

But if the stripes are centred on the pinwheels centres (shown with white dots in figure 11.3 Left) as in figure 11.3 Top Left, then the interpretation changes. Indeed,

[3] which involves the `erf` function

[4] by the wavevectors $\mathbf{k} = (k_1, k_2)$, $(-k_2, k_1)$, (k_2, k_1), $(-k_1, k_2)$.

[5] and also because $\mathbf{k} \to \hat{J}_{\mathbf{k}}$ is smooth

[6] It is unclear if this is true far from a bifurcation point. For example, the nodal structure of the spontaneous activity may be conserved along bifurcated branches but we have not been able to find such a general criterion. See also part II.

in this case, the hypercolumns are either not activated or entirely activated. For the ones entirely activated, we can suppose that all the orientations are present in the stimulus, *i.e.* that it is a small spot. The right column in figure 11.3 is the interpretation of the cortical activity in the left column. We represent spots with red squares centred on pinwheels (black dots). It follows that the first activity a) represents stripes of light and the second activity b) represents spots of light. These are called the non-contoured planforms in [Bressloff 2001b].

On the other hand, when only a fraction of the hypercolumn is activated, we determine which local contour produces such cortical activity by pooling[7] the orientations "that are activated". For example, in the case of thin stripes of activity in figure 11.3 c), we obtain an example of contoured planform.

Finally, there are activities that have an ambiguous interpretation. It is indeed difficult to see if the cortical activity in figure 11.3 d) Left is indeed represented by a mixture of contoured/non-contoured planforms as we have done in figure 11.3 d) Right. The interpretation is ambiguous because the local contours around the square should match the contours of the square. This might come from the fact that the spot of light is not really a square in this case.

11.4 Generalisation of the Ring Model

In this section, we adjust the parameters (a, σ, T) in order to produce the mechanism explained in chapter 8. One of the basic requirements of this mechanism is that the network must be able to spontaneously produce activity that looks like the LGN input when the nonlinear gain σ is high enough. As we have already computed the eigenvalues and eigenvectors, the basis of the mechanism is almost set. We start with the identification of an eigenvector that looks like the tuned component of a full field grating.

11.4.1 Identification of the critical wavevector

From figure 11.1, we see that $\cos(2\theta^{\mathbf{1}}(\mathbf{x})) \approx (\sin(x_1) + \sin(x_2))/2$ for the square lattice $\mathbf{1}$. Also we have (data not shown) that $\sin(2\theta^{\mathbf{1}}(\mathbf{x})) \approx (-\sin(x_1) + \sin(x_2))/2$. From $\cos(2\theta^{\mathbf{1}} - 2\theta_{aff}) = \cos 2\theta^{\mathbf{1}} \cos 2\theta_{aff} + \sin 2\theta^{\mathbf{1}} \sin 2\theta_{aff}$, we conclude that for all full field grating orientations, the input is composed of spots or stripes of wavelength 1. Hence, a candidate for the wavevector to be spontaneously selected is:

$$\mathbf{k}_c = (1, 0).$$

From the discussion in chapter 9, $\mathbf{k}_c$ must be the first wavevector to undergo a bifurcation when the nonlinear gain σ is varied: this happens if $\hat{J}_{\mathbf{k}_c}$ is the largest positive eigenvalue of J_{loc} (see lemma F.1.1) and the nonlinear gain that produces the bifurcation is written σ_0. Then, by symmetry, the static bifurcation is a Pitchfork bifurcation with symmetry group $\mathbf{D}_4 \ltimes \mathbb{T}^2$.

[7] This is done by computing the Fourier transform: $\arg \int V(\mathbf{x}) e^{2i\theta(\mathbf{x})} d\mathbf{x}$ around each pinwheel. The contour is validated if the total activity $|\int V(\mathbf{x}) e^{2i\theta(\mathbf{x})} d\mathbf{x}|$ is high enough.

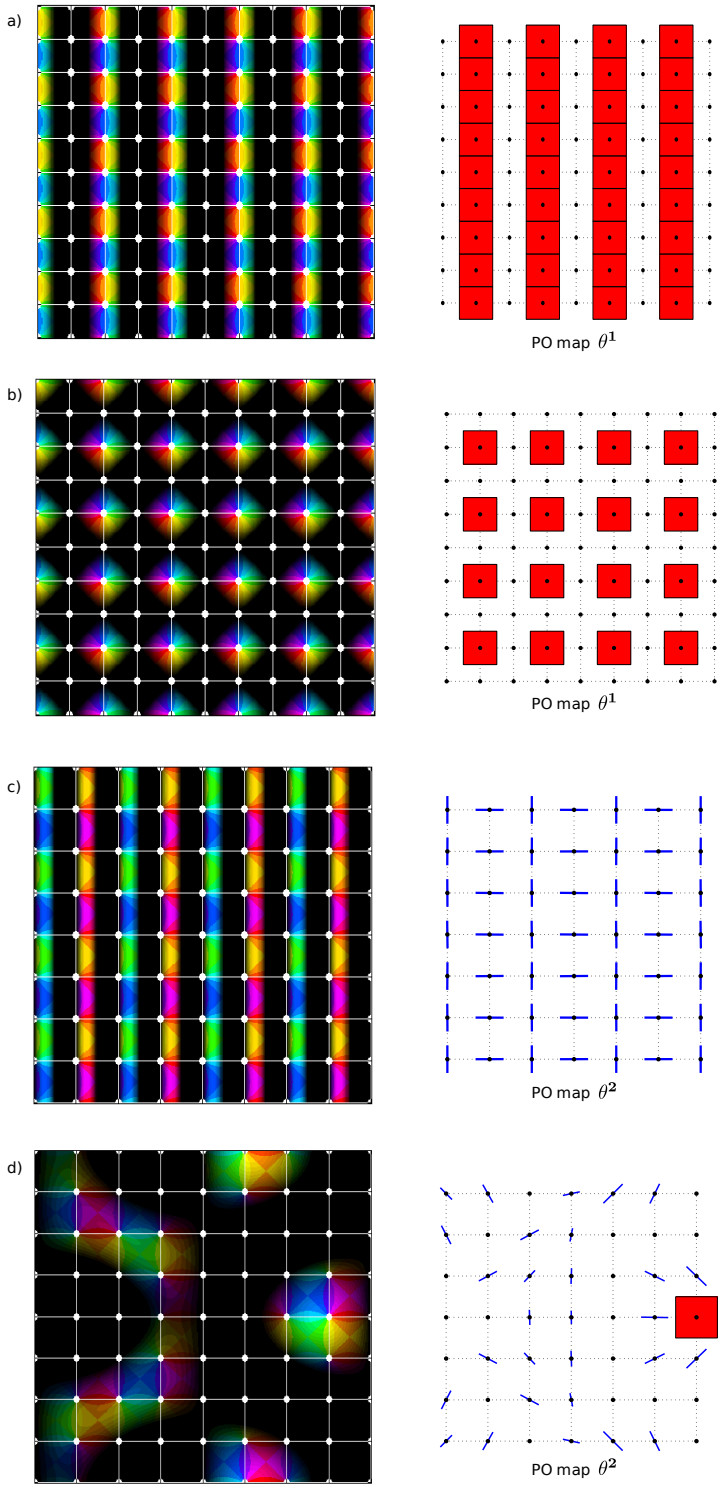

Figure 11.3: Plot of various plane wave membrane potential solutions. *a)* $\cos(x)$, *b)* $\cos(x)+\cos(y)$, *c)* $\sin(2x)$, *d)* $\cos(\frac{2x+y}{4})+\cos(\frac{-2x+y}{4})+\cos(\frac{2y+x}{4})+\cos(\frac{-2y+x}{4})$. See text for more information. Right: corresponding interpretation in terms of stripes, spots and contours (see text). The first two rows are for the PO map $\theta^{\mathbf{1}}$. The last two rows are for the PO map $\theta^{\mathbf{2}}$.

11.4.2 Parameter tuning and network behaviour

Once we have adjusted the connectivity parameters, it remains to tune the operating point of the network by tuning the nonlinear gain. In the case of the Ring Model, we chose a nonlinear gain close to a Pitchfork bifurcation $\sigma \leq \sigma_0$. Then, we studied the spontaneous activity depending on the nonlinear gain. This gave us a hint about the cortical responses to small contrasts. Indeed, the switching of the stimulus "opens" the Pitchfork (see section 3.3.2) and produces a turning point that we can follow as function of the contrast. This turning point arises for a nonlinear gain σ_c which is a decreasing function of the contrast: $\varepsilon \to \sigma_c(\varepsilon)$. For a particular value of the contrast ε_0, which we call the perception threshold, the turning point has the same value as the nonlinear gain of the network, *i.e.* $\sigma = \sigma_c(\varepsilon_0)$. Then, for larger contrasts, the network features a tuned response. The last important remark about the Ring Model is the rotation invariance. This invariance implies that the network responses are all the same $V^f(\theta) = f(\theta - \theta_{aff})$ where θ_{aff} is the stimulus orientation. For the Ring Model, we found up to three different functions f for a given stimulus and one of them is called the tuning curve (see definition 1.3.1). In the case here, we will only sketch the first part of this analysis, *i.e.* the study of the activity depending on the nonlinear gain. In particular we will not study the opening of the Pitchfork bifurcation. Note that we conjecture the present model to feature a perception threshold. However, because of the absence of the rotation symmetry, it has a finite number of cortical responses to a particular stimulus. However, we have not been able to derive the dependency of these responses on the stimulus angle θ_{aff} in a simple way. In particular, we are not able to compute the tuning curves analytically. Finally compared to the Ring Model, something new happens. As the network has spontaneous preferred orientations, when presented an arbitrary stimulus orientation, it will give a tuned response for contrasts above the perception threshold and the cortical response orientation will depend on the contrast. Hence, there could be a second perception threshold corresponding to the contrast value for which the cortical response aligns with the stimulus angle. This does not happen in the Ring Model because the cortical response is always aligned with the stimulus.

11.4.2.1 Tuning of the connectivity, J_{loc}

Having identified the critical wavevector, let us adjust the connectivity such that $\hat{J}_{\mathbf{k}_c}$ becomes the largest positive eigenvalue of J_{loc}. As the critical eigenvalue must be positive, this requires

$$\hat{J}_{\mathbf{k}_c} \approx 4\pi^2\sigma_{loc}^2 \left[ae^{-\sigma_{loc}^2/2} - 2e^{-\sigma_{loc}^2}\right] = 4\pi^2\sigma_{loc}^2 e^{-\sigma_{loc}^2/2}\left[a - 2e^{-\sigma_{loc}^2/2}\right] > 0 \quad (11.10)$$

which gives: $a > 2e^{-\sigma_{loc}^2/2}$. Also, we find that the extremum of $\mathbf{k} \to \hat{J}_{\mathbf{k}}$ occurs at $\|\mathbf{k}\| = \frac{1}{\sigma_{loc}}\sqrt{-2\log(a/4)}$. From $\|\mathbf{k}_c\| = 1$, we find:

$$a = 4e^{-\sigma_{loc}^2/2}. \quad (11.11)$$

To describe completely the connectivity J_{loc}, we need to fix the value of σ_{loc}. Rather, σ_{loc} will remain a free parameter that we adjust to have different network behaviours (see next sections). As σ_{loc} should not be too small compared to the square hypercolumn size ($\sigma_{loc} \approx \pi$), we shall assume that

$$\hat{J}_0 = 4\pi^2\sigma_{loc}^2\,[a-2] = \pi^2\sigma_{loc}^2\,[a-2] = 8\pi^2\sigma_{loc}^2\left[2e^{-\sigma_{loc}^2/2}-1\right] < 0,$$

i.e. $\sigma_{loc} > \sqrt{2\log(2)} \approx 1.1774$.

11.4.2.2 Tuning of the nonlinear gain, σ

Let us now operate as in chapter 8. We suppose that there is no input $\varepsilon = 0$ and look for a nonlinear gain $\sigma = \sigma_0$ such that the constant activity $V^f(\mathbf{x}) = v_0$ bifurcates. We find the equations (see (8.7) in chapter 8):

$$\left\{\begin{array}{rcl} v_0 &=& \hat{J}_0 S(\sigma_0 v_0) \\ 1 &=& \sigma_0 \hat{J}_{\mathbf{k}_c} DS(\sigma_0 v_0). \end{array}\right. \tag{11.12}$$

We proved in appendix E.3 that these equations have a unique solution (v_0, σ_0) if $\hat{J}_0 < 0$ which implies $a < 2$ and

$$\sigma_{loc} > \sqrt{2\log(2)} \approx 1.1774.$$

According to the discussion in section 9.5.2, the nonlinear gain σ of the network should be adjusted just below σ_0, *i.e.* $\sigma \precsim \sigma_0$. Indeed, in this case, when there is no input, the network does not have a tuned response.

The bifurcation point (v_0, σ_0) corresponds to a Pitchfork with the square symmetry group, it is called a $\mathbf{D}_4$-Pitchfork bifurcation. The critical eigenvectors are given by $(\cos(x_1), \sin(x_1), \cos(x_2), \sin(x_2))$. Let us write $V^f(\mathbf{x}) = v_0 + z_1 e^{ix_1} + z_2 e^{ix_2} + c.c.$[8].

Unlike in lemma 3.3.2 where we used the Lyapunov-Schmidt method to derive an equation in (z_1, z_2) for the stationary solutions, we are here interested in the local dynamics. We will see how this dynamics is changed when the delays are varied for example. This is why we apply the center manifold theorem (see remark 7) to the non-delayed neural fields equations to derive the reduced equation for (z_1, z_2) (see [Ermentrout 1991]):

$$\left\{\begin{array}{l} \dot{z}_1 = z_1\left(\frac{\sigma-\sigma_0}{\sigma_0} + \beta|z_1|^2 + \gamma|z_2|^2\right) + I_1 \\ \dot{z}_2 = z_2\left(\frac{\sigma-\sigma_0}{\sigma_0} + \beta|z_2|^2 + \gamma|z_1|^2\right) + I_2 \end{array}\right. \tag{11.13}$$

with $\beta, \gamma \in \mathbb{R}$ given in appendix F. We also find in section 3.3.2 that $I_1 = \int_\Omega I_{ext}(x_1, x_2) e^{-ix_1} dx_1 dx_2/(2\pi N_p)^2$ and $I_2 = \int_\Omega I_{ext}(x_1, x_2) e^{-ix_2} dx_1 dx_2/(2\pi N_p)^2$. In the case of full field gratings (*i.e.* $I_0 = 1$ in (11.6)) and the PO map $\theta^{\mathbf{1}}$, we have:

$$\begin{array}{l} I_1 = -i\frac{\varepsilon\beta}{4}\left(\cos 2\theta_{aff} - \sin 2\theta_{aff}\right) \\ I_2 = -i\frac{\varepsilon\beta}{4}\left(\cos 2\theta_{aff} + \sin 2\theta_{aff}\right). \end{array} \tag{11.14}$$

[8] complex conjugate.

It is known from [Golubitsky 1988] that the normal form (11.13) has two types of stationary solutions:

- the stripes $(e^{i\phi_1} z_1^f, 0),\ (0, e^{i\phi_2} z_1^f)$ with $z_1^f = \sqrt{\frac{\sigma_0 - \sigma}{\sigma_0 \beta}}$ and $\phi_1,\ \phi_2$ arbitrary,
- the spots $(z_1^f e^{i\phi_1}, z_1^f e^{i\phi_2})$ with $z_1^f = \sqrt{\frac{\sigma_c - \sigma}{\sigma_0(\beta+\gamma)}}$ and $\phi_1,\ \phi_2$ arbitrary,

when $I_1 = I_2 = 0$. Note that when the stimulus is switched on, the stationary solutions z_1^f, z_2^f of (11.13) are purely imaginary for the PO map $\theta^{\mathbf{1}}$. Hence there is a finite number[9] of cortical responses to a particular stimulus. In the case of no input, $\varepsilon = 0$, the spots are stable if and only if

$$\beta < -|\gamma| < 0 \tag{11.15}$$

whereas the stripes are stable if and only if

$$\gamma < \beta < 0. \tag{11.16}$$

It implies that the stripes and spots are mutually exclusive as stable patterns. We have plotted in figure 11.4 the two conditions (11.15)-(11.16) as function of the "threshold" T and the lateral extent of the local connectivity σ_{loc}. **In all cases, it requires the connectivity extent to be two to three times smaller than the hypercolumn extent.** This seems shorter than what is reported in the biology (see chapter 1).

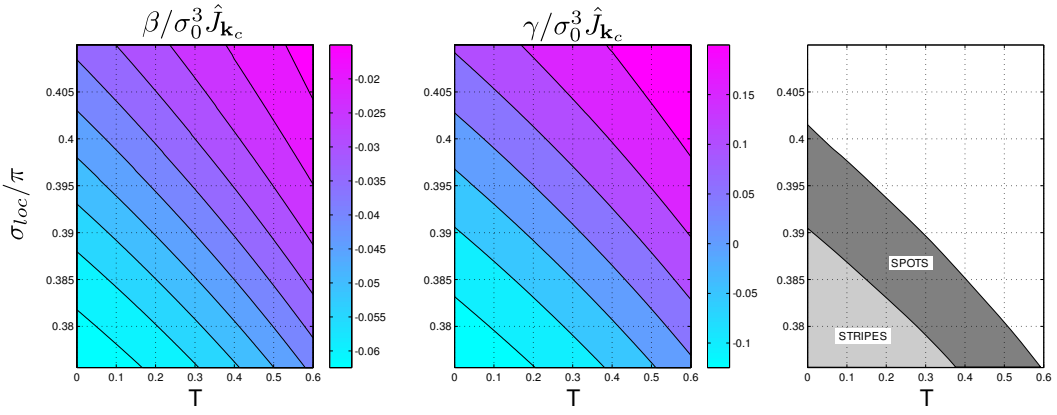

Figure 11.4: Left, Middle: Plot of the coefficients $\beta,\ \gamma$ of the $\mathbf{D}_4$-Pitchfork normal form as function of the threshold T and the spatial extent of the local connectivity σ_{loc}. Right: region in the parameter plane (T, σ_{loc}) where the spots or the stripes are stable in the case $\varepsilon = 0$.

Suppose that we have set the parameters such that the stripes are stable (for example). We have seen that depending on the stimulus orientation, the external

[9] Like in the previous chapter, this number is bounded by 9 by Bezout theorem.

input pattern is composed of stripes or spots. In the case of a horizontal full field grating ($\theta_{aff} = 0$), the input pattern is composed of spots for the PO map $\theta^{\mathbf{1}}$. This is a difficult task for the network to produce spots whereas it prefers stripes. The network is able to do so if the contrast is high enough. To understand this mechanism, *i.e.* how the network manages to give a "correct" response and for which contrast, requires a delicate study that we do not perform here. This would amount to solve (11.13) in (z_1, z_2) as function of $(\varepsilon, \theta_{aff})$. The main issue is that for a given contrast ε, there can be many solutions (z_1, z_2) and it is difficult, for example, to find an analytical condition on the contrast for a unique solution to exist. Also, at contrast fixed, the "tuning response" $\theta_{aff} \to (z_1, z_2)$ is more complicated than a cosine function as for the Ring Model.

We were not able to solve (11.13) and (11.14) as functions of $(\varepsilon, \theta_{aff})$, in particular, we were unable to compute the tuning curves. These equations could be numerically studied but this would lengthen too much the present study. Nevertheless, we can make the following two predictions. Let us call $z_1^f(\theta_{aff}, \varepsilon), z_2^f(\theta_{aff}, \varepsilon)$ a solution of (11.13). Then the firing rate at cortical location $\mathbf{x}_0$ is given by

$$TC(\theta_{aff}) = S\left[\sigma\left(v_0(\varepsilon) + 2\Re\left(z_1^f(\theta_{aff}, \varepsilon)e^{ix_1} + z_2^f(\theta_{aff}, \varepsilon)e^{ix_2}\right)\right)\right] \tag{11.17}$$

where the scalars $v_0, z_i^f(\theta_{aff}, \varepsilon)$, $i = 1, 2$, are independent of the cortical location $\mathbf{x}_0$. If the contrast is large enough, there is a unique cortical response to a stimulus oriented at θ_{aff}. The tuned component of this response looks like the tuned component of the input. Hence we should be able to write

$$TC(\theta_{aff}) \approx S\left[\sigma\left(v_0(\varepsilon) + 2\rho_1(\varepsilon)\cos 2(\theta(\mathbf{x}) - \theta_{aff})\right)\right]$$

where $\rho_1(\varepsilon)$ is real scalar. **It follows that the tuning width is the same at every cortical location for contrasts large enough to produce a cortical response which can be approximated by the above formula.** This is in contradiction with the experiments in [Nauhaus 2008] but in agreement with those in [Mariño 2005].

Another interesting effect is to look at the cortical response to a local oriented stimulus. Hence, we assume that the mask function I_0 in (11.6) is centred around $\mathbf{x} = 0$ and activates a feedforward region of 4 pinwheels: $I_0(\mathbf{x}) = \exp\left(-\frac{\|\mathbf{x}\|^2}{2(8\pi)^2}\right)$. Using the same argument, if the contrast is large enough, we have:

$$TC(\theta_{aff}) \approx S\left[\sigma\left(v_0(\varepsilon) + 2\rho_1(\varepsilon)I_0(\mathbf{x})\cos 2(\theta(\mathbf{r}) - \theta_{aff})\right)\right].$$

In particular, it is localized. But for smaller contrasts, the cortical response is given by (11.17): it is not localized and is regularly spatially organized at the hypercolumn scale. Hence, it looks like the cortical response to a full field grating. We conjecture that at small contrasts, the localized stimulus will excite populations of nearby hypercolumns with similar orientation (we do not know if this orientation is close to θ_{aff}). This seems in contradiction with recent experiments by Chavane *et al.* in [Chavane 2011]. Further numerical studies are required to understand the

link between the cortical response and the stimulus. However, we stop here our investigations in order to show how the tools, that we have developed for the delays in the previous part, apply to the present model.

11.5 Space dependent delays effects

In the two previous examples of this part, the Ring Model and the Blumenfeld *et al.* model, we have not looked at the delay dependent effects.

The Ring Model being a hypercolumn model without spatial extension, it is difficult to introduce propagation delays. Instead, we could have studied the effects of constant delays. This was done in chapter 6 although it was not a hypercolumn model. We found a Fold-Hopf bifurcation if the constant delay was large enough. In particular, around this bifurcation point, there can be bistability between stationary solutions and oscillating solutions.

We could have introduced constant delays in the Blumenfeld *et al.* model in the previous chapter. As the equations are very similar to those of the Ring Model, we expect similar conclusions to hold for the Blumenfeld *et al.* model.

Propagation delays in a V1 neural field model have only been studied once to our best knowledge in [Bressloff 2008]. This V1 model features a network of interacting Ring Models with a connectivity given by $J_{loc}(\theta-\bar{\theta})+\varepsilon_{LR}J_{LR}(\mathbf{x},\theta)$ where the local connectivity J_{loc} is the Ring Model connectivity and the long-range connectivity is basically the connectivity we use in section 11.6 up to the change $\theta \leftrightarrow \theta(\mathbf{x})$. The authors found a Fold-Hopf bifurcation for a particular propagation speed, the Hopf bifurcation occuring for the wavevector $\mathbf{k}=0$. Note that they did not look at the constant delays effects.

In this section, we take into consideration the delays as described in part III. More precisely, we modify (11.1) into:

$$\tau\frac{d}{dt}V(\mathbf{x},t) = -V(\mathbf{x},t) + \int_\Omega J(\mathbf{x},\mathbf{y})S\left[\sigma V(\mathbf{y},t-\tau(\mathbf{x},\mathbf{y}))\right]d\mathbf{y} + I_{ext}(\mathbf{x}) \tag{11.18}$$

where $\tau(\mathbf{x},\mathbf{y}) = D + c\left\|\mathbf{x}-\mathbf{y}\right\|_2$. As in the previous part, we make the distinction between the constant delays ($c=0$), the purely propagation delays ($D=0$) and the space dependent delays in the general case. Let us first characterize the spontaneous activity and see how the constant cortical activity $V^f(\mathbf{x},t)=v_0$ (which depends on the nonlinear gain σ) is altered by the introduction of delays. We study whether this stationary state can oscillate when delays are added. In this case, we write $V(\mathbf{x},t) = v_0 + z_0 e^{i\omega_H t}e^{i\mathbf{k}_H\cdot\mathbf{x}} + c.c.$ where z_0 is a scalar complex and call $\mathbf{k}_H$ the wavevector. The difficulty in finding this oscillating solution lies in finding the frequency ω_H and the wavevector. As explained in chapter 8 in the case of the static bifurcation, an oscillatory instability, called a Hopf bifurcation, arises when the linearised equation around the stationary state $V^f = v_0$

$$\tau\frac{d}{dt}\mathbf{U}(\mathbf{x},t) = -\mathbf{U}(\mathbf{x},t) + \sigma s_1\int_\Omega J(\mathbf{x},\mathbf{y})\mathbf{U}(\mathbf{y},t-\tau(\mathbf{x},\mathbf{y}))d\mathbf{y}, \tag{11.19}$$

with $s_1 = S^{(1)}(v_0)$, has solutions of the form $\mathbf{U}(t,\mathbf{x}) = e^{i\omega_H t}e^{i\mathbf{k}_H\cdot\mathbf{x}}$. The issue here is to find when such solutions defined by $(\omega_H, \mathbf{k}_H)$ exist. Fortunately, the model (11.18) belongs to the class of models for which we have found analytical formulas for the bifurcation point $(c_{\mathbf{k}}, D_{\mathbf{k}})$ at which solutions defined by $(\omega_H, \mathbf{k}_H)$ of (11.19) exist. As before in this Thesis, we start with the constant delays case.

11.5.1 Case of constant delays

In this section, we look for particular constant delays $D_{\mathbf{k}}$ such that (11.19) has an oscillating solution. We have seen in section 4.4.1.1 that this critical delay $D_{\mathbf{k}}$ for the wavevector $\mathbf{k}$ exists if and only if

$$\sigma s_1 \hat{J}_{\mathbf{k}} \leq -1. \tag{11.20}$$

From proposition 4.4.4, the smallest critical delay $D_{\mathbf{k}}$ is obtained for the largest eigenvalue $\hat{J}_{\mathbf{k}}$ which satisfies (11.20). We have adjusted J_{loc} in section 11.4.2 and the largest negative eigenvalue is $\hat{J}_0$, it follows that the most unstable wavevector is $\mathbf{k}_H = 0$. The model works close to the Pitchfork bifurcation point $\sigma = \sigma_0$. That is why we plot in figure 11.5, the values, in the parameter plane $(\|\mathbf{k}\|, \sigma_{loc})$, of the critical delay $D_{\mathbf{k}}/\tau$ at the Pitchfork point $\sigma = \sigma_0$. In this case, the condition (11.20) reduces to $\hat{J}_{\mathbf{k}}/\hat{J}_{\mathbf{k}_c} \leq -1$ because $\sigma_0 s_1 \hat{J}_{\mathbf{k}_c} = 1$. Under the curve labelled "∞", no critical delay exists whereas the critical delay values are indicated by the labels on the different isolevel curves.

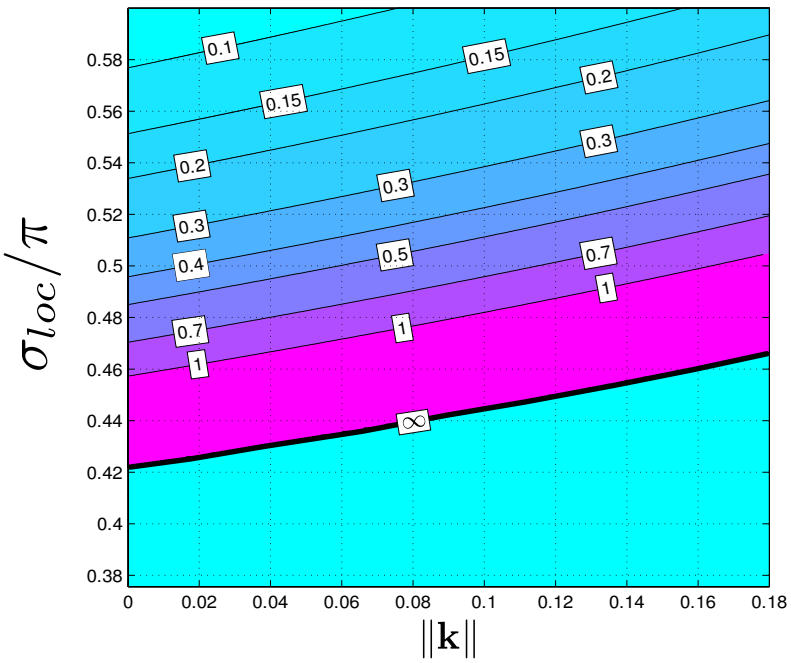

Figure 11.5: Plot of the critical delay values $D_{\mathbf{k}}/\tau$ as function of $(\|\mathbf{k}\|, \sigma_{loc})$ at the Pitchfork point $\sigma = \sigma_0$. Note that below the curve labelled "∞", no critical delay exists.

Lemma F.1.2 indicates that if no critical delay exists at the Pitchfork bifurcation point $\sigma = \sigma_0$, then no critical delay exists for smaller nonlinear gains $\sigma < \sigma_0$. On the other hand, if a critical delay exists at the Pitchfork bifurcation point, then this critical delay is a decreasing function of σ (from proposition 4.4.4 and lemma F.1.2). We find that the smallest local connectivity extent σ_{loc} for which there is an oscillating solution is given by $\sigma_{loc} \approx 0.42\pi$ for $\sigma = \sigma_0$.

The value $\sigma_0 s_1$ is independent of the threshold T as it equals $1/\hat{J}_{\mathbf{k}_c}$. Hence, the value of the critical delay does not depend on the threshold T for $\sigma = \sigma_0$. It implies that the critical delay never exists if the model operates in the spots regime (see figure 11.4 Right) or in the stripes regime because these regimes require the spatial extent of the local connectivity to be smaller than $\sigma_{loc} < 0.405$ (see figure 11.4 Right).

Having shown that no oscillating solutions can be found with constant delays at the Pitchfork bifurcation point $\sigma = \sigma_0$, we now turn to the study of space-dependent delays.

11.5.2 Case of space-dependent delays

In this section, we show that the introduction of propagation delays can produce oscillating solutions. Again, we use the result of section 4.4.1.2 to compute the Hopf bifurcation curves[10].

The Hopf bifurcation curves[11] should depend on the three parameters (σ_{loc}, c, D). As such, they form surfaces in the 3D parameter space. Instead of plotting these surfaces, we find it more convenient to show the bifurcation curves in the plane (D, c) for some particular σ_{loc}. This is done in figure 11.6 for $\sigma = \sigma_0$. Each Hopf curve corresponds to a wave vector $\mathbf{k} = (m, n)/N_p$ and the black dots mark the curve intersections which are Hopf-Hopf bifurcation points, *i.e.* the intersection between two Hopf curves. The first two panels ($\sigma_{loc} = 0.38\pi,\ 0.385\pi$) correspond to the stripes regime and the last panel ($\sigma_{loc} = 0.395\pi$) corresponds to the spots regime. We plot two panels in the first case because there is a Hopf-Hopf bifurcation point in the null wavevector if the local extent σ_{loc} is small enough. In the spots regime, there is no Hopf-Hopf bifurcation in the null wavevector. In both regimes, the most unstable wavevector is the null wavevector (corresponding to the blue curve) because it appears for the smallest critical delays. Hence, we do not consider the other Hopf-Hopf bifurcation points.

Finally, note that the first instabilities (c_0, D_0), *i.e.* the ones for the smallest delays, arise for $D_0 < \tau,\ c_0 \approx \tau$ on the blue curve for the null wavevector $\mathbf{k}_H = 0$. As $\tau \approx 10ms$, it gives a critical constant delay below $10ms$. In figure 11.6, the grey region indicates the parameter region where no oscillating solutions have bifurcated. Also the critical speed is in the range $c_0^{-1} = 0.1us/ms$ where us is the unit of space.

[10] Note that we have used the $C++$ library Cubature to compute the 2D Fourier transforms needed for the eigenvalues of $\mathbf{J}_{iy}$ in the Hopf curves formulas.

[11] They form a set in the parameter space (σ_{loc}, D, c) where a solution like $e^{i\omega_H t} e^{i\mathbf{k}\cdot\mathbf{x}}$ exists for (11.19).

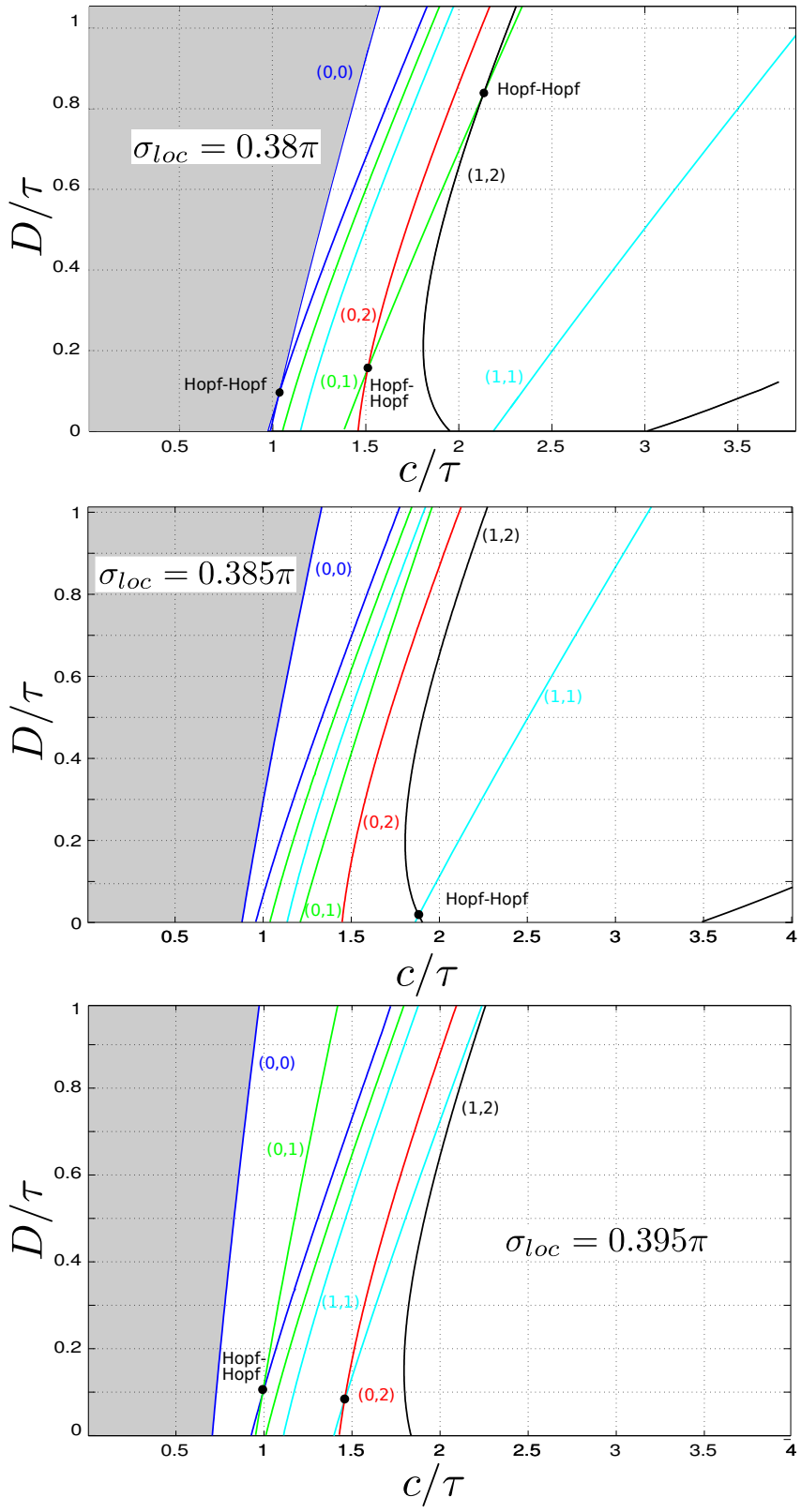

Figure 11.6: Plot of the Hopf curves in the parameter plane (c, D) for different local connectivity extent σ_{loc} and $N_p = 5$ at the Pitchfork point $\sigma = \sigma_c$. The labels (m, n) indicate the wavevector $\mathbf{k} = (m, n)/N_p$. The intersection of the curves is labelled with a black dot.

A hypercolumn has an extension of π $us \approx 1mm$ (see figure 11.1 Left). Hence, the critical speed is in the range $0.03mm/ms$ which is 30 times smaller then the speed seen in tissues. Hence, these instabilities should not be observed for biological values of the parameters.

Imagine that we can decrease the propagation speed pharmacologically, it increases c which can be larger than c_0. Then, the results in figure 11.6 indicate that, depending on the value of σ_{loc}, the $\mathbf{D}_4$-Pitchfork instability of the previous section, may degenerate into a $\mathbf{D}_4$-Pitchfork-Hopf instability[12] where the Hopf instability appears in the null wavevector $\mathbf{k} = 0$. We have already encountered this type of bifurcation in chapter 5 in the case of one-dimensional neural fields. Here, it is a bit more sophisticated because of the symmetries. More precisely, if we write $U(\mathbf{x}, t) = e^{i\omega_H t}$ the solution of (11.18) for $\mathbf{k} = 0$, then the membrane potential near the instability reads[13]:

$$V(\mathbf{x}, t) = v_0 + z_0 e^{i\omega_H t} + z_1 e^{ix_1} + z_2 e^{ix_2} + c.c. \tag{11.21}$$

and the normal formal form is given by[14]

$$\left\{ \begin{array}{lll} \dot{z}_0 = & z_0 \left(i\omega_H + \alpha_H^{(T)}(T - T_0) + \alpha_H^{(\sigma_{loc})}(\sigma_{loc} - \sigma_{loc,0}) + \beta_H |z_0|^2 + \alpha_1 |z_1|^2 + \alpha_1 |z_2|^2 \right) & +I_0 \\ \dot{z}_1 = & z_1 \left(\frac{\sigma - \sigma_c}{\sigma_c} + \alpha_2 |z_0|^2 + \beta |z_1|^2 + \gamma |z_2|^2 \right) & +I_1 \\ \dot{z}_2 = & z_2 \left(\frac{\sigma - \sigma_c}{\sigma_c} + \alpha_2 |z_0|^2 + \beta |z_2|^2 + \gamma |z_1|^2 \right) & +I_2 \end{array} \right. \tag{11.22}$$

where β, γ, I_1, I_2 are the same as in (11.13), $I_0 = \int_\Omega I_{ext}(\mathbf{x}) d\mathbf{x}/(2\pi N_p)^2$ and $(T_0, \sigma_{loc,0})$ are the critical parameters.

Remark 37. The equations satisfied by the amplitudes are the same as for the Hopf-Hopf bifurcation with $O(2)$ symmetry (see [Golubitsky 1988] and section 5.2.2.4). Hence, the equations for the amplitudes ρ_p and phases θ_p of the $z_p = \rho_p e^{i\theta_p}$s are decoupled and we find a 3D system for the amplitudes.

We will not study these equations because they are extremely sophisticated (see [Golubitsky 1988, Chossat 1986]). However we can give the general flavour of what can or cannot happen, leaving the complete analysis for future work. There are the static solutions $(0, z_1, z_1)$, $(0, z_1, 0)$, $(0, 0, z_1)$ studied in the previous section or the oscillating solution $(z_0, 0, 0)$. But more importantly, there are Mixed-Mode solutions (see also section 5.2.2.3) like:

$$V_{MM}(\mathbf{x}, t) = v_0 + 2\rho_0 \cos(\omega_H t + \phi_0) + 2\Re(z_1 e^{ix_1} + z_2 e^{ix_2}), \tag{11.23}$$

or quasi-periodic solutions (see also section 5.2.2.3) like:

$$V_{FH}(\mathbf{x}, t) = v_0 + 2\rho_0 \sin(\omega_H t) \sin(\omega_{FH} t) + 2\Re(z_1 e^{ix_1} + z_2 e^{ix_2}) \cos(\omega_{FH} t), \tag{11.24}$$

[12] We also found a $\mathbf{D}_4$-Pitchfork-Hopf-Hopf instability in the stripes regime in the null vector, *i.e.* the most unstable.

[13] where c.c. means complex conjugate.

[14] Recall that T is the threshold

where ω_{FH} is a frequency. Let us have a look at the Mixed-Mode solution for example. The membrane potential oscillates between the values $v_0 - 2\rho_0 + 2\Re(z_1 e^{ix_1} + z_2 e^{ix_2})$ and $v_0 + 2\rho_0 + 2\Re(z_1 e^{ix_1} + z_2 e^{ix_2})$. We can try to find a stimulus which produces such cortical responses. For example, we recognize in the Mixed-Mode solution, the tuned component of the cortical response to a full field grating while the untuned component is oscillating. If $v_0 - 2\rho_0 + 2\Re(z_1 e^{ix_1} + z_2 e^{ix_2}) < T$ and $v_0 + 2\rho_0 + 2\Re(z_1 e^{ix_1} + z_2 e^{ix_2}) > T$, then the firing rate $S\left(\sigma\left[v_0 - 2\rho_0 + 2\Re(z_1 e^{ix_1} + z_2 e^{ix_2})\right]\right)$ is low while $v_0 - 2\rho_0 + 2\Re(z_1 e^{ix_1} + z_2 e^{ix_2})$ is above threshold. Hence, V_{MM} could be produced by a drifting grating that is periodically switched on/off.

We stop here the investigation of these time periodic cortical responses as they require the in-depth study of their stability which requires the study of the system (11.22).

Finally, we would like to look at the last instability that can appear with the delays: the Bogdanov-Takens bifurcation. Its occurrence has been investigated in lemma 4.6.4 and is conditioned by the inequality:

$$0 > \frac{1}{\hat{J}_{\mathbf{k}_c}} \int_\Omega J_{loc}(\mathbf{x}) \left(D + c \left\|\mathbf{x}\right\|_2\right) \cos(x_1) d\mathbf{x} = D + \frac{c}{\hat{J}_{\mathbf{k}_c}} \int_\Omega J_{loc}(\mathbf{x}) \left\|\mathbf{x}\right\|_2 \cos(x_1) d\mathbf{x}. \tag{11.25}$$

Numerically, we find that $\frac{1}{\hat{J}_{\mathbf{k}_c}} \int_\Omega J_{loc}(\mathbf{x}) \left\|\mathbf{x}\right\|_2 \cos(x_1) d\mathbf{x}$ is an increasing function of σ_{loc} which maps $(0.375\pi, 0.405\pi)$ to $(1.515,\ 1.804)$. This rules out the possibility of a Bogdanov-Takens bifurcation.

In this section, we have studied the responses of the network, working close to the $\mathbf{D}_4$-Pitchfork bifurcation point, when the delays are added. In the case of constant delays, no oscillating response can be produced by the network if it works in the spots or stripes regime. In the case of space dependent delays, we have found oscillating solutions in the null wavevector $\mathbf{k}_H = 0$. This wavevector is the most unstable, *i.e.* by decreasing the propagation speed, this is the first mode to become unstable. If the speed is decreased around a critical speed, the model features a $\mathbf{D}_4$-Pitchfork-Hopf bifurcation. An analogue, yet simpler, bifurcation has been analysed in section 5.2.2.3. Here, the larger number of symmetries makes it difficult the study of this bifurcation which is postponed to future work. Recall that the authors in [Bressloff 2008] also found a Pitchfork-Hopf bifurcation with $\mathbf{k}_H = 0$ but they did not perform the study of the normal form.

11.6 Study of the long-range connections

We now take the long-range connections in consideration. Recall from section 1 that these connections are patchy, connect populations with similar preferred orientation and, depending on the species, present an anisotropy. Given a cortical position $\mathbf{x}$, we can connect the population at $\mathbf{x}$ with the other populations at $\mathbf{y}$ according to $J_{LR}(\mathbf{x}, \mathbf{y}) = G_{\sigma_\theta}(\theta(\mathbf{x}) - \theta(\mathbf{y}))$ with $\sigma_\theta \approx 30^o$. We obtain a patchy connectivity because the regions of similar preferred orientations are patchy in figure 11.1. Note that the patchiness of this connectivity depends on the cortical location $\mathbf{x}$.

Remark 38. There is another way to produce patchiness (see chapter 1), i.e. by using $G_{\sigma_\theta}(\theta(\mathbf{x}-\mathbf{y}+\mathbf{v})-\theta(\mathbf{v}))$ *where* $\mathbf{v} \notin \pi\mathbb{Z}^2$. *The vector* $\mathbf{v}$ *is used so that* $\theta(0+\mathbf{v})$ *is defined. Recall that* $\theta(0)$ *is undefined because* 0 *is right at the pinwheel. This type of connectivity produces a patchiness that is homogeneous: it does not depend on the cortical position* $\mathbf{x}$ *as opposed to the connectivity we are using in this chapter.*

Depending on the species, we have seen in section 1 that the long range connections present an anisotropy in that they tend to align with the preferred orientation $\theta(\mathbf{x}_0)$ at $\mathbf{x}_0$. This can be modeled by a term "à la" Bressloff *et al.* (see for example [Bressloff 2003, Baker 2009]) $J_0(\chi, R_{-2\theta(\mathbf{x}_0)}(\mathbf{x}_0 - \mathbf{y}))$ where $J_0(\chi, \mathbf{x}) = e^{-\left[(1-\chi)^2 x_1^2 + x_2^2\right]/2\sigma_{LR}^2}$. $R_{2\theta(\mathbf{x}_0)}$ is the counter-clockwise rotation[15] of angle $2\theta(\mathbf{x}_0)$ and σ_{LR} is the long-range connections extent.

Remark 39. There are two minor issues here. First, to agree with the network geometry, the function $\mathbf{x} \to J_0(\chi, \mathbf{x})$ *should satisfy the periodic boundary conditions assumed for* Ω. *Geometrically,* Ω *is a torus. Hence, in the expression of* $R_{-2\theta(\mathbf{x}_0)}(\mathbf{x}_0 - \mathbf{y})$, *we have to perform a rotation of the vector* $\mathbf{x}_0 - \mathbf{y}$ *which belongs to the torus. It is not possible to define a rotation on a torus. Hence,* $R_{-2\theta(\mathbf{x}_0)}(\mathbf{x}_0 - \mathbf{y})$ *is not well defined. The solution is to assume that the long-range connections are strictly contained in a disc of diameter smaller then* $2N_p\pi$.

If $\chi = 0$, then there is no anisotropy (as for the macaque for example) whereas for $\chi \in (0, 1)$, this connectivity presents an anisotropy along the preferred direction[16] (as for the tree shrew for example). All in all, the long-range connectivity reads:

$$J_{LR}(\mathbf{x}, \mathbf{y}) = J_0(\chi, R_{-2\theta(\mathbf{x})}(\mathbf{x} - \mathbf{y})) \cdot G_{\sigma_\theta}(\theta(\mathbf{x}) - \theta(\mathbf{y})) \tag{11.26}$$

Finally, we have seen that the long-range connections are modulatory, *i.e.* they are small compared to the local connections, hence, the connectivity in (11.1) is now:

$$J(\mathbf{x}, \mathbf{y}) = J_{loc}(\mathbf{x} - \mathbf{y}) + \varepsilon_{LR} J_{LR}(\mathbf{x}, \mathbf{y}) \tag{11.27}$$

where ε_{LR} is small compared to $a - 1 = J_{loc}(0)$. The long-range connections feature the following relations:

Lemma 11.6.1. *The long-range connections satisfy the following invariances. For the PO maps* $\pm\theta^{\mathbf{1}} + \theta_0$*:*

$$J_{LR}(R_\phi \mathbf{x}, R_\phi \mathbf{y}) = J_{LR}(\mathbf{x}, \mathbf{y}), \quad \phi \in \frac{\pi}{4}\mathbb{Z}$$

Proof. See appendix F.2.1. □

[15] *i.e.* $R_\theta = \begin{bmatrix} \cos(\theta) & -\sin(\theta) \\ \sin(\theta) & \cos(\theta) \end{bmatrix}$

[16] Indeed, when $\chi > 0$, the function $\mathbf{x} \to J_0(\chi, \mathbf{x})$ is close to one on the x-axis and has a contour plot similar to an ellipse aligned with the x-axis. Hence, the connectivity $J_0(\chi, R_{-2\theta(\mathbf{x}_0)}(\mathbf{x}_0 - \mathbf{y}))$ is non zero when $R_{-2\theta(\mathbf{x}_0)}(\mathbf{x}_0 - \mathbf{y})$ is on the x-axis *i.e.* $\mathbf{x}_0 - \mathbf{y} \propto \pm R_{2\theta(\mathbf{x}_0)} e_x$ where e_x is the unit vector of the x-axis. This last condition corresponds to $\mathbf{y}$ being along the preferred direction of the neurons located at $\mathbf{x}_0$.

Let us look at the $\mathbf{D}_4$-Pitchfork in (11.13) with the long-range connections. As these connections are small, we can apply the center manifold theorem (see appendix A.1) with the two parameters $(\sigma, \varepsilon_{LR})$ instead of just σ. It gives:

$$\begin{cases} \dot{z}_1 = z_1 \left(\frac{\sigma-\sigma_0}{\sigma_0} + \varepsilon_{LR} J_1^{(LR)} + \beta|z_1|^2 + \gamma|z_2|^2 \right) + I_1 \\ \dot{z}_2 = z_2 \left(\frac{\sigma-\sigma_0}{\sigma_0} + \varepsilon_{LR} J_2^{(LR)} + \beta|z_2|^2 + \gamma|z_1|^2 \right) + I_2 \end{cases} \tag{11.28}$$

with

$$\begin{cases} J_1^{(LR)} = \int\limits_{\Omega^2} J_{LR}(\mathbf{x}, \mathbf{y}) e^{i(x_1 - y_1)} d\mathbf{x} d\mathbf{y} / (2\pi N_p)^2 \\ J_2^{(LR)} = \int\limits_{\Omega^2} J_{LR}(\mathbf{x}, \mathbf{y}) e^{i(x_2 - y_2)} d\mathbf{x} d\mathbf{y} / (2\pi N_p)^2. \end{cases} \tag{11.29}$$

These coefficients govern the effects of the long-range connections. From the symmetries of J_{LR}, we find the following properties of the coefficients $J_k^{(LR)}$, $k = 1, 2$:

Lemma 11.6.2. *For the PO maps $\pm\boldsymbol{\theta}^{\mathbf{1}} + \theta_0$, we have:*

$$J_1^{(LR)} = J_2^{(LR)} \in \mathbb{R}.$$

Proof. See appendix F.2.2. □

We also need to study the dependency of $J_1^{(LR)}$ (which equals $J_2^{(LR)}$ by the previous lemma) on the anisotropy χ. This is done numerically by using the fact that the integrand in $J_1^{(LR)}$ is known analytically as a function of $\mathbf{x}, \mathbf{y}$. Indeed, we can use that

$$\begin{aligned} \cos(2\boldsymbol{\theta}^{\mathbf{1}}(\mathbf{x})) &\approx (\sin(x_1) + \sin(x_2))/2 \\ \sin(2\boldsymbol{\theta}^{\mathbf{1}}(\mathbf{x})) &\approx (-\sin(x_1) + \sin(x_2))/2 \end{aligned} \tag{11.30}$$

to express the integrand. The result is shown in figure 11.7. Two facts are interesting. First $J_1^{(LR)}$ is positive for $\chi \in [0,\ 1]$ and it is an increasing function of

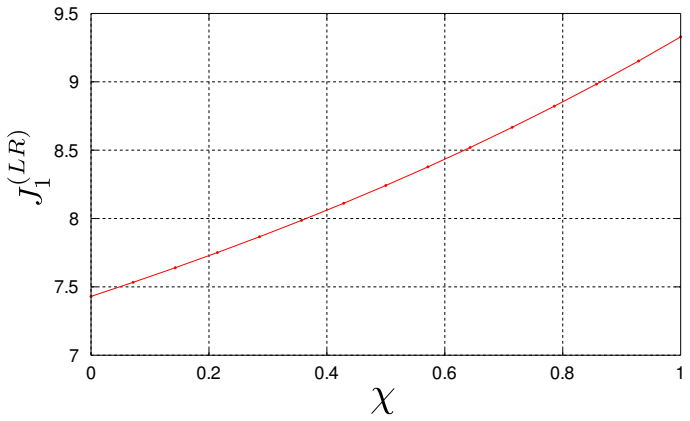

Figure 11.7: Plot of the coefficients $J_1^{(LR)}$ as function of the anisotropy χ for the map $\boldsymbol{\theta}^{\mathbf{1}}$. Computed with $N_p = 5$.

χ. Hence, from (11.28), the long-range connections improve the response: for a given stimulus, they increase the cortical response. This cortical response is further increased by the anisotropy χ for both local and full field stimuli.

We also provide the corrected normal form for the Pitchfork-Hopf bifurcation (11.22) with the long-range connections although we shall not push further its study:

$$\left\{\begin{array}{rl} \dot{z}_0 = & z_0\Big(i\omega_H + \alpha_H^{(T)}(T-T_0) + \alpha_H^{(\sigma_{loc})}(\sigma_{loc}-\sigma_{loc,0}) + \\ & \qquad \varepsilon_{LR}J_0^{(LR)} + \beta_H|z_0|^2 + \alpha_1|z_1|^2 + \alpha_1|z_2|^2\Big) \quad +I_0 \\ \dot{z}_1 = & z_1\left(\frac{\sigma-\sigma_0}{\sigma_0} + \varepsilon_{LR}J_1^{(LR)} + \alpha_2|z_0|^2 + \beta|z_1|^2 + \gamma|z_2|^2\right) \quad +I_1 \\ \dot{z}_2 = & z_2\left(\frac{\sigma-\sigma_0}{\sigma_0} + \varepsilon_{LR}J_2^{(LR)} + \alpha_2|z_0|^2 + \beta|z_2|^2 + \gamma|z_1|^2\right) \quad +I_2 \end{array}\right. \tag{11.31}$$

with $J_0^{(LR)} = e^{-i\omega_H D}\int\limits_{\Omega^2} d\mathbf{x}d\mathbf{y}J_{LR}(\mathbf{x},\mathbf{y})e^{-i\omega\|\mathbf{x}-\mathbf{y}\|_2}/(2\pi N_p)^2$.

11.7 Conclusion and extensions

We have shown how to implement the mechanism of Ben-Yishai *et al.* in a network with a biologically realistic connectivity on a PO square lattice. We have restricted the study to a one-population model and have found that it forced the (effective) connectivity to be a Mexican hat. Depending on the spatial extent of the local connectivity, the network spontaneously produces stripes or spots and this spontaneous response has to be adjusted in order to match the LGN input. The spatial extent of the local connectivity has to be two to three times smaller than the hypercolumn extent.

The study of the tuned responses has not been performed because of the difficulty to solve the equations. Note that this could be done numerically. We found that the width of the tuning curves was independent of the cortical position at large contrasts. We also found that the cortical response to a local oriented stimulus at θ_{aff} preferentially activated nearby populations of similar preferred orientation, this orientation was not linked to the stimulus angle θ_{aff}. In fact this dependency is a function of the contrast. Hence, it would be very interesting to look at the spontaneous responses and how they are altered by a stimulus. We expect something similar to the perception threshold of chapter 9 to hold but something new happens. There should be a perception threshold corresponding to the contrast value for which the cortical response aligns with the stimulus angle. Indeed, at small contrasts, the network has definite preferred orientations which are independent of the stimulus angle. For larger contrasts, there is a unique response which is (almost) aligned with the stimulus. At intermediate contrasts, the (stable) response angle is different from that of the stimulus angle. Hence, this suggests the existence of a threshold contrast at which the cortical response agrees with the stimulus. This does not happen in the Ring Model because the cortical response is always aligned with the stimulus. More study is needed to understand this mechanism. Note that this is central for the understanding of how much work is done by the recurrent connections compared to the LGN input in order to shape the cortical response.

We then studied how space-dependent delays could change the above conclusions. We found that if the model is insensitive to constant delays, it can be destabilized for particular pairs of constant-propagation delays. This requires a propagation speed that is 30 times smaller than the biological value. Hence, the model is insensitive to space-dependent delays as well. However, the delay-induced instabilities are very rich and could give rise to *time periodic planform*. We have not studied the resulting equations which, theoretically, support a wealth of behaviours. These behaviours could be seen if the propagation speed in tissues was pharmacologically reduced as with drugs for example. We have then considered long-range connections and showed that they increased the cortical response to drifting gratings and that the anisotropy further increased this response. However, they do not shape the spontaneous activity as they do in the work of Bressloff *et al.* .

Finally, this model has been a fantastic test-bed for the techniques we have developed in the two previous part. In particular, we have used the normal forms reduction for non-delayed/delayed neural fields and the analytical formulas for the Hopf bifurcation curves. Without this very last tool, the study of the model would have been far more difficult to achieve and would have relied on very intensive numerical computations.

This model could be extended in several ways in addition to the study of the reduced equations. The first step would be to study the pinwheel hexagonal lattice to see if it produces the same value for the local connectivity extent. Then it would be interesting to incorporate neuronal adaptation as it has been shown to be necessary for the orientation tuning in monkeys in [Nowak 2009]. Also a more detailed analysis of the Pitchfork-Hopf normal form is needed. Note that a study of centre-surround modulation is unlikely to reproduce biological data as it has been shown in [Seriès 2002a] that is requires at least two populations.

However, the real challenge is to make the model work with two excitatory/inhibitory populations with the same local spatial extent of the connectivity. The number of parameters is greatly increased but some other biological facts can be used to restrict their value. For example, contrast saturation of cortical responses, centre-surround modulations, motion streaks... These effects have already been widely modeled (see for example [Stetter 2000, Seriès 2002a, Lund 2003b]) but the idea here, would be to propose a working regime that rules out a huge set of possible parameters. To reach this goal, the tools developed in this Thesis will be essential.

Chapter 12

Conclusion

You can't always get what you want
But if you try sometimes you might find
You get what you need
(The Rolling Stones)

In this Thesis, we have used tools from dynamical systems theory to probe general neural field equations in the quest of understanding the more complex spiking neural networks. We decided to study these equations in the most general case with the minimal assumptions. This decision naturally split the Thesis in three main parts, two being "theoretical" and one collecting the applications to specific models of primary visual cortex.

In the part concerning the stationary cortical states, we found, by applying the degree theory, that the number of stationary solutions is odd for almost any parameters values. Moreover, the degree theory suggested a way of computing these solutions by deforming the nonlinearity to a new one, that we can treat analytically, and then following the solutions by deforming the nonlinearity back to the one we are interested in. This scheme can be parallelized on many computers to deal with large networks. Also, we found that by looking at the range of the integral operator linked to the connectivity function, we could describe without approximations the stationary solutions with potentially few variables.

Concerning the delays in the neural field, the two most important achievements have been the discovery of an analytical formula for the Hopf bifurcation curve and the proof of a center manifold theorem. The analytical formula provides the critical pair (effective delay, propagation delay) and the center manifold theorem allows to reduce the local dynamics around stationary solutions to ordinary differential equations. Then, various normal forms were computed in view of their use in the study of 1D simple neural networks. Despite their apparent simplicity, these networks can display sophisticated dynamics which require further investigations.

In the last part, we applied these results to particular models of the primary visual cortex (V1). The first application concerns the Ring Model, an hypercolumn model, to which we applied the Orbit Space Reduction to cope with the internal symmetries. Our bifurcation analysis provided a complete understanding of all parameters. We also identified a perception threshold, *i.e.* the minimal stimulus contrast that is required by the network to produce a cortical response in agreement with the stimulus. Finally, we found that the hypercolumn can be "fooled" by a well chosen sequence of stimuli. Then, we studied a V1 model which relies on experimental data and generalises the Ring Model. The idea was to see how many

of the results for the Ring Model extend to a network of hypercolumns. Also, we were interested in the effects of symmetries as experimental models do not display perfect symmetries. We conjectured the existence of a perception threshold but we failed to understand the mechanism in its full generality, it deserves further work. This understanding is of major importance because it gives the amount of cortical computation on top of the LGN input which is needed to shape the resulting cortical activity. The two previous models feature unrealistic connectivity between populations. We have then developed a new V1 model that generalises the previous two in the way they work, *i.e.* close to a static bifurcation, while modeling more closely biology. We have then used the analytical formulas for delays to arrive at the conclusion that the critical propagation speed is thirty times smaller than the experimental one whereas the critical effective delay is in the range of what is experimentally observed. Hence, the delay dependent effects cannot be seen without decreasing the propagation speed with drugs for example (see section 11.7).

Perspectives

The work concerning the stationary solutions can be pushed further. One could, for example, couple degree theory and equivariant theory to get results concerning the bifurcated branches in networks with symmetries. Also, in the 2D case, a criterion (such as the nodal structure of the cortical activity) is missing to describe the global structure of bifurcated branches. Such criterion, if it exists, would help the study of more realistic neural field models.

In the case of delays, a better understanding of the multiple effective delays case is required in order to avoid heavy simulations. Despite our proposition of a general numerical scheme applicable to any kind of delays, we think that the analytical study of two excitatory/inhibitory populations on 1D cortices with distinct effective delays and no propagation delays could be a first step to more sophisticated models well worth investigating. This would be particularly useful for the generalization of our V1 model to two populations for example.

On a more theoretical point of view, the study of the normal forms Fold-Hopf and Hopf-Hopf with $O(2)$-symmetry in the general case is lacking in our analysis. It would allow a complete understanding of the simple network with inverted Mexican-hat connectivity and delays.

An interesting aspect, not covered in this Thesis, is the interaction between neuronal/synaptic adaptation and delays. This has largely been ignored in the literature (we are only aware of the work of Venkov and co-workers) despite the usefulness and applicability to visual cortex models. Indeed, if after some intense period of activity, an hypercolumn is required to rest for some time δt regardless of its afferent inputs, it can only "see" hypercolumns at distance $v\delta t$, where v is the propagation speed of signals along axons. It seems that interesting behaviours, for biology and pattern theory could emerge from this interaction. The analysis of such models could be done with our tools without much change.

This suggests the move of neural fields modeling to a more dynamical stage. In the neuronal systems, and in particular in the visual system, there are many aspects which call for more dynamics. The first intriguing aspect of our vision system lies in the fixational eye movements (see the review [Martinez-Conde 2004]) that continuously modify - although without attention - the input to the network. These eye movements are driven by the Superior Colliculus which also sends the information to the visual area MT. The importance of the fixational eye movements for the visual system is crucial as it has been experimentally demonstrated that the blockade of eye movements paralyses our vision system in less than $100ms$ (see [Martinez-Conde 2004]). It is believed that the eye movements are necessary in order to counter the adaptation of the neuronal system to the external input. A first interesting remark is that by the spatial arrangement of the cortical neurons receptive fields, when the eye is pointing to an object of the visual field, a multi-scale representation of the scene is automatically generated. When looking at some contour, the activity is locally fluctuating (because of the eye movements) and is shaped by the phenomena of spike frequency adaptation and synaptic depression/facilitation. If one contour has been seen at a given location $\mathbf{r}_0$, it generates some high neuronal activity which is transmitted to the neighbourhood at a propagation speed of $v \approx 0.1-1 mm/ms$ (see section 2.2.5) while the neurons at $\mathbf{r}_0$ will be silent, because they spiked a lot, for a few hundreds of milliseconds. This activity wave will depolarize the neighbourhood and facilitates the detection of the contour (which has moved because of the eye movements) by the synchronization of the depolarization wave and the stimulus input (see also [Bringuier 1999, Seriès 2002b]) at the condition that the horizontal propagation speed and the eye movement speed are of the same order in cortical coordinates (for example). We think that the tools developed in this Thesis are mature enough to cope with these more dynamical questions about information processing in the first stages of the visual stream.

The work in part II is published in [Veltz 2010]. The analytical formula for the Hopf bifurcation curve in delayed neural field equations given in chapter 4 is published in [Veltz 2011a]. Finally, the stability analysis of stationary states in neural field equations through the use of fixed point methods is published in [Veltz 2011b].

Index

Part V

Appendix

Appendix A

Stationary properties

Definition A.0.1 (Stationary bifurcation point). *Let us consider an equation* $F(\mathbf{V},\sigma) = 0,\ \mathbf{V} \in \mathcal{B},\ \sigma \in \mathbb{R}^p$ *on a Banach space* $\mathcal{B}$. *Let us assume that* $\mathbf{V} = 0$ *is solution of this equation for all* σ. *Then,* σ_0 *is said to be a bifurcation point if there exists a sequence* $(\mathbf{V}_n, \sigma_n)$ *of solutions such that* $(\mathbf{V}_n, \sigma_n) \to (0, \sigma_0)$ *and* $(V_n)_n$ *is not a null sequence.*

If F is differentiable in the first variable, the Implicit functions theorem implies that σ_0 is a bifurcation point if the differential $D_{\mathbf{V}}F(0,\sigma_0)$ at $(0,\sigma_0)$ is not invertible.

Definition A.0.2 (Equivariant vector field). *A vector field* $F : \mathcal{B} \to \mathcal{B}$ *is said* G*-equivariant if* G *acts on* $\mathcal{B}$ *and* $\forall \mathbf{V} \in \mathcal{B},\ \forall g \in G,\ F(g \cdot \mathbf{V}) = g \cdot F(\mathbf{V})$.

A.1 The center manifold theorem from [Haragus 2010]

Let us consider the equation :

$$\frac{d}{dt}\mathbf{U} = \mathbf{L}\mathbf{U} + \mathbf{R}(\mathbf{U},\mu) \tag{A.1}$$

with 3 Banach spaces $\mathcal{Z} \to \mathcal{Y} \to \mathcal{X}$ with continuous embeddings. Let us assume that:

- $\mathbf{L} \in \mathcal{L}(\mathcal{Z},\mathcal{X})$.
- $\mathbf{R}(0,0) = 0,\ D_u\mathbf{R}(0,0) = 0$ and $\mathbf{R} \in C^k(\mathcal{V}_1 \times \mathcal{V}_2, \mathcal{Y})$, $k \geq 2$ with $\mathcal{V}_1 \times \mathcal{V}_2$, a neighbourhood of $(0,0)$ in $\mathbb{R}^{m_{par}} \times \mathcal{Z}$
- the spectrum of $\mathbf{L}$ is : $\Sigma(\mathbf{L}) = \Sigma_s - (\mathbf{L}) \cup \Sigma_c(\mathbf{L}) \cup \Sigma_u(\mathbf{L})$ with $\sup \Sigma_u(\mathbf{L}) > \gamma > 0$, $\sup \Sigma_s(\mathbf{L}) < -\gamma$. Moreover, $\Sigma_c(\mathbf{L})$ is the finite set of eigenvalues of finite algebraic multiplicities with zero real part.
- there are $\omega_0 > 0, c > 0, \alpha \in [0,1)$ such that $\forall \omega, |\omega| > \omega_0$, then $i\omega \notin \Sigma(\mathbf{L})$ and

$$\left\|(i\omega I - \mathbf{L})^{-1}\right\|_{\mathcal{L}(\mathcal{X})} \leq \frac{c}{|\omega|}$$

$$\left\|(i\omega I - \mathbf{L})^{-1}\right\|_{\mathcal{L}(\mathcal{Y},\mathcal{Z})} \leq \frac{c}{|\omega|^{1-\alpha}}$$

We write $\mathcal{X}_c$ the sum of the generalized eigenspaces for the eigenvalues in $\Sigma_c(\mathbf{L})$ and $\mathbf{P}_c$ the unique projector on $\mathcal{X}_c$ which commutes with $\mathbf{L}$. We also define the hyperbolic projector $\mathbf{P}_h \equiv \mathrm{Id} - \mathbf{P}_c$.

Theorem A.1.1 ([Haragus 2010]). *There is an application $\Psi \in C^k(\mathcal{X}_c \times \mathbb{R}^{m_{par}}, \mathbf{P}_h\mathcal{Z})$ with $\Psi(0,0) = 0$, $D\Psi(0,0) = 0$ and a neighbourhood $\mathcal{O}_u \times \mathcal{O}_\mu$ of $(0,0)$ in $\mathcal{Z} \times \mathbb{R}^{m_{par}}$ such that $\mu \in \mathcal{O}_\mu$ and a manifold $\mathcal{M}_0(\mu) = \{\mathbf{U}_c + \Psi(\mathbf{U}_c, \mu), \mathbf{U}_c \in \mathcal{X}_c\}$ such that :*

- *$\mathcal{M}(\mu)$ is locally invariant, i.e., if $\mathbf{U}$ is a solution of (A.1) satisfying $\mathbf{U}(0) \in \mathcal{M}(\mu) \cap \mathcal{O}_u$ and $\mathbf{U}(t) \in \mathcal{O}_u$ for all $t \in [0,T]$, then $\mathbf{U}(t) \in \mathcal{M}(\mu)$ for all $t \in [0,T]$.*
- *$\mathcal{M}(\mu)$ contains the set of bounded solutions of (A.1) staying in $\mathcal{O}_u$ for all $t \in \mathbb{R}$, i.e. if $\mathbf{U}$ is a solution of (A.1) satisfying for all $t \in \mathbb{R}$, $\mathbf{U}(t) \in \mathcal{O}_u$, then $\mathbf{U}(0) \in \mathcal{M}(\mu)$.*

A solution on the center manifold reads $\mathbf{U} = \mathbf{U}_0 + \Psi(\mathbf{U}_0, \mu)$ and satisfies

$$\frac{d}{dt}\mathbf{U}_0 = \mathbf{L}_0\mathbf{U}_c + \mathbf{P}_c\mathbf{R}(\mathbf{U}_c + \Psi(\mathbf{U}_c, \mu)). \tag{A.2}$$

A.2 Well-posedness of operators

We prove proposition A.2.1:

Proposition A.2.1. *If $\forall t,\ \mathbf{J}(t) \in \mathrm{L}^2(\Omega^2, \mathbb{R}^{\mathrm{p}\times\mathrm{p}})$, the linear integral operator $\mathbf{J}(t)$ is continuous from $\mathcal{F}$ to $\mathcal{F}$ and its norm $|||\mathbf{J}(t)|||_{\mathcal{F}}$ is bounded by $\|\mathbf{J}(t)\|_{\mathrm{L}^2(\Omega^2,\mathbb{R}^{\mathrm{p}\times\mathrm{p}})}$.*

Proof. The integral in the right-hand side of (3.2) exists because for almost all $\mathbf{r} \in \Omega$ the p^2 elements $J_{ij}(\mathbf{r}, \cdot, t)$, $i,j = 1, \cdots, p$ of $\mathbf{J}$ are in $\mathrm{L}^2(\Omega)$ for all $t > 0$ and the p coordinates of $\mathbf{V}(\cdot, t)$ are in $\mathrm{L}^2(\Omega)$ for all $t > 0$. Because of Fubini's theorem it is clear that $\mathbf{U}(t) = \mathbf{J}(t) \cdot \mathbf{V}(t)$ is an element of $\mathcal{F}$ for all $t > 0$. Next we have (we drop the time variable to simplify)

$$|U_i(\mathbf{r})| \leq \sum_j \left| \int_\Omega J_{ij}(\mathbf{r}, \mathbf{r}')\, V_j(\mathbf{r}')\, d\mathbf{r}' \right|$$

and (Cauchy-Schwarz):

$$|U_i(\mathbf{r})| \leq \sum_j \left(\int_\Omega J_{ij}^2(\mathbf{r}, \mathbf{r}')\, d\mathbf{r}' \right)^{1/2} \|V_j\|_2 ,$$

from where it follows that (Cauchy-Schwarz again, discrete version):

$$|U_i(\mathbf{r})| \leq \left(\sum_j \|V_j\|_2 \right)^{1/2} \left(\sum_j \int_\Omega J_{ij}^2(\mathbf{r}, \mathbf{r}')\, d\mathbf{r}' \right)^{1/2} = \|\mathbf{V}\|_{\mathcal{F}} \left(\sum_j \int_\Omega J_{ij}^2(\mathbf{r}, \mathbf{r}')\, d\mathbf{r}' \right)^{1/2} ,$$

from what it follows that $\mathbf{y}$ is in $\mathbf{L}^2_n(\Omega)$ (thanks again to Fubini's theorem) and

$$\|\mathbf{y}\|^2_{\mathcal{F}} \leq \|\mathbf{V}\|^2_{\mathcal{F}} \sum_{i,j} \int_{\Omega\times\Omega} J^2_{ij}(\mathbf{r},\mathbf{r}')\, d\mathbf{r}'\, d\mathbf{r} = \|\mathbf{V}\|^2_{\mathcal{F}}\, \|\mathbf{J}\|^2_{\mathrm{L}^2(\Omega^2,\mathbb{R}^{\mathrm{p}\times\mathrm{p}})}.$$

□

A.3 Fixed points theorems

We briefly describe some applications of Brouwer's and Leray-Schauder's degree theories. They are central in the proofs of parts 4 and 5 of proposition 3.2.7.

We first recall Schaeffer's theorem and provide a short proof based on the Leray-Schauder degree.

Theorem A.3.1 (Schaeffer). *Let X be a real Banach space. Suppose $M : X \to X$ is a compact mapping and*

$$\mathcal{S} = \{x \in X \,|\, \exists t \in [0,1] \text{ such that } x = tM(x)\}$$

is bounded. Then M has a fixed point.

Proof. We provide for completeness a short proof based on Leray-Schauder's degree theory. Taking $r > 0$ large enough such that $\mathcal{S} \subset B^\circ_r$, we define $m(x,t) = x - tM(x)$ on $\bar{B}_r \times [0,1]$. Then $0 \notin m(\partial B_r \times [0,1])$ by construction. According to the homotopy invariance of the Leray-Schauder degree

$$\deg_{\mathrm{LS}}(\mathrm{Id} - M, B_r, 0) = \deg_{\mathrm{LS}}(\mathrm{Id}, B_r, 0) = 1 \neq 0,$$

thus, according to the Kronecker property of the Leray-Schauder degree, there exists a solution to the equation $M(x) = x$. □

We can apply this theorem to prove existence of solutions to equation (3.9). We consider the function $\tilde{F} : \mathcal{F} \to \mathcal{F}$ defined by:

$$\tilde{F}(\mathbf{V},\sigma) = -F(\mathbf{V},\sigma) + \mathbf{V} = \mathbf{J}\cdot\mathbf{S}(\sigma\mathbf{V}) + \mathbf{I},$$

where F is defined in equation (3.9).

It is known that $\tilde{F}$ is a nonlinear compact operator of $\mathcal{F}$ [Faugeras 2009]. We can apply Schaeffer's theorem to the function $\tilde{F}$ since it is easy to prove (see [Faugeras 2009]) that for all $\mathbf{V}$ such that $\tilde{F}(\mathbf{V},\sigma) = t\mathbf{V}$ the following holds

$$\|\mathbf{V}\|_{\mathcal{F}} \leq t(\sigma\sqrt{p|\Omega|}\|\mathbf{J}\|_F + \|\mathbf{I}\|_{\mathcal{F}}), \tag{A.3}$$

where $\|\ \|_F$ is the Frobenius norm.

Hence for all σ there exists $\mathbf{V}^f_\sigma$ such that

$$\tilde{F}(\mathbf{V}^f_\sigma,\sigma) = \mathbf{V}^f_\sigma$$

The following easy consequence of the proof of theorem A.3.1 is used in the article.

Corollary A.3.2. *For each $\sigma \geq 0$ there exists an open bounded set $\mathcal{U}_\sigma$ containing $\mathcal{S}$ (defined in theorem A.3.1) such that* $\deg_{\mathrm{LS}}(\mathrm{Id} - \tilde{F}, \mathcal{U}_\sigma, 0) = 1$.

We next give without proof a theorem due to Leray and Schauder.

Theorem A.3.3 (Leray-Schauder). *Let X be a real normed space, $J = [a, b]$ and $M : X \times J \to X$ be of the form $Id + m$ with $m : X \times J \to X$ compact on $X \times J$. Let*

$$\Sigma = \{(x, \sigma) \in X \times J \ : \ M(x, \sigma) = 0\}$$

and for each $\sigma \in J$, let

$$\Sigma_\sigma = \{x \in X \ : \ (x, \sigma) \in \Sigma\}$$

Assume that Σ_a is bounded and that

$$\deg_{\mathrm{LS}}(M(., a), \mathcal{U}, 0) \neq 0$$

for some open bounded set $\mathcal{U} \supset \Sigma_a$.

Then Σ contains a connected component $\mathcal{C}$ intersecting $\Sigma_a \times \{a\}$ and which either intersects $\Sigma_b \times \{b\}$ or is unbounded.

A.4 Compact operators with simple eigenvalues

Proposition A.4.1. *For every $m \in \mathbb{N}^*$, the set of compact operators with m simple first eigenvalues is dense in the set of compact operators.*

Proof. The set $\mathcal{R}_f(\mathcal{F})$ of finite dimensional range linear operators is dense in the set $\mathcal{H}$ of the linear compact operators of $\mathcal{F}$ [Brezis 1983]. Thus we only need to prove the theorem for $\mathcal{R}_f(\mathcal{F})$. Let us consider $\mathbf{J} \in \mathcal{R}_f(\mathcal{F})$, and $R(\mathbf{J}) = Span(e_1, ..., e_k)$, $k \geq m$. Without loss of generality we assume that the first eigenvalue of $\mathbf{J}$ has multiplicity two, i.e. $\beta_1 = \beta_2$. Its corresponding Jordan block is then

$$\begin{bmatrix} \beta_1 & \varepsilon \\ 0 & \beta_1 \end{bmatrix}$$

Then if we define $\mathbf{J}_n = \mathbf{J} + \frac{1}{n} e_2 \otimes e_2$, we have $\lim_{n \to \infty} \mathbf{J}_n = \mathbf{J}$. The first two eigenvalues β_1 and $\beta_1 + \frac{1}{n}$ of $\mathbf{J}_n$ are simple, i.e. $\mathbf{J}_n e_1 = \beta_1 e_1$ and $\mathbf{J}_n(n\varepsilon e_1 + e_2) = (\beta_1 + \frac{1}{n})(n\varepsilon e_1 + e_2)$. We can do the same for the other eigenvalues, and define an operator $\mathbf{J}_n$ with m simple first eigenvalues, a finite dimensional rank, and which is arbitrarily close to $\mathbf{J}$. □

Proposition A.4.2. *The same proposition holds for operators of the type* $\mathrm{Id} + \mathbf{J}$ *where* $\mathbf{J}$ *is a compact operator.*

Proof. It follows from that of A.4.1. □

A.5 Reduction of the activity based model to a finite number of ordinary differential equations

We consider the equation for the activity-based model:

$$\begin{cases} \dot{\mathbf{A}} & = & -\mathbf{L}_a \cdot \mathbf{A} + \mathbf{S}_\sigma\left(\mathbf{J} \cdot \mathbf{A} + \mathbf{I}\right) \quad t > 0 \\ \mathbf{A}(\cdot, 0) & = & \mathbf{A}_0(\cdot) \end{cases} \tag{A.4}$$

We recall that $\mathbf{L}_a \neq \mathbf{L}$ (see [Ermentrout 1998]) because they do not have the same biological meaning: One is related to the synaptic time constant and the other to the cell membrane time constant. We let $\mathbf{L}_a = \mathrm{diag}(\alpha_1, \cdots, \alpha_p)$. We also recall the PG-kernel decomposition of $\mathbf{J} = \sum_k X_k \otimes Y_k$. Each of the p coordinates A_i, $i = 1, \cdots, p$ of $\mathbf{A}$ satisfies

$$\dot{A}_i + \alpha_i A_i = \mathbf{S}_\sigma(\mathbf{J} \cdot \mathbf{A} + \mathbf{I})_i \quad i = 1, \cdots, p$$

Similarly to the voltage case, let us consider the p finite dimensional subspaces F_i, $i = 1, \cdots, p$ of $\mathrm{L}^2(\Omega, \mathbb{R})$, where each F_i is generated by the N elements Y_k^i, $k = 1, \cdots, N$. We decompose $\mathrm{L}^2(\Omega, \mathbb{R})$ as the direct sum of F_i and its orthogonal complement for $\langle , \rangle_2$ $F_i^\perp$, $\mathrm{L}^2(\Omega, \mathbb{R}) = \mathrm{F_i} \oplus \mathrm{F_i^\perp}$ and write $A_i = A_i^\parallel + A_i^\perp$. We note $\prod_i^\parallel$ (respectively $\prod_i^\perp$) the projection from $\mathrm{L}^2(\Omega, \mathbb{R})$ to F_i (respectively to $F_i^\perp$) parallel to $F_i^\perp$ (respectively to F_i). This induces a decomposition of $\mathcal{F}$ as the direct sum of $F = \prod_{i=1}^p F_i$ and $F^\perp = \prod_{i=1}^p F_i^\perp$ such that for each vector $\mathbf{A}$ of $\mathcal{F}$ we can write $\mathbf{A} = \mathbf{A}^\parallel + \mathbf{A}^\perp$. By construction we also have

$$\mathbf{J} \cdot \mathbf{A}^\perp = 0,$$

and therefore

$$\begin{cases} \dot{A}_i^\parallel + \alpha_i A_i^\parallel = \prod_i^\parallel \mathbf{S}_\sigma(\mathbf{J} \cdot \mathbf{A}^\parallel + \mathbf{I})_i \\ \dot{A}_i^\perp + \alpha_i A_i^\perp = \prod_i^\perp \mathbf{S}_\sigma(\mathbf{J} \cdot \mathbf{A}_F + \mathbf{I})_i \end{cases} \quad i = 1, \cdots, p$$

which is a $2p$-dimensional non-autonomous system of ODEs:

$$\begin{cases} \dot{\mathbf{A}}^\parallel + \mathbf{L}_a \cdot \mathbf{A}^\parallel = \prod^\parallel \mathbf{S}_\sigma(\mathbf{J} \cdot \mathbf{A}^\parallel + \mathbf{I}) \\ \dot{\mathbf{A}}^\perp + \mathbf{L}_a \cdot \mathbf{A}^\perp = \prod^\perp \mathbf{S}_\sigma(\mathbf{J} \cdot \mathbf{A}^\parallel + \mathbf{I}) \end{cases},$$

where $\prod^\parallel \mathbf{A} = (\prod_i^\parallel A_i)_{i=1,\cdots,p}$ and $\prod^\perp \mathbf{A} = (\prod_i^\perp A_i)_{i=1,\cdots,p}$ are the projections of $\mathbf{A}$ on F and $F^\perp$. The first equation is a p-dimensional autonomous system of ODEs, which can be solved before solving the second one.

A.6 Lemmas for the general bounds

Lemma A.6.1. *For all x, $\sigma \in \mathbb{R}$ we have*

$$(S(\sigma x) - S(0))^2 \leq S(\sigma^2 x^2) - S(0)$$

Proof. We set $X = \sigma x$ and consider two cases.

$X > 1$ We have $e^{-X} > e^{-X^2}$ and therefore $S(X) - 1/2 < S(X^2) - 1/2$. Moreover, since $S(X) - 1/2 < 1$, $(S(X) - 1/2)^2 < S(X) - 1/2$ and we are done.

$0 < X < 1$ We let $X = \log y$, $1 < y < e$. We therefore have

$$S(X) - 1/2 = \frac{1}{2}\frac{y-1}{y+1} \quad S(X^2) - 1/2 = \frac{1}{2}\frac{y^{\log y} - 1}{y^{\log y} + 1}$$

We consider the expression $(y-1)^2(y^{\log y}+1) - 2(y+1)^2(y^{\log y}-1)$ and prove it is negative. Because $y^{\log y} < y$ it is upperbounded by $(y-1)^2(y^{\log y}+1) - 2(y^{\log y}+1)^2(y^{\log y}-1)$ which has the sign of $(y-1)^2 - 2(y^{2\log y}-1)$. The last expression is upperbounded by $(y-1)^2 - 2(y^{\log y}-1) = (e^X - 1)^2 - 2(e^{X^2}-1)$ which is negative for $0 < X < 1$.

□

Proposition A.6.2. *The solutions of equation (3.9) satisfy the following inequalities for all* $\sigma \geq 0$

$$\left\|\mathbf{V}_\sigma^f\right\|_{\mathcal{F}} \leq \sqrt{p|\Omega|}\,\|\mathbf{J}\|_{\mathcal{F}} + \|\mathbf{I}_{\text{ext}}\|_{\mathcal{F}} \stackrel{\text{def}}{=} B_1$$

$$\left\|\mathbf{V}_\sigma^f - \mathbf{V}_0^f\right\|_{\mathcal{F}} \leq \frac{1}{2}\sqrt{p|\Omega|}\,\|\mathbf{J}\|_{\mathcal{F}} \stackrel{\text{def}}{=} B_2,$$

as well as

$$\left\|\mathbf{V}_\sigma^f - \mathbf{V}_0^f\right\|_{\mathcal{F}} \leq \frac{\sigma}{4}\,\|\mathbf{J}\|_{\mathcal{F}}\,B_1$$

Proof. The first inequality is a straightforward consequence of equation (3.9), taking the $\mathcal{F}$-norm and using the fact that $0 \leq S(x) \leq 1$ for all $x \in \mathbb{R}$.http://fidji.inria.fr/biblio For the second one we write $\mathbf{V}_\sigma^f - \mathbf{V}_0^f = \mathbf{J} \cdot (\mathbf{S}(\sigma\mathbf{V}_\sigma^f) - \mathbf{S}(0))$, take the $\mathcal{F}$-norm of both sides of the equality and use the Cauchy-Schwarz inequality. We find $\left\|\mathbf{V}_\sigma^f - \mathbf{V}_0^f\right\|_{\mathcal{F}} \leq \|\mathbf{J}\|_{\mathcal{F}} \cdot \left\|\mathbf{S}(\sigma\mathbf{V}_\sigma^f) - \mathbf{S}(0)\right\|_{\mathrm{L}^2(\Omega,\mathbb{R}^p)}$. But since $\forall x \in \mathbb{R},\ -\frac{1}{2} \leq S(x) - S(0) \leq \frac{1}{2}$, we have $\left\|\mathbf{S}(\mathbf{V}_\sigma^f) - \mathbf{S}(0)\right\|_{\mathrm{L}^2(\Omega,\mathbb{R}^p)} \leq \frac{1}{2}\sqrt{p|\Omega|}$, which proves the first inequality.

The third inequality can be obtained as follows. It is easy to see that $S(\sigma x) - S(0) \leq \frac{\sigma}{4}|x|$ for all $x \in \mathbb{R}$ and all $\sigma \geq 0$. This implies that $\left\|\mathbf{S}(\mathbf{V}_\sigma^f) - \mathbf{S}(0)\right\| \leq \frac{\sigma}{4}\left\|\mathbf{V}_\sigma^f\right\|$. The first inequality yields the third. □

A.7 The size of the basin of attraction of a stable persistent state

In order to get a rough estimate of the size of the basin of attraction of a stable stationary solution of the neural field equations we prove the following, general, lemma.

Lemma A.7.1.*Let* x^f *be a stable stationary solution of the finite dimensional dynamical system* $\dot{x} = f(x)$ *at which the Jacobian matrix* A *is symmetric. If the*

second order derivative $D^2 f$ is bounded ($\left\|D^2 f\right\|_\infty < \infty$), the stable manifold of x^f contains the open ball $B(x^f, R)$ with $R = 2\frac{\min|\sigma(A)|}{\|D^2 f\|_\infty}$, where $\sigma(A)$ is the spectrum of the Jacobian matrix A.

Proof. We assume w.l.g. that $x^f = 0$. We write $A = Df(0)$ and $f(x) = Ax + \varepsilon(x)$, then it is known, and easy to verify, that $L(x) = \int_0^\infty \left\|e^{sA}x\right\|^2 ds$ is a Lyapunov function. Moreover, because of the Taylor's formula without remainder we have

$$\varepsilon(x) = \left(\int_0^1 (1-s)D^2 f(sx)\, ds\right) \cdot (x, x),$$

from which we deduce that

$$\|\varepsilon(x)\| \leq \frac{1}{2} \|x\|^2 \left\|D^2 f\right\|_\infty .$$

Let us compute

$$DL(x) \cdot f(x) = DL(x) \cdot (Ax + \varepsilon(x)) = -\|x\|^2 + DL(x) \cdot \varepsilon(x)$$

Now $DL(x) \cdot h = -\left\langle A^{-1}x, h\right\rangle$ and since A is symmetric, we obtain $|DL(x) \cdot h| \leq \frac{1}{\min|\sigma(A)|} \|x\| \|h\|$ and finally

$$DL(x) \cdot f(x) \leq \|x\|^2 \left(-1 + \frac{1}{2}\left\|D^2 f\right\|_\infty \frac{1}{\min|\sigma(A)|}\|x\|\right) < 0$$

if $\|x\| < 2\frac{\min|\sigma A|}{\|D^2 f\|_\infty} \equiv R$ □

Appendix B

Theory of delays

B.1 Operators and their spectra

We recall and gather in this appendix a number of definitions, results and hypotheses that are used in the body of the Thesis to make it more self-sufficient.

Definition B.1.1. *We note* $|||\mathbf{J}|||_{\mathcal{F}}$ *the operator norm of a bounded operator* $\mathbf{J} \in \mathcal{L}(\mathcal{F}, \mathcal{F})$*, ie*

$$\sup_{\|\mathbf{V}\|_{\mathcal{F}} \leq 1} \frac{\|\mathbf{J} \cdot \mathbf{V}\|_{\mathcal{F}}}{\|\mathbf{V}\|_{\mathcal{F}}}$$

It is known, see e.g. [Kato 1995], that

$$|||\mathbf{J}|||_{\mathcal{F}} \leq \|\mathbf{J}\|_{\mathrm{L}^2(\Omega^2, \mathbf{R}^{\mathrm{p}\times\mathrm{p}})}$$

Definition B.1.2. *A semigroup* $(\mathbf{T}(t))_{t\geq 0}$ *on a Banach space* X *is strongly continuous if* $\forall x \in X$*,* $t \to T(t)x$ *is continuous from* $\mathbb{R}_+$ *to* X*.*

Definition B.1.3. *A semigroup* $(T(t))_{t\geq 0}$ *on a Banach space* X *is norm continuous if* $t \to T(t)$ *is continuous from* $\mathbb{R}_+$ *to* $L(X)$*. It is said eventually norm continuous if* $t \to \mathbf{T}(t)$ *is norm continuous from* (t_0, ∞) *to* $\mathcal{L}(X)$*. If* t_0 *can be chosen to be* 0*, we say that* $(T(t))_{t\geq 0}$ *is immediately norm continuous.*

Theorem B.1.4. *Let* $(T(t))_{t\geq 0}$ *be a strongly continuous semigroup on a Banach space* X *with generator* $(\mathbf{A}, D(\mathbf{A}))$*. Moreover, assume that* $(T(t))_{t\geq 0}$ *is eventually norm continuous. Then the Spectral Mapping Theorem*

$$\Sigma(T(t)) \setminus \{0\} = e^{t\Sigma(\mathbf{A})}$$

holds for all $t \geq 0$*. As a consequence, if* $-\infty < \sup \Re\Sigma(\mathbf{A}) < 0$*, then there exists* $M \geq 1$ *such that:*

$$|||T(t)||| \leq M e^{\frac{t}{2} \sup \Re\Sigma(\mathbf{A})}, \quad \forall t \geq 0.$$

Theorem B.1.5 (Miyadera-Voigt,[Engel 2001]). *Let* $(A, D(A))$ *be the generator of a strongly contiuous semigroup* $(T(t))_{t\geq 0}$ *on a Banach space* X *and let* $C \in \mathcal{L}((D(A), \|\cdot\|_A), X)$ *with* $\|x\|_A \equiv \|x\| + \|Ax\|$*. Assume that there exist contants* $t_0 > 0$*,* $0 \leq q < 1$ *such that*

$$\int_0^{t_0} \|CT(s)x\| \, ds \leq q \|x\|, \ \forall x \in D(A)$$

Then $(A+C, D(A))$ generates a strongly continuous semigroup $(U(t))_{t\geq 0}$ on X which satifies $\forall x \in D(A)$:

$$\begin{aligned} U(t)x &= T(t)x + \int_0^t T(t-s)CU(s)xds \\ &= T(t)x + \int_0^t U(t-s)CT(s)xds. \end{aligned}$$

Theorem B.1.6 ([Bátkai 2005]). *Let $(A, D(A))$ be the generator of a strongly contiuous semigroup $(T(t))_{t\geq 0}$ on a Banach space X and let $C \in \mathcal{L}((D(A), \|\cdot\|_A), X)$ with $\|x\|_A \equiv \|x\| + \|Ax\|$. Define the abstract Volterra operator $V : C^0(\mathbb{R}_+, \mathcal{L}(X)) \to C^0(\mathbb{R}_+, \mathcal{L}(X))$ by $VF \equiv t \to \int_0^t F(t-s)CT(s)ds$ on $D(A)$ and by its continuous extension on X. If the following assumptions are satisfied:*

- *there exist a contant $\varepsilon > 0$ and a function $q : [0, \varepsilon) \to \mathbb{R}_+$ such that*

$$\int_0^t \|CT(s)x\| \, ds \leq q(t) \|x\|, \ \forall x \in D(A), \forall t \in [0, \varepsilon)$$

  with $\lim_{t \searrow 0} q(t) = 0$.

- *$(T(t))_{t\geq 0}$ is norm continuous for $t > \alpha$*

- *there exists $n \in \mathbb{N}$ such that $V^n T$ is norm continuous for $t > 0$*

Then $(A+C, D(A))$ generates a strongly continuous semigroup on X which is norm continuous for $t > n\alpha$.

Definition B.1.7. *A closed operator $T \in \mathcal{L}(X)$ of a Banach space X is Fredholm if $dim\mathcal{N}(T)$* and *$codim\mathcal{R}(T)$ are finite and $\mathcal{R}(T)$ is closed in X.*

Definition B.1.8. *A closed operator $T \in \mathcal{L}(X)$ of a Banach space X is semi-Fredholm if $dim\mathcal{N}(T)$* or *$codim\mathcal{R}(T)$ is finite and $\mathcal{R}(T)$ is closed in X.*

Definition B.1.9. *If $T \in \mathcal{L}(X)$ is a closed operator of a Banach space X the essential spectrum $\Sigma_{ess}(T)$ is the set of λs in $\mathbb{C}$ such that $\lambda\mathrm{Id} - T$ is not semi-Fredholm i.e. either $\mathcal{R}(\lambda\mathrm{Id}-T)$ is not closed or $\mathcal{R}(\lambda\mathrm{Id}-T)$ is closed but $dim\mathcal{N}(\lambda\mathrm{Id}-T) = codim\mathcal{R}(\lambda\mathrm{Id} - T) = \infty$.*

Definition B.1.10 ([Hale 1993]). *If $K(\lambda) : \mathcal{B}_1 \to \mathcal{B}_2$, the $\mathcal{B}_i$ being complex Banach spaces, be a linear operator-valued functions that depends analytically on $\lambda \in \mathbb{C}$. A point λ_0 is a characteristic value of K if $\exists x_0 \in \mathcal{B}_1 \setminus \{0\}$ such that $K(\lambda_0)x_0 = 0$. An ordered set $(x_0, \cdots, x_{k-1}) \subset \mathcal{B}_1$ is a Jordan chain for $K(\lambda_0)$ if $x_0 \neq 0$ and $K(z)\alpha(z) = O((z-\lambda_0)^k)$ where α is the root function:*

$$\alpha(z) = \sum_{i=0}^{k-1} (z-\lambda_0)^i x_i$$

The maximum length of the Jordan chains starting at x_0 is called the rank of x_0.

Definition B.1.11 ([Hale 1993]). *We call $(x_{1,0}, \cdots, x_{1,r_1-1}, \cdots, x_{p,0}, \cdots, x_{p,r_p-1})$ a canonical system of Jordan chains for $K(\lambda_0)$ if $(x_{1,0}, \cdots, x_{p,0})$ is a basis of $Ker\ K(\lambda_0)$ and for each k, $(x_{k,0}, \cdots, x_{k,r_k-1})$ is a Jordan chain of rank r_k.*

Lemma B.1.12 ([Hale 1993]). *$(x_0, \cdots, x_{p-1})$ is Jordan chain of length p for $K(\lambda_0)$ if and only if $(x_0, \cdots, x_{p-1}) \in Ker\ K_p$ with*

$$K_p = \begin{bmatrix} K(\lambda_0) & 0 & \cdots & 0 \\ \frac{d}{dz}K(\lambda_0) & K(\lambda_0) & \cdots & 0 \\ \vdots & & \ddots & \vdots \\ \frac{1}{(p-1)!}\frac{d^{p-1}}{dz^{p-1}}K(\lambda_0) & \frac{1}{(p-2)!}\frac{d^{p-2}}{dz^{p-2}}K(\lambda_0) & \cdots & K(\lambda_0) \end{bmatrix}$$

Proof. Easy to prove from a Taylor expansion of $\lambda \to K(\lambda)$ at $\lambda = \lambda_0$. □

B.2 Boundedness in $\mathcal{F}$

Lemma B.2.1. *We have* $|\langle \mathbf{L}_1 S(\mathbf{V}_t), \mathbf{V}(t)\rangle_{\mathcal{F}}| \leq \sqrt{p|\Omega|} \cdot |||\mathbf{J}|||_{\mathcal{F}} \|\mathbf{V}(t)\|_{\mathcal{F}}$.

Proof. By the Cauchy-Schwarz inequality:

$|\langle \mathbf{L}_1 S(\mathbf{V}_t), \mathbf{V}(t)\rangle_{\mathcal{F}}| \leq \|\mathbf{L}_1 S(\mathbf{V}_t)\|_{\mathcal{F}} \|\mathbf{V}(t)\|_{\mathcal{F}} \leq \sqrt{p|\Omega|} \cdot |||\mathbf{J}|||_{\mathcal{F}} \|\mathbf{V}(t)\|_{\mathcal{F}}$ because S is bounded by 1. □

B.3 Regularity

Lemma B.3.1. *If we define* $\mathrm{L}^{\mathrm{q}} \equiv \mathrm{L}^{\mathrm{q}}(\Omega, \mathbf{R}^{\mathrm{p}})$ *(recall that $\mathcal{F} \equiv \mathrm{L}^2$). Then, we have* $\forall \phi \in W^{1,q}(-\tau_m, 0; \mathrm{L}^{\mathrm{q}})$,

$$\mathbf{L}_1 \phi = \mathbf{J}\phi(0) - \int_{-\tau_m}^{0} \mathbf{J}[s]\dot{\phi}(s)ds$$

where $\forall s \in [-\tau_m, 0]$, $J_{ij}(\mathbf{r}, \mathbf{r}')[s] \equiv J_{ij}(\mathbf{r}, \mathbf{r}')H(s + \tau_{ij}(\mathbf{r}, \mathbf{r}'))$ *and H is the Heaviside function.*

Proof.

$$\begin{aligned}
((\mathbf{L}_1\phi)(\mathbf{r}))_i &= \sum_{j=1}^{p} \int_{\Omega} J_{ij}(\mathbf{r}, \bar{\mathbf{r}})\phi_j(\bar{\mathbf{r}}, -\tau_{ij}(\mathbf{r}, \bar{\mathbf{r}}))d\bar{\mathbf{r}} \\
&= -\sum_{j=1}^{p} \int_{\Omega} J_{ij}(\mathbf{r}, \bar{\mathbf{r}}) \left[\int_{-\tau_{ij}(\mathbf{r}, \bar{\mathbf{r}})}^{0} \dot{\phi}_j(\mathbf{r}, s)ds - \phi_j(\mathbf{r}, 0) \right] \\
&= \sum_{j=1}^{p} J_{ij}\phi_j(0) - \sum_{j=1}^{p} \int_{\Omega} J_{ij}(\mathbf{r}, \bar{\mathbf{r}}) \int_{-\tau_m}^{0} \dot{\phi}_j(\mathbf{r}, s)H(s + \tau_{ij}(\mathbf{r}, \bar{\mathbf{r}}))ds \\
&= (\mathbf{J}\phi(0))_i - \int_{-\tau_m}^{0} \left(\int_{\Omega} \mathbf{J}(\mathbf{r}, \bar{\mathbf{r}})H(s + \boldsymbol{\tau}(\mathbf{r}, \bar{\mathbf{r}}))\dot{\phi}(\mathbf{r}, s) \right) \quad \text{(B.1)}
\end{aligned}$$

As $\boldsymbol{\tau}$ is continuous, $\mathbf{J}(\mathbf{r},\mathbf{r}')[s] \in \mathrm{L}^{\mathrm{q}}(\Omega^2 \times [-\tau_{\mathrm{m}},0],\mathbb{R}^{\mathrm{p}\times\mathrm{p}})$. □

Let us define the operator:

$$\forall \mathbf{U} \in \mathrm{L}^{\mathrm{q}}, \forall \theta \in [-\tau_{\mathrm{m}},0], \quad (\mathrm{S_t}\mathbf{U})(\theta) = \begin{cases} e^{-(t+\theta)\mathbf{L}_0}\mathbf{U} & \text{if} \quad -t < \theta \leq 0 \\ 0 & \text{if} \quad -\tau_m < \theta \leq -t \end{cases}$$

and the nilpotent semigroup

$$\forall \phi \in \mathrm{L}^{\mathrm{q}}(-\tau_{\mathrm{m}},0;\mathrm{L}^{\mathrm{q}}), \forall \theta \in [-\tau_{\mathrm{m}},0], \quad (\mathrm{T}_0(\mathrm{t})\phi)(\theta) = \begin{cases} \phi(t+\theta) & \text{if} \quad t+\theta \leq 0 \\ 0 & \text{if} \quad t+\theta > 0 \end{cases}$$

Hence $T_0(t) = 0$ if $t > \tau_m$. We show that the property (M) in [Bátkai 2005] is true:

Lemma B.3.2. *If* $\mathbf{J} \in \mathrm{L}^\infty(\Omega^2,\mathbb{R}^{\mathrm{p}})$, *then for each space* $\mathcal{X}^{(q)} \equiv \mathrm{L}^{\mathrm{q}} \times \mathrm{L}^{\mathrm{q}}(-\tau_{\mathrm{m}},0;\mathrm{L}^{\mathrm{q}})$ *where* $\mathrm{L}^{\mathrm{q}} \equiv \mathrm{L}^{\mathrm{q}}(\Omega,\mathbf{R}^{\mathrm{p}})$ *and* $2 \leq q < \infty$, *there exists* $Q : \mathbb{R}_+ \to \mathbb{R}_+$ *with* $\lim_{t\to 0^+} Q(t) = 0$ *such that*

$$\forall \begin{bmatrix} x \\ \phi \end{bmatrix} \in D(\mathbf{A}) \quad \int_0^t \|\mathbf{L}_1(S_s x + T_0(s)\phi)\|_{\mathrm{L}^{\mathrm{q}}}\, ds \leq Q(t) \left\| \begin{bmatrix} x \\ \phi \end{bmatrix} \right\|_{\mathcal{X}^{(q)}}.$$

Proof. Let us first focus on the term $\int_0^t \|\mathbf{L}_1(S_s x)\|_{\mathrm{L}^{\mathrm{q}}}\, ds$. As $t \geq 0$, we find $(\mathbf{L}_1(S_s x))(\mathbf{r}) = \int d\bar{\mathbf{r}} \mathbf{1}_{[\tau(\mathbf{r},\bar{\mathbf{r}}),\infty)}(s)\mathbf{J}(\mathbf{r},\bar{\mathbf{r}})e^{-(s-\tau(\mathbf{r},\bar{\mathbf{r}})\mathbf{L}_0}x(\bar{\mathbf{r}})$. For s fixed, $\mathbf{J}_2(s) : (\mathbf{r},\bar{\mathbf{r}}) \to \mathbf{1}_{[\tau(\mathbf{r},\bar{\mathbf{r}}),\infty)}(s)\mathbf{J}(\mathbf{r},\bar{\mathbf{r}})e^{-(s-\tau(\mathbf{r},\bar{\mathbf{r}})\mathbf{L}_0}$ defines an integral operator on L^{q} such that $\mathbf{L}_1(S_s x) = \mathbf{J}_2(s)x$. Its norm is bounded[1] by: $|||\mathbf{J}_2(s)|||_{\mathrm{L}^{\mathrm{q}}} \leq |\Omega|\sqrt{p}\,\|\mathbf{J}\|_{L^\infty(\Omega^2,\mathbb{R}^p)}$. This gives $\int_0^t \|\mathbf{L}_1(S_s x)\|_{\mathcal{F}}\, ds \leq t|\Omega|\sqrt{p}\,\|\mathbf{J}\|_{L^\infty(\Omega^2,\mathbb{R}^p)}$.

Let us look at the second term $\int_0^t \|\mathbf{L}_1(T_0(s)\phi)\|_{\mathrm{L}^{\mathrm{q}}}\, ds$. As $t \geq 0$, we find $(\mathbf{L}_1(T_0(s)\phi))(\mathbf{r}) = \int d\bar{\mathbf{r}} \mathbf{1}_{[0,\tau(\mathbf{r},\bar{\mathbf{r}})]}(s)\mathbf{J}(\mathbf{r},\bar{\mathbf{r}})\phi(s-\tau(\mathbf{r},\bar{\mathbf{r}}),\bar{\mathbf{r}})$. We write $\int_0^t ds\, \|\mathbf{L}_1(T_0(s)\phi)\|_{\mathrm{L}^{\mathrm{q}}} = \int_0^t h^{1/q}$ with

$$h(s) \equiv \int_\Omega d\mathbf{r} \left\| \int_\Omega d\bar{\mathbf{r}}\ \mathbf{1}_{[0,\tau(\mathbf{r},\bar{\mathbf{r}})]}(s)\mathbf{J}(\mathbf{r},\bar{\mathbf{r}})\phi(s-\tau(\mathbf{r},\bar{\mathbf{r}}),\bar{\mathbf{r}}) \right\|_{\mathbb{R}^p}^q.$$

We apply the Hölder inequality with $\bar{q}$ such that $q^{-1} + \bar{q}^{-1} = 1$:

$$\begin{aligned} \forall \mathbf{r},\ & \left\| \int_\Omega d\bar{\mathbf{r}}\ \mathbf{1}_{[0,\tau(\mathbf{r},\bar{\mathbf{r}})]}(s)\mathbf{J}(\mathbf{r},\bar{\mathbf{r}})\phi(s-\tau(\mathbf{r},\bar{\mathbf{r}}),\bar{\mathbf{r}}) \right\|_{\mathbb{R}^p} \\ &\leq \int_\Omega d\bar{\mathbf{r}}\ \mathbf{1}_{[0,\tau(\mathbf{r},\bar{\mathbf{r}})]}(s)\, \|\mathbf{J}(\mathbf{r},\bar{\mathbf{r}})\phi(s-\tau(\mathbf{r},\bar{\mathbf{r}}),\bar{\mathbf{r}})\|_{\mathbb{R}^p} \\ &\leq \int_\Omega d\bar{\mathbf{r}}\ \mathbf{1}_{[0,\tau(\mathbf{r},\bar{\mathbf{r}})]}(s)|||\mathbf{J}(\mathbf{r},\bar{\mathbf{r}})|||_{\mathbb{R}^p}\, \|\phi(s-\tau(\mathbf{r},\bar{\mathbf{r}}),\bar{\mathbf{r}})\|_{\mathbb{R}^p} \\ &\leq \sqrt{p}\,\|\mathbf{J}\|_{L^\infty(\Omega^2,\mathbb{R}^p)} \int_\Omega d\bar{\mathbf{r}}\ \mathbf{1}_{[0,\tau(\mathbf{r},\bar{\mathbf{r}})]}(s)\, \|\phi(s-\tau(\mathbf{r},\bar{\mathbf{r}}),\bar{\mathbf{r}})\|_{\mathbb{R}^p} \\ &\overset{Holder}{\leq} \sqrt{p}\,\|\mathbf{J}\|_{L^\infty(\Omega^2,\mathbb{R}^p)} \left(\int_\Omega d\bar{\mathbf{r}} \right)^{1/\bar{q}} \left(\int_\Omega d\bar{\mathbf{r}}\ \mathbf{1}_{[0,\tau(\mathbf{r},\bar{\mathbf{r}})]}(s)\, \|\phi(s-\tau(\mathbf{r},\bar{\mathbf{r}}),\bar{\mathbf{r}})\|_{\mathbb{R}^p}^q \right)^{1/q}. \end{aligned}$$

[1] Using the Cauchy-Schwarz inequality followed by the Hölder inequality.

This gives:

$$h(s) \;\leq\; \left(\sqrt{p}\,\|\mathbf{J}\|_{L^\infty(\Omega^2,\mathbb{R}^p)}\,|\Omega|^{1/\bar{q}}\right)^q \int_\Omega d\mathbf{r} \int_\Omega d\bar{\mathbf{r}}\;\; \mathbf{1}_{[0,\tau(\mathbf{r},\bar{\mathbf{r}})]}(s)\,\|\phi(s-\tau(\mathbf{r},\bar{\mathbf{r}}),\bar{\mathbf{r}})\|^q_{\mathbb{R}^p}$$

Again, we apply the Hölder inequality with $\bar{q}$ such that $q^{-1}+\bar{q}^{-1}=1$:

$$\int_0^t h^{1/q} \leq \left[\int_0^t 1\right]^{1/\bar{q}} \left[\int_0^t h\right]^{1/q} \leq$$

$$\sqrt{p}\,\|\mathbf{J}\|_{L^\infty(\Omega^2,\mathbb{R}^p)}\,|\Omega|^{1/\bar{q}} t^{1/\bar{q}} \left[\int_0^t ds \int_\Omega d\mathbf{r} \int_\Omega d\bar{\mathbf{r}}\;\mathbf{1}_{[0,\tau(\mathbf{r},\bar{\mathbf{r}})]}(s)\,\|\phi(s-\tau(\mathbf{r},\bar{\mathbf{r}}),\bar{\mathbf{r}})\|^q_{\mathbb{R}^p}\right]^{1/q}$$

$$\overset{Fubini}{=} \sqrt{p}\,\|\mathbf{J}\|_{L^\infty(\Omega^2,\mathbb{R}^p)}\,|\Omega|^{1/\bar{q}} t^{1/\bar{q}} \left[\int_\Omega d\mathbf{r} \int_\Omega d\bar{\mathbf{r}} \int_0^t ds\;\mathbf{1}_{[0,\tau(\mathbf{r},\bar{\mathbf{r}})]}(s)\,\|\phi(s-\tau(\mathbf{r},\bar{\mathbf{r}}),\bar{\mathbf{r}})\|^q_{\mathbb{R}^p}\right]^{1/q}$$

$$\leq \sqrt{p}\,\|\mathbf{J}\|_{L^\infty(\Omega^2,\mathbb{R}^p)}\,|\Omega|^{1/\bar{q}} t^{1/\bar{q}} \left[\int_\Omega d\mathbf{r} \int_\Omega d\bar{\mathbf{r}} \int_{-\tau_m}^0 d\theta\,\|\phi(\theta,\bar{\mathbf{r}})\|^q_{\mathbb{R}^p}\right]^{1/q}$$

$$\overset{Fubini}{=} \sqrt{p}\,\|\mathbf{J}\|_{L^\infty(\Omega^2,\mathbb{R}^p)}\,|\Omega|^{1/\bar{q}} t^{1/\bar{q}} \left[|\Omega| \int_{-\tau_m}^0 d\theta\,\|\phi(\theta)\|^q_{\mathrm{L^q}}\right]^{1/q}$$

$$= \sqrt{p}\,\|\mathbf{J}\|_{L^\infty(\Omega^2,\mathbb{R}^p)}\,|\Omega| t^{1/\bar{q}}\,\|\phi\|_{\mathrm{L^q}(-\tau_m,0;\mathrm{L^q})}$$

Finally we find:

$$\int_0^t \|\mathbf{L}_1(S_s x + T_0(s)\phi)\|_{\mathrm{L^q}}\,ds \leq \sqrt{p}\,\|\mathbf{J}\|_{L^\infty(\Omega^2,\mathbb{R}^p)}\,|\Omega|\max(t,t^{1/\bar{q}}) \left\|\begin{bmatrix} x \\ \phi \end{bmatrix}\right\|_{\mathcal{X}^{(q)}}$$

which concludes the proof. □

B.4 Analytical formula for the Hopf bifurcation curve in the parameter plane (D, c)

These formulae rely on the following lemma:

Lemma B.4.1. *If $J = |J|e^{i\psi}$, $\psi \in (-\pi,\pi]$, there is a (unique) solution $X_0 > 0$ to $\Re W_0(JX) = W_0(X)$ iff $1 \leq |J|$ and $\arccos\left(\frac{1}{|J|}\right) \leq |\psi|$. This solution is given by $X_0 = \xi_0 e^{\xi_0}$ with*

$$\xi_0 = \frac{1}{\sqrt{|J|^2-1}}\left(|\psi| - \arccos\left(\frac{1}{|J|}\right)\right).$$

Then $\frac{\Im W_0(JX_0)}{W_0(X)} = \frac{sign(\psi)}{\sqrt{|J|^2-1}}$.

Proof. Let us define $\Psi(z) = ze^z$, by definition $\Psi(W_0(z)) = z$, hence the equation becomes $\Psi(\Re W_0(JX)) = X > 0$. We write $W_0(JX) = \xi + i\eta$ with $\eta \in (-\pi,\pi]$ (by definition of the principal branch) and $JX = |J|Xe^{i\psi}$, $\psi \in (-\pi,\pi]$. As $sign\,(\Im(W_0(z))) = sign\,(\arg z)$ (see [Corless 1996]), we find that $sign(\psi) = sign(\eta)$. From the symmetry $\overline{W_0(z)} = W_0(\bar{z})$, we conclude that $\eta(\psi)$ can be written

$sign(\psi)\eta(|\psi|)$: we can suppose that $\psi \geq 0$ and thus that $\eta \geq 0$. By definition of W_0, $JX = \Psi(\xi + i\eta)$, it gives:

$$\begin{cases} |J|Xcos(\psi) = e^{\xi}(\xi cos(\eta) - \eta sin(\eta)) \\ |J|Xsin(\psi) = e^{\xi}(\xi sin(\eta) + \eta cos(\eta)) \end{cases}$$

Using $\xi e^{\xi} = X$, we find $\left(\frac{\eta}{\xi}\right)^2 = |J|^2 - 1 \Rightarrow \frac{\eta}{\xi} = \sqrt{|J|^2 - 1}$ and the two equations reduce to

$$e^{i(\psi-\eta)} = \frac{1}{|J|}\left[1 + i\sqrt{|J|^2 - 1}\right] = e^{i\phi},\ \phi = \arccos\left(\frac{1}{|J|}\right) \in \left[0, \frac{\pi}{2}\right]$$

This gives $\eta = \psi - \phi\ [2\pi]$. If $\psi - \phi \geq 0$, then we have a solution $\eta = \psi - \phi$. However, if $\psi - \phi < 0$, the only potential solution is $\eta = \psi - \phi + 2\pi$, but $\psi - \phi + 2\pi \geq -\frac{\pi}{2} + 2\pi > \pi$ but $\eta \leq \pi$. Hence there is a (unique) solution iff $\psi - \phi \geq 0$ which is $\eta = \psi - \phi$. In this case $\xi = \frac{\psi - \arccos\left(\frac{1}{|J|}\right)}{\sqrt{|J|^2-1}}$.

□

B.5 Study of the adjoint $\mathbf{A}^*$

Lemma B.5.1. *The adjoint* $\mathbf{A}^*$ *of* $\mathbf{A}$ *for* $\langle\ ,\ \rangle_{\mathcal{X}}$ *satisfies*

$$\mathbf{A}^* \begin{bmatrix} y \\ \psi \end{bmatrix} = \begin{bmatrix} -\mathbf{L}_0^* y + \psi(0) \\ \frac{d}{d\theta}\left(\mathbf{J}^*[\theta]y - \psi\right) \end{bmatrix}$$

with domain

$$D(\mathbf{A}^*) = \left\{ \begin{bmatrix} y \\ \psi \end{bmatrix} \in \mathcal{X}, \psi(s) - (\mathbf{J}[s])^* y \in W^{1,2}(-\tau_m, 0; \mathcal{F})\ \textit{and}\ \psi(-\tau_m) = (\mathbf{J}[-\tau_m])^* y \right\}$$

.

Proof. The proof follows [Nakagiri 1988]. For all $\begin{bmatrix} x \\ \phi \end{bmatrix} \in D(\mathbf{A})$, let us write $\langle \mathbf{A}\begin{bmatrix} x \\ \phi \end{bmatrix}, \begin{bmatrix} y \\ \psi \end{bmatrix} \rangle_{\mathcal{X}} = \langle \begin{bmatrix} x \\ \phi \end{bmatrix}, \begin{bmatrix} z \\ \eta \end{bmatrix} \rangle_{\mathcal{X}}$ and look for $\begin{bmatrix} z \\ \eta \end{bmatrix}$. Using lemma B.3.1, we have :

$$\begin{aligned} \langle \mathbf{A}\begin{bmatrix} x \\ \phi \end{bmatrix}, \begin{bmatrix} y \\ \psi \end{bmatrix} \rangle_{\mathcal{X}} &= \langle y, -\mathbf{L}_0 x + \mathbf{J}x \rangle_{\mathcal{F}} - \int_{-\tau_m}^{0} \langle y, \mathbf{J}[s]\dot{\phi}(s) \rangle_{\mathcal{F}} ds + \int_{-\tau_m}^{0} \langle \dot{\phi}(s), \psi(s) \rangle_{\mathcal{F}} ds \\ &= \langle x, z \rangle_{\mathcal{F}} + \int_{-\tau_m}^{0} \langle \phi(s), \eta(s) \rangle_{\mathcal{F}} ds \end{aligned}$$

In the scalar product $\int_{-\tau_m}^{0} \langle \phi(s), \eta(s) \rangle_{\mathcal{F}} ds$, we would like to make appear $\dot{\phi}$. Thus we set $M(s) = \int_{-\tau_m}^{s} \eta$, then

$$\int_{-\tau_m}^{0} \langle \phi(s), \eta(s) \rangle_{\mathcal{F}} ds = \langle \phi(0), M(0) \rangle_{\mathcal{F}} - \int_{-\tau_m}^{0} \langle \dot{\phi}, M \rangle_{\mathcal{F}}$$

Also:

$$\int_{-\tau_m}^{0} \langle (\mathbf{J}[s])^* y, \dot{\phi}(s) \rangle_{\mathcal{F}} ds = \langle \phi(0), \mathbf{J}^* y \rangle_{\mathcal{F}} - \langle \mathbf{L}_1 \phi, y \rangle_{\mathcal{F}}$$

because $(\mathbf{J}[0])^* = \mathbf{J}^*$. Then:

$$\int_{-\tau_m}^{0} \langle \dot{\phi}(s), -\psi(s) + (\mathbf{J}[s])^* y - M(s) \rangle_{\mathcal{F}} ds = \langle x, z + \mathbf{L}_0^* y - \mathbf{J}^* y + M(0) \rangle_{\mathcal{F}}.$$

This last equality is true $\forall \begin{bmatrix} x \\ \phi \end{bmatrix} \in D(\mathbf{A})$, if we choose the constant function $\phi(\theta) = x \in \mathcal{F}$, it gives:

$$z = -\mathbf{L}_0^* y + \mathbf{J}^* y - M(0)$$

then

$$\psi(s) - (\mathbf{J}[s])^* y + M(s) = 0 \quad \forall s \in [-\tau_m, 0].$$

It follows that

$$\psi(-\tau_m) = (\mathbf{J}[-\tau_m])^* y$$

and

$$M(0) = -\psi(0) + (\mathbf{J}(0))^* y = -\psi(0) + \mathbf{J}^* y.$$

We still need to find η to finish the proof. Because M is C^1, we have

$$\eta(s) = -\frac{d}{ds} \left[\psi(s) - (\mathbf{J}[s])^* y \right].$$

□

B.6 Linear analysis

B.6.1 Stability

In this section we prove lemma B.6.1 which is central in establishing the first sufficient condition in proposition 4.5.7.

Lemma B.6.1. *Let $\beta > 0$ be such that $\frac{1}{\boldsymbol{\tau}^\beta} \in \mathrm{L}^2(\Omega^2, \mathbb{R}^{\mathrm{p}\times\mathrm{p}})$). Then we have the following bound:*

$$\|\mathbf{Z}(t)\|_{\mathcal{F}} \leq {\tau_m}^{\frac{3}{2}+\beta} \|\mathbf{U}_t\|_{\mathcal{C}} \sqrt{\sum_{i,j} \int_{\Omega^2} \mathbf{J}_{ij}(\mathbf{r}, \bar{\mathbf{r}})^2 / \tau_{ij}(\mathbf{r}, \bar{\mathbf{r}})^{2\beta}} \equiv {\tau_m}^{\frac{3}{2}+\beta} \left\| \frac{\mathbf{J}}{\boldsymbol{\tau}^\beta} \right\|_{\mathrm{L}^2(\Omega^2, \mathbb{R}^{\mathrm{p}\times\mathrm{p}})} \|\mathbf{U}_t\|_{\mathcal{C}}$$

Proof.
We have:

$$\left\| \int_{\Omega} d\bar{\mathbf{r}} \mathbf{J}(\cdot, \bar{\mathbf{r}}) \int_{t-\boldsymbol{\tau}(\cdot,\bar{\mathbf{r}})}^{t} \mathbf{U}(\bar{\mathbf{r}}, s) ds \right\|_{\mathcal{F}}^2 = \int_{\Omega} d\mathbf{r} \sum_i \left[\sum_j \int_{\Omega} d\bar{\mathbf{r}} \mathbf{J}_{ij}(\mathbf{r}, \bar{\mathbf{r}}) \int_{t-\tau_{ij}(\mathbf{r},\bar{\mathbf{r}})}^{t} \mathbf{U}_j(\bar{\mathbf{r}}, s) ds \right]^2 \tag{B.2}$$

and if we set $y_i(\mathbf{r}) = \sum_j \int_\Omega d\bar{\mathbf{r}} \mathbf{J}_{ij}(\mathbf{r},\bar{\mathbf{r}}) \int_{t-\tau_{ij}(\mathbf{r},\bar{\mathbf{r}})}^{t} \mathbf{U}_j(\bar{\mathbf{r}},s)ds$, we have : $|y_i(\mathbf{r})| \leq \sum_j |\int_\Omega d\bar{\mathbf{r}} \mathbf{J}_{ij}(\mathbf{r},\bar{\mathbf{r}}) \int_{t-\tau_{ij}(\mathbf{r},\bar{\mathbf{r}})}^{t} \mathbf{U}_j(\bar{\mathbf{r}},s)ds|$ and from the Cauchy-Schwartz inequality:

$$\int_\Omega d\bar{\mathbf{r}} \mathbf{J}_{ij}(\mathbf{r},\bar{\mathbf{r}}) \int_{t-\tau_{ij}(\mathbf{r},\bar{\mathbf{r}})}^{t} \mathbf{U}_j(\bar{\mathbf{r}},s)ds \leq \sqrt{\int_\Omega d\bar{\mathbf{r}} \frac{\mathbf{J}_{ij}(\mathbf{r},\bar{\mathbf{r}})^2}{\tau_{ij}(\mathbf{r},\bar{\mathbf{r}})^{2\beta}}} \sqrt{\int_\Omega d\bar{\mathbf{r}} \tau_{ij}(\mathbf{r},\bar{\mathbf{r}})^{2\beta} \left\{ \int_{t-\tau_{ij}(\mathbf{r},\bar{\mathbf{r}})}^{t} \mathbf{U}_j(\bar{\mathbf{r}},s)ds \right\}^2}$$

Again, from the Cauchy-Schwartz inequality applied to $\left\{ \int_{t-\tau_{ij}(\mathbf{r},\bar{\mathbf{r}})}^{t} \mathbf{U}_j(\bar{\mathbf{r}},s)ds \right\}^2$:

$$\begin{aligned} \int_\Omega d\bar{\mathbf{r}} \tau_{ij}(\mathbf{r},\bar{\mathbf{r}})^{2\beta} \left\{ \int_{t-\tau_{ij}(\mathbf{r},\bar{\mathbf{r}})}^{t} \mathbf{U}_j(\bar{\mathbf{r}},s)ds \right\}^2 &\leq \int_\Omega d\bar{\mathbf{r}} \tau_{ij}(\mathbf{r},\bar{\mathbf{r}})^{2\beta+2} \int_{t-\tau_m}^{t} \mathbf{U}_j(\bar{\mathbf{r}},s)^2 ds \\ &\leq \tau_m^{2\beta+2} \int_\Omega d\bar{\mathbf{r}} \int_{t-\tau_m}^{t} \mathbf{U}_j(\bar{\mathbf{r}},s)^2 ds = \tau_m^{2\beta+2} \int_{t-\tau_m}^{t} \int_\Omega d\bar{\mathbf{r}} \mathbf{U}_j(\bar{\mathbf{r}},s)^2 ds \end{aligned} \quad \text{(B.3)}$$

Then, from the discrete Cauchy-Schwartz inequality:

$$\begin{aligned} |y_i(\mathbf{r})| &\leq \tau_m^{\beta+1} \sum_j \sqrt{\int_{t-\tau_m}^{t} ds \int_\Omega d\bar{\mathbf{r}} \mathbf{U}_j(\bar{\mathbf{r}},s)^2} \sqrt{\int_\Omega d\bar{\mathbf{r}} \mathbf{J}_{ij}(\mathbf{r},\bar{\mathbf{r}})^2 / \tau_{ij}(\mathbf{r},\bar{\mathbf{r}})^{2\beta}} \\ &\leq \tau_m^{\beta+1} \sqrt{\sum_j \int_{t-\tau_m}^{t} ds \int_\Omega d\bar{\mathbf{r}} \mathbf{U}_j(\bar{\mathbf{r}},s)^2} \sqrt{\sum_j \int_\Omega d\bar{\mathbf{r}} \mathbf{J}_{ij}(\mathbf{r},\bar{\mathbf{r}})^2 / \tau_{ij}(\mathbf{r},\bar{\mathbf{r}})^{2\beta}} \\ &= \tau_m^{\beta+1} \sqrt{\int_{t-\tau_m}^{t} ds \|\mathbf{U}(s)\|_{\mathcal{F}}^2} \sqrt{\sum_j \int_\Omega d\bar{\mathbf{r}} \mathbf{J}_{ij}(\mathbf{r},\bar{\mathbf{r}})^2 / \tau_{ij}(\mathbf{r},\bar{\mathbf{r}})^{2\beta}} \\ &\leq \tau_m^{\beta+\frac{3}{2}} \|\mathbf{U}_t\|_{\mathcal{C}} \sqrt{\sum_j \int_\Omega d\bar{\mathbf{r}} \mathbf{J}_{ij}(\mathbf{r},\bar{\mathbf{r}})^2 / \tau_{ij}(\mathbf{r},\bar{\mathbf{r}})^{2\beta}} \end{aligned} \quad \text{(B.4)}$$

which gives as stated:

$$\sum_i \int_\Omega y_j(\mathbf{r})^2 d\mathbf{r} \leq \tau_m^{2\beta+3} \|\mathbf{U}_t\|_{\mathcal{C}}^2 \sum_i \sum_j \int_\Omega d\bar{\mathbf{r}} \mathbf{J}_{ij}(\mathbf{r},\bar{\mathbf{r}})^2 / \tau_{ij}(\mathbf{r},\bar{\mathbf{r}})^{2\beta}$$

and allows us to conclude. □

B.7 The Cauchy problem

B.7.1 Regularity of R

Lemma B.7.1. *Let us assume that* $\mathbf{J} \in \mathrm{L}^\infty(\Omega^2, \mathbb{R}^{\mathrm{p}\times\mathrm{p}})$. *Then* $\mathbf{L}_1$ *is a continuous operator from* $C^0(-\tau_m, 0; \mathrm{L}^1(\Omega, \mathbb{R}^{\mathrm{p}}))$ *to* $\mathrm{L}^{\mathrm{q}}(\Omega, \mathbb{R}^{\mathrm{p}})$.

Proof. We take $\phi \in C^0(-\tau_m, 0; \mathrm{L}^1(\Omega, \mathbb{R}^{\mathrm{p}}))$ and write, for convenience, $\phi^d(\mathbf{r}, \bar{\mathbf{r}}) = \phi(-\tau(\mathbf{r}, \bar{\mathbf{r}}), \bar{\mathbf{r}})$. If $\mathbf{U} \equiv \mathbf{L}_1\phi$, we have:

$$|U_i(\mathbf{r})| = \Big| \sum_j \int_\Omega d\bar{\mathbf{r}}\ J_{ij}(\mathbf{r}, \bar{\mathbf{r}})\phi_j^d(\mathbf{r}, \bar{\mathbf{r}}) \Big| \leq \|\mathbf{J}\|_{\mathrm{L}^\infty(\Omega^2, \mathbb{R}^{\mathrm{p}\times\mathrm{p}})} \int_\Omega \sum_j \Big|\phi_j^d(\mathbf{r}, \bar{\mathbf{r}})\Big| d\bar{\mathbf{r}}$$
$$\overset{Cauchy-Schwarz}{\leq} \sqrt{p}\, \|\mathbf{J}\|_{\mathrm{L}^\infty(\Omega^2, \mathbb{R}^{\mathrm{p}\times\mathrm{p}})} \int_\Omega \Big\|\phi^d(\mathbf{r}, \bar{\mathbf{r}})\Big\|_{\mathbb{R}^p} d\bar{\mathbf{r}}$$

Also, we find:

$$\int_\Omega \Big\|\phi^d(\mathbf{r}, \bar{\mathbf{r}})\Big\|_{\mathbb{R}^p} d\bar{\mathbf{r}} \leq \sup_{\mathbf{r}\in\Omega} \int_\Omega \Big\|\phi^d(\mathbf{r}, \bar{\mathbf{r}})\Big\|_{\mathbb{R}^p} d\bar{\mathbf{r}} \leq$$
$$\sup_{\theta\in[-\tau_m,0]} \int_\Omega \|\phi(\theta, \bar{\mathbf{r}})\|_{\mathbb{R}^p}\, d\bar{\mathbf{r}} = \sup_{\theta\in[-\tau_m,0]} \|\phi(\theta)\|_{\mathrm{L}^1(\Omega,\mathbb{R}^{\mathrm{p}})} \equiv \|\phi\|_{C^0(-\tau_m,0;\mathrm{L}^1(\Omega,\mathbb{R}^{\mathrm{p}}))}$$

which gives $|U_i(\mathbf{r})| \leq \sqrt{p}\, \|\mathbf{J}\|_{\mathrm{L}^\infty(\Omega^2,\mathbb{R}^{\mathrm{p}\times\mathrm{p}})}\, \|\phi\|_{C^0(-\tau_m,0;\mathrm{L}^1(\Omega,\mathbb{R}^{\mathrm{p}}))}$. It follows that

$$\|\mathbf{U}\|_{\mathrm{L}^{\mathrm{q}}(\Omega,\mathbb{R})} \leq p\sqrt{p}|\Omega|^{1/q}\, \|\mathbf{J}\|_{\mathrm{L}^\infty(\Omega^2,\mathbb{R}^{\mathrm{p}\times\mathrm{p}})}\, \|\phi\|_{C^0(-\tau_m,0;\mathrm{L}^1(\Omega,\mathbb{R}))}$$

which concludes the proof. □

B.7.2 The inhomogeneous equation

Lemma B.7.2. *Let* $(\mathcal{T}_0(t))$ *be the* C^0*-semigroup with generator* $\mathbf{A}_0 = \begin{bmatrix} -\mathbf{L}_0 & 0 \\ 0 & \frac{d}{d\theta} \end{bmatrix}$, $D(\mathbf{A}_0) = D(\mathbf{A})$ *and* $\mathbf{B} \equiv \begin{bmatrix} 0 & \mathbf{L}_1 \\ 0 & 0 \end{bmatrix} \in \mathcal{L}(D(\mathbf{A}), \mathcal{X})$. *It is known from [Bátkai 2005][theorem 3.25] that* $\mathbf{A}_0$ *generates the strongly continuous semigroup* $\mathcal{T}_0(t) = \begin{bmatrix} S(t) & 0 \\ S_t & T_0(t) \end{bmatrix} \in \mathcal{L}(\mathcal{X})$ *where* $S(t) \equiv e^{-\mathbf{L}_0 t}, S_t, T_0(t)$ *are defined in appendix B.3. Then we have:*

$$\begin{array}{rcl} \mathbf{T}(t) & = & \mathcal{T}_0(t) + \int_0^t \mathcal{T}_0(t-s)\mathbf{B}\mathbf{T}(s)ds \\ & = & \mathcal{T}_0(t) + \int_0^t \mathbf{T}(t-s)\mathbf{B}\mathcal{T}_0(s)ds. \end{array} \tag{B.5}$$

on $D(\mathbf{A}) \oplus (\mathcal{F} \times \{0\})$.

Proof. There are 3 main parts in the proof. First, we find the regularity of $\pi_2\mathbf{T}(t)\begin{bmatrix} x \\ 0 \end{bmatrix}$. Then we use the Miyadera-Voigt perturbation theorem to prove the lemma on $D(\mathbf{A})$. Finally, we extend the formula to $D(\mathbf{A}) \oplus (\mathcal{F} \times \{0\})$ by continuity.

1. Let us write $\begin{bmatrix} f(t) \\ \xi(t) \end{bmatrix} \equiv \mathbf{T}(t) \begin{bmatrix} x \\ 0 \end{bmatrix}$. We consider a sequence $D(\mathbf{A}) \ni \begin{bmatrix} x \\ \phi_n \end{bmatrix} \to \begin{bmatrix} x \\ 0 \end{bmatrix}$ in $\mathcal{X}$. Then, $\begin{bmatrix} f_n(t) \\ \xi_n(t) \end{bmatrix} \equiv \mathbf{T}(t) \begin{bmatrix} x \\ \phi_n \end{bmatrix} \in D(\mathbf{A})$ is a classical solution of:

$$\left\{ \begin{array}{rcl} \dot{f}_n & = & -\mathbf{L}_0 f_n + \mathbf{L}_1 \xi_n \\ \dot{\xi}_n & = & \frac{\partial \xi_n}{\partial \theta} \end{array} \right. \tag{B.6}$$

where the second equation is solved by $\xi_n(t,\theta) = H_n(t+\theta)$. From the initial condition $\xi_n(0,\theta) = \phi_n(\theta)$ and the belonging to $D(\mathbf{A})$, $\xi_n(t,0) = f_n(t)$, we find:

$$H_n(t) = \left\{ \begin{array}{l} f_n(t) \text{ if } t \geq 0 \\ \phi_n(t) \text{ if } t \leq 0. \end{array} \right. \tag{B.7}$$

As $\mathbf{T}(t) \begin{bmatrix} x \\ \phi_n \end{bmatrix} \to \mathbf{T}(t) \begin{bmatrix} x \\ 0 \end{bmatrix}$ in $\mathcal{X}$ for all $t \geq 0$, we have:

$$\xi(t,\theta) = \left\{ \begin{array}{lll} f(t+\theta) & \text{if} & t+\theta \geq 0 \\ 0 & \text{otherwise} & . \end{array} \right. \tag{B.8}$$

As $\mathbf{T}$ is strongly continuous on $\mathcal{X}$, it gives $f \in C^0(\mathbb{R}_+, \mathrm{L}^{\mathrm{q}})$ and $\xi(t,\cdot)$ has one discontinuity point if and only if $t < \tau_m$.

2. We apply the perturbation theorem B.1.5 to $\mathbf{A}_0+\mathbf{B}$ (see [Bátkai 2005][theorem 3.26] and lemma B.3.2). We find $\forall u \in D(\mathbf{A})$:

$$\begin{array}{rcl} \mathbf{T}(t)u & = & \mathcal{T}_0(t)u + \int_0^t \mathcal{T}_0(t-s)\mathbf{B}\mathbf{T}(s)u \, ds \\ & = & \mathcal{T}_0(t)u + \int_0^t \mathbf{T}(t-s)\mathbf{B}\mathcal{T}_0(s)u \, ds. \end{array}$$

3. Then, we extend by continuity the above formulas. Let us notice that $\mathcal{F} \times \{0\}$ is in the closure of $D(\mathbf{A})$ in $\mathcal{X}$ and write (for example) $\delta(t) = \mathbf{T}(t) - \mathcal{T}_0(t) - \int_0^t \mathcal{T}_0(t-s)\mathbf{B}\mathbf{T}(s)ds$. We wish to extend $\delta(t)$ to $\mathcal{F} \times \{0\}$. Let us first notice that $\delta(t)$ is bounded on $\mathcal{F} \times \{0\}$ for $\|\cdot\|_{\mathcal{X}}$. Indeed, this comes from $\mathbf{L}_1$ being bounded on history segment like $\pi_2 \mathbf{T}(t) \begin{bmatrix} x \\ 0 \end{bmatrix}$. Then, we consider a sequence $D(\mathbf{A}) \ni u_n \to u \in \mathcal{F} \times \{0\}$ in $\mathcal{X}$. We have $\delta(t)u_n = 0$ and as $\delta(t)$ is bounded on $D(\mathbf{A}) \oplus \mathcal{F} \times \{0\}$, we have:

$$\left\| \underbrace{\delta(t)u_n}_{=0} - \delta(t)u) \right\|_{\mathcal{X}} \leq K \left\| u_n - u \right\|_{\mathcal{X}}$$

which gives $\delta(t)u = 0$. the other formula is similar. This concludes the proof of the lemma.

□

We need the following estimations for the main proposition that follows.

Lemma B.7.3. *For $f \in C^0_\eta(\mathbb{R}, \mathrm{L}^{\mathrm{q}})$, we have:*

1. $\int_t^{t+\varepsilon} S_{t+\varepsilon-r} f(r)dr \overset{\varepsilon\to 0^+}{=} O(\varepsilon^{1+1/q})$ *in* $\mathrm{L}^{\mathrm{q}}(-\tau_{\mathrm{m}}, 0; \mathrm{L}^{\mathrm{q}})$,

2. $\forall \lambda \in \mathbb{C}$ *such that* $\Re\lambda \geq 0$, $\int_t^{t+\varepsilon} T_0(t+\varepsilon-r) f(r) e^{\lambda\cdot} dr \overset{\varepsilon\to 0^+}{\sim} \varepsilon f(t) e^{\lambda\cdot}$ *in* $\mathrm{L}^{\mathrm{q}}(-\tau_{\mathrm{m}}, 0; \mathrm{L}^{\mathrm{q}})$.

Proof.

1. Let us write $U_1(t;\cdot) = \int_t^{t+\varepsilon} S_{t+\varepsilon-r} f(r)dr$. From the definition of S_t, we find:

$$\begin{aligned}
\|U_1(t;\cdot)\|^q_{L^q(-\tau_m,0;\mathrm{L}^{\mathrm{q}})} &= \int_{-\tau_m}^{0} d\theta \left\| \int_t^{t+\varepsilon} S(t+\varepsilon-r+\theta) f(r) H(t+\varepsilon-r+\theta) dr \right\|^q_{\mathrm{L}^{\mathrm{q}}} \\
&= \int_{-\varepsilon}^{0} d\theta \left\| \int_0^{\theta+\varepsilon} S(\varepsilon-r+\theta) f(t+r) dr \right\|^q_{\mathrm{L}^{\mathrm{q}}} \\
&\leq \int_{-\varepsilon}^{0} d\theta \left(\int_0^{\theta+\varepsilon} \|S(\varepsilon-r+\theta) f(t+r)\|_{\mathrm{L}^{\mathrm{q}}} dr \right)^q \\
&= O\left(\int_{-\varepsilon}^{0} d\theta \left(\int_0^{\theta+\varepsilon} 1 dr \right)^q \right) = O(\varepsilon^{q+1})
\end{aligned}$$

where H is the Heaviside function. Hence, we have:

$$U_1(t;\cdot) = O(\varepsilon^{1+1/q}) = o(\varepsilon).$$

2. Let us write $U_2(t;\theta) = \int_t^{t+\varepsilon} (T_0(t+\varepsilon-r)(f(r)e^{\lambda\cdot}))(\theta) dr$. From the definition[2] of $T_0(t)$,

$$\begin{aligned}
U_2(t;\theta) &= \int_t^{t+\varepsilon} f(r) e^{\lambda(t+\theta+\varepsilon-r)} H(-(t+\theta+\varepsilon-r)) dr = \int_{\max(t,t+\varepsilon+\theta)}^{t+\varepsilon} f(r) e^{\lambda(t+\theta+\varepsilon-r)} dr \\
&\equiv U_{2,1}(t;\theta) + U_{2,2}(t;\theta)
\end{aligned}$$

with:

$$U_{2,1}(t;\theta) \equiv \begin{cases} \int_{t+\varepsilon+\theta}^{t+\varepsilon} f(r) e^{\lambda(t+\theta+\varepsilon-r)} dr & \text{if} \quad \theta > -\varepsilon \\ 0 & \text{if} \quad \theta \leq -\varepsilon \end{cases} \tag{B.9}$$

and

$$U_{2,2}(t;\theta) \equiv \begin{cases} \int_t^{t+\varepsilon} f(r) e^{\lambda(t+\theta+\varepsilon-r)} dr & \text{if} \quad \theta < -\varepsilon \\ 0 & \text{if} \quad \theta \geq -\varepsilon. \end{cases} \tag{B.10}$$

For the first term, we find:

$$\begin{aligned}
\|U_{2,1}(t;\cdot)\|^q_{L^q(-\tau_m,0;\mathrm{L}^{\mathrm{q}})} &= \int_{-\varepsilon}^{0} d\theta \left\| \int_{t+\theta+\varepsilon}^{t+\varepsilon} f(r) e^{\lambda(t+\theta+\varepsilon-r)} dr \right\|^q_{\mathrm{L}^{\mathrm{q}}} \\
&= O\left(\int_{-\varepsilon}^{0} d\theta \left(\int_{t+\theta+\varepsilon}^{t+\varepsilon} 1 dr \right)^q \right) = O(\varepsilon^{q+1}).
\end{aligned}$$

Hence, we have:

$$U_{2,1}(t;\cdot) = o(\varepsilon).$$

[2] see appendix B.3

For the second term, it is easy to show that:

$$\forall \theta \in [-\tau_m, 0],\ \frac{1}{\varepsilon} U_{2,2}(t;\theta) \overset{\varepsilon \to 0^+}{\to} f(t)e^{\lambda\theta} \text{ in } \mathrm{L}^{\mathrm{q}}(-\tau_{\mathrm{m}}, 0; \mathrm{L}^{\mathrm{q}})$$

which concludes the proof.

□

Proposition B.7.4. *For all $\eta \in [0, \gamma]$ and $F = \begin{bmatrix} f \\ 0 \end{bmatrix} \in C^0_\eta(\mathbb{R}, \mathcal{Y})$, we consider*

$$u(t) = \int_{-\infty}^{t} \mathbf{T}(t-r) P_s \begin{bmatrix} f(r) \\ 0 \end{bmatrix} dr.$$

Then, u satisfies the following properties:

1. *$u \in C^0_\eta(\mathbb{R}, \mathcal{Z})$ and $\|u\|_{C^0_\eta(\mathbb{R},\mathcal{Z})} \leq K(\eta) \|f\|_{C^0_\eta(\mathbb{R},\mathcal{Y})}$ with $\eta \to K(\eta)$ positive continuous,*
2. *$u \in C^1(\mathbb{R}, \mathcal{X})$,*
3. *u satifies $\dot{u} = \mathbf{A}u + P_s \begin{bmatrix} f \\ 0 \end{bmatrix}$ on $\mathcal{X}$, i.e. is a classical solution.*

Proof. Choose $\gamma' > \gamma$ such that the spectral splitting (see section 4.4.4) is still valid with γ'. It gives

$$|||\mathbf{T}(t)P_s|||_{\mathcal{X}} \leq Me^{-\gamma' t},\ t > 0. \tag{B.11}$$

Note that the group $S(t) = e^{-\mathbf{L}_0 t}$ satifies:

$$\|S(t)\|_{\mathcal{L}(\mathrm{L}^{\mathrm{q}})} \leq e^{-lt},\ l > \gamma',\ \forall t. \tag{B.12}$$

Let us prove that $u(t)$ exists for all $t \in \mathbb{R}$. From (B.11), we find $\left\| \mathbf{T}(t-r) P_s \begin{bmatrix} f(r) \\ 0 \end{bmatrix} \right\|_{\mathcal{X}} \leq Me^{-\gamma'(t-r)+\eta|r|} \|f\|_{C^0_\eta(\mathbb{R},\mathcal{Y})}$ which gives:

$$\|u(t)\|_{\mathcal{X}} \leq M \|f\|_{C^0_\eta(\mathbb{R},\mathcal{Y})} \int_{-\infty}^{t} e^{-\gamma'(t-r)+\eta|r|} dr.$$

We change of variable in the integral to find

$$\int_{-\infty}^{0} e^{\gamma' r + \eta|t+r|} dr \leq \int_{-\infty}^{0} e^{\gamma' r + \eta|t| + \eta|r|} dr = \frac{e^{\eta|t|}}{\gamma' - \eta}.$$

This gives:

$$\|u(t)\|_{\mathcal{X}} \leq M \|f\|_{C^0_\eta(\mathbb{R},\mathcal{Y})} \frac{e^{\eta|t|}}{\gamma' - \eta}. \tag{B.13}$$

1. From lemma B.7.2, we find

$$\begin{aligned} u(t) &= \int_{-\infty}^{t} \left(\mathcal{T}_0(t-r) P_s \begin{bmatrix} f(r) \\ 0 \end{bmatrix} + \int_0^{t-r} \mathcal{T}_0(t-r-v) \mathbf{BT}(v) P_s \begin{bmatrix} f(r) \\ 0 \end{bmatrix} dv \right) dr \\ &\equiv u_1(t) + u_2(t). \end{aligned} \tag{B.14}$$

We shall prove Point 1. for each $u_i(t),\ i = 1, 2$.

Case of u_1. The first term is:

$$u_1(t) = \int_{-\infty}^{t} \mathcal{T}_0(t-r) P_s \begin{bmatrix} f(r) \\ 0 \end{bmatrix} dr.$$

Recall from proposition 4.4.10 that

$$P_s(u) = u - \sum_i \langle\langle \psi_i, u \rangle\rangle \phi_i$$

where $\phi_i = \begin{bmatrix} x_i \\ x_i e^{\lambda_i \theta} \end{bmatrix}$ are the generalized eigenvectors of $\mathbf{A}$ for the eigenvalues λ_i such that $\Re\lambda_i \geq 0$. Write $\psi_i = \begin{bmatrix} y_i \\ \pi_2 \psi_i \end{bmatrix}$, $f_i(r) \equiv \langle y_i, f(r) \rangle_{\mathcal{F}} x_i$ and H the Heaviside function. Note that:

$$\|f_i(r)\|_{\mathcal{X}} = O\left(\|f(r)\|_{\mathcal{X}}\right) = O(e^{\eta|r|}) \tag{B.15}$$

because $\mathcal{X}^{(q)} \hookrightarrow \mathcal{X}^{(2)}$ for $q \geq 2$. Then, we have:

$$\begin{aligned} \mathcal{T}_0(t-r) P_s \begin{bmatrix} f(r) \\ 0 \end{bmatrix} &= \mathcal{T}_0(t-r) \begin{bmatrix} f(r) - \sum_i f_i(r) \\ -\sum_i f_i(r) e^{\lambda_i \theta} \end{bmatrix} \\ &= \begin{bmatrix} S(t-r) \left(f(r) - \sum_i f_i(r) \right) \\ S_{t-r} \left(f(r) - \sum_i f_i(r) \right) - \sum_i f_i(r) e^{\lambda_i (t-r+\theta)} H(-(t-r+\theta)) \end{bmatrix}. \end{aligned}$$

We shall see that the second component is continuous in θ. It is then easy to see that the two components are equal when $\theta = 0$. We have for the second component:

$$\theta \to \int_{-\infty}^{t+\theta} S(t-r+\theta) \left(f(r) - \sum_i f_i(r) \right) dr - \sum_i \int_{t+\theta}^{t} f_i(r) e^{\lambda_i (t-r+\theta)} dr.$$

The second term is C^1 on $[-\tau_m, 0]$. We wish to apply the dominated convergence theorem to the first integral term. Hence, we need to bound the norm of the derivative of its integrand by an integrable function of r. This derivative is

$$-\mathbf{L}_0 S(t-r+\theta) \left(f(r) - \sum_i f_i(r) \right)$$

which is bounded[3] by $K |||\mathbf{L}_0|||_{\mathcal{F}} \|f\|_{C^0_\eta(\mathbb{R}, \mathcal{Y})} e^{l\tau_m} e^{-l(t-r+\tau_m)+\eta|r|}$ which is

[3] for some constant K depending on x_i, y_i.

r-integrable. Hence, the dominated convergence theorem shows that the second component belongs to $C^1(-\tau_m, 0; \mathrm{L}^q)$ for all time t. This implies that

$$\boxed{\forall t \in \mathbb{R},\ u_1(t) \in \mathcal{Z}}$$

because $\pi_1 u_1(t) = (\pi_2 u_1)(0)$. Finally:

$$\begin{aligned}
\|u_1(t)\|_{\mathcal{Z}} \leq & \left\| \int_{-\infty}^{t} S(t-r) \left(f(r) - \sum_i f_i(r) \right) dr \right\|_{\mathrm{L}^q} \\
+ & \left\| \int_{-\infty}^{t} S_{t-r} \left(f(r) - \sum_i f_i(r) \right) - \sum_i f_i(r) e^{\lambda_i (t-r+\theta)} H(-(t-r+\theta)) dr \right\|_{\mathrm{W}^{1,q}(-\tau_m, 0; \mathrm{L}^q)} \\
& \leq \left\| \int_{-\infty}^{t} S(t-r) \left(f(r) - \sum_i f_i(r) \right) dr \right\|_{\mathrm{L}^q} \\
& \quad + \left\| \int_{-\infty}^{t} S_{t-r} \left(f(r) - \sum_i f_i(r) \right) \right\|_{\mathrm{W}^{1,q}(-\tau_m, 0; \mathrm{L}^q)} \\
& + \left\| \int_{-\infty}^{t} \sum_i f_i(r) e^{\lambda_i (t-r+\theta)} H(-(t-r+\theta)) dr \right\|_{\mathrm{W}^{1,q}(-\tau_m, 0; \mathrm{L}^q)} . \qquad \text{(B.16)}
\end{aligned}$$

The first term is bounded by[4] by $K \|f\|_{C^0_\eta(\mathbb{R},\mathcal{Y})} \int_{-\infty}^{t} e^{-l(t-r)+\eta|r|} dr \leq K \|f\|_{C^0_\eta(\mathbb{R},\mathcal{Y})} \int_{-\infty}^{t} e^{-\gamma'(t-r)+\eta|r|} dr \leq K \|f\|_{C^0_\eta(\mathbb{R},\mathcal{Y})} \frac{e^{\eta|t|}}{\gamma'-\eta}$. Let us write:

$$\left\| f(r) - \sum_i f_i(r) \right\|_{\mathcal{X}} \leq K_f \|f\|_{C^0_\eta(\mathbb{R},\mathcal{Y})} e^{\eta|r|}$$

for some constant K_f. For the second term in (B.16), we have:

$$\begin{aligned}
& \left\| \int_{-\infty}^{t} S_{t-r} \left(f(r) - \sum_i f_i(r) \right) dr \right\|^q_{\mathrm{L}^q(-\tau_m, 0; \mathrm{L}^q)} \\
& \quad = \int_{-\tau_m}^{0} \left\| \int_{-\infty}^{t+\theta} S(t-r+\theta) \left(f(r) - \sum_i f_i(r) \right) dr \right\|^q_{\mathrm{L}^q} d\theta \\
& \quad \leq \int_{-\tau_m}^{0} \left(\int_{-\infty}^{t+\theta} K_f \|f\|_{C^0_\eta(\mathbb{R},\mathcal{Y})} e^{\eta|t| - l(t-r+\theta)} dr \right)^q d\theta \\
& \quad \leq \tau_m \left(K_f \|f\|_{C^0_\eta(\mathbb{R},\mathcal{Y})} \frac{e^{\eta|t| + l\tau_m}}{\gamma' - \eta} \right)^q
\end{aligned}$$

[4] for some constant K

and

$$\begin{aligned}
&\left\| \frac{d}{d\theta} \int_{-\infty}^{t} S_{t-r} \left(f(r) - \sum_i f_i(r) \right) dr \right\|^q_{\mathrm{L^q}(-\tau_\mathrm{m},0;\mathrm{L^q})} \\
&= \int_{-\tau_m}^{0} \left\| \left(f(t+\theta) - \sum_i f_i(t+\theta) \right) - \int_{-\infty}^{t+\theta} \mathbf{L}_0 S(t-r+\theta) \left(f(r) - \sum_i f_i(r) \right) dr \right\|^q_{\mathrm{L^q}} d\theta \\
&\overset{|a+b|^q \le 2^{q-1}(|a|^q+|b|^q)}{\le} 2^{q-1} \int_{-\tau_m}^{0} \left\| f(t+\theta) - \sum_i f_i(t+\theta) \right\|^q_{\mathrm{L^q}} \\
&\quad + 2^{q-1} \left(\int_{-\infty}^{t+\theta} \left\| \mathbf{L}_0 S(t-r+\theta) \left(f(r) - \sum_i f_i(r) \right) \right\|_{\mathrm{L^q}} dr \right)^q d\theta \\
&\le K_f^q \left\| f \right\|^q_{C^0_\eta(\mathbb{R},\mathcal{Y})} \left(\int_{-\tau_m}^{0} e^{q\eta|t+\theta|} d\theta + |||\mathbf{L}_0|||^q \int_{-\tau_m}^{0} d\theta \left(\int_{-\infty}^{t+\theta} e^{-l(t-r+\theta)+\eta|r|} dr \right)^q \right) \\
&\le K_f^q \left\| f \right\|^q_{C^0_\eta(\mathbb{R},\mathcal{Y})} e^{q\eta|t|} \tau_m e^{q\eta\tau_m} \left(1 + \left(\frac{|||\mathbf{L}_0|||}{\gamma' - \eta} \right)^q \right). \quad \text{(B.17)}
\end{aligned}$$

The third term in (B.17) is very similar. This allows to conclude that:

$$\boxed{\left\| u_1(t) \right\|_{\mathcal{Z}} \le K_1(\eta) \left\| f \right\|_{C^0_\eta(\mathbb{R},\mathcal{Y})} e^{\eta|t|}.}$$

Finally, let us write for $t > s$:

$$\begin{aligned}
u_1(t) - u_1(s) = &\int_{-\infty}^{t} \left(\mathcal{T}_0(t-r) - \mathcal{T}_0(s-r) \right) P_s \begin{bmatrix} f(r) \\ 0 \end{bmatrix} dr \\
&+ \int_{s}^{t} \mathcal{T}_0(t-r) P_s \begin{bmatrix} f(r) \\ 0 \end{bmatrix} dr
\end{aligned}$$

Using the same arguments as above, it is straightforward to show that:

$$\left\| \int_{s}^{t} \mathcal{T}_0(t-r) \begin{bmatrix} f(r) \\ 0 \end{bmatrix} dr \right\|_{\mathcal{Z}} = O(|t-s|)$$

and

$$\left\| \int_{-\infty}^{t} \left(\mathcal{T}_0(t-r) - \mathcal{T}_0(s-r) \right) \begin{bmatrix} f(r) \\ 0 \end{bmatrix} dr \right\|_{\mathcal{Z}} = O(|t-s|)$$

because $t \to S(t)$ is C^1. This shows that $\left\| u_1(t) - u_1(s) \right\|_{\mathcal{Z}} \le K|t-s|$, hence $t \to u_1(t)$ is continuous in $\mathcal{Z}$. It follows that

$$\boxed{u_1 \in C^0_\eta(\mathbb{R}, \mathcal{Z}).}$$

Case of u_2. We start with the introduction of convenient notations:

$$\begin{bmatrix} h(v,r) \\ 0 \end{bmatrix} \equiv \mathbf{BT}(v) P_s \begin{bmatrix} f(r) \\ 0 \end{bmatrix}.$$

Note from (B.11) that

$$\|h(v,r)\|_{\mathrm{L}^{\mathrm{q}}} \leq K \|f\|_{C^0_\eta(\mathbb{R},\mathcal{Y})} e^{-\gamma' v+\eta|r|} \tag{B.18}$$

for some constant K. It follows that u_2 is given by:

$$u_2(t) = \int_{-\infty}^{t} dr \int_0^{t-r} dv \begin{bmatrix} S(t-r-v)h(v,r) \\ S_{t-r-v}h(v,r) \end{bmatrix} \tag{B.19}$$

and

$$\begin{aligned} \pi_2 u_2(t;\theta) &= \int_{-\infty}^{t} dr \int_0^{t-r} dv\ S(t-r-v+\theta)h(v,r)H(t-r-v+\theta) \\ &= \int_{-\infty}^{t+\theta} dr \int_0^{t-r+\theta} dv\ S(t-r-v+\theta)h(v,r). \end{aligned}$$

We want to show that this function is C^1 on $[-\tau_m, 0]$ by applying the dominated convergence theorem. The integrand is C^1 in θ. Taking the derivative w.r.t. θ gives:

$$h(t-r+\theta,r) - \int_0^{t-r+\theta} dv\ \mathbf{L}_0 S(t-r-v+\theta)h(v,r).$$

The first term is bounded by $K\|f\|_{C^0_\eta(\mathbb{R},\mathcal{Y})} e^{-\gamma'(t-r)+\eta|r|}$ and the second term is bounded by

$$K\|f\|_{C^0_\eta(\mathbb{R},\mathcal{Y})} |||\mathbf{L}_0||| \int_0^{t-r+\theta} dv\, e^{-l(t-r-v-\tau_m)} e^{-\gamma' v+\eta|r|} = O(e^{-\gamma'(t-r)+\eta|r|}).$$

Hence, the derivative is $O(e^{-\gamma'(t-r)+\eta|r|})$ which is r-integrable. It follows from the dominated convergence theorem that $\pi_2 u_2(t)$ is C^1 on $[-\tau_m, 0]$ for all time t. We find that:

$$\boxed{\forall t \in \mathbb{R},\ u_2(t) \in \mathcal{Z}.}$$

We can now compute the norm $\|u_2(t)\|_{\mathcal{Z}}$:

$$\begin{aligned} \|u_2(t)\|_{\mathcal{Z}} = &\left\| \int_{-\infty}^{t} dr \int_0^{t-r} S(t-r-v)h(v,r)dv \right\|_{\mathrm{L}^{\mathrm{q}}} \\ &+ \left\| \int_{-\infty}^{t} dr \int_0^{t-r} S_{t-r-v}h(v,r)dv \right\|_{\mathrm{W}^{1,\mathrm{q}}(-\tau_{\mathrm{m}},0;\mathrm{L}^{\mathrm{q}})}. \end{aligned} \tag{B.20}$$

From computations similar to the ones for $\|u_1(t)\|_{\mathcal{Z}}$ and by using the bound (B.18), we find that

$$\boxed{\|u_2(t)\|_{\mathcal{Z}} \leq M(\eta)\|f\|_{C^0_\eta(\mathbb{R},\mathcal{Y})} e^{\eta|t|}}$$

where $\eta \to M(\eta)$ is a positive continuous function of η. Finally, we have for $\delta > 0$ (for example):

$$u_2(t+\delta) - u_2(t) = \int_{-\infty}^{t} dr \Big(\int_0^{t-r} dv \, [\mathcal{T}_0(t+\delta-r-v) - \mathcal{T}_0(t-r-v)] \begin{bmatrix} h(v,r) \\ 0 \end{bmatrix} + \int_{t-r}^{t+\delta-r} dv \, \mathcal{T}_0(t+\delta-r-v) \begin{bmatrix} h(v,r) \\ 0 \end{bmatrix} \Big) + \int_t^{t+\delta} dr \int_0^{t+\delta-r} dv \, \mathcal{T}_0(t+\delta-r-v) \begin{bmatrix} h(v,r) \\ 0 \end{bmatrix}.$$

By bounding each term, it can be shown, albeit being lengthy, that $\|u_2(t+\delta) - u_2(t)\| \overset{\delta}{=\!\sim} 0 \; O(|\delta|)$. It follows that

$$\boxed{u_2 \in C^0(\mathbb{R}, \mathcal{Z}).}$$

Combining the results for u_1 and u_2, we have shown that $u \in C^0_\eta(\mathbb{R}, \mathcal{Z})$ and that

$$\|u\|_{C^0_\eta(\mathbb{R},\mathcal{Z})} \leq K(\eta) \, \|f\|_{C^0_\eta(\mathbb{R},\mathcal{Y})}$$

for some positive continuous function $\eta \to K(\eta)$.

2. As in Point 1., we have:

$$\begin{aligned} u(t) &= \int_{-\infty}^{t} \begin{bmatrix} S(t-r)\left(f(r) - \sum_i f_i(r)\right) \\ S_{t-r}\left(f(r) - \sum_i f_i(r)\right) - \sum_i f_i(r) e^{\lambda_i(t-r+\theta)} H(-(t-r+\theta)) \end{bmatrix} dr \\ &+ \int_{-\infty}^{t} dr \int_0^{t-r} dv \begin{bmatrix} S(t-r-v)h(v,r) \\ S_{t-r-v}h(v,r) \end{bmatrix}. \end{aligned}$$

The only difficulty in showing that $t \to u(t)$ is C^1 in $\mathcal{X}$ comes from the second component because $t \to S(t)$ is analytical on L^{q}. To keep the proof small, we shall only prove that

$$t \to U(t) \equiv \int_{-\infty}^{t} S_{t-r} f(r) dr$$

is C^1, the other terms being very similar. We write:

$$U(t;\theta) = \int_{-\infty}^{t+\theta} S(t+\theta-r) f(r) dr.$$

Using the dominated convergence theorem, we find:

$$\frac{d}{dt} U(t;\theta) = f(t+\theta) - \int_{-\infty}^{t+\theta} \mathbf{L}_0 S(t+\theta-r) f(r) dr = f(t+\theta) - \mathbf{L}_0 U(t;\theta).$$

As $\theta \to \frac{d}{dt} U(t;\theta) \in \mathrm{L}^{\mathrm{q}}(-\tau_{\mathrm{m}}, 0; \mathrm{L}^{\mathrm{q}})$, we have that

$$U'(t) = -\mathbf{L}_0 U(t) + f(t+\cdot).$$

Doing similar estimations with the other terms of the second component of $u(t)$, we find that:

$$\boxed{u \in C^1(\mathbb{R}, \mathcal{X}).}$$

3. Let us consider $a > 0$. From the definition of $u(t)$, we find:

$$u(t+a) = \mathbf{T}(a)u(t) + \int_t^{t+a} \mathbf{T}(a+t-r)P_s \begin{bmatrix} f(r) \\ 0 \end{bmatrix} dr.$$

As u is in $C^1(\mathbb{R}, \mathcal{X}) \cap C^0(\mathbb{R}, \mathcal{Z})$, we can take the derivative w.r.t. a and find:

$$\frac{d}{da}u(t+a) = \frac{d}{dt}u(t+a) = \mathbf{A}u(t+a) + \frac{d}{da}\int_t^{t+a} \mathbf{T}(a+t-r)P_s \begin{bmatrix} f(r) \\ 0 \end{bmatrix} dr.$$

Then, taking the limit $a \to 0$ in $\mathcal{X}$:

$$\dot{u}(t) = \mathbf{A}u(t) + \lim_{a\to 0} \frac{d}{da}\int_t^{t+a} \mathbf{T}(a+t-r)P_s \begin{bmatrix} f(r) \\ 0 \end{bmatrix} dr.$$

Hence we need to compute

$$\lim_{a\to 0^+} \frac{1}{a}\int_t^{t+a} \mathbf{T}(a+t-r)P_s \begin{bmatrix} f(r) \\ 0 \end{bmatrix} dr.$$

Let us write $u_a(t) = \int_t^{t+a} \mathbf{T}(a+t-r)P_s \begin{bmatrix} f(r) \\ 0 \end{bmatrix} dr$. As in Point 2., we find:

$$u_a(t) = \int_t^{t+a} \begin{bmatrix} S(t+a-r)\left(f(r) - \sum_i f_i(r)\right) \\ S_{t+a-r}\left(f(r) - \sum_i f_i(r)\right) - \sum_i f_i(r)T_0(t+a-r)e^{\lambda_i \cdot} \end{bmatrix} dr \\ + \int_t^{t+a} dr \int_0^{t+a-r} dv \begin{bmatrix} S(t+a-r-v)h(v,r) \\ S_{t+a-r-v}h(v,r) \end{bmatrix}$$

First term. We start by the first component which gives the limit (it is differentiable):

$$\lim_{a\to 0^+} \frac{1}{a}\int_t^{t+a} S(t+a-r)\left(f(r) - \sum_i f_i(r)\right) = f(t) - \sum_i f_i(t).$$

Using lemma B.7.3, we find

$$\lim_{a\to 0^+} \frac{1}{a}\int_t^{t+a} S_{t+a-r}\left(f(r) - \sum_i f_i(r)\right) - \sum_i f_i(r)T_0(t+a-r)e^{\lambda_i \cdot} \\ = -\sum_i f_i(r)T_0(t+a-r)e^{\lambda_i \cdot}.$$

Hence, the limit of the first term is $P_s \begin{bmatrix} f(t) \\ 0 \end{bmatrix}$.

Second term. Using lemma B.7.3, we find that the second term is $o(\varepsilon^2)$.

Because $u \in C^1(\mathbb{R}, \mathcal{X})$, we have shown that $\forall t \in \mathbb{R}$,

$$\dot{u} = \mathbf{A}u + P_s \begin{bmatrix} f \\ 0 \end{bmatrix}.$$

This concludes the proof of the proposition. □

B.7.3 The inhomogeneous equation (Parabolic case)

We would like to show that the center manifold is attracting when the unstable spectrum is empty $\Sigma_u(\mathbf{A}) = \emptyset$. This requires to check two properties like we did in appendix B.7.2. We start with a definition for a given Banach space $\mathcal{E}$:

$$\mathcal{F}_\eta(\mathbb{R}, \mathcal{E}) \equiv \left\{ \phi \in C^0(\mathbb{R}, \mathcal{E}), \|\phi\|_{\mathcal{F}_\eta(\mathbb{R},\mathcal{E})} \equiv \sup_{t\in\mathbb{R}} e^{\eta t}\|\phi(t)\|_{\mathcal{E}} < \infty \right\}.$$

Then, we have the following proposition (analog to proposition 4.6.2)

Proposition B.7.5. *Let us assume that the unstable spectrum is empty $\Sigma_u(\mathbf{A}) = \emptyset$. Define for all integer $2 \leq q < \infty$, $\mathcal{Y}_h = P_h\mathcal{Y}^{(q)}$, $\mathcal{Z}_h = P_h\mathcal{Z}^{(q)}$. For any $\eta \in [0, \gamma]$,*

1. *and for any $u_0 \in \mathcal{Z}_h$, the problem $\dot{u} = \mathbf{A}u$ with initial condition u_0 has a unique solution $u \in C^0(\mathbb{R}^+, \mathcal{Z}_h)$ and $\|u(t)\|_{\mathcal{Z}} \leq c_\eta e^{-\eta t}$ for all $t \geq 0$ and some positive constant c_η.*

2. *and for any function $F = P_h \begin{bmatrix} f \\ 0 \end{bmatrix} \in \mathcal{F}_\eta(\mathbb{R}, \mathcal{Y}_h)$, the problem*

$$\dot{u} = \mathbf{A}u + F(t) \tag{B.21}$$

has a unique solution $u = \mathbf{K}_h F \in \mathcal{F}_\eta(\mathbb{R}, \mathcal{Z}_h)$ and

$$|||\mathbf{K}_h|||_{\mathcal{L}(\mathcal{F}_\eta(\mathbb{R},\mathcal{Y}_h),\mathcal{F}_\eta(\mathbb{R},\mathcal{Z}_h))} \leq C(\eta)$$

with $C \in C^0([0, \gamma], \mathbb{R})$.

Proof. Choose $\gamma' > \gamma$ such that the spectral splitting (see section 4.4.4) is still valid with γ'.

1. Let us write $u_0 = \begin{bmatrix} x_0 \\ \phi_0 \end{bmatrix}$. The solution u is given by $u(t) = \mathbf{T}(t)u_0$. From $\mathcal{Z}^{(q)} = D(\mathbf{A}_{(q)})$, we find that u is a strong solution and that $u(t) \in \mathcal{Z}_h$. Using the same trick as in proposition B.7.4, we write $u(t) = \mathcal{T}_0(t)u_0 + \int_0^t \mathcal{T}_0(t-s)\mathbf{B}\mathbf{T}(s)u_0 ds \equiv u_1(t) + u_2(t)$. For $u_0 \in \mathcal{Z}_h$, we find $u_1(t) \in \mathcal{Z}_h$. Also, for $t > \tau_m$, we have $u_1(t) = \begin{bmatrix} S(t)x_0 \\ S_t x_0 \end{bmatrix}$, where $S(t) \equiv e^{-\mathbf{L}_0 t}$, which gives

$\|u_1(t)\|_{\mathcal{Z}} = O(e^{-lt})$. Let us look at the expression $u_2(t)$. From $\mathbf{BT}(s)u_0 \equiv \begin{bmatrix} h(s) \\ 0 \end{bmatrix}$, we have $\|h(s)\|_{\mathrm{L}^{\mathrm{q}}} \leq Ke^{-\gamma' s} \|u_0\|_{\mathcal{Z}}$. We find

$$u_2(t) = \int_0^t \begin{bmatrix} S(t-s)h(s) \\ S_{t-s}h(s) \end{bmatrix} ds$$

which belongs to $\mathcal{Z}$. Using the estimate of h, it is straightforward to show that $\|u_2(t)\|_{\mathcal{Z}} = O(e^{-\eta t})$ (see the proof of proposition B.7.4). This allows to conclude the proof of the first part.

2. Let us consider

$$u(t) = \int_{-\infty}^t \mathbf{T}(t-r)P_s \begin{bmatrix} f(r) \\ 0 \end{bmatrix} dr.$$

As $\mathcal{F}_\eta(\mathbb{R}, \mathcal{Y}_h)$ is continuously embedded in $C^0_\eta(\mathbb{R}, \mathcal{Y}_h)$, proposition 4.6.2 shows that $u \in C^0_\eta(\mathbb{R}, \mathcal{Z}_h) \cap C^1(\mathbb{R}, \mathcal{X})$ and that u is a classical solution of (B.21). In order to prove that $u \in \mathcal{F}_\eta(\mathbb{R}, \mathcal{Z}_h)$ and the inequality on $|||\mathbf{K}_h|||_{\mathcal{L}(\mathcal{F}_\eta(\mathbb{R},\mathcal{Y}_h),\mathcal{F}_\eta(\mathbb{R},\mathcal{Z}_h))}$, we have to modify the estimates in proposition 4.6.2 although the general plan of the proof is exactly the same. Changing the norms $\|\cdot\|_{C^0_\eta(\mathbb{R},\cdot)}$ into $\|\cdot\|_{\mathcal{F}_\eta(\mathbb{R},\cdot)}$ in the estimates of proposition 4.6.2 is straightforward but lengthy and we shall only show how to do this for the first one of them, the other being very similar. The inequality we shall consider is the first that arises in the proof of proposition 4.6.2. We find: $\left\| \mathbf{T}(t-r)P_s \begin{bmatrix} f(r) \\ 0 \end{bmatrix} \right\|_{\mathcal{X}} \leq Me^{-\gamma'(t-r)-\eta r} \|f\|_{\mathcal{F}_\eta(\mathbb{R},\mathcal{Y}_h)}$ which gives:

$$\|u(t)\|_{\mathcal{X}} \leq M \|f\|_{\mathcal{F}_\eta(\mathbb{R},\mathcal{Y}_h)} \int_{-\infty}^t e^{-\gamma'(t-r)-\eta r} dr \leq M \|f\|_{\mathcal{F}_\eta(\mathbb{R},\mathcal{Y}_h)} \frac{e^{-\eta t}}{\gamma' - \eta}.$$

Following the proof of proposition 4.6.2, we can prove of the second part of the present proposition.

□

Appendix C

Numerics of delays

C.1 Definitions

Definition C.1.1 (trace-class). *A bounded linear operator* $\mathbf{J}$ *over a separable Hilbert space* $\mathcal{F}$ *is said to be in the trace-class if for some (and hence all) orthonormal bases* $(e_k)_{k\in\mathbb{N}}$ *of* $\mathcal{F}$*, the sum of positive terms* $\|\mathbf{J}\|_1 := \sum_k \langle (\mathbf{J}^*\mathbf{J})^{1/2} e_k, e_k\rangle$ *is finite. In this case, the sum* $\sum_k \langle \mathbf{J}e_k, e_k\rangle$ *is absolutely convergent and is independent of the choice of the orthonormal basis. This value is called the trace of* $\mathbf{J}$*, denoted by* $\mathrm{Tr}(\mathbf{J})$.

Proposition C.1.2 (Fredholm determinant). *The Fredholm determinant of the perturbation of identity by a trace-class operator* $\mathbf{J}$ *satisfies* $\det_F(\mathrm{Id}+\mathbf{J}) = \prod_k (1+\lambda_k(\mathbf{J}))$ *where* $(\lambda_k(\mathbf{J}))_k$ *is the punctual spectrum of* $\mathbf{J}$.

C.2 Normal form computation

C.2.1 The Hopf bifurcation

We have the following normal form coefficients:

Lemma C.2.1. *The coefficients are given*[1] *by:*

$$\begin{cases} \alpha = \pi\overline{\beta_1}\frac{i\omega_H}{c_H} \\ \beta = \pi\overline{\beta_1}\frac{i\omega_H+1}{s_1}\sigma_H^2\left[\frac{s_3}{2} + \sigma_H s_2^2\left(\frac{J_0}{1-\sigma_H s_1 J_0} + \frac{(Je^{-2i\omega_H\tau_H})_{2n}}{2(2i\omega_H+1-\sigma_H s_1(Je^{-2i\omega_H\tau_H})_{2n})}\right)\right] \\ \gamma = \pi\overline{\beta_1}\frac{i\omega_H+1}{s_1}\sigma_H^2\left[s_3 + \sigma_H s_2^2\left(\frac{J_0}{1-\sigma_H s_1 J_0} + \frac{J_{2n}}{1-\sigma_H s_1 J_{2n}} + \frac{(Je^{-2i\omega_H\tau_H})_0}{2i\omega_H+1-\sigma_H s_1(Je^{-2i\omega_H\tau_H})_0}\right)\right] \end{cases}$$

Proof. The bifurcation is studied in [Haragus 2010] where it is shown that:

$$\begin{cases} \alpha = \langle \phi_1^*, \mathbf{R}_{11}(\phi_1) + 2\mathbf{R}_{20}(\phi_1, \Psi_{00001})\rangle_{\mathcal{X}} \\ \beta = \langle \phi_1^*, 3\mathbf{R}_{30}(\phi_1,\phi_1,\overline{\phi_1}) + 2\mathbf{R}_{20}(\overline{\phi_1}, \Psi_{20000}) + 2\mathbf{R}_{20}(\phi_1, \Psi_{11000})\rangle_{\mathcal{X}} \\ \gamma = \langle \phi_1^*, 6\mathbf{R}_{30}(\phi_1,\phi_2,\overline{\phi_2}) + 2\mathbf{R}_{20}(\phi_1, \Psi_{00110}) + 2\mathbf{R}_{20}(\phi_2, \Psi_{10010}) + 2\mathbf{R}_{20}(\overline{\phi_2}, \Psi_{10100})\rangle_{\mathcal{X}} \end{cases}$$

with $\mathbf{R}_{ql} = \frac{1}{q!l!}\frac{\partial^{q+l}}{\partial^q u \partial^l c}\mathbf{R}$. Recall that the expression of $\mathbf{R}_{i0}$ have been given in lemma 4.6.1. For example, $\mathbf{R}_{01} = \partial_c \mathbf{R}(0,c) = 0$. The equations for the Ψ coefficients are also given in [Haragus 2010]. They are solved below and we only show

[1] Recall that $(Je^{-2i\omega_H\tau_H})_n \equiv \int Je^{-2i\omega_H\tau_H}\cos_n$.

how to solve one of them.

$$\begin{cases} \mathbf{A}\Psi_{00001} = -\mathbf{R}_{01} = 0 & \Rightarrow \quad \pi_2\Psi_{00001} = 0 \\ (2i\omega_H - \mathbf{A})\Psi_{20000} = \mathbf{R}_{20}(\phi_1,\phi_1) & \Rightarrow \quad \pi_2\Psi_{20000} = \sigma_H^2 s_2 \frac{(Je^{-2i\omega_H\tau})_{2n}}{2(2i\omega_H+1-\sigma_H s_1 (Je^{-2i\omega_H\tau})_{2n})} e^{2i\omega_H\theta} e_{2n} \\ \mathbf{A}\Psi_{11000} = -2\mathbf{R}_{20}(\phi_1,\overline{\phi_1}) & \Rightarrow \quad \pi_2\Psi_{11000} = \sigma_H^2 s_2 \frac{-J_0}{-1+\sigma_H s_1 J_0} e_0 \\ (2i\omega_H - \mathbf{A})\Psi_{10100} = 2\mathbf{R}_{20}(\phi_1,\phi_2) & \Rightarrow \quad \pi_2\Psi_{10100} = \sigma_H^2 s_2 \frac{(Je^{-2i\omega_H\tau})_0}{2i\omega_H+1-\sigma_H s_1 (Je^{-2i\omega_H\tau})_0} e^{2i\omega_H\theta} e_0 \\ \mathbf{A}\Psi_{10010} = -2\mathbf{R}_{20}(\phi_1,\overline{\phi_2}) & \Rightarrow \quad \pi_2\Psi_{10010} = \sigma_H^2 s_2 \frac{-J_{2n}}{-1+\sigma_H^2 s_2 J_{2n}} e_{2n} \\ \Psi_{00110} = S\cdot\Psi_{11000} \text{ (reflexion)} & \Rightarrow \quad \Psi_{00110} = \Psi_{11000} \end{cases}$$

Recall that the Ψ_{ijklm} belongs to $\mathcal{Z} = D(\mathbf{A})$. This is why we only give the second component of the Ψ coefficients in the above equations. Let us show, for example, how to solve the second equation $(2i\omega_H - \mathbf{A})\Psi_{20000} = \mathbf{R}_{20}(\phi_1,\phi_1)$. From $(2i\omega_H - \frac{d}{d\theta})\pi_2\Psi_{20000} = 0$, we find that $(\pi_2\Psi_{20000})(\theta) = (\pi_1\Psi_{20000})e^{2i\omega_H\theta}$. Using $\mathbf{R}_{20}(\phi_1,\phi_1) = \begin{bmatrix} \frac{s_2}{2}(Je^{-2i\omega_H\tau})_{2n}e_{2n} \\ 0 \end{bmatrix}$, the equation for the first component is:

$$\frac{s_2}{2}(Je^{-2i\omega_H\tau})_{2n}e_{2n} = (2i\omega_H + 1 - \sigma_H s_1 J(2i\omega_H))\pi_1\Psi_{20000}$$

This convolutional equation shows that Ψ_{20000} is colinear to e_{2n} which then gives the solution:

$$\pi_2\Psi_{20000} = \sigma_H^2 s_2 \frac{(Je^{-2i\omega_H\tau_H})_{2n}}{2(2i\omega_H + 1 - \sigma_H s_1 (Je^{-2i\omega_H\tau})_{2n})} e^{2i\omega_H\theta} e_{2n}$$

The expressions for β,γ follow easily. The case of α is a bit more different according to the first remark in section 5.2.2.2. As the varying parameter is c, we shall rescale the time by c. It is easy to show that the normalisation factor β_1 is the same in the rescaled/not-rescaled case. In this case, the eigenvector e_n solves:

$$(i\tilde{\omega}_H + c_H)e_n = c_H s_1 \sigma_H \int J(\cdot - y)e^{-i\tilde{\omega}_H|\cdot - y|_\pi} e_n(y)dy$$

and we find that $\tilde{\omega}_H = c_H\omega_H$. Then, we find that $\pi_1\mathbf{R}_{11}\phi_1 = i\omega_H e_n$ which gives the linear term $i\omega_H\pi\overline{\beta_1}(c - c_H)$ in the reduced equation for the rescaled time $c_H t$. If we go back to the original equation by using $ct \to t$, it gives the linear factor $i\omega_H\pi\overline{\beta_1}\frac{c-c_H}{c_H}$. Recall that to the third order, the coefficients β,γ do not depend on c. This is why we did not use the rescaled time trick for their computation.

□

C.2.2 Fold-Hopf bifurcation

Lemma C.2.2. *The Fold-Hopf normal form:*

$$\begin{cases} \dot{z}_1 &= (a_1 + b_1|z_1|^2 + c_1|z_2|^2)z_1 \\ \dot{z}_2 &= (i\omega_{FH} + a_2 + b_2|z_2|^2 + c_2|z_1|^2)z_2 \end{cases}$$

has the following coefficients:

$$\begin{cases} \frac{b_1}{\pi\beta_1} = \sigma_{FH}^3 J_n \left[\frac{s_3}{2} + \sigma_{FH} s_2^2 \left(\frac{J_0}{1-J_0/J_n} + \frac{J_{2n}}{2(1-J_{2n}/J_n)}\right)\right] \\ \frac{c_1}{\pi\beta_1} = \sigma_{FH}^3 J_n \left[s_3 + \sigma_{FH} s_2^2 \left(\frac{J_0}{1-J_0/J_n} + \frac{(Je^{-i\omega_{FH}\tau_{FH}})_n}{i\omega_{FH}+1-(Je^{-i\omega_{FH}\tau_{FH}})_n/J_n} + \frac{(Je^{i\omega_{FH}\tau_{FH}})_n}{-i\omega_{FH}+1-(Je^{i\omega_{FH}\tau_{FH}})_n/J_n}\right)\right] \\ \frac{b_2}{\pi\beta_2} = (i\omega_{FH}+1)J_n\sigma_{FH}^3 \left[\frac{s_3}{2} + \sigma_{FH} s_2^2 \left(\frac{J_0}{1-J_0/J_n} + \frac{(Je^{-2i\omega_{FH}\tau_{FH}})_0}{2(2i\omega_{FH}+1-(Je^{-2i\omega_{FH}\tau_{FH}})_0/J_n)}\right)\right] \\ \frac{c_2}{\pi\beta_2} = (i\omega_{FH}+1)J_n\sigma_{FH}^3 \left[s_3 + \sigma_{FH} s_2^2 \left(\frac{J_0}{1-J_0/J_n} + 2\frac{(Je^{-i\omega_{FH}\tau_{FH}})_n}{i\omega_{FH}+1-(Je^{-i\omega_{FH}\tau_{FH}})_n/J_n}\right)\right] \end{cases}$$

where $J\cdot e_n \equiv J_n e_n,\ \sigma_{FH} = \frac{1}{s_1 J_n},\ (Je^{-i\omega_{FH}\tau_{FH}})_0 = \frac{i\omega_{FH}+1}{\sigma_{FH} s_1} = (i\omega_{FH}+1)J_n.$

Proof.

Let us write the nonlinear change of variable $\tilde{\Psi}$ to bring the delayed neural field equations to the normal form (5.17). We Taylor expand $\tilde{\Psi}$ as in section 5.2.1:

$$\tilde{\Psi}(v_0,\mu) = \sum_{l_1+l_2+p_1+p_2+r>1} z_1^{l_1}\bar{z}_1^{l_2} z_2^{p_1}\bar{z}_2^{p_2}\mu^r \tilde{\Psi}_{l_1,l_2,p_1,p_2,r},\ \ \tilde{\Psi}_{l_1,l_2,p_1,p_2,r}\in\mathcal{Z},$$

where $\tilde{\Psi}$ satisfies $\tilde{\Psi}(0,0)=0,\ D_{v_0}\tilde{\Psi}(0,0)=0$. Using the equation (5.9) satisfied by $\tilde{\Psi}$ and a Maple program similar to the one given in section 5.2.1, we find the following equations. For convenience, we have indicated, in brackets, the monomials that are used to find the equation.

$$\begin{array}{rcll}
-a_1\phi_1 &=& -\mathbf{A}\tilde{\Psi}_{1,0,0,0,1} - \mathbf{R}_{0,1}(\phi_1) - 2\,\mathbf{R}_2(\phi_1,\tilde{\Psi}_{0,0,0,0,1}) & [z_1]\\
-a_2\phi_2 &=& (i\omega_{FH}-\mathbf{A})\tilde{\Psi}_{0,0,1,0,1} - \mathbf{R}_{0,1}(\phi_2) - 2\,\mathbf{R}_2(\phi_2,\tilde{\Psi}_{0,0,0,0,1}) & [z_2]\\
-2b_1\phi_1 &=& -2\,\mathbf{L}\tilde{\Psi}_{2,1,0,0,0} - 4\,\mathbf{R}_2(\phi_1,\tilde{\Psi}_{1,1,0,0,0}) - 4\,\mathbf{R}_2(\overline{\phi_1},\tilde{\Psi}_{2,0,0,0,0}) & \\
&& -6\,\mathbf{R}_3(\overline{\phi_1},\phi_1,\phi_1) & [{z_1}^2\bar{z}_1]\\
-c_2\phi_2 &=& (i\omega_{FH}-\mathbf{A})\tilde{\Psi}_{1,1,1,0,0} - 2\mathbf{R}_2(\tilde{\Psi}_{0,1,1,0,0},\phi_1) & \\
&& -2\mathbf{R}_2(\overline{\phi_1},\tilde{\Psi}_{1,0,1,0,0}) - 2\mathbf{R}_2(\phi_2,\tilde{\Psi}_{1,1,0,0,0}) - 6\mathbf{R}_3(\phi_2,\phi_1,\overline{\phi_1}) & [z_1\bar{z}_1\,z_2]\\
-c_1\phi_1 &=& -2\,\mathbf{A}\tilde{\Psi}_{1,0,1,1,0} - 2\,\mathbf{R}_2(\tilde{\Psi}_{1,0,0,1,0},\phi_2) & \\
&& -2\,\mathbf{R}_2(\overline{\phi_2},\tilde{\Psi}_{1,0,1,0,0}) - 2\,\mathbf{R}_2(\phi_1,\tilde{\Psi}_{0,0,1,1,0}) - 6\,\mathbf{R}_3(\phi_2,\phi_1,\overline{\phi_2}) & [z_2\bar{z}_2\,z_1]\\
-2\,b_2\,\phi_2 &=& 2\,(i\omega_{FH}-\mathbf{A})\tilde{\Psi}_{0,0,2,1,0} - 4\,\mathbf{R}_2(\tilde{\Psi}_{0,0,1,1,0},\phi_2) - 4\,\mathbf{R}_2(\overline{\phi_2},\tilde{\Psi}_{0,0,2,0,0}) & \\
&& -6\,\mathbf{R}_3(\phi_2,\phi_2,\overline{\phi_2}) & [\bar{z}_2\,z_2^2]
\end{array}$$

Thus, using the Fredholm alternative in[2] $\mathcal{X}=\mathcal{X}^{(2)}$:

$$\begin{array}{rcl}
a_1 &=& \langle\phi_1^*, \mathbf{R}_{0,1}(\phi_1) + 2\mathbf{R}_2(\phi_1,\tilde{\Psi}_{0,0,0,0,1})\rangle_{\mathcal{X}}\\
a_2 &=& \langle\phi_2^*, \mathbf{R}_{0,1}(\phi_2) + 2\mathbf{R}_2(\phi_2,\tilde{\Psi}_{0,0,0,0,1})\rangle_{\mathcal{X}}\\
b_1 &=& \langle\phi_1^*, 2\,\mathbf{R}_2(\phi_1,\tilde{\Psi}_{1,1,0,0,0}) + 2\mathbf{R}_2(\overline{\phi_1},\tilde{\Psi}_{2,0,0,0,0}) + 3\mathbf{R}_3(\overline{\phi_1},\phi_1,\phi_1)\rangle_{\mathcal{X}}\\
c_2 &=& \langle\phi_2^*, 2\mathbf{R}_2(\tilde{\Psi}_{0,1,1,0,0},\phi_1) + 2\mathbf{R}_2(\overline{\phi_1},\tilde{\Psi}_{1,0,1,0,0}) + 2\mathbf{R}_2(\phi_2,\tilde{\Psi}_{1,1,0,0,0})\\
&& +6\mathbf{R}_3(\phi_2,\phi_1,\overline{\phi_1})\rangle_{\mathcal{X}}\\
c_1 &=& \langle\phi_1^*, 2\,\mathbf{R}_2(\tilde{\Psi}_{1,0,0,1,0},\phi_2) + 2\,\mathbf{R}_2(\overline{\phi_2},\tilde{\Psi}_{1,0,1,0,0}) + 2\,\mathbf{R}_2(\phi_1,\tilde{\Psi}_{0,0,1,1,0})\\
&& +6\,\mathbf{R}_3(\phi_2,\phi_1,\overline{\phi_2})\rangle_{\mathcal{X}}\\
b_2 &=& \langle\phi_2^*, 2\,\mathbf{R}_2(\tilde{\Psi}_{0,0,1,1,0},\phi_2) + 2\,\mathbf{R}_2(\overline{\phi_2},\tilde{\Psi}_{0,0,2,0,0}) + 3\,\mathbf{R}_3(\,\phi_2,\phi_2,\overline{\phi_2})\rangle_{\mathcal{X}}
\end{array}$$

[2]Recall that we are working with three spaces $\mathcal{X}^{(q)},\mathcal{Y}^{(q)},\mathcal{Z}^{(q)}$. Solving the equations in $\mathcal{X}^{(2)}$ gives the solutions in $\mathcal{X}^{(q)}$ for $q\geq 2$.

where $\mathbf{R}_{ql} = \frac{1}{q!l!}\frac{\partial^{q+l}}{\partial^q u \partial^l c}\mathbf{R}$. In order to find the coefficients of the normal form, we are led to compute some of the coefficients of $\tilde{\Psi}$. By taking the second order monomials, we find:

$$
\begin{aligned}
\mathbf{A}\tilde{\Psi}_{0,0,0,0,1} = 0 \quad &\Rightarrow \quad \pi_2\tilde{\Psi}_{0,0,0,0,1} \in \mathbb{C}\phi_1 \\
\mathbf{A}\tilde{\Psi}_{1,1,0,0,0} \quad &= \quad -2\mathbf{R}_2(\phi_1,\bar{\phi_1}) = -2\tfrac{\sigma_{FH}^2 s_2}{2} J_0 \begin{bmatrix} e_0 \\ 0 \end{bmatrix} \\
&\Rightarrow \quad \pi_2\tilde{\Psi}_{1,1,0,0,0} = -\tfrac{\sigma_{FH}^2 s_2 J_0}{-1+\sigma_{FH}s_1 J_0} e_0 \\
&\qquad + \mathbb{C}\phi_1 \\
(i\omega_{FH} - \mathbf{A})\tilde{\Psi}_{1,0,1,0,0} \quad &= \quad 2\mathbf{R}_2(\phi_1,\phi_2) = 2\tfrac{\sigma_{FH}^2 s_2}{2}(Je^{-i\omega_{FH}\tau_{FH}})_n \begin{bmatrix} e_n \\ 0 \end{bmatrix} \\
&\Rightarrow \quad \pi_2\tilde{\Psi}_{1,0,1,0,0} = \tfrac{\sigma_{FH}^2 s_2 (Je^{-i\omega_{FH}\tau_{FH}})_n}{i\omega_{FH}+1-\sigma_{FH}s_1(Je^{-i\omega_{FH}\tau_{FH}})_n} e_n e^{i\omega_{FH}\theta} \\
&\qquad + \mathbb{C}\phi_2 \\
\mathbf{A}\tilde{\Psi}_{0,0,1,1,0} \quad &= \quad -2\mathbf{R}_2(\phi_2,\bar{\phi_2}) = -2\tfrac{\sigma_{FH}^2 s_2 J_0}{2} \begin{bmatrix} e_0 \\ 0 \end{bmatrix} \\
&\Rightarrow \quad \pi_2\tilde{\Psi}_{0,0,1,1,0} = -\tfrac{\sigma_{FH}^2 s_2 J_0}{-1+\sigma_{FH}s_1 J_0} e_0 \\
&\qquad + \mathbb{C}\phi_1 \\
(2i\omega_{FH} - \mathbf{A})\tilde{\Psi}_{0,0,2,0,0} \quad &= \quad \mathbf{R}_2(\phi_2,\phi_2) = \tfrac{\sigma_{FH}^2 s_2}{2}(Je^{-2i\omega_{FH}\tau_{FH}})_0 \begin{bmatrix} e_0 \\ 0 \end{bmatrix} \\
&\Rightarrow \quad \pi_2\tilde{\Psi}_{0,0,2,0,0} = \tfrac{\sigma_{FH}^2 s_2 (Je^{-2i\omega_{FH}\tau_{FH}})_0}{2(2i\omega_{FH}+1-\sigma_{FH}s_1(Je^{-2i\omega_{FH}\tau_{FH}})_0)} e^{2i\omega_{FH}\theta} e_0 \\
\mathbf{A}\tilde{\Psi}_{2,0,0,0,0} \quad &= \quad -\mathbf{R}_2(\phi_1,\phi_1) = -\tfrac{\sigma_{FH}^2 s_2}{2} J_{2n} \begin{bmatrix} e_{2n} \\ 0 \end{bmatrix} \\
&\Rightarrow \quad \pi_2\tilde{\Psi}_{2,0,0,0,0} = -\tfrac{\sigma_{FH}^2 s_2}{2(-1+\sigma_{FH}s_1 J_{2n})} J_{2n} e_{2n} \\
&\qquad + \mathbb{C}\phi_1 \\
(i\omega_{FH} + \mathbf{A})\tilde{\Psi}_{1,0,0,1,0} \quad &= \quad -2\mathbf{R}_2(\phi_1,\bar{\phi_2}) = -2\tfrac{\sigma_{FH}^2 s_2}{2}(Je^{i\omega_{FH}\tau_{FH}})_n \begin{bmatrix} e_n \\ 0 \end{bmatrix} \\
&\Rightarrow \quad \pi_2\tilde{\Psi}_{1,0,0,1,0} = \tfrac{-\sigma_{FH}^2 s_2 (Je^{i\omega_{FH}\tau_{FH}})_n}{i\omega_{FH}-1+\sigma_{FH}s_1(Je^{i\omega_{FH}\tau_{FH}})_n} e_n e^{-i\omega_{FH}\theta} \\
&\qquad + \mathbb{C}\overline{\phi_2} \\
(i\omega_{FH} - \mathbf{A})\tilde{\Psi}_{0,1,1,0,0} \quad &= \quad 2\mathbf{R}_2(\phi_2,\bar{\phi_1}) = 2\tfrac{\sigma_{FH}^2 s_2}{2}(Je^{-i\omega_{FH}\tau_{FH}})_{-n} \begin{bmatrix} e_{-n} \\ 0 \end{bmatrix} \\
&\Rightarrow \quad \pi_2\tilde{\Psi}_{0,1,1,0,0} = \tfrac{\sigma_{FH}^2 s_2 (Je^{-2i\omega_{FH}\tau_{FH}})_{-n}}{i\omega_{FH}+1-\sigma_{FH}s_1(Je^{-i\omega_{FH}\tau_{FH}})_{-n}} e_{-n} e^{i\omega_{FH}\theta} \\
&\qquad + \mathbb{C}\phi_2
\end{aligned}
$$

Let us just indicate how to solve the third equation $(i\omega_{FH} - \mathbf{A})\tilde{\Psi}_{1,0,1,0,0} = 2\mathbf{R}_2(\phi_1,\phi_2)$. The second component of the equation: $(i\omega_{FH} - \frac{d}{d\theta})\pi_2\tilde{\Psi}_{1,0,1,0,0} = 0$ gives $\pi_2\tilde{\Psi}_{1,0,1,0,0} = \pi_1\tilde{\Psi}_{1,0,1,0,0}e^{i\omega_{FH}\theta}$. If we insert this solution in the first component of the equation, we find:

$$(i\omega_{FH} + 1 - \sigma_{FH}s_1 J(i\omega_{FH}))\pi_1\tilde{\Psi}_{1,0,1,0,0} = 2\frac{\sigma_{FH}^2 s_2}{2}(Je^{-i\omega_{FH}\tau_{FH}})_n e_n.$$

The kernel is $\ker(i\omega_{FH} + 1 - \sigma_{FH}s_1 J(i\omega_{FH})) = \mathbb{C}e_0$ and we find: $\pi_2\tilde{\Psi}_{1,0,1,0,0}(\theta) = \frac{\sigma_{FH}^2 s_2 (Je^{-i\omega_{FH}\tau_{FH}})_n}{i\omega_{FH}+1-\sigma_{FH}s_1(Je^{-i\omega_{FH}\tau_{FH}})_n} e_n e^{i\omega_{FH}\theta} + \mathbb{C}e_0 e^{i\omega_{FH}t}$. Using the previous formulas and

$J \cdot e_n \equiv J_n e_n$, $\sigma_{FH} = \frac{1}{s_1 J_n}$, $(Je^{-i\omega_{FH}\tau_{FH}})_0 = \frac{i\omega_{FH}+1}{\sigma_{FH}s_1} = (i\omega_{FH}+1)J_n$, it is staightforward to obtain the lemma. □

C.2.3 Hopf-Hopf normal form

Lemma C.2.3. *The Hopf-Hopf normal form*

$$\begin{cases} \dot{z}_0 = z_0\left(i\omega_0 + a_0 + b_0|z_0|^2 + c_0|z_1|^2 + d_0|z_2|^2\right) \\ \dot{z}_1 = z_1\left(i\omega_1 + a_1 + b_1|z_0|^2 + c_1|z_1|^2 + d_1|z_2|^2\right) \\ \dot{z}_2 = z_2\left(i\omega_1 + a_1 + b_1|z_0|^2 + d_1|z_1|^2 + c_1|z_2|^2\right) \end{cases} \tag{C.1}$$

has the following coefficients:

$$\begin{aligned}
b_0/\pi\overline{\beta_0}(Je^{-i\omega_0\tau})_0 &= \tfrac{\sigma_{FH}^3 s_3}{2} + \sigma_{FH}^4 s_2^2\left[\tfrac{J_0}{1-\sigma_{FH}s_1J_0} + \tfrac{(Je^{-2i\omega_0\tau})_0}{2(2i\omega_0+1-\sigma_{FH}s_1(Je^{-2i\omega_0\tau})_0)}\right] \\
c_0/\pi\overline{\beta_0}(Je^{-i\omega_0\tau})_0 &= \sigma_{FH}^3 s_3 + \sigma_{FH}^4 s_2^2 \\
&\quad \left[\tfrac{(Je^{-i(\omega_0-\omega_1)\tau})_n}{i(\omega_0-\omega_1)+1-\sigma_{FH}s_1(Je^{-i(\omega_0-\omega_1)\tau})_n} + \tfrac{(Je^{-i(\omega_0+\omega_1)\tau})_n}{i(\omega_0+\omega_1)+1-\sigma_{FH}s_1(Je^{-i(\omega_0+\omega_1)\tau})_n}\right. \\
&\quad \left. + \tfrac{J_0}{1-\sigma_{FH}s_1J_0}\right] \\
d_0 &= c_0 \\
b_1/\pi\overline{\beta_1}(Je^{-i\omega_1\tau})_n &= \sigma_{FH}^3 s_3 + \sigma_{FH}^4 s_2^2 \\
&\quad \left[\tfrac{(Je^{-i(\omega_1-\omega_0)\tau})_n}{i(\omega_1-\omega_0)+1-\sigma_{FH}s_1(Je^{-i(\omega_1-\omega_0)\tau})_n} + \tfrac{(Je^{-i(\omega_0+\omega_1)\tau})_n}{i(\omega_0+\omega_1)+1-\sigma_{FH}s_1(Je^{-i(\omega_0+\omega_1)\tau})_n}\right. \\
&\quad \left. + \tfrac{J_0}{1-\sigma_{FH}s_1J_0}\right] \\
c_1/\pi\overline{\beta_1}(Je^{-i\omega_1\tau})_n &= \tfrac{\sigma_{FH}^3 s_3}{2} + \sigma_{FH}^4 s_2^2\left[\tfrac{J_0}{1-\sigma_{FH}s_1J_0} + \tfrac{(Je^{-2i\omega_1\tau})_{2n}}{2(2i\omega_1+1-\sigma_{FH}s_1(Je^{-2i\omega_1\tau})_{2n})}\right] \\
d_1/\pi\overline{\beta_1}(Je^{-i\omega_1\tau})_n &= \sigma_{FH}^3 s_3 + \sigma_{FH}^4 s_2^2\left[\tfrac{J_{2n}}{1-\sigma_{FH}s_1J_{2n}} + \tfrac{(Je^{-2i\omega_1\tau})_0}{2i\omega_1+1-\sigma_{FH}s_1(Je^{-2i\omega_1\tau})_0} + \tfrac{J_0}{1-\sigma_{FH}s_1J_0}\right]
\end{aligned}$$

Proof. The normal form for the Hopf-Hopf bifurcation between the 0-mode and the n-mode in the non-resonant case where $\frac{\omega_0}{\omega_n} \notin \mathbb{Q}$ is given in [Golubitsky 1988]:

$$\begin{cases} \dot{z}_0 = z_0\left(i\omega_0 + a_0 + b_0|z_0|^2 + c_0|z_1|^2 + d_0|z_2|^2\right) \\ \dot{z}_1 = z_1\left(i\omega_1 + a_1 + b_1|z_0|^2 + c_1|z_1|^2 + d_1|z_2|^2\right) \\ \dot{z}_2 = z_2\left(i\omega_1 + a_1 + b_1|z_0|^2 + d_1|z_1|^2 + c_1|z_2|^2\right) \end{cases}$$

Recall that the eigenvalue $i\omega_0$ has the eigenvector $\phi_0 = \begin{bmatrix} e_0 \\ e^{i\omega_0\theta}e_0 \end{bmatrix}$ and that $i\omega_1$ has the eigenvectors $\phi_1 = \begin{bmatrix} e_n \\ e^{i\omega_1\theta}e_n \end{bmatrix}, \phi_2 = \begin{bmatrix} e_{-n} \\ e^{i\omega_1\theta}e_{-n} \end{bmatrix}$. Let us write the nonlinear change of variable $\tilde{\Psi}$ to bring the delayed neural field equations to the normal form (C.1). We Taylor expand $\tilde{\Psi}$ as in section 5.2.1:

$$\tilde{\Psi}(v_0,\mu) = \sum_{k_1+k_2+l_1+l_2+p_1+p_2+r>1} z_0^{k_1}\bar{z}_0^{k_2}z_1^{l_1}\bar{z}_1^{l_2}z_2^{p_1}\bar{z}_2^{p_2}\mu^r\tilde{\Psi}_{k_1,k_2,l_1,l_2,p_1,p_2,r},\ \tilde{\Psi}_{k_1,k_2,l_1,l_2,p_1,p_2,r} \in \mathcal{Z},$$

where $\tilde{\Psi}$ satisfies $\tilde{\Psi}(0,0)=0,\ D_{v_0}\tilde{\Psi}(0,0)=0$. Using the equation (5.9) satisfied by $\tilde{\Psi}$ and a Maple program similar to the one given in section 5.2.1, we find the next equations.

$$
\begin{aligned}
0 &= 2(i\omega_0-\mathbf{A})\tilde{\Psi}_{2,1,0,0,0,0,0}+2b_0\phi_0-4\mathbf{R}_2(\tilde{\Psi}_{1,1,0,0,0,0,0},\phi_0)-4\mathbf{R}_2(\overline{\phi_0},\tilde{\Psi}_{2,0,0,0,0,0,0})\\
&\quad -6\mathbf{R}_3(\phi_0,\phi_0,\overline{\phi_0})\\
0 &= (i\omega_0-\mathbf{A})\tilde{\Psi}_{1,0,1,1,0,0,0}+c_0\phi_0-2\mathbf{R}_2(\tilde{\Psi}_{1,0,0,1,0,0,0},\phi_1)-2\mathbf{R}_2(\overline{\phi_1},\tilde{\Psi}_{1,0,1,0,0,0,0})\\
&\quad -2\mathbf{R}_2(\phi_0,\tilde{\Psi}_{0,0,1,1,0,0,0})-6\mathbf{R}_3(\phi_0,\phi_1,\overline{\phi_1})\\
0 &= (i\omega_0-\mathbf{A})\tilde{\Psi}_{1,0,0,0,1,1,0}+d_0\phi_0-2\mathbf{R}_2(\tilde{\Psi}_{1,0,0,0,0,1,0},\phi_2)-2\mathbf{R}_2(\overline{\phi_2},\tilde{\Psi}_{1,0,0,0,1,0,0})\\
&\quad -2\mathbf{R}_2(\phi_0,\tilde{\Psi}_{0,0,0,0,1,1,0})-6\mathbf{R}_3(\phi_0,\phi_2,\overline{\phi_2})\\
0 &= (i\omega_1-\mathbf{A})\tilde{\Psi}_{1,1,1,0,0,0,0}+b_1\phi_1-2\mathbf{R}_2(\tilde{\Psi}_{0,1,1,0,0,0,0},\phi_0)-2\mathbf{R}_2(\overline{\phi_0},\tilde{\Psi}_{1,0,1,0,0,0,0})\\
&\quad -2\mathbf{R}_2(\phi_1,\tilde{\Psi}_{1,1,0,0,0,0,0})-6\mathbf{R}_3(\phi_1,\phi_0,\overline{\phi_0})\\
0 &= 2(i\omega_1-\mathbf{A})\tilde{\Psi}_{0,0,2,1,0,0,0}+2c_1\phi_1-4\mathbf{R}_2(\tilde{\Psi}_{0,0,1,1,0,0,0},\phi_1)-4\mathbf{R}_2(\overline{\phi_1},\tilde{\Psi}_{0,0,2,0,0,0,0})\\
&\quad -6\mathbf{R}_3(\phi_1,\phi_1,\overline{\phi_1})\\
0 &= (i\omega_1-\mathbf{A})\tilde{\Psi}_{0,0,1,0,1,1,0}+d_1\phi_1-2\mathbf{R}_2(\tilde{\Psi}_{0,0,1,0,0,1,0},\phi_2)-2\mathbf{R}_2(\overline{\phi_2},\tilde{\Psi}_{0,0,1,0,1,0,0})\\
&\quad -2\mathbf{R}_2(\phi_1,\tilde{\Psi}_{0,0,0,0,1,1,0})-6\mathbf{R}_3(\phi_1,\phi_2,\overline{\phi_2})\\
0 &= (i\omega_1-\mathbf{A})\tilde{\Psi}_{1,1,0,0,1,0,0}+b_1\phi_2-2\mathbf{R}_2(\tilde{\Psi}_{0,1,0,0,1,0,0},\phi_0)-2\mathbf{R}_2(\overline{\phi_0},\tilde{\Psi}_{1,0,0,0,1,0,0})\\
&\quad -2\mathbf{R}_2(\phi_2,\tilde{\Psi}_{1,1,0,0,0,0,0})-6\mathbf{R}_3(\phi_2,\phi_0,\overline{\phi_0})\\
0 &= (i\omega_1-\mathbf{A})\tilde{\Psi}_{0,0,1,1,1,0,0}+d_1\phi_2-2\mathbf{R}_2(\tilde{\Psi}_{0,0,0,1,1,0,0},\phi_1)-2\mathbf{R}_2(\overline{\phi_1},\tilde{\Psi}_{0,0,1,0,1,0,0})\\
&\quad -2\mathbf{R}_2(\phi_2,\tilde{\Psi}_{0,0,1,1,0,0,0})-6\mathbf{R}_3(\phi_2,\phi_1,\overline{\phi_1})\\
0 &= 2(i\omega_1-\mathbf{A})\tilde{\Psi}_{0,0,0,0,2,1,0}+2c_1\phi_2-4\mathbf{R}_2(\tilde{\Psi}_{0,0,0,0,1,1,0},\phi_2)\\
&\quad -4\mathbf{R}_2(\overline{\phi_2},\tilde{\Psi}_{0,0,0,0,2,0,0})-6\mathbf{R}_3(\phi_2,\phi_2,\overline{\phi_2})
\end{aligned}
$$

Notice that the equations for b_1, c_1, d_1 are redundent: because of the symmetries, they give the same result. Using the Fredholm alternative in[3] $\mathcal{X}=\mathcal{X}^{(2)}$, we find:

$$
\begin{aligned}
2b_0 &= \langle\psi_0, 4\mathbf{R}_2(\tilde{\Psi}_{1,1,0,0,0,0,0},\phi_0)+4\mathbf{R}_2(\overline{\phi_0},\tilde{\Psi}_{2,0,0,0,0,0,0})+6\mathbf{R}_3(\phi_0,\phi_0,\overline{\phi_0})\rangle_{\mathcal{X}}\\
c_0 &= \langle\psi_0, 2\mathbf{R}_2(\tilde{\Psi}_{1,0,0,1,0,0,0},\phi_1)+2\mathbf{R}_2(\overline{\phi_1},\tilde{\Psi}_{1,0,1,0,0,0,0})+2\mathbf{R}_2(\phi_0,\tilde{\Psi}_{0,0,1,1,0,0,0})\\
&\quad +6\mathbf{R}_3(\phi_0,\phi_1,\overline{\phi_1})\rangle_{\mathcal{X}}\\
d_0 &= \langle\psi_0, 2\mathbf{R}_2(\tilde{\Psi}_{1,0,0,0,0,1,0},\phi_2)+2\mathbf{R}_2(\overline{\phi_2},\tilde{\Psi}_{1,0,0,0,1,0,0})+2\mathbf{R}_2(\phi_0,\tilde{\Psi}_{0,0,0,0,1,1,0})\\
&\quad +6\mathbf{R}_3(\phi_0,\phi_2,\overline{\phi_2})\rangle_{\mathcal{X}}\\
b_1 &= \langle\psi_1, 2\mathbf{R}_2(\tilde{\Psi}_{0,1,1,0,0,0,0},\phi_0)+2\mathbf{R}_2(\overline{\phi_0},\tilde{\Psi}_{1,0,1,0,0,0,0})+2\mathbf{R}_2(\phi_1,\tilde{\Psi}_{1,1,0,0,0,0,0})\\
&\quad +6\mathbf{R}_3(\phi_1,\phi_0,\overline{\phi_0})\rangle_{\mathcal{X}}\\
2c_1 &= \langle\psi_1, 4\mathbf{R}_2(\tilde{\Psi}_{0,0,1,1,0,0,0},\phi_1)+4\mathbf{R}_2(\overline{\phi_1},\tilde{\Psi}_{0,0,2,0,0,0,0})+6\mathbf{R}_3(\phi_1,\phi_1,\overline{\phi_1})\rangle_{\mathcal{X}}\\
d_1 &= \langle\psi_1, 2\mathbf{R}_2(\tilde{\Psi}_{0,0,1,0,0,1,0},\phi_2)+2\mathbf{R}_2(\overline{\phi_2},\tilde{\Psi}_{0,0,1,0,1,0,0})+2\mathbf{R}_2(\phi_1,\tilde{\Psi}_{0,0,0,0,1,1,0})\\
&\quad +6\mathbf{R}_3(\phi_1,\phi_2,\overline{\phi_2})\rangle_{\mathcal{X}}
\end{aligned}
$$

where $\mathbf{R}_{ql}=\frac{1}{q!l!}\frac{\partial^{q+l}}{\partial^q u\partial^l c}\mathbf{R}$. In order to find the coefficients of the normal form, we are led to compute some of the coefficients of $\tilde{\Psi}$. By taking the second order terms, we find the next equations and using the fact that $\phi_0=\begin{bmatrix} e_0 \\ e^{i\omega_0\phi_1\theta}e_0\end{bmatrix}, \phi_1=$

[3] Recall that we are working with three spaces $\mathcal{X}^{(q)},\mathcal{Y}^{(q)},\mathcal{Z}^{(q)}$. Solving the equations in $\mathcal{X}^{(2)}$ gives the solutions in $\mathcal{X}^{(q)}$ for $q\geq 2$.

$\begin{bmatrix} e_n \\ e^{i\omega_1\theta}e_n \end{bmatrix}, \phi_2 = \begin{bmatrix} e_{-n} \\ e^{i\omega_1\theta}e_{-n} \end{bmatrix}$:

$$
\begin{aligned}
\mathbf{A}\tilde{\Psi}_{1100000} &= -2\mathbf{R}_2(\overline{\phi_0}, \phi_0) \\
&= -2\tfrac{\sigma_{HH}^2 s_2}{2} J_0 \begin{bmatrix} e_0 \\ 0 \end{bmatrix} \Rightarrow \pi_2\tilde{\Psi}_{1100000} = -\tfrac{\sigma_{HH}^2 s_2 J_0}{-1+\sigma_{FH}s_1 J_0} e_0 \\
(4i\omega_0 - 2\mathbf{A})\tilde{\Psi}_{2000000} &= 2\mathbf{R}_2(\phi_0, \phi_0) \\
&= 2\tfrac{\sigma_{HH}^2 s_2}{2} (Je^{-2i\omega_0\tau})_0 \begin{bmatrix} e_0 \\ 0 \end{bmatrix} \\
&\Rightarrow \pi_2\tilde{\Psi}_{2000000} = \tfrac{\sigma_{HH}^2 s_2 (Je^{-2i\omega_0\tau})_0 e^{2i\omega_0\theta}}{2(2i\omega_0+1-\sigma_{FH}s_1(Je^{-2i\omega_0\tau})_0)} e_0 \\
(i\omega_0 - i\omega_1 - \mathbf{A})\tilde{\Psi}_{1001000} &= 2\mathbf{R}_2(\overline{\phi_1}, \phi_0) \\
&= \sigma_{HH}^2 s_2 (Je^{-i(\omega_0-\omega_1)\tau})_n \begin{bmatrix} e_{-n} \\ 0 \end{bmatrix} \\
&\Rightarrow \pi_2\tilde{\Psi}_{1001000} = \tfrac{\sigma_{HH}^2 s_2 (Je^{-i(\omega_0-\omega_1)\tau})_n e^{i(\omega_0-\omega_1)\theta}}{i(\omega_0-\omega_1)+1-\sigma_{FH}s_1(Je^{-i(\omega_0-\omega_1)\tau})_n} e_{-n} \\
(i\omega_1 + i\omega_0 - \mathbf{A})\tilde{\Psi}_{1010000} &= 2\mathbf{R}_2(\phi_1, \phi_0) \\
&= 2\tfrac{\sigma_{HH}^2 s_2}{2} (Je^{-i(\omega_0+\omega_1)\tau})_n \begin{bmatrix} e_n \\ 0 \end{bmatrix} \\
&\Rightarrow \pi_2\tilde{\Psi}_{1010000} = \tfrac{\sigma_{HH}^2 s_2 (Je^{-i(\omega_0+\omega_1)\tau})_n e^{i(\omega_0+\omega_1)\theta}}{i(\omega_0+\omega_1)+1-\sigma_{FH}s_1(Je^{-i(\omega_0+\omega_1)\tau})_n} e_n \\
\mathbf{A}\tilde{\Psi}_{0011000} &= -2\mathbf{R}_2(\overline{\phi_1}, \phi_1) \\
&= -2\tfrac{\sigma_{HH}^2 s_2}{2} J_0 \begin{bmatrix} e_0 \\ 0 \end{bmatrix} \Rightarrow \pi_2\tilde{\Psi}_{0011000} = -\tfrac{\sigma_{HH}^2 s_2 J_0}{-1+\sigma_{FH}s_1 J_0} e_0 \\
(-i\omega_1 + i\omega_0 - \mathbf{A})\tilde{\Psi}_{1000010} &= 2\mathbf{R}_2(\overline{\phi_2}, \phi_0) \\
&= 2\tfrac{\sigma_{HH}^2 s_2}{2} (Je^{-i(\omega_0-\omega_1)\tau})_n \begin{bmatrix} e_n \\ 0 \end{bmatrix} \\
&\Rightarrow \pi_2\tilde{\Psi}_{1000010} = \tfrac{\sigma_{HH}^2 s_2 (Je^{-i(\omega_0-\omega_1)\tau})_n e^{i(\omega_0-\omega_1)\theta}}{i(\omega_0-\omega_1)+1-\sigma_{FH}s_1(Je^{-i(\omega_0-\omega_1)\tau})_n} e_n \\
(i\omega_1 + i\omega_0 - \mathbf{A})\tilde{\Psi}_{1000100} &= 2\mathbf{R}_2(\phi_2, \phi_0) \\
&= 2\tfrac{\sigma_{HH}^2 s_2}{2} (Je^{-i(\omega_0+\omega_1)\tau})_n \begin{bmatrix} e_{-n} \\ 0 \end{bmatrix} \\
&\Rightarrow \pi_2\tilde{\Psi}_{1000100} = \tfrac{\sigma_{HH}^2 s_2 (Je^{-i(\omega_0+\omega_1)\tau})_n e^{i(\omega_0+\omega_1)\theta}}{i(\omega_0+\omega_1)+1-\sigma_{FH}s_1(Je^{-i(\omega_0+\omega_1)\tau})_n} e_{-n} \\
\mathbf{A}\tilde{\Psi}_{0000110} &= -2\mathbf{R}_2(\overline{\phi_2}, \phi_2) \\
&= -2\tfrac{\sigma_{HH}^2 s_2}{2} J_0 \begin{bmatrix} e_0 \\ 0 \end{bmatrix} \Rightarrow \pi_2\tilde{\Psi}_{0000110} = -\tfrac{\sigma_{HH}^2 s_2 J_0}{-1+\sigma_{FH}s_1 J_0} e_0 \\
(i\omega_1 - i\omega_0 - \mathbf{A})\tilde{\Psi}_{0110000} &= 2\mathbf{R}_2(\phi_1, \overline{\phi_0}) \\
&= 2\tfrac{\sigma_{HH}^2 s_2}{2} (Je^{-i(\omega_1-\omega_0)\tau})_n \begin{bmatrix} e_n \\ 0 \end{bmatrix} \\
&\Rightarrow \pi_2\tilde{\Psi}_{0110000} = \tfrac{\sigma_{HH}^2 s_2 (Je^{-i(\omega_1-\omega_0)\tau})_n e^{i(\omega_1-\omega_0)\theta}}{i(\omega_1-\omega_0)+1-\sigma_{FH}s_1(Je^{-i(\omega_1-\omega_0)\tau})_n} e_n \\
(4i\omega_1 - 2\mathbf{A})\tilde{\Psi}_{0020000} &= 2\mathbf{R}_2(\phi_1, \phi_1) \\
&= 2\tfrac{\sigma_{HH}^2 s_2}{2} (Je^{-2i\omega_1\tau})_{2n} \begin{bmatrix} e_{2n} \\ 0 \end{bmatrix} \\
&\Rightarrow \pi_2\tilde{\Psi}_{0020000} = \tfrac{\sigma_{HH}^2 s_2 (Je^{-2i\omega_1\tau})_{2n} e^{2i\omega_1\theta}}{2(2i\omega_1+1-\sigma_{FH}s_1(Je^{-2i\omega_1\tau})_{2n})} e_{2n}
\end{aligned}
$$

$$
\begin{aligned}
\mathbf{A}\tilde{\Psi}_{0010010} &= -2\mathbf{R}_2(\overline{\phi_2}, \phi_1) \\
&= -2\tfrac{\sigma_{HH}^2 s_2}{2} J_{2n} \begin{bmatrix} e_{2n} \\ 0 \end{bmatrix} \Rightarrow \pi_2 \Psi_{0010010} = -\tfrac{\sigma_{HH}^2 s_2 J_{2n}}{-1+\sigma_{FH} s_1 J_{2n}} e_{2n} \\
(2i\omega_1 - \mathbf{A})\tilde{\Psi}_{0010100} &= 2\mathbf{R}_2(\phi_2, \phi_1) \\
&= 2\tfrac{\sigma_{HH}^2 s_2}{2} (J e^{-2i\omega_1 \tau})_0 \begin{bmatrix} e_0 \\ 0 \end{bmatrix} \\
&\Rightarrow \pi_2 \tilde{\Psi}_{0010100} = \tfrac{\sigma_{HH}^2 s_2 (J e^{-2i\omega_1 \tau})_0 e^{2i\omega_1 \theta}}{2i\omega_1 + 1 - \sigma_{FH} s_1 (J e^{-2i\omega_1 \tau})_0} e_0
\end{aligned}
$$

which gives the lemma. □

Appendix D

The Deco-Roland model of long range apparant motion in the ferret

D.1 Eigenvalues and linearized equation

We assume that the stationary activity is $(A^{(1)}, A^{(2)}) = (0, 0)$. The jacobian of (7.1) is given by:

$$L = \frac{1}{\tau}\begin{bmatrix} -\mathrm{Id} + S'(0)J^{(1)} & S'(0)f^b W \\ S'(0)W & -\mathrm{Id} + S'(0)J^{(2)} \end{bmatrix}. \tag{D.1}$$

Because the connectivities functions $J^{(1)}, J^{(2)}, W$ are homogeneous, the eigenvectors of L have the form: $\begin{bmatrix} v_n^1 \cos_n \\ v_p^2 \cos_p \end{bmatrix}$. Then necessarilly, we find that $n = p$. Hence, looking for the eigenvalues amounts to diagonalize the following matrices:

$$L_n = \frac{1}{\tau}\begin{bmatrix} -1 + S'(0)\hat{J}_n^{(1)} & S'(0)f_b\hat{W}_n \\ S'(0)\hat{W}_n & -1 + S'(0)\hat{J}_n^{(2)} \end{bmatrix}. \tag{D.2}$$

where, for example $\hat{J}_n^{(1)} = \int_{-\pi}^{\pi} J^{(1)}(x)cos(nx)dx$. Finally, we have:

$$\Sigma(\mathbf{L}) = \bigcup_n \left\{ \beta_{n,\pm} \equiv \frac{1}{\tau}\left(-1 + S'(0)\frac{\hat{J}_n^{(1)} + \hat{J}_n^{(2)}}{2} \pm \frac{S'(0)}{2}\sqrt{(\hat{J}_n^{(1)} - \hat{J}_n^{(2)})^2 + 4f^b\hat{W}_n^2} \right) \right\}$$

Remark 40. *We have:* $\beta_{n,-} < -1 + S'(0)\hat{J}_n^{(2)} < -1 + S'(0)\hat{J}_n^{(1)} < \beta_{n,+}$.

D.2 Computation of the bifurcation curves

Lemma D.2.1. *The pitchfork bifurcation curves are located on parabolas* (f_b, J_2)

$$f_b^c = \frac{1}{\hat{W}_n^2 s_1^2}\left[1 - S'(0)\hat{J}_n^{(1)}\right]\left[1 - S'(0)\hat{J}_n^{(2)}\right]$$

A condition to slow down the dynamical system, is to be close to this bifurcation curve, i.e.:

$$f \leq f_c$$

Proof. First, we compute the Fourier coefficients and give the approximations from the parameters used in the model:

$$\hat{J}_n^{(i)} = \int_{-\pi}^{\pi} J^{(i)} \cos_n = \begin{cases} -4\pi^2 \frac{J_0}{\lambda} + 4\pi J_2 (1 - e^{-\frac{\pi}{\lambda_i}}) \approx -4\pi^2 \frac{J_0}{\lambda_i} + 4\pi J_2, & n = 0 \\ \frac{4\pi J_2 e^{-\frac{\pi}{\lambda_i}}}{1+n^2\lambda_i^2} \left(e^{\frac{\pi}{\lambda_i}} + (-1)^{n+1} \right) \approx \frac{4\pi J_2}{1+n^2\lambda_i^2} < 4\pi J_2, & n > 0 \end{cases} \tag{D.3}$$

and

$$\hat{W}_n = \int_{-\pi}^{\pi} W \cos_n = \begin{cases} 4\pi(1 - e^{-\frac{\pi}{\alpha}}) \approx 4\pi, & n = 0 \\ \frac{4\pi e^{-\frac{\pi}{\alpha}}}{1+n^2\alpha^2} \left(e^{\frac{\pi}{\alpha}} + (-1)^{n+1} \right) \approx \frac{4\pi}{1+n^2\alpha^2} < 4\pi, & n > 0 \end{cases} \tag{D.4}$$

Notice that $e^{-\frac{\pi}{\alpha}} \approx 4e^{-4}$ and $\hat{W}_n > 0$, idem for $\hat{J}_n^{(i)}$, $n > 0$, which justifies the above approximations. We look for a relashionship such that $\beta_n = 0$. It gives:

$$f_b = \frac{1}{\hat{W}_n^2 s_1^2} \left[1 - S'(0) \hat{J}_n^{(1)} \right] \left[1 - S'(0) \hat{J}_n^{(2)} \right]$$

which is a parabola in (f_b, J_2). On each parabola P_n, the smallest value of J_2 such that $f_b = 0$ is given by $J_2 = \frac{1+n^2\lambda^2}{4\pi S'(0)} \geq \frac{1+\lambda^2}{4\pi S'(0)}, n > 0$ and $J_2 = \frac{1+\frac{4\pi^2 S'(0)}{\lambda'} J_0}{4\pi S'(0)}$ otherwise. Hence, there are $\sqrt{\frac{4\pi^2 S'(0)}{\lambda'\lambda^2}} J_0 \approx 6$ parabolas 'before' P_0. □

D.3 Effect of the intra-cortical propagation delays

From appendix 7.4, we need to compute :

$$\frac{1}{v_{propa}} \int_{-\pi}^{\pi} J^{(1)}(x)|x| \cos(x) dy + \frac{1}{v_{propa}} \int_{-\pi}^{\pi} J^{(2)}(x)|x| \cos(x) dy$$

By neglecting $e^{-\pi/\lambda}$, we find:

$$D(\lambda_1) = \int_{-\pi}^{\pi} J^{(1)}(x)|x| \cos(x) dy \approx 4\pi \frac{(2J_0 - J_2)\lambda_1^4 + (4J_0 + J_2)\lambda_1^2 + 2J_0}{\lambda_1(\lambda_1^4 + 2\lambda_1^2 + 1)}$$

It is positive for $J_0 = 0.2,\ J_2 = 0.9$ and $\lambda_1 \in (0, 1)$. The same is true for $D(\lambda_2)$.

D.4 Study of the Hopf bifurcation curves for constant delays

From chapter B, we need to find the characteristic values $s = i\omega \in i\mathbb{R}$ such that the linearized operator

$$L(s) = \begin{bmatrix} -\tau s - 1 + S'(0) J^{(1)} & S'(0) f^b W e^{-s\tau_2} \\ S'(0) W e^{-s\tau_1} & -\tau s - 1 + S'(0) J^{(2)} \end{bmatrix} \tag{D.5}$$

has a nontrivial kernel. We find that the null vector has to be $\begin{bmatrix}\cos_n\\ \cos_n\end{bmatrix}$ (or the same but with cos → sin). Hence, we find the following equations for the characteristic values

$$\begin{aligned} 0 &= \det\begin{bmatrix} -s-1+s_1\hat{J}_n^{(1)} & s_1 f^b \hat{W}_n e^{-s\tau_2/\tau} \\ s_1\hat{W}_n e^{-s\tau_1/\tau} & -s-1+s_1\hat{J}_n^{(2)} \end{bmatrix} \\ &\equiv \det\begin{bmatrix} -s-a & s_1 f^b \hat{W}_n e^{-s\tau_2/\tau} \\ s_1\hat{W}_n e^{-s\tau_1/\tau} & -s-b \end{bmatrix} = (s+a)(s+b) - Ae^{-sB} \end{aligned} \tag{D.6}$$

with $s_1 = S'(0)$, $a = 1-s_1\hat{J}_n^{(1)} > 0$, $b = 1-s_1\hat{J}_n^{(2)} > 0$, $A = s_1^2 f_b \hat{W}_n^2 > 0, B = \frac{\tau_1+\tau_2}{\tau}$. We find a purely imaginary characteristic value $s = i\omega$ i.f.f.

$$\begin{cases} A\cos(\omega D) = -\omega^2 + ab \\ A\sin(\omega D) = \omega(a+b) \end{cases} \tag{D.7}$$

which give $2\omega^2 = -(a^2+b^2) \pm \sqrt{(a^2-b^2)^2+4A^2}$. As $\omega^2 > 0$, it forces

$$2\omega^2 = -(a^2+b^2) + \sqrt{(a^2-b^2)^2+4A^2} > 0.$$

This is possible exists i.f.f. $(a^2+b^2)^2 < (a^2-b^2)^2 + 4A^2$ *i.e.* $|ab| < A$. Notice that the pitchfork bifurcation curves read:

$$A_n = a_n b_n$$

Hence, above each pitchfork curve P_n, there is a Hopf bifurcation for some delay critical B which is infinite on the parabola and decreases as we move away from the parabola. Hence, no oscillatory patterns can be found in the parameter regime of the model.

D.5 Study of the apparent speed/contrast relationship

Close to the pitchfork bifurcation point (J_2^{bif}, f_{bif}^b), the dynamics is well approximated by $(A^{(1)}(t), A^{(2)}(t)) \approx z_1(t)\begin{bmatrix}\cos\\ \cos\end{bmatrix} + z_2(t)\begin{bmatrix}\sin\\ \sin\end{bmatrix}$. If we write $\varepsilon\beta e^{i\theta}$, the projection of the external input on $Span\left(\begin{bmatrix}\cos\\ \cos\end{bmatrix}, \begin{bmatrix}\sin\\ \sin\end{bmatrix}\right)$ where ε is the contrast, we find $\dot{z}/\beta_2 = \beta_1 z + \chi_3|z|^2 z + \varepsilon I e^{i\theta}$ where χ_3 can be computed analogously as in section E.5, $\beta_2 = 1+S'(0)\hat{W}_1(f_b\tau_2+\tau_1)$ from section 5.2.2.1 and $\beta_1 = \frac{J_2-J_2^{bif}}{J_2^{bif}} + \frac{f^b-f_{bif}^b}{f_{bif}^b}$. A solution $z = \rho e^{i\phi}$ satisfies:

$$\begin{cases} \tau\dot{\rho}/\beta_2 &= \beta_1\rho + \chi_3\rho^3 + \varepsilon\beta\cos(\theta-\phi) \\ \tau\rho\dot{\phi}/\beta_2 &= \varepsilon\beta\sin(\theta-\phi) \end{cases} \tag{D.8}$$

Then speed of the apparent motion, for which ρ is almost constant, is given by:

$$\omega_0 = \frac{\varepsilon\beta}{\beta_2\tau\rho^f} \approx \frac{\varepsilon\beta}{(1+S'(0)\hat{W}_1(f_b\tau_2+\tau_1))(\sqrt{\frac{\beta_1}{\chi_3}}+\varepsilon/2\beta_1)} \approx \frac{\varepsilon\beta}{(1+1+S'(0)\hat{W}_1(f_b\tau_2+\tau_1))\sqrt{\frac{\beta_1}{\chi_3}}}.$$

Appendix E

The Ring Model

E.1 Numerical computation of the invariant functions

Let us say a few words about the practical computation of the invariant functions $\tilde{B}_0, a, b, c, d$. As we are interested in the tuning curves, using the estimates in prop A.6.2, we obtain that the L^2-norm $\left\|V^f\right\|_2$ of the tuning curve is upperbounded by 14 for the connectivity function shown in figure 9.5. The relation $\left\|V^f\right\|_2^2 = \pi\left(v_0^2 + \frac{J_1}{2}\pi_1 + \frac{J_2}{2}\pi_2\right)$ yields the estimation:

$$\left\|V^f\right\|_\infty \leq |v_0| + \sqrt{J_1}(|v_1^{(1)}| + |v_1^{(2)}|) + \sqrt{|J_2|}(|v_2^{(1)}| + |v_2^{(2)}|) \overset{\text{Cauchy-Schwarz}}{\leq} \frac{3}{\sqrt{\pi}}\left\|V^f\right\|_2 \leq 6.75$$

for the same values of the parameters. The next step is to approximate the sigmoid S by a polynomial P on some interval $[-\alpha, \alpha]$ where the value of α is chosen so that $\sigma\left\|V^f\right\|_\infty \leq \alpha$. As we need to observe the first two Pitchfork bifurcations, reached for the values $\sigma_1 < \sigma_2$ of σ, see remark E.2, we need at least $\sigma = \sigma_2$ and, being a little bit conservative, we end up computing the solutions for $\sigma \in [0, 1.6]$. This in turn requires $\alpha \approx 11$. Note that the more accurate the approximation of S, the higher the degree of P with the consequence that some numerical instabilities may develop since this implies raising small numbers to high powers.

P is then expressed in the basis of the Chebychev polynomials as $P = \sum_i \alpha_i T_i$. The reason for this is that the Chebychev polynomials having rational coefficients, we can use, for example, the Groebner basis package of the symbolic computation package Maple to express the invariants B_0, B_1, B_2 as functions of $(v_0, \vec{\pi})$. For example, we have:

$$\begin{aligned}
B_0 &= \frac{\varepsilon_0}{\pi}\int_{-\frac{\pi}{2}}^{\frac{\pi}{2}} S\left[\sigma v_0 + \sigma\Re\left(\sqrt{J_1}z_1 e^{-2piy} + \sqrt{J_1}z_2 e^{-4piy}\right)\right] dy \\
&\approx \frac{\varepsilon_0}{\pi}\int_{-\frac{\pi}{2}}^{\frac{\pi}{2}} P\left[\sigma v_0 + \sigma\Re\left(\sqrt{J_1}z_1 e^{-2piy} + \sqrt{J_1}z_2 e^{-4piy}\right)\right] dy \\
&= \frac{\varepsilon_0}{\pi}\sum_i \alpha_i \int_{-\frac{\pi}{2}}^{\frac{\pi}{2}} T_i\left[\sigma v_0 + \sigma\Re\left(\sqrt{J_1}z_1 e^{-2piy} + \sqrt{J_1}z_2 e^{-4piy}\right)\right] dy \\
&\overset{Maple}{=} \frac{\varepsilon_0}{\pi}\sum_i \alpha_i \tilde{T}_i(v_0, \vec{\pi})
\end{aligned}$$

The computation of $\tilde{T}_i(v_0, \vec{\pi}) = \int_{-\frac{\pi}{2}}^{\frac{\pi}{2}} T_i\left[\sigma v_0 + \sigma\Re\left(\sqrt{J_1}z_1 e^{-2piy} + \sqrt{J_1}z_2 e^{-4piy}\right)\right] dy$ is done automatically by the Groebner basis package but requires that the coefficients

of the polynomial T_i be rational, not real. This justifies the Chebychev approximation. For $\alpha = 14$ and an approximation error of 0.01 ($\|S - P\|_{\infty,[-14,14]} < 0.01$), it yields a polynomials P of degree 19. One important advantage of this method is that it does not require the vector $(v_0, \vec{\pi})$ to be on the Orbit Space to do the computations, i.e. we can compute $\tilde{B}_0, a, b, c, d$ even for values of $(v_0, \vec{\pi})$ that make no sense, e.g. $\pi_1 < 0$, and then project the result on the Orbit Space. Note that the method is coherent since the results shown in figures 9.5 and 9.6 obtained by numerical continuation do satisfy $\sigma \left\|V^f\right\|_\infty < 11$, that is, are consistent with the numerical approximation.

E.2 Numerical computation of the solutions of the nonlinear equations in the case $N = 2$

In order to solve the nonlinear equations (9.14) for the tuning curves, we apply the strategy of section 3.3. The idea is to use a homotopy to solve the problem: we introduce a new parameter μ which translates S, i.e. $S_{(\mu)} \overset{def}{=} S_0 + \mu S(0)$. Thus $S_{(0)} = S_0$ and $S_{(1)} = S$. This way we change the nonlinearity in (9.8) in order to find the tuning curves analytically (notice that this translation only affects the first equation of (9.8)). Indeed, when the nonlinearity is the centered sigmoid S_0 we obtain the trivial solution $V^f = 0$ and we can also compute the values of the nonlinear gain σ where the Pitchfork bifurcations occur. We can then numerically continue this trivial solution with respect to the parameters (σ, μ) to find the solutions of the equations with the "correct" nonlinearity, namely S. We then simply take a slice of the output of the continuation program for $\mu = 1$ and obtain the dependency of the solutions w.r.t. the nonlinear gain σ. This approach, though numerically intensive, is very convenient because it automatically gives the bifurcated branches. It also allows to compute some non-connected branches of solutions. This strategy relies on the library TRILINOS, see the acknowledgements below.

E.3 Existence of the Pitchfork bifurcation

In this appendix we prove that there is always a Pitchfork bifurcation for some nonlinear gain $\sigma = \sigma_0$.

Lemma E.3.1. *For every pair (T, J_1), there exists a unique pair $(\sigma_0 > 0, v_0^f)$ such that*

$$(E) : \begin{cases} v_0^f &= \varepsilon_0 S(\sigma_0 v_0^f) \\ 1 &= \sigma_0 S'(\sigma_0 v_0^f)\frac{J_1}{2} \end{cases}$$

when $\varepsilon_0 = -1$.

Proof. **We do the case $\varepsilon_0 = -1$.** As $S' = S(1-S)$, the second equation (E.2) becomes : $1 = \frac{\sigma J_1}{2} S(1-S) \overset{\text{using}(E.1)}{=} \frac{\sigma J_1}{2}(-U)(1+U)$ where $U \overset{\text{def}}{=} v_0^f$. This quadratic

equation in U has real solutions if and only if $\sigma J_1 \geq 8$, and they are given by

$$U_\pm(\sigma) = \frac{-1 \pm \sqrt{1 - \frac{8}{\sigma J_1}}}{2}$$

We still have to verify that (E.1) is satisfied for at least one of these solutions.

For example, for U_+, we obtain the equation in (σ, J_1, T) : $U_+(\sigma) = -S(\sigma U_+(\sigma) - T)$. Notice that $\sigma \to U_+(\sigma)$ is increasing from $\frac{-1}{2}$ to 0^- and that $\sigma \to \sigma U_+(\sigma)$ is increasing from $-\frac{4}{J_1}$ to $-\frac{2}{J_1}$. Hence $\sigma \to -S(\sigma U_+ - T)$ is decreasing from $-S(-\frac{4}{J_1} - T)$ to $-S(-\frac{2}{J_1} - T) < 0$. We conclude that there is always a unique intersection point σ_0 between these two curves. By using similar arguments, the equation $U_- = -S(\sigma U_- - T)$ has no solution in σ.

□

E.4 The width of the tuning curves

Lemma E.4.1. *The width δ_c at half-height of the tuning curve is given by*

$$\cos(\delta_c) = \frac{-1}{4b}\left(4\,a - T + \ln\left(\frac{\mathrm{e}^{-4\,a+4\,b+T} + \mathrm{e}^{-4\,a-4\,b+T} + 2\,\mathrm{e}^{-8\,a+2\,T}}{2 + \mathrm{e}^{-4\,a+4\,b+T} + \mathrm{e}^{-4\,a-4\,b+T}}\right)\right)$$

where $a = \sigma v_0^f$ and $b = \sigma\sqrt{J_1}\rho^f$.

Proof. From the definition of the width δ_c at half-height,. we find:

$$S(4(a+b) - T) - S(4(a-b) - T) = 2\left[S(4(a + \cos(\delta_c)b) - T) - S(4(a-b) - T)\right].$$

Using some algebra, the equation $S(4(a+b) - T) + S(4(a-b) - T) = 2S(4(a + \cos(\delta_c)b) - T)$ yields the result. □

E.5 Computation of the coefficient χ_3

Let us call σ_0 the bifurcation point solution of:

$$\begin{cases} v_0^f &= \varepsilon_0 S(\sigma v_0^f) \\ 1 &= \sigma S'(\sigma v_0^f)\frac{J_1}{2} \end{cases}$$

By symmetry, this (static) bifurcation is a Pitchfork bifurcation. The kernel is written:

$$\mathcal{X}_0 = Span(cos_2, sin_2) = \ker \mathbf{L}_{\sigma_0}$$

where $\mathbf{L}_\sigma \equiv -\mathrm{Id} + \sigma S'(\sigma v(\sigma)^f)J$. The reduced equation obtained with the Equivariant Lyapunov-Schmidt reduction (see [Golubitsky 1984]) is also equivariant. Using the coordinates $\mathbf{U}_0 = A\cos_2 + B\sin_2$ with $A, B \in \mathbb{R}$, the reduced equation is given by (see [Golubitsky 1984, Haragus 2010]):

$$\begin{aligned} 0 &= \left(\beta(\sigma) + \chi_3(A^2 + B^2)\right) A \\ 0 &= \left(\beta(\sigma) + \chi_3(A^2 + B^2)\right) B. \end{aligned}$$

Let us write the equation to solve $0 = \mathbf{F}(\mathbf{U};\sigma) \equiv -\mathbf{U} + \mathbf{J}\cdot\mathbf{S}(\sigma v_0^f + \sigma\mathbf{U}) + v_0^f$. From [Golubitsky 1984][chapter VII.1.d], we have the following expression:

$$6\chi_3 = \langle \frac{2}{\pi}\cos_2, D^3\mathbf{F}(0;\sigma_0)[\cos_2,\cos_2,\cos_2] - 3D^3\mathbf{F}(0;\sigma_0)[\cos_2,\mathbf{W}]\rangle_2 \tag{E.1}$$

with

$$\mathbf{L}_{\sigma_0}\mathbf{W} = (\mathrm{Id} - \mathbf{P}_{\mathcal{X}_0})D^2\mathbf{F}(0;\sigma_0)[\cos_2,\cos_2].$$

From $D^3\mathbf{F}(0;\sigma_0)[\cos_2,\cos_2,\cos_2] = S^{(3)}\sigma_0^3\mathbf{J}\cdot\cos_2^2$ where we have written $S^{(3)}$ for $S^{(3)}(\sigma_0 v_0^f)$, we find:

$$\langle \frac{2}{\pi}\cos_2, D^3\mathbf{F}(0;\sigma_0)[\cos_2,\cos_2,\cos_2]\rangle_2 = \frac{3}{8}S^{(3)}\sigma_0^3 J_1.$$

E.5.1 Computation of W

From $D^2\mathbf{F}(0;\sigma_0)[\cos_2,\cos_2] = S''\sigma_0^2\mathbf{J}\cdot\cos_2^2$ where we have written S'' for $S^{(2)}(\sigma_0 v_0^f)$, we find:

$$D^2\mathbf{F}(0;\sigma_0)[\cos_2,\cos_2] = \frac{S''\sigma_0^2}{8}\left(J_0 + \frac{J_2}{2}\cos_4\right).$$

By using a Fourier expansion of $\mathbf{W}$, we find:

$$\mathbf{W} = \left(\frac{J_0}{-1+S'\sigma_0 J_0} + \frac{J_2}{2(-1+S'\sigma_0 J_2/2)}\cos_4\right)\frac{S''\sigma_0^2}{2}$$

where we have written S' for $S^{(1)}(\sigma_0 v_0^f)$. Using the equality $1 = \sigma_0 S'\frac{J_1}{2}$, we have:

$$\mathbf{W} = \left(\frac{J_0}{-1+2J_0/J_1} + \frac{J_2}{2(-1+J_2/J_1)}\cos_4\right)\frac{S''\sigma_0^2}{2}$$

E.5.2 Finding χ_3

Using the above expressions of $\mathbf{W}$ and $D^2\mathbf{F}$, we find:

$$\chi_3 = \sigma_0^3\left(\frac{S^{(3)}}{2} + \sigma_0 S''^2\left[\frac{J_0}{1-2J_0/J_1} + \frac{J_2/2}{2(1-J_2/J_1)}\right]\right)\frac{J_1}{8}$$

If we simplify this expression for the case $J = \varepsilon_0 + J_1\cos_2$, $J_1 > 0$ of section 9.3.1 and using the coordinates $\mathbf{U}_0 = \sqrt{J_1}v_1\cos_2 + \sqrt{J_1}v_2\sin_2$, we find:

$$\chi_3 = \sigma_0^3\left(\frac{S^{(3)}}{2} + \sigma_0 S''^2\frac{\varepsilon_0}{1-2\varepsilon_0/J_1}\right)\frac{J_1^2}{8}.$$

E.6 Stability of the tuning curves with external input turned on

Consider a nonlinear gain σ high enough to generate the O(2)-Pitchfork bifurcation. If we turn on the external input, for small contrasts, we can derive an equation on the center manifold as (3.20). We find:

$$\dot{z} = z\left(\frac{\sigma - \sigma_0}{\sigma_0} + \chi_3|z|^2\right) + \varepsilon\frac{\beta}{\sqrt{|J_1|}} \equiv z\left(\tilde{\sigma} + \chi_3|z|^2\right) + \varepsilon\frac{\beta}{\sqrt{|J_1|}} \tag{E.2}$$

which shows that z is real. We assume here that $\chi_3 < 0$. When $\varepsilon = 0$, there is a circle of solutions given by $|z_0|^2 = \frac{\tilde{\sigma}}{-\chi_3}$ in addition to the untuned solution $z = 0$. Now if $\varepsilon > 0$ is small, we obtain three solutions, two arising from the previous circle. They are given, up to the first order in ε, by: $z^f_\pm = \pm\sqrt{\frac{\tilde{\sigma}}{-\chi_3}} + \frac{\varepsilon}{2\tilde{\sigma}}\frac{\beta}{\sqrt{|J_1|}} \in \mathbb{R}$. Computing the Jacobian of the system (E.2) in real coordinates at the two nontrivial stationary solutions $z^f_\pm$, we find a diagonal matrix with diagonal elements:

$$\mathrm{Jac}(z^f_\pm) = \left\{-2\tilde{\sigma} \mp 3\frac{\varepsilon}{|z_0|}\frac{\beta}{\sqrt{|J_1|}}, \mp\frac{\varepsilon}{|z_0|}\frac{\beta}{\sqrt{|J_1|}}\right\}$$

Hence z^f_+ is stable and z^f_- is unstable.

Appendix F

A model of V1 without feature-based connectivity

F.1 Lemmas for the bifurcation points

Lemma F.1.1. *Let v_0 be the stationary membrane potential solution of $v_0 = \hat{J}_0 S(v_0)$ with $\hat{J}_0 < 0$. Then there is a unique bifurcation point σ_0 for the wavevector $\mathbf{k}_c$ with positive eigenvalue $\hat{J}_{\mathbf{k}_c}$. Moreover, σ_0 is a decreasing function of $\hat{J}_{\mathbf{k}_c}$.*

Proof. The bifurcation point reads

$$\left\{ \begin{array}{rcl} v_0 & = & -S(\sigma_0 v_0) \\ 1 & = & \sigma_0 \hat{J}_{\mathbf{k}_c} DS(\sigma_0 v_0) \end{array} \right. \tag{F.1}$$

were we have supposed that $\hat{J}_0 = -1$ (a rescaling in v_0 allows this assumption). We proved in appendix E.3 that these equations have a unique solution (v_0, σ_0). Let us look at $\sigma_0' \equiv \frac{d}{d\hat{J}_{\mathbf{k}_c}}\sigma_0$. We write $v_0' \equiv \frac{d}{d\hat{J}_{\mathbf{k}_c}} v_0$, $s_1 = DS(\sigma v_0)$ and $s_2 = D^2 S(\sigma v_0)$. Then taking the derivative of (F.1) Top:

$$v_0' = -(\sigma_0 v_0)' s_1 = -(\sigma_0' v_0 + \sigma_0 v_0') s_1 \tag{F.2}$$

which gives

$$v_0' = -\frac{\sigma_0' v_0 s_1}{1 + \sigma_0 s_1}$$

and

$$(\sigma_0 v_0)' = \sigma_0' v_0 + \sigma_0 v_0' = \sigma_0' v_0 - \sigma_0 \frac{\sigma_0' v_0 s_1}{1 + \sigma_0 s_1} = \sigma_0' v_0 \frac{1}{1 + \sigma_0 s_1}.$$

Also, from the derivative of (F.1) Bottom, $-\sigma_0' s_1 \hat{J}_{\mathbf{k}_c} = \sigma_0 s_1 + \sigma_0 (\sigma_0 v_0)' s_2 \hat{J}_{\mathbf{k}_c}$ which gives:

$$-\sigma_0' \hat{J}_{\mathbf{k}_c} \left(s_1 + \frac{\sigma_0 v_0 s_2}{1 + \sigma_0 s_1} \right) = \sigma_0 s_1 = \frac{1}{\hat{J}_{\mathbf{k}_c}} > 0.$$

Hence the sign of $-\sigma_0'$ is the sign of $s_1 + \frac{\sigma_0 v_0 s_2}{1+\sigma_0 s_1}$. But:

$$\begin{array}{rcl} s_1 + \frac{s_2 v_0 \sigma_0}{1+\sigma_0 s_1} & = & \frac{1}{1+\sigma_0 s_1} \left[s_1 + \sigma_0 s_1^2 \left(1 + \frac{s_2}{s_1^2} v_0 \right) \right] \\ & = & \frac{1}{1+\sigma_0 s_1} \left[s_1 + \sigma_0 s_1^2 \left(1 - \frac{s_2}{s_1^2} S(\sigma_0 v_0) \right) \right] \\ & = & \frac{1}{1+\sigma_0 s_1} \left[s_1 + \sigma_0 s_1^2 e^{\sigma_0 v_0 - T} \right] > 0 \end{array} \tag{F.3}$$

This concludes the proof. □

Lemma F.1.2. *Let v_0 be the stationary membrane potential solution of $v_0 = \hat{J}_0 S(v_0)$ with $\hat{J}_0 < 0$. Then, the v_0 is unique, negative and the function $\sigma \to v_0(\sigma) DS(v_0(\sigma))$ is increasing.*

Proof. The activity is solution of $v_0 = \hat{J}_0 S(v_0)$ with $\hat{J}_0 < 0$. When can, up to a rescaling of σ, v_0 assume that $\hat{J}_0 = -1$. Hence we look at the equation $v_0 = -S(\sigma v_0)$ which have only one solution v_0 for each σ. Write $s_1 = DS(\sigma v_0)$ and $s_2 = D^2 S(\sigma v_0)$:

$$\frac{d}{d\sigma}(\sigma s_1) = s_1 + \sigma s_1' = s_1 + \sigma(\sigma v_0)' s_2 \tag{F.4}$$

Also $(\sigma v_0)' = v_0 + \sigma v_0' = v_0 - \sigma(\sigma v_0)' s_1$ and $(\sigma v_0)' = \frac{v_0}{1+\sigma s_1}$ which gives

$$\begin{aligned} (\sigma s_1)' &= s_1 + v_0 \tfrac{s_2 \sigma}{1+\sigma s_1} = \tfrac{1}{1+\sigma s_1}\left[s_1 + \sigma s_1^2 \left(1 + \tfrac{s_2}{s_1^2} v_0\right)\right] \\ &= \tfrac{1}{1+\sigma s_1}\left[s_1 + \sigma s_1^2 \left(1 - \tfrac{s_2}{s_1^2} S(v_0)\right)\right] \\ &= \tfrac{1}{1+\sigma s_1}\left[s_1 + \sigma s_1^2 e^{\sigma v_0 - T}\right] > 0 \end{aligned} \tag{F.5}$$

This concludes the proof. □

F.2 The case of the long-range connections

Lemma F.2.1. *The long-range connections features the following invariances. For the PO maps $\pm\theta^{\mathbf{1}} + \theta_0$:*

$$J_{LR}(R_\phi \mathbf{x}, R_\phi \mathbf{y}) = J_{LR}(\mathbf{x}, \mathbf{y}), \quad \phi \in \frac{\pi}{4}\mathbb{Z}$$

Proof. We start by the PO map $\theta^{\mathbf{1}} + \theta_0$ using (11.8):

$$\begin{aligned} J_{LR}(R_{2\phi}\mathbf{x}, R_{2\phi}\mathbf{y}) &= J_0\left(\chi, R_{-2\theta(R_{2\phi}\mathbf{x})} R_{2\phi}(\mathbf{x} - \mathbf{y})\right) \\ &= J_0\left(\chi, R_{-2\theta(\mathbf{x})-2\phi} R_{2\phi}(\mathbf{x} - \mathbf{y})\right) \\ &= J_0\left(\chi, R_{-2\theta(\mathbf{x})}(\mathbf{x} - \mathbf{y})\right) = J_{LR}(\mathbf{x}, \mathbf{y}). \end{aligned}$$

For the PO map $-\theta^{\mathbf{1}} + \theta_0$ using (11.9):

$$\begin{aligned} J_{LR}(R_{2\phi}\mathbf{x}, R_{2\phi}\mathbf{y}) &= J_0\left(\chi, R_{-2\theta(R_{2\phi}\mathbf{x})} R_{2\phi}(\mathbf{x} - \mathbf{y})\right) \\ &= J_0\left(\chi, R_{-2\theta(\mathbf{x})+2\phi} R_{2\phi}(\mathbf{x} - \mathbf{y})\right) \\ &= J_0\left(\chi, R_{4\phi} R_{-2\theta(\mathbf{x})}(\mathbf{x} - \mathbf{y})\right) = J_{LR}(\mathbf{x}, \mathbf{y}) \end{aligned}$$

because J_0 is even. □

Lemma F.2.2. *For the maps $\pm\theta^{\mathbf{1}} + \theta_0$, we have:*

$$J_1^{(LR)} = J_2^{(LR)} \in \mathbb{R}.$$

Proof. We first note that $G_{\sigma_\theta}(\theta(\mathbf{x}) - \theta(\mathbf{y}))$ is invariant by $R_\pi, R_{\pi/2}$. The fact that J_{LR} is invariant by R_π implies that the coefficients are real numbers. The facts that J_{LR} is invariant by $R_{\pi/2}$ (which is the map $(x, y) \to (-y, x)$) and that the coefficients are real imply that the two coefficients are equal. □

F.3 Computation of the D_4-Pitchfork normal form

Lemma F.3.1. *The* $\mathbf{D}_4$*-Pitchfork normal form:*

$$\left\{\begin{array}{l}\dot{z}_1 = z_1\left(\frac{\sigma-\sigma_0}{\sigma_0} + \beta|z_1|^2 + \gamma|z_2|^2\right)\\ \dot{z}_2 = z_2\left(\frac{\sigma-\sigma_0}{\sigma_0} + \beta|z_2|^2 + \gamma|z_1|^2\right)\end{array}\right. \tag{F.6}$$

has the following coefficients:

$$\begin{array}{rcl}\beta/\sigma_0^3\hat{\mathbf{J}}_{\mathbf{k}_c} = \sigma_0 s_2^2 & \left[\frac{\hat{\mathbf{J}}_0}{1-\hat{\mathbf{J}}_0/\mathbf{J}_{\mathbf{k}_c}} + \frac{\hat{\mathbf{J}}_{2\mathbf{k}_c}}{2(1-\hat{\mathbf{J}}_{2\mathbf{k}_c}/\hat{\mathbf{J}}_{\mathbf{k}_c})}\right] & + \quad s_3/2\\ \gamma/\sigma_0^3\hat{\mathbf{J}}_{\mathbf{k}_c} = \sigma_0 s_2^2 & \left[\frac{\hat{\mathbf{J}}_0}{1-\hat{\mathbf{J}}_0/\mathbf{J}_{\mathbf{k}_c}} + 2\frac{\hat{\mathbf{J}}_{(1,1)}}{1-\hat{\mathbf{J}}_{(1,1)}/\hat{\mathbf{J}}_{\mathbf{k}_c}}\right] & + \quad s_3\end{array} \tag{F.7}$$

and $s_2 \equiv \mathbf{S}^{(2)}(v_0),\ s_3 \equiv \mathbf{S}^{(3)}(v_0)$.

Proof. The linear part is the same as in lemma 3.3.2. Let us write the nonlinear change of variable $\tilde{\Psi}$ to bring the neural field equations to the normal form (F.6). We Taylor expand $\tilde{\Psi}$ as in section 5.2.1:

$$\tilde{\Psi}(v_0,\mu) = \sum_{l_1+l_2+p_1+p_2+r>1} z_1^{l_1}\bar{z}_1^{l_2}z_2^{p_1}\bar{z}_2^{p_2}\mu^r\tilde{\Psi}_{l_1,l_2,p_1,p_2,r},\ \ \tilde{\Psi}_{l_1,l_2,p_1,p_2,r}\in\mathcal{Z},$$

where $\tilde{\Psi}$ satisfies $\tilde{\Psi}(0,0)=0,\ D_{v_0}\tilde{\Psi}(0,0)=0$. Using the equation (5.9) satisfied by $\tilde{\Psi}$ and a Maple program similar to the one given in section 5.2.1, we find the following equations with $e^{ix}\equiv\zeta_1,\ e^{iy}\equiv\zeta_2,\ \zeta_1^*\equiv\frac{1}{(2\pi N_p)^2}e^{-ix},\ \zeta_2^*\equiv\frac{1}{(2\pi N_p)^2}e^{-iy}$:

$$\begin{array}{rcl}0 &=& -2L\Psi_{2,1,0,0,0} + 2\beta\zeta_1 - 4\mathbf{R}_2(\Psi_{1,1,0,0,0},\zeta_1) - 4\mathbf{R}_2(\bar{\zeta}_1,\Psi_{2,0,0,0,0} - 6\mathbf{R}_3(\zeta_1.\zeta_1,\bar{\zeta}_1)\\ 0 &=& -L\Psi_{1,1,1,0,0} + \gamma\zeta_2 - 2\mathbf{R}_2(\Psi_{0,1,1,0,0},\zeta_1) - 2\mathbf{R}_2(\bar{\zeta}_1,\Psi_{1,0,1,0,0}) - 2\mathbf{R}_2(\zeta_2,\Psi_{1,1,0,0,0})\\ && -6\mathbf{R}_3(\zeta_2,\zeta_1,\bar{\zeta}_1)\end{array}$$

where the differentials $\mathbf{R}_p \equiv \frac{1}{p!}D^p\mathbf{R}(0,\sigma_0)$ are given in lemma 3.2.1 and $L=-\mathrm{Id}+\sigma_0 s_1\mathbf{J}$. From the Fredholm alternative, we find:

$$\begin{array}{rcl}\beta &=& \langle\zeta_1^*, 2\mathbf{R}_2(\Psi_{1,1,0,0,0},\zeta_1) + 2\mathbf{R}_2(\bar{\zeta}_1,\Psi_{2,0,0,0,0}) + 3\mathbf{R}_3(\zeta_1.\zeta_1,\bar{\zeta}_1)\rangle_2\\ \gamma &=& \langle\zeta_2^*, 2\mathbf{R}_2(\Psi_{0,1,1,0,0},\zeta_1) + 2\mathbf{R}_2(\bar{\zeta}_1,\Psi_{1,0,1,0,0}) + 2\mathbf{R}_2(\zeta_2,\Psi_{1,1,0,0,0}) \ .\\ && + 6\mathbf{R}_3(\zeta_2,\zeta_1,\bar{\zeta}_1)\rangle_2\end{array}$$

In order to find the coefficients of the normal form, we are led to compute some of the coefficients of $\tilde{\Psi}$. By taking the second order monomials, we find:

$$\begin{array}{rcl}0 &=& 2L\Psi_{2,0,0,0,0} + 2\mathbf{R}_2(\zeta_1,\zeta_1)\\ 0 &=& L\Psi_{1,1,0,0,0} + 2\mathbf{R}_2(\zeta_1,\bar{\zeta}_1)\\ 0 &=& L\Psi_{0,1,1,0,0} + 2\mathbf{R}_2(\zeta_2,\bar{\zeta}_1)\\ 0 &=& L\Psi_{1,0,1,0,0} + 2\mathbf{R}_2(\zeta_1,\zeta_2)\end{array}$$

which are solved by

$$\begin{array}{rcl}\Psi_{2,0,0,0,0} &=& Span(\zeta_1,\zeta_2,\bar{\zeta}_1,\bar{\zeta}_2) + \frac{\sigma_0^2 s_2}{2}\frac{\hat{\mathbf{J}}_{2\mathbf{k}_c}}{1-s_1\sigma_0\hat{\mathbf{J}}_{2\mathbf{k}_c}}\zeta_1^2\\ \Psi_{1,1,0,0,0} &=& Span(\zeta_1,\zeta_2,\bar{\zeta}_1,\bar{\zeta}_2) + 2\frac{\sigma_0^2 s_2}{2}\frac{\hat{\mathbf{J}}_0}{1-s_1\sigma_0\hat{\mathbf{J}}_0}\\ \Psi_{0,1,1,0,0} &=& Span(\zeta_1,\zeta_2,\bar{\zeta}_1,\bar{\zeta}_2) + 2\frac{\sigma_0^2 s_2}{2}\frac{\hat{\mathbf{J}}_{(1,1)}}{1-s_1\sigma_0\hat{\mathbf{J}}_{(1,1)}}\zeta_2\bar{\zeta}_1\\ \Psi_{1,0,1,0,0} &=& Span(\zeta_1,\zeta_2,\bar{\zeta}_1,\bar{\zeta}_2) + 2\frac{\sigma_0^2 s_2}{2}\frac{\hat{\mathbf{J}}_{(1,1)}}{1-s_1\sigma_0\hat{\mathbf{J}}_{(1,1)}}\zeta_1\zeta_2.\end{array}$$

Let us indicate how to solve the first equation for example. Note that $\mathbf{R}_2(\zeta_1, \zeta_1) = \frac{\sigma_0^2 s_2}{2}\mathbf{J} \cdot \zeta_1^2 = \frac{\sigma_0^2 s_2}{2}\hat{\mathbf{J}}_{2\mathbf{k}_c}\zeta_1^2$. A particular solution is given by $A\zeta_1^2$ where A satisfies $(1 - s_1\sigma_0\hat{\mathbf{J}}_{2\mathbf{k}_c})A = \frac{\sigma_0^2 s_2}{2}\hat{\mathbf{J}}_{2\mathbf{k}_c}$ to which we must add any null vector of L. This gives the coefficient $\Psi_{2,0,0,0,0}$.

It is then straightforward to obtain β and γ. □

Bibliography

[Adelson 1985] E.H. Adelson and J.R. Bergen. *Spatiotemporal energy models for the perception of motion.* Journal of the Optical Society of America A, vol. 2, pages 284–299, 1985. 165

[Ahmed 2008] B. Ahmed, A. Hanazawa, C. Undeman, D. Eriksson, S. Valentiniene and P.E. Roland. *Cortical dynamics subserving visual apparent motion.* Cerebral Cortex, vol. 18, no. 12, page 2796, 2008. 166, 169

[Albrecht 1982] Duane G. Albrecht and David B. Hamilton. *Striate cortex of monkey and cat: contrast response function.* Journal of Neurophysiology, vol. 48, no. 1, pages 217–233, July 1982. 18

[Albright 1987] T.D. Albright and R. Desimone. *Local precision of visuotopic organization in the middle temporal area (MT) of the macaque.* Experimental Brain Research, vol. 65, no. 3, pages 582–592, 1987. 172

[Alitto 2004] H.J. Alitto and W.M. Usrey. *Influence of contrast on orientation and temporal frequency tuning in ferret primary visual cortex.* Journal of neurophysiology, vol. 91, no. 6, page 2797, 2004. 184

[Allgower 2003] E.L. Allgower and K. Georg. Introduction to numerical continuation methods, volume 45. Society for Industrial Mathematics, 2003. 57

[Amari 1977] S.-I. Amari. *Dynamics of pattern formation in lateral-inhibition type neural fields.* Biological Cybernetics, vol. 27, no. 2, pages 77–87, June 1977. 23, 32, 40, 85

[Angelucci 2002] A. Angelucci, J.B. Levitt, E.J. Walton, J.M. Hupe, J. Bullier and J.S. Lund. *Circuits for local and global signal integration in primary visual cortex.* The Journal of Neuroscience, vol. 22, no. 19, pages 8633–8646, October 2002. 15, 16, 17

[Appell 2006] J. Appell and C.-J Chen. *How to solve Hammerstein equations.* Journal of integral equations and applications, vol. 18, no. 3, pages 287–296, 2006. 32

[Arino 2006] O. Arino, ML Hbid and E.A. Dads. Delay differential equations and applications. Springer, 2006. 90, 91, 93, 95, 101, 128

[Atay 2005] Fatihcan M. Atay and Axel Hutt. *Stability and bifurcations in neural fields with finite propagation speed and general connectivity.* SIAM Journal on Applied Mathematics, vol. 65, no. 2, pages 644–666, 2005. 41, 87, 108, 111, 118

[Atay 2006] Fatihcan M. Atay and Axel Hutt. *Neural fields with distributed transmission speeds and long-range feedback delays.* SIAM Journal of Applied Dynamical Systems, vol. 5, no. 4, pages 670–698, 2006. 87, 108

[Baker 2009] T.I. Baker and J.D. Cowan. *Spontaneous pattern formation and pinning in the primary visual cortex.* Journal of Physiology-Paris, vol. 103, no. 1-2, pages 52–68, 2009. 228, 248

[Balanov 2006] Z. Balanov, W. Krawcewicz and H. Steinlein. Applied equivariant degree. American Institute of Mathematical Sciences, 2006. 77

[Barlow 1961] H.B. Barlow. *Possible principles underlying the transformation of sensory messages.* Sensory communication, pages 217–234, 1961. ix, xiii

[Bátkai 2005] A. Bátkai and S. Piazzera. Semigroups for delay equations. AK Peters, Ltd., 2005. 89, 95, 97, 102, 103, 105, 123, 128, 129, 272, 274, 279, 280

[Bayerl 2004] P. Bayerl and H. Neumann. *Disambiguating visual motion through contextual feedback modulation.* Neural Computation, vol. 16, no. 10, pages 2041–2066, 2004. 172

[Bélair 1994] J. Bélair and S.A. Campbell. *Stability and bifurcations of equilibria in a multiple-delayed differential equation.* SIAM Journal on Applied Mathematics, pages 1402–1424, 1994. 86

[Bélair 1996] J. Bélair, S.A. Campbell and P. Van Den Driessche. *Frustration, stability, and delay-induced oscillations in a neural network model.* SIAM Journal on Applied Mathematics, pages 245–255, 1996. 86

[Ben-Yishai 1995] R. Ben-Yishai, RL Bar-Or and H. Sompolinsky. *Theory of orientation tuning in visual cortex.* Proceedings of the National Academy of Sciences, vol. 92, no. 9, pages 3844–3848, 1995. 20, 40, 60, 61, 80, 86, 88, 127, 142, 153, 176, 184, 185, 186, 187, 192, 207, 210, 228

[Benucci 2009] A. Benucci, D.L. Ringach and M. Carandini. *Coding of stimulus sequences by population responses in visual cortex.* Nature neuroscience, vol. 12, no. 10, pages 1317–1324, 2009. 216

[Beurle 1956] R.L. Beurle. *Properties of a mass of cells capable of regenerating pulses.* Philosophical Transactions of the Royal Society of London. Series B, Biological Sciences, vol. 240, no. 669, page 55, 1956. 23

[Blasdel 1986a] G.G. Blasdel and G. Salama. *Voltage-sensitive dyes reveal a modular organization in monkey striate cortex.* Nature, vol. 321, pages 579—585, 1986. 9

[Blasdel 1986b] G.G. Blasdel and G. Salama. *Voltage-sensitive dyes reveal a modular organization in monkey striate cortex.* Nature, vol. 321, no. 6070, pages 579–585, 1986. 213

[Blasdel 1992a] G.G. Blasdel. *Differential imaging of ocular dominance and orientation selectivity in monkey striate cortex.* The Journal of neuroscience, vol. 12, no. 8, page 3115, 1992. 9

[Blasdel 1992b] G.G. Blasdel. *Orientation selectivity, preference, and continuity in monkey striate cortex.* Journal of Neuroscience, vol. 12, no. 8, pages 3139–3161, 1992. 9

[Blomquist 2005] P. Blomquist, J. Wyller and G.T. Einevoll. *Localized activity patterns in two-population neuronal networks.* Physica D, vol. 206, pages 180–212, 2005. 32, 41

[Blumenfeld 2006] B. Blumenfeld, D. Bibitchkov and M. Tsodyks. *Neural network model of the primary visual cortex: From functional architecture to lateral connectivity and back.* Journal of computational neuroscience, vol. 20, no. 2, pages 219–241, 2006. 61, 211, 213, 214, 216, 218, 225, 226, 228

[Bojak 2010] I. Bojak and D.T.J. Liley. *Axonal velocity distributions in neural field equations.* PLOS Comp. Bio., 2010. 87

[Bonhoeffer 1991] T. Bonhoeffer and A. Grinvald. *Orientation columns in cat are organized in pinwheel like patterns.* Nature, vol. 364, no. 353, pages 429–431, 1991. 9

[Born 2005] R.T. Born and D.C. Bradley. *Structure and Function of Visual Area MT.* Annu. Rev. Neurosci, vol. 28, pages 157–189, 2005. 8, 11

[Bosking 1997] W.H. Bosking, Y. Zhang, B. Schofield and D. Fitzpatrick. *Orientation Selectivity and the Arrangement of Horizontal Connections in Tree Shrew Striate Cortex.* The Journal of Neuroscience, vol. 17, no. 6, pages 2112–2127, 1997. 10, 17, 217, 229

[Breda 2006] D. Breda, S. Maset and R. Vermiglio. *Pseudospectral approximation of eigenvalues of derivative operators with non-local boundary conditions.* Applied numerical mathematics, vol. 56, no. 3-4, pages 318–331, 2006. 132, 133

[Breda 2009] D. Breda, S. Maset and R. Vermiglio. *TRACE-DDE: a Tool for Robust Analysis and Characteristic Equations for Delay Differential Equations.* Topics in Time Delay Systems, pages 145–155, 2009. 132, 135

[Bressloff 2000] P.C. Bressloff, N.W. Bressloff and J.D. Cowan. *Dynamical mechanism for sharp orientation tuning in an integrate-and-fire model of a cortical hypercolumn.* Neural computation, vol. 12, no. 11, pages 2473–2511, 2000. 60, 61, 86, 92, 153, 184, 186, 187, 228

[Bressloff 2001a] P.C. Bressloff. *Traveling fronts and wave propagation failure in an inhomogeneous neural network*. Physica D: Nonlinear Phenomena, vol. 155, no. 1-2, pages 83–100, 2001. 41

[Bressloff 2001b] P.C. Bressloff, J.D. Cowan, M. Golubitsky, P.J. Thomas and M.C. Wiener. *Geometric visual hallucinations, Euclidean symmetry and the functional architecture of striate cortex*. Phil. Trans. R. Soc. Lond. B, vol. 306, no. 1407, pages 299–330, March 2001. 40, 60, 61, 73, 79, 86, 88, 92, 127, 153, 184, 186, 187, 189, 210, 211, 227, 228, 236

[Bressloff 2002a] P.C. Bressloff and J.D. Cowan. *An amplitude equation approach to contextual effects in visual cortex*. Neural computation, vol. 14, no. 3, pages 493–525, 2002. 73, 211

[Bressloff 2002b] P.C. Bressloff and J.D. Cowan. Spontaneous pattern formation in primary visual cortex. Institute of Physics: Bristol, 2002. In: Nonlinear dynamics: where do we go from here? Chap 11. 211

[Bressloff 2003] P.C. Bressloff. *Spatially periodic modulation of cortical patterns by long-range horizontal connections*. Physica D: Nonlinear Phenomena, vol. 185, no. 3-4, pages 131–157, 2003. 41, 86, 228, 248

[Bressloff 2005a] P. Bressloff. *Spontaneous symmetry breaking in self–organizing neural fields*. Biological Cybernetics, vol. 93, no. 4, pages 256–274, October 2005. 32, 53

[Bressloff 2005b] P.C. Bressloff. *Course 11 Pattern formation in visual cortex*. Les Houches, vol. 80, pages 477–574, 2005. 211

[Bressloff 2006] P.C. Bressloff. *Weakly interacting pulses in synaptically coupled neural media*. SIAM Journal on Applied Mathematics, vol. 66, no. 1, pages 57–81, 2006. 41

[Bressloff 2008] P.C. Bressloff and Z.P. Kilpatrick. *Nonlocal Ginzburg-Landau equation for cortical pattern formation*. Physical Review E, vol. 78, no. 4, pages 41916:1–16, 2008. 87, 99, 228, 229, 242, 247

[Brezis 1983] H. Brezis. Analyse fonctionnelle. théorie et applications. Masson, 1983. 53, 58, 266

[Bringuier 1999] V. Bringuier, F. Chavane, L. Glaeser and Y. Frégnac. *Horizontal propagation of visual activity in the synaptic integration field of area 17 neurons*. Science, vol. 283, no. 5402, page 695, 1999. 168, 255

[Brodmann 1909] K. Brodmann. Vergleichende lokalisationslehre der grobhirnrinde. J.A.Barth, Leipzig, 1909. 7

[Budd 2010] J.M.L. Budd, K. Kovács, A.S. Ferecskó, P. Buzás, U.T. Eysel and Z.F. Kisvárday. *Neocortical Axon Arbors Trade-off Material and Conduction Delay Conservation.* PLoS Comput Biol, vol. 6, no. 3, page e1000711, 2010. 33

[Burton 2006] TA Burton. Stability by fixed point theory for functional differential equations. Dover Publications, Mineola, NY, 2006. 111

[Campbell 2005] S.A. Campbell, Y. Yuan and S.D. Bungay. *Equivariant Hopf bifurcation in a ring of identical cells with delayed coupling.* Nonlinearity, vol. 18, page 2827, 2005. 99

[Campbell 2008] S.A. Campbell and Y. Yuan. *Zero singularities of codimension two and three in delay differential equations.* Nonlinearity, vol. 21, page 2671, 2008. 88

[Carandini 1997] M. Carandini and D.L. Ringach. *Predictions of a recurrent model of orientation selectivity.* Vision Research, vol. 37, no. 21, pages 3061–3071, 1997. 20, 61, 185, 210, 228

[Carandini 2007] M. Carandini. *Melting the iceberg: contrast invariance in visual cortex.* Neuron, vol. 54, no. 1, pages 11–13, 2007. 20

[Chalupa 2004] L. M. Chalupa and J.S. Werner, editeurs. The visual neurosciences. MIT Press, 2004. Two volumes. 31, 199

[Chavane 2011] F. Chavane, D. Sharon, D. Jancke, O. Marre, Y. Frégnac and A. Grinvald. *Lateral spread of orientation selectivity in V1 is controlled by intracortical cooperativity.* Frontiers in Systems Neuroscience, vol. 5, 2011. 18, 229, 241

[Chemla 2010a] S. Chemla and F. Chavane. *Voltage-sensitive dye imaging: Technique review and models.* Journal of Physiology-Paris, vol. 104, no. 1-2, pages 40–50, 2010. 214

[Chemla 2010b] Sandrine Chemla. *A biophysical cortical column model for optical signal analysis.* PhD thesis, School of Information and Communication Sciences, 2010. 3, 15, 228

[Choquet 1969] G. Choquet. Cours d'analyse, volume II. Masson, 1969. 50

[Chossat 1986] P. Chossat, M. Golubitsky and B.L. Keyfitz. *Hopf-Hopf mode interactions with O (2) symmetry.* Dynamical Systems, vol. 1, no. 4, pages 255–292, 1986. 246

[Chossat 2000] P. Chossat and R. Lauterbach. Methods in Equivariant Bifurcations and Dynamical Systems. World Scientific Publishing Company, 2000. 140, 143, 145, 187, 194, 195, 196

[Chossat 2009] Pascal Chossat and Olivier Faugeras. *Hyperbolic planforms in relation to visual edges and textures perception.* Plos Comput Biol, vol. 5, no. 12, page e1000625, December 2009. 228

[Colby 1995] C.L. Colby, J.R. Duhamel and M.E. Goldberg. *Oculocentric spatial representation in parietal cortex.* Cereb. Cortex, vol. 5, pages 470–481, 1995. 40

[Conway 1978] J.B. Conway. Functions of one complex variable, volume 11. Springer, 2 édition, 1978. 135

[Coombes 2003] S. Coombes, G.J. Lord and M.R. Owen. *Waves and bumps in neuronal networks with axo-dendritic synaptic interactions.* Physica D: Nonlinear Phenomena, vol. 178, no. 3-4, pages 219–241, 2003. 23, 27

[Coombes 2004] S. Coombes and M. R. Owen. *Evans Functions for Integral Neural Field Equations with Heaviside Firing Rate Function.* SIAM Journal on Applied Dynamical Systems, vol. 3, no. 4, pages 574–600, 2004. 41

[Coombes 2005a] S. Coombes and M. R. Owen. *Bumps, Breathers, and Waves in a Neural Network with Spike Frequency Adaptation.* Phys. Rev. Lett., vol. 94, no. 14, 2005. 23

[Coombes 2005b] Stephen Coombes. *Waves, bumps, and patterns in neural fields theories.* Biological Cybernetics, vol. 93, no. 2, pages 91–108, 2005. 23, 32, 53, 85, 86, 92

[Coombes 2007] S. Coombes, N.A Venkov, L. Shiau, I. Bojak, D.T.J. Liley and C.R. Laing. *Modeling electrocortical activity through local approximations of integral neural field equations.* Physical Review E, vol. 76, no. 5, page 51901, 2007. 86, 87, 99

[Coombes 2009] S. Coombes and C. Laing. *Delays in activity based neural networks.* Philosophical Transactions of the Royal Society A., vol. 367, pages 1117–1129, 2009. 86

[Corless 1996] R.M. Corless, G.H. Gonnet, D.E.G. Hare, D.J. Jeffrey and D.E. Knuth. *On the LambertW function.* Advances in Computational mathematics, vol. 5, no. 1, pages 329–359, 1996. 98, 275

[Curtu 2004] R. Curtu and B. Ermentrout. *Pattern Formation in a Network of Excitatory and Inhibitory Cells with Adaptation.* SIAM Journal on Applied Dynamical Systems, vol. 3, page 191, 2004. 23, 144

[Das 1999] A. Das and C.D. Gilbert. *Topography of contextual modulations mediated by short-range interactions in primary visual cortex.* Nature, vol. 399, no. 6737, pages 655–661, 1999. 15

[Dayan 2001a] P. Dayan and L.F. Abbott. Theoretical neuroscience : Computational and mathematical modeling of neural systems. MIT Press, 2001. 24, 27, 60, 61

[Dayan 2001b] P. Dayan and L.F. Abbott. Theoretical neuroscience : Computational and mathematical modeling of neural systems. MIT Press, 2001. 184, 187

[Dean 1981] AF Dean. *The relationship between response amplitude and contrast for cat striate cortical neurones.* The Journal of Physiology, vol. 318, no. 1, page 413, 1981. 184

[DeAngelis 1999] G.C. DeAngelis and W.T. Newsome. *Organization of disparity-selective neurons in macaque area MT.* The Journal of neuroscience, vol. 19, no. 4, page 1398, 1999. 8

[Deco 2010] G. Deco and P. Roland. *The role of multi-area interactions for the computation of apparent motion.* NeuroImage, vol. 51, no. 3, pages 1018–1026, 2010. 165, 166, 167, 168, 169, 170

[DeYoe 1996] E.A. DeYoe, G.J. Carman, P. Bandettini, S. Glickman, J. Wieser, R. Cox, D. Miller and J. Neitz. *Mapping striate and extrastriate visual areas in human cerebral cortex.* Proceedings of the National Academy of Sciences of the United States of America, vol. 93, no. 6, page 2382, 1996. 8

[Diekmann 1995] O. Diekmann. Delay equations: functional-, complex-, and nonlinear analysis. Springer, 1995. 86, 95, 101

[Diogo 2003] A.C.M. Diogo, J.G.M. Soares, A. Koulakov, T.D. Albright and R. Gattass. *Electrophysiological imaging of functional architecture in the cortical middle temporal visual area of Cebus apella monkey.* The Journal of neuroscience, vol. 23, no. 9, page 3881, 2003. 11, 12

[Doubrovinski 2005] K. Doubrovinski. *Dynamics, Stability and Bifurcation Phenomena in the Nonlocal Model of Cortical Activity.* U.u.d.m. project report 2005:8, Uppsala University, Department of Mathematics, June 2005. 32

[Douglas 1995] R.J. Douglas, C. Koch, M. Mahowald, KA Martin and H.H. Suarez. *Recurrent excitation in neocortical circuits.* Science, vol. 269, no. 5226, page 981, 1995. 15, 20, 185

[Dragoi 2000a] V. Dragoi, J. Sharma and M. Sur. *Adaptation-induced plasticity of orientation tuning in adult visual cortex.* Neuron, vol. 28, no. 1, pages 287–298, 2000. 11, 13

[Dragoi 2000b] V. Dragoi and M. Sur. *Dynamic properties of recurrent inhibition in primary visual cortex: contrast and orientation dependence of contextual effects.* Journal of Neurophysiology, vol. 83, no. 2, page 1019, 2000. 228

[Dragoi 2001] V. Dragoi, C. Rivadulla and M. Sur. *Foci of orientation plasticity in visual cortex.* Nature, vol. 411, no. 6833, pages 80–86, 2001. 11

[Dunford 1988] N. Dunford and J.T. Schwartz. Linear operators: Spectral operators, volume 7. Wiley-Interscience, 1988. 94

[Enculescu 2007] M. Enculescu and M. Bestehorn. *Liapunov functional for a delayed integro-differential equation model of a neural field.* EPL (Europhysics Letters), vol. 77, page 68007, 2007. 161

[Engel 2001] K.J. Engel and R. Nagel. One-parameter semigroups for linear evolution equations, volume 63. Springer, 2001. 95, 97, 107, 128, 129, 271

[Ermentrout 1979] GB Ermentrout and J.D. Cowan. *Temporal oscillations in neuronal nets.* Journal of mathematical biology, vol. 7, no. 3, pages 265–280, 1979. 86, 228

[Ermentrout 1980] G.B. Ermentrout and J.D. Cowan. *Large scale spatially organized activity in neural nets.* SIAM Journal on Applied Mathematics, pages 1–21, 1980. 74, 80, 86, 92, 108

[Ermentrout 1991] B. Ermentrout. *Stripes or spots? Nonlinear effects in bifurcation of reaction-diffusion equations on the square.* Proceedings: Mathematical and Physical Sciences, vol. 434, no. 1891, pages 413–417, 1991. 239

[Ermentrout 1993] GB Ermentrout and JB McLeod. *Existence and uniqueness of travelling waves for a neural network.* In Royal Society(Edinburgh), Proceedings, volume 123, pages 461–478, 1993. 41

[Ermentrout 1998] Bard Ermentrout. *Neural networks as spatio-temporal pattern-forming systems.* Reports on Progress in Physics, vol. 61, pages 353–430, 1998. 23, 27, 29, 40, 53, 60, 61, 184, 187, 211, 267

[Ermentrout 2009] B. Ermentrout and T.W. Ko. *Delays and weakly coupled neuronal oscillators.* Philosophical Transactions of the Royal Society A: Mathematical, Physical and Engineering Sciences, vol. 367, no. 1891, page 1097, 2009. 26

[Ernst 2001] UA Ernst, KR Pawelzik, C. Sahar-Pikielny and MV Tsodyks. *Intracortical origin of visual maps.* nature neuroscience, vol. 4, no. 4, pages 431–436, 2001. 228, 229

[Exner 1875] S. Exner and K.A. der Wissenschaften.
"Uber das sehen von bewegungen und theorie des zusammengesetzten auges. aus der kk Hof-und Staatsdruckerei, 1875. 165

[Faria 1995] T. Faria and LT Magalhaes. *Normal forms for retarded functional differential equations with parameters and applications to Hopf bifurcation.*

Journal of differential equations, vol. 122, no. 2, pages 181–200, 1995. 87, 90, 93, 126, 129

[Faria 2001] T. Faria. *Normal forms for semilinear functional differential equations in Banach spaces and applications. Part II.* Discrete and Continuous Dynamical Systems (DCDS-A), vol. 7, no. 1, pages 155–176, 2001. 87, 90, 127

[Faria 2002] T. Faria, W. Huang and J. Wu. *Smoothness of center manifolds for maps and formal adjoints for semilinear FDEs in general Banach spaces.* SIAM Journal on Mathematical Analysis, vol. 34, page 173, 2002. 87

[Faugeras 2007] O. Faugeras, F. Grimbert and F. Chavane. *Neural field model of vsd optical imaging signals.* In W. R. Holmes, R. Jung and F. Skinner, editeurs, Sixteenth Annual Computational Neuroscience Meeting (CNS), volume 8, Suppl 2 of *BMC Neuroscience*, July 2007. 214, 216

[Faugeras 2008] O. Faugeras, F. Grimbert and J.-J. Slotine. *Abolute stability and complete synchronization in a class of neural fields models.* SIAM Journal of Applied Mathematics, vol. 61, no. 1, pages 205–250, September 2008. 49, 61, 80, 86

[Faugeras 2009] Olivier Faugeras, Romain Veltz and Francois Grimbert. *Persistent neural states: stationary localized activity patterns in nonlinear continuous n-population, q-dimensional neural networks.* Neural Computation, vol. 21, no. 1, pages 147–187, 2009. 41, 42, 45, 46, 47, 49, 73, 74, 80, 118, 265

[Faye 2010] Grégory Faye and Olivier Faugeras. *Some theoretical and numerical results for delayed neural field equations.* Physica D, vol. 239, no. 9, pages 561–578, May 2010. Special issue on Mathematical Neuroscience. 108

[Felleman 1991] D.J. Felleman and D.C. Van Essen. *Distributed hierarchical processing in the primate cerebral cortex.* Cereb Cortex, vol. 1, pages 1–47, 1991. 8

[Felten 2010] D.L. Felten and A.N. Shetty. Netter's atlas of neuroscience. Saunders/Elsevier, 2010. 5, 24

[Ferster 2000] D. Ferster and K. D. Miller. *Neural Mechanisms of Orientation Selectivity in the Visual Cortex.* Annual Review of Neuroscience, vol. 23, pages 441–471, March 2000. 18

[Finn 2007] I.M. Finn, N.J. Priebe and D. Ferster. *The emergence of contrast-invariant orientation tuning in simple cells of cat visual cortex.* Neuron, vol. 54, no. 1, pages 137–152, 2007. 20

[Fitzpatrick 1996] D. Fitzpatrick. *The functional organization of local circuits in visual cortex: insights from the study of tree shrew striate cortex.* Cerebral Cortex, vol. 6, no. 3, page 329, 1996. 15, 17

[Fourcaud-Trocme 2003] N. Fourcaud-Trocme, D. Hansel, C. van Vreeswijk and N. Brunel. *How Spike Generation Mechanisms Determine the Neuronal Response to Fluctuating Inputs.* Journal of Neuroscience, vol. 23, no. 37, page 11628, 2003. 25

[Fregnac 2010] Y. Fregnac, P. Baudot, F. Chavane, J. Lorenceau, O. Marre, C. Monier, M. Pananceau, P.V. Carelli and G. Sadoc. *Multiscale functional imaging in V1 and cortical correlates of apparent motion.* Dynamics of Visual Motion Processing, pages 73–93, 2010. 165

[Funahashi 1989] S. Funahashi, C.J. Bruce and P.S. Goldman-Rakic. *Mnemonic coding of visual space in the monkey's dorsolateral prefrontal cortex.* J. Neurophysiol., vol. 61, pages 331–349, 1989. 40

[Geisler 2001] W.S. Geisler, D.G. Albrecht, A.M. Crane and L. Stern. *Motion direction signals in the primary visual cortex of cat and monkey.* Visual Neuroscience, vol. 18, no. 04, pages 501–516, 2001. 8

[Gerstner 2002] W. Gerstner and W. M. Kistler. *Mathematical formulations of Hebbian learning.* Biological Cybernetics, vol. 87, pages 404–415, 2002. 27

[Gilbert 1989] C.D. Gilbert and T.N. Wiesel. *Columnar specificity of intrinsic horizontal and corticocortical connections in cat visual cortex.* The Journal of Neuroscience, vol. 9, no. 7, page 2432, 1989. 217, 226

[Goldberg 2004] J.A. Goldberg, U. Rokni and H. Sompolinsky. *Patterns of ongoing activity and the functional architecture of the primary visual cortex.* Neuron, vol. 42, no. 3, pages 489–500, 2004. 217

[Golubitsky 1984] M. Golubitsky and D.G. Schaeffer. Singularities and groups in bifurcation theory, volume I. Springer, 1984. 54, 57, 71, 139, 187, 309, 310

[Golubitsky 1985] M. Golubitsky and I. Stewart. *Hopf bifurcation in the presence of symmetry.* Archive for Rational Mechanics and Analysis, vol. 87, no. 2, pages 107–165, 1985. 145

[Golubitsky 1988] M. Golubitsky, I. Stewart and D.G. Schaeffer. Singularities and groups in bifurcation theory, volume II. Springer, 1988. 54, 57, 71, 139, 143, 144, 147, 149, 151, 152, 195, 240, 246, 295, 298

[Gouras 1968] P. Gouras. *Identification of cone mechanisms in monkey ganglion cells.* The Journal of Physiology, vol. 199, no. 3, page 533, 1968. 5

[Grimbert 2008] F. Grimbert. *Mesoscopic models of cortical structures.* PhD thesis, University of Nice Sophia-Antipolis, February 2008. x, 3, 15

[Grinvald 1986] A. Grinvald, E. Lieke, R.D. Frostig, C.D. Gilbert and T.N. Wiesel. *Functional architecture of cortex revealed by optical imaging of intrinsic signals.* Nature, 1986. 9, 213

[Grinvald 2004] Amiram Grinvald and Rina Hildesheim. *VSDI: A new era in functional imaging of cortical dynamics*. Nature, vol. 5, pages 874–885, November 2004. 214

[Grothendieck 1956] A. Grothendieck. *La théorie de Fredholm*. Bull. Soc. Math. France, vol. 84, pages 319–384, 1956. 133

[Guckenheimer 1983] J. Guckenheimer and P. J. Holmes. Nonlinear oscillations, dynamical systems and bifurcations of vector fields, volume 42 of *Applied mathematical sciences*. Springer, 1983. 41, 42, 57, 87, 120, 137, 139, 149, 150, 156, 157, 158

[Guo 2005a] Y. Guo and C.C. Chow. *Existence and Stability of Standing Pulses in Neural Networks: II Stability*. SIAM Journal on Applied Dynamical Systems, vol. 4, pages 249–281, 2005. 32

[Guo 2005b] Yixin Guo and Carson C. Chow. *Existence and Stability of Standing Pulses in Neural Networks: I. Existence*. SIAM Journal on Applied Dynamical Systems, vol. 4, no. 2, pages 217–248, 2005. 32

[Gutkin 2000] B.S. Gutkin, G.B. Ermentrout and J. O'Sullivan. *Layer 3 patchy recurrent excitatory connections may determine the spatial organization of sustained activity in the primate prefrontal cortex*. Neurocomputing, vol. 32-33, pages 391–400, 2000. 32

[Haeusler 2007] Stefan Haeusler and Wolfgang Maass. *A Statistical Analysis of Information-Processing Properties of Lamina-Specific Cortical Microcircuits Models*. Cerebral Cortex, vol. 17, pages 149–162, January 2007. 27, 228

[Hale 1993] J.K. Hale and S.M.V. Lunel. Introduction to functional differential equations. Springer Verlag, 1993. 86, 87, 90, 91, 93, 95, 101, 103, 126, 127, 128, 272, 273

[Hammerstein 1930] A. Hammerstein. *Nichtlineare Integralgleichungen nebst Anwendungen*. Acta Math., vol. 54, pages 117–176, 1930. 32

[Hansel 1997] D. Hansel and H. Sompolinsky. *Modeling feature selectivity in local cortical circuits*. Methods of neuronal modeling, pages 499–567, 1997. 20, 40, 60, 142, 184, 187, 192

[Haragus 2010] M. Haragus and G. Iooss. Local bifurcations, center manifolds, and normal forms in infinite dimensional systems. EDP Sci. Springer Verlag UTX series, 2010. xxi, 42, 54, 56, 87, 90, 93, 119, 120, 123, 124, 125, 126, 127, 129, 139, 140, 143, 145, 146, 147, 149, 157, 187, 188, 196, 263, 264, 291, 309

[Hazewinkel 2001] Michiel Hazewinkel, editeur. Encyclopaedia of mathematics. Springer, 2001. 32

[Hodgkin 1952] A.L. Hodgkin and A.F. Huxley. *A quantitative description of membrane current and its application to conduction and excitation in nerve.* Journal of Physiology, vol. 117, pages 500–544, 1952. 85

[Hopfield 1984] J. J. Hopfield. *Neurons with Graded Response Have Collective Computational Properties like Those of Two-State Neurons.* Proceedings of the National Academy of Sciences, USA, vol. 81, no. 10, pages 3088–3092, 1984. 29, 46

[Hubel 1962] D.H. Hubel and T.N. Wiesel. *Receptive fields, binocular interaction and functional architecture in the cat visual cortex.* J Physiol, vol. 160, pages 106–154, 1962. 8, 9, 184

[Hubel 1965] D.H. Hubel and T.N. Wiesel. *Receptive fields and functional architecture in two nonstriate visual areas (18 and 19) of the cat.* Journal of Neurophysiology, vol. 28, pages 229–289, 1965. 8

[Hubel 1968] D.H. Hubel and T.N. Wiesel. *Receptive fields and functional architecture of monkey striate cortex.* The Journal of Physiology, vol. 195, no. 1, page 215, 1968. 8

[Hubel 1977] D.H. Hubel and T.N. Wiesel. *Functional architecture of macaque monkey.* Proceedings of the Royal Society, London [B], pages 1–59, 1977. 8, 9

[Hubener 1997] M. Hubener, D. Shoham, A. Grinvald and T. Bonhoeffer. *Spatial Relationships among Three Columnar Systems in Cat Area 17.* Journal of Neuroscience, vol. 17, no. 23, pages 9270–9284, 1997. 9, 11

[Hupé 1998] J.M. Hupé, A.C. James, B.R. Payne, S.G. Lomber, P. Girard and J. Bullier. *Cortical feedback improves discrimination between figure and background by V1, V2 and V3 neurons.* Nature, vol. 394, pages 784–791, 1998. 172

[Hupé 2001] J.M. Hupé, A.C. James, P. Girard, S.G. Lomber, B.R. Payne and J. Bullier. *Feedback connections act on the early part of the responses in monkey visual cortex.* Journal of Neurophysiology, vol. 85, no. 1, page 134, 2001. 166

[Hutt 2003] A. Hutt, M. Bestehorn and T. Wennekers. *Pattern formation in intracortical neuronal fields.* Network: Computation in Neural Systems, vol. 14, pages 351–368, 2003. 132

[Hutt 2006] A. Hutt and F.M. Atay. *Effects of distributed transmission speeds on propagating activity in neural populations.* Physical Review E, vol. 73, no. 021906, pages 1–5, 2006. 87, 108

[Hutt 2008] A. Hutt. *Local excitation-lateral inhibition interaction yields oscillatory instabilities in nonlocally interacting systems involving finite propagation delays.* Physics Letters A, vol. 372, pages 541–546, 2008. 87, 108, 153

[Hutt 2009] A. Hutt. *Finite Propagation Speeds in Spatially Extended Systems.* Complex Time-Delay Systems: Theory and Applications, page 151, 2009. 87

[Hutt 2010] A. Hutt and N. Rougier. *Activity spread and breathers induced by finite transmission speeds in two-dimensional neural fields.* Physical Review E, vol. 82, no. 5, page 055701, 2010. 86, 132

[Iooss 2000] G. Iooss and K. Kirchgassner. *Travelling waves in a chain of coupled nonlinear oscillators.* Communications in Mathematical Physics, vol. 211, no. 2, pages 439–464, 2000. 123

[Ize 2003] J. Ize and A. Vignoli. Equivariant degree theory. de Gruyter, 2003. 77

[Izhikevich 2000] E.M. Izhikevich. *Neural Excitability, Spiking, and Bursting.* International Journal of Bifurcation and Chaos, vol. 10, pages 1171–1266, 2000. 80

[Izhikevich 2007] E.M. Izhikevich. Dynamical Systems in Neuroscience: The Geometry of Excitability And Bursting. MIT Press, 2007. 24

[Izhikevich 2008] Eugene M Izhikevich and Gerald M Edelman. *Large-scale model of mammalian thalamocortical systems.* Proc Natl Acad Sci U S A, vol. 105, no. 9, pages 3593–3598, March 2008. ix, xiii

[Jancke 2004] D. Jancke, F. Chavane, S. Naaman and A. Grinvald. *Imaging cortical correlates of illusion in early visual cortex.* Nature, vol. 428, pages 423–426, 2004. 168

[Jarlebring 2010] E. Jarlebring, K. Meerbergen and W. Michiels. *An Arnoldi like method for the delay eigenvalue problem.* status: published, 2010. 96, 132, 136

[Jin 2011] J. Jin, Y. Wang, H.A. Swadlow and J.M. Alonso. *Population receptive fields of ON and OFF thalamic inputs to an orientation column in visual cortex.* Nature neuroscience, 2011. 14

[Jirsa 2000] VK Jirsa and JAS Kelso. *Spatiotemporal pattern formation in neural systems with heterogeneous connection topologies.* Physical Review E, vol. 62, no. 6, pages 8462–8465, 2000. 41, 87

[Kandel 2000] E.R. Kandel, J.H. Schwartz and T.M. Jessel. Principles of neural science. McGraw-Hill, 4th édition, 2000. 3, 5, 6, 14, 31

[Kang 2003] K. Kang, M. Shelley and H. Sompolinsky. *Mexican hats and pinwheels in visual cortex.* Proceedings of the National Academy of Sciences of the United States of America, vol. 100, no. 5, page 2848, 2003. 20, 33, 228

[Kato 1995] T. Kato. Perturbation Theory for Linear Operators. Springer, 1995. 95, 96, 126, 271

[Kenet 2003] T. Kenet, D. Bibitchkov, M. Tsodyks, A. Grinvald and A. Arieli. *Spontaneously emerging cortical representations of visual attributes.* Nature, vol. 425, no. 6961, pages 954–956, 2003. 213, 214, 226

[Kielhöfer 2003] H. Kielhöfer. Bifurcation theory: An introduction with applications to pdes. Springer, 2003. 41, 42, 54, 55, 57, 71

[Kilpatrick 2008] Z.P. Kilpatrick, S.E. Folias and P.C. Bressloff. *Traveling pulses and wave propagation failure in inhomogeneous neural media.* SIAM Journal on Applied Dynamical Systems, vol. 7, no. 1, pages 161–185, 2008. 41

[Kilpatrick 2010a] Z.P. Kilpatrick and P.C. Bressloff. *Effects of synaptic depression and adaptation on spatiotemporal dynamics of an excitatory neuronal network.* Physica D: Nonlinear Phenomena, vol. 239, no. 9, pages 547–560, 2010. 23

[Kilpatrick 2010b] Z.P. Kilpatrick and P.C. Bressloff. *Spatially structured oscillations in a two-dimensional excitatory neuronal network with synaptic depression.* Journal of computational neuroscience, vol. 28, no. 2, pages 193–209, 2010. 23

[Kishimoto 1979] K. Kishimoto and S. Amari. *Existence and stability of local excitations in homogeneous neural fields.* Journal of Mathematical Biology, vol. 7, no. 4, pages 303–318, 1979. 41

[Kisvarday 1997] ZF Kisvarday, E. Toth, M. Rausch and UT Eysel. *Orientation-specific relationship between populations of excitatory and inhibitory lateral connections in the visual cortex of the cat.* Cerebral Cortex, vol. 7, no. 7, page 605, 1997. 217, 226

[Kl"uver 1966] H. Kl
"uver. Mescal, and mechanisms of hallucinations. University of Chicago Press Chicago, 1966. 228

[Koch 2005] C. Koch. Biophysics of computation: information processing in single neurons. Oxford University Press, USA, 2005. 24

[Kolers 1964] P.A. Kolers. *The illusion of movement.* Scientific American, 1964. 165

[Kress 1999] R. Kress. Linear integral equations, volume 82. Springer Verlag, 1999. 74

[Kuznetsov 1998] Yuri A. Kuznetsov. Elements of applied bifurcation theory. Applied Mathematical Sciences. Springer, 2nd édition, 1998. 41, 42, 56, 57, 65, 87, 120, 127, 137, 139, 156

[Laing 2002] C.L. Laing, W.C. Troy, B. Gutkin and G.B. Ermentrout. *Multiple bumps in a neuronal model of working memory.* SIAM J. Appl. Math., vol. 63, no. 1, pages 62–97, 2002. 32, 41

[Laing 2003a] Carlo R. Laing and William C. Troy. *PDE Methods for Nonlocal Models.* SIAM Journal on Applied Dynamical Systems, vol. 2, no. 3, pages 487–516, 2003. 41

[Laing 2003b] C.R. Laing and W.C. Troy. *Two-bump solutions of Amari-type models of neuronal pattern formation.* Physica D, vol. 178, no. 3, pages 190–218, April 2003. 32

[Langford 1980] W.-F. Langford and G. Iooss. *Interactions of Hopf and pitchfork bifurcations.* Bifurcation Problems and their Numerical Solution. HD Mittelmann and H. Weber editors, ISNM, vol. 54, pages 103–134, 1980. 149

[Levitt 1997] J.B. Levitt and J.S. Lund. *Contrast dependence of contextual effects in primate visual cortex.* Nature, vol. 387, no. 6628, pages 73–76, 1997. 18

[Lund 1988] J.S. Lund. *Anatomical organization of macaque monkey striate visual cortex.* Annual Review of Neuroscience, vol. 11, no. 1, pages 253–288, 1988. 14

[Lund 2003a] Jennifer S. Lund, Alessandra Angelucci and Paul C. Bressloff. *Anatomical Substrates for Functional Columns in Macaque Monkey Primary Visual Cortex.* Cerebral Cortex, vol. 12, pages 15–24, 2003. 14, 16, 17, 86, 153, 229, 230

[Lund 2003b] J.S. Lund, A. Angelucci and P.C. Bressloff. *Anatomical substrates for functional columns in macaque monkey primary visual cortex.* Cerebral Cortex, vol. 13, no. 1, page 15, 2003. 251

[Ma 2005] Tian Ma and Shouhong Wang. Bifurcarion theory and applications, volume 53 of *Nonlinear Science.* World Scientific, 2005. 55

[Malach 1993] R. Malach, Y. Amir, M. Harel and A. Grinvald. *Relationship between intrinsic connections and functional architecture revealed by optical imaging and in vivo targeted biocytin injections in primate striate cortex.* Proceedings of the National Academy of Sciences, vol. 90, no. 22, page 10469, 1993. 15, 16

[Mariño 2005] J. Mariño, J. Schummers, D.C. Lyon, L. Schwabe, O. Beck, P. Wiesing, K. Obermayer and M. Sur. *Invariant computations in local cortical networks with balanced excitation and inhibition.* Nature neuroscience, vol. 8, no. 2, pages 194–201, 2005. 15, 19, 34, 217, 226, 230, 241

[Markounikau 2010] V. Markounikau, C. Igel, A. Grinvald and D. Jancke. *A dynamic neural field model of mesoscopic cortical activity captured with voltage-sensitive dye imaging.* PLoS Comput Biol, vol. 6, no. 9, page e1000919, 2010. 86, 214

[Markram 2004] H. Markram, M. Toledo-Rodriguez, Y. Wang, A. Gupta, G. Silberberg and C. Wu. *Interneurons of the neocortical inhibitory system.* Nature Reviews Neuroscience, vol. 5, pages 793–804, 2004. 15

[Markram 2006] H. Markram. *The blue brain project.* Nat Rev Neurosci, vol. 7, no. 2, pages 153–60, 2006. ix, xiii, 15

[Martin 2002] K.A.C. Martin. *Microcircuits in visual cortex.* Current opinion in neurobiology, vol. 12, no. 4, pages 418–425, 2002. 18

[Martinez-Conde 2004] Susana Martinez-Conde, Stephen L. Macknik and David H. Hubel. *The role of fixational eye movements in visual perception.* Nature Reviews Neuroscience, vol. 5, pages 229–240, 2004. 255

[Masson 2010] G.S. Masson and U.J. Ilg, editeurs. Dynamics of visual motion processing. Neuronal, Behavioral, and Computational Approaches. Springer Verlag, 1 édition, 2010. 11

[McCormick 1985] D.A. McCormick, B.W. Connors, J.W. Lighthall and D.A. Prince. *Comparative electrophysiology of pyramidal and sparsely spiny stellate neurons of the neocortex.* Journal of Neurophysiology, vol. 54, no. 4, page 782, 1985. 33

[Meister 2001] M. Meister and T. Bonhoeffer. *Tuning and topography in an odor map on the rat olfactory bulb.* The journal of neuroscience, vol. 21, no. 4, page 1351, 2001. 9

[Merchant 2004] H. Merchant, A. Battaglia-Mayer and A.P. Georgopoulos. *Neural responses in motor cortex and area 7a to real and apparent motion.* Experimental brain research, vol. 154, no. 3, pages 291–307, 2004. 166

[Miikkulainen 2005] R. Miikkulainen, J.A. Bednar, Y. Choe and J. Sirosh. Computational maps in the visual cortex. Springer, New York, 2005. 228

[Miller 1996] E.K. Miller, C.A. Erickson and R. Desimone. *Neural mechanisms of visual working memory in prefrontal cortex of the Macaque.* J. Neurosci., vol. 16, pages 5154–5167, 1996. 40

[Monier 2002] C. Monier. *Diversité fonctionnelle de l'intégration synaptique dans le cortex visuel primaire.* PhD thesis, Université Paris 6, 2002. 18

[Mountcastle 1957] V.B. Mountcastle. *Modality and topographic properties of single neurons of cat's somatosensory cortex.* Journal of Neurophysiology, vol. 20, pages 408–434, 1957. 8

[Muckli 2002] L. Muckli, N. Kriegeskorte, H. Lanfermann, F.E. Zanella, W. Singer and R. Goebel. *Apparent motion: event-related functional magnetic resonance imaging of perceptual switches and states.* J Neurosci, vol. 22, no. 9, 2002. 166

[Murphy 1996] P.C. Murphy and A.M. Sillito. *Functional morphology of the feedback pathway from area 17 of the cat visual cortex to the lateral geniculate nucleus.* The Journal of neuroscience, vol. 16, no. 3, page 1180, 1996. 14

[Nakagiri 1988] S. Nakagiri. *Structural properties of functional differential equations in Banach spaces.* Osaka J. Math, vol. 25, pages 353–398, 1988. 276

[Nauhaus 2008] I. Nauhaus, A. Benucci, M. Carandini and D.L. Ringach. *Neuronal selectivity and local map structure in visual cortex.* Neuron, vol. 57, no. 5, pages 673–679, 2008. 15, 19, 241

[Newsome 1986] W.T. Newsome, A. Mikami and R.H. Wurtz. *Motion selectivity in macaque visual cortex. III. Psychophysics and physiology of apparent motion.* Journal of Neurophysiology, vol. 55, no. 6, page 1340, 1986. 165, 166

[Nowak 1997] L.G. Nowak and J. Bullier. The timing of information transfer in the visual system, volume 12 of *Cerebral Cortex*, chapitre 5, pages 205–241. Plenum Press, New York, 1997. 15

[Nowak 2009] L.G. Nowak and P. Barone. *Contrast adaptation contributes to contrast-invariance of orientation tuning of primate V1 cells.* PLoS one, vol. 4, no. 3, page e4781, 2009. 18, 251

[Nunez 1995] P.L. Nunez. Neocortical dynamics and human eeg rhythms. Oxford University Press, USA, 1995. 33

[Obermayer 1993] K. Obermayer and G.G. Blasdel. *Geometry of orientation and ocular dominance columns in monkey striate cortex.* The Journal of neuroscience, vol. 13, no. 10, page 4114, 1993. 9

[Ohki 2005] K. Ohki, S. Chung, Y.H. Ch'ng, P. Kara and R.C. Reid. *Functional imaging with cellular resolution reveals precise micro-architecture in visual cortex.* Nature, vol. 433, pages 597–603, 2005. 9

[Ohki 2006] K. Ohki, S. Chung, P. Kara, M. H
"ubener, T. Bonhoeffer and R.C. Reid. *Highly ordered arrangement of single neurons in orientation pinwheels.* Nature, vol. 442, no. 7105, pages 925–928, 2006. 9

[Pazy 1983] A. Pazy. Semigroups of linear operators and applications to partial differential equations. Springer–Verlag, 1983. 109

[Perkel 1986] D.J. Perkel, J. Bullier and H. Kennedy. *Topography of the afferent connectivity of area 17 in the macaque monkey: A double-labelling study.* The Journal of comparative neurology, vol. 253, no. 3, pages 374–402, 1986. 14

[Pinto 1996] D.J. Pinto, J.C. Brumberg, D.J. Simons, G.B. Ermentrout and R. Traub. *A quantitative population model of whisker barrels: re-examining the Wilson-Cowan equations.* Journal of Computational Neuroscience, vol. 3, no. 3, pages 247–264, 1996. 29, 31, 85

[Pinto 2001a] D.J. Pinto and G.B. Ermentrout. *Spatially structured activity in synaptically coupled neuronal networks: 1. Traveling fronts and pulses.* SIAM J. of Appl. Math., vol. 62, pages 206–225, 2001. 32, 41

[Pinto 2001b] D.J. Pinto and G.B. Ermentrout. *Spatially structured activity in synaptically coupled neuronal networks: 2. Standing pulses.* SIAM J. of Appl. Math., vol. 62, pages 226–243, 2001. 32, 33

[Poincaré 1924] H. Poincaré. Science et méthode. E. Flammarion, 1924. ix, xiii

[Purves 2004] D. Purves, G.J. Augustine, D. Fitzpatrick, W.C. Hall, LaMantia A-S., McNamara J.O. and Williams S.M. Neuroscience. Sinauer Associates, Inc, 3rd édition, 2004. 3, 5, 24

[Qubbaj 2007] M.R. Qubbaj and V.K. Jirsa. *Neural field dynamics with heterogeneous connection topology.* Physical review letters, vol. 98, no. 23, page 238102, 2007. 41

[Rabinowitz 1971] P.H. Rabinowitz. *Some global results for nonlinear eigenvalue problems.* J. Funct. Anal, vol. 7, pages 487–513, 1971. 55, 56

[Rangan 2005] A.V. Rangan, D. Cai and D.W. McLaughlin. *Modeling the spatiotemporal cortical activity associated with the line-motion illusion in primary visual cortex.* Proceedings of the National Academy of Sciences of the United States of America, vol. 102, no. 52, page 18793, 2005. 228

[Reid 1995] R.C. Reid and J.M. Alonso. *Specificity of monosynaptic connections from thalamus to visual cortex.* Nature, vol. 378, no. 6554, pages 281–283, 1995. 14

[Reynaud 2011] Alexandre Reynaud. *Role fonctionnel des interactions laterales dans l'integration du mouvement visuel : etude en imagerie optique au niveau du cortex visuel primaire du singe eveille.* PhD thesis, Universite de la Mediterranee - Aix-Marseille II, 2011. 3

[Rockland 1983] K.S. Rockland and J.S. Lund. *Intrinsic laminar lattice connections in primate visual cortex.* The Journal of Comparative Neurology, vol. 216, no. 3, pages 303–318, 1983. 15

[Roland 2006] P.E. Roland, A. Hanazawa, C. Undeman, D. Eriksson, T. Tompa, H. Nakamura, S. Valentiniene and B. Ahmed. *Cortical feedback depolarization waves: a mechanism of top-down influence on early visual areas.* Proceedings of the National Academy of Sciences, vol. 103, no. 33, page 12586, 2006. 166

[Rolls 2002] Edmund T. Rolls and Gustavo Deco. Computational neuroscience of vision. Oxford university press, 2002. 3

[Rose 1974] D. Rose and C. Blakemore. *An analysis of orientation selectivity in the cat's visual cortex.* Experimental Brain Research, vol. 20, no. 1, pages 1–17, 1974. 20

[Roxin 2005] A. Roxin, N. Brunel and D. Hansel. *Role of Delays in Shaping Spatiotemporal Dynamics of Neuronal Activity in Large Networks.* Physical Review Letters, vol. 94, no. 23, page 238103, 2005. x, xiv, 25, 86, 98, 142

[Roxin 2011] A. Roxin and E. Montbrió. *How effective delays shape oscillatory dynamics in neuronal networks.* Physica. D, vol. 240, no. 3, pages 323–345, 2011. 25, 86, 87, 98, 99, 142, 144, 149, 155

[Rubin 2004] J.E. Rubin and W.C. Troy. *Sustained spatial patterns of activity in neuronal populations without recurrent excitation.* SIAM journal on applied mathematics, vol. 64, no. 5, pages 1609–1635, 2004. 32, 41

[Sala 2004] Marzio Sala, Michael A. Heroux and David M. Day. *Trilinos Tutorial.* Rapport technique SAND2004-2189, Sandia National Laboratories, 2004. 65, 66, 75

[Salin 1995] P.A. Salin and J. Bullier. *Corticocortical connections in the visual system: structure and function.* Psychol. Bull., vol. 75, pages 107–154, 1995. 15

[Schummers 2002] J. Schummers, J. Mariño and M. Sur. *Synaptic integration by V1 neurons depends on location within the orientation map.* Neuron, vol. 36, no. 5, pages 969–978, 2002. 11, 19

[Schwabe 2006] L. Schwabe, K. Obermayer, A. Angelucci and P.C. Bressloff. *The role of feedback in shaping the extra–classical receptive field of cortical neurons: a recurrent network model.* The Journal of Neuroscience, vol. 26, no. 36, pages 9117–9129, September 2006. 228

[Schwartz 1977] E.L. Schwartz. *Spatial mapping in the primate sensory projection: Analytic structure and relevance to perception.* Biological cybernetics, vol. 25, no. 4, pages 181–194, 1977. 7

[Sclar 1982] G. Sclar and R.D. Freeman. *Orientation selectivity in the cat's striate cortex is invariant with stimulus contrast.* Experimental Brain Research, vol. 46, no. 3, pages 457–461, 1982. 18, 19, 184

[Seriès 2002a] P. Seriès. *A theoretical study of center/ surround modulations of V1 receptive fields: circuits, dynamics and perceptual correlates.* PhD thesis, Paris VI, 2002. 3, 251

[Seriès 2002b] P. Seriès, S. Georges, J. Lorenceau and Y. Frégnac. *Orientation dependent modulation of apparent speed: a model based on the dynamics of feedforward and horizontal connectivity in V1 cortex.* Vision Research, vol. 42, no. 25, pages 2781–2798, 2002. 165, 255

[Shampine 2001] L.F. Shampine and S. Thompson. *Solving DDEs in MATLAB.* Applied Numerical Mathematics, vol. 37, pages 441–458, 2001. 86

[Sharon 2002] D. Sharon and A. Grinvald. *Dynamics and constancy in cortical spatiotemporal patterns of orientation processing.* Science, vol. 295, no. 5554, page 512, 2002. 214

[Shayer 2000] L.P. Shayer and S.A. Campbell. *Stability, bifurcation, and multistability in a system of two coupled neurons with multiple time delays.* SIAM Journal on Applied Mathematics, vol. 61, no. 2, pages 673–700, 2000. 86

[Shelley 2002] M. Shelley and D. McLaughlin. *Coarse-grained reduction and analysis of a network model of cortical response: I. Drifting grating stimuli.* Journal of Computational Neuroscience, vol. 12, no. 2, pages 97–122, 2002. 15, 20, 211, 228, 231

[Sherman 1996] S.M. Sherman and R.W. Guillery. *The functional organization of thalamocortical relays.* J. Neurophysiol.,, vol. 76, pages 1367–1395, 1996. 7

[Sherman 2001] S.M. Sherman and R.W. Guillery. Exploring the thalamus. Academic Pr, 2001. 7

[Shinozaki 2007] Hiroshi Shinozaki. Lambert w function approach to stability and stabilization problems for linear time- delay systems. Master's thesis, Kyoto Institute of Technology, 2007. 98

[Shriki 2003] O. Shriki, D. Hansel and H. Sompolinsky. *Rate models for conductance-based cortical neuronal networks.* Neural Computation, vol. 15, no. 8, pages 1809–1841, 2003. 60, 184

[Sillito 2006] A.M. Sillito, J. Cudeiro and H.E. Jones. *Always returning: feedback and sensory processing in visual cortex and thalamus.* TRENDS in Neurosciences, vol. 29, no. 6, pages 307–316, June 2006. 172

[Simon 2010] B. Simon. Trace ideals and their applications. AMS Bookstore, 2010. 133

[Skottun 1987] B.C. Skottun, A. Bradley, G. Sclar, I. Ohzawa and R.D. Freeman. *The effects of contrast on visual orientation and spatial frequency discrimination: a comparison of single cells and behavior.* Journal of Neurophysiology, vol. 57, no. 3, page 773, 1987. 184

[Solomon 2002] S.G. Solomon, A.J.R. White and P.R. Martin. *Extraclassical receptive field properties of parvocellular, magnocellular, and koniocellular cells in the primate lateral geniculate nucleus.* The Journal of neuroscience, vol. 22, no. 1, pages 338–349, 2002. 14

[Somers 1995] D.C. Somers, S.B. Nelson and M. Sur. *An emergent model of orientation selectivity in cat visual cortical simple cells.* Journal of Neuroscience, vol. 15, no. 8, page 5448, 1995. 20, 184, 185, 210, 228

[Somers 1998] D.C. Somers, E.V. Todorov, A.G. Siapas, L.J. Toth, D.S. Kim and M. Sur. *A local circuit approach to understanding integration of long-range inputs in primary visual cortex.* Cerebral Cortex, vol. 8, no. 3, page 204, 1998. 228

[Sterratt 2011] D. Sterratt, B. Graham, A. Gillies and D. Willshaw. Principles of computational modelling in neuroscience. Cambridge Univ Pr, 2011. 24, 25

[Stetter 2000] M. Stetter, H. Bartsch and K. Obermayer. *A mean-field model for orientation tuning, contrast saturation, and contextual effects in the primary visual cortex.* Biological cybernetics, vol. 82, no. 4, pages 291–304, 2000. 33, 172, 228, 251

[Stetter 2002] M. Stetter. Exploration of cortical function: Imaging and modeling cortical population coding strategies. Kluwer Academic Pub, 2002. 172

[Stettler 2002] D.D. Stettler, A. Das, J. Bennett and C.D. Gilbert. *Lateral connectivity and contextual interactions in macaque primary visual cortex.* Neuron, vol. 36, no. 4, pages 739–750, 2002. 16

[Steyn-Ross 2007] M.L. Steyn-Ross, D.A. Steyn-Ross, MT Wilson and J.W. Sleigh. *Gap junctions mediate large-scale Turing structures in a mean-field cortex driven by subcortical noise.* Physical Review E, vol. 76, no. 1, page 11916, 2007. 24

[Suarez 1995] H. Suarez, C. Koch and R. Douglas. *Modeling direction selectivity of simple cells in striate visual cortex within the framework of the canonical microcircuit.* The Journal of neuroscience, vol. 15, no. 10, page 6700, 1995. 228

[Swindale 2003] N.V. Swindale, A. Grinvald and A. Shmuel. *The spatial pattern of response magnitude and selectivity for orientation and direction in cat visual cortex.* Cerebral Cortex, vol. 13, no. 3, page 225, 2003. 9

[Tao 2004] L. Tao, M. Shelley, D. McLaughlin and R. Shapley. *An egalitarian network model for the emergence of simple and complex cells in visual cortex.* Proc Natl Acad Sci, vol. 101, no. 1, pages 366–371, January 2004. 228

[Thomson 2002] Alex M. Thomson, A. Peter Bannister, Audrey Mercer and Oliver T. Morris. *Target and temporal pattern selection at neocortical synapses.* The Royal Society, vol. 357, pages 1781–1791, 2002. 15

[Thomson 2003] Alex M. Thomson and A. Peter Bannister. *Interlaminar Connections in the Neocortex.* Cerebral Cortex, vol. 13, pages 5–14, January 2003. 15, 27

[Thomson 2007] A.M. Thomson and C. Lamy. *Functional maps of neocortical local circuitry.* Frontiers in Neuroscience, vol. 1, no. 1, pages 19–42, November 2007. 15

[Tlapale 2011] Emilien Tlapale. *Modelling the dynamics of contextual motion integration in the primate.* PhD thesis, Université Nice Sophia Antipolis, January 2011. 11

[Travis 1974] CC Travis and GF Webb. *Existence and stability for partial functional differential equations.* AMERICAN MATHEMATICAL SOCIETY, vol. 200, 1974. 91

[Tricomi 1985] F.G. Tricomi. Integral equations. Dover, 1985. Reprint. 32, 42, 58

[Troyer 1998] T.W. Troyer, A.E. Krukowski, N.J. Priebe and K.D. Miller. *Contrast-invariant orientation tuning in cat visual cortex: thalamocortical input tuning and correlation-based intracortical connectivity.* The Journal of neuroscience, vol. 18, no. 15, page 5908, 1998. 20

[Tsodyks 1998] Misha Tsodyks, Klaus Pawelzik and Henry Markeam. *Neural Networks with Dynamic Synapses.* Neural Computation, vol. 10, pages 821–835, 1998. 23

[Tuckwell 1988] H. C. Tuckwell. Introduction to theoretical neurobiology. Cambridge University Press, 1988. 24

[Vanzetta 2008] I. Vanzetta and A. Grinvald. *Coupling between neuronal activity and microcirculation: implications for functional brain imaging.* HSFP Journal, vol. 2, pages 79–88, 2008. 213

[Veltz 2010] Romain Veltz and Olivier Faugeras. *Local/Global Analysis of the Stationary Solutions of Some Neural Field Equations.* SIAM Journal on Applied Dynamical Systems, vol. 9, no. 3, pages 954–998, August 2010. 86, 92, 108, 255

[Veltz 2011a] Romain Veltz. *An analytical method for computing Hopf bifurcation curves in neural field networks with space-dependent delays.* Comptes Rendus Mathematique, vol. 349, pages 749–752, July 2011. 100, 255

[Veltz 2011b] Romain Veltz and Olivier Faugeras. *Stability of the stationary solutions of neural field equations with propagation delays.* The Journal of Mathematical Neuroscience, vol. 1, no. 1, page 1, 2011. 87, 95, 132, 255

[Venkov 2007] N.A. Venkov, S. Coombes and P.C. Matthews. *Dynamic instabilities in scalar neural field equations with space-dependent delays.* Physica D: Nonlinear Phenomena, vol. 232, pages 1–15, 2007. 41, 87, 99, 153

[Venkov 2008] N.A. Venkov. *Dynamics of Neural Field Models.* PhD thesis, University of Nottingham, 2008. URL: http://www.maths.nottingham.ac.uk/personal/pmxnav/nikola venkov 09 - neural fields - phd thesis.pdf. 27, 132

[Voges 2010] N. Voges, C. Guijarro, A. Aertsen and S. Rotter. *Models of cortical networks with long-range patchy projections.* Journal of computational neuroscience, vol. 28, no. 1, pages 137–154, 2010. 18

[Wang 2006] W. Wang, H.E. Jones, I.M. Andolina, T.E. Salt and A.M. Sillito. *Functional alignment of feedback effects from visual cortex to thalamus.* Nature neuroscience, vol. 9, no. 10, pages 1330–1336, 2006. 14, 16

[Werner 2001] Herrad Werner and Tim Richter. *Circular stationary solutions in two-dimensional neural fields.* Biological Cybernetics, vol. 85, no. 3, pages 211–217, September 2001. 32

[Wertheimer 1912] M. Wertheimer. *Experimentelle studien "uber das sehen von bewegung.* Zeitschrift f "ur Psychologie, vol. 61, pages 161–265, 1912. 165

[Wilson 1972] H.R. Wilson and J.D. Cowan. *Excitatory and inhibitory interactions in localized populations of model neurons.* Biophys. J., vol. 12, pages 1–24, 1972. 23

[Wilson 1973] H.R. Wilson and J.D. Cowan. *A mathematical theory of the functional dynamics of cortical and thalamic nervous tissue.* Biological Cybernetics, vol. 13, no. 2, pages 55–80, September 1973. 23, 32, 40, 85

[Wohrer 2008] Adrien Wohrer. *The vertebrate retina: A functional review.* Research Report 6532, INRIA, May 2008. 3, 6

[Wu 1996] J. Wu. Theory and applications of partial functional differential equations. Springer, 1996. 90, 91, 95, 101, 109, 126

[Wu 1998] J. Wu. *Symmetric functional differential equations and neural networks with memory.* Transactions of the American Mathematical Society, vol. 350, no. 12, pages 4799–4838, 1998. 86, 95

[Wu 2001] J. Wu. Introduction to neural dynamics and signal transmission delay. Walter de Gruyter, 2001. 86

[Yoshioka 1996] T. Yoshioka, G.G. Blasdel, J.B. Levitt and J.S. Lund. *Relation between patterns of intrinsic lateral connectivity, ocular dominance, and cytochrome oxidase-reactive regions in macaque monkey striate cortex.* Cerebral Cortex, vol. 6, no. 2, page 297, 1996. 15, 16

[Yosida 1980] K. Yosida. Functional Analysis. 6th ed., volume XII of *Grundlehren der mathematischen Wissenschaften.* Springer–Verlag, 1980. 94, 106

[Yousef 2001] T. Yousef, É. Tóth, M. Rausch, U.T. Eysel and Z.F. Kisvárday. *Topography of orientation centre connections in the primary visual cortex of the cat.* Neuroreport, vol. 12, no. 8, page 1693, 2001. 217, 226

[Zhuo 2003] Y. Zhuo, T.G. Zhou, H.Y. Rao, J.J. Wang, M. Meng, M. Chen, C. Zhou and L. Chen. *Contributions of the visual ventral pathway to long-range apparent motion.* Science, vol. 299, no. 5605, page 417, 2003. 166